IDENTIFICATION OF BRANCH-POINT RESTRICTIONS IN MICROBIAL METABOLISM THROUGH METABOLIC FLUX ANALYSIS AND LOCAL NETWORK PERTURBATIONS

by

Joseph John Vallino

B.S. Chemical Engineering
University of California, Berkeley
(1983)

M.S. Chemical Engineering
California Institute of Technology
(1985)

Submitted to the Department of Chemical Engineering in
Partial Fulfillment of the Requirements for the Degree of

DOCTOR OF PHILOSOPHY
in Chemical Engineering

at the

MASSACHUSETTS INSTITUTE OF TECHNOLOGY
February, 1991

Signature of Author 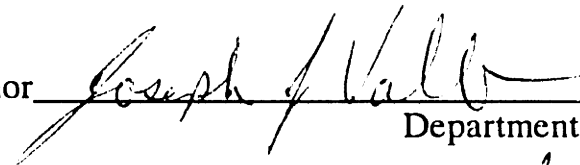
Department of Chemical Engineering
November 6, 1990

Certified by 
Gregory N. Stephanopoulos
Professor of Chemical Engineering
Thesis Supervisor

Accepted by 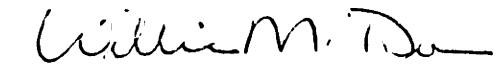
William M. Deen
Chairman, Departmental Committee on Graduate Students

— Blank Page —

IDENTIFICATION OF BRANCH-POINT RESTRICTIONS IN MICROBIAL METABOLISM THROUGH METABOLIC FLUX ANALYSIS AND LOCAL NETWORK PERTURBATIONS

by

Joseph John Vallino

Submitted to the Department of Chemical Engineering
on November 6, 1990 in partial fulfillment of the
requirements for the Degree of Doctor of Philosophy in
Chemical Engineering

ABSTRACT

To enhance metabolic engineering efforts, a general, non-invasive procedure has been developed by which the primary metabolism of an organism (*i.e.*, glycolysis, tricarboxylic acid cycle, pentose phosphate pathway, etc.) can be represented in a simple mathematical framework that permits metabolic carbon-flux distributions to be estimated from the measured accumulation rates of extracellular metabolites. The approach is based solely on biochemically constrained metabolite balances and a pseudo-steady state approximation for intracellular metabolite accumulation rate; consequently, knowledge of enzyme kinetics is not required. This representation allows metabolic networks to be readily analyzed for singularity and sensitivity problems, and incorporates a measurement consistency routine, which insures that measurements properly comply with biochemical constraints and the pseudo-steady state approximation. Theoretical flux distributions are readily determined and are employed to calculate the maximum product yield sustainable by the assumed biochemistry. Analysis of theoretical flux distributions facilitate the identification of key branch-points in the metabolism where flux alterations must occur in order to achieve improvements in product yield. If any of these key branch-points, referred to as principal nodes, are regulated *in vivo* such that flux partitioning at a node is maintained constant or otherwise bounded, then the overall metabolic network will appear rigid to flux alterations, and improvements in product yield may not be realizable by simple enzyme attenuation or deletion techniques commonly employed for strain improvement. To assess the degree by which a principal node may limit product yield, its response to a local metabolic perturbation is examined. Possible nodal responses are classified as: 1) flexible, if flux partitioning is not bounded; 2) weakly rigid, if flux partitioning is bounded but not controlled; and 3) strongly rigid, if flux partition is actively controlled.

To demonstrate these techniques, lysine production from glucose by *Corynebacterium glutamicum* ATCC 21253 is examined. Analysis of the metabolic network of *C. glutamicum* reveals two singular groups associated with 1) the TCA cycle and the glyoxylate shunt, and 2) four carboxylation reactions. These network singularities,

however, are easily removed since *in vitro* assays demonstrate that the glyoxylate shunt in not expressed in the presence of glucose and that phosphoenolpyruvate (PEP) carboxylase (PPC) is the only significant carboxylation reaction. Flux distributions generated from a controlled lysine fermentation are consistent with the preconceived operation of the metabolic pathways and agree well with tracer-based flux estimates documented in the literature. Theoretical flux analysis of the network reveals that the maximum molar lysine yield from glucose is 75%. Three principal nodes are identified at the glucose-6-phosphate (Glc6P), PEP, and pyruvate (Pyr) branch-points.

Flux analysis of a Glc6P isomerase attenuated mutant, isolated from *C. glutamicum* ATCC 21253, during a lysine fermentation indicates that the Glc6P node is not weakly rigid. Analysis of the ATCC 21253 strain cultivated on gluconate indicates that lysine yield is not limited by NADPH supply. It is concluded that the Glc6P node is flexible. Examination of the flux distributions in a pyruvate dehydrogenase complex (PDC) attenuated mutant, isolated from the ATCC 21253 strain, reveals that the Pyr node is not weakly rigid. Diversion of pyruvate from the TCA cycle following the addition of arsenite or fluoropyruvate during a fermentation indicates that the Pyr node in not strongly rigid and that Pyr does not limit lysine yield, which implicates the PEP node as the source of the network rigidity.

To examine the cause of the PEP node rigidity, a kinetic-based model is constructed incorporating enzyme kinetics for enolase, PPC, Pyr kinase (PK), aspartate (Asp) aminotransferase, PDC, Asp kinase (AT), and citrate synthase. Analysis of this model indicates that the PEP node is strongly rigid due to the allosteric control of PPC activity by Asp and acetyl coenzyme A (AcCoA). Since PPC requires activation by AcCoA to overcome inhibition by Asp, diversion of carbon from the TCA cycle results in a loss of PPC activation and a collapse of the PPC flux. As a result, attempts to enhance lysine yield via attenuation of PK or PDC activity only result in overall network flux attenuation. Furthermore, the rigidity of the PEP node is enhanced by the poor affinity of AK for Asp and the strong affinity of PK for PEP. To circumvent the strong rigidity of the PEP node, it is recommended that *C. glutamicum* be transformed with a gene that encodes for a PPC that is resistant to inhibition by Asp and does not require activation by AcCoA.

Thesis Supervisor: Dr. Gregory N. Stephanopoulos

Title: Professor of Chemical Engineering

Acknowledgements

This thesis is the culmination of several years of research, and as such, many people have contributed to it. Some have directly assisted and are easily acknowledged, while many others have contributed in more subtle ways to the development of new ideas or to the maintenance of my sanity. Although it is not possible to acknowledge everyone to which I am indebted (I probably couldn't spell all their names correctly anyway), I will attempt to scratch the surface.

First of all, I would like to express my gratitude to Greg Stephanopoulos, my advisor, for allowing me the freedom, with the proper dash of guidance, to formulate my own research objectives and approaches. Although such freedom can often extend ones tenure, it is an experience, I feel, that will prove invaluable in the future. I have also appreciated working with an advisor who is easy to talk to, not only in regards to research, but on aspects of life in general. Appreciation also goes to the members of my committee, Arnold Demain, Mark Kramer, Anthony Sinskey, and Daniel I. C. Wang, who have provided encouragement for more and more research as well as an implicit education on the presentation of research results.

I greatly acknowledge the assistance and camaraderie of my lab-mates, who have not only made late nights in the lab pleasurable (ok, bearable), but were also instrumental in providing suggestions. Thanks go to: Bob Kiss (the) for providing the fermentation monitoring program and his perspectives on the lysine fermentation, as well as for keeping the lab running smoothly; John David Chung for his infinite discussions and debates on the meaning of Chemical Engineering, research, and life (add an extra year, but well worth it); Craig Zupke for his input on the flux analysis routines; Ron Grosz for setting up the lab after our move from CalTech; and Sung Park for his discussions pertaining to this work. Much appreciation is also extended to the rest of the group for making seminars not only enlightening, but a pleasure to

attend. This goes equal well to the members of BPEC, and similar groups, who have provided constructive critiques, as well as friendship. I also thank Max Follettie for sharing his experience and knowledge on the microbiology of *Corynebacterium glutamicum.*

Without the support I received from many dear friends, both new and old, it is doubtful if completion of this work would have been possible (or meaningful). Foremost, utmost, and mostmost on this list is my "wefe" Cindy (BF). Not only did she translate this manuscript from "Joe" into English, she has been truly understanding and supportive, especially near the end. Three cheers go to Jim McMillian for his dear friendship and his Northern California perspectives, and to Greg O'Connor for his friendship and support. Special thanks also go to the Berkeley inmates, Matt Croughan and Fred Lam, for making the transition to Boston and MIT fun. Thanks also go to my buddies at (ok, were at) Caltech and to many dear friends back home.

If it were not for my parents (Mom and Dad), I may never have passed elementary school. To them I can only say, "You think it's easy..."

Finally, I would like to acknowledge Sulzer Biotech Systems for their gracious donation of the fermentation equipment that was used extensively in this research.

Contents

List of Figures

List of Tables

— Blank Page —

Chapter 1

Introduction

'I don't know what you mean by "glory,"' Alice said. Humpty Dumpty smiled contemptuously. 'Of course you don't—till I tell you. I meant "there's a nice knock-down argument for you!"'

'But "glory" doesn't mean "a nice knock-down argument,"' Alice objected.

'When *I* use a word,' Humpty Dumpty said, in rather a scornful tone, 'it means just what I choose it to mean—neither more nor less.'

'The question is,' said Alice, 'whether you *can* make words mean so many different things.'

'The question is,' said Humpty Dumpty, 'which is to be master——that's all.'

—Lewis Carrol, 1871
Through the Looking-Glass

Biochemical engineering covers a multitude of disciplines; hence, for brevity (or perhaps arrogance), there is a tendency to mix jargon between disciplines, which, of course, can be rather confusing. To make matters worse, I have introduced some new terminology, where needed, to facilitate discussion on the analysis of metabolic networks. Hopefully, the reader will not be as confused as poor Alice.

1.1 Motivation

In order to obtain high yields in the microbial production of primary metabolites, such as amino acids, the flow of carbon through the primary metabolism (*i.e.*, glycolysis, the TCA cycle, the pentose phosphate pathway, etc.) must be radically redirected from the pathways that normally support balanced growth. Such metabolic flux alterations directly oppose the enzyme level control mechanisms that are responsible for maintaining flux distributions optimal for growth. We refer to this

resistance as metabolic or network rigidity, which must be removed in order to attain improvements in product yield. Although modifications of the primary metabolism can now be achieved through molecular biology, the choice of enzymes to be amplified or attenuated to mitigate network rigidity remains uncertain, and yield enhancements via metabolic modifications are largely pursued by trial and error. Hence, there is a clear need to develop a robust technique to identify limitations in the primary metabolism.

Kinetic-based models of cellular metabolism and their analysis can sometimes reveal potential limiting enzymes or metabolic control architectures that may be responsible for network rigidity. These approaches, however, require detailed kinetic information that is often unavailable or severely limited for all but a few well-studied organisms. Consequently, the kinetic-based approach cannot be widely applied. Experimental techniques based on stable or radioactive isotope traces have been utilized to estimate flux distributions through metabolic networks. Unfortunately, these techniques can be experimentally taxing and are not easily extended beyond shaker flask studies or employed for on-line monitoring due to the expense or radioactivity of the tracer. Furthermore, a general framework has not been developed to utilized the information from metabolic flux distributions to identify limitations in the primary metabolism.

1.2 Objectives

- Develop a general procedure by which flux distributions in the primary metabolic pathways can be estimated from measurements that can be readily attained during the course of a fermentation.

- Develop a technique by which flux distribution estimates can be employed to identify limitations in the primary metabolism that constrain product yield.

- Apply these techniques to identify metabolic limitations that affect lysine yield.

1.3 Approach

To estimate the carbon flow through the primary metabolic pathways, we have extended and generalized *ad hoc* methodologies based on metabolite (*i.e.*, mass) balances that have been previously employed to examine fermentation processes. The approach, which is conceptually identical to tracer-based methods, utilizes constraints imposed by the biochemistry, a pseudo-steady state approximation for intracellular metabolites, and the measured accumulation rates of extracellular metabolites to generate flux distribution maps during the course of a fermentation. However, as inferred above, flux distribution maps, whether constructed from metabolite balances or tracers, do not directly identify limitations in the primary metabolism. To address this fundamental problem, general mechanisms are proposed by which the primary metabolism may limit product yield.

It will be demonstrated that the metabolite balance technique can be readily used to calculate theoretical flux distributions in the primary metabolism, which facilitates the identification of key metabolic branch-points where flux alterations must occur in order to achieve improvements in product yield. Although a considerable amount of research has focused on identifying "bottleneck" enzymes in a pathway (provided enzyme kinetics are available), relatively little emphasis has been placed on how branch-point flux partitioning is controlled, even though maximizing product yield ultimately relies on redirecting flux distributions at these key points. If any of these key branch-points, referred to as principal nodes, are regulated *in vivo* such that flux partitioning at the node is maintained constant, then the overall metabolic network will appear rigid and improvements in product yield will not be realizable by simple enzyme attenuation or deletion techniques commonly employed for strain improvement. Therefore, if a rigid principal node is present, its identification is imperative. Based on this premise, techniques are presented to examine principal node rigidity from local metabolic perturbations.

To demonstrate these techniques, we have chosen to investigate the microbial production of lysine from glucose by *Corynebacterium glutamicum* ATCC 21253. This organism displays characteristics of metabolic rigidity since deregulation of lysine synthesis typically results in lysine yields that are only 50% of the theoretical

maximum. Numerous attempts to perturb the metabolism, via enzyme attenuation, in favor of lysine synthesis have been met with only marginal success, and it is believed that the suboptimal lysine yield is due to nodal rigidity in the primary metabolism that supplies lysine precursors. We have focussed our research interests on 1) estimating flux distributions, 2) identifying the principal nodes in lysine synthesis, and 3) assessing principal node rigidity through metabolic perturbations.

1.4 Thesis Organization

Kinetic-based techniques employed for metabolic flux estimation and analysis are reviewed in the first sections of Chapter 2. Although most of the techniques presented in these sections were not employed in this study, they represent alternative methods to that developed in Chapter 4. Hence, the review provides the background by which the techniques developed Chapter 4 may be gauged. The last section of Chapter 2 reviews experimental techniques of metabolic flux estimation, including the metabolite balance techniques that are extended in Chapter 4. The first part of Chapter 3 reviews the primary biochemistry of glutamic acid bacteria as well as the pathways necessary to support biomass and lysine synthesis. Section 3.3 reviews the metabolic modifications that have been attempted to improve lysine producing strains. The last section of Chapter 3 briefly reviews the lysine fermentation. In Chapter 4, metabolic flux estimation and analysis techniques are thoroughly developed, and applied to the lysine network reviewed in Chapter 3. In Section 4.2, techniques for estimating theoretical yields are presented, and in Section 4.3, the basic premiss underlying metabolic rigidity is formulated. The framework present in Section 4.3 is crucial since it forms the justification of the experimental approach proposed for the identification of metabolic branch-point limitations. Although the procedures for enzyme assays, strain isolation, and fermentation operation occupy the bulk of Chapter 5, in Section 5.3, results are presented on the dominate pathways present in *C. glutamicum* ATCC 21253. In Chapter 6, results are presented on the metabolic perturbations used to asses the rigidity in the lysine metabolic network. In Section 6.5, a kinetic model is developed to illustrated the cause of the metabolic rigidity.

Chapter 2

Metabolic Flux Estimation Review

There are two general techniques employed to estimate flux distributions in metabolic networks. The first technique, discussed in Section 2.1, relies on kinetic expressions to represent the enzymatic reactions that comprise the metabolic pathways. These expressions, coupled with reaction stoichiometry, are used to construct a kinetic based-model of cellular metabolism, which can be solved numerically for the flux distributions. The advantage of a kinetic-based description of metabolism is that it can be analyzed for control architecture, as well as rate limiting reactions. Such analysis techniques are reviewed in Section 2.2. The obvious disadvantage to the kinetic-based approach is that detailed kinetic expressions for enzymatic reactions are often unavailable. Furthermore, the analysis of large kinetic models can tax numerical techniques and is often not amenable by analytical techniques. To circumvent such constraints, experimental base techniques can be employed for metabolic flux estimation, which are reviewed in Section 2.3. These techniques only require knowledge of the biochemistry; however, they cannot be used to predict metabolic response to enzymatic perturbations. Such perturbations must be conducted experimentally, as discussed in Chapters 4 and 6.

2.1 Kinetic-Based Models

2.1.1 Degree of Complexity

The kinetics of a metabolic network can be represented at two basic levels of complexity. Consider the following enzyme catalyzed reaction

$$E + S \underset{k_{-1}}{\overset{k_1}{\rightleftarrows}} ES \underset{k_{-2}}{\overset{k_2}{\rightleftarrows}} E + P \qquad (2.1)$$

where E, S, ES, P represent the enzyme, substrate, enzyme-substrate complex, and product, respectively, and k_i are rate constants. From the law of mass action, the overall rate of product formation is given by the following set of equations

$$\frac{d[S]}{dt} = k_{-1}[ES] + k_1[S][ES] - k_1[E_t][S] \qquad (2.2)$$

$$\frac{d[P]}{dt} \quad k_2[ES] - k_2[E_t][P] + k_{-2}[ES][P] \qquad (2.3)$$

$$\frac{d[ES]}{dt} = k_1[S][E_t] + k_{-2}[P][E_t] - (k_{-1} + k_2 + k_1[S] + k_{-2}[P])[ES] \qquad (2.4)$$

where $[E_t]$ is the total enzyme concentration given by [E] + [ES]. We will refer to such expressions as microkinetic representations since the various enzyme complexes are described in detail. Although a microkinetic expression can accurately capture the true dynamics of an enzyme catalyzed reaction, the dimensionality of these expressions can become extremely large (on the order of twenty differential equations or more) when complex enzymes, such as allosteric enzymes, are involved [see Hayashi and Sakamoto (1986) for examples]. If the desired goal is to model a metabolic network, which may consist of 10 to 100 or more enzymatic reactions, then the microkinetic representation of the network can become prohibitively large, particularly if several allosteric enzymes are present. Furthermore, the rate constants associated with the formation and breakdown of the enzyme complex are such that they often introduce significant time scale separation into the corresponding differential equations. Systems with significant time scale separation are referred to as stiff, and can introduce computational problems if not properly handled [Hayashi and Sakamoto, 1986]. Another disadvantage to the microkinetic representation is the lack of information on rate constants for the various enzyme-complex reactions associated with the detailed kinetics. Nevertheless, microkinetic representations are

often the only recourse for certain applications and have been employed to model metabolic networks, as we will see below.

If a quasi-steady state approximation is invoked for the ES complex (*i.e.*, Equation (2.4) is set to zero) [Alberty, 1959], then Equation (2.3) can be simplified to:

$$\frac{d[P]}{dt} = \frac{(k_1k_2[S] - k_{-1}k_{-2}[P])[E_t]}{k_{-1} + k_2 + k_1[S] + k_{-2}[P]} \tag{2.5}$$

This equation further simplifies to the classic Michaelis-Menten expression if the decomposition of the enzyme complex to product is assumed irreversible (*i.e.*, $k_{-2} = 0$) [Briggs and Haldane, 1925]. Although Equation (2.5) is an approximate solution to Equations (2.2)-(2.4), it is often a valid approximation [Vergonet and Berendsen, 1970; Segel, 1988]. We will refer to such a representation of an enzymatic reaction as a macrokinetic expression, in order to differentiate it from the microkinetic expression. The two main advantages of the macrokinetic representation are 1) the extreme reduction in system dimensionality, and 2) the availability of kinetic parameters from Lineweaver-Burk plots, Hill plots, etc. [Segel, 1975]†. For example, whereas the microkinetic representation of an allosteric enzyme may consist of 10 to 20 differential equations, the macrokinetic representation would only consist of one algebraic expression, whose rate parameters could be obtained from a Hill plot. Furthermore, if determining the steady state flux distribution and metabolite concentrations are the main objectives, then the macrokinetic expression is preferable, as both micro and macro representations yield the same steady-state results.

---

† Segel is also an excellent reference on the development of macrokinetic rate law expressions.

2.1.2 Metabolic Models

Although modeling of biochemical kinetics dates back to ca. 1900, it was not until the advent of computational methods (*i.e.*, analog and digital computers) that significant advances in quantitative metabolic kinetics were attained [Garfinkel, 1981]. Computational methods are required since the representation, either micro- or macrokinetic, of a system of enzymatic reactions is highly nonlinear and analytical solutions can seldom be obtained. Furthermore, studies on cognition have revealed that the mind can simultaneously follow only a few unrelated variables or feedback loops [Miller, 1956]. Hence the requirement for computational solutions.

Some of the first computer models were employed to study the enzyme kinetics associated with state transitions observed in the respiratory chain [Chance and Williams, 1956]. Using an analog computer, the authors where able to simulate experimentally observed respiratory transitions from State 4 to State 3, and back to State 4, upon the addition of a phosphate acceptor (ADP). These simulations validated the crossover theorem and the proposed phosphorylation sites of the respiratory chain [Chance *et al.*, 1955, 1958].

Shortly following the above publications, a microkinetic model was developed on a digital computer to simulate glycolysis and respiration in ascites tumor cells [Chance *et al.*, 1960]. The model was fairly simplistic due to computer limitations, and the microkinetic approach was required since the model was intended to simulate fast transients. Only a few reactions were used to represent glucose phosphorylation and glycolysis, and all the enzymes of the TCA cycle were lumped into one reaction. However, oxidative phosphorylation was well represented and accounted for the effects of uncoupling agents. Another salient feature of the model was the compartmentalization of ATP into two isolated—nonmixing—pools, representing the mitochondrial and cytoplasmic ATP reserves. The simulation presented illustrated the transients associated with endogenous metabolism and its response to the addition of glucose and subsequent addition of an oxidative phosphorylation uncoupling agent. Although the kinetic model was fairly simplistic, it was able to capture the general dynamics observed experimentally, including responses similar to the Pasteur and Crabtree effects. These effects, as well as the overall metabolic control, were

attributed to the compartmentalization of ATP and the availability of ADP. Even though this paper was one of the first in the field, it concisely demonstrated the usefulness of kinetic models in confirming hypothesis regarding metabolic control.

In a subsequent study, the above model was vastly expanded to account for all the enzymes of glycolysis, including reversibility of reactions and feedback inhibition by metabolites [Garfinkel and Hess, 1964]. Despite the lack of the TCA cycle or pentose phosphate pathway, the increased number of enzymatic reactions and the microkinetic representation produced a model consisting of 89 differential equations and 65 chemical species. Not surprisingly, computational problems were encountered, undoubtedly due to significant time scale separation in the model—*i.e.*, stiffness. Although the increase in complexity resulted in better agreement between experimental data and model predictions, the adenine nucleotides were still found to be the most important controlling factors in the model. If nothing else, this second paper illustrates the general trend in the field to construct metabolic models with ever increasing complexity.

Other systems that have been modeled by Garfinkel *et al.* include the TCA cycle [Garfinkel, 1971a,b] and the gluconeogenesis pathway [Achs *et al.*, 1971; Anderson *et al.*, 1971] in perfused rat livers, and a relatively complete metabolic model for perfused rate heart [Achs and Garfinkel, 1977a,b]. These models differ from those discussed above in that they appear to rely on macrokinetic representations (complete details of the models are not provided and are difficult to assess) and experimental data is used to fine tune model parameters. Once the model is constructed it is evaluated for controlling reactions by simply observing the response of the model to induced perturbations, a somewhat ad hoc, though fairly effective, sensitivity analysis. For instance, it was found from the studies on perfused rat livers that the TCA cycle is strongly affected by pyruvate carboxylase activity and oxaloacetate concentration, and gluconeogenesis is governed by the supply of phosphoenolpyruvate rather than by nucleotide concentrations. Studies on the perfused rat heart have provided a considerable amount of data on the transient responses of the metabolism to anoxia and glucose addition, the description of which is beyond the scope of this review. Furthermore, the authors were able to construct

flux distribution maps, similar to those described in Chapter 6, during the induced transients†. In general, however, these complex models appear similar to those developed earlier.

Recently, an extensive macrokinetic model has been constructed for the Human red blood cell—or erythrocyte—[Joshi and Palsson, 1989a,b,1990a,b]. The model consists of 33 differential equations (mass balances) and 41 macrokinetic rate expressions, and accounts for glycolysis, the pentose phosphate pathway, nucleotide metabolism, the Na^+/K^+ ion pump, osmotic balance and electroneutrality (the TCA cycle does not exist in erythrocytes). Predicted steady-state intracellular metabolite concentrations agree well with experimental measurements, and steady-state fluxes appear acceptable and agree with the limited data available. However, many aspects of the model were not compared to experimental data, and the usefulness of the model, other than as a review and compilation of previous results, was not significantly discussed. This is unfortunate as the model appears to incorporate sufficient rigorous information to be employed as a predictive tool, which could be used to formulate conditions for enlightening experimental work.

2.1.3 Cellular Models

Cellular models are similar to the macrokinetic models discussed above, in the sense that kinetic rate expressions and mass balance constraints are utilized to construct a set of differential equations intended to represent cellular functions. The main difference between cellular models and those discussed in the previous section resides on the scope of the model. Cellular models are intended to integrate the fundamental processes of a single cell, including synthesis of precursor metabolites, transcription, translation, cellular volume and composition, and replication and sporulation (where applicable). Such representations are basically the extreme of structured growth models. Cellular models are typically employed to obtain estimates for macroscopic parameters, such as growth rate under varying conditions, cell

---

† Although the flux distribution map is constructed from transient conditions, no significant violation of the pseudo-steady state approximation is observable (see Chapter 4).

volume, DNA replication rate, etc., as well as to elucidate the mechanisms of the overall cellular control. These models not only account for the synthesis of primary metabolites, but also the synthesis of protein, cell wall components, RNA, and DNA. To minimize the dimensionality of these models, enzymatic reactions of an entire pathway are often lumped into one overall rate expression and many metabolites are pooled into one group, such as "amino acids". Consequently, cellular models do not typically contain enough detail on the primary metabolism to be useful for metabolic studies, so the results obtained from such modeling will not be reviewed here. The interested reader is referred to the cellular models constructed for *Escherichia coli* [Domach *et al.*, 1984; Peretti and Bailey, 1986] and *Bacillus subtilis* [Jeong *et al.*, 1990] for more information.

2.1.4 Summary

Kinetic models not only provide estimates for steady-state flux distributions and metabolite concentrations, but are also useful in elucidating metabolic controls. Furthermore, since kinetic models are predictive, the effects of metabolic modifications, such as attenuation or amplification of enzyme activity, can be studied. There are several problems, however, associated with such models. Often, the detailed kinetic information required is unavailable, and even if it is, there is no guarantee that the expressions are comprehensive. It is quite conceivable that published kinetics on a particular enzyme may not account for the affects of a crucial inhibitor or activator. Since the response of a metabolic network strongly depends on the feedback architecture and/or enzyme regulation, incorrect kinetic information can lead to erroneous conclusions regarding metabolic control or rate limiting reactions. Even if accurate kinetic expressions are available, the identification of the controlling reactions in a complex metabolic network can be quite difficult. It is somewhat ironic that the kinetic models intended to elucidate cellular metabolism have become as complex and as difficult to comprehend as the organisms themselves. Not surprisingly, techniques for simplifying kinetic model expressions and identifying rate limiting reactions have received extensive attention in the literature, as reviewed in the next section.

2.2 Analysis of Kinetic Based Models

Once the metabolic functions of the cell are cast into a mathematical representation, they can be manipulated to the extent permitted by mathematical analysis. Consequently, there are quite literally hundreds of papers covering the topic of metabolic network analysis, a tutorial review of which is given by Heinrich *et al.* (1977). These papers generally fall into two main categories: 1) those that attempt to simplify the kinetic models so that the overall dynamics of the metabolism can be analyzed; and 2) techniques that attempt to identify controlling or rate limiting reactions. Although neither of these techniques are employed in this thesis, they represent alternative network analysis methods to that developed in Chapter 4. Therefore, they justify a brief review.

2.2.1 Analysis of Model Dynamics

Several similar techniques, based on traditional systems analysis, have been developed to simplify and analyze kinetic-based models of metabolism. In general, these techniques are not well suited for the purpose of uniquely identifying product limiting enzymes; they do, however, elucidate inherent metabolic controls that also need to be understood to optimize the metabolism leading to product synthesis. Since the techniques are based on modal analysis, this is briefly reviewed first [also see Luenberger (1979) and references given below].

The set of differential equations that describe macro- or microkinetic models, such as Equations (2.2)-(2.3), can be expressed as

$$\frac{d\boldsymbol{S}'}{dt} = \boldsymbol{F}(\boldsymbol{S}') \tag{2.6}$$

where $\mathbf{S}'$ is a vector of metabolite concentrations (and enzyme concentrations if a microkinetic description is used) and $\mathbf{F}$ is a vector of nonlinear functions in $\mathbf{S}'$. This equation can be linearized around the steady state, $\mathbf{S}'_{ss}$, which satisfies $\mathbf{F}(\mathbf{S}'_{ss}) = \mathbf{0}$, to give the following linear equation

$$\frac{d\mathbf{S}}{dt} = \mathbf{JS} \tag{2.7}$$

where **J** is the well known Jacobian matrix of **F** and **S** is now the deviation from steady state variable, given by $\mathbf{S} = \mathbf{S}' - \mathbf{S}'_{SS}$. This linearization is required since analytical solutions to the nonlinear expression, Equation (2.6), do not typically exist and analysis techniques have only been developed for linear systems. If the proper linear transformation is applied, Equation (2.7) can be expressed as

$$\frac{d\mathbf{m}}{dt} = \mathbf{\Lambda m} \tag{2.8}$$

where **m** is a vector of modes and **Λ** is a diagonal matrix composed of the eigenvalues of **J**. The linear transformation which accomplishes this is given by

$$\mathbf{m} = \mathbf{M}^{-1}\mathbf{S} \tag{2.9}$$

where **M** is referred to as the modal matrix whose columns are the eigenvectors of **J**. As evident from Equation (2.8), the linear transformation describes a basis in which the modes of the system are decoupled. Consequently, the solution to Equation (2.8) is readily determined and given by

$$m_i = m_{i,o}\exp(\lambda_i t) \quad \text{for } i = 1,..., k \tag{2.10}$$

where m_i are elements of **m**, $m_{i,o}$ are their initial conditions, λ_i are the diagonal elements of **Λ** (eigenvalues), and k is the dimension of **S**. Each mode has its own dynamics and moves at a characteristic time, or time constant, τ_i, given by $1/|\mathrm{Re}(\lambda_i)|$. The solution in terms of **S** is easily obtained by applying the inverse transformation to Equation (2.10), shown here

$$\mathbf{S} = \mathbf{Mm} = m_{1,o}\exp(\lambda_1 t)\mathbf{M}_1 + m_{2,o}\exp(\lambda_2 t)\mathbf{M}_2 + ... + m_{k,o}\exp(\lambda_k t)\mathbf{M}_k \tag{2.11}$$

where $\mathbf{M}_i$ are the column vectors of $\mathbf{M}$. Although the dynamics of each mode is characterized by a single time constant, it is clear from Equation (2.11) that the concentration of any particular metabolite is characterized by a spectrum of time constants. Consequently, it is easier to analyze systems in modal space and then transform the result back to concentration space. It is important to realize that Equation (2.11) accurately represents the true system only in the neighborhood of the steady state, *i.e.*, near $\mathbf{S} = \mathbf{0}$. To our knowledge, the extent a metabolic system can be perturbed from its steady state and still be described by Equation (2.7) has received relatively little attention. This is unfortunate since most metabolic modifications, such as enzyme deregulation, amplification, or attenuation, represent significant metabolic perturbations. Nevertheless, analysis of Equations (2.10) or (2.11) have proved to be insightful, as reviewed below.

It is not the actual solution of Equation (2.7), given by Equation (2.11), that is of interest here since it too will be fairly complex. If the solution was the only objective, then the above analysis is needless since the original nonlinear system can almost always be solved numerically, as reviewed in Section 2.1. Rather, it is how the linear solution may be approximated and how these approximations affect the original nonlinear system that are of interest. One of the first simplifications that can be investigated is that of time scale separation. If certain modes of Equation (2.10) have fast time scales (τ_F) and others have slow time scales (τ_S) such that $\tau_F \ll \tau_S$, then those modes with fast time scales will reach their steady state values much sooner than those modes with slow dynamics. Furthermore, if τ_F is small compared to time scales of interest, then those modes with times scales τ_F or smaller may be relaxed (*i.e.*, set to zero). Consequently, differential equations may be replaced with algebraic expressions. Time scale separation has been found to be predominant in both macro and microkinetic based models [Heinrich and Sonntag, 1982; Reich and Selkov, 1975]. In macroscopic models, time scale separation has been used to remove enzymatic reactions with fast dynamics and to lump metabolites into appropriate pools [Liao and Lightfoot, 1988b; Palsson and Joshi, 1987]. With this analysis, macrokinetic models, such as those reviewed in Section 2.1, which consist of many metabolites and differential equations, may be reduced to just a few. Palsson

and Lightfoot (1984) have used time scale separation to demonstrate the validity of the quasi-steady state approximation and when its use is inappropriate.

The above analysis also employs another separation technique to simplify Equation (2.11). If **M** is diagonal, the metabolites themselves are the modes and can be readily evaluated since they are not coupled. The off-diagonal terms of **M** indicate the extent of interaction between the metabolites, as given by Equation (2.11), and their magnitudes are a function of the system parameters. Although **M**, in general, is not diagonal, with proper scaling of the system, Palsson and Lightfoot demonstrated that the diagonal terms of **M** vanish or are easily evaluated at various limits. This allowed them to examine the limits under which the quasi-steady state approximation is valid. They have also examined enzyme cooperativity in dimeric enzymes [Palsson *et al.*, 1984].

Liao and Lightfoot (1988a) have developed an experimentally coupled technique that exploits systems with time scale separation to estimate selected *in vivo* kinetic parameters. The essence of the technique can best be explained by a simple example. Consider a three component system whose linearized solution, as given by Equation (2.11), is

$$\begin{aligned} S_1 &= \alpha \exp(\lambda_1 t) + 0 + \beta \exp(\lambda_3 t) \\ S_2 &= 0 + \gamma \exp(\lambda_2 t) + \delta \exp(\lambda_3 t) \\ S_3 &: \text{ irrelevant} \end{aligned} \tag{2.12}$$

where α, β, γ, and δ are constants produced from the linearization and the initial conditions. If S_1 and S_2 were plotted on a phase diagram, the general solution would produce a nonlinear curve that exponentially approached the origin with increasing time (assume that all three eigenvalues have negative real parts). However, if there was significant time scale separation in the system, such that $\tau_1, \tau_2 \ll \tau_3$, then the first two modes could be relaxed and S_1 and S_2 could be expressed as $S_1 = \beta S_2/\delta$ for $t > \tau_1$ and τ_2. Therefore, from any initial conditions, the phase diagram of S_1 versus S_2 would exhibit a fast transient decay to a straight line given of slope β/δ, and then would exponentially decay along this line to the origin. The straight line so formed

is referred to as the characteristic reaction path (CRP), and is only exhibited by systems with time scale separation. Since the terms in Equation (2.11), such as α, β, γ, and δ in the example, are derived from kinetic expressions of the model, the slope of the CRP is an indirect measure of these parameters. Consequently, if one plots intracellular metabolite concentrations parameterized by time on a phase diagram, some information about the *in vivo* kinetics may be discerned from the slope and position of the CRP, if it is observable. These techniques have been applied to study the kinetics of phosphofructokinase in Yeast [Liao *et al.*, 1988] and of pyruvate kinase and phosphofructokinase in human red blood cells [Liao and Lightfoot, 1987]. Although this technique is promising, since it couples analysis with experiments, it is still quite limited by observability and sensitivity problems.

Other approaches have focused directly on elucidating the dynamics of metabolic feedback loops. Since these systems are inherently nonlinear, only extremely simplified subsystems are examined in depth. The typical metabolic control loop examined is a linear sequence of enzymatic reactions where the last metabolite in the sequence is an inhibitor of the first enzyme, and the first metabolite in the sequence, or its production rate, can be manipulated. Such systems closely resemble those studied in the chemical, electronic, and aerospace fields which are employed for systems control. Consequently, control theory has been extensively developed and has recently been employed to study control in metabolic networks. The goal of this type of analysis is to study how the metabolic control system reacts to changes in operating conditions, such as concentration of the first metabolite, inhibition type, enzyme amount, etc. For example, one teleologic view holds that the flux through a pathway should approach the maximum supportable since this would most efficiently utilize the enzyme resources. However, Majewski and Domach (1985) have employed control theory to demonstrate that there is a tradeoff between enzyme capacity utilization and flux controllability. Near enzyme capacity—maximum flux—the response of the network becomes sluggish, while fast response time can only be attained under low enzyme capacity. Majewski and Domach (1990b) have also demonstrated that TCA cycle flux control by modulation of an enzyme's apparent K_M (K-type regulation) is superior to modulation of its V_{MAX} (V-type regulation) for

enzymes with hyperbolic kinetics. It was further shown that different control architectures affect pathway coordination and scavenging functions. Similar control analysis techniques have been used to examine multiple steady states and acetate production in *E. coli* [Majewski and Domach, 1990a,c]. Palsson and Lightfoot have employed linear analysis and control theory to study the stability of simple networks and to examine conditions when a macrokinetic model can be used in place of a microkinetic description [Palsson and Lightfoot, 1985a,b; Palsson *et al.*, 1985]. Although these techniques are rather elegant, their applicability to complete metabolic networks remains questionable.

2.2.2 Metabolic Control and Biochemical Systems Theories

Approximately twenty years ago, two separate theoretical techniques were independently developed to facilitate and standardize the analysis of metabolic networks, which, as we have described above, are highly non-linear and difficult to analyze without resorting to numerical techniques. Currently, these two techniques are referred to as metabolic control theory (MCT) and biochemical systems theory (BST).

2.2.2.1 Metabolic Control Theory

Although the development of MCT is usually attributed to Kacser and Burns (1973) and Heinrich and Rapoport (1974a,b), it is conceptually no different than that originally presented by Higgins (1965). The primary impetus behind the development of MCT was to quantify the strength by which each enzyme in a metabolic pathway controls the overall flux through the pathway. Since this is accomplished via standard sensitivity analysis, we will agree with Savageau *et al.* (1987a) that MCT is somewhat of a misnomer. To systematically examine the effects of modulating an enzyme's concentration (E_i) on the flux (J) and metabolite concentrations (S_i) in a non-branching pathway, such as

$$S_0 \overset{E_1}{\rightleftarrows} S_1 \overset{E_2}{\rightleftarrows} S_2 \rightleftarrows \cdots \overset{E_n}{\rightleftarrows} S_n \rightarrow \qquad (2.13)$$

several sensitivity coefficients were defined, which have since been standardized [Westerhoff *et al.*, 1984], as reviewed below.

The elasticity coefficient for an isolated enzyme is a measure of how its activity changes with respect to slight perturbations of a selected metabolite or parameter (kinetic constant, inhibitor, etc.) at a particular point in concentration and parameter space under otherwise constant conditions, and is defined by

$$\epsilon^{i}_{S_k} = \frac{S_k}{v_i}\frac{\partial v_i}{\partial S_k} \tag{2.14}$$

In other words, the elasticity coefficient is the slope, with respect to S_k (or some other selected parameter), of the reaction velocity (v_i) at a given point in concentration space, which can be obtained from *in vitro* kinetic experiments or by differentiating the rate law expression with respect to S_k. It should be noted that the elasticity coefficient is not constant but varies as a function of location in concentration and parameter space.

The flux control coefficient expresses the sensitivity of the steady state pathway flux to slight perturbations in the concentration of a selected enzyme and is defined as

$$C^{J}_{E_i} = \frac{E_i}{J}\frac{dJ}{dE_i} \tag{2.15}$$

As with the elasticity coefficients, the value of flux control coefficients of a pathway, such as that of Equation (2.13), strongly depend on the operating point at which the coefficients are evaluated. Since the flux control coefficients are pathway dependent variables, they are not easily measurable; however, algebraic expressions can be derived for linear pathways that allow one to calculate the flux control coefficients from the elasticity coefficients that, in theory, can be measured.

Under steady state conditions, it can be shown [Kacser and Burns, 1973] for the linear pathway of Equation (2.13) (where S_0 is held constant and S_n is removed at its synthesis rate) that

$$\sum_{i=1}^{n} C_{E_i}^{J} = 1 \tag{2.16}$$

provided that v_i is proportional to E_i, which is often the case. Referred to as the flux-control summation theorem, Equation (2.16) indicates that if a particular enzyme in the pathway has a flux control coefficient close to unity, then it will have a dominating or controlling effect on the pathway. Another algebraic expression which can be derived for each metabolite (S) in the pathway (except S_n) is given by

$$\sum_{k=1}^{n-1} \sum_{i=1}^{n} C_{E_i}^{J} \epsilon_{S_k}^{i} = 0 \tag{2.17}$$

and is called the flux-control connectivity theorem. Between Equations (2.16) and (2.17) there are *n* linear equations from which the flux control coefficient can be determined if the elasticity coefficients are known. Recently, these relationships have been described in matrix notation and extended to complex pathways [Fell and Sauro, 1985; Small and Fell, 1989; Cascante *et al.*, 1989a,b] although the technique appears somewhat cumbersome.

Metabolic control theory has received extensive discussion in the literature as well as some criticism [Groen and Tager, 1988; Kacser and Porteous, 1987; Crabtree and Newsholme, 1987; Welch *et al.*, 1987]. Its usefulness, however, in clarifying metabolic controls or as a metabolic engineering tool remains unclear at best. (We will not even consider the obvious fact that one could construct a complete macrokinetic model from the information required to apply MCT.) Based on the flux-control summation theory and the observation that flux control coefficients of a pathway are often of similar order, Kacser and Burns (1979) have proposed that cellular metabolism can be characterized as a "Molecular Democracy" where control

of a pathway flux is distributed in a relatively equal manner to all the enzymes in the pathway. This has led to the philosophy that a rate limiting enzyme does not exist in a pathway, which, however, is misleading since the flux control coefficients represent flux sensitivity to the enzyme amount, not to feedback control architecture. A simple thought experiment illustrates the point. Consider a simple linear pathway in which the last metabolite in the network inhibits the first enzyme. Since the pathway is regulated by negative feedback control, it is not expected that amplification or attenuation of any enzyme in the pathway (including the first) will lead to significant alterations in pathway flux. These results imply that all of the flux control coefficients would be of similar order, which could lead one to the incorrect conclusion that a rate limiting enzyme does not exist. However, if we perturb the network architecture by releasing the feedback inhibition of the first enzyme, a significant increase in flux throughput could be achieved. Indeed, enzyme deregulation is the primary technique by which overproduction of primary metabolites is attained (see Chapter 3). Since feedback loops are pervasive in metabolic networks, flux control coefficients are not very enlightening and can be misleading. In our opinion, the philosophy of molecular democracy is inappropriate. Furthermore, due to the highly nonlinear nature of metabolic networks (which is extensively utilized to achieve cellular control) flux control coefficients for a pathway can vary radically between different operating points of the system, which was demonstrated even when the technique was first developed [Kacser and Burns, 1973]. Consequently, it is unlikely that the application of MCT to one or two operating points would reveal the ultrasensitivity that can arise at a branch-point [LaPorte *et al.*, 1984] or the branch-point control that we have observed (see Chapter 6). To capture such nonlinear phenomena, one must calculate flux control coefficients or related sensitivity coefficients at many different operating points; however, this is an arduous task and one would be better off utilizing numerical sensitivity techniques.

It is not surprising the MCT falls short of its intended task since it is merely a sensitivity analysis routine, which is applied to a highly nonlinear system. Its popularity in the literature can probably be attributed to two points: 1) a quantitative analysis routine for metabolic networks does not exist, yet there is always a desire to

attain one; and 2) the technique allows the user to publish "milestones" in the form of flux control coefficients that are viewed as worthwhile by the proponents of MCT†.

2.2.2.2 Biochemical Systems Theory

Biochemical systems theory (BST), developed by Savageau (1969a,b,1970), is a technique to reduce the complexity of macrokinetic metabolic models, so that they are amenable to analytical techniques. As passionately discussed by Savageau *et al.* (1987a,b), many of the techniques developed in MCT can be readily derived from BST; therefore, they claim that MCT is merely a special case of BST, a point that is still debated [Cornish-Bowden, 1989].

The foundation of BST resides in the representation of complex rate equations, such as Equation (2.5), by power law expressions. It is based on the assertion [Savageau, 1969b, 1987a] that enzyme kinetics can be approximated over a wide range by a straight line if plotted on a log-log plot. When the fitted line (at a particular operating point) is translated back into Cartesian coordinates, the following power law expression emerges

$$v_i(S_1,\ldots,S_n) = \alpha_i \prod_{j=1}^{n} S_j^{g_{ij}} \tag{2.18}$$

where α_i depends on the operating point (S_o) and g_{ij} are obtained by the partial derivatives of the rate expression with respect to S_j evaluated at the operating point. In other words, the power law expression represents the linear approximation, in the log-log domain, of the kinetic expression at some fixed point. For example, the well known Michaelis-Menten rate law can be expressed as

$$v = \alpha S^g \tag{2.19}$$

---

† Anyone who has examined a paper on numerical sensitivity methods can attest that a short table of numbers (*i.e.*, control coefficients) is more appealing than cause and effects relationships interpreted from a plethora of simulations, even though the later is often more enlightening.

where

$$g = \frac{K_M}{K_M + S_O} \quad \text{and} \quad \alpha = \frac{V_M S_O}{K_M + S_O} S_O^{-g} \tag{2.20}$$

Dynamic mass balances are still used to represent the metabolic network, as given by

$$\frac{dS_i}{dt} = \alpha_i \prod_{k=1}^{n} S_k^{g_{ik}} - \beta_i \prod_{j=1}^{n} S_j^{h_{ij}} \quad \text{for} \quad i = 1,..., n \tag{2.21}$$

where the first and second power product terms represent reactions producing and consuming S_i, respectively. The main advantage of the power law approximation is that it preserves some of the inherent nonlinear nature of enzyme kinetics [Savageau, 1970], while standardizing the format of kinetic expressions in a form that is more amenable to general theories of analysis. For instance, Savageau (1969b) shows that an analytical expression for the steady state solution of Equation (2.21) can be easily obtained and the existence of multiple steady states can be readily predicted.

Although BST is based on a foundation (the power law representation) that has potential for expansion [see Sorribas and Savageau (1989a,b) and references therein for latest developments], the techniques are still at their infancy with respect to those developed for linear analysis discussed in the preceding section. Furthermore, neither linear nor nonlinear analysis techniques can be easy applied to complete metabolic networks, and it is questionable if subnetworks can be realistically analyzed in isolation from the complete network. With the wide range of operating conditions and the chaotic behavior a metabolic network can achieve, it is uncertain if any technique that relies on expansion around a single operating point will ever render more insight into metabolic controls than standard numerical analysis.

2.3 Measurement Based Techniques

There are basically three different measurement techniques that can be used to estimate flux distributions in metabolic pathways: 1) tracer based techniques in which elements of a substrate are labeled with a stable or radioactive isotope; 2)

nuclear magnetic resonance (NMR) techniques in which magnetized nuclei serve as the label; and 3) metabolite balance techniques in which the consumption and accumulation rates of substrates and products are used to estimate the metabolic flux distributions. Metabolite balances and tracers are indirect techniques in the sense that a flux supported by a particular enzyme is not actually measured. Although NMR magnetization transfer and isotope exchange techniques directly measure a unidirectional reaction rate, they have not been used to estimate pathway fluxes, and have only been applied to a few enzymes. Each of these techniques are reviewed below. The mass balance technique is further developed in Chapter 4 and is used to study flux distributions in *Corynebacterium glutamicum* during lysine production, as presented in Chapter 6.

2.3.1 Tracer Based Techniques

Radioisotope traces have been extensively used in metabolic studies and were originally employed to elucidate pathway structure as opposed to pathway flux. However, once a metabolic pathway has been constructed and verified (by no means a trivial task), radioisotope tracers can be used to estimate the extent by which the various metabolic pathways are involved in the assimilation of the substrate(s). Although the methodology to accomplish this is fairly straight forward, it can be quite taxing, experimentally.

The general technique is as follows. The organism is incubated with a radioactive substrate, such as glucose, which has been specifically labeled at a designated carbon position with ^{14}C. After enough time has elapsed, the experiment is terminated and the incorporation of radioactivity into products, such as CO_2, biomass, excreted amino or organic acids, etc., is measured. If necessary, the amount of radioactivity incorporated into various carbon positions of the product can also be measured, but this increases dramatically the experimental effort. These experiments can then be repeated with the same substrate, but labeled at a different position, or with a different substrate. This experimental data by itself, however, does not define the metabolic flux distributions, which is why we refer to this approach as an indirect measurement technique. To obtain the flux distributions, one must utilize the

knowledge of the biochemical pathways along with information on how the carbon label is passed from one metabolite to the next to construct a set of algebraic equations that relate the metabolic fluxes to the product radioactivity. A complete and thorough description of the construction of flux distribution maps from radioisotope tracers has be published by Blum and Stein (1982). Blum *et al.* have also generated the most comprehensive metabolic flux distribution maps yet published, where *Tetrahymena pyriformis* [Connett and Blum, 1971; Stein and Blum, 1979] and hepatocytes [Crawford and Blum, 1983] served as the experimental systems. Their latest model has accounted for compartmentalization in the mitochondria and the peroxisomes. Although they have been able to construct quite detailed flux distribution maps from radioactivity measurements from only a few products, this required approximate 20 different ^{14}C-label combinations of 9 different substrates—not a simple task. Although radioisotope tracers have been extensively used to study flux partitioning between the pentose phosphate pathway and glycolysis, except for Blum *et al.*, radioisotope tracers have not been utilized to construct complete metabolic flux distribution maps, which may indicate that the effort required is not justified by the returns. Furthermore, the inherent safety issues associated with radioactive compounds often precludes their use in a controlled culture environment, such as a fermentor. As for glutamic acid bacteria, radioisotope tracers have not been extensively used except for early studies [Shiio *et al.*, 1960a,b; Shiio and Tsunoda, 1961a,b; Oishi and Aida, 1965; Otsuka *et al.*, 1965a].

The same approach discussed above for probing metabolic networks can also be accomplished with stable isotope labels, such as ^{13}C. Instead of measuring the radioactivity of the product, however, an NMR spectrum of the culture medium is used to determine the extent to which the label has been distributed among the products (this method should not be confused with *in vivo* NMR studies discussed below). Unlike radioactivity measurements, the intensity of the label at each carbon position of a metabolite can often be determined from the NMR spectrum, which dramatically increases the amount of information that can be extracted from the tracer study. As a result, fairly complete flux distribution maps can often be constructed from relatively few experiments. The only real disadvantage to the NMR

based technique is the high cost of the labeled substrates and the low sensitivity (compared to radioactivity) of NMR, which is compounded by the high background level of ^{13}C, approximately 1%. However, other stable labels, such as ^{1}H, ^{15}N, and ^{31}P, can also be employed. Recently, stable isotope tracers and NMR have been used to examine metabolic flux distributions in glutamic acid bacteria [Yamaguchi *et al.*, 1986; Inbar and Lapidot, 1987; Walker *et al.*, 1982; Inbar *et al.*, 1985; Ishino *et al.*, 1986; Walker and London, 1987]. The results, however, in several of these papers are corrupted by one or more of the general errors discussed below.

Anaplerotic reactions, such as phosphoenolpyruvate (PEP) carboxylase, can fix substantial amounts of CO_2 (see Chapter 6), especially if large amounts of TCA-related metabolites are secreted to the culture medium. The degree to which CO_2 (or HCO_3^-) is labeled in the micro-environment around the cell is uncertain; however, it is likely to be significant. Consequently, flux estimates will be corrupted if label fixing by CO_2 assimilating reactions is not accounted for. This problem is compounded by exchange reactions, such as

$$OAA \rightarrow Pyr + CO_2$$
$$PEP + CO_2 \rightarrow OAA + P_i$$

since label enrichment in CO_2 released by oxaloacetate (OAA) can be different than that assimilated by PEP carboxylase.

To support growth and product synthesis, metabolites are continuously drained from the primary metabolism, often at a high enough rate to dramatically affect flux and label distributions (see Chapter 6). Many investigators, however, do not account for the synthesis of by-products or biomass, and they implicitly assume that only complete substrate oxidation (or substrate oxidation coupled with the synthesis of the product of interest) occurs. As a result of these mass balance discrepancies and the unaccounted for CO_2 assimilation discussed above, flux estimates generated from repeated label experiments, such as using [1-^{14}C] versus [6-^{14}C] glucose, often show poor agreement. In an attempt to correct these errors, some investigators resort to assuming that some metabolic cycles, such as the TCA cycle or the glyoxylate shunt,

can be operated in a "single turn" or in "multiple turns". These unrealistic assumptions increase the number of degrees of freedom, so that a good fit to the tracer data can be artificially obtained. In our opinion, such assumptions would not have to be invoked if mass balances were properly closed, as discussed by Blum and Stein (1982) and also in Chapter 4.

Although tracer techniques are quite powerful tools for flux estimation, it should be emphasized that they are indirect measurements of flux distributions and will produce erroneous results if incorrect or incomplete metabolic pathways are used. Furthermore, there are no significant differences between flux estimation based on tracer methods or that based on metabolite balances discussed below. As for direct flux measurements, *in vivo* NMR techniques hold some promise, as discussed below.

2.3.2 NMR Techniques

Although it is beyond the scope of this review to discuss *in vivo* NMR applications in general [see review by Fernandez and Clark, (1987) and references therein], two *in vivo* NMR techniques, magnetization transfer and isotope exchange [Alger and Shulman, 1984; Brindle and Campbell, 1987], deserve some comment since they can be potentially employed for direct flux estimation. These techniques are both based on the same principle. Consider a reaction involving two species, such as $A \rightleftarrows B$, that are in equilibrium. If at $t = 0$ species A is labeled with a marker that is distinguishable when transferred to B, then one can measure the rate of the forward reaction as the label in the two pools approaches equilibrium. The difference between the two techniques resides in the label used. For magnetization transfer technique, the NMR device is used to impart a net magnetization of specific nuclei associated with the substrate or product of the enzyme under study. The decay of the induced magnetization can then be followed with NMR spectroscopy, and the rate of label decay can be used to estimate a unidirectional reaction rate. In the isotope exchange technique, a labeled substrate is added to the culture and its rate of incorporation into a particular metabolite pool is monitored.

These techniques cannot be easily applied to reactions at branch-points and are limited to substrates or products that are observable via NMR. As a result, only a few enzymes have been studied using these techniques [Brindle and Campbell, 1987], and the emphasis has been on measuring unidirectional enzyme kinetics as opposed to net flux. Another fundamental problem associated with *in vivo* NMR techniques is the control of a proper culture environment within the confines of the instrument [Fernandez and Clark, 1987]. Faced with these problems, *in vivo* NMR techniques are currently not considered viable methods for the measurement of metabolic fluxes; however, this field is rapidly advancing and it is conceivable that many of these obstacles will be overcome.

2.3.3 Metabolite Balance Techniques

Since this technique is fully developed in Chapter 4, only the basis of its foundation is reviewed here. The use of mass balance constraints on the growth of a microorganism became popular in estimation and control after it was observed that the elemental composition of the biomass remains relatively constant during growth [Minkevich and Eroshin, 1973]. This permits one to construct a general equation of stoichiometric growth, such as

$$aC_6H_{12}O_6 + bO_2 + cNH_3 \rightarrow dC_\alpha H_\beta O_\gamma N_\delta + eH_2O + fCO_2 + gC_wH_xO_yN_z \quad (2.22)$$

Glucose Biomass Product

In this equation the only unknowns are the seven (a-g) stoichiometric coefficients. There are not seven degrees of freedom, however, since four elemental balance equations can be constructed around carbon, hydrogen, nitrogen, and oxygen. Consequently, if production or consumption rates of three compounds, such as glucose, O_2, and CO_2, are measured, then the production or consumption rates of the remaining four compounds can be estimated. The classic example of such stoichiometric based control is that for the production of Yeast [Cooney *et al.*, 1977; Wang *et al.*, 1977], where it was demonstrated that controlling the respiratory quotient (f/b) at 1.04 would minimize ethanol synthesis and thereby maximize biomass

production. Stoichiometrically based estimation techniques have since been improved by incorporating the use of a Kalman filter algorithm [San and Stephanopoulos, 1984a,b; Stephanopoulos and San, 1984; Grosz and Stephanopoulos, 1984; Vallino and Stephanopoulos, 1987]. Wang and Stephanopoulos (1983) demonstrated that the elemental balance constraints can be used to identify gross measurement errors if there are more measurements than required to close the system.

Around the same period it was also demonstrated that the elemental balance constraints could be used to estimate flux distributions in the TCA cycle during citric acid production by *Aspergillus niger* and *Candida lipolytica* [Verhoff and Spradlin, 1976; Aiba and Matsuoka, 1979]. It was also demonstrated that flux estimates based on different pathway architectures could be used to discriminate between proposed pathways. These same techniques were also employed to estimate flux distributions and organic acid and alcohol production in *Clostridium acetobutylicum* [Papoutsakis, 1984; Papoutsakis and Meyer, 1985; Reardon *et al.*, 1987]. A similar technique (based on a metabolite balance) was used to estimate flux distributions in a crude metabolic pathway of *Brevibacterium flavum* during lysine production [Simon, 1984]. In all these applications, the mass or metabolite balance technique was applied in a rather *ad hoc* manner, and none of the cases utilized a complete metabolic pathway. To fill this void and to examine whether flux distributions in a complete metabolic network can be observed from the accumulation rates of extracellular metabolite alone, we have developed a systematic method for the mathematical representation and analysis of metabolic networks from standard enzymatic reactions [Vallino and Stephanopoulos, 1987, 1989], which is also presented in Chapter 4 and used to examine lysine production by *Corynebacterium glutamicum* (Chapter 6). Approximately the same methodology has also been developed independently by others [Tsai and Lee, 1988; Niranjan and San, 1989], but they have not applied it to a complete metabolic network nor have they examined its experimental implications.

It should be reemphasized that flux estimates based on metabolite balances are no less accurate or prone to error that those based on radio or stable isotope tracers. Since accumulation rates of extracellular metabolites are readily measured under normal fermentations conditions, metabolite balance techniques are the

method of first choice. If flux distributions cannot be completely observed from metabolite accumulation rates only (due to singularities, see Chapter 4), then tracers can be used as supplemental measurements. In any case, flux estimation based on tracer methods can always be improved by utilizing mass balance constraints as well. It is also important to realize that the metabolite balance techniques can also be used in conjunction with kinetic based models reviewed in Section 2.1. Since both models utilize the exact same biochemistry, the steady state flux distributions obtained from the kinetic simulations must match that obtained experimentally from the metabolite based model. If the two flux distributions disagree, then the kinetic model can be fine-tuned to match the experimental results (which is seldom done however). Chapter 6 provides for an example of such kinetic model tuning.

Chapter 3

Lysine Biosynthesis Review

Lysine is found in limiting amounts in most animal feed grains, such as corn, rice, and wheat; consequently, the nutritional value of these grains can be greatly improved if they are supplemented with lysine. Although several methods exist for the industrial production of lysine [Nakayama, 1972], it is predominately produced by microbial fermentation from inexpensive carbon sources, such as cane molasses [Minoda, 1986]. Since the microbial production of lysine (as well as most amino acids) has been extensively reviewed [Kinoshita, 1985; Nakayama, 1982; Kinoshita and Nakayama, 1978; Nakayama, 1972; Kikuchi and Nakao, 1986; Enie *et al.*, 1982; Hirose and Okada, 1979; Hirose *et al.*, 1978], this chapter will only review those aspects of lysine biosynthesis that are required in subsequent chapters, namely: 1) the glutamic acid bacteria; 2) their biochemistry; 3) techniques for strain improvement; and 4) the lysine fermentation.

3.1 Glutamic Acid Bacteria

Since the original publications on the microbial production of glutamate and lysine by *Micrococcus glutamicus* [Kinoshita *et al.*, 1957a; Kinoshita *et al.*, 1958a] and its characterization [Kinoshita *et al.*, 1958b] (later reclassified to *Corynebacterium glutamicum* [Kinoshita, 1962]), numerous organisms have been identified or isolated that can excrete glutamate or lysine [Abe and Takayama, 1972]. As a group, these bacteria are referred to as the glutamic acid bacteria and have been classified in many groups, a partial list of which is displayed in Table 3.1. Although this group appears to span several different genera, this has been found to be unwarranted

[Kinoshita, 1985; Abe *et al.* 1967], and the majority of the glutamic acid bacteria can be classified under the genus *Corynebacterium sensu stricto* [Minnikin *et al.*, 1978]. Specific studies have demonstrated that *Brevibacterium flavum* 22 and ATCC 14067, and *C. glutamicum* ATCC 13032 should all be classified as *C. glutamicum* [Kvashnikov *et al.*, 1984; Otsuka *et al.*, 1965a,b]. These taxonomic similarities among the glutamic acid bacteria is quite important since research groups typically study one specific strain. Consequently, the information published on one particular strain can be assumed (if no other data is available) to be true for all the glutamic acid bacteria. In particular, we will be working solely with *C. glutamicum* ATCC 21253 but will rely heavily on literature from *B. flavum* and *B. lactofermentum* since all three species exhibit nearly 100% DNA homology [Suzuki *et al.*, 1981; Kinoshita, 1985].

Table 3.1 Partial list of glutamic acid bacteria, from Abe and Takayama (1972).

Genus	Species	
Corynebacterium	*glutamicum* *lilium*	*callunae* *herculis*
Brevibacterium	*flavum* *lactofermentum* *thiogenitalis*	*divaricatum* *ammoniagenes*
Microbacterium	*ammoniaphilum* *salicinovolum*	*flavum*
Arthrobacter	*globiformis*	*aminofaciens*

Glutamic acid bacteria are gram-positive, non-sporulating, non-motile, short rods or cocci, require biotin for growth, and all have a propensity to excrete glutamate under a biotin limitation. Most strains can utilize acetate or ethanol as a primary carbon source and a few species can catabolize hydrocarbons (but are probably of the genus *Nocardia* [Kinoshita, 1985]). Most stains will grow between pH 6 and 9 and optimally between pH 7 to 8. Their optimum temperature for growth is between 25 to 37 °C and are typically cultured at 30°C [Abe and Takayama, 1972].

For a complete review of these organisms, the reader is referred to any of the eight reviews listed at the beginning of this chapter.

3.2 Biochemistry

The biochemistry reviewed in this section covers the primary metabolism of *C. glutamicum* necessary to support lysine and biomass synthesis from glucose. Also discussed, with reference to Chapter 5, are the pathways that have been elucidated in this study. Since the details of certain pathways have not been confirmed in *C. glutamicum*, we will rely on literature data from *B. flavum* and other glutamic acid bacteria to supplement the biochemistry where needed. A condensed form of the biochemical reactions, discussed in Chapter 4, is listed as the preliminary biochemistry set (PBS) in Appendix B.

3.2.1 Primary Pathways

These pathways form the primary metabolism of *C. glutamicum* and are quite similar to those documented for *Escherichia coli*, Yeast, etc, that can be found in standard biochemistry texts [Mandelstam *et al.*, 1982; Gottschalk, 1986; Lehninger, 1975].

3.2.1.1 Embden-Meyerhof-Parnas Pathway

The Embden-Meyerhof-Parnas (EMP) pathway (or glycolysis) catalyzes the conversion of glucose-6-phosphate (Glc6P) to pyruvate (Pyr), as illustrated in Table 3.2. All enzymes of the EMP pathway have been detected in *B. flavum* [Shiio *et al.*, 1959a, 1961b], and have been indirectly verified in *C. glutamicum* [Otsuka *et al.*, 1965a; Kinoshita, 1962]. In general, most of the enzymes of the EMP pathway have not been characterized; however, an early study on pyruvate kinase in *B. flavum* [Ozaki and Shiio, 1969] reveals that it is an allosteric enzyme which is activated by AMP and inhibited by ATP. Recently, 6-phosphofructokinase was isolated and characterized in *B. flavum* [Sugimoto and Shiio, 1989], where it was found that the enzyme exhibits normal Michaelis-Menten kinetics and is inhibited by ADP only. Glucose-6-phosphate isomerase was also recently purified and characterized in *B. flavum* [Sugimoto and Shiio, 1989b], and was found to exhibit normal hyperbolic

kinetics and is strongly inhibited by E4P. There is also some evidence that the enzymes of EMP pathway are expressed constitutively [Ruklish *et al.*, 1978]. The EMP pathway is represented by Reactions (3-7:PBS)†.

Table 3.2 Reactions of the Embden-Meyerhof-Parnas pathway.

Glc6P isomerase	Glc6P ⇄ Fru6P
Phosphofructokinase	Fru6P + ATP → Fru16dP + ADP
Fru16dP aldolase	Fru16dP ⇄ DHAP + GAP
Triose phosphate isomerase	DHAP ⇄ GAP
GAP dehydrogenase	GAP + NAD + P_i ⇄ PGP + NADH
PGP kinase	PGP + ADP ⇄ G3P + ATP
Phosphoglycerate mutase	G3P ⇄ 2PG
Enolase	2PG ⇄ PEP + H2O
Pyruvate kinase	PEP + ADP → Pyr + ATP

3.2.1.2 Tricarboxylic Acid Cycle

The tricarboxylic acid (TCA) cycle is primarily responsible for the generation of NADH through the oxidation of acetyl coenzyme A (AcCoA), as well as the synthesis of precursor metabolites, such as oxaloacetate (OAA) and α-ketoglutarate (αKG), provided an anaplerotic reaction is active (see Section 3.2.2 below). The EMP pathway is coupled to the TCA cycle via the pyruvate dehydrogenase complex (PDC). The PDC and TCA reactions are summarized in Table 3.3.

The PDC has been detected in *B. flavum* [Shiio and Ujigawa, 1978] and *B. lactofermentum* [Tosaka *et al.*, 1985], and its presence is implied in *C. glutamicum* [Kinoshita, 1962]. However, the kinetics of the enzyme have not been established, and only the apparent Michaelis constant for the three PDC substrates has been determined [Shiio *et al.*, 1984b].

Initial reports on *B. flavum* [Shiio *et al.*, 1959a] and *C. glutamicum* [Kinoshita *et al.*, 1957a; Kinoshita, 1962; Otsuka *et al.*, 1965b] indicate that all enzymes of the TCA cycle are present, except for α-ketoglutarate dehydrogenase (αKGDH) and succinate thiokinase (P-enzyme) [Shiio *et al.*, 1961d; 1962c]. As a result of these

† The nomenclature (3-7:PBS) refers to Reactions (3) to (7) in the biochemistry set PBS listed in Appendix B.

Table 3.3 Coupling reaction (PDC) and the reactions of the TCA cycle.

Pyr dehydrogenase complex	Pyr + NAD + CoA → AcCoA + NADH + CO2
Citrate synthase	AcCoA + OAA + H2O → Cit + CoA
Aconitase	Cit ⇄ IsoCit
IsoCit dehydrogenase	IsoCit + NADP → αKG + CO2 + NADPH
αKG dehydrogenase complex	αKG + NAD + CoA → SucCoA + CO2 + NADH
Succinate thiokinase	SucCoA + P_i + ADP ⇄ Suc + ATP + CoA
Succinate dehydrogenase	Suc + FAD ⇄ Fum + FADH
Fumarate hydratase	Fum + H2O ⇄ Mal
Malate dehydrogenase	Mal + NAD ← OAA + NADH

preliminary findings, a modified TCA cycle (also called the DCA cycle) was proposed [Shiio *et al.*, 1960b; 1961c; Shiio and Tsunoda, 1961b] for the oxidation of AcCoA, as illustrated in Figure 3.1. In this modified pathway, the glyoxylate shunt and oxaloacetate decarboxylase (OAADC) (see below) effectively by-pass αKGDH and succinate thiokinase, so that CO_2 is produced by PDC and OAADC instead of isocitrate dehydrogenase (ICDH) and αKGDH, which is demonstrated in Chapter 4. Recently, however, αKGDH has been detected in *B. flavum* [Shiio and Ujigawa-Takeda, 1980]. Furthermore, the induction of the glyoxylate shunt by glucose does not occur in *C. glutamicum*, and its induction in *B. flavum* remains ambiguous (see Section 3.2.2 below). Therefore, current evidence supports the normal operation of the TCA cycle without the aid of the glyoxylate shunt in *C. glutamicum*. Operation of the DCA cycle in *B. flavum* also appears unlikely since mutants that lack αKGDH do not grow on glutamate [Shiio *et al.*, 1982b]; however, some uncertainty remains regarding the extent of TCA cycle operation in *B. flavum*. It is important to realize that denunciation of the DCA cycle in glutamic acid bacteria has not occurred. As a result, articles on glutamic acid bacteria are still published that illustrate the DCA cycle as the dominate or the only oxidation pathway. The difference between the TCA and DCA cycle model is not inconsequential since the two models produce dramatically different flux distribution estimates, as demonstrated in Chapter 4.

Several enzymes of the TCA cycle have also been characterized in *B. flavum*. Citrate synthase exhibits normal Michaelis-Menten kinetics and is inhibited by *cis*-

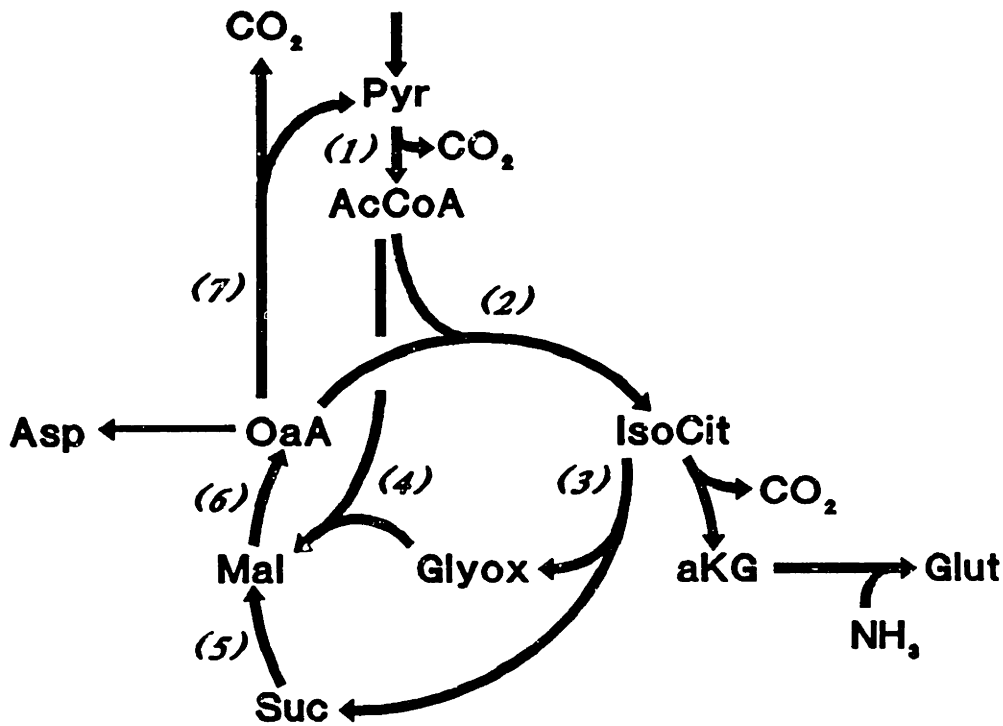

Figure 3.1 Pathways and reactions of the dicarboxylic acid (DCA) cycle originally proposed for glutamic acid bacteria. Reactions are: (1) pyruvate dehydrogenase complex (PDC); (2) citrate synthase; (3) isocitrate lyase; (4) malate synthase; (5) succinate dehydrogenase plus fumarate hydratase; (6) malate dehydrogenase; and (7) oxaloacetate decarboxylase (OAADC). For each pyruvate that is completely oxidized by the DCA cycle, two CO_2 molecules are produced by PDC and one by OAADC.

aconitate, isocitrate, and weakly by ATP [Shiio *et al.*, 1977], and is repressed by glutamate [Shiio and Ujigawa, 1978]. Isocitrate dehydrogenase is specific for NADP and is synergistically inhibited by glyoxylate plus oxaloacetate and exhibits standard hyperbolic kinetics [Shiio and Ozaki, 1968; Ozaki and Shiio, 1968]. α-Ketoglutarate dehydrogenase is significantly inhibited by several metabolites of the primary metabolism, exhibits normal hyperbolic kinetics, and appears to be quite labile. The enzyme appears inducible by glutamate and repressed by citrate, and its *in vitro* activity drops considerably during the stationary phase [Shiio and Ujigawa-Takeda, 1980; Shiio *et al.*, 1982c]. Ruklish *et al.* (1978) have demonstrated that succinate dehydrogenase is membrane associated, and ICDH is inducible at the transcription level by glucose, but malate dehydrogenase is expressed constitutively. They have

also documented that ICDH activity decreases and glycolytic activity increases as respiration is reduced [Ruklisha *et al.*, 1981]. Since the original work, no other studies have been published on succinate thiokinase. Activity of TCA cycle enzymes have also been demonstrated in other Coryneform bacteria [Baryshnikova *et al.*, 1979; Krulwich and Pelliccione, 1979]. The TCA cycle is represented by Reactions (13-19) in the PBS.

3.2.1.3 Pentose Phosphate Pathway

The pentose phosphate pathway (PPP) produces NADPH for biosynthesis (the oxidative branch) and metabolites for nucleic acid synthesis. The pathway can operate in a completely cyclic or linear (*i.e.*, one pass) manner. The reactions of this pathway are illustrated in Table 3.4. Initial evidence for the existence of the PPP came from radio isotope tracer studies on *B. flavum* [Shiio *et al.*, 1960a], *C. glutamicum* [Otsuka *et al.*, 1965a] and *B. ammoniagenes* [Oishi and Aida, 1965], and the detection of an NADP specific Glc6P dehydrogenase [Shiio *et al.*, 1959a]. Recent studies on *C. glutamicum* with ^{13}C tracers and NMR also support the existence of the PPP [Ishino *et al.*, 1986; Yamaguchi *et al.*, 1986]. Both Glc6P and Glcn6P dehydrogenases (G6PDH, GN6PDH) have been isolated and characterized in *B. flavum* [Sugimoto and Shiio 1987a,b]. Both enzymes are NADP specific, inhibited by NADPH, and exhibit hyperbolic kinetics. G6PDH is inducible by glucose, while GN6PDH is induced by gluconate. Although both enzymes are inhibited by several metabolites, OAA and Fru16dP elicit the strongest inhibition of G6PDH and GN6PDH, respectively. The transketolase (TK) and transaldolase (TA) have been detected in *B. flavum*, and the TK has been isolated and characterized [Sugimoto and Shiio, 1989b]. The TK exhibits normal hyperbolic kinetics and a specific inhibitor has yet to be identified. The TK also appears inducible by acetate, fructose and citrate. Sugimoto and Shiio have also detected some activity of Sed7P kinase and sedoheptulose 1,7-bisphosphate aldolase, but these reactions have not been included in the biochemistry set. To our knowledge, the remaining enzymes of the PPP have not been assayed for although their existence is implied by the tracer studies. Several PPP enzymes have also been detected on other Coryneform bacteria [Baryshnikova

et al., 1979; Krulwich and Pelliccione, 1979]. The PPP is represented by Reactions (27-32:PBS).

Table 3.4 Enzymatic reactions of the pentose phosphate pathway.

Glc6P dehydrogenase	Glc6P + NADP ⇄ NADPH + 6PGL
6-Phosphogluconolactonase	6PGL + H2O → Glcn6P
Glcn6P dehydrogenase	Glcn6P + NADP ⇄ Ribu5P + NADPH + CO2
Rib5P isomerase	Ribu5P ⇄ Rib5P
Ribu5P 3-epimerase	Ribu5P ⇄ Xyl5P
Transketolase	Xyl5P + Rib5P ⇄ Sed7P + GAP
Transaldolase	Sed7P + GAP ⇄ Fru6P + E4P
Transketolase	Xyl5P + E4P ⇄ Fru6P + GAP

3.2.2 Anaplerotic Pathways

Anaplerotic reactions are required for the sustained operation of the TCA cycle since metabolites cannot be removed from the cycle without replenishment, as thoroughly reviewed by Kornberg (1966). Four anaplerotic reactions have been detected in glutamic acid bacteria, which are listed in Table 3.5 and represented by Reactions (9,10,12,21,21:PBS). Although some evidence exists that PEP carboxykinase (EC 4.1.1.32) and PEP carboxytransphosphorylase (EC 4.1.1.38) are present in *B. ammoniagenes* [Baryshnikova and Loginova, 1979], the findings are not well supported; therefore, these two enzymes will not be considered. Even without their consideration, the degree of activity or expression of the enzymes listed in Table 3.5 appear to vary from species to species, as explained below.

Table 3.5 Anaplerotic reactions detected in glutamic acid bacteria.

PEP carboxylase	PEP + CO2 → OAA + P_i
Pyruvate carboxylase	Pyr + CO2 + ATP ⇄ OAA + ADP + P_i
Malic enzyme	Mal + NADP ⇄ Pyr + NADPH + CO2
Glyoxylate shunt:	
IsoCit lyase	IsoCit ⇄ Suc + Glyox
Malate synthase	Glyox + AcCoA + H2O → Mal + CoA

3.2.2.1 Phosphoenolpyruvate Carboxylase

PEP carboxylase (PPC) (EC 4.1.1.31) has been detected at high activity in *C. glutamicum* [O'Regan *et al.*, 1989], *B. flavum* [Shiio *et al.*, 1960b], and *B. lactofermentum* [Tosaka *et al.*, 1979c]. Our own experiments have also detected high activity of PPC in *C. glutamicum* ATCC 21253 (Section 5.3). However, PPC is lacking in *Arthrobacter globiformis* [Gurr and Jones, 1977]. The kinetics of the PPC enzyme in *B. flavum* have been extensively studied [Ozaki and Shiio, 1969; Shiio and Ujigawa, 1979; Mori and Shiio, 1985a, b, 1986], and the gene has been cloned and sequenced in *C. glutamicum* [Eikmanns *et al.*, 1989; O'Regan *et al.*, 1989] and cloned in *B. lactofermentum* [Sano *et al.*, 1987]. PPC is an allosteric enzyme which is strongly activated by AcCoA and Fru16dP and inhibited by aspartate and αKG. In *B. flavum*, activity of PPC has been shown to be correlated with the activity of ICDH and lysine production [Ruklish *et al.*, 1982] and is repressed by either glutamate or aspartate [Shiio and Ujigawa, 1978].

3.2.2.2 Pyruvate Carboxylase

Pyruvate carboxylase (PC) (EC 6.4.1.1) catalyzes a reaction similar to PPC, but utilizes Pyr as a substrate and requires ATP and biotin as cofactors. PC has not been detected in *B. flavum* [Ozaki and Shiio, 1969], nor have we detected appreciable levels of it in *C. glutamicum* (Section 5.3). However, PC has been detected in *A. globiformis* [Gurr and Jones, 1977] and *B. lactofermentum* (along with PPC) [Tosaka *et al.*, 1979c]. PC in *A. globiformis* has characteristics similar to PPC in *B. flavum*, while PC in *B. lactofermentum* is not inhibited or activated by aspartate or AcCoA, respectively. It is possible that PC in *B. lactofermentum* is under transcription or translation control while PPC is under metabolite control although this has not been conclusively demonstrated. Nevertheless, there appears to be significant differences in carboxylation reactions employed by the various species of glutamic acid bacteria; such variability in carboxylation reactions, however, is not unprecedented [Baryshnikova and Loginova, 1979; Scrutton, 1978].

3.2.2.3 Malic Enzyme

The malic enzyme (ME) (EC 1.1.1.40) catalyzes the carboxylation reaction between pyruvate and malate. Original studies on *B. flavum* [Shiio *et al.*, 1959a,

1960b; Shiio, 1960] detected the presence of the ME and demonstrated it is specific for NADP. ME has also been detected in *B. lactofermentum* [Tosaka *et al.*, 1979c], and we have detected it in *C. glutamicum* (Section 5.3). However, the ability to detect ME in *B. flavum* seems to vary with publication, some report ME activity [Shiio *et al.*, 1982b; Mori and Shiio, 1987a], while others do not [Ozaki and Shiio, 1969, Ruklish *et al.*, 1982]. Nevertheless, in all reports on the ME from glucose culture cell extracts (including our own) the activity of the enzyme is always much smaller than the activity observed for PPC or PC (when present). Therefore, the ME is not believed to support a significant anaplerotic role. Furthermore, the ME is not believed to act in a carboxylating mode *in vivo* [Kornberg, 1966]. Inducibility of the ME in glutamic acid bacteria from malate or other TCA related metabolites has not been reported although it has been mentioned that glutamate induces ME in *B. flavum* [Mori and Shiio, 1987a].

3.2.2.4 Glyoxylate Shunt

The glyoxylate shunt is composed of two enzymes, isocitrate lyase (EC 4.1.3.1) and malate synthase (EC 4.1.3.2), as illustrated in Table 3.5. Since the glyoxylate shunt effectively by-passes the two CO_2 producing steps of the TCA cycle, a net synthesis of C_4 metabolites can be attained from AcCoA catabolism, which can be used in the anaplerotic sense [Kornberg, 1966]. Although the glyoxylate shunt enzymes are typically only induced by acetate, initial studies on *B. flavum* [Shiio *et al.*, 1959a, 1961a] indicated that the glyoxylate shunt may be operative even when glucose is utilized as the primary carbon source. This hypothesis was later confirmed from radio isotope tracer studies [Shiio and Tsunoda, 1961a,b]. Furthermore, isocitrate lyase has also been isolated and characterized in *B. flavum* and has been shown to be inhibited by several TCA related metabolites [Ozaki and Shiio, 1968]. The existence of the glyoxylate shunt is undisputable; however, its degree of induction on glucose remains ambiguous, especially in *C. glutamicum*. Although isocitrate lyase activity is always high in acetate cultured glutamic acid bacteria, its reported activity varies considerably for glucose cultured organisms, as evident from Table 3.6. Since we could not rely on literature data, we directly measured the activity of isocitrate lyase in *C. glutamicum* ATCC 21253 under normal culture conditions. The results

indicate (Table 3.6, but see Section 5.3.2) that the glyoxylate shunt is induced by acetate, but repressed by glucose.

To summarize, of the four anaplerotic reactions listed in Table 3.5, only PEP carboxylase appears active in *C. glutamicum* ATCC 21253 when cultured on glucose, which has also been found for *B. flavum* 22LD [Ruklish *et al.*, 1978]. However, these results cannot be generalized to all the species grouped under glutamic acid bacteria.

Table 3.6 Isocitrate lyase activity (nmole/min/mg-protein) reported for various strains of glutamic acid bacteria cultured on either glucose or acetate.

Carbon source			
Glucose	Acetate	Organism	Reference
6*	—§	*B. flavum* ATCC 14067	Shiio *et al.*, 1959a
146	783	*B. flavum* ATCC 14067	Shiio *et al.*, 1962c
50†	—	*B. flavum* ATCC 14067	Otsuka *et al.*, 1965b
112‡	—	"	"
0.8†	—	*C. glutamicum* ATCC 13032	"
69‡	—	"	"
—	770	*B. flavum* ATCC 14067	Ozaki and Shiio, 1968
0	222	*B. flavum* 22LD	Ruklish *et al.*, 1978
0	524	*C. glutamicum* ATCC 21253	Section 5.3.2

§ Not measured.
* Estimated from data.
† Cultured under low biotin (2 μg/l).
‡ Cultured under high biotin (30 μg/l).

3.2.3 Sugar Transport and Phosphorylation

The original study on *B. flavum* [Shiio *et al.*, 1959a] demonstrated the presence of glucokinase. Recently, however, it has been found that three PEP:sugar phosphotransferase systems (PTS) are present in *B. flavum* [Mori and Shiio, 1987a,b; Shiio *et al.*, 1990], which catalyze the following reaction:

$$\text{Sugar} + \text{PEP} \rightarrow \text{Pyr} + \text{Sugar-P}$$

The glucose-PTS catalyzes the transport and phosphorylation of glucose and is expressed constitutively. This PTS also acts on mannose (although *B. flavum* cannot grow on mannose), glucosamine, and 2-deoxyglucose, but not on fructose. A fructose

inducible fructose-PTS acts on fructose to form fructose-1-P, which is converted to Fru16dP by 1-phosphofructokinase. This PTS also acts on xylitol and slightly on glucose. The sucrose-PTS specifically acts on sucrose, which is then hydrolyzed to fructose and Glc6P by hydrolase, as illustrated in Table 3.7. The fructose so produced is acted on by the fructose-PTS, since fructokinase has not been detected in *B. flavum*. Although present, glucokinase is not believed to be involved with the transport or phosphorylation of extracellular glucose since the activity of glucokinase is low compared to that of the glucose-PTS. Furthermore, glucose-PTS plus fructose-PTS lacking mutants are unable to grow on glucose [Mori and Shiio, 1987a,b]. Consequently, the glucose-PTS is assumed to transport and phosphorylate all glucose in *C glutamicum*. This system is represented by Reaction (1:PBS).

Table 3.7 Enzymes associated with the uptake of various sugars.

Glucose-PTS*	Glc + PEP → Glc6P + Pyr
Fructose-PTS¶‡	Frc + PEP → Fru1P + Pyr
Sucrose-PTS‡	Sucrose + PEP → Sucrose-P + Pyr
Glucokinase†	Glc + ATP → Glc6P + ADP
1-phosphofructokinase	Fru1P + ATP → Fru16dP + ADP
Hydrolase§	Sucrose-P → Frc + Glc6P
Mannitol dehydrogenase	Mann + NAD → Frc + NADH
Maltase	Maltose → 2 Glc
Gluconokinase‡	Glcn + ATP → Glcn6P + ADP
Ribokinase‡	Ribose + ATP → Rib5P + ADP

* Also acts on mannose, glucosamine, and 2-deoxyglucose.
¶ Also acts on xylitol and to some extent on glucose.
† Believed to act on intracellular glucose only.
§ Exhibits invertase activity as well.
‡ Induced by the corresponding substrate.

Other sugar processing enzymes detected in *B. flavum* by Mori and Shiio (1987a,b) and Shiio *et al.* (1990) are listed in Table 3.7. Mannitol is converted to fructose by a NAD specific mannitol dehydrogenase; mannitol kinase has not been detected in *B. flavum*. Neither ribose nor gluconate participate in any of the three PTS; however, high activity of ribokinase or gluconokinase is present when *B. flavum* is culture on ribose or gluconate, respectively. Consequently, these two metabolites

enter the primary metabolism through the pentose phosphate pathway. Maltose is converted to glucose by maltase, which may be converted, intracellularly, to Glc6P by glucokinase. The enzymes glucose dehydrogenase and isomerase were not detected in *B. flavum*.

Marauska *et al.* (1981) have proposed that the membrane electrochemical potential is the energy donor for glucose transport, and hexokinase is responsible for glucose phosphorylation in *B. flavum* 22LD. They also conclude that the PTS is not present; however, the evidence presented is not strong enough to displace the conclusions drawn by Shiio and Mori discussed above. Consequently, the PTS is assumed to be the dominate glucose transport reaction. Ruklish (1987) has demonstrated that glucose uptake is greater in *B. flavum* 22LD when glycolysis activity is high and TCA activity is low. Saturation and maximum rate constants for glucose uptake have also been determined.

3.2.4 Ammonium Uptake and Aminotransferases

The main routes of ammonium assimilation (at high ammonium concentrations) in bacteria are via glutamate dehydrogenase, glutamine synthetase or aspartase. Since aspartase exhibits little to no activity in *C. glutamicum* [Kinoshita *et al.*, 1957b; Menkel *et al.*, 1989] and alanine and leucine dehydrogenases have not been detected either [Kinoshita, 1985], none of these reactions will be considered. Even though glutamate synthase activity has been reported in glutamic acid bacteria [Vandecasteele *et al.*, 1975], the GS/GOGAT ammonium assimilation route [Gottschalk, 1986, p. 40] will not be included, as ammonium concentrations in lysine fermentations are extremely high (ca. 0.6 M). The two ammonium assimilation reactions are given by

$$\alpha KG + NADPH + NH3 \rightleftarrows Glut + NADP + H2O \qquad (23:PBS)$$

$$Glut + NH3 + ATP \rightleftarrows Glum + ATP \qquad (24:PBS)$$

Glutamate dehydrogenase (GDH) (Reaction (23:PBS)) has been characterized in *B. flavum* [Shiio and Ozaki, 1970] and is the primary route for glutamate overproduction

in glutamic acid bacteria [Kinoshita, 1985]. GDH is specific for NADPH and does not appear to be inhibited by amino or organic acids, which may account for glutamate overproduction. Early reports concluded that glutamate excretion under low biotin conditions occurs via passive diffusion [Demain and Birnbaum, 1968]; however, recent reports indicate that glutamate excretion may be due to inversion of the uptake process [Clement and Laneelle, 1986] or by a special efflux carrier system [Hoischen and Kramer, 1989]. Glutamate accumulation, however, is not observed in the lysine fermentations examined in Chapter 6.

Five amino acid transferases have been isolated and partially characterized in *B. flavum* [Shiio *et al.*, 1982c]. Of these five, aspartate aminotransferase (AT) accounts for 90% of the overall observed activity and specifically reacts with oxaloacetate,

$$OAA + Glut \rightleftarrows Asp + AKG \qquad (35:PBS)$$

Aspartate aminotransferase is required for aspartate synthesis [Shiio and Ujigawa, 1978] as well as glutamate assimilation [Shiio *et al.*, 1982b]. The other aminotransferases detected exhibited activity for branched-chain keto-acids, prephenate, phenylpyruvate and p-hydroxylphenylpyruvate. In *B. lactofermentum* the presence of pyruvate aminotransferase has been detected [Tosaka *et al.*, 1978c].

3.2.5 Respiratory Chain

The respiratory—or electron transport—chain in bacteria is associate with the cellular membrane and facilitates the transfer of electrons from reduced compounds, such as NADH, FADH, etc., to oxygen. In so doing, the electron transport chain harnesses the free energy from the redox reaction to translocate protons from the cytoplasm to the environment, which sets up a proton gradient and a membrane potential, collectively referred to as the protonmotive force. This protonmotive force can then be utilized by the cell to generate ATP from ADP + P_i via ATP synthase (or ATPase) or to transport nutrients across the cell membrane. The number of ADP atoms phosphorylate to ATP per atom of oxygen (O not O_2) reduced is

referred to as the P/O number, which depends on the number of proton translocation sites (coupling sites) in the respiratory chain. The number of protons translocated per atom of oxygen consumed is also given by H^+/O, which is typically twice the number of coupling sites or P/O. The number of coupling sites, in turn, depends on the number and type of cytochromes present in the respiratory chain. The reader is referred to Haddock and Jones (1977) for a thorough review of bacterial respiration.

Studies on the respiratory chain in *B. thiogenitalis* [Sugiyama *et al.*, 1973], *B. lactofermentum* [Kawahara *et al.*, 1988], and *B. flavum* [Shvinka *et al.*, 1979] has reveal that all three organisms contain menaquinone and cytochromes a, b, and c. Cytochrome d has also been detected in copper deficient cells of *B. thiogenitalis*. In *B. flavum*, two cytochrome oxidases have also been identified: cyt. o (420, 569 nm) and cyt. a_3 (435, 569 nm). The alpha absorption peaks of the three cytochromes identified in *B. flavum*, cyt. c_{555}, b_{567}, and a_{604}, closely match those found in *B. thiogenitalis*, cyt. c_{552}, b_{563}, a_{602} and in *B. lactofermentum*, c_{552}, b_{561}, and a_{603}. Shvinka *et al.* have also identified two branches in the respiratory chain of *B. flavum*, as illustrated in Figure 3.2. These alternate branches may be utilized in order to regulate phosphorylation efficiency or to rapidly turnover NADH. Such respiratory control has been documented in *B. flavum* [Shvinka *et al.*, 1982; Kalnenieks *et al.*, 1989]. Although three energy-coupling sites could be supported in the respiratory chain illustrated in Figure 3.2, Kawahara *et al.* has found in *B. lactofermentum* that only sites 1 (NADH-MQ) and 2 (MQ-cyt. c) translocate protons. Site 3 (cyt. c-aa_3) does not appear to pump protons. These results imply that the maximum P/O ratio in glutamic acid bacteria is 2. Therefore, to represent oxidative phosphorylation, the following reactions were added to the preliminary biochemistry set,

$$2\ NADH + O2 + 4\ ADP \rightarrow 2\ H2O + 4\ ATP + 2\ NAD \qquad (33{:}PBS)$$

$$2\ FADH + O2 + 2\ ADP \rightarrow 2\ H2O + 2\ ATP + 2\ FAD \qquad (34{:}PBS)$$

where the by-pass of the first energy-coupling site (NADH dehydrogenase) by succinate oxidation (which produces FADH) has been accounted for in Reaction (34:PBS).

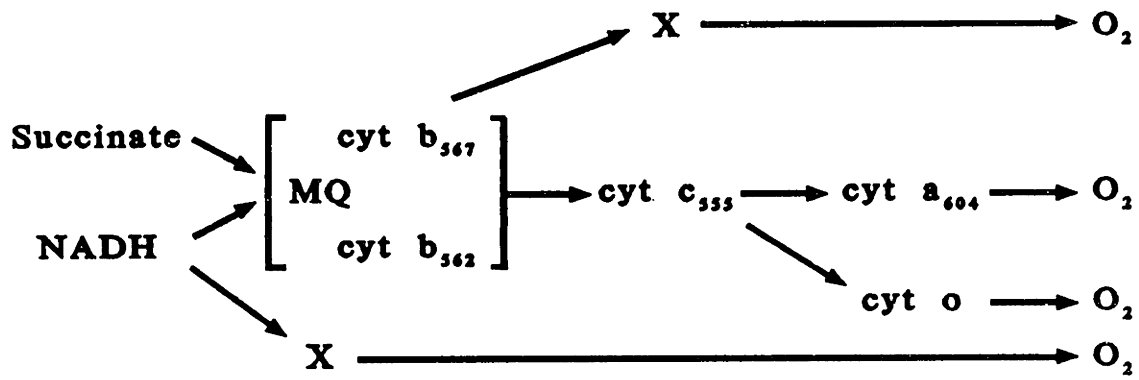

Figure 3.2 Respiratory chain for *Brevibacterium flavum* as proposed by Shvinka *et al.* (1979), where MQ is menaquinone and X represents unidentified transmitters.

3.2.6 Coupling Pathways

3.2.6.1 Entner-Doudoroff Pathway

The Entner-Doudoroff (ED) pathway [Entner and Doudoroff, 1952] is an alternate route by which glucose or gluconate can be assimilated. The pathway consists of two enzymatic steps

$$\text{Glcn6P} \rightarrow \text{KDPG} + \text{H2O}$$
$$\text{KDPG} \rightarrow \text{Pyr} + \text{GAP}$$

which are catalyzed by 6-phosphogluconate dehydratase and 2-keto-3-deoxy-6-phosphogluconate (KDPG) aldolase, respectively. The ED pathway effectively couples together the pentose phosphate and the EMP pathways since Glcn6P is produced from Glc6P dehydrogenase (when glucose is the carbon source) and the Pyr and GAP produced are further metabolized via the enzymes of the EMP. However, initial tracer studies in *B. flavum* [Shiio *et al.*, 1960a] and *C. glutamicum* [Otsuka *et al.*, 1965a] indicate that the ED pathway is not present in either of these bacteria. Furthermore, our studies (Sections 5.3 and 6.3.2.1) also indicate that the ED pathway

is not present in *C. glutamicum* ATCC 21253 when cultured on glucose, nor is it induced by gluconate. Consequently, the ED pathway was not included in the PBS.

3.2.6.2 Oxaloacetate Decarboxylase

Oxaloacetate decarboxylase (OAADC) (EC 4.1.1.3) catalyzes the decarboxylation of oxaloacetate (OAA) as shown here

$$OAA \rightarrow Pyr + CO2 \qquad (11:PBS)$$

OAADC has been detected at high activity in *B. flavum* [Shiio *et al.*, 1959a; Mori and Shiio, 1987a], *B. lactofermentum* [Tosaka *et al.*, 1979c], and *C. glutamicum* [see Section 5.3.3], and may require biotin for activity [Tosaka *et al.*, 1979c]. We have found that OAADC appears to be expressed constitutively but does not require biotin for activity. Although OAADC activity assayed in cell-free extract is quite high, its *in vivo* metabolic function is uncertain. The enzyme would be required for the operation of the DCA cycle (Figure 3.1), but the lack of the glyoxylate shunt precludes this. It is possible that the enzyme is required for growth on acetate (since the DCA cycle is operative then), but this does not explain why it is present in glucose cultured cell-free extracts. Furthermore, it is not believed to support significant Pyr synthesis since mutants which lack pyruvate kinase are unable to grow on ribose or gluconate [Mori and Shiio, 1987a]. It could be speculated that OAADC functions to maintain low OAA concentration since OAA is a potent inhibitor of many enzyme reactions. Nevertheless, OAADC is included in the preliminary biochemistry set, although it will be later removed from the working biochemistry set (BS1), as discussed in Chapter 4.

3.2.6.3 Nucleotide Transhydrogenase.

Some organisms possess a pyridine dinucleotide transhydrogenase which catalyzes the following reaction:

$$NADP + NADH \rightleftarrows NADPH + NAD \qquad (43:PBS)$$

Two basic types of this enzyme exist. One is watersoluble and does not participate in energy production while the other is membrane-associated and can translocate protons across the membrane to produce ATP [see Hoek and Rydstrom (1988), and the reviews references therein]. From a flux mapping point of view, the presence of this enzyme effectively renders NADPH indistinguishable from NADH, and so introduces flux observability problems (see Chapter 4). Although both energy and non-energy linked transhydrogenases have been extensively studied, these studies have focused on relatively few organisms. Consequently, information regarding the existence of either transhydrogenase in glutamic acid bacteria is lacking. The only information currently available are reports that the cell-free extract of *C. glutamicum* is unable to oxidize NADPH in the presence of citrate or glutamate but oxidizes NADH readily [Kinoshita *et al.*, 1960; Shiio *et al.*, 1959b; Kinoshita, 1972, pp. 298, 300], which implies the absence of a nucleotide transhydrogenase in these organisms. Our studies were also unable to detect a soluble nucleotide transhydrogenase (Section 5.3.1). Nevertheless, a nucleotide transhydrogenase is included in the PBS to facilitate discussion on non-observable pathways, presented in Chapter 4 (it will later be removed from the working biochemistry set).

3.2.6.4 Gluconeogenesis

To grow on C_4 carbon compounds, organisms that utilized the EMP pathway must be able to by-pass the pyruvate dehydrogenase complex, pyruvate kinase, and phosphofructokinase catalyzed reactions (Tables 3.2 and 3.3), as the free energy associated with these reactions strongly favors their forward direction (see Lehninger (1975), pg. 624). Although glutamic acid bacteria can sustain growth on C_2, C_3, and C_4 compounds, the gluconeogenesis pathway in these organisms has not been directly studied. However, fructose diphosphatase, which by-passes phosphofructokinase via

$$Fru16dP + H2O \rightleftarrows Fru6P + P_i$$

has been recently demonstrated in *B. flavum* [Sugimoto and Shiio, 1989; Shiio *et al.*, 1990] and exhibits Michaelis-Menten kinetics but is inhibited by its substrate at more that 30 μM [Sugimoto and Shiio, 1989b]. Two possible routes exist for by-passing

PDC and PK. The first is by PEP carboxykinase (EC 4.1.1.32), which is similar to PPC, but utilizes ATP as a cofactor to render the reaction reversible, as shown here:

$$PEP + CO2 + ATP \rightleftarrows OAA + ADP$$

The second possible route involves OAADC to by-pass PDC and PEP synthetase (EC 2.7.9.2)

$$Pyr + ATP \rightarrow PEP + AMP + P_i$$

to by-pass PK. The second route is likely to operate *in vivo* since OAADC is expressed at high levels and some activity of PEP synthetase has been detected in *C. glutamicum* (see Section 5.3.2). Since the theoretical lysine yield is affected by the existence of PEP synthetase (Chapter 4), the operation of the proposed pathway should be investigated in more detail in future studies.

3.2.7 Aspartate and Lysine synthesis

3.2.7.1 Pathway

Original studies on the lysine producing strain of *C. glutamicum* [Nakayama and Kinoshita, 1961a,b] indicated that lysine biosynthesis occurs via the diaminopimelate (DAP) pathway and not the α-aminoadipate pathway (see Rodwell (1969) for both pathways) since DAP and DAP carboxylase could be detected. The reactions of the DAP pathway for lysine synthesis are illustrated in Figure 3.3. Later studies on *C. glutamicum* [Nakayama *et al.*, 1966] have detected the presence of aspartate kinase (AK) and dihydrodipicolinate (DDP) synthase, the first enzyme of the lysine branch. Recent studies on *C. glutamicum* [Cremer *et al.* 1988] have demonstrated the presence of AK, aspartate semialdehyde (ASA) dehydrogenase, DDP synthase, DDP reductase, DAP dehydrogenase and carboxylase. Studies in *B. flavum* have demonstrated the presence of AK, ASA dehydrogenase, DDP synthetase and reductase [Miyajima *et al.*, 1968; Shiio and Miyajima, 1969; Miyajima and Shiio, 1970b]. In *B. lactofermentum* [Tosaka and Takinami, 1978], the presence of AK,

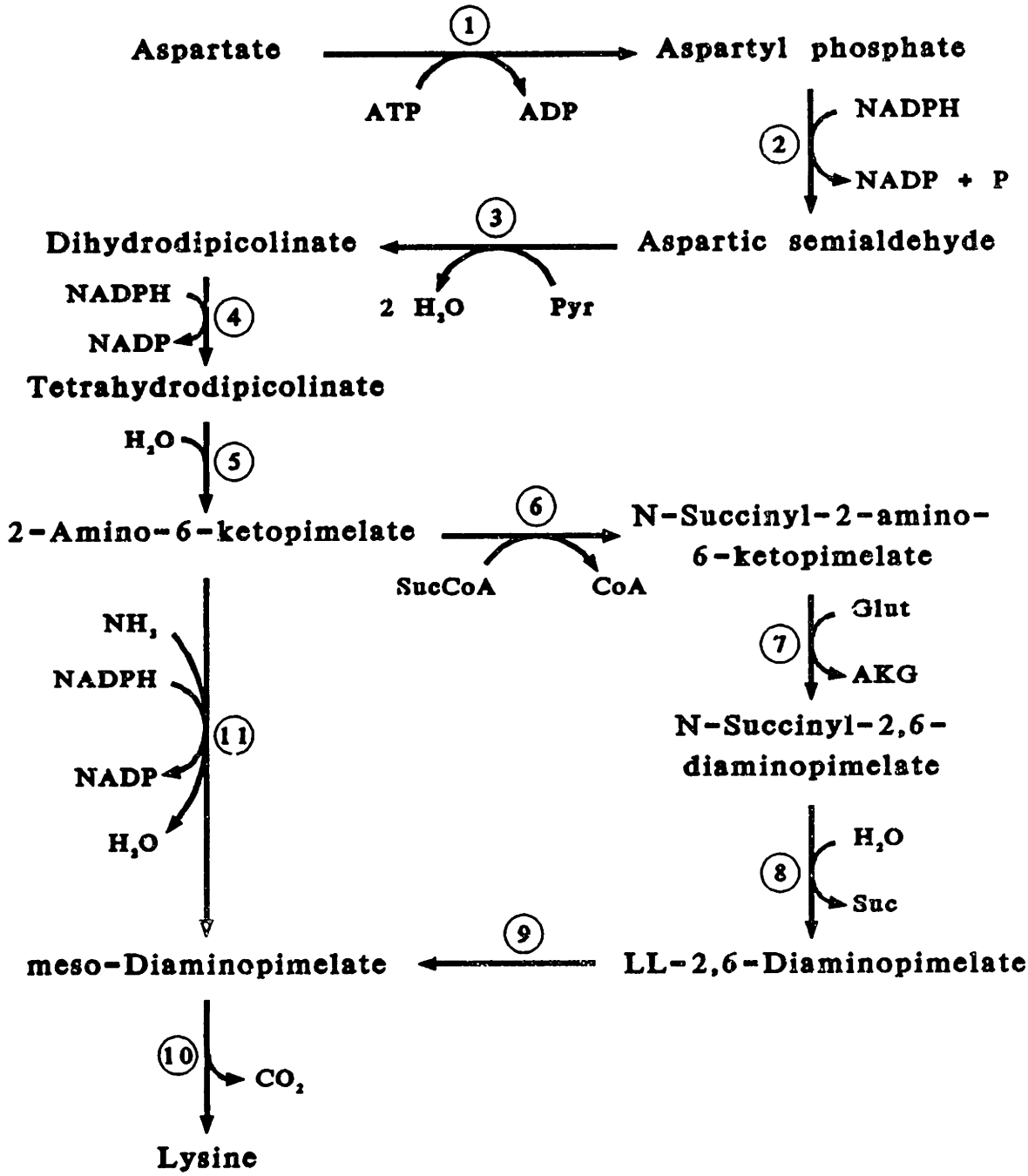

Figure 3.3 Diaminopimelate pathway for lysine synthesis in glutamic acid bacteria. The enzymes are: 1) aspartate kinase; 2) aspartic β-semialdehyde dehydrogenase; 3) dihydrodipicolinate synthase; 4) dihydrodipicolinate reductase; 5) nonenzymatic (?) ring opening step; 6) N-succinyl (or acetyl)-2-amino-6-ketopimelate synthetase (or tetrahydrodipicolinate succinylase); 7) N-succinyl (or acetyl)-aminoketopimelate:glutamate aminotransferase; 8) N-succinyl (or acetyl) diaminopimelate desuccinylase; 9) diaminopimelate epimerase; 10) diaminopimelate decarboxylase; and the alternate route 11) *meso*-α,ϵ-diaminopimelate D-dehydrogenase.

DDP synthase and reductase, and N-acetyl-ϵ-keto-α-aminopimelate (AKAP) synthase have been demonstrated. They have also established that AKAP synthase can utilize either AcCoA or SucCoA.

An alternate pathway for the direct conversion of 2-amino-6-ketopimelate (AKP) from meso-DAP has also been identified in glutamic acid bacteria (shown as Reaction (11) in Figure 3.3). This pathway was originally detected by Oshima *et al.* (1964), but they attributed it to the catalytic action of glutamate dehydrogenase. It was later identified [Misono *et al.*, 1979] as meso-α,ϵ-diaminopimelate dehydrogenase and was found to be present in both *Corynebacterium* and *Brevibacterium* species, and has been purified in *C. glutamicum* [Misono *et al.*, 1986]. Unlike *Bacillus sphaericus*, which only has mDAP dehydrogenase [White, 1983], evidence suggests that both the standard pathway and mDAP dehydrogenase significantly contributed to lysine synthesis (ca. 50% each) [Leadlay, 1978; Ishino *et al.*, 1984].

The mechanism by which lysine is assimilated or secreted has gone largely uninvestigated in glutamic acid bacteria, and relatively little information is available in general [Milner, *et al.*, 1987]. A recently published article on *C. glutamicum* [Luntz *et al.* 1986] indicates that lysine secretion may occur via active transport through lysine-specific channels or pores, and not by passive diffusion. However, more research is required on the subject before specifics of the transport mechanisms can be deduced. In this study, it is assumed that lysine secretion is not energy dependent. Whether intracellular or extracellular, lysine is not degraded since *C. glutamicum* appears to lack lysine decarboxylase [Nakayama and Kinoshita, 1961a]. The enzymes of the lysine synthesis pathways are represented by Reactions (36-40:PBS).

3.2.7.2 Regulation

The original studies on lysine synthesis from *C. glutamicum* indicated that lysine production could be inhibited by the addition of homoserine (Homo) or threonine (Thr) to the culture medium [Nakayama *et al.*, 1961], which was later attributed to inhibition of aspartate kinase [Nakayama *et al.*, 1966]. It was found that AK is subject to concerted—multivalent—feedback inhibition by threonine plus lysine, as illustrated in Figure 3.4, but is not significantly inhibited by either amino acid

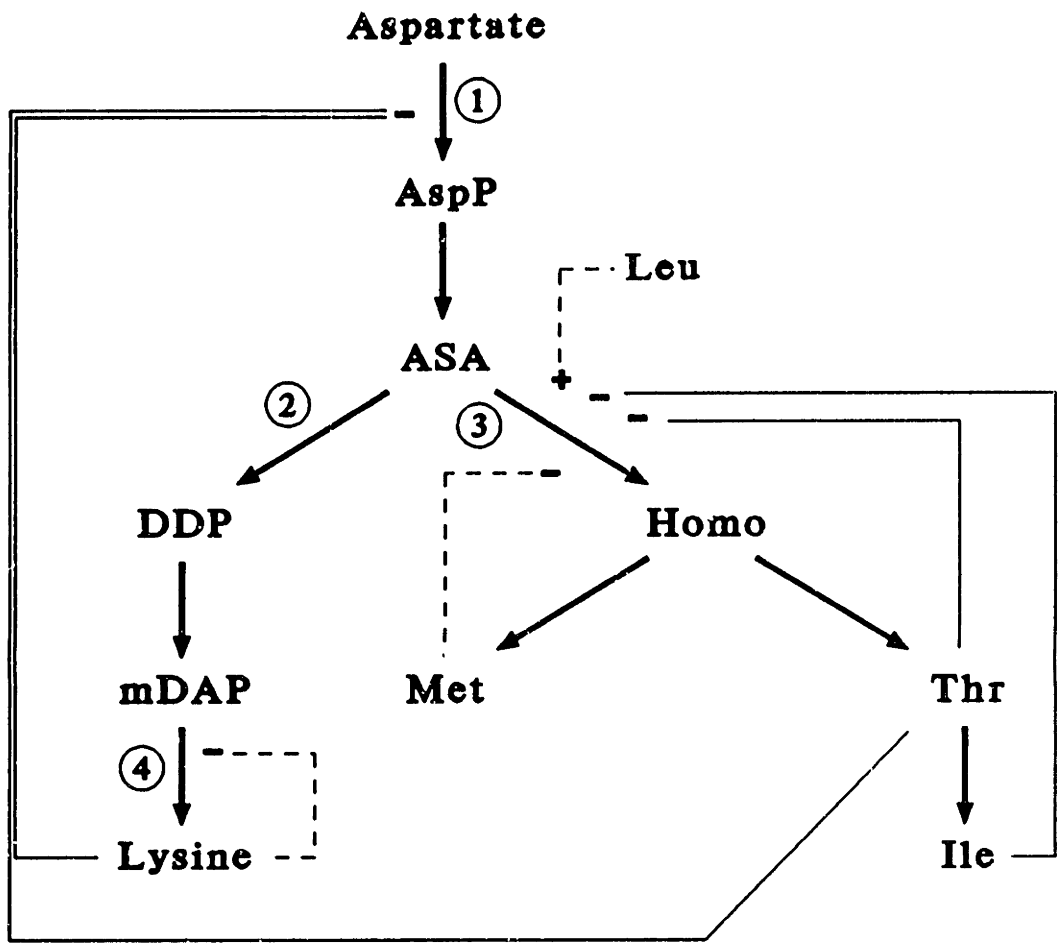

Figure 3.4 Regulation of the aspartate amino acid family in *Corynebacterium glutamicum*. The regulated enzymes are: 1) aspartate kinase; 2) dihydrodipicolinate synthase; 3) homoserine dehydrogenase; 4) diaminopimelate decarboxylase. Solid lines illustrate inhibition (-) or activation (+) and dashed lines illustrate repression (-) or induction (+).

separately. This inhibition can be slightly relieved by either methionine or isoleucine. Similar feedback inhibition of AK has also been documented in *B. flavum* [Miyajima *et al.*, 1968; Shiio and Miyajima, 1969] and *B. lactofermentum* [Tosaka and Takinami, 1978]; however, *B. lactofermentum* differs in that AK inhibition also results from the addition of lysine or threonine separately, and two AK isozymes may exist [Tosaka *et al.*, 1978a]. Homoserine dehydrogenase (ASA branch-point enzyme) is strongly inhibited by threonine and slightly by isoleucine and is repressed by methionine in *C. glutamicum* [Nara *et al.*, 1961, Cremer *et al.*, 1988], *B. flavum* [Miyajima and Shiio, 1971; Miyajima *et al.*, 1968] and *B. lactofermentum* [Tosaka *et al.*, 1978a, 1979a]. It has been documented as an allosteric enzyme in *B. flavum* [Miyajima and Shiio, 1970a]. In *B. lactofermentum*, leucine has been found to repress the synthesis of DDP synthetase [Tosaka *et al.*, 1978b]. A recent study on *C. glutamicum* [Cremer *et al.*, 1988] has demonstrated that leucine induces the synthesis of homoserine dehydrogenase while lysine represses the synthesis of DAP carboxylase. Since mDAP is required in cell wall synthesis, regulation of DAP carboxylase is understandable. However, Yeh *et al.* (1988) reported that DAP carboxylase is expressed constitutively in *C. glutamicum*; consequently, some uncertainty exists on the regulation of DAP carboxylase. The current regulatory picture for lysine synthesis in *C. glutamicum* is illustrated in Figure 3.4. Note, pathway regulation for *B. lactofermentum* is slightly different from that illustrated in Figure 3.4. Although *B. flavum* may have the same regulation architecture as *C. glutamicum*, it has not been completely confirmed.

3.2.8 Other Products

This section reviews the biochemistry associated with by-products that have been observed to accumulated along with lysine. It is not a comprehensive review; only those by-products observed to accumulate in the lysine fermentations discussed in Chapters 5 and 6 are examined. The biosynthesis of trehalose, acetate, lactate, alanine, valine, are reviewed below.

Trehalose (Trehal) is a disaccharide of two glucose residues that is typically synthesized intracellularly as a storage compound; however, it has been observed to accumulate extracellularly in glutamate and lysine fermentations [Walker *et al.*, 1982;

Inbar *et al.*, 1985], and we have observed large amounts in our lysine fermentation. In Yeast, trehalose phosphate is synthesized from Glc6P and uridine diphosphate glucose (UDPG) [Cabib and Leloir, 1959]. Since UDPG is ultimately synthesized from Glc6P and ATP [Lehninger, 1975, p. 643], the synthesis of trehalose is represented by:

$$2\ \text{Glc6P} + \text{ATP} \rightarrow \text{Trehal} + \text{ADP} + 3\ P_i \qquad \text{(2:PBS)}$$

Two routes exist for the production of acetate (Ac) from the primary metabolism. One is by the reversal of AcCoA synthetase and the other is via phosphotransacetylase plus acetate kinase. A mutation study on *B. flavum* [Shiio *et al.*, 1969] indicates that acetate is produced and consumed via the later pathway, which can be expressed in one reaction as:

$$\text{AcCoA} + \text{ADP} \rightleftarrows \text{Ac} + \text{CoA} + \text{ATP} \qquad \text{(20:PBS)}$$

Lactate (Lac) synthesis is assumed to catalyzed by the well known lactate dehydrogenase enzyme:

$$\text{Pyr} + \text{NADH} \rightleftarrows \text{Lac} + \text{NAD} \qquad \text{(8:PBS)}$$

In *B. lactofermentum* [Tosaka *et al.*, 1978c] it has been demonstrated that alanine (Ala) is synthesized predominately via pyruvate aminotransferase with glutamate as the amino donor, and not by alanine dehydrogenase or aspartate decarboxylation. Thus, alanine synthesis is given by

$$\text{Pyr} + \text{Glut} \rightleftarrows \text{Ala} + \text{AKG} \qquad \text{(25:PBS)}$$

Valine (Val) synthesis in *B. lactofermentum* [Tsuchida and Momose, 1975] has been implied to occur via the reaction sequence identified in *E. coli* [Mandelstam *et*

al., 1982, p. 172]. Although the pathway consists of four enzymatic reactions, it is expressed as one, shown here:

$$2\ Pyr + NADPH + Glut \rightarrow Val + CO2 + H2O + NADP + AKG \quad (26{:}PBS)$$

3.3 Strain Improvements

This section reviews the various metabolic modifications that have been attained or attempted in glutamic acid bacteria to improve lysine production. Since there are three main research groups that have published techniques for strain improvement in *C. glutamicum* (mostly Kinoshita and Nakayama; Kyowa Fermentation Industry Co., Tokyo Japan), *B. flavum* (Shiio; Ajinomoto Co., Kawasaki Japan), and *B. lactofermentum* (Tosaka; Ajinomoto, Kawasaki Japan), strain improvements in each species will be reviewed separately and in a case history manner. In almost all the cases reviewed below, strain improvement has been attained through mutation (by exposure to UV radiation, X-ray radiation, or N-methyl-N'-nitro-N-nitrosoguanidine (NTG), currently the preferred mutagen) and strain isolation or selection based on a phenotype intended to improve lysine production. Those strains which match the desired phenotype are then tested for lysine productivity and not genotype since the ultimate goal of the above mentioned companies is to improve lysine yield and titer. Although this technique works extremely well, it does produce some ambiguity on the metabolic alterations that actually lead to the strain improvement. For example, one may hypothesize that attenuation of PDC activity may divert pyruvate from the TCA cycle to lysine synthesis and thereby improve yield. Based on the techniques typically employed, a few hundred mutants would be isolated with phenotypes that correspond to a PDC attenuated genotype. If any of the few hundred isolated mutants exhibited improved lysine yield, it would be concluded that PDC activity attenuation improves lysine yield. However, isolation or selection techniques are imperfect; strains will inevitably be selected with multiple mutations or mutations that differ from the desired genotype. Although the improved strains can be characterized (and often are), there is always the possibility that the crucial alterations go undetected, especially for modifications

of the primary metabolism. Such scenarios will be exemplified below. Nevertheless, the mutation and characterizations studies reviewed below are extremely informative on the nature of lysine regulation in glutamic acid bacteria.

3.3.1 *Corynebacterium glutamicum*

It was discovered that homoserine or threonine auxotrophic strains of *C. glutamicum* ATCC 13032 secreted large amounts of lysine when cultured on a glucose plus ammonium chloride minimal medium supplemented with homoserine or threonine [Kinoshita *et al.*, 1958a]. Lysine overproduction, however, could be severely inhibited by the addition of either threonine or homoserine [Nakayama *et al.*, 1961]. Although not completely understood at the time, these results are easily explained in light of the biochemical regulation of lysine synthesis discussed previously and illustrated in Figure 3.4. Since homoserine auxotrophic strains are unable to synthesize threonine (or methionine or isoleucine), the concerted feedback on aspartate kinase is relieved and lysine synthesis becomes deregulated. However, if too much threonine or homoserine is added to the medium, then the feedback is reestablished and lysine overproduction is inhibited. Although strains that lack any of the enzymes between ASA and threonine will produce lysine, those strains which lack homoserine dehydrogenase (HDH) (first enzyme of threonine branch) produce the most lysine [Nakayama *et al.*, 1966] since deletion of HDH does not produce a dead-end pathway. Strains with mutations other than at HDH also excrete by-product (such as phosphohomoserine) since these mutations lead to dead-end pathways that are unregulated. These inferior strains are better documented in *B. flavum* discussed below.

Although other techniques for strain improvement have been applied to *C. glutamicum*, the procedures are described in US patents, so are not well documented. These procedures, however, have been documented (or were originally established) in *B. flavum* or *B. lactofermentum* discussed below, so they will not be described here. For additional information on *C. glutamicum*, the reader is referred to United States Patents: 2,979,439 (1961); 3,595,751 (1971); 3,687,810 (1972); 3,707,441 (1972); 3,708,395 (1973); 3,732,144 (1973); 3,959,075.

Recently, attempts have been made to increase lysine production in *C. glutamicum* by introducing the genes coding for DDP synthase [Cremer *et al.*, 1988] and aspartase [Menkel *et al.*, 1989] from *E. coli*; however, improvements in lysine production by the transformed strains are minimal and poorly documented (only final lysine titers are reported). Consequently, it is difficult to determined if the transformations are viable methods for improving lysine production.

3.3.2 *Brevibacterium flavum*

Homoserine auxotrophic strains of *B. flavum* 2247 (or ATCC 14067) also excrete large amounts of lysine into the culture medium [Sano and Shiio, 1967] since the regulation of lysine synthesis in *B. flavum* is basically identical to that of *C. glutamicum*. It was also discovered that some prototrophic revertants of homoserine auxotrophs also produced large amounts of lysine without requiring amino acid supplements for growth [Shiio and Sano, 1969]. The growth rate of these strains are similar to the wild strain; however, their growth can be completely inhibited by the addition of relatively small amounts of either methionine or threonine. Referred to as methionine sensitive (Met^S), these strains have very low HDH activity, approximately 2% of the wild type. It is hypothesized that the reduced activity of HDH is high enough to support normal growth but causes the intracellular threonine concentration to drop below AK inhibition levels. The loss in AK regulation results in lysine overproduction as in the $Homo^-$ strains. The addition of methionine or threonine to the medium completely represses or inhibits the reduced *in vivo* HDH activity, so that the cell becomes starved of either threonine or methionine, respectively, and ceases to grow. As expected, addition of both amino acids promotes growth but inhibits lysine production if excess threonine is added. Although Met^S strains were useful to the understanding of lysine regulation, they are not typically employed in industrial settings.

In the lysine secreting strains mentioned above, the feedback inhibition of AK is still operative and has only been by-passed by regulating threonine availability. The best method currently available, however, for quickly selecting good lysine producers focuses on deregulating AK feedback directly. This method, originally published by

Sano and Shiio (1970), selects those strains that are able to grow in the presence of threonine plus S-(2-aminoethyl)-L-cysteine (AEC), a sulfur analog of lysine—an antimetabolite [Cavallini *et al*, 1955]. Since AEC resembles lysine, it elicits similar inhibitory effects, such as the arrest of lysine synthesis, but AEC cannot be incorporated into protein. As a result, cells which have normal lysine regulation cannot grow in the presence of AEC. Although AEC strongly inhibits the growth of *Lactobacillus* sp. [Shiota *et al.*, 1958], threonine is also required as a supplement to achieve strong growth inhibition in glutamic acid bacteria. Strains which are resistent to AEC plus threonine (AEC^R) secrete large amounts of lysine and possess feedback resistent AK (AK^R) enzymes. Since methionine and threonine are regulated at HDH, only lysine is overproduced. A similar technique that employs α-amino-β-hydroxyvaleric acid (AHV), a threonine analog, is useful for selecting threonine producers [Shiio and Nakamori, 1970], although threonine accumulation is small compared to lysine accumulation by AEC^R strains. An advantage of both techniques is that they rely on strain selection as opposed to strain isolation.

Both AEC^R and $Homo^-$ strains of either *C. glutamicum* or *B. flavum* accumulate approximately 30 g/l lysine•HCl/l from 100 g/l glucose or 29.5% molar yield (note, yields can vary considerable depending on culture conditions). Although this yield is considered high, it is still less than half of the theoretical maximum, which is considered to be 75% (see Chapter 4 for theoretical lysine yields). Since lysine synthesis has been deregulated or by-passed in lysine producing strains, it is believed that the suboptimal yield is due to inadequate synthesis of lysine precursors: PEP, Pyr, NADPH. It should be noted that AcCoA (or SucCoA) and Glut are sometimes improperly categorized as precursors; however, there is no net consumption of these metabolites and their regeneration does not alter flux distribution in the primary metabolism (see Chapter 4). To address potential precursor limitations, attempts have been made to modify the primary metabolism of *B. flavum*. Although lysine overproduction by AEC^R and $Homo^-$ strains is relatively well documented and understood, modifications of the primary metabolism that increase lysine production are plagued by the ambiguities discussed at the beginning of this section. Nevertheless, modifications of the primary metabolism have lead to significant

improvements in lysine yield, so it is important to attempt to decipher the results documented for *B. flavum.*

The first attempt to improve lysine producing strains via modifications of the primary metabolism was a spinoff from a citrate synthase lacking (CS^L) mutant (No. 214) that required glutamate for growth and was used to study glutamate producers [Shiio and Ujigawa, 1978]. It was found that two prototrophic revertants (No. 15 and 15-8) of the CS^L mutant (No. 214) excrete aspartate and have attenuated CS (CS^A) activity [Shiio *et al.*, 1982a]. Since aspartate is a precursor to lysine, strains were selected from the CS^A mutants that were AEC^R (No. 1-231) or $Homo^-$ and overproduced lysine. When the lysine yields of these new strains were compared to strains which were only AEC^R or $Homo^-$, it was found that the new strains accumulated more lysine [Shiio *et al.*, 1982a]. It was, therefore, concluded that CS^A is a viable method for improving lysine production in lysine excreting strains. It should be noted that it is not useful to state the actual improvement in lysine yield since the yields for a given strain vary significantly under different culture conditions. Consequently, it will be assumed that the lysine productivity classifications concluded by the investigators are valid.

Based on findings from Tosaka's group (discussed below), strains of *B. flavum* 1-231 (which is AEC^R, CS^A) were isolated for sensitivity to fluoropyruvate (FP) since FP sensitive (FP^S) strains usually have attenuated activity of the pyruvate dehydrogenase complex (PDC^A), which was demonstrated to increase lysine yields in *B. lactofermentum.* Two strains were selected (No. 22 and 2-11) from 1-231 that are FP^S and accumulated large amounts of lysine•HCl, 51 g/l from 100 g/l glucose [Ozaki and Shiio, 1983]. However, when these strains, as well as their parent strains, were examined for enzyme activities, they were radically different than expected. First, the original parent strain No. 15-8 not only is CS^A but also possesses a PEP carboxylase enzyme that exhibits reduced inhibition by aspartate. This feedback resistent PPC (PPC^R) was not directly selected for and was simply good fortune. The lysine producing strain No. 1-231, selected from 15-8 based on AEC^R, has a feedback sensitive AK, which is inconsistent with the AEC^R phenotype. Instead, strain No. 1-231 displays severely attenuated HDH activity and is Met^S. Furthermore, the activity

of PK in this stain is less than 10% of the PK activity of the parent strain, No. 15-8, which was also not selected for. A revertant of strain No. 1-231, with normal HDH activity (No. 70), was demonstrated to accumulate large amounts of aspartate instead of lysine due to the PPC^R and CS^A genotypes [Mori and Shiio, 1984]. Finally, strain No. 22, isolated from 1-231 based on FP^S, possesses normal activity of PDC, which is inconsistent with FP^S phenotype; however, this strain completely lacks HDH activity. It was concluded [Ozaki and Shiio, 1983] that the difference in lysine productivity between strains No. 1-231 (41%) and 22 (51%) is due to the lack of HDH activity in strain No. 22. They also stated that attenuation of PK accounts for the high lysine yields in both strains, but they did not consider the PPC^R genotype to be important. Subsequent analysis of strains No. 1-231 and 22 revealed that strain 1-231 is Met^S while strain No. 22 is not FP^S [Shiio *et al.*, 1984]. They also concluded that PPC^R does not enhance lysine productivity since strain No. 22 has lower PPC activity than No. 1-231. They did, however, not consider the fact that the inhibition of PPC by Asp in strain No. 22 is significantly less than that in strain No. 1-231. All points considered, they were unable to determine why strain No. 22 produces more lysine than strain No. 1-231.

Since PDC^A mutants of *B. flavum* could not be obtained by isolating strains with FP^S phenotypes (or at least none were reported), a second method was developed which relies on prototrophic revertants of acetate requiring mutants. Strains which lack PDC require acetate supplement for growth to synthesize AcCoA. Consequently, those strains which lose the AC requirement must have regained some PDC activity. When this isolation procedure was applied to strain No. 22, the strain KD-11 was obtained which produced the highest lysine yield yet reported, 55% (g lysine•HCl/g glucose) and exhibited altered kinetics of PDC [Shiio *et al.*, 1984]. It was concluded that attenuating PDC in lysine producing strains can increase lysine productivity. It is interesting to note that PPC activity in strain KD-11 has also been slightly amplified and is less sensitive to aspartate inhibition when compared to strain No. 22. Also, both strains KD-11 and No. 22 have fairly low OAA decarboxylase activity compared to the wild strain, No. 2247.

Although strain KD-11 accumulates large amounts of lysine, the metabolic modifications that lead to its enhanced lysine productivity remain uncertain since it is descended from strain No. 22. To address some of these uncertainties, the affects of PK attenuation on lysine yield were reinvestigated by employing a new technique for isolating PK^A mutants. This technique, published by Shiio *et al.* (1987), relies on the properties of the three sugar:PEP phosphotransferase systems discussed in Section 3.1. It should be recalled that ribose (or gluconate) is not acted upon by any of the three PTSs and is instead phosphorylated by ribokinase (or gluconokinase), while the transport and phosphorylation of glucose via the PTS also converts PEP to Pyr. Consequently, strains which have reduced PK activity are still able to grow on glucose (or other PTS transported sugars) but are unable to grow on ribose (or gluconate), which provides a viable selection marker for PK^A mutants. This technique was applied to a strain No. 2-190 [Ozaki and Shiio, 1983], which is similar to No. 1-231 but has full activity of PK and is truly AEC^R. The resulting strain, KL-18, exhibited increased lysine yield compared to its parent, No. 2-190 [Shiio *et al.*, 1987]. The results conclusively demonstrated that PK attenuation by the ribose selection marker will improve lysine yields, but this only pertains to stains that are already CS^A, AEC^R, and PPC^R. Effects of PK^A on AEC^R strains has not been investigated.

In a recent study to better quantify the effects of CS^A plus PPC^R traits on lysine yields, strains of No. 15-8 (CS^A, PPC^R and AEC^R, but AK sensitive to concerted feedback [Ozaki and Shiio, 1983]) were selected for AK^R [Yokota and Shiio, 1988]. It was hypothesized that strain No. 15-8 could be $(AEC + Thr)^R$ without AK^R if the partial deregulation of PPC increased the intracellular Asp concentration such that AEC + Thr no longer inhibited growth. This hypothesis was partially confirmed by the investigators who demonstrated that strain No. 15-8 is sensitive to AEC + Thr when cultured on acetate, which is metabolized via the glyoxylate shunt and not PPC. From strain No. 15-8 cultured on acetate, six AEC^R strains were selected and all exhibited improvements in lysine yield when compared to strains that were only AEC^R. These results indicate that CS^A plus PPC^R are desirable traits in lysine producing strains.

Although significant improvements in lysine yields have been attained through modifications of the primary metabolism, it is still not clear which single modification will produce the greatest result. For example, the first step in attaining lysine producing strains of glutamic acid bacteria is to select strains with AEC^R phenotypes; however, the second stage selection remains ambiguous. Although one could apply all the selection techniques reviewed above, there is a high probability that some are superfluous so the effort invested would not be worth the improvements attained. This thesis attempts to determine, in a novel manner, which pathways in the primary metabolism should be modified in the second stage of selection.

3.3.3 *Brevibacterium lactofermentum*

B. lactofermentum strains that are either AEC^R or $Homo^-$ also secrete lysine into the culture medium; however, it was also found that lysine production by AEC^R strains could be improved by further isolating strains that are $(AHV + Lys)^R$ [Tosaka and Takinami, 1978; Tosaka *et al.*, 1978a]. Aspartate kinase activity in AEC^R or AHV^R strains is subject to inhibition by lysine or threonine, respectively, while AEC^R plus AHV^R strains exhibited only slight inhibition by either metabolite, added separately or together. These results indicate that AK in *B. lactofermentum* may exist as isozymes although this has not been confirmed.

From studies on AEC^R strains, it was found that the addition of leucine to the culture medium inhibited lysine accumulation and that leucine auxotrophs (Leu^-) accumulated more lysine than standard AEC^R strains [Tosaka *et al.*, 1978d]. The improvements in lysine production from Leu^- strains is attributed to the removal of DDP synthase repression by Leu [Tosaka *et al.*, 1978b]. They also demonstrated that Leu^- of AEC^R strains of *C. glutamicum* also accumulated more lysine, even though Leu repression of DDP synthase does not occur in this organism. It is uncertain how Leu auxotrophy improves lysine production in *C. glutamicum*, but two possibilities are: 1) since Leu is derived from Pyr, Leu^- increase the availability of Pyr for lysine synthesis; or 2) Leu activation of homoserine dehydrogenase (see Section 3.2) may elevate the intracellular threonine pool, and thereby increase AK inhibition. Lysine production improvements by Leu^- strains of *C. glutamicum* has also been

documented in the US patents cited previously. In a similarly study, alanine auxotrophs (Ala^-) of AEC^R strains of *B. lactofermentum* also increase lysine production [Tosaka *et al.*, 1978c]. In this case, however, lysine improvement is believed to be due to increasing Pyr availability for lysine synthesis.

Although glutamic acid bacteria require biotin for growth and biotin concentration is crucial in glutamate fermentations, biotin typically does not affect lysine production provided it is supplied in sufficient quantities. However, it was found that increasing biotin concentration from 50 to 500 μg/l increased lysine yield in *B. lactofermentum* by 24% [Tosaka *et al.*, 1979b]. This improvement in lysine yield has been attributed to the increase in pyruvate carboxylase (PC) activity since PC requires biotin as a cofactor [Tosaka *et al.*, 1979c]. The increase has only been observed in *B. lactofermentum* as *C. glutamicum* and *B. flavum* lack PC. Based on these results, it was hypothesized that increased pyruvate availability, through attenuation of PDC activity, could permit more pyruvate to enter the PC catalyzed reaction which could enhance lysine yield [Tosaka *et al.*, 1985]. PDC attenuated (PDC^A) strains of *B. lactofermentum* were isolated for their sensitivity to fluoropyruvate (FP), which has been demonstrated to be a strong competitive inhibitor of pyruvate dehydrogenase (PDH) in the PDC [Tosaka *et al.*, 1985]. At low concentrations, FP does not severely inhibit growth of strains with nominal PDC activity; however, FP inhibition of PDH in PDC^A stains is strong enough to render PDC inactive, which, in turn, inhibits growth. Studies of several PDC^A strains of *B. lactofermentum* indicated that an optimum attenuation of PDC exists for lysine production, which was found to be 27% of the parent strain's PDC activity. The best strain accumulated large amounts of lysine•HCl (70 g/l) at a high yield (50% g/g). As discussed above, PDC attenuation also appears to increase lysine yield in *B. flavum* stains.

Recently, PPC in *B. lactofermentum* has been cloned and reintroduced, at a slightly higher copy number, to increase OAA availability [Sano *et al.*, 1987]. The recombinant strains exhibited increases in threonine and proline production, but affects on lysine production were not reported.

3.3.4 Summary

There are two basic techniques for deregulating lysine synthesis: 1) isolate HDH lacking strains from Homo$^-$ strains; and 2) directly select AK^R strains based on their (AEC + threonine)^R phenotype, the preferred method. Several enzymes of the primary metabolism have been modified in an attempt to increase lysine precursor availability. Pyruvate kinase attenuated strains can be isolated from colonies able to grow on glucose, but unable to grow on ribose. PDC^A strains can be isolated from colonies that are either FP^S or are prototrophic revertants of acetate auxotrophs. CS^A strains can be isolated from prototrophic revertants of glutamate auxotrophs. Although PPC^R strains are believed to enhance lysine yield, a good method for their isolation has not been presented. Modifications of the primary metabolism has definitely enhanced lysine yield. However, of the numerous possibilities, it is not known which modification will produce the best results. The frequency at which improved strains are isolated by the above techniques (except for AEC^R and Homo$^-$ methods) is fairly low, which may indicate that an undetected mutation is responsible for improvements in lysine yield. An interesting question then is, if one were to randomly select mutants from AEC^R strains and test them for lysine production (brute force), would one obtain strain improvements at the same frequency?

3.4 Fermentation

Lysine fermentations are, in general, relatively easy to conduct since the fermentation can be operated in batch mode and no special controllers are needed. As a result, most research effort has focused on strain improvements as discussed in Section 3.3. Since the primary objective of this thesis is to elucidate the relationship between carbon-flux distributions in the primary metabolism and lysine yield, an attempt has not been made to optimize the fermentation process. Consequently, only the fundamentals of the standard fermentation are reviewed here.

3.4.1 Media

By far the most important factor in attaining high lysine yields, aside from the strain, is the composition of the culture medium. Although optimization of a medium depends on the strain employed, the base compositions of media are fairly similar. Industrial scale production of lysine [Nakayama, 1972] usually begins with an initial seed culture consisting of 20 g/l glucose, 10 g/l peptone, 5 g/l meat extract, and 2.5 g/l NaCl in tap water. This seed is used to inoculate a second seed culture consisting of 50 g/l cane blackstrap molasses, 20 g/l $(NH_4)_2SO_4$, 50 g/l corn steep liquor, and 10 g/l $CaCO_3$ (to maintain pH) in tap water, which is then used to inoculate the fermentor: 200 g/l cane blackstrap molasses and 18 g/l soybean meal hydrolyzate.

For analytical studies, a seed medium consisting of 10 g/l polypeptone, 10 g/l yeast extract, and 5 g/l NaCl is usually used, while a defined fermentation medium typically consist of 100 g/l glucose, 40 g/l $(NH_4)_2SO_4$, 1 g/l KH_2PO_4, 0.4 g/l $MgSO_4 \cdot 7H_2O$, 2 mg/l Fe^{2+}, 2 mg/l Mn^{2+}, 300 µg/l biotin, 200 µg/l thiamine, and threonine plus methionine if the strain is $Homo^-$. Iron availability has been found to limit growth [Nakayama *et al.*, 1964a] which may be due to a poor iron uptake system since autoclaving iron with glucose [Nakayama *et al.*, 1964b] or the addition of citrate (a chelating agent) [von der Osten *et al.*, 1989] improves growth.

In terms of lysine production, threonine concentrations above 325 mg/l strongly inhibits lysine accumulation in $Homo^-$ strains of *C. glutamicum* [Daoust and Stoudt, 1961]. This inhibition, however, can be dramatically reduced by the addition of methionine. The optimum threonine and methionine concentrations for lysine production were found to be 300 and 100 mg/l, respectively. Daoust and Stoudt also found that the addition of glutamate (ca. 200 mg/l) can significantly increase lysine accumulation although this has not been well supported by other investigators. The addition of isoleucine has also been reported to enhance lysine production [Nakayama *et al.*, 1961]. Other studies have shown that the addition of small amounts of antibiotics [Zaki *et al.*, 1982] or dimethyl sulfoxide (DMSO) [Tang *et al.*, 1989] can improve lysine yield by altering cellular permeability, but both results are questionable due to the low lysine yields they observed.

3.4.2 Operating Conditions

Lysine fermentations are typically operated at approximately 30°C [Nakayama, 1972], although a recent report has demonstrated the production of lysine at 50°C from methanol by a thermophilic Homo$^-$, AEC^R strain of *Bacillus* sp. [Schendel *et al.*, 1990]. The pH is controlled close to neutrality by the addition of NH_4OH, urea, or introducing NH_3 with the air inlet. Typical industrially observed yields for "good" lysine producers range from 30-40% (g lysine•HCL/g glucose). However, yields for newly isolated strains, discussed in Section 3.3, may be as high as 55%. The rate of respiration during growth and lysine production is fairly high during these fermentations; consequently, even under high agitation and air flow rates, oxygen limitations can occur, especially in industrial size fermentors. Under oxygen limitations, lysine synthesis diminishes and is replaced by the accumulation of lactate and succinate [Hirose and Okada, 1979]. Even if the oxygen limitation is removed later in the fermentation, after growth has ceased, lysine synthesis remains attenuated [Hilliger and Hanel, 1981]. Oxygen deprivation appears to increase cell membrane phospholipid content as well as intracellular lysine concentration [Hanel *et al.*, 1981]. It is speculated that this increase in intracellular lysine concentration may inhibit AK and thereby elicit the reduction in lysine production. There is also some evidence that the reduction in lysine syntheses may be due to the repression of TCA cycle enzymes and an induction of glycolytic enzymes [Ruklisha *et al.*, 1981], but how this leads to inhibition of lysine synthesis has not been established.

In terms of optimum oxygen concentration, Enie *et al.* (1982) provides a concise review. They group amino acids into three categories: I) arginine, glutamine, glutamate, and proline; II) isoleucine, lysine, and threonine; and III) leucine, valine, and phenylalanine. For Type I and II amino acids ("TCA cycle-related amino acids"), any oxygen concentration above the critical level results in optimum production of these amino acids, where the critical oxygen concentration has been found to be 0.0002 atm (or 0.1% of saturation) for *B. lactofermentum* [Akashi *et al.*, 1978]. It has also been found that Type II amino acids are less sensitive to oxygen limitations than Type I (also see [Akashi *et al.*, 1979c]). Since Type III amino acids are derived from the EMP pathway metabolites, a slight oxygen limitation results in the optimum

production of these amino acids. Since oxygen probes are typically not reliable below 5% of saturation (0.01 atm), redox potential is used to control the respiration rate of the culture in Type III amino acid fermentations. Although the production of some amino acids, such as arginine [Akashi, *et al.*, 1979a] and glutamate [Hirose *et al.*, 1967], are inhibited at high oxygen concentrations (much greater than 0.21 atm or 100% saturation), this effect has not been reported for lysine production and such extreme operating conditions are seldom observed in practice. There has also been a report that lysine and biomass production are dramatically affected by dissolved oxygen concentrations between 5 and 50% sat. and by agitation speed between 500 and 1300 rpm [Beker *et al.*, 1973]. Unfortunately, the investigators did not present actual data and their conclusions have not been supported by others. Based on current understanding, stringent dissolved-oxygen (DO) control is unnecessary in lysine fermentations and DO need only be maintained above the critical value and below 100% sat.

3.4.3 Process Improvements

There is some evidence from a AEC^R strain of *Corynebacterium* sp. that growth rate and biomass yield on glucose may be slightly inhibited at high glucose concentrations, whereas lysine yield may be maximized under such conditions [Hadj *et al.*, 1988]. Although poorly documented, the authors demonstrate that controlling glucose concentration between 90 and 140 g/l can improve lysine titer and yield. Improvements from fed-batch operations have also been mentioned by Shvinka *et al.* (1980). They also state that induction of the glyoxylate shunt by feeding acetate can improve lysine yield as well. Similarly, an investigator in our laboratory has found significant improvements in both lysine titer and yield under fed-batch conditions [Kiss, In preparation].

Although there are relatively few reports on lysine production from continuous culture, a recent publication has demonstrated that lysine can be produced at high rates and yields under continuous operation [Hirao *et al.*, 1989]. At a glucose feed concentration of 280 g/l and a dilution rate of ca. 0.02 h^{-1}, the exit stream of the chemostat reached a maximum lysine•HCl concentration of 105 g/l at a 37.9%

(molar) yield. The highest lysine•HCl volumetric productivity observed was 5.6 g/l/h at a glucose feed concentration of 120 g/l and a dilution rate of ca. 0.16 h^{-1}. Wash out conditions varied significantly with glucose feed concentration, and oxygen was found to be the limiting nutrient except at fairly low dilution rates. The isolated strain, which is resistent to AEC, rifampicin, streptomycin and 6-azauracil, proved to be exceptionally stable, with fermentations exceeding 500 h of operation. It should be noted, however, exceptionally stable strains are difficult to isolated and strain reversion is the main problem associated with continuous cultures. Reversions can even present problems in batch fermentations [Nakayama, 1972].

A recent study has demonstrated that lysine can be produced from *Corynebacterium* sp. immobilized in calcium alginate beads [Nasri *et al.*, 1989]. Although this is a preliminary study, it indicates that the immobilized cells accumulate more lysine and at a slightly higher yield than cells in free suspension.

Chapter 4

Analysis of Metabolic Networks

A general methodology, and its analysis, for the estimation of the carbon-flux distribution in the primary metabolic pathways that support biomass synthesis is developed in the first section of this chapter. The technique, referred to collectively as the Bioreaction Network Algorithm (BRNA), is applied to lysine production by *Corynebacterium glutamicum*, but can be readily extended to other organisms or products. It is demonstrated in Section 4.2 that the BRNA can be used to predict metabolic flux distributions that must be realized in order to satisfy theoretical lysine yields. This analysis reveals potential branch-point limitations in the network that may constrain lysine yield. The identification and classification of these branch-point limitations are described in Section 4.3 and for basis of the experimental approach, the results of which are presented in Chapter 6.

4.1 Mathematical Representation of Metabolism

This section describes the methodology by which the biochemistry reviewed in Chapter 3 can be represented mathematically, so that the carbon-fluxes (*i.e.*, reaction rate or extent) through the biochemical pathways can be estimated by measuring the accumulation rates of extracellular metabolites only. The methodology relies solely on metabolite balances (*i.e.*, elemental balances), biochemical constraints, and a pseudo-steady state approximation for intracellular metabolites.

4.1.1 Metabolite Balances

Metabolite balances (or related techniques) have been used quite extensively for various estimation routines, as reviewed in Chapter 2. A brief example will illustrated how these balances can be further applied for metabolic flux estimation. A given set of reactions, stoichiometrically balanced, such as

$$A \rightarrow B \quad (1)$$
$$B \rightarrow C \quad (2)$$
$$B \rightarrow D \quad (3)$$

can easily be represented by evaluating the accumulation rate of each compound in the set. For the simple reaction set above, the following set of equations are obtained from such a "metabolite balance";

$$r_A(t) = -x_1(t) \quad (4)$$
$$r_B(t) = x_1(t) - x_2(t) - x_3(t) \quad (5)$$
$$r_C(t) = x_2(t) \quad (6)$$
$$r_D(t) = x_3(t) \quad (7)$$

where $x_i(t)$ is the rate (or flux) at time t of Reaction (i) above and $r_M(t)$ is the rate of accumulation for metabolite M at time t. Consequently, if the metabolite accumulation rates (r_A-r_D) can be measured, the reaction fluxes can be estimated. Even if one metabolite cannot be measured, the fluxes can still be obtained, as there are more equations than unknowns. Such a system is referred to as overdetermined, and the extra—or redundant—equation is quite useful for identifying measurement inconsistencies, as will be explained in Section 4.1.9. Although this example might seem trivial, the exact same technique can be applied to the entire set of metabolic reactions reviewed in Chapter 3, where accumulation rates for extracellular metabolites are obtained from fermentation data, and a pseudo-steady state approximation (PSSA) is invoked for intracellular metabolites. The net result is the ability to estimate the carbon-flux distribution in the primary metabolism throughout the course of the fermentation from extracellular measurements only.

The remainder of this section describes the details and assumptions that are necessary to estimate flux distributions through the primary metabolism from metabolite balances, as well as the typical problems encountered.

4.1.2 Network Closure and Reaction Condensation

The number of biochemical reactions chosen to represent the metabolism of an organism largely rests on the details required for the desired goals, but is always constrained by the pathways actively expressed by the organism under the culture conditions employed. Although the methodology developed in this chapter is quite general, an emphasis will be placed on the primary metabolism of *C. glutamicum* during lysine overproduction as reviewed in Chapter 3. Once the representative biochemistry set is defined for the particular objectives, however, it must meet closure conditions, and the dimension of the set can often be reduced, as discussed below. In the discussions to follow, it is assumed that all reactions have been stoichiometrically balanced with respect to the metabolites in the measurement set. Reactions do not have to meet elemental stoichiometry since some metabolites, such as water, will not be included in the measurement set.

Since flux estimation will be based on metabolite balances, it is necessary that all intracellular metabolites synthesized are properly consumed, as they would be in the cell, so that a pseudo-steady state approximation can be invoked for these metabolites. The inclusion of such regenerating reactions in the biochemistry set (BS) is referred to as network closure. For instance, in the biosynthesis of lysine from oxaloacetate, reactions must be included to produce the required precursors (Glut, Pyr, NADPH, SucCoA, and ATP) and to regenerate, or integrate into the primary metabolism, the spent metabolites (αKG, Suc, NADP, CoA, and ADP). However, closure reactions do not need to be included for those metabolites that will not be part of the balance, such as H_2O. Reactions that lead to the production of extracellular metabolites (such as CO_2, by-products, etc.) must also be included in the BS (the synthesis of biomass is deferred to the next section).

After a biochemistry set is constructed and properly closed, the dimensionality of the system can often be dramatically reduced—condensed—by removing those

intracellular metabolites that are not branch-points. A metabolite is considered a branch-point if it is involved in three or more reactions. For example, the following sequence of intracellular reactions

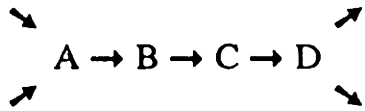

(8)

can be reduced to

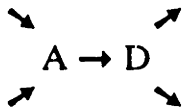

(9)

since the three reactions that convert A to D in Equation (8) comprise a nonbranching sequence that must all proceed at the same rate under the PSSA. Before the BS can be condensed, however, the synthesis of biomass must be considered as its inclusion will introduce more branch-points.

4.1.3 Biomass Synthesis and Maintenance

Although hundreds of reactions are required to synthesize all the necessary constituents of biomass from the primary metabolites, it is unlikely that the fluxes through these peripheral reactions could be accurately estimated since the flux through any one of these reaction will be quite small. Furthermore, we are only interested in the primary metabolism so inclusion of such reactions would unnecessarily increase the dimension of the network. In this analysis, it is helpful to consider biomass as just another metabolite (such as lysine) that is drawn off the primary metabolism. Although biomass synthesis can be represented by one reaction in which glucose (or some other primary carbon source), ammonium, NADPH, and ATP are the only substrates [Minkevich and Eroshin, 1973; Papoutsakis, 1984; Reardon *et al.*, 1987; Vallino, 1987], this approximation does not distribute the biomass burden realistically over the primary metabolism. Under this approximation, part of the glucose that enters the cell is immediately removed for biomass synthesis, and only the remaining glucose enters the pathways of the primary metabolism. Such

a simple expression for biomass synthesis is, of course, a gross simplification since the glucose that actually leads to biomass is removed at various points throughout the primary metabolism. A more accurate representation of metabolic burden of biomass synthesis can be obtained if biomass is expressed as a summation of primary precursor metabolites, where the amount of each metabolite required is given by yield a coefficient. Such a description has been developed by Ingraham *et al.* (1983) for *E. coli*, where biomass composition is expressed in terms of 12 "building block" metabolites. Although there are significant differences between *E. coli* and *C. glutamicum* (*E. coli* is gram negative for one), the composition of the two procaryotes is not expected to be significantly different at the "building block" level. Indeed, amino acid composition of *E. coli* [Stouthamer, 1973; Ingraham *et al.*, 1983] is similar to that of *C. glutamicum* [Kimura, 1963]. Furthermore, it will be demonstrated in Section 4.1.8 that the flux distributions through the primary metabolism are not very sensitive to alterations in the biomass yield coefficients. The use of *E. coli* biomass composition for *C. glutamicum* is therefore warranted. Although Ingraham *et al.* decomposed *E. coli* down to 12 precursor metabolites, biomass decomposition to this extent is not always necessary. For instance, if the network representation of the primary metabolism extends to the synthesis of all 20 amino acids, then biomass composition should be expressed in terms of amino acids, and not in terms of keto acids. If biomass was expressed in terms of keto acids, then the flux to the amino acids would be underestimated. (In fact, the simple biomass reaction described at the beginning of this section, that was considered inadequate, represents the decomposition of biomass all the way back to glucose.)

Based on Ingraham *et al.* (1983, Table 9 p. 122 and Table 11 p. 128), the primary metabolites, as well as ATP, NAD, and NADPH, required to synthesize 1.0 mole of *C. glutamicum* are displayed in Table 4.1. The derivation of the data presented in this table is as follows. The data provide by Ingraham *et al.* (1983, Table 11, p. 128) was adjusted (NH_3 and NADPH subtracted from substrate pools, and CO_2 added as a product) so that the calculated elemental composition of the *C. glutamicum* from Table 4.1 would match the experimentally observed composition of $C_{3.97}H_{6.16}O_{1.94}N_{0.845}$, 3.02% ash (MW = 100), given in Table 5.13 (Section 5.5.5.1).

Table 4.1 Primary metabolites required to synthesize 1.0 mole of *C. glutamicum*, see text for details.

Substrates (mmole)						Products (mmole)	
21	Glc6P	52	PEP	25	Glum	1000	Biomas
7	Fru6P	30	Pyr	54	Ala	143	CO2
90	Rib5P	332	AcCoA	40	Val	364	AKG
36	E4P	80	Asp	3820	ATP	3820	ADP
13	GAP	33	LysI	476	NADPH	476	NADP
150	G3P	446	Glut	312	NAD	312	NADH
52	Thr¶	15	Met¶	43	Leu¶		

¶ Amino acids supplied in medium.

Next, NH_3 (and the corresponding amount of NADPH) was removed from the substrate pool and replaced by Glut to AKG conversion since *C. glutamicum* fixes all NH_3 via glutamate dehydrogenase. Since *C. glutamicum* ATCC 21253 does not synthesize isoleucine, leucine, methionine or threonine from primary metabolites (culture medium is supplemented with leucine, methionine, and threonine, due to the auxotrophic requirements of ATCC 21253), these amino acids (and their corresponding energy and reducing equivalent requirements) were subtracted from the substrate pool. Finally, the amino acids aspartate, lysine, glutamate, glutamine, alanine, and valine were added to the substrate pool (and the corresponding amounts of keto acids, ATP, etc, were removed) since the reactions leading to the direct synthesis of these amino acids are included in the metabolic network. The resulting reaction (Table 4.1) is referred to as the biomass reaction. Although not required in this study, integration of complex products into the primary metabolism, such as proteins, can be handled in a similar manner as that described for biomass synthesis.

The ATP requirement for biomass synthesis given in Table 4.1 is the theoretical value and is basically identical to the theoretical Y_{ATP}^{MAX} of 28.8 g DCW/mole ATP calculated by Stouthamer (1973) for growth of *E. coli* on glucose and minimal salts. Consequently, ATP requirements for maintenance [Mallette, 1963; Marr *et al.*, 1963] have not been accounted for. Although we could account for

maintenance related ATP consumption by introducing the typically observed ATP yield (Y_{ATP}) of 10.5 g DCW/mole ATP [Bauchop and Elsden, 1960], this yield is known to vary with culture conditions [Stouthamer, 1978; Stouthamer and Bettenhaussen, 1973], and would be expected to drop dramatically, due to the operation of futile cycles [Leiser and Blum, 1987; Katz and Rognstad, 1976], when *C. glutamicum* enters the threonine limited stationary phase. To avoid these uncertainties, a different approach was taken. It can be shown (see Section 4.1.5 below) that the metabolic flux distributions can still be determined if the ATP metabolite balance is removed from the network. Although removal of the ATP balance would solve the problem, the extent of ATP overproduction could not be determined then. Consequently the following reaction was added to the biochemistry set

$$ATP \rightarrow ADP \qquad (42:PBS)$$

so that the ATP balance could be maintained, without actually constraining the flux distributions. The flux supported by this reaction, referred to as ATP dissipation, represents the amount of ATP that is synthesized over that which is theoretically required, and is equal to the amount of ATP that is required for cellular maintenance and expended in futile cycles. Although the working lower bound for the flux in this reaction is unknown, the flux certainly cannot be less that zero, and a large flux implies substantial operation of futile cycles (see Section 6.1.3.2.3 for typically observed values).

Closure and condensation of the metabolic reactions reviewed in Chapter 3 along with the biomass equation (Table 4.1) and the ATP dissipation reaction constitute the preliminary metabolic network of *C. glutamicum* for lysine overproduction. This preliminary biochemistry set (PBS) is listed in Appendix B. In the following sections the mathematical representation and analysis of this biochemistry set is presented.

4.1.4 Bioreaction Network Equation

The preliminary biochemistry set list in Appendix B can now be expressed mathematically by constructing a metabolite balance (Section 4.1.1) for each metabolite that occurs in the set. The resulting set of equations can be expressed in matrix form, as

$$\mathbf{A}\mathbf{x}(t) = \mathbf{r}(t) \tag{4.1}$$

which is referred to as the Bioreaction Network Equation (BRNE). The matrix **A** contains the stoichiometry of the metabolic network and is referred to the biochemistry matrix. The dimension of **A**, D(**A**), is $m \times n$, where m is the number of equations (*i.e.*, number of metabolites) and n is the number of unknown fluxes. For a solution of the BRNE to exist, it is necessary for m to be greater than or equal to n; however, this is not a sufficient condition as will be explained in the next section. If m is less than n, then there are more unknowns than equations, so $n-m$ reactions must be removed or lumped together, as explained in the next section. The n-dimensional vector $\mathbf{x}(t)$ represents the unknown fluxes supported by the reactions in the PBS at time t. The m-dimensional vector $\mathbf{r}(t)$ contains the measured or approximated accumulation rates of each metabolite in the BRNE at time t, and is referred to as the metabolite accumulation rate vector, or simply the measurement vector. Construction of this vector is deferred to Section 4.1.6 below.

Although a balance can be constructed around each metabolite in a BS, some metabolites cannot be measured, or do not provide additional information. For example, production or consumption of water (H2O) occurs in several reactions; however, the accumulation rate of water cannot be measured. Similarly, balance equations around the complements of several cofactors (such as NAD, NADP, CoA, etc) do not provide additional information and should not be included in the BRNE (they are dependant equations that will be examined in more detail in Section 4.1.9). Consequently, it is sometimes necessary to remove a metabolite balance from the BRNE, which can easily be accomplished by deleting the row(s) from **A** and $\mathbf{r}(t)$ that correspond to the metabolite(s) to be removed. Occasionally the measurements of extracellular metabolites are unavailable (*e.g.*, glucose, O_2, CO_2, etc.), but their

accumulation rates can still be estimated from the BRNE. The unmeasured metabolites can be deleted for the BRNE to produce

$$\mathbf{A}'\hat{\mathbf{x}}(t) = \mathbf{r}'(t) \tag{4.2}$$

$$\mathbf{r}_D(t) = \mathbf{A}_D\hat{\mathbf{x}}(t) \tag{4.3}$$

where $\mathbf{A}'$ and $\mathbf{r}'(t)$ are the same as in Equation (4.1), except that rows $\mathbf{A}_D$ has been deleted from $\mathbf{A}$ and $\mathbf{r}_D(t)$ has been deleted from $\mathbf{r}(t)$. The fluxes can then be estimated ($\hat{\mathbf{x}}(t)$) from Equation (4.2) (provided $\mathbf{A}'$ is not singular) and plugged into Equation (4.3) to provide an estimate of the accumulation rates for the unmeasured metabolites. This analysis is just a generalization of some of the estimation techniques reviewed in Chapter 2.

It is quite apparent from the above discussion that one must keep track of the metabolites that comprise the BRNE as they will usually form a subset of metabolites listed in the biochemistry set. This is easily accomplished by constructing a metabolite set (MS) that consists of the metabolites of the BS that are actually balanced around, and corresponds, on a one-to-one basis, with the elements of $\mathbf{r}(t)$. The BRNE equation, therefore, is completely defined by one BS and one MS, which can be modified as needed. The preliminary metabolite set (PMS) for lysine production by *C. glutamicum* (along with the PBS) is listed in Appendix B. The corresponding biochemistry matrix ($\mathbf{A}$) of the BRNE has dimensions of 40 (m) × 43 (n). Since m is less than n, $\mathbf{A}$ is singular and must be modified in order to obtain a solution of the BRNE, as explained below.

4.1.5 Singularities

Since the BRNE is a simple linear expression, we can take advantage of the wealth of information known about these systems from linear algebra. Although $\mathbf{A}$ is inherently a sparse matrix, it is not ordered (*i.e.*, band diagonal, symmetric, etc.), so that manipulations of $\mathbf{A}$ must involve the entire matrix. This does not introduce a problem, however, for these systems are typically small and can easily be handled

on personal computers. The techniques and terms referred to in this section, and those that follow, can be found in Strang (1980) or Noble and Daniel (1977), except where noted.

4.1.5.1 Identification

For a unique solution of the BRNE to exist, the rank of **A**, R(**A**) (or number of independent equations), must equal the column dimension of **A**, given by *n*. If this is true, then **A** is said to be of full rank or nonsingular. The rank of **A** can be determined from a singular value decomposition of **A**, where R(**A**) equals the number of nonzero singular values (with respect to machine precision). However, since **A** is, by nature, properly scaled (most elements are either zero or one), R(**A**) can often be accurately determined by gaussian elimination, where R(**A**) equals the number of nonzero rows of the transformed matrix. If R(**A**) does not equal *n*, then **A** is said to be singular, and some or all of the fluxes cannot be uniquely determined from the metabolite balances alone, which can also be regarded as an observability problem. The set of reactions—fluxes—that are affected by the singularity (*i.e.*, cannot be uniquely determined) will be referred to as a singular group. The existence of a singular group or groups means that an infinite set of fluxes exists that produce the same metabolite accumulation rate vector. Consider for example the simplified network displayed in Figure 4.1 (A). The correspond biochemistry matrix (**A**) has a dimension of 6 × 6; however, R(**A**) equals 5, so **A** is singular. It is easy to see that fluxes x_1, x_5, and x_6, are uniquely defined by r_X, r_Y, and r_Z, respectively. However, fluxes x_2, x_3, and x_4, comprise a singular group as shown here

$$x_2 = f_1(\mathbf{r}) - \alpha \tag{10}$$
$$x_3 = f_2(\mathbf{r}) - \alpha \tag{11}$$
$$x_4 = \alpha \tag{12}$$

where α is any real number and $f_i(\mathbf{r})$ are functions of r_i. In essence, the singular network of Figure 4.1 (A) is actually a linear composite of the three nonsingular subnetworks illustrated in Figure 4.1 (B). To obtain a unique solution, either α must be set or an additional independent equation must be added to **A**.

A)

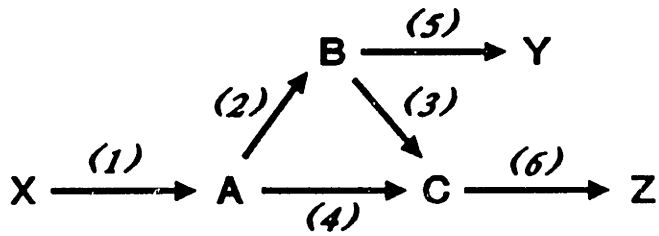

B)

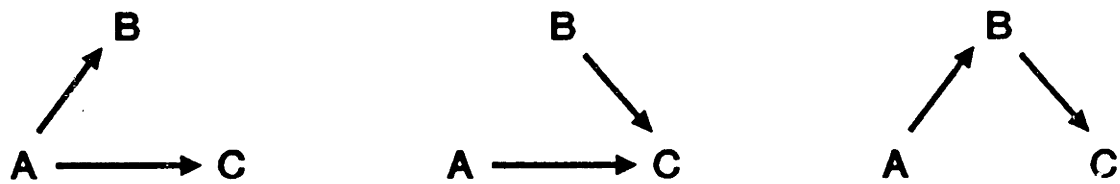

Figure 4.1 Example of a singular network. (A) Reactions (2), (3), and (4) comprise a singular group. (B) Nonsingular reaction groups that form the basis of the singular group in (A).

The general solution of any BRNE, $\mathbf{x}_G$, is given by

$$\mathbf{x}_G = \mathbf{x}_R + \sum_{i=1}^{q} \alpha_i \mathbf{x}_{N,i} \tag{4.4}$$

where $\mathbf{x}_R$ is the solution to the BRNE with the minimum norm; $\mathbf{x}_{N,i}$ span the null-space of $\mathbf{A}$ (*i.e.*, $\mathbf{A}\mathbf{x}_{N,i} = \mathbf{0}$); α_i are any real scalars; and q is the dimension of the null-space of $\mathbf{A}$ (*i.e.*, $q = n - \mathrm{R}(\mathbf{A})$). Therefore, the number of singular groups equals q, and each singular group, i, involves the reactions that correspond to the nonzero elements of $\mathbf{x}_{N,i}$ for that singular group. The network of Figure 4.1 (A), for example, has one dependant equation and the reactions of the singular group are given by $\mathbf{x}_N = [0\ -1\ -1\ 1\ 0\ 0]^T$, or reactions x_2, x_3, and x_4, as illustrated in Equations (10-12) above. It should be noted that singular reaction groups are analogous to dependant

reactions as given by the Gibbs' rule of stoichiometry [Aris and Mah, 1963], where each singular group consists of one dependent reaction.

4.1.5.2 Removal

There are two basic approaches to removing singularities from the BRNE. The first consists of removing reactions or lumping them together. For instance, the network of Figure 4.1 (A) can be rendered nonsingular by removing either Reaction (2), (3), or (4) from the network. Such a network modification would be justified if one of the three reactions exhibits low activity, or is not expressed under the conditions of the study. Removal of reactions is also equivalent to lumping reactions together. The removal of Reaction (3) in Figure 4.1 (A), for example, can be interpreted as the lumping of the A-to-C-via-B flux with Reaction (4).

The second approach in the removal of singularities is to set the flux-partitioning at a particular branch-point to a constant value. For example, if independent measurements or kinetic analysis of the network in Figure 4.1 (A) indicate that the flux supported by Reaction (2), divided by the flux of Reaction (1), is always approximately ϕ, then the following equation could be added to the BRNE

$$x_2 - \phi x_1 = 0 \tag{13}$$

which would effectively remove the singularity. Similarly, if certain fluxes are actually known, $\mathbf{x}_K$, (*i.e.*, from direct measurements), then Equation (4.1) can be expressed as

$$[\mathbf{A}_U \; \mathbf{A}_K] \begin{bmatrix} \mathbf{x}_U \\ \mathbf{x}_K \end{bmatrix} = \mathbf{r} \tag{4.5}$$

where $\mathbf{x}_U$ are the unknown fluxes and $\mathbf{A}$ has been partitioned to $[\mathbf{A}_U \; \mathbf{A}_K]$. Equation (4.5) can be rearranged to give

$$\mathbf{A}_U \mathbf{x}_U = \mathbf{r}' \quad \text{where} \quad \mathbf{r}' = \mathbf{r} - \mathbf{A}_K \mathbf{x}_K \tag{4.6}$$

which can be solved for the unknown fluxes, provided $\mathbf{A}_U$ is not singular.

In either case, the network fluxes that are affected by such modifications depends on the number of reactions involved in the singular groups, which are given by $\mathbf{x}_{N,i}$. Although a singular group often consists of only of few reactions, it can involve the entire network. Consequently, the removal or lumping of reactions or the addition of supplementary equations can have global effects and should be examined carefully. All supplementary information on the metabolism, such as *in vitro* assays, should be consulted to properly mitigate singularities. Such metabolic studies need not focus on the entire network since the singularity analysis identifies the reactions that form a singular group.

4.1.5.3 *C. glutamicum* Network

The techniques described above can now be applied to the preliminary biochemistry and metabolite sets (PBS and PMS) listed in. Since m is less than n ($D(\mathbf{A}) = 40 \times 43$), three reactions must be immediately removed. As reviewed in Chapter 3, a dinucleotide transhydrogenase has not been detected in *C. glutamicum*; consequently, Reaction (43:PBS)† was removed. Although two pathways exit for the conversion of AKP to lysine, and both may support a significant flux [Leadlay, 1979], either one can be removed with negligible effects on the network (*i.e.*, this singular group only involves a few reactions). Consequently, mDAP dehydrogenase (Reaction (39:PBS)) was removed. The malate enzyme (Reaction (12:PBS)) was also removed from the network since it exhibits almost no activity when *C. glutamicum* is cultured on glucose (see Chapter 3 and Section 5.3.1). Deleting these three reactions from the PBS reduces $D(\mathbf{A})$ to 40×40. Singularity analysis of the resulting network, however, indicates that $R(\mathbf{A})$ is only 37, which means three more reactions must be removed. These three singular groups involve practically every reaction in the network, so one cannot rely on the elements of $\mathbf{x}_{N,i}$ to determine which reactions to consider for deletion. Consequently, it is necessary to rely on the preconceived operation of the metabolism to isolate those reactions that should be investigated for possible removal.

---

† This nomenclature, Reaction (#:BS), which will be used throughout the thesis, refers to Reaction (#) of biochemistry set BS listed in Appendix B, in this case Reaction (43) of the PBS.

Examination of the PBS reveals that there are three anabolic reaction sets present: PEP carboxylase (PPC), Reaction (9:PBS); pyruvate carboxylase (PC), Reaction (10:PBS); and the glyoxylate shunt, Reactions (21:PBS) and (22:PBS). As reviewed in Section 3.2, the primary metabolism can function in either the TCA or DCA cycle mode, which largely depends on the expression level of the above enzymes. It was found (see Section 5.3.2), however, that the first enzyme of the glyoxylate shunt (isocitrate lyase, Reaction (21:PBS)) appears repressed when *C. glutamicum* is cultured in the presence of glucose; therefore, Reactions (21:PBS) and (22:PBS) were deleted from the PBS. However, this only removes one of the singular groups in $\mathbf{A}$, since $R(\mathbf{A})$ was reduced to 36 due to the removal of the GLYOX balance from the BRNE. Examination of the remaining null vectors (given by $\mathbf{x}_{N,1}$ and $\mathbf{x}_{N,2}$) indicate that the reactions comprising the remaining two singular groups are pyruvate kinase (PK, Reaction (7:PBS)), PPC, PC, oxaloacetate decarboxylase (OAADC, Reaction (11:PBS)), and the ATP dissipation reaction (Reaction (42:PBS)). Since PK is a well-established enzyme in *C. glutamicum*, and the ATP dissipation reaction can not realistically be removed (ATP dissipation certainly occurs), the activities of PC, PPC, and OAADC were assayed for. It was found (see Section 5.3.1) that while PPC and OAADC exhibited high activity, PC could not be detected. Consequently, PC was removed from the network, leaving one singular group (note, even though $m > n$, $\mathbf{A}$ is still singular). The presence of high, constitutive activity of OAADC remains somewhat a mystery. Although OAADC is required for the operation of the DCA cycle for acetate catabolism, it should not be required for TCA cycle operation. It is possible the OAADC has a high Michaelis constant for OAA, so that under glucose catabolism, OAADC does not support a significant flux. Nevertheless, the PEP-to-Pyr flux supported by PPC and OAADC can be lumped with PK, so that OAADC can be removed from the network, as illustrated in Figure 4.2. A summary of the dependent reactions removed from the PBS are illustrated in Figure 4.3, and the remaining reactions, after condensation, form biochemistry and metabolite sets no. 1 (BS1 and MS1) listed in Appendix B. The associated biochemistry matrix has dimensions given by $D(\mathbf{A}) = 37 \times 34$. The sets BS1 and MS1 constitute the BRNE and will form the basis for all subsequent

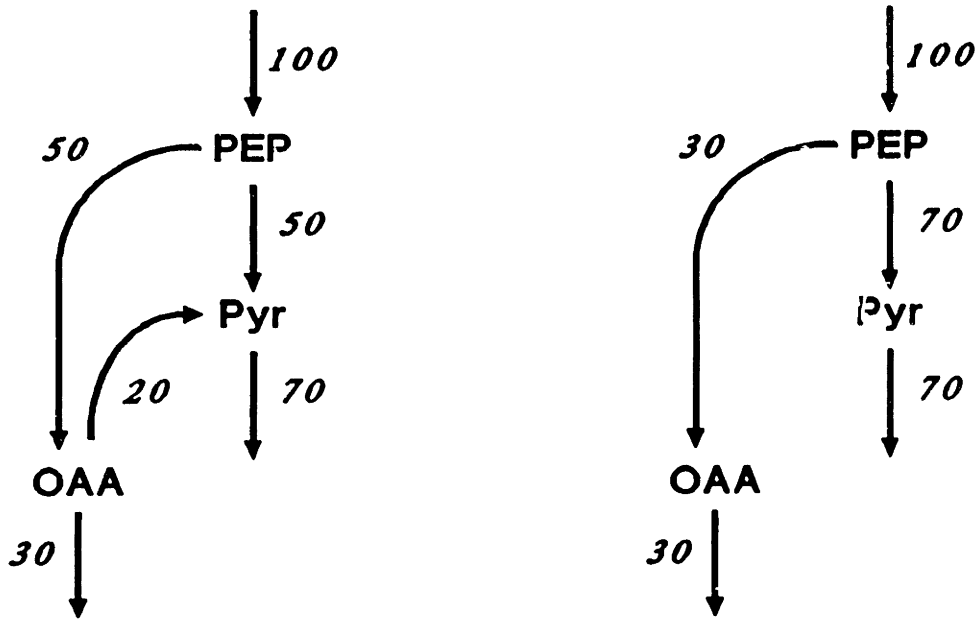

Figure 4.2 Effect of removing OAADC from the PPC-PK-OAADC singular group. Diagram on the left represents actual flux distribution (not observable), while the diagram on the right is the estimated flux distribution after removal of OAADC.

analyses.

As previously mentioned, removal of dependant reactions (*i.e.*, choice of α_i in Equation (4.4)) can dramatically affect flux distributions throughout a network, as dictated by $\mathbf{x}_{N,i}$. The two flux distribution maps illustrated in Figures 4.4 and 4.5, for example, were calculated from the same measurement vector, $\mathbf{r}$; yet, the distributions exhibit radically different characteristics. The flux distribution map of Figure 4.4 is based on BS1 and MS1 developed above, while the distribution map of Figure 4.5 is based on the DCA cycle model (glyoxylate shunt and OAADC replace PPC and αKG dehydrogenase, now established as incorrect). Not surprisingly, flux distributions in the TCA (or DCA) cycle are radically different in the two models. The two networks, however, also predict extremely different fluxes in the pentose phosphate pathway (Reactions (22-27:BS1)), due to the difference in the ICDH flux (Reaction (12:BS1)). Radically different flux distributions can present quite a problem as metabolic modifications intended to enhance lysine yield in one network could be inappropriate for the other network, with possible deleterious effects. Although flux

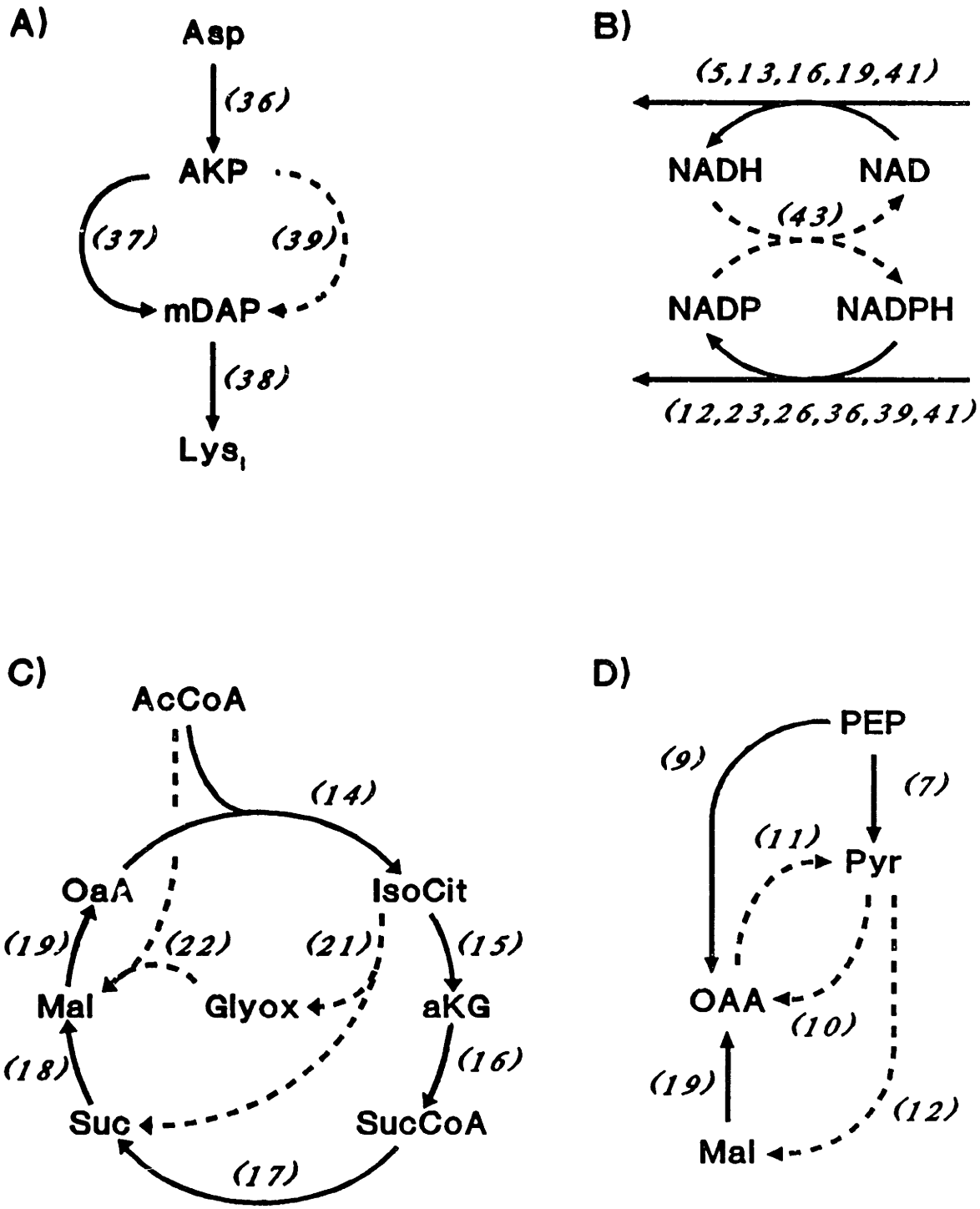

Figure 4.3 Reactions (numbers shown in parentheses) removed from the preliminary biochemistry set (PBS) to alleviate singularity problems: (A) mDAP dehydrogenase (39); (B) dinucleotide transhydrogenase; (C) isocitrate lyase (21) and malate synthase; (D) pyruvate carboxylase (10), oxaloacetate decarboxylase (11), and malate enzyme (12).

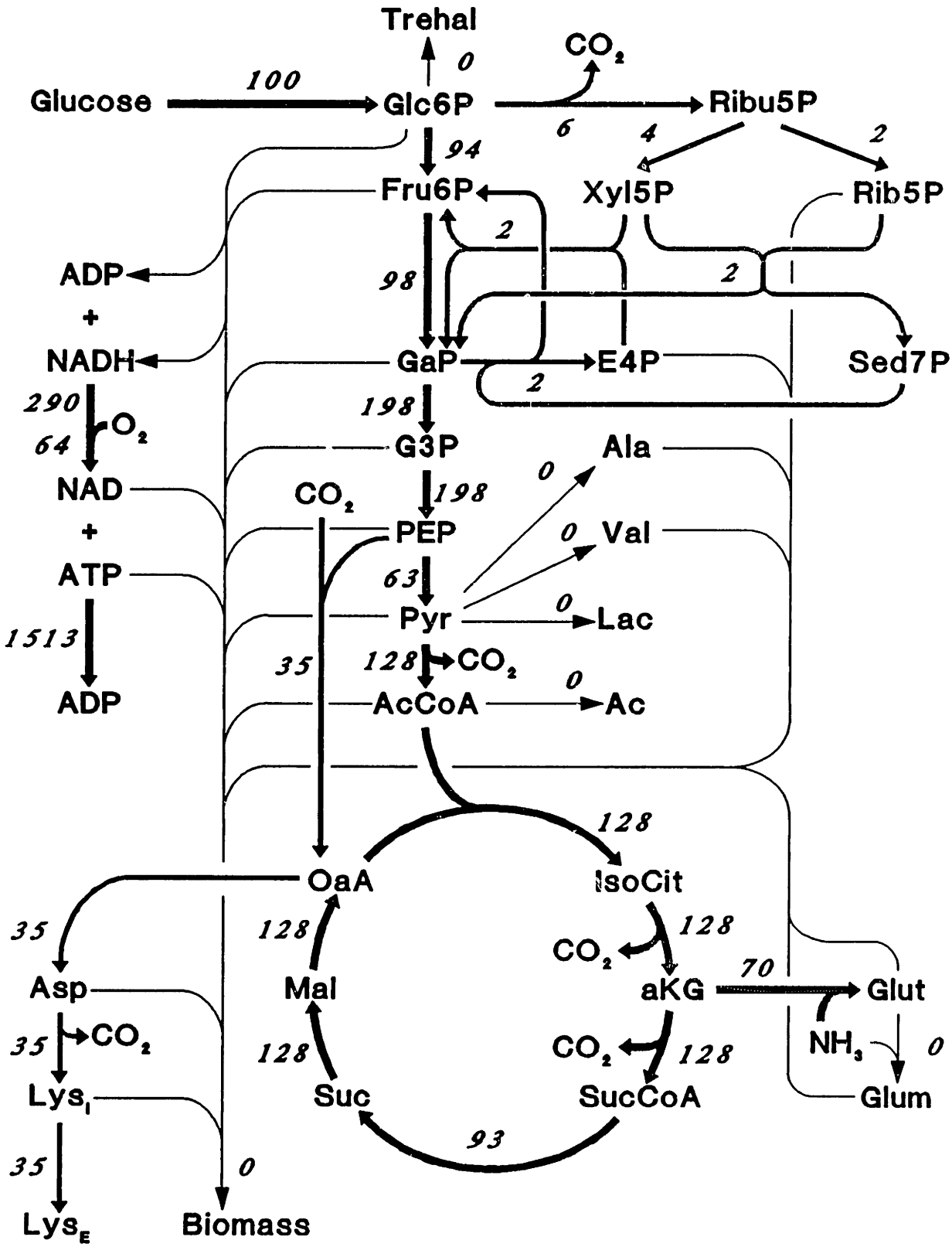

Figure 4.4 Theoretical flux distributions (arbitrary molar units) in the TCA cycle model (BS1 and MS1) for a 35% lysine yield with no biomass or by-product accumulation.

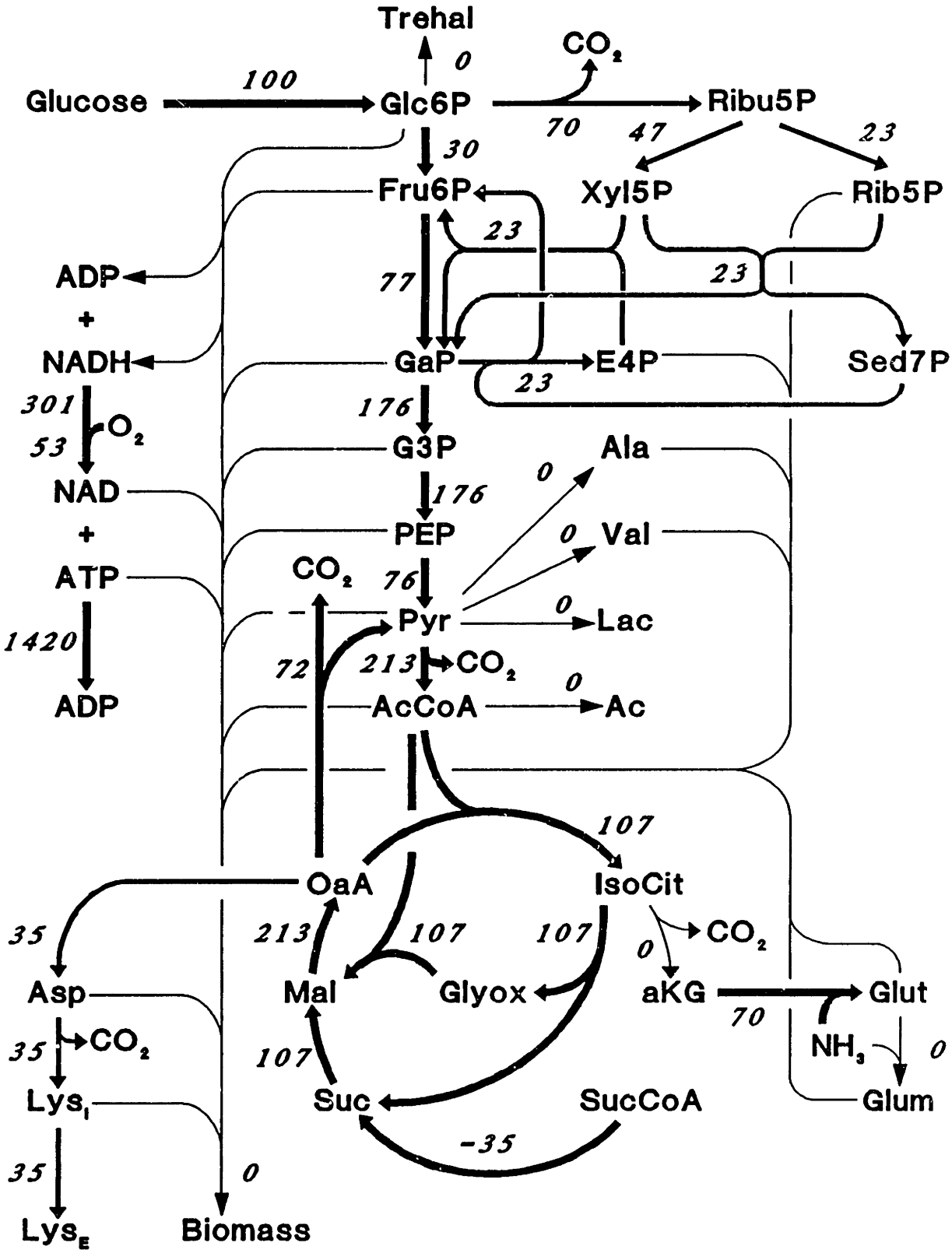

Figure 4.5 Theoretical flux distributions (arbitrary molar units) in the DCA cycle model (PPC and αKGDH of BS1 replaced by the glyoxylate shunt and OAADC) for a 35% lysine yield with no biomass or by-product accumulation. Note the elevated pentose phosphate pathway flux.

discrepancies can lead to erroneous conclusions regarding appropriate metabolic modifications, significantly different flux predictions can also be used for network discrimination, as demonstrated for citric acid production [Aiba and Matsuoka, 1979]. Since the DCA cycle model supports a much greater pentose phosphate pathway (PPP) flux than the TCA cycle model, the participation of the glyoxylate shunt can be assessed by measuring the fraction of glucose that enters the PPP, which can easily be determined from stable or radio isotope tracer studies. As discussed in Section 6.1.3.2.2, such studies indicate a PPP flux consistent with the TCA cycle model (BS1 and MS1). Internal consistency of a network can sometimes be confirmed without the aid of addition measurements by examining the feasibility of predicted flux distributions. A particular network arrangement can be regarded as inadequate if flux distributions, constructed from consistent data, predict negative flows for reactions considered irreversible.

4.1.5.4 Suggestions

Although glucose metabolism in *C. glutamicum* (PBS) was rendered observable (BS1 and MS1) without relying on ambiguous assumptions (intracellular assays were required however), this may not always be the case for other organisms. Consequently, the following few suggestions regarding reactions associated with singular groups may be useful: 1) One of two pathways at a branch-point can sometimes be removed by examining the kinetics of the branch enzymes. If the lead enzyme of a branch has poor affinity for the branch metabolite, or exhibits low activity compared to the competing enzyme, then it may be acceptable to delete the branch from the network. Likewise, if two competing branches exhibit similar activities and metabolite affinities, then it may be acceptable to set the branch splits, as discussed above. 2) The presence of a dinucleotide transhydrogenase (such as Reaction (43:PBS)) renders NADH and NADPH indistinguishable from the stand point of metabolite balances. If the transhydrogenase is capable of supporting a significant flux, the singularity can be removed, with minimal network perturbation, by replacing the oxidative branch of the PPP (Reaction (27:PBS)) with the transhydrogenase reaction. 3) The Entner-Doudoroff pathway can be incorporated by deleting Glc6P isomerase (Reaction (3:PBS)). 4) The carboxylase-decarboxylase

reactions between PEP or Pyr and OAA or Mal can usually be lumped into one reaction with minimal network flux alterations. 5) If the reactions of a pathway depend on flux directionality (*i.e.*, glycolysis versus gluconeogenesis), then the appropriate reactions can be swapped in or out of the BS depending on the flux estimates.

4.1.6 Metabolite Accumulation Rate Vector

Since biomass composition, as given in Table 4.1, also accounts for all free intracellular metabolites pools, the measurement vector **r** represents the total accumulation rate for each metabolite listed in MS1 minus the intracellular accumulation rate that is account for in the measurement of the biomass accumulation rate.

4.1.6.1 Balanced Growth

If $C_j^T(t)$ is the total concentration of metabolite j (total mmoles of metabolite j per liter of fermentation broth) in the MS, excluding biomass, $C_B(t)$ is the biomass concentration, and Y_j is the fraction of free metabolite j in biomass (implicit in Table 4.1), then

$$r_j(t) = \frac{dC_j^T(t)}{dt} - Y_j r_{BIO}(t) \quad \text{and} \quad r_{BIO}(t) = \frac{dC_B(t)}{dt} \tag{4.7}$$

or

$$r_j(t) = \frac{dC_j^E(t)}{dt} + \frac{dC_j^I(t)}{dt} - Y_j r_{BIO}(t) \quad \text{and} \quad r_{BIO}(t) = \frac{dC_B(t)}{dt} \tag{4.8}$$

where $C_j^T(t) = C_j^E(t) + C_j^I(t)$ and the superscripts E and I refer to extracellular and intracellular components of metabolite j, respectively. Under balance growth [Bailey and Ollis, 1977, p. 347], the composition of the biomass remains constant, so $C_j^I(t) = Y_j C_B(t)$, where Y_j is a constant. Therefore, balance growth implies

$$\frac{dC_j^I(t)}{dt} = \frac{d(Y_j C_B(t))}{dt} = Y_j r_{BIO}(t) \tag{4.9}$$

and Equation (4.8) can be expressed as

$$r(t) = \begin{bmatrix} r_I(t) \\ r_E(t) \end{bmatrix} \quad \text{where} \quad \begin{aligned} r_I(t) &= 0 \\ r_E(t) &= \frac{dC^E(t)}{dt} \end{aligned} \tag{4.10}$$

where I corresponds to all intracellular metabolites and E refers to all extracellular metabolites, including biomass. Consequently, only those metabolites that have extracellular complements need monitoring, which greatly reduces the number of measurements required to estimate the flux distributions through the primary metabolism, given by the BS. The above derivation is for batch fermentations, but can be easily extended to fed-batch and continuous operations by accounting for dilution effects. Although Equation (4.10) is exact, by definition of balance growth, it is a valid approximation over a much wider range of growth.

4.1.6.2 Pseudo-Steady State

If the rate of accumulation of an intracellular metabolite (minus that accounted for by $Y_i\, r_{BIO}(t)$) is small compared to the reactions producing or consuming it, then a pseudo-steady state (PSS) approximation (PSSA) can be invoked for that metabolite, and Equation (4.10) is valid even if growth is unbalanced. Consider the following reaction

$$\rightarrow M \rightarrow \tag{14}$$

where M is any intracellular metabolite produced at rate $x_P(t)$ and consumed at rate $x_C(t)$. We will assume, without loss of generality, that $r_{BIO} = 0$. For the PSSA to be valid $dC_M(t)/dt$ must be significantly less than $x_P(t)$ or $x_C(t)$, where $C_M(t)$ is the intracellular concentration of M (*i.e.*, not based on total fermentor volume). Since it is acceptable to have some error in the flux estimates, the PSSA will be considered valid under the following criteria

$$|x_P(t) - x_C(t)| \leq \tfrac{1}{2}\delta|x_P(t) + x_C(t)| \tag{15}$$

where a value of 0.05 (5% of flux) is considered acceptable for δ. The lower bound on specific fluxes (see Chapter 6) is approximately 1.0 mmole/g DCW/h.

Hoischen and Kramer (1989) have measured the specific intracellular water volume (v_{CELL}) of *C. glutamicum* to be 1 μl/mg DCW, which is approximately 3 to 4 times greater than that given by packed cell density (ρ_{CELL} = 270 mg DCW/ml [Inbar *et al.*, 1985]). Therefore, typical intracellular fluxes ($x_P(t)$ or $x_C(t)$), in intracellular concentration units, are approximately 1000 mM/h (x / v_{CELL}), and are often much greater. Based on the PSSA limit given by Equation (15), the concentration of an intracellular metabolite can change at a rate of approximately 50 mM/h without introducing significant errors in the flux estimates. This rate is extremely large compared to the typical concentration ranges exhibited by intracellular metabolites. For the cell to maintain a stable, yet responsive metabolism, the concentration of an intracellular metabolite in a reaction sequence usually ranges from 20% to 100% of its respective Michaelis constant (K_M) [Atkinson, 1977, pp. 116-118]. Michaelis (or saturation) constants for most reactions in the primary network are typically less than 1 mM and almost never exceed 10 mM [Domach *et al.*, 1984; Jeong *et al.*, 1990]. Even though intracellular metabolite concentrations might change significantly and rapidly to affect the metabolic control directives of the cell, these changes do not result in a significant violation of the PSSA (flux distributions may be radically altered however). This is also supported experimentally.

Measurements of the intracellular concentrations of Pyr, Glc6P, and Cit in *Saccharomyces cerevisiae* [Weibel *et al.*, 1974] during a diauxic growth perturbation exhibit maximum rates of change of only 5 μmole/g DCW/h, which is only 0.5% of typical flux rates. Although variations in intracellular metabolite concentrations, measured at growth rates from 0.02 to 0.22 1/h for *S. cerevisiae* [Franco *et al.*, 1984], change significantly, the variations are easily attained without any violation of the PSSA. Even under extreme metabolic transients [Shanks and Bailey, 1990], the PSSA is still applicable without significant losses in accuracy. Consequently, the metabolic fluxes can be far from steady state but still observable from metabolite balances. The PSSA approximation refers to the concentration of intracellular metabolites, but not the macromolecular composition of the biomass.

Although biomass composition is known to change under different growth conditions [Mandelstam *et al.*, 1982], it is not expected that the biomass yield coefficients, given in Table 4.1, should change to such an extent that they would dramatically alter predicted flux distributions. Furthermore, changes in biomass composition usually occur when growth rate is quite small. Under low to moderate growth rates, however, the affect of biomass synthesis on flux distributions is negligible since Reaction (33:PS1) would be small compared to the glucose uptake rate. Sensitivity of flux estimates to the biomass measurement is further discussed in Section 4.1.8 below.

In general, the PSSA is an extremely accurate representation of the accumulation rate for intracellular metabolites. Even if a violation of the PSSA occurs, it is often observable from redundancy analysis, discussed in Section 4.1.9. A much greater uncertainty exists with the assumptions regarding the existence of certain metabolic pathways. Consequently, inconsistent results or incomplete closure of metabolite balance is more likely due to the inaccurate representation of the cellular metabolism or the accumulation of unidentified extracellular metabolites, than actual violation of the PSSA.

4.1.6.3 Measurements Uncertainty

For batch, fed-batch, or continuous fermentations, extracellular metabolite accumulation rates are calculated from the following expression

$$r_e(t)\,V(t) = \frac{d(C_e(t)\,V(t))}{dt} + F_o(t)\,C_e(t) - F_i(t)\,C_e^f \qquad (4.11)$$

where $F_i(t)$ and $F_o(t)$ are the inlet and outlet feed rates (l/h), C_e^f is the concentration of metabolite e in the feed, and $V(t)$ is the fermentor volume. Independent of the type of process, however, accumulation rates are basically a temporal or spacial function of concentration differences, such as $\mathbf{r}(t) = \mathbf{f}(\Delta\mathbf{C}(t,x,...))$. Consequently, each rate calculation has associated with it a measurement error, which can be quite large since the calculations often involve the subtraction of two large numbers. Therefore, experiments should be design to minimize such errors. Continuous processes, of

course, produce the most accurate rate data; yet, a continuous process may not be the best representation of the process since most industrial fermentations are conducted in a batch or fed-batch mode.

Each accumulation rate, r_j, has an associated uncertainty or standard deviation (σ_j), which is correlated with the measurement error of the metabolite. The actual measurement vector (symbolized as $\bar{\mathbf{r}}(t)$ to denote a measured variable), then, has a covariance matrix $\boldsymbol{\Psi}$ whose diagonal terms are the variance ($E\{r_j r_j\} = \sigma_j^2$) of r_j and off diagonal terms represent the covariance in noise between measured rates ($E\{r_i r_j\}$). Although some covariance is associated with the measurements noise (such as in OUR and CER), it can usually be ignored without serious consequences [Wang and Stephanopoulos, 1983]. Therefore, $\boldsymbol{\Psi}$ will be assumed diagonal unless otherwise noted. Measurement uncertainties and the calculation of σ_j^2 for the lysine fermentation are discussed in Section 5.5.4.

4.1.7 Flux Calculations

Flux distributions are given by the solution ($\mathbf{x}(t)$) of the BRNE (Equation (4.1)). However, as these systems are often overdetermined ($m > n$), a solution does not usually exist for a given measurement vector $\bar{\mathbf{r}}(t)$. A unique estimate of the solution ($\hat{\mathbf{x}}(t)$), that minimizes the sum of the squared residuals, J, given by

$$J = [\boldsymbol{A}\boldsymbol{x}(t) - \bar{\boldsymbol{r}}(t)]^T \boldsymbol{\Psi}^{-1} [\boldsymbol{A}\boldsymbol{x}(t) - \bar{\boldsymbol{r}}(t)] \tag{4.12}$$

is easily obtain, and is the well known weight least-squares solution shown below:

$$\hat{\boldsymbol{x}}(t) = (\boldsymbol{A}^T \boldsymbol{\Psi}^{-1} \boldsymbol{A})^{-1} \boldsymbol{A}^T \boldsymbol{\Psi}^{-1} \bar{\boldsymbol{r}}(t) \tag{4.13}$$

As mentioned above, these systems are small enough (such as BS1 and MS1) that the matrix calculations are easily handled on a personal computer. To minimize possible computational rounding errors, Equation (4.13) should be calculated via a QR or singular value decomposition.

On consideration of the thermodynamics of the biochemistry, one is lead to the expectation that a more realistic solution of the BRNE can be obtained if constraints are imposed on the flux estimates, such that the directionality of irreversible reactions are not violated. This can be accomplished if the minimization of Equation (4.12) is subject to the constraint $\mathbf{C}\mathbf{x}(t) \geq \mathbf{b}$, where $\mathbf{C}$ is a $k \times n$ matrix that specifies those reactions whose flux must equal or exceed $\mathbf{b}$, which is usually taken as the null vector for irreversible reactions. The solution to the quadratic problem, refer to as inequality constrained least-squares, is not amenable by analytical methods and must be solved numerically. The optimal solution (provided $\mathbf{A}$ is nonsingular) is given by

$$\hat{\boldsymbol{x}}(t) = (\boldsymbol{A}^T\boldsymbol{A})^{-1}\boldsymbol{A}^T\bar{\boldsymbol{r}}(t) + (\boldsymbol{A}^T\boldsymbol{A})^{-1}\boldsymbol{C}^T\boldsymbol{z}(t) \tag{4.14}$$

which is obtained by a modified simplex method [Liew, 1976] (although other methods do exist [Boot, 1963b]), where $\mathbf{z}(t)$ is a numerically determined k-dimensional dual vector. (Note, Ψ has been set to the identity matrix in this analysis).

Constraining the reaction fluxes in the manner described above, however, may be an inappropriate method to achieve thermodynamic consistency. If the objective function J exhibited a local as well as a global minimum, then the optimal solution to the constrained problem could lie off the constraint plane ($\mathbf{C}\mathbf{x} = \mathbf{b}$), even if the solution to the unconstrained problem violated the constraints, as illustrated in Figure 4.6 (A). The objective function for the BRNE, however, is quadratic (Equation (4.12)) and only exhibits a single minimum (as $\mathbf{A}^T\mathbf{A}$ is positive definite). Consequently, if the solution to the unconstrained problem (Equation (4.13)) violates any of the constraints ($\mathbf{C}\mathbf{x} \geq \mathbf{b}$), then the solution to the constrained problem (Equation (4.14)) must lie, at least partially, on the constrain plane, as illustrated in Figure 4.6 (B). Fluxes that violate reaction directionality, therefore, will be forced to zero. Although a constrained solution does not violate thermodynamic laws, simply constraining a reaction to zero flux is not necessarily justified. As explained in Section 4.1.5, an irreversible reaction that supports a negative flux is indicative of

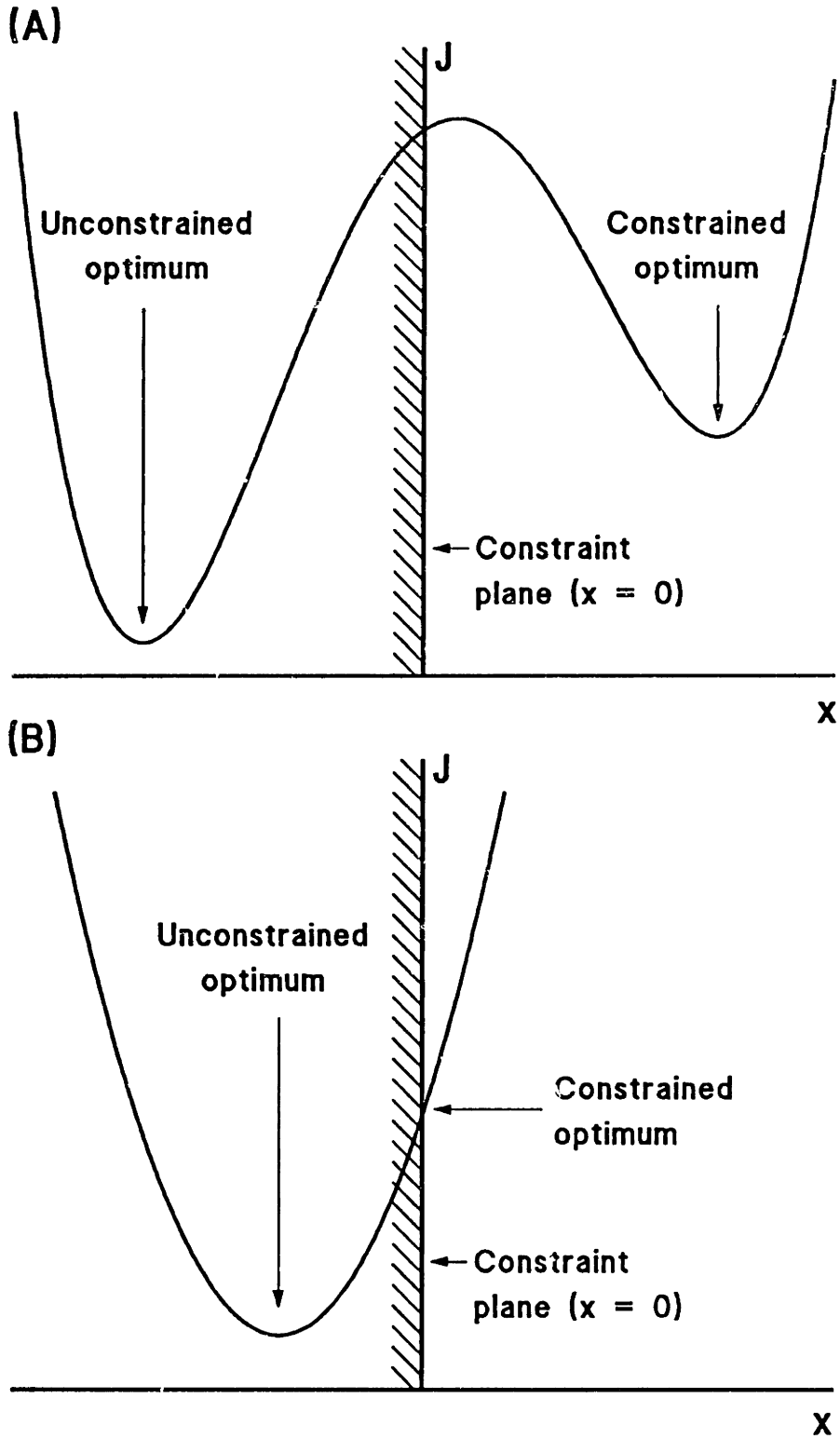

Figure 4.6 Effect of constraints ($x \geq 0$) on different objective functions, *J*. Optimum solution of a quartic objective function (A) does not have to intercept constraint plane if constraints are violated, but optimum solution of a quadratic objective function (B) must intercept constraint plane if constraints are violated.

inappropriate representation of the cellular metabolism, and should be mitigated through refinements of the biochemistry set. Thus, constraints must be used with caution.

Although not investigated in this thesis, flux constraints may be useful in theoretical studies on flux attenuation. For example, if Ψ is constructed to represent the probability that a metabolite may accumulate, then the network response to the attenuation of enzyme activity could be examined, where the constraints could be used to place a maximum on the activity of the attenuated enzyme. The difficulty in this assessment, of course, resides in the proper choice for the elements of Ψ. Unless otherwise noted, flux distributions calculated in all subsequent studies are based on the unconstrained solution to the BRNE given by Equation (4.13).

4.1.8 Sensitivity Analysis

Although it has been demonstrated above that a unique solution to the BRNE exists, provided **A** is nonsingular, it is possible that the solution (Equation (4.13)) may be quite sensitive to slight perturbations in **A** or **r**, given by $\mathbf{A} + \delta\mathbf{A}$ and $\mathbf{r} + \delta\mathbf{r}$, respectively. If the BRNE is ill-conditioned (*i.e.* sensitive to slight perturbations in **A** or **r**) then the biochemistry and metabolite sets must be modified such that the resulting system is well-conditioned. Removal of sensitivity problems are dealt with in the same manner as singularities, discussed previously.

The affect of perturbations in **A** or **r** on the flux distributions are evaluated by solving the following normal equation (where Ψ has been set to **I**) for $\delta\mathbf{x}$:

$$A^T(A + \delta A)(x + \delta x) = A^T(r + \delta r) \tag{4.15}$$

If the perturbation of **A** is small, such that $\|(\mathbf{A}^T\mathbf{A})^{-1}\mathbf{A}^T\delta\mathbf{A}\| < 1$, then it can be shown that [see Noble and Daniel (1977) p. 170, for similar example]

$$\frac{\|\delta x\|}{\|x\|} \leq C(A)M\left[\frac{\|A^T\|\|\delta r\|}{\|A^T r\|} + \frac{\|\delta A\|}{\|A\|}\right] \tag{4.16}$$

where

$$C(A) = \|A\|\|(A^T A)^{-1} A^T\| = \frac{\theta_{MAX}(A)}{\theta_{MIN}(A)} \tag{4.17}$$

$M = [1 - \|(\mathbf{A}^T\mathbf{A})^{-1}\mathbf{A}^T\delta\mathbf{A}\|]^{-1}$, and $\| \|$ is the Euclidian norm. Equation (4.16) clearly illustrates that if the condition number, C(**A**), is large, then slight perturbations in **A** or **r** may lead to large perturbations in the fluxes. In general, the condition number can be regarded as measure of the singularity of **A**, where a large value indicates **A** is close to being singular. For computational reasons, it is better to calculate the condition number from the maximum and minimum singular values of **A** (θ_{MAX} and θ_{MIN}, respectively), as illustrated in Equation (4.17).

The overall condition of the BRNE, therefore, can be assessed by examining the condition number of **A**, which is dictated by the biochemistry and metabolite sets. If the condition number is small (less than ca. 100), then the BRNE is considered well-conditioned; however, if the C(**A**) is large (greater than ca. 1000), then the BRNE is ill-conditioned, and the possibility exists that measurement noise may produce significant alterations in $\mathbf{x}(t)$. It is possible, however, that even if C(**A**) is large, the system may not exhibit sensitivity problems due to the inequality of Equation (4.16). The condition number for the BS1-MS1 system is 59 (θ_{MAX} = 6.9, θ_{MIN} = 0.12); consequently, this representation of the metabolism is well-conditioned. Since **A** from BS1-MS1 is overdetermined by three equations (D(**A**) = 37 × 34), up to three metabolite balances—equations—can be deleted from MS1 without necessarily introducing singularities in **A**. This redundancy is quite useful, as all extracellular metabolites are not always measured or may be difficult to measure. However, deleting balances from the BRNE (as given by Equations (4.2) and (4.3)) often increases C(**A**) of the resulting biochemistry matrix. For example, condition numbers for the BS1-MS1 system with various extracellular metabolites deleted from MS1 are displayed in Table 4.2.

Although the condition of the BRNE is tolerable with three metabolite balances deleted, it is quite obvious that deletion of the O2 and CO2 measurements significantly diminish the accuracy of the flux estimates. Consequently, analysis of

Table 4.2 Condition number (Equation (4.17)) of the BRNE, constructed from BS1 and MS1, with selected extracellular metabolites deleted from MS1.

Metabolites deleted from MS1			C(A)
None			59
BIOMAS (7)			140
CO2 (8)			59
GLC (14)			61
LYSE (20)			60
NH3 (25)			61
O2 (26)			132
GLC	O2		136
NH3	O2		138
BIOMAS	CO2		143
LYSE	O2		144
BIOMAS	GLC		155
BIOMAS	NH3		174
BIOMAS	O2		207
BIOMAS	LYSE		445
CO2	O2		762
BIOMAS	LYSE	NH3	462
BIOMAS	GLC	NH3	519
BIOMAS	GLC	LYSE	726
BIOMAS	CO2	O2	845
CO2	NH3	O2	881

C(**A**) provides a means of identifying those extracellular metabolites that greatly improve the sensitivity of the BRNE, and those measurements that can be deleted with little affect on the flux estimates. This analysis is similar to that discussed by Grosz *et al.* (1984). However, as discussed in the next section, all extracellular metabolites should be measured, if possible, since the redundant measurements are very useful in identifying inconsistencies.

If a sensitivity problem is indicated by the condition number, it is often useful to examine the sensitivity of the BRNE in more detail. Sensitivity of the BRNE to perturbations in **A** is given by the derivative of Equation (4.13) with respect to an element of **A**, given by a_{ij}. If a matrix lemma [Boot, 1963a] is used to express the

derivative of $(\mathbf{A}^T\mathbf{A})^{-1}$ in terms of the derivatives of $\mathbf{A}$ and $\mathbf{A}^T$, then the following equation is produced for the sensitivity of $\mathbf{x}(t)$ with respect to a_{ij} (Ψ has been dropped)

$$\frac{\partial \hat{x}(t)}{\partial a_{ij}} = (A^T A)^{-1}\left[\frac{\partial A^T}{\partial a_{ij}} - \left(\frac{\partial A^T}{\partial a_{ij}}A + A^T\frac{\partial A}{\partial a_{ij}}\right)(A^T A)^{-1}A^T\right]\bar{r}(t) \qquad (4.18)$$

where $\frac{\partial A}{\partial a_{ij}}$ represents an $m \times n$ matrix in which the element a_{ij} of $\mathbf{A}$ is set to 1 and all other elements are set to 0. As can be seen from Equation (4.18), an n-dimensional vector is generated for each element of $\mathbf{A}$ (and an $n \times m$ matrix if $\mathbf{r}$ is left as a variable); consequently, the data produced by this equation cannot be easily scanned at leisure. The analysis is best used to examine the effects of modifying a particular stoichiometric coefficient. For example, one can example the effect of change biomass yields (Table 4.1) or the P/O ratio in oxidative phosphorylation (Reactions (28:BS1) and (29:BS1)).

Sensitivity of the flux vector with respect to perturbations in the measurement vector is given by the following derivative

$$\frac{\partial \hat{x}(t)}{\partial \bar{r}(t)} = (A^T\Psi^{-1}A)^{-1}A^T\Psi^{-1} \qquad (4.19)$$

where the right side of this expression is known as the generalized inverse of $\mathbf{A}$. The analysis of this equation, which generates an $n \times m$ matrix, allows one to examine the effects of individual measurements on the flux distributions. For example, the sensitivity of the flux estimates with respect to biomass accumulation rate, listed in Table 4.3, clearly illustrate that even substantial measurement errors in biomass accumulation rate will not significantly alter flux estimates, except for fluxes x_{33} and x_{34}. These low sensitivities also indicate that alterations in biomass composition should not significantly affect flux estimates, unless the biomass synthesis rate is extremely high relative to glucose consumption. Evaluation of Equation (4.19) can

also be used to establish the reliability of flux distribution estimates in ill-conditions metabolic networks. If the sensitive variables in these networks, indicated by Equation (4.19), are stable, then fluxes can be estimated with greater confidence than dictated by C(**A**). For instance, evaluation of Equation (4.19) may indicate that flux estimates are only sensitive to Glc6P accumulation rate; however, since r_{Glc6P} is approximately 0 under the PSSA, the sensitivity problem is significantly diminished.

Table 4.3 Sensitivity of the flux estimates to perturbations in biomass accumulation rate for the BS1-MS1 defined BRNE.

	x_i) $\partial x_i / \partial r_{BIOMAS\,(7)}$						
1)	0.02	10)	0.13	19)	-0.05	27)	0.05
2)	-0.07	11)	-0.18	20)	0.01	28)	0.07
3)	-0.11	12)	-0.19	21)	-0.02	29)	-0.08
4)	0.02	13)	-0.18	22)	0.19	30)	-0.11
5)	0.05	14)	-0.02	23)	0.12	31)	-0.16
6)	-0.09	15)	-0.17	24)	0.08	32)	-0.09
7)	-0.06	16)	-0.18	25)	0.05	33)	0.96
8)	-0.01	17)	-0.01	26)	0.07	34)	-3.38
9)	-0.10	18)	0.08				

With respect to the bioreaction network of *C. glutamicum*, given by BS1 and MS1, the generalized inverse of **A** does not exhibit any large elements; hence, the flux estimates appear not to be sensitive to measurement errors, which is consistent with the condition number of **A**, as listed in Table 4.2. It should be noted that the sensitivity analysis of the BRNE (Equations (4.17)-(4.19)) can be preformed without the measurement vector. Therefore, metabolic networks can be evaluated before experimental work, and experimental design can be based on the results of the analysis.

4.1.9 Consistency Analysis

Since each reaction in a metabolic network must involve two or more metabolites, the biochemistry matrix **A** of the BRNE is often overdetermined (*i.e.*, more equations than unknowns, $m > n$). We have demonstrated in Section 4.1.8 that

these extra balances—or redundant equations—often improve the condition number of **A** and reduce sensitivity problems associated with flux estimation. However, the redundant equations can also be used to identify inconsistencies in the measurement vector ($\mathbf{r}(t)$) and, under proper conditions, incorrect metabolic stoichiometry (**A**). This analysis follows the original work of Romagnoli and Stephanopoulos (1981) and its application to fermentation data discussed by Wang and Stephanopoulos (1983). Consequently, this section will only discuss the general concepts of consistency analysis and its application to flux estimation in metabolic networks.

4.1.9.1 Redundant Equations

We will assume throughout this section that the biochemistry matrix, **A**, is of full column rank (nonsingular, $R(\mathbf{A}) = n$), or has been rendered so, and that $m > n$. The redundant equations expressed as functions of $\mathbf{r}(t)$ result from the linear dependent equations of **A**, of which there are $m - n$ (or ℓ) since **A** is of full rank. However, the redundant equations are implicitly expressed and must be extracted from **A** as follows. Through Gaussian elimination, the **A** matrix can be partitioned into an upper $n \times n$ triangular matrix, **U**, and an lower $\ell \times n$ null matrix. This manipulation can be expressed by the multiplication of the BRNE by an $m \times m$ permutation matrix **P**, as shown here

$$\boldsymbol{PAx}(t) = \begin{bmatrix} \boldsymbol{U} \\ \mathbf{0} \end{bmatrix} \boldsymbol{x}(t) = \boldsymbol{Pr}(t) \tag{4.20}$$

The permutation matrix is then partitioned into an upper $n \times m$ matrix **S** and a lower $\ell \times m$ matrix **Z**, as given by $\mathbf{P} = [\mathbf{S}\ \mathbf{Z}]^T$. Therefore, Equation (4.20) can be expressed as

$$\mathbf{Ux}(t) = \mathbf{Sr}(t) \tag{4.21}$$

$$\mathbf{Zr}(t) = \mathbf{0} \tag{4.22}$$

where we will refer to **Z** as the redundancy matrix. Equation (4.22) represents mass balance constraints on the measurements, $\mathbf{r}(t)$, as dictated by the assumed

biochemistry, and is in the proper form required for the consistency analysis as described by Wang and Stephanopoulos (1983). Equation (4.21) is only included for completeness, and should not be used to calculate the fluxes from raw data (unless Equation (4.22) is exactly satisfied) since it does not represent the least-squares solution (**S** is not unique and depends on the pivots chosen in the Gaussian elimination). It should be noted that some columns of **Z** may contain only zeros, which means that the metabolites that correspond to these columns are not constrained or involved in the consistency analysis. Null columns of **Z** are superfluous and should be removed, along with the corresponding elements of $\mathbf{r}(t)$. For the discussions to follow, we will assume, without loss of generality, that **Z** does not contain any null columns. Finally, since **P** is the product of a series of elementary matrices, it is nonsingular; therefore, **Z** will always have full rank ℓ.

From the above discussion, it would appear that one would want to include balance equations for all intracellular metabolites since this would increase the number of redundant equations (*i.e.*, ℓ). While this is the case, the addition of some metabolite balances produce redundant equations that are fairly useless. For example, if both NAD and NADH are included in MS1, then one of redundant equations can be expressed as $r_{NAD} + r_{NADH} = 0$. Since a PSSA is used for both metabolites, this redundant equation is never violated. Therefore, it is not necessary to include both NAD and NADH in MS1; one is sufficient. The existence of superfluous metabolite balances can be checked as follows. All columns of **Z** which correspond to unmeasured metabolites (*i.e.*, those in which a PSSA replaces actual measurement) are deleted. If $R(\mathbf{Z}^*)$ denotes the rank of the resulting matrix, then the number of superfluous balances are given by $\ell - R(\mathbf{Z}^*)$. For MS1, the following complementary cofactors were dropped: ADP, CoA, FAD, NAD, NADP

4.1.9.2 Framework

Due to the presence of measurement noise, Equation (4.22) will seldom be satisfied by the actual measurements, $\bar{\mathbf{r}}(t)$, that is

$$\mathbf{Z}\bar{\mathbf{r}}(t) = \epsilon \tag{4.23}$$

Since Equation (4.22) represents mass balance constraints, it is desirable to find an estimate of $\mathbf{r}(t)$, denoted $\hat{\mathbf{r}}(t)$, that satisfies

$$\begin{aligned} &\text{Minimize } J = (r(t) - \bar{r}(t))^T \Psi^{-1} (r(t) - \bar{r}(t)) \\ &\text{subject to } Zr(t) = 0 \end{aligned} \tag{4.24}$$

The estimated measurement vector $\hat{\mathbf{r}}(t)$, given by

$$\hat{r}(t) = (I - \Psi Z^T (Z \Psi Z^T)^{-1} Z) \bar{r}(t) \tag{4.25}$$

is the vector that exactly satisfies the mass balance constraints (Equation (4.22)) with the smallest deviation from the original measurements, $\bar{\mathbf{r}}(t)$. With Equation (4.22) satisfied, Equation (4.25) coupled with Equation (4.21) could be used to estimate the flux vector, although this is not done in practice, as numerical sensitivity of the solution has not been investigated. It should be noted that $\hat{\mathbf{r}}(t)$ given by Equation (4.25) is identical to $\hat{\mathbf{r}}(t)$ calculated from Equations (4.13) and (4.1). However, since $\mathbf{ZZ}^T$ is an $\ell \times \ell$ matrix while $\mathbf{A}^T\mathbf{A}$ is an $n \times n$ matrix and $\ell < n$, $\hat{\mathbf{r}}(t)$ can be calculated and manipulated with far fewer operations if Equation (4.25) is used.

The consistency of the original measurements can now be determined if we examine the magnitude by which the original measurements were displaced (the residuals) in order to meet the constraints of Equation (4.22). Since the measurement covariance matrix, Ψ, is assumed diagonal, the magnitude of the

displacement is given by

$$h = \sum_{i=1}^{m} \frac{(\hat{r}_i(t) - \bar{r}_i(t))^2}{\sigma_i^2} \tag{4.26}$$

where h is referred to as the consistency index and σ_i^2 are the diagonal terms of Ψ. It follows from Equation (4.26) that the greater the discrepancy between the actual measurements ($\overline{\mathbf{r}}$) and the constrained estimates ($\hat{\mathbf{r}}$), the larger the consistency index. We must determined, however, the point at which the consistency index is considered larger than is warranted by the known uncertainty in the measurements. Since each term in the summation of Equation (4.26) is a standardized normal variate, the consistency index can be characterized by a Chi-square variate with ℓ degrees of freedom†, denoted $\chi^2(\ell)$. The area under the probability density function of a $\chi^2(\ell)$ distribution, integrated from zero to $\chi_p^2(\ell)$, equals the probability, p, that a randomly sampled Chi-square variate will be less than $\chi_p^2(\ell)$; that is, $P\{\chi^2(\ell) < \chi_p^2(\ell)\} = p$. Therefore, if $h \geq \chi_p^2(\ell)$, then there is a p probability (or level of confidence) that the variance in the measurement set ($\overline{\mathbf{r}}$) is larger than that given by Ψ (p is usually taken to be 0.9 to 0.95; we will use the value of 0.9). Such a measurement set is said to be inconsistent, or harbor gross measurement errors. Although often exercised in practice, the contrary statement is not true: if $h < \chi_p^2(\ell)$, then $\overline{\mathbf{r}}(t)$ is consistent. If inconsistencies in the measurement set are not found, then the analysis is ended and $\hat{\mathbf{r}}(t)$ is used to calculate the fluxes from Equation (4.13), although Ψ can be dropped from this equation since $\mathbf{Z}\hat{\mathbf{r}}(t) = 0$ is exactly satisfied. On the other hand, if the measurement set is inconsistent, the flux estimates must be viewed with skepticism since it is not known how the error will be propagated. Fortunately, it is often possible to identify and remove the inconsistent measurements, so that fluxes can be reliable estimated, even if some measurements harbor gross errors in the original set.

---

† See Wang and Stephanopoulos (1983) for discussion on degrees freedom.

To systematically isolate an inconsistency, one measurement at a time is deleted from $\mathbf{r}(t)$, and the consistency index of the reduced system is reevaluated as given by Equations (4.25) and (4.26). If the resulting measurement set passes the consistency test (*i.e.*, $h < \chi^2_p(\ell-1)$), then there is a high probability that the deleted measurement is corrupted. Since a redundant equation is required to calculate the value of the deleted measurement, the row dimension of $\mathbf{Z}$ and the number of degrees of freedom are reduced by one for each measurement deleted in any given iteration. Consequently, if the measurement set remains inconsistent after the systematic deletion of each measurement, the procedure can be repeated with the deletion of two or more measurements at a time. The maximum number of measurements that can be deleted in any one pass is give by $\ell - 1$. Conceptually, the deletion of a measurement is equivalent to setting its variance to ∞, so the degree by which the measurement can be altered to meet the constraints of Equation (4.22) is unbounded. As a result, the deleted measurement has a tendency to act as a sink for all measurement errors. The deletion of a measurement is rather drastic, and should be avoid if possible, as described in the next section.

If an inconsistency repeatedly arises in different measurement sets, then the possibility exists that the inconsistency is due to an error in the representation of the biochemistry (*i.e.*, in **A**). A biochemistry error can be observed (*i.e.*, produce inconsistencies) if the number of reactions in the BS is less than the maximum number in independent reactions possible, as given by Gibbs' law of stoichiometry [Tsai and Lee (in preparation)]. Such an inconsistency must be rectified by modifying the BS. (For a thorough discussion and implementation of consistency analysis, the interested reader is referred to the above cited references.)

4.1.9.3 Applications

The above analysis was originally developed to detect and isolate gross measurement errors that occur in the monitoring of large scale processes, where the errors are mostly attributed to equipment malfunctions which can go unnoticed due to the large dimensionality of the process involved. However, we are primarily interested in analytical scale experiments to elucidate flux distributions, so the likelihood of gross measurement errors occurring due to equipment malfunction is

fairly low. Yet, due to the nature of the measurement vector, we have found some extensions of the consistency analysis that are quite useful for improving flux estimation. A typical measurement vector associated with the BRNE not only contains the measurements of the extracellular metabolites, but also contains the "measurements" of many intracellular metabolites. For instance, only 12 of the 37 metabolites listed in MS1 are ever observed extracellularly. The intracellular metabolites are, of course, not actually measured, but the PSSA can certainly be regarded as such. If an intracellular metabolite begins to accumulate (violating the PSSA), the consistency analysis can often detect the accumulation, and, to a limited extent, identify the accumulating metabolite. The offending metabolite cannot always be exactly identified since typical networks consist of a large number of metabolites but only a few redundant equations (for instance, $m = 37$ and $\ell = 3$ for the BS1-MS1 system). Consequently, the analysis may identify a few closely related metabolites whose deletion would alleviate the inconsistency.

Another slight extension of the consistency analysis can be used to monitor by-production accumulation. In most fermentations there are usually only a handful of extracellular metabolites that are considered the primary products or substrates, such as glucose, ammonium, biomass, oxygen, etc. These primary metabolites are often the only metabolites that are actually measured or monitored. However, under certain conditions, the culture may excrete various by-products that are not specifically monitored. For example, if the culture experiences a slightly anaerobic environment, lactate may be excreted. If the primary metabolites are the only measurements included in the consistency analysis, then by-product accumulation may cause an inconsistency, but it will not be locatable. This problem can be alleviated by including the typically observed by-product metabolites in the measurement vector (with modifications to BS, of course) and setting their accumulation rate to zero (that is, if they are not actually measured). Thus, if an unmonitored by-product begins to accumulate, it will be detected and identified by the consistency analysis. For the lysine fermentation, the metabolites Ac, Ala, Lac, Pyr, Trehal, and Val have been included in MS1 since these metabolites have been observed to accumulate late in the fermentation.

There is a potential problem, however, in detecting inconsistencies in measurement vectors with artificially high dimensions. If the assigned standard deviations for metabolites under the PSSA are too large, it is possible that a significant error in the accumulation rate of one metabolite may go undetected. Since there are many metabolites under the PSSA, a large error in one measurement can sometimes be distributed as a slight error in several metabolites, which can lower the consistency index to a passing level. To avoid this problem, most of the metabolites that have a zero accumulation rate are removed from the consistency routine for the first pass. This can easily be accomplished by deleting the columns of $\mathbf{Z}$ and the elements of $\mathbf{r}(t)$ that correspond to metabolites of precisely zero accumulation rate. These deletions are permissible since the columns of $\mathbf{Z}$ are multiplied by the zero elements of $\mathbf{r}(t)$. The same effect could be attained by setting the standard deviations of the PSS measurements to zero, although this would introduce singularities in Ψ. The reduced measurement set is then checked for consistency, as described above. If an inconsistency arises that cannot be identified in the reduced measurement set, then the complete measurement vector is restored and searched for the inconsistent measurement or PSSA.

There is an additional reason for using a partial measurement set in the consistency routine. It is presumed that intracellular metabolites that are occasionally excreted as by-products (such as pyruvate) are more likely to accumulate intracellularly or go undetected than those metabolites that are never observed to be excreted. Consequently, if a slight inconsistency arises in a measurement set, it is often preferable to alleviate the inconsistency by slightly increasing the uncertainty (*i.e.*, standard deviation) in those intracellular metabolites that are routinely excreted, rather than to delete a measurement altogether (unless deletion is warranted). Therefore, those metabolites that are considered by-products should also be included in the reduced measurement set and assigned a standard deviation that will allow for acceptable accumulation. This cannot be applied to every metabolite in the measurement set due to the distribution of error problem discussed above. For the lysine fermentation, the metabolites of MS1 that usually comprise the reduced

measurement set, denoted $\mathbf{r}_E(t)$, are: Ac (1), Ala (4), Biomas (7), CO2 (8), Glc (14), Lac (19), LysE (20), NH3 (25), O2 (26), Pyr (29), Trehal (35), and Val (36).

4.1.10 Implementation and Summary

This section has described the methodology by which the flux distributions through the primary metabolic pathways of an organism can be estimated solely from the measurements of extracellular metabolites. The overall procedure, referred to as the bioreaction network algorithm (BRNA), is implemented in two main loops.

The first iteration involves the mathematical representation of the cellular metabolism. The basic biochemical reactions chosen to represent the metabolism of the organism depends on the desired objectives; however, once the biochemistry set is defined (from the literature and *in vitro* assays) it is checked for closure, and condensed to produce the metabolite set, as described in Section 4.1.1. A metabolite balance is then employed to generate the Bioreaction Network Equation (4.1). The resulting biochemistry matrix **A** is checked for singularity and sensitivity problems, both of which must be removed through modifications of the biochemistry set or by the addition of supplementary information. Once the BRNE is rendered well-conditioned, the second loop of the iteration is entered. It should be noted that this loop is seldom reentered for a given system, provided realizable flux distributions are obtained in the second loop.

The second loop constitutes the main iteration sequence of the BRNA. At a given time t during the course of a fermentation the metabolite accumulation rate vector $\overline{\mathbf{r}}(t)$ is constructed based on extracellular measurements and the PSSA. Equations (4.25) and (4.26) are then used to check the consistency of the measurement vector before flux estimates are generated. If the measurements pass the consistency test, then Equation (4.13) (without Ψ) is used to estimate the fluxes from $\hat{\mathbf{r}}(t)$. If the measurements fail the consistency test, then an attempt is made to isolate the inconsistent measurement in the reduced measurement set. If the inconsistency is not located, then the entire measurement set is restored, and the search is continued. The inconsistent measurement is either deleted or its variance increased, and the fluxes are estimated from the updated measurement vector, $\hat{\mathbf{r}}(t)$.

If the inconsistency cannot be located, then the resulting flux distributions must be treated with caution. After the flux estimates are obtained, they are checked for proper directionality. If negative fluxes are observed in irreversible reactions, then the biochemistry set must be reevaluated via the first iteration loop. Although constraints (Equation (4.14)) can be used to mitigate the problem, they are not recommended. This loop is then repeated for each measurement vector constructed. A menu driven PC based computer program (BIONET) has been written to facilitate implementation of all the procedures discussed in this section. A manual of this program is provided in Appendix C.

The BRNA has been applied to the metabolic network of *C. glutamicum* to examine the effects of lysine overproduction on the primary metabolism. The biochemistry reviewed in Chapter 3 has been condensed to form BS1 and MS1 listed in Appendix B. The resulting biochemistry matrix is well-conditioned and the estimated flux distributions do not violate thermodynamic constraints (see Chapter 6).

4.2 Theoretical Flux Distributions and Maximum Yields

As discussed in Sections 4.1.4, 4.1.8, and 4.1.9, when **A** is overdetermined, which often occurs, metabolite balances can be deleted from the BRNE and flux distributions can be estimated from incomplete measurement sets. Therefore, theoretical flux distributions can be generated if all redundant metabolite balances are removed from MS (so that **A** is square, but nonsingular) and the accumulation rates of the remaining metabolites are specified. Furthermore, maximum theoretical yields can be determined by finding the theoretical flux distribution that produces the highest yield within thermodynamic constraints. Such flux distributions are easily found, as described below for the metabolic network of *C. glutamicum* given by BS1 and MS1.

4.2.1 Lysine Yield

As a first estimate, the maximum theoretical yield for a product is typically determined from an overall stoichiometric equation that relates the substrates to the

desired product, where the maximum yield can be calculated from elemental balance constraints. The conversion of glucose to lysine, for example, can be expressed as:

$$C_6H_{12}O_6 + aNH_3 + bO_2 \rightarrow cC_6H_{14}O_2N_2 + dCO_2 + eH_2O \qquad (16)$$

Since there are five unknown stoichiometric coefficients (a-e) and only four elemental balance equations (on C, H, O, and N), one more equation must be specified in order to determine the lysine yield, given by the coefficient c. In this case it is easy to show that if b is set to zero, the maximum lysine yield of 85.7% (mole lysine/mole glucose) is obtained (for $b \geq 0$). This yield will be refer to as the elemental maximum. However, with a metabolic intensive product such as lysine, the maximum yield calculated in this manner may not be realizable under the constraints of the biochemistry, even if Equation (16) is thermodynamically favorable. Consequently, one often resorts to calculating theoretical yields based on the cofactor requirements of the product, and the cofactor generating potential of the substrate as govern by the biochemistry. Such an analysis has been conducted by Shvinka *et al.* (1980) for lysine production by *Brevibacterium flavum*. The main problem associated with calculating yields in this manner is the high probability of constructing an infeasible metabolic flux distribution or violating reaction directionality constraints (or just making computational errors). For example, Shvinka *et al.* assume that lysine biosynthesis from glucose or acetate can occur through the operation of the TCA cycle only (variants A and C); however, it is impossible to sustain operation of the TCA cycle if metabolites (such as oxaloacetate) are drained off the TCA cycle without replenishment from an anabolic reaction, such as PEP carboxylase or the glyoxylate shunt. Consequently, the results they obtain for variants A and C are meaningless. To avoid such problems, we have found that biochemically constrained maximum theoretical yields can easily be obtained from the BRNE, as discussed below for lysine synthesis based on BS1 and MS1.

To calculate a theoretical flux distribution for a given lysine yield, the metabolite balances for CO2, NH3, and O2 are deleted from MS1, and the accumulation rates for BIOMAS, GLC, and LYSE are set to 0, -100, and Y_{LYS},

respectively, where Y_{LYS} is the percent molar lysine yield. The accumulation rates of the remaining metabolites in MS1 are set to zero. Although the deletion of CO2, NH3, and O2 from MS1 dramatically increases the condition number (Table 4.2), it is not critical since the value is still acceptable with respect to numerical computation, and there is no uncertainty in **r**. The resulting flux distribution is checked for feasibility by examining the directionality of the fluxes. If all fluxes meet thermodynamic constraints (*i.e.*, acceptable flows in irreversible reactions) then Y_{LYS} is considered a feasible yield.

Figure 4.4 illustrates a theoretical flux distribution for a 35% lysine yield. The procedure may be repeated with increasing values of Y_{LYS} until an infeasible flux distribution occurs, at which point Y_{LYS} represents the maximum theoretical yield (Y_{LYS}^{MAX}) under the constraints of the biochemistry. Under the constraints of the BS1-MS1 system, the first infeasible flux distribution occurs when the flux supported by pyruvate kinase (PK; Reaction 7:BS1)) reaches zero, which corresponds to a Y_{LYS} of 64% (as illustrated in Figure 4.7). The zero PK flux is attributed to the presence of the glucose:PEP phosphotransferase system (Reaction (1:BS1)) which converts PEP to Pyr in the phosphorylation of glucose. If PEP synthetase (EC 2.7.9.2) or pyruvate dikinase (EC 2.7.9.1) are not expressed in *C. glutamicum* when it is cultured on glucose, then the 64% yield represents the maximum. However, we have detected slight *in vitro* activity of PEP synthetase in *C. glutamicum* when it is cultured on glucose (see Section 5.3.2). Consequently, we will assume that 64% yield does not correspond to a true infeasible flux distribution. If the irreversibility constraint on PK is relaxed, the next infeasible flux distribution occurs when Y_{LYS} equals 75%. As illustrated in Figure 4.8, to achieve a 75% lysine yield the flux supported by the TCA cycle drops to zero, and any further increase in Y_{LYS} results in a negative TCA cycle flux. Consequently, the 75% yield will be considered the theoretical maximum (Y_{LYS}^{MAX}) under the constrains of BS1. Examination of Figure 4.8† reveals that Y_{LYS}^{MAX} is not constrained by ATP or NADH availability since the ATP dissipation reaction (Reaction (34:BS1)) and respiration (Reactions (28BS1)) are nonzero. Rather, Y_{LYS}^{MAX}

† See Appendix B and Section 6.1.3.2 for the details in reading these flux distribution maps.

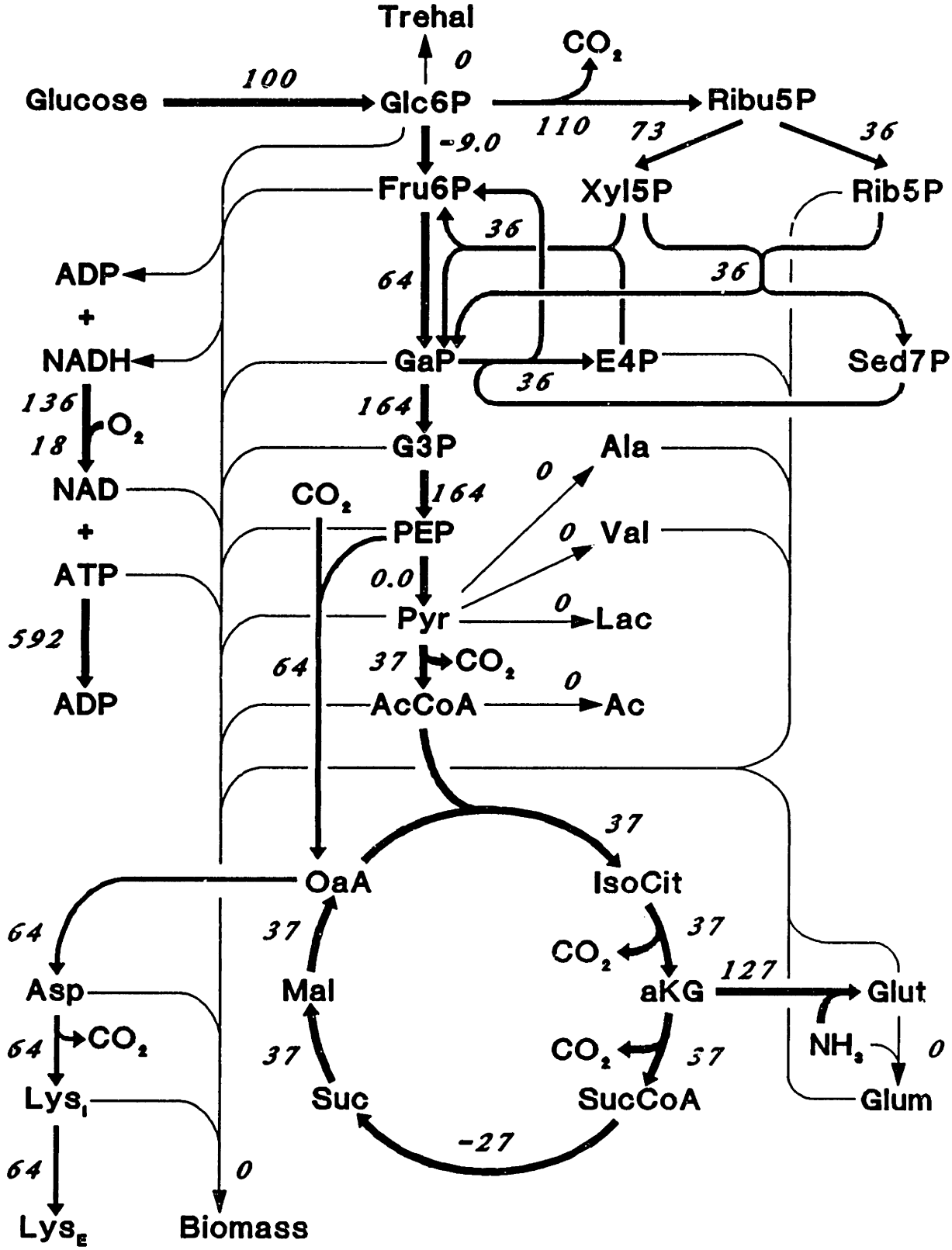

Figure 4.7 Theoretical flux distribution for a 64% molar lysine yield, based on constraints dictated by BS1. Limitation is due to irreversibility of pyruvate kinase (Reaction (7:BS1)). See Appendix B and Section 6.1.3.2 for a complete description of flux maps.

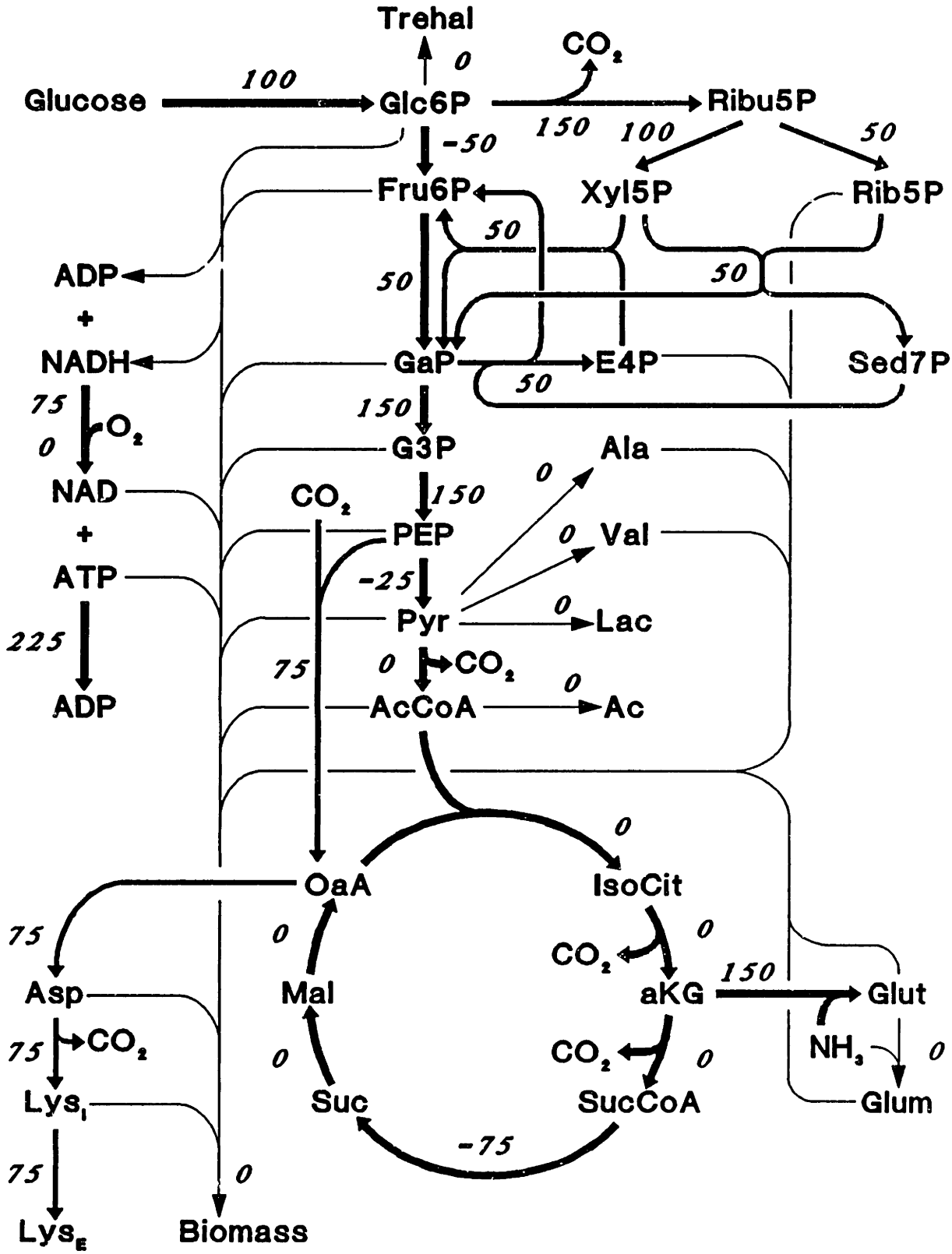

Figure 4.8 Theoretical flux distribution at 75% lysine yield. Limitation is due to constraints of TCA cycle flux (PK irreversibility constraint relaxed). See caption of Figure 4.7 for details.

ultimately results from the constraint that NADH and NADPH are not interconvertible. As a result, the excess NADH produced in glycolysis cannot be used to drive the NADPH requiring biosynthetic reactions associated with lysine synthesis. The required NADPH must be synthesized from the oxidative branch of the PPP (Reaction (22:BS1)), which leads to some carbon loss, due to CO_2 production, and a Y_{LYS}^{MAX} that is lower than the elemental maximum. If a transhydrogenase is added (such as Reaction (43:PBS)) and PDC (Reaction (10:BS1)) is deleted from BS1 (to removed singularity problems), the lysine yield can be increased to 82% before an ATP limit occurs (not shown). However, as discussed in Chapter 3, a transhydrogenase has not been observed in *C. glutamicum* or related species, so the Y_{LYS}^{MAX} of 75% will be considered the theoretical maximum.

It becomes clear from the above discussion that the concept of "theoretical maximum yield", so widely used, is not as concrete as one is lead to believe. To be precise, the reported theoretical maximum yield should always be accompanied by the biochemistry set used to ascertain the yield and the limitation incurred. A summary of the encountered theoretical lysine yields is listed in Table 4.4.

Table 4.4 Theoretical lysine yields under different constraints of biochemistry set 1.

Constraint (reaction #)	Yield %
Pyruvate kinase (7)	64
TCA cycle† (10-16)	75
ATP production‡ (34)	82
Elemental maximum§	85.7

† Considered true maximum.
‡ With dinucleotide transhydrogenase.
§ From Equation (16)

It should be realized that true iteration is not required to determined theoretical yields since the BRNE is linear. If it is known, by observation, that a particular reaction will limit the theoretical yield, such as PK, then the exact flux distribution can be determined from interpolation or extrapolation between two flux distributions. Other useful information can be extracted from theoretical flux

distribution as follows. Since production rates for the deleted metabolites can be calculated from Equation (4.3) after a theoretical flux distribution is constructed, the respiratory quotient (RQ) that accompanies a particular yield can also be determined. For example, at the Y_{LYS}^{MAX} of 75%, the RQ equals 2.0. Knowledge of RQ values can be quite useful for fermentation control, as discussed by Kiss.

It is important to realize that theoretical flux distributions are easily determined by swapping or removing reactions and metabolites from BS1 and MS1. These techniques are extremely useful in determining theoretical yields for different substrates or for different products, provided the biochemistry is properly modified. Alternate biochemical pathways can also be easily investigated. Examples of lysine yield on acetate and biomass yield are described below.

4.2.2 Lysine Yield on Acetate

As discussed in Chapter 3 and Section 5.3.2, cultivation of *C. glutamicum* on a minimal acetate medium induces the glyoxylate shunt (Reactions (21 & 22:PBS)), which introduces a singularity in **A**. This singularity can be removed, however, if α-ketoglutarate dehydrogenase (αKGDH) is deleted (Reaction (13:BS1)) and replaced by oxaloacetate decarboxylase (Reaction (11:PBS)). The resulting network is referred to the DCA cycle model. The calculation of theoretical lysine yields on acetate follows that described above for glucose except, that the rate of accumulation of AC is set to -100 and that for glucose is set to zero. Also, ATP consumption in Reaction (4:BS1) is removed and an additional mole of ATP is added to Reaction (7:BS1) to account for the gluconeogenesis pathway for acetate metabolism. The maximum lysine yield on acetate is found to 19% (mole/mole), where the limiting reaction becomes PDC (Reaction (10:BS1)), as illustrated in Figure 4.9. Even if the malic enzyme (Reaction (12:PBS)) or αKGDH are added (with the PDC deleted), the yield does not significantly improve (the yield increases to 21% and is ATP limited, not shown). As before, these flux distributions are easily calculated and manipulated with the BRNE.

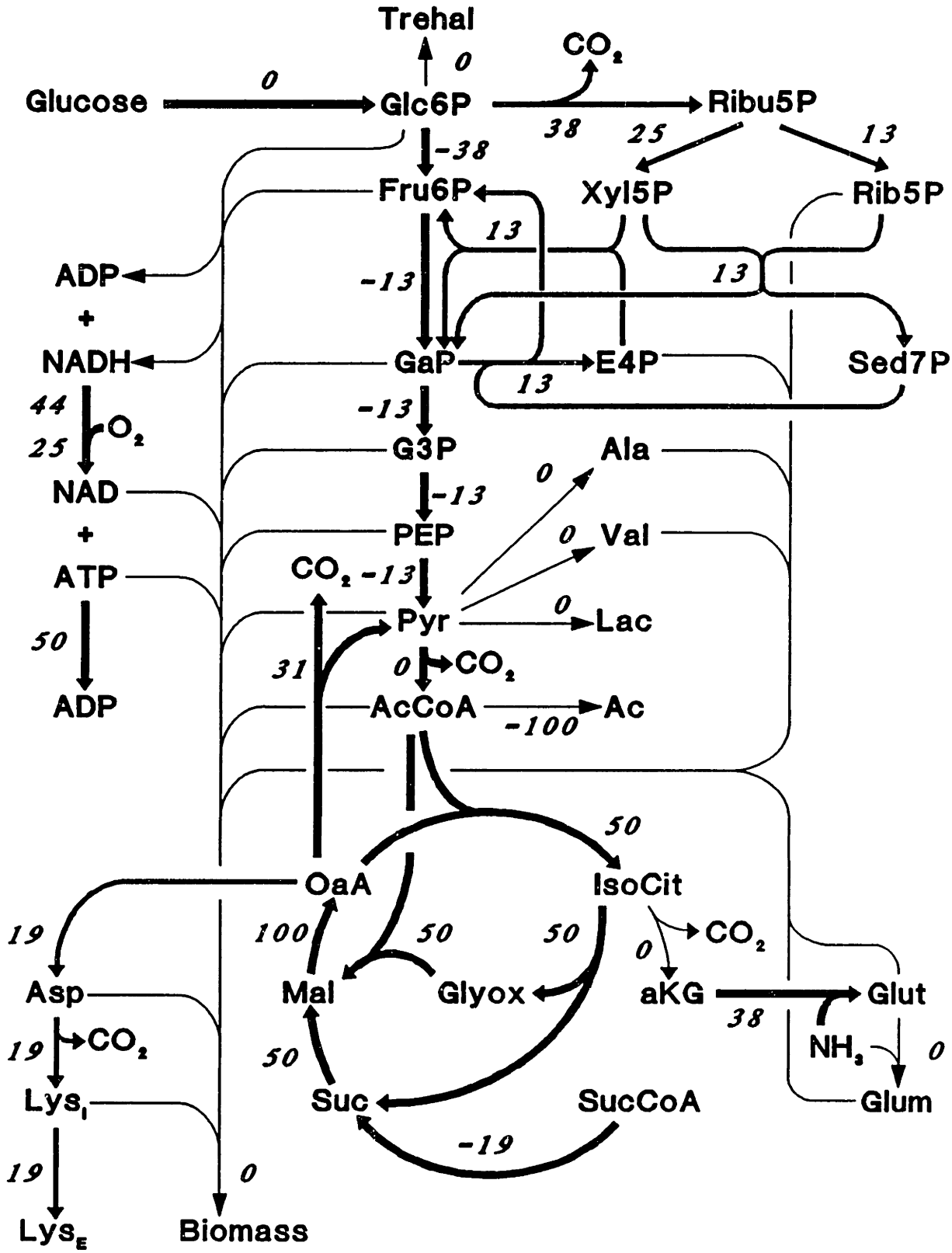

Figure 4.9 Theoretical flux distribution for 19% lysine yield on acetate. Network is based on DCA cycle model (glyoxylate shunt and OAADC replace PPC and αKGDH in BS1). Constraint is imposed by irreversibility of PDC flux (Reaction (10:BS1)).

4.2.3 Biomass yield

Examination of theoretical flux distributions at increasing biomass yields clearly illustrates the effects of biomass burden on the primary metabolism. Theoretical flux distributions are calculated as above, except r_{GLC} and r_{LYSE} are set to -100 and 0, respectively, and $r_{BIOMASS}$ becomes the manipulated variable. If we relax the directionality constraints on PK again, the maximum biomass yield (in g biomass/g glucose) is 73%, as illustrated in Figure 4.10. It is interesting to note that the limitation occurs due to the TCA cycle flux and not ATP availability. This biomass yield in not realistic since maintenance has not been accounted for (as discussed in Section 4.1.3); real biomass yields on glucose are typically 50% (g/g) (see Chapter 6, Figure 6.6). Nevertheless, the hypothetical biomass flux distribution illustrates how metabolites are drained off the primary metabolism to the extent that very little carbon actually reaches the TCA cycle.

4.2.4 Summary

It has been demonstrated that maximum theoretical yields can be easily and unambiguously predicted from theoretical flux distributions generated from the BRNE. For the metabolism dictated by BS1, we have established that the realizable maximum theoretical lysine yield from glucose is 75% (provided PK irreversibility constraint is relaxed). Furthermore, the technique is easily extended to other products or substrates, and is a useful tool for examining the effects of biochemical modifications. As we will see in the next section, theoretical flux distributions can also be used to identify the key metabolic branch-points of product synthesis.

4.3 Nodal Analysis

In this section we discuss how the flux mapping techniques developed in Sections 4.1 and 4.2 can be used to identify areas in the primary metabolism that can potentially limit product yield, and how these potential limitations can be experimentally assessed. Although lysine overproduction by *C. glutamicum* is used to illustrate the ideas, the concepts are general enough to be applicable to most

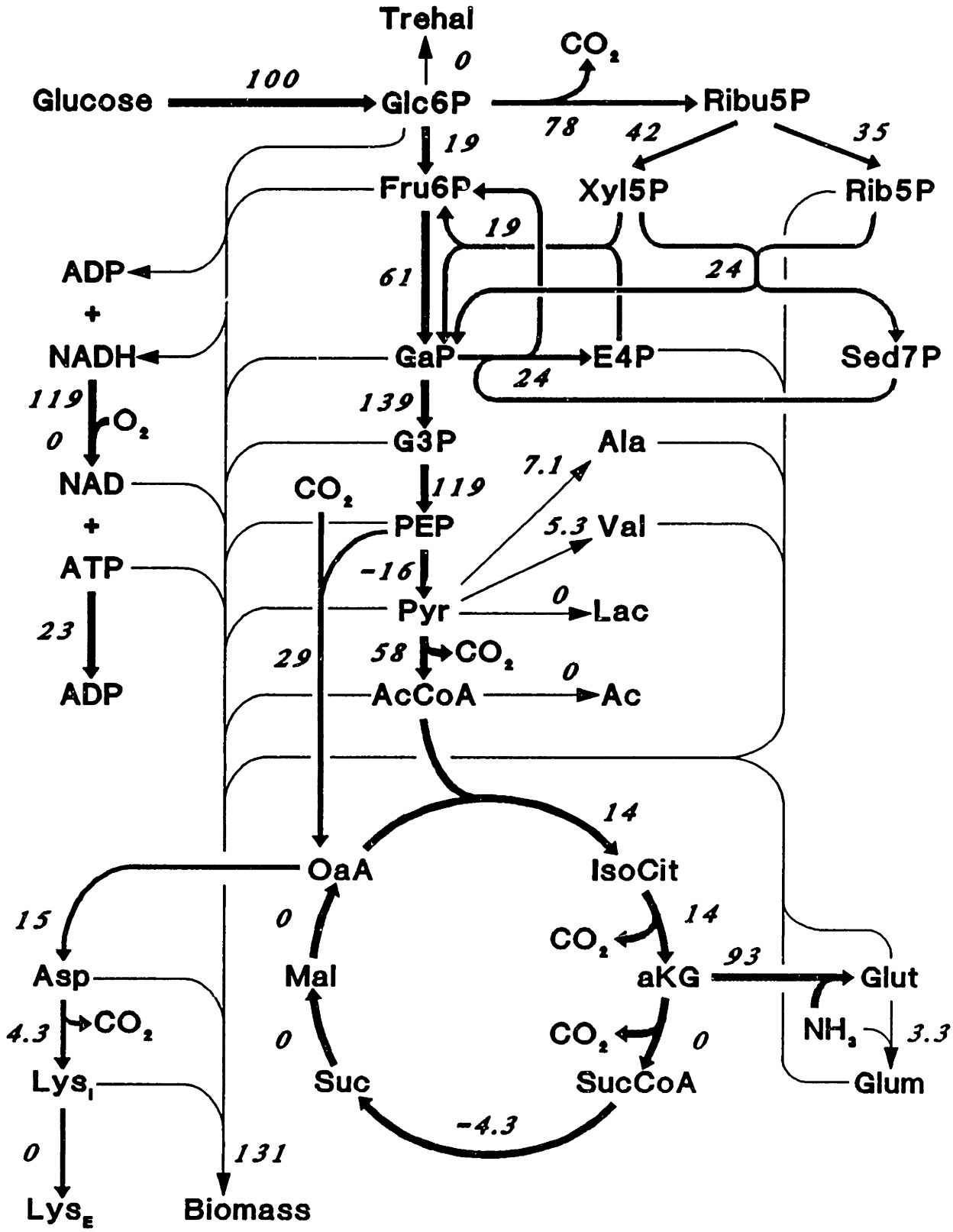

Figure 4.10 Theoretical flux distribution that corresponds to a biomass yield of 73% (g/g) as constrained by BS1. Maximum yield dictated by constraints on TCA cycle flux. It should be noted that ATP requirements for maintenance are not accounted for.

products of the primary metabolism. To facilitate subsequent discussion, it is useful to define the following terms:

(i) A *trunk* will refer to a sequence of reactions that produce a particular metabolite, and a *branch* will refer to a sequence of reactions that consume a particular metabolite. Trunks and branches are only defined with respect to a particular metabolite and each may be composed of several enzymatic reactions.

(ii) A *node*† is defined by a metabolite with two or more branches, while a *condensation-point* is defined by a metabolite with more than one trunk but at most one branch.

(iii) A *network* is composed of multiple reactions which are interconnected by nodes and condensation-points. If a metabolite has only one branch and one trunk, then it should be removed from the network, as described in Section 4.1.2.

(iv) The *split-ratio* at a node is defined as the flux of a branch normalized by the summation of the trunk fluxes. A node has as many split-ratios as branches, which sum to unity under pseudo-steady state conditions.

4.3.1 Principal Nodes

It is often assumed that poor product yield results from an enzyme or enzymes in a reaction sequence (*i.e.*, the reactions that lead from aspartate to lysine) that limit the throughput to the product. Consequently, a fair amount of research effort has been focused on identifying the controlling enzymes in a reaction sequence, such as metabolic control theory (MCT) reviewed in Chapter 2. Although overall activity of the product branch can certainly govern product synthesis rate, product yield is ultimately a function of the split-ratios at the intermediate nodes. For example, in the network given by A→B, B→C, and B→D, the yield of D strictly depends on the split-ratios at the B node, and not on the activity of the B to D branch. Although amplifying limiting enzymes in the product branch may affect nodal split-ratios, if the split-ratios of certain nodes are insensitive to product branch activity, then the yield may not be enhanced. Furthermore, if the product is synthesized at adequate rates under nominal conditions, then it may be more proficient to affect split-ratios by

† Branch-point is a synonym of node.

attenuating by-product branches. If the goal is to improve product yield, then the focus of any metabolic engineering study should be on affecting nodal split-ratios (assuming that product inhibition has already been removed). Therefore, it is essential to identify the nodes in the network that are crucial to product synthesis or lead to by-product formation, for these nodes constitute the limiting points of the network. Identification of these nodes in the network of *C. glutamicum* defined by BS1 and MS1 is described below.

Although a network may consist of a large number of nodes, we have found that the split-ratios at relatively few nodes actually change as a function of product yield. These nodes are referred to as the *principal nodes* since they directly affect product yield and will be the focus for subsequent studies. The split-ratios at the remaining nodes are independent of product yield and require no modifications. Although the location of the principal nodes in a network is a function of the product, by-products, and substrate, the nodes are easily identified by examining theoretical flux distributions constructed at various product yields. For example, the theoretical flux distributions at 35%, 64%, and 75% lysine yield developed in Section 4.2, and illustrated in condensed format in Figure 4.11, identify five nodes whose split-ratios alter as a function of lysine yield, namely, Glc6P, Fru6P, PEP, Pyr, and OAA. Of these five nodes, however, only three, Glc6P, PEP, and Pyr are considered principal nodes of interest for the following reasons. Examination of Fru6P revels that it is only a condensation-point for lysine yields less than 60%. Greater than 60% yield, the isomerase reaction (Reaction (3:BS1)) reverses and Fru6P becomes the principal node while Glc6P converts to a condensation-point. Since typically observed lysine yields are close to 30%, the Fru6P condensation-point is not a target for metabolic modification until observed yield approaches 60%. Above 60% yield, however, emphasis switches from the Glc6P to the Fru6P node. Although by definition OAA is a principal node, close inspection of the node reveals that it is a trivial one, for all OAA consumed by citrate synthase (Reaction (11:BS1), first enzyme of TCA cycle) is returned via malate dehydrogenase (Reaction (16:BS1), last enzyme of TCA cycle). In essence, the TCA cycle flux simply "passes through" the OAA node. As a result, all OAA produced by PEP carboxylase (Reaction (9:BS1))

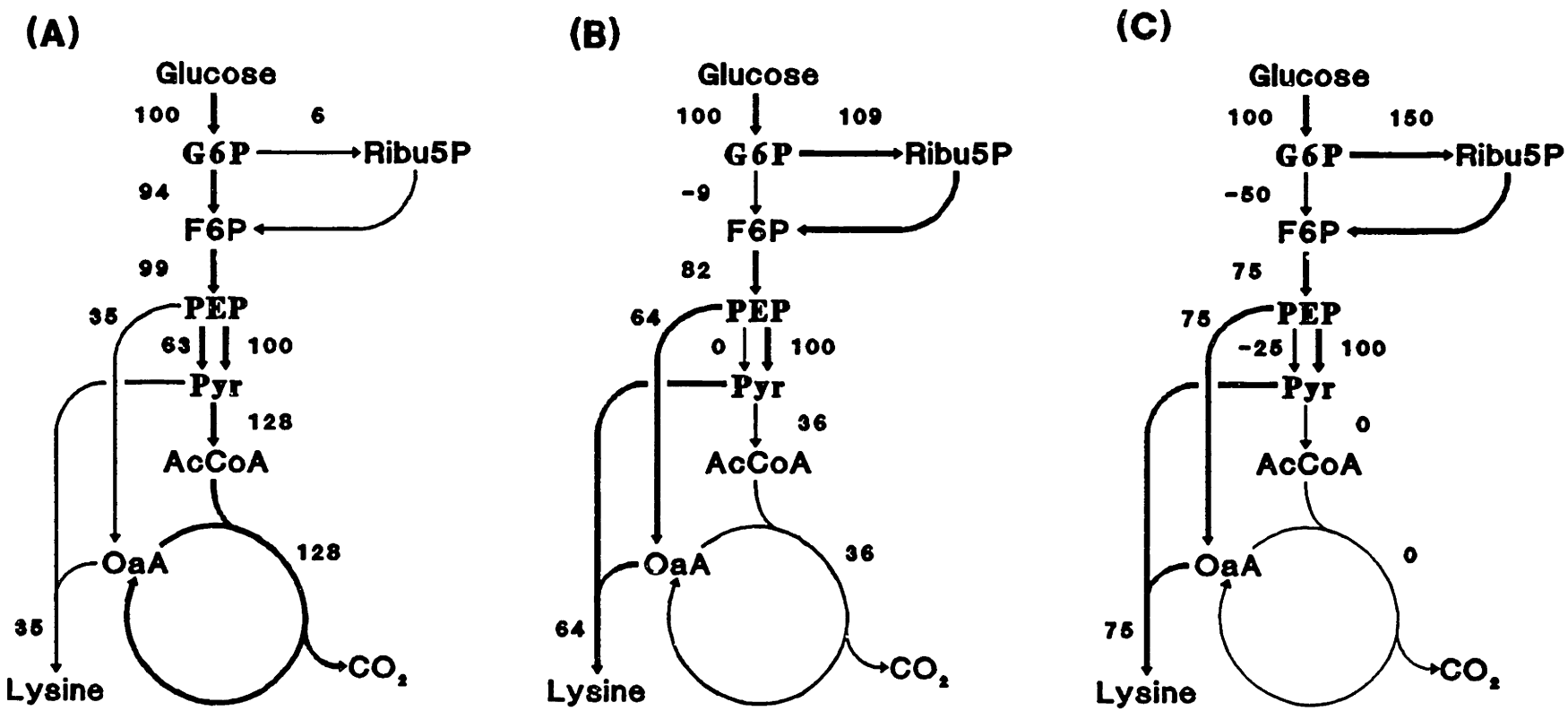

Figure 4.11 Theoretical flux distribution at 35% (A), 64% (B), and 75% (C) lysine yield condensed from Figures 4.4, 4.7, and 4.8, respectively. A negative flux indicates that the flow is in the opposite direction indicated by the arrow. Notice how the split-ratios at the glucose-6-phosphate (G6P), phosphoenolpyruvate (PEP), and pyruvate (Pyr) nodes change as lysine yield is increased. Both PK and PTS fluxes illustrated.

is consumed for lysine synthesis, as depicted in Figure 4.11. The OAA node would be a principal node if other TCA related by-products were produced, such as glutamate, but this is not observed experimentally.

The importance of understanding the mass balance constraints on the operation of the TCA cycle and associated anaplerotic reaction (PPC), as defined by BS1, should be emphasized, as it is often misperceived that net OAA production can occur from malate dehydrogenase. For example, Menkel *et al.* (1989) assumed that the introduction of aspartase (EC 4.3.1.1) would improve aspartate availability since aspartase taps into the fumarate pool. Fumarate, however, is no more "available" than OAA since the net production of either is govern by the PEP node split-ratio. Thus, the introduction of aspartase is basically identical to amplifying aspartate aminotransferase (Reaction (30:BS1)), which is several enzymes removed from the PEP principal node. It should also be noted that all carbon that enters the TCA cycle via AcCoA must be oxidized to CO_2, while carbon that enters the TCA cycle from any other point cannot be oxidized and must eventually leave the TCA cycle. In other words, the addition of a TCA intermediate is equivalent to increasing the PEP node split-ratio. Menkel *et al.* (1989) also demonstrated that lysine yield is improved by fumarate addition, which would, in our opinion, indicates that net OAA synthesis (hence aspartate) limits lysine yield. This, however, is contrary to their conclusions that aspartate availability does not limit lysine synthesis. Also, the aspartate excretion they observe may be due to a suboptimal split-ratio at the Pyr node, as described below. This example serves to illustrate how the flux mapping technique can be used to assess proposed metabolic modifications.

To summarize the dependence of lysine yield on the split-ratios at the three principal nodes, each will be independently examined in turn below. It is also helpful to study the condensed networks illustrated in Figure 4.11. As the lysine yield increases, a higher fraction of the glucose that enters the Glc6P node must be diverted into the pentose phosphate pathway to meet the increasing NADPH requirements of lysine synthesis. If the kinetics at this node are such that glycolysis outcompetes the pentose phosphate pathway for Glc6P, then lysine will be NADPH limited, and the excess carbon entering the network must ultimately lead to by-

product formation. However, if the Glc6P node split-ratio varies so as to exactly meet NADPH burdens, then lysine yield limitations must be caused by suboptimal splits at the other two principal nodes. The next principal node encountered is the PEP node. Since PEP and pyruvate are the two carbon-precursors for lysine synthesis, if the split-ratio of the PPC branch is less than 50%, then in sufficient OAA will be synthesized and excess Pyr will be formed, which will most likely be oxidized in the TCA cycle. If the PPC branch split-ratio is greater than 50%, then excessive amounts of OAA will be synthesized (although this has never observed), which could lead to aspartate or glutamate by-products. Assuming optimal splits at the Glc6P and PEP nodes, if the pyruvate dehydrogenase complex branch (Reaction (10:BS1)) split-ratio at the Pyr node is greater than zero, lysine synthesis will be limited by pyruvate, and once again accumulation of TCA related metabolites could result. Simply stated, suboptimal split-ratios at any of the three principal nodes leads to suboptimal lysine yields. We now wish to consider the factors which may limit nodal split-ratios.

4.3.2 Nodal and Network Flexibility

Since enzymes in the network are expressed in such a way as to lead to optimal biomass synthesis, it is likely that the split-ratios at some or all of the principal nodes will be suboptimal with respect to lysine synthesis. As for analogy, consider a pipe network where the flow in a particular branch of pipes is solely governed by the diameter of the pipes. Consequently, the split-ratio at any node will be governed by the relative diameters of the branch pipes. A pipe network for "biomass synthesis" would be designed such that pipe diameters would be a function of biomass metabolite requirements. If this pipe network was then switched over to "lysine synthesis" by increasing the diameters of the lysine trunk pipes, one would not expect maximum lysine yield to result since pipes at the principal nodes leading to by-products have not been resized. In such a simple analogy the obvious solution would be to decrease—or attenuate—those pipes that lead to by-products. The premise of this technique closely paraliels the approach typically followed for increasing yield in lysine producing strains, as reviewed in Chapter 3. Such an

approach, however, inherently assumes that the split-ratios at the principal nodes can be easily modified through amplification or attenuation of enzyme activity.

4.3.2.1 Classification of Nodes

In vivo metabolic control is, of course, much more complicated than a pipe network. It can be anticipated, considering enzyme kinetics, that the split-ratios of certain nodes may be easily altered while the split-ratios of other nodes may be quite difficult to alter. Therefore, we need to consider the factors which might affect nodal split-ratios. The ease at which a nodal split-ratio may be altered is defined as follows:

(v) A node is defined as *flexible* if the split-ratio for each branch solely depends on the demand for the branch metabolites, and any branch can attain a split-ratio of 100% if such a metabolite demand occurs.

(vi) A node is considered *rigid* if the split-ratio of one or more branches is fixed or bounded. Such a node is *weakly rigid* if the split-ratio bound of the affected branch can be mitigated by attenuating the remaining branches of the node. If the split-ratio cannot be significantly improved through branch attenuation, the node is defined as *strongly rigid*, which implies active split-ratio control.

Although these definitions are mutually exclusive, in practice nodes may exhibit varying degrees of flexibility or rigidity. For the sake of clarity, however, such "fuzziness" will not be considered. To understand the origins of the above definitions, it is useful to considered the kinetic mechanisms that form their foundations. In the following discussion, kinetics of a branch refers to the lumped-response of all the enzymes that constitute the branch. A flexible node results if all branches of the node exhibit product regulation (such as feed back inhibition), have similar affinities for the node metabolite, and display similar activities.

As an example, consider the nodal architecture illustrated in Figure 4.12 (A). If both branches meet the conditions described above, then the split-ratio at the node solely depends on the demands on the two products (P_1 and P_2). If P_1 is deregulated, the majority of the flux will enter the P_1 branch, and vice versa for P_2. By definition, a flexible node will not limit product yield. If the three principal nodes in the lysine network were completely flexible, then deregulation of lysine would result in maximum yield. Since this does not occur, some nodal rigidity must exist in the

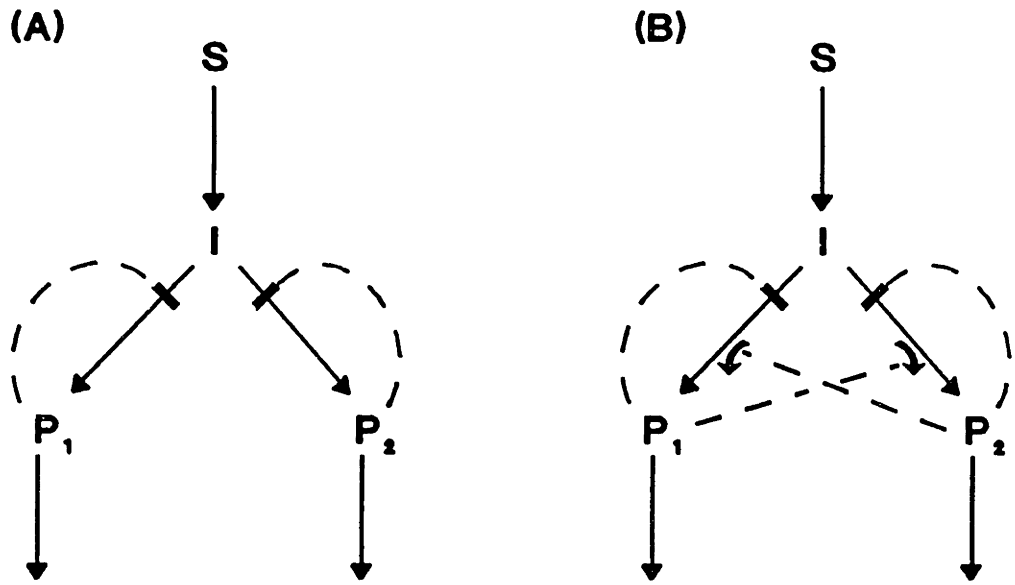

Figure 4.12 Hypothetical node control architectures where dashed line indicates positive (➡) or negative (▮) feedback. (A) Flexible or weakly rigid node and (B) strongly rigid node. See text for details.

network. A weakly rigid node is similar to a flexible node, allowing that some branches may exhibit dominance. For example, if one of the branches in of the node illustrated in Figure 4.12 (A) had a much higher activity (or higher affinity for the node metabolite) and was not strongly inhibited by its product, then even complete deregulation of the subordinate branch would not significantly redirect the flux. However, the split-ratio of the subordinate branch could be significantly increased if the activity of the dominate branch was attenuated. The pipe network previously described would consist of weakly rigid nodes. Therefore, a weakly rigid node can limit product yield, but can be mitigated via enzyme attenuation. Finally, a node which is strongly rigid has branches whose split-ratios are actively controlled, which implies that some feedback must exist between competing branches. Consider the node illustrated in Figure 4.12 (B). In this example a metabolite of one branch (P_1 or P_2) acts as an activator of the opposing branch, where it is assumed that the activator can mitigate the action of the inhibitor (P_2 or P_1), as observed in many

allosteric enzymes [Kurganov, 1982]. The rigidity of the node may be demonstrated by examining the nodal response to a perturbation.

Let us assume that increasing the P_1 branch split-ratio is the desired goal. Furthermore, we may assume that the steady state concentration of P_1 is high enough to strongly inhibit its own synthesis in the absence of the activator, P_2. To increase the split-ratio of the P_1 branch, the flux in the P_2 branch must be attenuated; however, if the synthesis of P_2 is blocked, then the P_1 branch will lose its activation, and end-product inhibition will severely attenuate the synthesis of P_1. Consequently, attenuating one branch results in the attenuation of the opposing branch (overall collapse), and the split-ratios for each branch remain relatively unaffected. Since the node depicted in Figure 4.12 (B) is symmetric, the same effect occurs for attenuation of P_1 synthesis.

Although other possible control architectures could be postulated that would produce a rigid node, the key aspects to any such control is the presence of a feedback mechanism between competing branches that will have the tendency of maintaining a constant split-ratio, as demonstrated in Figure 4.12 (B). Not only can a rigid node limit product yield, but its effects are not easily mitigated via simple enzyme activity attenuation. Although a great deal of information has been published on metabolic feedback, most seem to emphasis end-product inhibition [Umbarger, 1969; Cohen, 1965] and relatively few focus on split-ratio control [LaPorte *et al.*, 1984; Attkinson, 1977, pp. 193-199]. An actual rigid node in the *C. glutamicum* network is described in Section 6.5. The translation of nodal rigidity to network response is discussed below.

4.3.2.2 Network Response

How networks are affected by the presence of a strongly rigid node may be demonstrated through the use of a simple network composed of only two nodes as depicted in Figures 4.13 and 4.14. First, we will consider only those networks that lack condensing branches as in Figure 4.13, which will be referred to as *independent networks* since the split-ratios at any node may change without resulting in the accumulation of an intermediate. In the following discussion, the desired objective is to increase the yield of product (P) over the by-products (B_i) through attenuation

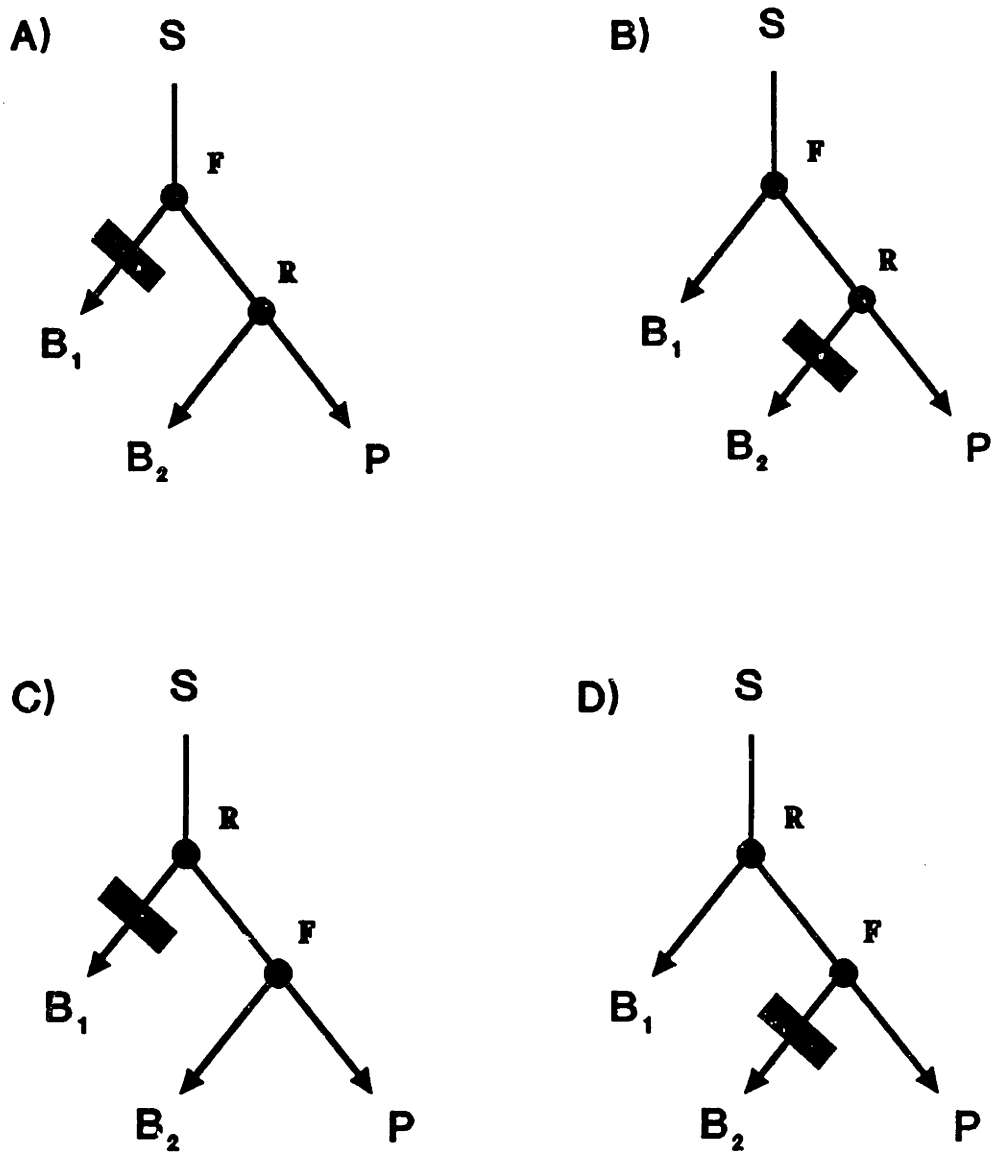

Figure 4.13 Independent networks composed of one rigid (R) and one flexible (F) node, where B_1 and B_2 represent by-products and P the desired product. The rectangle represents a flux attenuation point intended to enhance product yield. The network responses are: (A) yield enhancement; (B) yield reduction; (C) yield unaffected but overall network attenuated; and (D) yield enhancement.

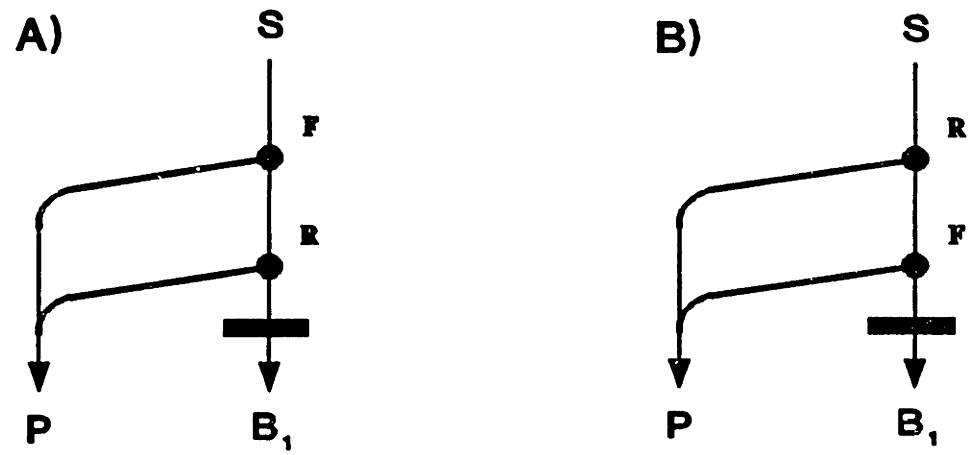

Figure 4.14 Dependent networks. (See caption of Figure 4.14 for details.) Both networks would exhibit overall attenuation to the indicated perturbation, but the yield would be unaffected.

of the indicated branch (illustrated in Figure 4.13). In the first scenario, the flexible node (**F**) precedes the strongly rigid node (**R**), as depicted in Figure 4.13 (A,B). In Figure 4.13 (A), blocking the synthesis of B_1 at the flexible node results in a rechanneling of the substrate to the rigid node. Since the split-ratio at the rigid node remains unchanged and B_1 synthesis is reduced, the net result is an increase in the yield of P. However, if the synthesis of B_2 is attenuated (as shown in Figure 4.13 (B)), then by the definition of a rigid node, product synthesis also becomes equally attenuated. Attenuation of both branches of the rigid node results in a higher conversion of substrate to by-product B_1, causing an actual reduction in product yield to occur. If the nodes are flipped such that the rigid node feeds into the flexible node (as shown in Figure 4.13 (C,D)), then attenuation of B_1 synthesis (Figure 4.13 (C)) causes the substrate to be consumed at an attenuated rate since the flux through the opposing branch is also attenuated by definition. As the split-ratio at the subsequent flexible node is unaffected, the overall yield remains unchanged; however, the synthesis rate of P is attenuated by the same amount as the synthesis of B_1. If synthesis of B_2 is blocked (Figure 4.13 (D)), then the carbon entering the flexible node can be completely redirected to the product, which results in product yield

enhancement. This final scenario (Figure 4.13 (D)) also concisely illustrates the hypothesized limitations in lysine synthesis. The flexible node represents aspartate semialdehyde (ASA), where one branch leads to lysine, the other to homoserine. In the ATCC 21253 strain, the undesirable branch has been blocked through mutation of homoserine dehydrogenase, which results in homoserine—or threonine plus methionine—auxotrophy, and the overproduction of lysine when supplemented threonine is exhausted. Therefore, all carbon entering the ASA node—the flexible node—is redirected to lysine synthesis in these strains. The yield is not maximum due to what is hypothesized as a rigid node somewhere in the primary metabolism preceding aspartate, where B_1 would represent CO_2.

We have demonstrated that the presence of the rigid node in the independent network produces three distinct results from perturbations intended to enhance product yield: 1) yield improvement, Figure 4.13 (A,D); 2) yield reduction, Figure 4.13 (B); 3) yield unaffected and overall flux attenuated, Figure 4.13 (C). Furthermore, the type of response depends on the location of the rigid node since the results from Figures 4.13 (A,B) differ from those in Figures 4.13 (C,D).

The final consideration is the affect of rigid nodes on *dependent networks* illustrated in Figures 4.14 (A,B). A network is considered dependent if it contains nodes whose branches condense to form a metabolite, such as the condensation of PEP and PYR to produce lysine. In these networks, the flux in all condensing branches must be equal; otherwise, accumulation (or excretion) of intracellular components would result. (We will assume, without loss of generality, that the network is regulated such that intracellular metabolite accumulation cannot occur.) Under this constraint, the split-ratios of all branches that are a part of the dependent network must vary proportionately in order to satisfy mass balance constraints. Consequently, the split-ratio at one node in a dependent network or sub-network cannot be arbitrarily change without affecting all associated nodes. Under both node architectures, illustrated in Figures 4.14 (A,B), attenuation of B_1 results in attenuation of the overall network without altering the yield. Since the split-ratio of all nodes in a dependent network must vary in unison, the presence of one or more rigid nodes constrains the flexibility of all nodes so associated. These results imply that if a

network is dependent and contains one or more rigid nodes, then the observed product yield cannot be easily affected by metabolic perturbations. For such situations, product yield enhancement may only be achieved by transforming the rigid node into a flexible one.

Examination of the lysine biosynthetic network of *C. glutamicum* (described by BS1 and MS1 and depicted in condensed format in Figure 4.11) reveals that it is a dependent network since the products of the principal nodes—NADPH, OAA and PYR—all condense to form lysine. Consequently, if any of the principal nodes are weakly or strongly rigid, then lysine yield will be limited. Attempts to redirect the carbon flow may result in overall network collapse due the dependent network architecture. Therefore, to improve lysine yield, the extent of principal node rigidity must be assessed.

4.3.3 Assessment of Nodal Rigidity

Since the BRNE does not contain information on enzyme kinetics, nodal rigidity cannot be determined from analysis of the equation, nor is nodal rigidity easily assessed from steady state fermentation data. However, nodal rigidity can often be inferred from the response of the network to metabolic perturbations. The general objective is to locally perturb a principal node and observe the resulting flux distributions. If the perturbation results in significant improvement in product yield, then the perturbed node must be either weakly or strongly rigid. On the other hand, if the product branch split-ratio can be significantly† increased without affecting product yield (*i.e.* intermediate accumulates instead), then the node is probably flexible and the rigidity lies elsewhere. It is also possible in dependent networks that a local perturbation of a node will induce overall network attenuation as discussed above. In this case, either the perturbed node is strongly rigid, or some other principal node is rigid.

---

† Significantly in this context is relative to the node under investigation since the split-ratio of some nodes are much more sensitive to alterations in product yield than others.

Potential scenarios are as numerous as there are nodes in a network since nodal response in actuality forms a continuum that cannot be easily quantified as either rigid or flexible, black or white, and is subject to the interpretation of the investigator. Nevertheless, the technique is still quite useful in identifying areas in a network that may be potentially rigid and limiting product yield. The technique allows the investigator to hone-in on the potential problem areas in the network and apply techniques, such as MCT, that are difficult to apply to an entire network.

Types of perturbations that can be employed to assess nodal rigidity basically fall into three categories: 1) attenuation of enzyme activity via addition of specific inhibitors; 2) amplification or attenuation of enzyme activity via genetic modifications; and 3) environmental modifications, such as a different carbon source, temperature, etc. Although classic mutation-selection techniques can be used to introduce genetic modifications, such techniques should be avoided when possible since mutagens can often introduce multiple mutations. Consequently, it is preferable to alter enzyme activity via techniques of molecular biology or with specific enzyme inhibitors. Furthermore, the enzyme perturbed should be as close to the node as possible; otherwise, intermediates may accumulate which complicates the interpretation of the results.

The above techniques have been employed to study the rigidity of the Glc6P, PEP and Pyr principal nodes. The results of these experiments are presented in Chapter 6.

4.3.4 Summary

We have demonstrated in this section that it is inappropriate to attribute product yield limitations to a controlling enzyme in a branch. Rather, product yield limitations occur from suboptimal product branch spit-ratios at the principal nodes of the network. Therefore, attempts to improve product yield should address the factors which affect nodal split-ratios. To this end, we have defined two types of nodes, flexible and rigid, and have characterized their relative effects on dependent and independent networks. Examination of lysine overproduction from the metabolic network of *C. glutamicum*, defined by BS1 and MS1, reveals the presence of three

principal nodes located at the Glc6P, PEP, and Pyr branch-points. Since the products of the principal nodes condense to form lysine, the network is classified as dependent. Experimental perturbations coupled with the flux mapping techniques developed in Section 4.1 have been outlined to assess nodal rigidity. The results of such experiments are presented in Chapter 6.

Chapter 5

Materials and Methods

5.1 Culture Preparations

5.1.1 Organisms

Corynebacterium glutamicum ATCC 21253, obtained from the American Type Culture Collection (Rockville MD), is the organism employed in all lysine fermentations (except the industrial-type fermentation) and serves as the parent strain in the mutation and selection studies discussed in Section 5.4 below. *C. glutamicum* ATCC 21253 requires biotin, homoserine (or threonine plus methionine), and leucine for growth and is directly descended from ATCC 13287, a homoserine auxotroph and lysine producer, which is descended from the wild-type glutamate producing strain ATCC 13032 (see United States Patent 3,708,395 as well as Chapter 3).

Stock cultures of this organism, and its descendants, are maintained at 4°C on LB5G medium (Table 5.1) plates or slants and transferred at approximately one month intervals. Backup cultures are stored at -70°C in LB5G medium (no Agar) supplemented with 10% (v/v) glycerol. Bacto Yeast Extract, Tryptone, and Agar are from Difco Laboratories (Detroit MI).

An industrial strain of *Brevibacterium flavum*, which is Thr^-, Trp^-, and AEC^R, was obtained from Roquette Freres (Lestrem, France). Since this strain is only employed in one fermentation (B3) and is not used in any other study, it is only discussed in Section 5.5.5.5.

Table 5.1 LB5G medium for propagation and seed cultures.

Component	Concentration (g/l)
Glucose	5
Yeast Extract	5
Tryptone	10
NaCl	5
Agar (plates)	18

5.1.2 Cultivation of Seed and Preculture

Cultures for fermentation inoculation, growth studies, or intracellular assays are started from a seed culture consisting of 50 ml of LB5G medium (Table 5.1, without Agar) in a 250 ml triple baffled Erlenmeyer flask (Belco, Vineland NJ). The seed culture is inoculated from a loop of the stock culture that has been grown overnight on a LB5G plate at 30°C. The seed culture is allowed to grow at 30°C under agitation (ca. 200 rpm) for 10 hours and is then used to inoculate the preculture.

The basal preculture medium (PMB) is listed in Table 5.2. The preculture medium is based on that given by von der Osten (1989), but is supplemented with threonine, methionine and leucine to meet the auxotrophic requirements of *C. glutamicum* ATCC 21253. Based on biomass yields from methionine, leucine, and threonine of 7.9, 20, and 29 mg amino acid/g biomass, respectively [Kiss, Manuscript in preparation], the preculture medium should support a final biomass titer of approximately 5 g/l before an amino acid limitation is encountered.

PMB medium is prepared as required except for the 100x mineral salts and 10x B&T solutions which are prepared beforehand and stored non-sterile at 4°C. The 10x B&T solution is kept covered as thiamine is light sensitive. While the 100x mineral salts solution can be stored indefinitely, the biotin plus thiamine solution is discarded after four weeks or if any growth is evident. The preculture medium is autoclaved at 121°C for 20 min in three separate parts (as indicated in Table 5.2),

which are aseptically combined after sufficiently cooled. The volume of the preculture as well as the inoculation volume of the seed culture depends on the particular experiment, but a tripled baffled Erlenmeyer flask is always used, in which the liquid volume never exceeds 25% of the flask volume. All precultures are cultivated at 30°C under agitation of ca. 150 to 200 rpm (better mixing in 4 l flasks is obtained at lower agitation speeds due to resonance).

Shaker flasks are periodically monitored by aseptically withdrawing a 5 to 10 ml sample which is measured for optical density (OD) and pH, and is examined for contamination. Optical density is measured in a square 4.0 ml cuvette at 660 nm against a water blank, where an OD of 1.0 corresponds to a dry cell weight of 0.28 g/l (see Figure 6.5 (A) and Section 6.1.3.1). Samples are properly diluted with water such that the absorbance at 660 nm does not exceed 0.5.

Optical density and pH profiles for a typical preculture run are illustrated in Figure 5.1. In this case, a 4 l shaker flask with 1 l of medium was used and was inoculated with 50 ml (all) of the seed culture. An oxygen limitation is encountered at approximately 10 h which results in lactic acid production (not shown), growth termination, and a drop in pH. The maximum growth rate attained was 0.7 h^{-1} and the final biomass titer was 3.1 g DCW/l (an OD of 10.9).

It is quite apparent from Figure 5.1 that the preculture, under the conditions described above, can only be maintained for approximately 8 to 10 h before an oxygen limitation is encountered. Although the final biomass titer and the duration of the exponential phase can be increased by reducing the liquid volume in the shaker flask, this was not required in most studies since the final biomass titer is adequate for enzymatic assays (Section 5.2.2) or fermentation inoculation (Section 5.5.2.2). It should be noted that if a shaker flask culture is to be run longer than 12 h (*e.g.*, lysine studies), $CaCO_3$ must be added to Part A of the medium (ca. 30 g/l) to maintain pH around 6.5. Furthermore, the threonine concentration must be reduced, so that it is the limiting nutrient.

Table 5.2 Basal preculture medium (PMB).

Component		Amount	
Part A	Glucose	20	g
	Citrate•Na_3•$2H_2O$	1.14	g
	$CaCl_2$	55	mg
	$MgSO_4$•$7H_2O$	200	mg
	$FeSO_4$•$7H_2O$	20	mg
	NaCl	1	g
	100x Mineral Salts	10	ml
	pH (adjusted w/ HCl)	5.0	
	Volume	800	ml
Part B	K_2HPO_4	8	g
	KH_2PO_4	1	g
	Threonine	150	mg
	Leucine	100	mg
	Methionine	40	mg
	10x B&T	10	ml
	Volume	100	ml
Part C	$(NH_4)_2SO_4$	5	g
	Volume	100	ml

100x Mineral Salts		10x B&T	
Component	Amount	Component	Amount
$FeCl_3$•$6H_2O$	200. mg	Biotin	5.0 mg
$MnSO_4$•H_2O	200. mg	Thiamine•HCl	10.0 mg
$ZnSO_4$•$7H_2O$	50. mg	Volume	100.0 ml
$CuCl_2$•$2H_2O$	20. mg		
$Na_2B_4O_7$•$10H_2O$	20. mg		
$(NH_4)_6Mo_7O_{24}$•$4H_2O$	10. mg		
pH (by HCl)	1.5		
Volume	1000. ml		

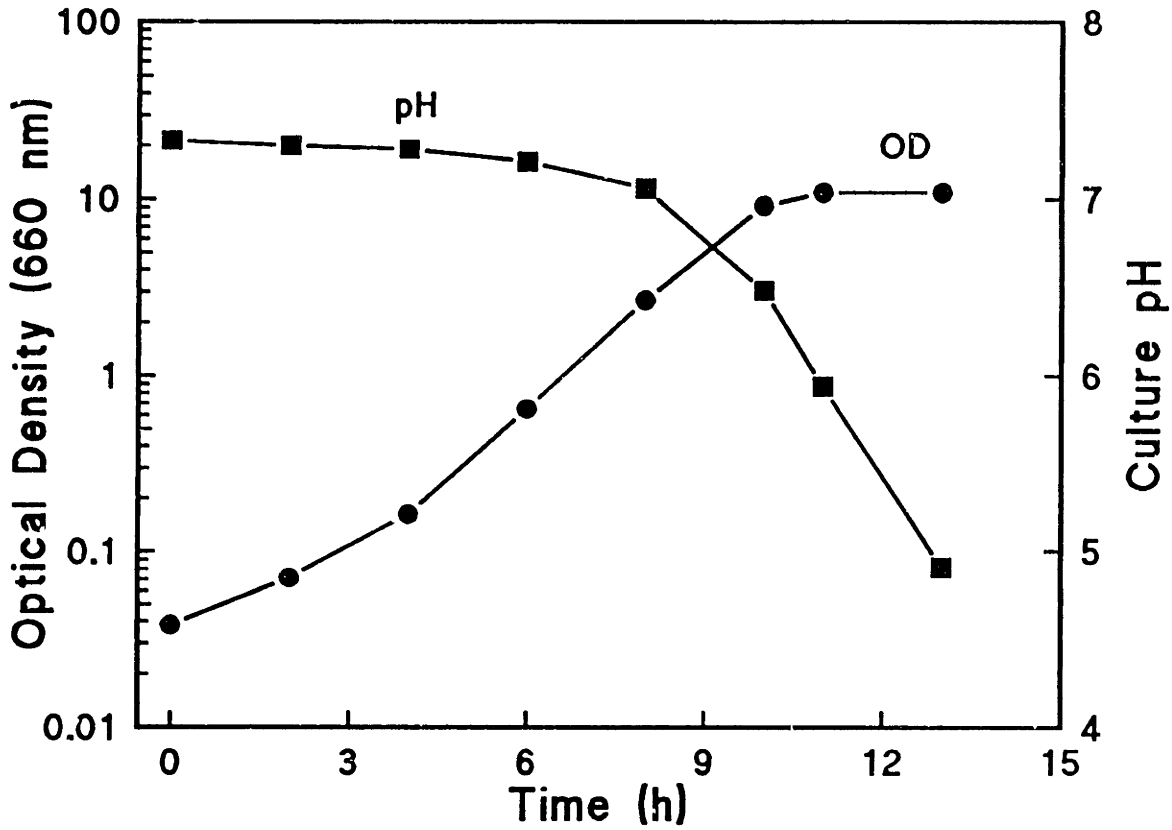

Figure 5.1 Optical density (OD) and pH profiles of *C. glutamicum* ATCC 21253 cultured in 1.0 l of medium PMB in a 4 l flask and inoculated with 50 ml of seed culture.

5.2 Intracellular Enzyme Assays

5.2.1 Cell Homogenization

Cells in late exponential growth phase are cooled on ice to 4°C and centrifuged at 5000-7000 × g at 4°C (J2-21 centrifuge, Beckman, Palo Alto CA). The pellet is washed twice with cold **extract buffer** (100 mM Tris•HCl pH 7.5, 100 mM KCl, 10 mM $MgCl_2$) and resuspended to a final volume of 15 ml. The amount of culture broth harvested is such that the biomass concentration in the washed cell concentrate is approximately 30 to 60 g DCW/l (this usually requires approximately 1 l of the preculture at an OD of 3.6).

Cell homogenization is accomplished by ballistic disintegration with a MSK cell homogenizer (B. Braun Melsungen AG, W. Germany). A 50 ml glass shaking bottle

is used, to which 40.0 g of 0.10-0.11 mm glass beads are added, then placed on ice. After being sufficiently cooled, 15 ml of the cell concentrate is added to the bottle which is placed in the cell homogenizer and shaken at 4000 rpm for 2 min. To maintain the bead and cell suspension at approximately 4°C, liquid CO_2 is sparged around the shaker bottle with the aid of a capillary attachment (B. Braun) and a cylinder of liquid CO_2, which must incorporate a liquid syphon (*i.e.*, riser tube). The control of the flask temperature is not always satisfactory and must balance two opposing effects (a high flow rate of liquid CO_2 will freeze the sample, while a zero flow rate will allow the temperature of the sample to exceed 50°C). Although the manufacturer suggests a continuous flow of liquid CO_2, we found this to be unsatisfactory, as the flow rate cannot be controlled accurately. We obtained the best results from pulses of liquid CO_2, in which the valve on the capillary attachment is opened 1/8 to 1/4 of a turn for a given duration and at a given frequency. For the sample conditions described above, adequate cooling is achieved by first cooling the homogenizer for 5 to 10 sec, then pulsing the liquid CO_2 on for 10 sec out of ever 30 sec of operation (*i.e.*, 10 sec on followed by 20 sec off). It should be noted that the cooling cycle strongly depends on the sample volume and bead weight used, so the cooling cycle cannot be extrapolated to other flask configurations.

To separate the glass beads from the cell homogenate, the mixture is poured into a 60 cc plastic syringe in which a thin layer of glass wool has been placed inside the syringe at the exit to trap the beads. The cell homogenate is forced through the syringe (leaving the beads behind) into a 16 ml polycarbonate Sepcor centrifuge tube (Labcor Products, Inc., Gaithersburg MD) that is packed on ice. The centrifuge tubes are placed in a JA-20 rotor with rubber adaptor sleeves (Beckman) and centrifuged at 20,000 rpm (48,000 × g) at 4°C for 45 min. The cell-free extract is pipetted from the centrifuge tubes and placed in a glass vial that is packed in ice for subsequent assays.

Total Protein

Due to the high protein concentrations obtained in the cell free extract, total protein is assayed with biuret reagent (Sigma, St. Louis MO), in which 300 µl of cell-free extract or extract buffer (blank) is incubated with 5.0 ml of biuret reagent for 15

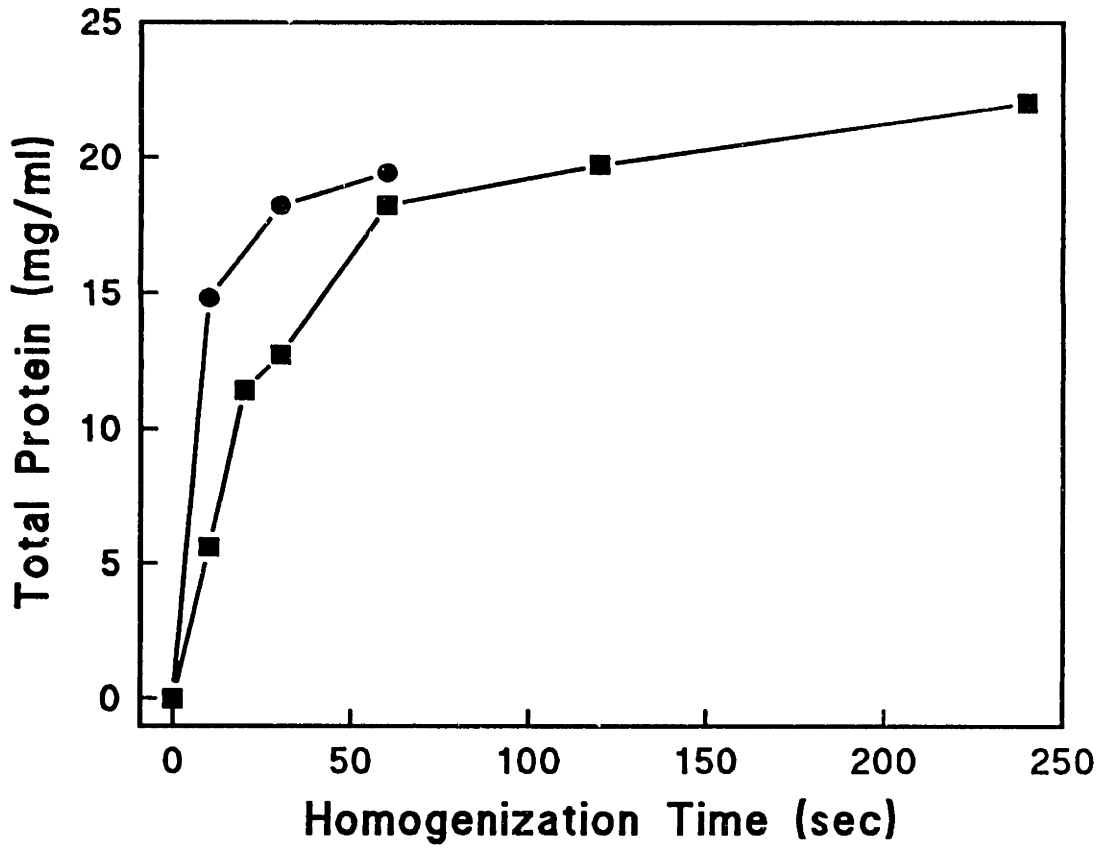

Figure 5.2 Release of soluble protein as a function of homogenization time for cells grow in a complex medium (●) or in PMB medium (■). Complex medium contains (in g/l): glucose, 20; tryptone, 15; yeast extract, 5; NaCl, 5; $(NH_4)_2SO_4$, 5.

min at ambient temperature. Sample absorbance is measured at 545 nm and blanked against the extract buffer. Standards are made with bovine serum albumin (Serva, Westbury NY) in extract buffer at 5, 10, 20, and 30 mg/ml.

The release of soluble protein as a function of homogenization time is illustrated in Figure 5.2. It has been observed that cells grown in a complex medium [20 g/l glucose, 15 g/l tryptone, 5 g/l yeast extract, 5 g/l NaCl, 5 g/l $(NH_4)_2SO_4$] appear to rupture faster than those grown in PMB medium, as evident from Figure 5.2. In either case, a significant fraction of total soluble protein is released into the extract buffer after 2 min of homogenization.

5.2.2 Enzyme Assays

Only the assay procedures are discussed in this section. Results from intracellular assays of *C. glutamicum* are presented in Sections 5.3, 5.4, and Chapter 6. All biochemical reagents were obtained from Sigma (St. Louis MO) and assays are of the crude cell-free extract (no dialysis, etc.), unless otherwise noted. All cofactors and unstable metabolites are prepared fresh or stored for not more that 4 days. As a result, most reagents are made in small amounts (1 to 2 ml). Activity is reported in nmole/min/mg-protein.

5.2.2.1 Glucose-6-phosphate isomerase (GPI)

GPI activity is measured in the reverse direction (*i.e.*, formation of Glc6P) by coupling it with glucose-6-P dehydrogenase and measuring the rate of NADPH formation spectrophotometrically at 340 nm [Noltmann, 1966].

To a 4.0 ml cuvette add:

2.5−x ml		Water
100 µl	1.5 M	Tris•HCl, pH 7.5
100 µl	150 mM	$MgCl_2$
100 µl	60 mM	Fructose-6-P•Na_2
100 µl	10 U/ml	Glucose-6-P dehydrogenase (Sigma G-63-78) in 15 mM Tris•HCl, pH 7.5
100 µl	12.5 mM	NADP in 50 mM Tris•HCl, pH 7.5

Allow to incubate at 30°C for 5 min, then add:

x ml	Enzyme extract (ca. 0.2-0.4 mg protein)

Measure rate of absorbance change per minute (dA/dt) at 340 nm.

Enzyme activity is given by the following expression

$$\text{Activity [nmole/min/mg-protein]} = \frac{1000\,V}{\epsilon_{340}\,l\,[P]\,x}\,\frac{dA}{dt} \qquad (5.1)$$

where V is the volume in ml of the assay mixture (3 ml), ϵ_{340} is the molar absorptivity of NADPH or NADH at 340 nm (both are 6.22 $mM^{-1}\,cm^{-1}$), l is the cuvette path length (1 cm), x is the volume (in ml) of cell-free extract added, and [P] is the total

protein concentration in the cell-free extract (in mg/ml). It should be noted that GPI activity as calculated from Equation (5.1) may be twice the actual value due to native gluconate-6-P dehydrogenase activity in the crude extract.

5.2.2.2 Glucose-6-phosphate dehydrogenase (G6PDH)

Activity of G6PDH is assayed by measuring the rate of NADPH formation spectrophotometrically [Deutsch, 1983].

To a 4 ml cuvette add:

2.6−x ml		Water
100 µl	1.5 M	Tris•HCl, pH 7.5
100 µl	150 mM	$MgCl_2$
100 µl	12.5 mM	NADP (see GPI assay)
x ml		Enzyme extract (ca. 1 mg protein)

Incubate for 5 min at 30°C, then add

100 l	150 mM	Glucose-6-P Na_2

Measure rate of absorbance change at 340 nm.

Activity is given by Equation (5.1). As with GPI, activity calculated in this manner may be twice the actual value. Sugimoto and Shiio (1987a) have noted that the activity of G6PDH in *B. flavum* decays rapidly if the extraction buffer does not contain either KCl or $MgCl_2$.

5.2.2.3 Gluconate-6-phosphate dehydrogenase (GN6PDH)

Activity of GN6PDH is assayed by the method given for G6PDH except that glucose-6-P is replaced by an equivalent amount of gluconate-6-P•Na_3. Unlike G6PDH, GN6PDH is fairly stable without the addition of KCl or $MgCl_2$.

5.2.2.4 6-Phosphogluconolactonase (lactonase)

The activity of lactonase has been measured in the forward direction [Bauer *et al.*, 1983], however, to our knowledge, the reverse reaction has not been assayed, even though the enzyme has been reported to be irreversible [Lehninger, 1975]. In order to determine if gluconate-6-P can be converted to glucose-6-P in cell-free extracts of *C. glutamicum*, gluconate-6-P is incubated with the enzyme extract for a

specified amount of time. The reaction is stopped and the mixture is assayed for glucose-6-P. The specifics are as follows.

To a 1.5 ml micro-centrifuge tube add:

0.767−x ml		Water
67 µl	1.5 M	Tris•HCl, pH 7.5
33 µl	150 mM	$MgCl_2$
67 µl	7.33 mM	NADPH in water
x ml		Enzyme extract (ca. 0.6 mg protein)

Incubate at 30°C for 5 min, then add

67 µl	150 mM	Gluconate-6-P•Na_3 or water (blank)

Allow to reaction to proceed for 5-10 min (Δt), then terminate it with

200 µl	12%(w/v)	Trichloroacetic acid

Remove precipitated protein by centrifugation.

Assay for glucose-6-Phosphate

To a 4 ml cuvette add:

2.40 ml		Water
200 µl	1.5 M	Tris•HCl, pH7.5
100 µl	150 mM	$MgCl_2$
100 µl	12.5 mM	NADP (see GPI assay)
100 µl		Sample from micro-centrifuge tube

Measure absorbance at 340 nm (A_1) then add:

100 µl	10 U/ml	Glucose-6-P dehydrogenase (see GPI assay)

Remeasure absorbance at 340 nm (A_2) after 10 min.

The concentration (in M) in the original sample, after the addition of trichloroacetic acid, is given by $[Glcn6P] = 4823(A_2 - A_1)$. The activity of the reverse lactonase reaction is $1.2[Glcn6P]/(x[P]\Delta t)$. Two blanks, one without enzyme, the other without

Glcn6P, are also be run such that background levels of Glc6P can be properly subtracted out.

5.2.2.5 Isocitrate dehydrogenase (ICDH)

Activity of ICDH is assayed by measuring the rate of NADPH formation [Goldberg and Ellis, 1983].

To a 4 ml cuvette add:

2.6−x ml		Water
100 µl	1.5 M	Tris•HCl, pH 7.5
100 µl	150 mM	$MnCl_2$
100 µl	12.5 mM	NADP (see GPI assay)
x ml		Enzyme extract (ca. 0.02-0.1 mg protein)

Incubate for 5 min at 30°C, then add

100 µl	150 mM	DL-Isocitrate•Na_3

Measure rate of absorbance change at 340 nm.

Activity is calculated from Equation (5.1).

5.2.2.6 Aconitase

Aconitase is assayed by coupling it to ICDH and measuring the change in absorbance at 340 nm. Since ICDH exhibits high activity in the cell-free extract of *C. glutamicum*, no ICDH needs to be added. Although the assay of aconitase is basically identical to the ICDH assay, a few changes are made so that fluorocitrate inhibition can be studied.

To a 4 ml cuvette add:

2.4−x ml		Water
100 µl	1.5 M	Tris•HCl, pH 7.5
100 µl	150 mM	$MnCl_2$
100 µl	150 mM	Citrate•Na_3
100 µl	0-60 mM	Fluorocitrate barium salt (Sigma F-9634)
100 µl	3 M	Na_2SO_4

Filter out $BaSO_4$ precipitate if fluorocitrate is used, then add:

x ml		Enzyme extract (ca. 0.5 mg protein)

Incubate at 30°C for 5 min, then add:

100 µl	12.5 mM	NADP (see GPI assay)

Measure rate of change in absorbance at 340 nm.

To precipitate the barium ion out of solution before the addition of the extract (addition of extract with barium ion results in precipitate), Na_2SO_4 is added and the solution is filtered through 0.22 µm Millex-GV filter unit (Millipore, Bedford MA). The addition of the Na_2SO_4 also increases the observed aconitase activity by a factor of 2 to 3. Unlike other organisms [Fansler and Lowenstein, 1969; Rokita, 1983], aconitase in *C. glutamicum* is fairly stable and does not appear to require activation with iron. It should be noted that fluorocitrate is extremely toxic and must be handled with extreme care.

5.2.2.7 Isocitrate lyase (ICLY)

Activity of ICLY is measured by an end-point method in which the glyoxylate formed from isocitrate is determined by reacting it with 2,4-dinitrophenylhydrazine [Darton and Gunsalus, 1962]. The method is composed of two steps, in which the enzymatic reaction is first performed, followed by an assay for glyoxylate.

Step 1. To a 1.5 ml micro-centrifuge tube add:

0.7−x ml		Water
100 µl	1.5 M	Tris•HCl, pH 7.5
33.3 µl	150 mM	$MgCl_2$
100 µl	200 mM	Glutathione, reduced
x ml		Enzyme extract (ca. 0.2 mg protein)

Incubate for 5 min at 30 °C, then add:

66.6 µl	150 mM	DL-Isocitrate•Na_3

Allow reaction to proceed at 30°C for 5-10 min (Δt), then add:

200 µl	12%(w/v)	Trichloroacetic acid

Remove precipitated protein by centrifugation.

Step 2. To a 18 × 150 mm test tube add:

1.0 ml		Aliquot of sample from Step 1.
1.0 ml	0.1%(w/v)	2,4-Dinitrophenylhydrazine in 2 N HCl

Incubate at ambient temperature for 10 min, then add:

2.0 ml	95%(v/v)	Ethanol
1.0 ml		Water
5.0 ml	1.5 N	NaOH

Incubate at ambient temperature for 10 min, then measure absorbance at 540 nm.

To account for background in the cell-free extract, an assay is run in which isocitrate is omitted. A standard curve is constructed with glyoxylate samples at 0.1, 0.5, and 1.0 μmole/ml processed through Step 2. Both the standard curve and the assay samples are blanked against a water sample processed through Step 2. The molar extinction coefficient (ϵ_{540}) obtained from the standard curve was found to be 0.997 $mM^{-1}cm^{-1}$ (this number relates the concentration of the sample in Step 1 to the absorbance of the 10.0 ml sample in Step 2). ICLY activity is given by $1200[glyoxylate]/(\epsilon_{540}[P]x)$.

5.2.2.8 Oxaloacetate decarboxylase (OAADC)

Activity of OAADC is measured with an end-point assay in which the formation of pyruvate and/or the removal of oxaloacetate is measured [Mori and Shiio, 1987a].

Step 1. To a 1.5 ml micro-centrifuge tube add:

0.8−x ml		Water
100 μl	Buffer	500 mM Tris•HCl, pH 8.0, 250 mM NaCl, 100 mM $MgSO_4$
x ml		Enzyme extract (ca. 1 mg protein)

Incubate at 30°C for 5-10 min, then add:

100 µl	100 mM	Oxaloacetic acid, freshly made and neutralized with KOH

Allow reaction to proceed at 30°C for 5-10 min, then add:

200 µl	12%(w/v)	Trichloroacetic acid

Enzymatically measure formation of pyruvate or removal of oxaloacetate.

Assay for Oxaloacetate or Pyruvate

To a 4.0 ml cuvette add:

2.65 ml	Buffer	250 mM Triethanolamine•HCl, 2.5 mM EDTA•Na_2•$2H_2O$, pH 7.6 (NaOH)
100 µl	6.4 mM	NADH in buffer
50 µl		Sample at 0-10 mM OAA or Pyruvate

Measure absorbance at 340 nm against water (A_1), then add:

10 µl	100 U/ml	Malic dehydrogenase (Sigma M-9004) in 3 M $(NH_4)_2SO_4$, for OAA assay.
or 10 µl	100 U/ml	Lactate dehydrogenase (Sigma L-1254) in 3 M $(NH_4)_2SO_4$, for Pyr assay.

Allow reaction to proceed for 10 min then remeasure absorbance (A_2).

The concentration of OAA or Pyr in the original sample (in mM) is given by [OAA] or [Pyr] = $9.04(A_1 - A_1)$. The activity of OAADC is obtained as discussed for lactonase above. Two blank assays are also run, one which lacks enzyme and the other which lacks OAA. It should be noted that oxaloacetate is very unstable and readily decomposes to form pyruvate.

5.2.2.9 Phosphoenolpyruvate decarboxylase (PPC)

The activity of PPC is assayed by coupling it with malate dehydrogenase and measuring the decrease in absorbance at 340 nm that accompanies NADH consumption [Tosaka *et al.*, 1979c].

To a 4.0 ml cuvette add:

2.39 ml		Water
100 µl	1.5 M	Tris•HCL, pH 7.5
100 µl	300 mM	$KHCO_3$
100 µl	150 mM	$MnCl_2$
100 µl	6 mM	Acetyl-coenzyme A (do not add to blank)
100 µl	6.4 mM	NADH in 50 mM Tris•HCl, pH7.5
100 µl	150 mM	Phosphoenolpyruvate•K or water (Blank)
10 µl	1000 U/ml	Malate dehydrogenase (Sigma M-9004)

Place "blank" in sample side of spectrophotometer, sample in reference side of spec., allow to reach 30°C, then add:

x ml	Enzyme extract (ca. 0.8 mg protein)

Measure rate of change in absorbance at 340 nm.

A blank (no PEP) is run simultaneously with the sample due to the presence of NADH oxidase in the cell-free extract. For this same reason, the extract must be the last item added; otherwise, NADH will be completely oxidized before the assay can be started.

5.2.2.10 Pyruvate carboxylase (PC)

The PPC assay described above is also used to determined the activity of PC, except pyruvate•Na replaces PEP, $MgCl_2$ is used in place of $MnCl_2$, and acetyl-coenzyme A is replaced with 100 µl of 60 mM ATP•Na_2. It should be noted that this assay is complicated if the cell-free extract contains high activity of lactate dehydrogenase (LDH). If the extract contains high LDH activity, then ATP can be omitted from the blank instead of pyruvate; however, PC activity may be underestimated, as ATP often inhibits LDH.

5.2.2.11 Malic Enzyme (ME)

The activity of the ME is assayed by measuring the increase or decrease (depending on directionality of reaction) in absorbance at 340 nm [Hsu and Lardy, 1969; Mori and Shiio, 1987a].

Malic enzyme assay in decarboxylating direction

To a 4.0 ml cuvette add:

2.2−x ml		Water
0.5 ml	0.4 M	Triethanolamine pH 7.4 adjust w/ KOH
100 µl	150 mM	$MnCl_2$
100 µl	12.5 mM	NADP (see GPI assay)
x ml		Enzyme extract (ca. 1 mg protein)

Incubate at 30°C for 5 min, then add:

100 µl	300 mM	L-Malic acid neutralized with KOH

Measure rate of increase in absorbance at 340 nm.

Malic enzyme assay in carboxylating direction

To a 4.0 ml cuvette add:

1.90−x ml		Water
100 µl	1.5 M	Tris•HCl, pH 7.5
100 µl	150 mM	$MnCL_2$
600 µl	1 M	KCl
100 µl	300 mM	$KHCO_3$
100 µl	7.33 mM	NADPH in 50 mM Tris•HCL, pH 7.5
x ml		Enzyme extract (ca. 1 mg protein)

Incubate at 30°C for 5 min, then add:

100 µl	300 mM	Pyruvate•Na or water (blank)

Measure rate of decrease in absorbance at 340 nm.

A blank (water in place of malate or pyruvate) is placed in the reference side of the spectrophotometer if absorbance changes significantly before the addition of substrate. Activity is calculated by Equation (5.1).

5.2.2.12 Phosphoenolpyruvate synthetase (PPS)

The activity of PPS is assayed by an end-point method, in which the ATP dependent removal of pyruvate is measured [Cooper and Kornberg, 1969]. The presence pyruvate is determined by reacting it with 2,4-dinitrophenylhydrazine.

To a 1.5 ml micro-centrifuge tube add:

0.167−x ml		Water
33 µl	150 mM	$MgCl_2$
50 µl	100 mM	$ATP{\bullet}Na_2$ or Water (blank)
150 µl	5 mM	Pyruvate•Na

Incubate at 30°C for 5 min, then add:

x ml	Enzyme extract (ca. 0.2 mg protein)

After 5-10 min of reaction (Δt), remove 100 µl of sample and add it to a 13 × 100 mm test tube which contains, premixed, the following:

0.9 ml		Water
0.33 ml	0.1%(w/v)	2,4-Dinitrophenylhydrazine in 2 N HCl

Allow reaction to proceed for 10 min at ambient temperature, then add:

1.67 ml	10%(w/v)	NaOH in water

Incubate for 10 min, then measure absorbance at 445 nm.

A sample is run without enzyme, pyruvate, or ATP to blank spectrophotometer, and an additional sample is run without ATP to account for background pyruvate removal. Under the assay conditions, 1 µmole of pyruvate has an extinction of 6 absorbance units [Cooper and Kornberg, 1969]. PPS activity is given by $833[A(w/o\ ATP)-A(w/\ ATP)]/(\Delta t[P]x)$.

5.2.2.13 Pyruvate dehydrogenase complex (PDC)

An attempt was made to assay PDC via tetrazolium dye reduction [Hinman and Blass, 1981]; however, this method failed because a component in the cell-free extract was able to couple dye reduction to dithiothreitol oxidation which resulted in rapid increase in absorbance. As a result of this problem, an end-point method,

developed by Reed and Willms (1966), was used to assay PDC activity. The assay is based on the measurement of acetyl phosphate that is produced from acetyl coenzyme A by phosphotransacetylase.

To a 15 ml centrifuge tube add:

0.55−x ml		Water
100 µl	1 M	KH_2PO_4 adjusted to pH 7.0 with KOH
20 µl	200 mM	$MgSO_4$
20 µl	500 U/ml	Phosphotransacetylase (Sigma P-5907) in 100 mM Tris•HCl pH 8.0
10 µl	7000 U/ml	Lactate dehydrogenase (Serva 27389)
100 µl		14.3 mM NAD, 10 mM Thiamine pyrophosphate
100 µl	10 mM	Acetyl coenzyme A in 64 mM Cysteine, free base
x ml		Enzyme extract (ca. 1 mg protein)

Incubate for 5 min at 30°C, then add

100 µl	500 mM	Pyruvate•Na or Water (blank)

Allow reaction to proceed for 30 min. Prepare separately:

1 ml	4 M	Hydroxylamine•HCl (store at 4°C)
1 ml	3.5 M	NaOH

After 30 min, add the following to the assay reaction:

1 ml	100 mM	Citric acid adjusted to pH 5.4 w/ KOH
1 ml	4 M	Neutralized hydroxylamine solution above

Incubate for 10 min at ambient temperature, then add:

1 ml	3 M	HCl
1 ml	12%(w/v)	Trichloroacetic acid
1 ml	5%(w/v)	$FeCl_3$ in 0.1 N HCl

Centrifuge solution and read absorbance at 540 nm after 7 min.

A standard curve is constructed as follows: to 1.0 g succinic anhydride, 40 ml of the neutralized hydroxylamine solution is added and allowed to react for 10 min. This solution is diluted to 100 ml and is equivalent to 80 mM acetyl phosphate. Dilutions of this standard are substituted for the enzyme solution to construct the standard

curve. Under the above assay conditions, 1.0 mM acetyl phosphate in the original produces an absorbance of 0.131 at 540 nm. The spectrophotometer and assay are blanked with a sample in which pyruvate is omitted. Although slight improvement in assay linearity was obtained by dialyzing (6000-8000 MWCO) the sample against 100 mM Tris•HCl, pH 7.5, some PDC activity was lost and the improvement in linearity did not warrant the extra effort. Inhibition of PDC by fluoropyruvate (FP) is assayed as above, except FP is added to the incubation mixture.

5.2.2.14 Entner-Doutoroff pathway (ED)

The ED pathway [Entner and Doudoroff, 1952] is assayed by measuring the rate of pyruvate formation from gluconate-6-P. The rate of pyruvate formation is measured by coupling the assay to lactate dehydrogenase and the oxidation of NADH. Assay conditions are based on the work of Kovachevich and Wood (1955a,b).

To a 4.0 ml cuvette add:

2.49−x ml		Water
100 µl	1.5 M	Tris•HCl, pH 7.5
100 µl	150 mM	Gluconate-6-P•Na_3 or Water (blank)
10 µl	1000 U/ml	Lactate dehydrogenase (Sigma L-1254) in 2.1 M $(NH_4)_2SO_4$, pH 6.0
100 µl	60 mM	Glutathione, reduced
100 µl	150 mM	$MnCl_2$

Incubate for 5 min at 30°C, then add:

x ml	Enzyme extract (ca. 1 mg protein)

Measure rate of decrease in absorbance at 340 nm.

Due to the presence of NADH oxidase, a blank (without Glcn6P) is placed in the sample position and the sample is run in the reference position of the spectrophotometer. Activity is calculated from Equation (5.1).

5.2.2.15 NADH or NADPH oxidase

These assays measure the rate of NAD(P)H oxidation in the presence of enzyme extract only.

To a 4.0 ml cuvette add:

2.8−x ml		Water
100 µl	1.5 M	Tris•HCl, pH 7.5
100 µl	6.4 mM	NADH or NADPH

Incubate tc reach 30°C, then add:

x ml	Enzyme extract (ca. 1 mg protein)

Measure rate of decrease in absorbance at 340 nm.

Activity of either oxidase is calculated from Equation (5.1). It should be noted that ultracentrifugation (150,000 × g) will reduced NADH oxidase activity in *C. glutamicum* by a factor of 2 to 3. Similar results have been reported for *B. flavum* [Shiio *et al.*, 1984b].

5.2.2.16 Dinucleotide transhydrogenase

Activity of soluble transhydrogenase is measured with the NADPH oxidase assay, except that 100 µl of 7.2 mM NAD is also added to the reaction solution. Since NADH oxidase activity in cell-free extracts of *C. glutamicum* is much greater than NADPH oxidase activity, the addition of NAD couples the transhydrogenase to the NADH oxidase. In this assay, the observed activity of the transhydrogenase is bounded by the activity of the NADH oxidase.

5.3 Characterization of *C. glutamicum*

As discussed in Chapters 3 and 4, there is some ambiguity in the literature with regards to the anaplerotic pathways that are expressed in *C. glutamicum* when cultured on a glucose medium. Since the lack or presence of certain pathways or enzymes can dramatically alter metabolic flux distributions, assays for several enzymes were conducted as discussed below.

5.3.1 Summary of Enzyme Activities

Table 5.3 summarizes the enzymes of *C. glutamicum* ATCC 21253 that have been assayed during the course of this research. Although some of the enzymes presented in this table were assayed to address the ambiguities associated with the anaplerotic pathways, others were assayed to characterize mutants or to examine the effects of inhibitors or alternate carbon sources on enzyme activities, the results of which are discussed in Section 5.4 and Section 6.3. Therefore, the results presented in Table 5.3 are not from one preparation of cell-free extract.

Enzyme activity reported in Table 5.3 represents averaged activity assayed from a particular cell-free extract, but does not represent averaged activity between different extract preparations. Similarly, the reported errors reflect the uncertainties in the assay and not variance between different extract preparations. Furthermore, since a statistically significant number of assays was not examined, the associated errors represent either limits of detectability or maximum observed fluctuations.

It is quite apparent from Table 5.3 that the only significant anaplerotic reaction present in *C. glutamicum* when cultured on a glucose minimal medium is PEP carboxylase. It is not believed that pyruvate carboxylase, malic enzyme, or isocitrate lyase exhibit enough activity to support a significant metabolic flux. The Entner-Doudoroff pathway could not be detected, and results presented in Section 6.3.2.1 indicate that the ED pathway is not induced by gluconate either. Consequently the ED pathway is not present in *C. glutamicum*. Although a soluble dinucleotide transhydrogenase could not be detected, the results are by no means rigorous, and the existence of this enzyme should be further examined in future studies.

5.3.2 Glyoxylate Shunt Induction

To examine the induction of the glyoxylate shunt by acetate, three cell-free extracts were prepared from cells cultured on the following modified PMB media: 1) 10 g/l glucose; 2) 20 g/l potassium acetate; and 3) 10 g/l glucose plus 20 g/l potassium acetate. Other components of the media are as given in Table 5.1, except that citrate was replaced by 50 mg/l EDTA•Na_2•$2H_2O$. All cultures were grown in 500 ml of medium in 2 l triple baffled shaker flasks and were each inoculated with

Table 5.3 Enzyme activities in *C. glutamicum* ATCC 21253 cultured on PMB medium.

Enzyme Assayed	Activity*	Error
Glucose-6-P isomerase	1064	±50
Glucose-6-P dehydrogenase	133	±7
Gluconate-6-P dehydrogenase	271	±10
Pyruvate dehydrogenase complex	28	±10
Isocitrate dehydrogenase	1710	±50
Aconitase	95	±10
Phosphoenolpyruvate carboxylase	270	±5
Oxaloacetate decarboxylase	275	±40
Pyruvate carboxylase‡	~0	±5
Malic enzyme (carboxylating)	~1.3	±5
Malic enzyme (decarboxylating)	4.9	±5
Isocitrate lyase	~4	±7
Phosphoenolpyruvate synthetase	17	±10
Entner-Doudoroff pathway	~0	±5
NADH oxidase	57	±5
NADPH oxidase	16	±5
NADH oxidase†	23	±5
NADPH oxidase†	1.4	±5
Soluble transhydrogenase†	~0	±5

* Activity reported in nmole/min/mg-protein.
‡ The ~ indicates activity is at the lower bound of detectability.
† Cells cultured in complex medium: 20 g/l glucose, 15 g/l tryptone, 5 g/l yeast extract, 5 g/l NaCl, 5 g/l $(NH_4)_2SO_4$.

15 ml of seed culture. Optical density, glucose, acetate, and lactate were monitored every few hours and are reported in Figure 5.3. Cultures grown on glucose or glucose plus acetate were harvested at 7.5 h, while the acetate grown culture was harvested at 12.5 h due to its slower growth rate. Although it is difficult to determined in this experiment, it appears that glucose and acetate are consumed simultaneously by *C. glutamicum.*

The activities of isocitrate lyase and PEP synthetase for the three cultures are listed in Table 5.4. The results on isocitrate lyase conclusively indicate that the glyoxylate shunt is not operative in *C. glutamicum* when cultured on a minimal

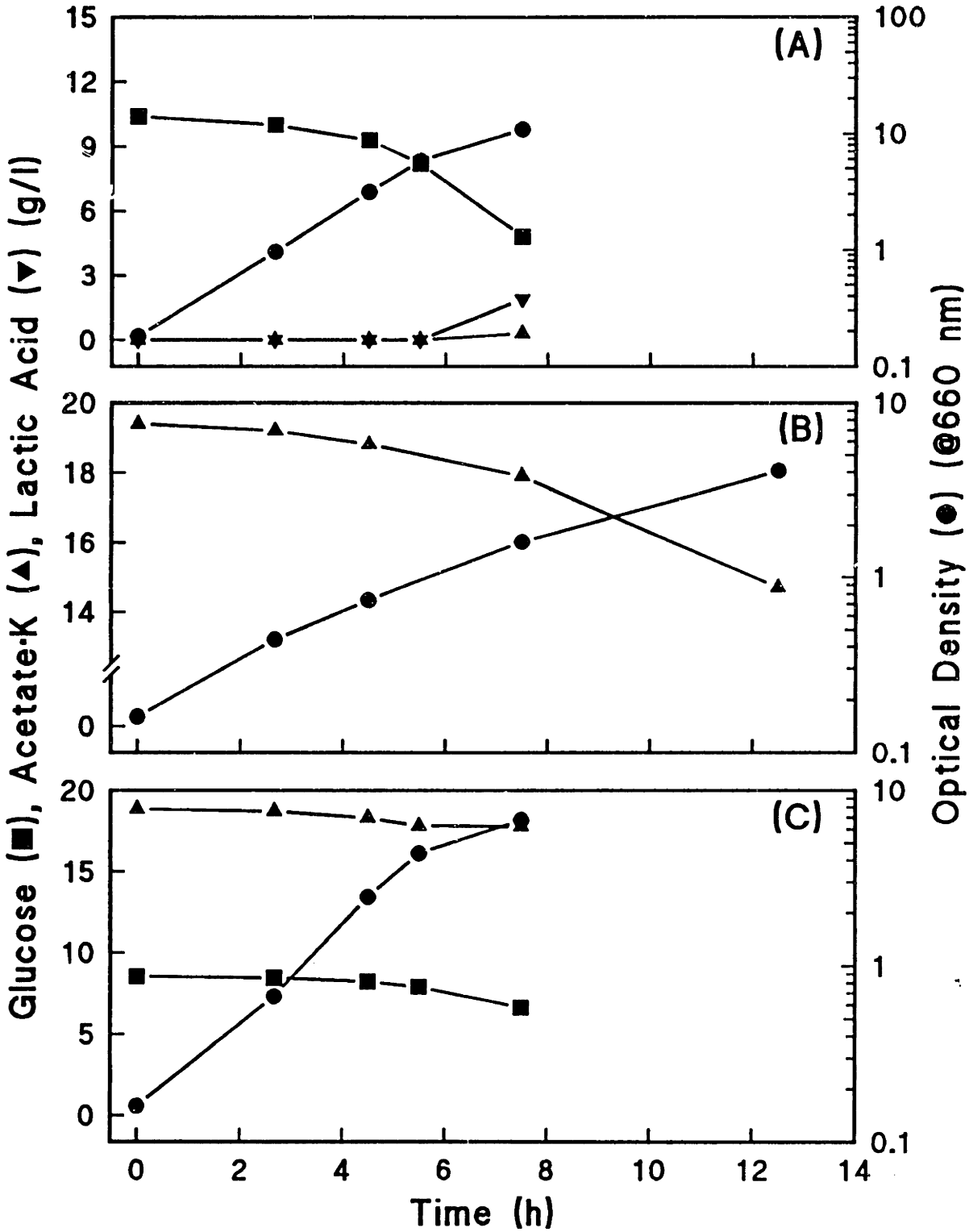

Figure 5.3 Growth and metabolite concentration profiles in shaker flask cultures of *C. glutamicum* ATCC 21253 grown on PMB medium modified to contain (A) 10 g/l glucose, (B) 20 g/l potassium acetate, or (C) 10 g/l glucose plus 20 g/l potassium acetate.

glucose medium. Furthermore, glucose appears to repress isocitrate lyase, while acetate is a strong inducer. The increase in PEP synthetase activity in acetate cultivated cells is consistent with the operation of this enzyme. It is postulated that growth on C_2, C_3, and C_4 carbon sources is accomplished by oxaloacetate decarboxylase, PEP synthetase, and the glyoxylate shunt. Existence of fructose diphosphatase has already been demonstrated, as discussed in Section 3.2.6.4.

Table 5.4 Activity of isocitrate lyase and PEP synthetase in *C. glutamicum* ATCC 21253 cultivated on glucose or acetate PMB medium.

	Activity (nmole/min/mg-protein)		
Enzyme	Glucose	Acetate	Glucose + Acetate
Isocitrate lyase	-2.7	524	15
PEP synthetase	17	39	12

5.3.3 Oxaloacetate Decarboxylase

As discussed in Chapter 3, the function of OAADC in the metabolic assimilation of glucose is uncertain since the glyoxylate shunt (*i.e.*, the DCA cycle) does not support a significant metabolic flux, as demonstrated above. To investigate the properties of OAADC, its activity was assayed under several conditions described below.

To ensure that the catalytic decarboxylation of OAA was enzymatic in nature and not due to divalent cations, the OAADC assay was run on cell-free extract that had been heated at 121°C for 10 min. Compared to an OAA blank without enzyme, the heat-treated extract did not exhibit any OAADC activity, while the unheated extract exhibited an OAADC activity of 250 U/mg, which confirms that OAA decarboxylation is due to an enzyme-catalyzed reaction. It was also found that the first order decay rate of OAA under the assay conditions without enzyme is 1.25 h^{-1}. Consequently, OAA standards without enzyme must be run under the assay conditions so that the nonenzymatic decarboxylation of OAA can be accurately

Table 5.5 Effect of inhibitors on oxaloacetate decarboxylase activity in crude cell-free extract.

Inhibitor added	Activity*	% Inhibition
Standard Assay, #1	275	0
5 U/ml Avidin	287	-4
10 μg/ml Biotin	279	-1
100 μM P-Chloromercuribenzoate	155	44
10 mM NaF	242	12
10 mM 8-Hydroxyquinoline	201	27
100 μM Oxalate	177	36
Standard Assay #2	226	0
10 mM ATP	194	14
10 mM ATP + 1 U/ml Avidin	211	7
1 U/ml Avidin	269	-19

* in nmole/min/mg-protein

accounted for.

The activity of OAA was also assayed in cells that were cultured in SLB medium (Table 5.6) in which 20 g/l of glucose, acetate, or pyruvate were added. The activity of OAA from these cultures (not shown) was statistically identical to OAA activity from cultures grown in PMB medium. Since the activity of OAADC appears independent of the culture medium, it is probably a constitutive enzyme, which is consistent with results from *Pseudomonas ovalis* [Horton and Kornberg, 1964].

As a further characterization, the effects of several inhibitors on OAADC activity were investigated and are summarized in Table 5.5. The effects of avidin and biotin indicate that OAADC in *C. glutamicum* does not require biotin as a cofactor, which is similar to OAADC found in cod muscle [Schmitt *et al.*, 1966], but unlike that in *Salmonella typhimurium* [Wifling and Dimroth, 1989]. The presence of ATP does not appear to significantly effect OAADC activity, except for slight inhibition. The effects of the other inhibitors are similar to those observed for OAADC in rat liver mitochondria [Corwin, 1959].

Although it is possible the OAADC may be inhibited by AcCoA [Horton and Kornberg, 1964], this was not investigated. In general, more research is required to determine the *in vivo* function of OAADC.

5.4 Isolation of Modified Strains

Strains FPS009 (PDC^A) and NFG068 (GPI^A) were isolated from *C. glutamicum* ATCC 21253 for fermentation studies as explained below.

5.4.1 Mutagens

The first mutagen investigated was UV radiation, as this mutagen can produce a wide spectrum of mutations [Gerhardt *et al.*, 1981, p. 225]. A 4 Watt, short wave (254 nm) UV source is used (Spectroline Model EF-140C, Westbury NY), which is placed 22 cm above the sample. A survival rate curve is constructed as follows [also see Nakayama *et al.* (1961b)]. A seed culture of *C. glutamicum* ATCC 21253 is grown to an OD of 0.3, which corresponds to a cell density of 3×10^7 cells/ml (1.0 OD = 1×10^8 cells/ml, or 1 g-DCW = 4×10^{11} cells). The seed culture is separated into 5 ml aliquots, which are each centrifuged at 5000 × g for 5 min and resuspended in 2.5 ml diluent (50 mM $MgSO_4$) and transferred to sterile 100 × 15 mm glass petri dishes. Each petri dish sample is exposed to the UV source for 0 to 60 sec and kept under dim light to minimize photoreactivation. A 100 µl of an irradiated sample is spread, at the proper serial dilution to obtain 30 to 300 colonies per plate, on LB5G plates and incubated at 30°C until colonies can be counted (2-3 days). The survival curve for the above procedure is illustrated in the Figure 5.4 and indicates that a 25 to 30 sec exposure time is required to achieve a 0.1 to 1 % survival rate under the above conditions.

Cultures for isolation or selection studies are prepared as above, with the exception of one sample which is irradiated for 25 to 30 sec. A 100 µl sample of the irradiated culture is spread (after serial dilution) on LB5G plates as above to determine the survival rate, and 100 µl aliquots of the remaining culture are used to inoculate five to ten 10 ml LB5G culture tubes. To insure that each bacteria has a homogenous genome, the test tube cultures are grown in the dark for approximately 8 to 10 hours. After the outgrowth period, cell density in each culture tube is determined from colony counts. In the meantime, the cultures are stored at 4°C until the colonies are observable for counting (ca. 24 h). Cell density information is then used to determined the proper dilution necessary to obtain 50 to 100 colonies per

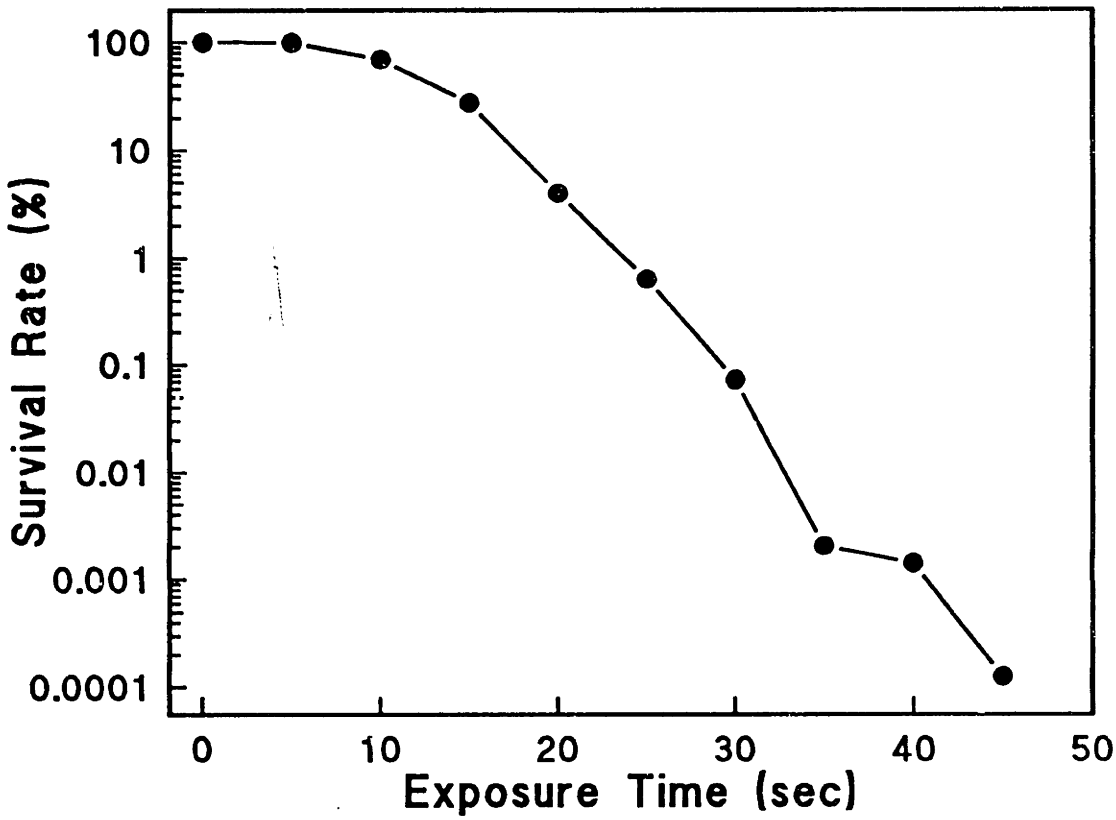

Figure 5.4 Survival curve for *C. glutamicum* ATCC 21253 exposed to UV radiation (254 nm) at an initial cell concentration of 4.8×10^7 cells/ml. See text for details.

plate. Viability of cultures that are maintained in suspension at 4°C for several days is approximately 50%.

To examine mutation rates obtained from UV irradiated samples, the stored cultures are spread on LB5G plates then replicated with RepliPlate transfer pads (FMC, Rockland ME) onto PMB plates. From approximately 4300 colonies, only 60 mutant colonies (or 1.4%) were unable grow on the PMB plates. Since several thousand *mutant* colonies must be tested for the realistic isolation of a desired strain, the UV induced mutation rate was considered too low. Consequently, N-methyl-N'-nitro-N-nitrosoguanidine (NTG) was used in place of UV radiation.

Mutants were derived from NTG as follows. A 50 ml seed culture of *C. glutamicum* ATCC 21253 is grown to an OD of 4.8 and transferred to five 15 ml centrifuge tubes. The samples are centrifuged for 5 min at 5000 × g and washed once with 10 ml of 0.1 M citrate buffer, pH 6.0. Four of the centrifuge tubes are

resuspended in 9 ml of citrate buffer, and the fifth tube (control) is suspended in 10 ml. To the four 9 ml tubes, 1 ml of 2 mg/ml NTG, dissolved in water and filter sterilized, is added. All five tubes are incubated at 30°C for 30 min, then washed three times with citrate buffer and resuspended in 10 ml LB5G medium. The four samples exposed to NTG are mixed together with 4 ml of sterile glycerol, to give a total volume 44 ml. One milliliter aliquots of the treated cells are placed in cryovials and stored at -40°C for future use. Colony counts from the control and the NTG exposed cells give a survival rate of 55%, and exhibit mutations rates in excess of 25%. All materials and liquids exposed to NTG are soaked in 0.1 N HCl to decompose the NTG.

For isolation studies, a vial of stock NTG treated cells is thawed and 100 µl samples are removed to inoculate five to ten culture tubes containing 10 ml of LB5G medium. These cultures are allowed to grow overnight.

5.4.2 Isolation of PDC^{A} Mutants

The isolation of *C. glutamicum* ATCC 21253 mutants with attenuated activity of the pyruvate dehydrogenase complex (PDC) is based on the work of Tosaka *et al.* (1985). Since fluoropyruvate (FP) is a strong competitive inhibitor of PDC, those strains which have reduced activity of PDC may not be able to grow in the presence of FP. Such strains are referred to as FP sensitive (FP^{S}). Isolation of FP^{S} strains is as follows.

After culturing an NTG treated stock of *C. glutamicum* in 10 ml of LB5G medium, the cultures are spun down and resuspended in 10 ml of PMB medium supplemented with 40 µM FP and 500 U/ml penicillin G to enrich FP^{S} strains. These culture tubes are incubated under agitation for 6 h, at which time 10 U of penicillinase is added to each culture tube and then incubated for another 1/2 h before being resuspended in 10 ml of LB5G medium. These cultures are then plated out on LB5G plates to determine cell density and stored at 4°C. After the cell density is determined, the cultures are plated out on LB5G plates to a density of 50 to 100 colonies per plate and replica plated with RepliPlate pads onto PMB plates and PMB plates supplemented with 50 µM FP. Colonies which exhibit growth on

PMB plates but not on the PMB plates supplemented with FP are examined for PDC activity.

Out of 2900 colonies examined, 13 exhibited sensitivity to FP at 50 μM. Of these 13 strains, 5 were cultured on SLB medium (Table 5.6) and assayed for PDC activity, the results of which are listed in Table 5.7. Of these strains, FPS009 exhibited a 98% attenuation of PDC activity and was selected for fermentation studies.

Table 5.6 SLB medium.

Component	g/l
Glucose	20
Tryptone	20
Yeast extract	15
NaCl	5

Table 5.7 Activity of PDC in selected FP^S mutants of *C. glutamicum* ATCC 21253.

Strain	PDC Activity*
ATCC 21253	27.9
FPS002	17.9
FPS008	25.4
FPS009	0.45
FPS012	21.2
FPS013	32.8

* in nmole/min/mg-protein

Although FPS009 will grow on PMB plates, its does not grow well in PMB suspension medium. However, if 5 g/l potassium acetate is added to the PMB suspension medium, then growth is significantly improved although it is still severely attenuated with respect to ATCC 21253. Growth stimulation by acetate addition supports the hypothesis that PDC attenuation is the growth limiting mutation.

5.4.3 Isolation of GPI^A Mutants

Isolation of *C. glutamicum* ATCC 21253 mutants with attenuated glucose-6-P isomerase activity (GPI^A) is based on the work of Fraenkel and Levisohn (1967), in which they selected GPI-lacking mutants of *E. coli* from mutants that exhibited impaired glucose assimilation. This selection precess is based on the premise that if a strain lacks GPI, then it must catabolize glucose via the pentose phosphate pathway which will impair growth. In their study, strains with impaired glucose assimilation

were identified as red colonies on tetrazolium indicator plates. However, it was found that growth of *C. glutamicum* is inhibited by the tetrazolium dye, so growth on other fermentation indicator plates was investigated.

To test fermentation indicator plates, three strains of *C. glutamicum*, ATCC 21253, FPS009, and MUT003, were employed. Strain MUT003 is an uncharacterized UV-induced mutant that will not grow on PMB plates where acetate or citrate is the primary carbon source and exhibits attenuated growth on glucose PMB plates. Strains FPS009 and MUT003 were chosen since they both exhibit impaired glucose assimilation rates compared to the parent strain, ATCC 21253. Two fermentation indicator plates, EMB [Lederberg, 1950] and PRED [MacFaddin, 1985, p. 620] (Table 5.8), were found to distinguish between ATCC 21253 and FPS009 or MUT003. When *C. glutamicum* ATCC 21253 is replica-plated from LB5G plates onto EMB plates, the colonies developed extremely slowly and exhibited an almost black appearance on the dark purple background. Colonies of ATCC 21253 never exceed 2-3 mm in diameter, and their attenuated growth is probably due to methylene blue and eosin Y, which are known to be inhibitory to gram positive organisms [MacFaddin, 1985, p. 294]. However, when either FPS009 or MUT003 are plated onto EMB plates, they both exhibit good growth and take on a light pinkish color on the dark purple background, and colony size is close to that observed on LB5G plates. Consequently, EMB plates were found to provide a satisfactory means of isolating mutants with attenuated glucose assimilation rates. Similarly, when ATCC 21253 is plated on PRED plates, the colonies developed as normal, but their growth turns the orange-colored agar to yellow, while FPS009 colonies turn the agar to a red color. Strain MUT003 did not affect the color of the agar. In all three strains, colony color remains pale yellow to white. Nevertheless, the PRED plates also provided a satisfactory indication of poor glucose fermentors.

The procedure for isolating GPI^A mutants of *C. glutamicum* ATCC 21253 is as follows. NTG treat stocks of *C. glutamicum* are thawed and 100 µl samples are removed to inoculate twelve 10 ml LB5G culture tubes that contained 2.5 g/l glucose plus 2.5 g/l fructose instead of 5 g/l glucose. The cultures are grown, plated and stored at 4 °C as explained above. After cell densities are determined, 100 µl

Table 5.8 Fermentation indicator plates.

EMB Plates		PRED Plates	
Component	(g/l)	Component	(g/l)
Glucose	10	Glucose	10
Tryptone	8	Tryptone	10
Yeast extract	1	Yeast extract	1
NaCl	5	NaCl	5
K_2HPO_4	2	Phenol red	0.020
Eosin Y	0.4	Agar	18
Methylene blue	0.065	pH	7.2
Agar	18		

samples, at the appropriate dilution, from each culture tube are spread on four EMB and four PRED plates, producing a total of 96 plates at a colony density of 50 to 200 colonies per plate. Colonies are then examined for their ability to ferment glucose.

Out of approximately 11,000 colonies, 96 exhibited some extent of attenuated ability to ferment glucose on the EMB or PRED plates. Each of the 96 non-fermenting glucose (NFG) strains were isolated and streaked on four PMB plates that contained either glucose, fructose, gluconate or malate as the sole carbon source. The isolation philosophy was that strains that have attenuated activity of GPI will grow slowly on glucose and malate plates, but rapidly on fructose and gluconate plates since the assimilation of gluconate and fructose does not require GPI. However, unlike *E. coli* [Fraenkel and Levisohn, 1967], none of the isolated NFG strains exhibited the desired phenotype. Instead, strains were selected that exhibited good growth on gluconate, but attenuated growth on glucose, and variable growth on fructose or malate. Of the 96 NFG strains, 9 exhibited the desired traits and were cultured in SLB medium, supplemented with 10 g/l fructose and 10 g/l potassium gluconate, and assayed for GPI activity. The results are illustrated in Table 5.9.

Of the 9 strains assayed, only one (NFG068) exhibited attenuated GPI activity. This strain was reassayed for GPI as well as other NADPH producing enzymes, the results of which are listed in Table 5.10. Although activity of GPI, G6PDH, and possible ICDH, appear to be inducible by gluconate, the assays indicate that GPI in NFG068 is only approximately 7% as active as GPI in ATCC 21253. Growth studies

Table 5.9 Activity of GPI in mutant strains of *C. glutamicum* ATCC 21253.

Strain	Activity*
ATCC 21253	1051
NFG006	830
NFG013	1191
NFG021	1015
NFG058	1009
NFG068	178
NFG070	1270
NFG071	982
NFG079	889
NFG087	962

* in nmole/min/mg-protein

on NFG068 have shown that this strain grows well on gluconate, poorly on glucose, and almost not at all on fructose or malate PMB plates. Furthermore, revertants have not been observed, which indicates that the mutation is fairly stable. Although EMB plates are better indicators of glucose fermentation mutants, NFG068 was isolated from a PRED plate.

Table 5.10 Activity of selected enzymes in *C. glutamicum* ATCC 21253 and NFG068 cultured on various media.

Strain	Medium	Activity* GPI	G6PDH	ICDH
ATCC 21253	PMB	966	107	--
NFG068	PMB	67.6	170	--
NFG068	SLBG†	180	210	1194
NFG068	SLB	37.8	155	852

* in nmole/min/mg-protein
† SLB with gluconate•K instead of glucose

5.5 Fermentations

5.5.1 Equipment and Configuration

The fermentor and associated equipment configuration is illustrated in Figure 5.5.

5.5.1.1 Fermentor

All fermentations were carried out in a MBR Laboratory Bioreactor equipped with an MCS 10 control unit and donated to our laboratory by MBR Bio Reactor AG (division of Sulzer Bros., Inc., Wetzikon, Switzerland). The vessel is of stainless steel with a 19.5 cm inner diameter and has a capacity of 15 l and a working volume of approximately 12 l. The vessel is equipped with one 25 mm bottom port that is occupied by a steam sterilizable harvest/drain valve and four 25 mm side ports which are occupied by a temperature probe, a pH probe, a dissolved oxygen probe, and a steam sterilizable sampling valve. The stainless steel head plate has five 19 mm and eight 12 mm ports through which air, base, antifoam, and supplementary components are added by 5 and 8 mm (dia.) hypodermic needles. The center 19 mm port is occupied by a reflux cooler (condenser) and an exhaust air filter assembly which is stuffed with cotton. A vessel pressure gauge and air sparger occupy two 19 mm ports, and a 1.5 bar safety valve occupies a 12 mm port. Agitation is by direct drive in which vessel integrity is maintained by a double mechanical seal that is steam sterilizable. Four six-blade Rushton-type impellers are mounted on the impeller shaft and a baffle assembly is mounted to the vessel wall. The vessel is sterilized in place and temperature control for both cultivation and sterilization is maintained by a water jacket that is built into the vessel's outer wall. The entire vessel assembly sits atop two load cells which are calibrated to monitor the weight of the liquid within the vessel. Steam for sterilizing the sample valves and the mechanical seal is supplied externally by a steam generator model PP-4 (Steamaster Co., Inc., Rutherford NJ), also donated by MBR Bio Reactor AG.

5.5.1.2 Probes and Controllers

The MCS 10 control unit is equipped with amplifiers and controllers for temperature (PID), impeller shaft rpm (PI), pH (PI), dissolved oxygen (PID), and load cell (PID). The temperature probe is supplied by MBR and temperature

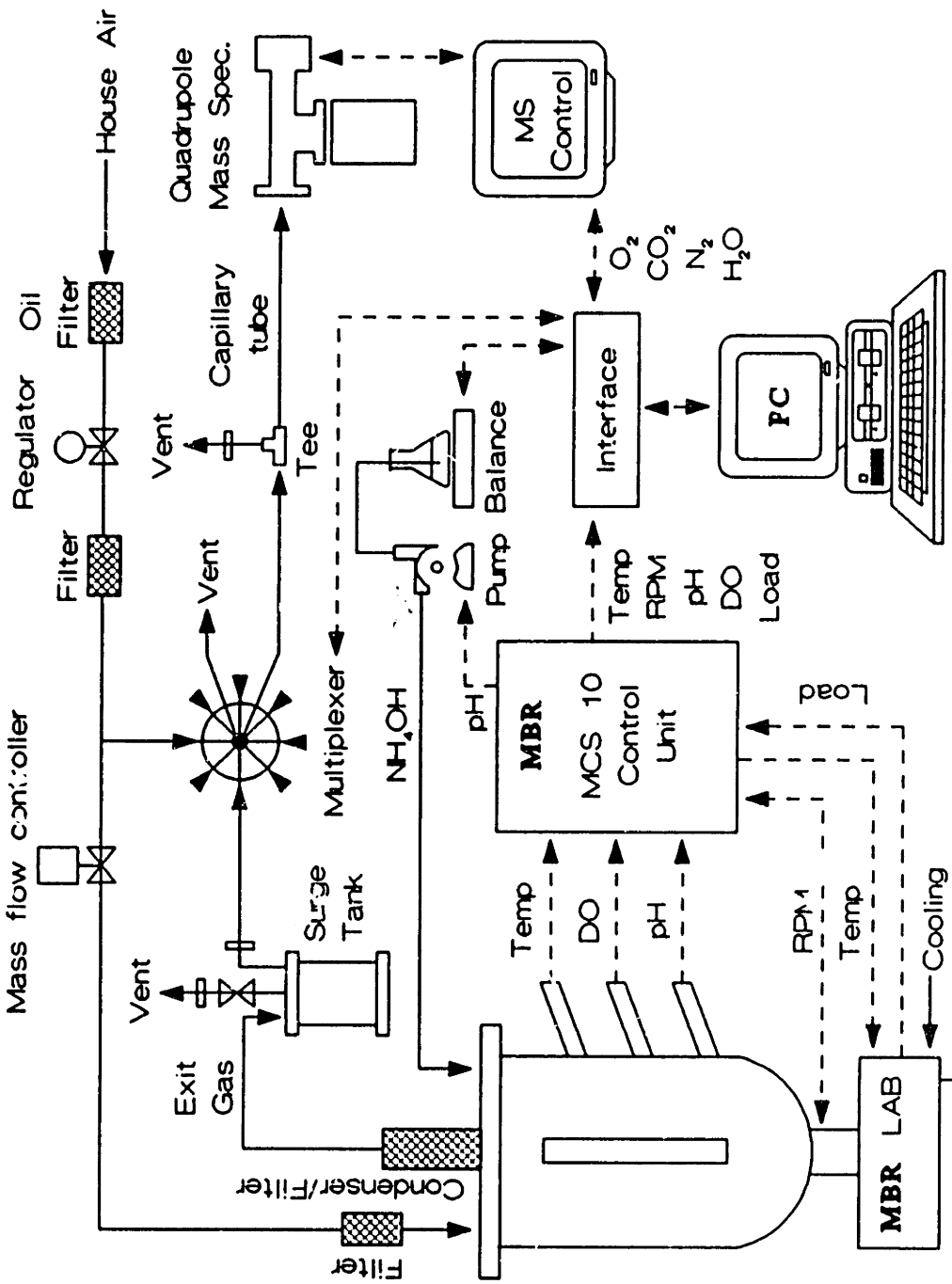

Figure 5.5 Fermentation equipment and configuration. Solid lines represent physical connections and dashed lines represent control or sensor signals.

control is accomplished by either heating the water that circulates in the outer shell or by exchanging it with external cooling water. The impeller drive motor is equipped with a tachometer such that impeller shaft speed is directly controlled. The pH probe is from Ingold (Ingold Electrodes Inc., Type 765, Wilmington MA) and is equipped with a pressure chamber (Type 764-31) that allows the probe to be sterilized in place. The pH probe is calibrated at pH 4 and 7 with standard buffers. An MBR peristaltic pump, which is controlled in an on-off manner by the MBR pH controller, is used for the addition of ammonium hydroxide (26% (w/w) NH_3) to maintain proper pH. To minimize loss of NH_3 in exit gas and delays caused by holdup of NH_4OH on foam, NH_4OH is added directly to the fermentation broth through an immersed MBR chemostat tube. A sterile connection to the chemostat tube is made with a 5 mm MBR hypodermic needle through a rubber diaphragm and Masterflex C-Flex tubing, size 14 (Cole-Parmer, Chicago IL) connects the needle to the NH_4OH vessel. Although the tubing and needle are separately autoclaved, the NH_4OH and its container are not. The weight of NH_4OH added for pH control is monitored by an Ohaus G 4000-S0 balance (Ohaus Scale Corp., Florham Park NJ). Dissolved oxygen is measured with a sterilizable 25 mm Ingold O_2 electrode (No. 322756800), which is calibrated to 0% air saturation during sterilization and to 100% air (ca. 3-4 psig) saturation under gas sparging, prior to inoculation. Although possible, dissolved oxygen is not controlled. The fermentor load cell is provided by MBR and the load cell reading is adjusted to match the weight of the fermentation broth added prior to inoculation.

5.5.1.3 Off-Gas Analysis

Equipment setup for the monitoring of culture oxygen uptake rate (OUR) and carbon dioxide evolution rate (CER) is closely based on that described by Coppella and Dhurjati (1987). Building-supplied air is passed through an oil filter and regulator (Johnson Controls, Milwaukee WI) which is adjusted to deliver air at 20 psig. Following the regulator, air flows through a 5 Å molecular sieve filter (Pierce Chemical Co., Rockford IL) and a 0.2 μm particle filter (No. 6164-T4, Matheson Gas Prod., Gloucester MA) before entering a 5850E mass flow controller (Brooks Instrument Division, Hatfield PA), that is calibrated for N_2, has a maximum

throughput of 20 l/min at 21.1°C and 14.7 psia, and is controlled and powered by a Brooks Model 5878 controller. The metered air is sterilized through a 0.2 μm filter (No. 12122, Gelman Sciences Inc., Ann Arbor MI) before entering the fermentor air-sparger via a 8 mm hypodermic needle connection through a head plate port. Fermentor exit gas is passed through the reflux condenser and filter assembly and into a 0.6 l surge tank as described by Coppella and Dhurjati. A pressure relieve valve on the surge tank maintains a 3-4 psig back pressure on the fermentor, which provides a 1 to 2 l/min gas flow rate to a E3SC8P multiplexer valve (Valco Instruments Inc., Houston TX) whose temperature is controlled at 110°C (ITC10399 Valco). The multiplexer valve is computer controlled and allows the simultaneous monitoring of off-gas from more than one fermentor (currently, two fermentors have been successfully connected). The gas stream selected by the multiplexer enters a standard pipe tee, of which one end is vented through a bacterial filter (No. 4210 Gelman Sciences) to the laboratory and the other end is connected to a 1 m × 50 μm ID fused silica capillary tube (25VS-050 Scientific Glass Engineering Inc., Austin TX) that leads to the mass spectrometer. The capillary tube provides the required pressure drop to the Dycor quadruple mass spectrometer (Ametex, Thermox Instruments Division, Pittsburgh PA) which is employed to measure ion currents at mass to charge ratios of 44, 32, 28, and 18, that are generated by CO_2, O_2, N_2, and H_2O, respectively, in the gas stream (other mass to charge channels were not utilized; see Coppella and Dhurjati for details). The mass spectrometer is calibrated as described by Coppella and Dhurjati where the gas mixture typically employed consists of 2% CO_2, 20% O_2, and the balance N_2 (Matheson). For our setup, we typically obtained a S2844 split ratio of 0.060, and O_2 and CO_2 response factors of 1.045 and 0.47 respectively. See Section 5.5.4.1 for OUR and CER calculations.

5.5.1.4 Data Acquisition

Isolated signals (isolation amplifiers from MBR) from the MBR MCS 10 control unit for medium temperature, impeller RPM, dissolved oxygen, medium pH, and fermentor load are communicated to an IBM PC (WYSE clone) via A/D channels (differential) on a DT2801 Data Translation (Marlboro MA) board that is plugged into one of the expansion slots of the PC. Communications between the PC

and the Valco multiplexer valve is via the digital channels on the DT2801 board. A Data Translation DT707 screw terminal board is used to make the physical connections between the DT2801 board and the peripheral equipment. Standard RS232 serial communication lines are used to connect the Ohaus balance and the Dycor mass spectrometer controller to the PC.

A copy of a fermentation monitoring program written to interface with the Dycor mass spectrometer (STEVE and STEVE2) was obtained from Steve Coppella (Department of Chemical Engineering, University of Delaware, Newark DE) and was modified [Kiss, in preparation] to better meet our needs. This program, which runs on a IBM PC or clone, simultaneously monitors and stores on-line variables from up to four fermentations and graphically displays selected variables in real-time. The program also calculates OUR and CER from the raw mass spectrometer data (see Section 5.5.4.1).

5.5.2 Fermentation Procedures

All the fermentations were conducted in batch mode under basically the same conditions as that described below for the control fermentation. The specifics of each fermentation are detailed in Section 5.5.5.

5.5.2.1 Fermentation Medium

The standard fermentation medium (FM4: listed in Table 5.11) is designed to produce 10.0 l of medium after the addition of a 1.0 l inoculum. This medium is similar to the PMB medium, except that all components (with the exception of phosphate and citrate) have been significantly increased so that higher cell densities can be achieved. Glucose and ammonium sulfate concentrates have been raised to 150 g/l and 40 g/l, respectively, so that high lysine titers can be attained. The medium is designed such that threonine is the limiting nutrient, and methionine and leucine are in excess. Based on the amino acid composition *C. glutamicum* [Kimura, 1963], each of the supplied amino acids should support exponential growth to 7.3 g DCW/l (if Thr+Ile limiting), 56 g DCW/l (if Met limiting), and 32 g DCW/l (if Leu limiting) of biomass. However, since biomass can increase after a limiting amino acid is depleted [Tonnies, 1965], these biomass yields do not reflect attainable final biomass

titers. In most fermentations, exponential growth terminates at approximately 10 g DCW/l biomass, but continues to a final value of 17-18 g DCW/l (see Section 6.1.1).

Table 5.11 Fermentation medium FM4.

Part A: in fermentor			Part B: separate		
Component	Amount		Component	Amount	
Glucose	1500	g	K_2HPO_4	40	g
Citric Acid	10	g	KH_2PO_4	20	g
$MgSO_4 \cdot 7H_2O$	6	g	Threonine	7.33	g
$FeSO_4 \cdot 7H_2O$	500	mg	Leucine	15	g
NaCl	20	g	Methionine	6	g
$CaCl_2$	1	g	Biotin	10	mg
100x Mineral Salts†	200	ml	Thiamine•HCl	20	mg
Antifoam PEG 2000	10	ml	$(NH_4)_2SO_4$	400	g
pH	3-4		Volume	2	l
Volume	7	l			

† See Table 5.2.

Even though ammonium sulfate concentration is high and ammonium hydroxide is used for pH control, it is still possible that ammonium may limit lysine synthesis if it is produced at high yields. This can occur because NH_4OH added does not completely compensate for $(NH_4)_2SO_4$ consumed for lysine production. For example, if lysine is produced solely from added NH_4OH, as shown here (50% lysine yield)

$$2 \text{ Glucose} + 2 NH_4OH + 5 O_2 \rightarrow \text{Lysine} + 6 CO_2 + 10 H_2O$$

the net result is an increase in pH since lysine is basic. Consequently, base addition will stop and NH_4 will be consumed from $(NH_4)_2SO_4$, which will result in H_2SO_4 production. As a result, a net consumption of $(NH_4)_2SO_4$ will occur during lysine production. Nevertheless, in all fermentations conducted (except the *B. flavum* run), ammonium sulfate did not become limiting. It is important to realize that the

medium has not been optimized for lysine production. See Section 5.5.5.1 for further discussion on medium design.

The fermentation medium is made in two parts (Table 5.11), of which Part A is sterilized at 121 °C in the fermentor for 40 min. Part B of the medium is sterilized separately for 30 min, and aseptically added to the fermentor via a 8 mm hypodermic needle after both media have sufficiently cooled. The antifoam used is poly(propylene glycol) with an average molecular weight of 2000 (Polysciences, Inc., Warrington PA), and the amino acids and vitamins are from Sigma (St. Louis MO). Glucose used is anhydrous and obtained from J. T. Baker, Inc. (Jackson TN). Undiluted ammonium hydroxide (29% NH_3, but slightly lower when assayed) (Mallinckrodt, Inc., Paris, KY) is used as the base for pH control. Additional antifoam is also autoclaved in a 20 cc disposable syringe which is connected to an MBR 5 mm hypodermic needle. This syringe is connected to the head plate of the fermentor and antifoam is added (in 1 ml aliquots) as needed in the later stages of the fermentation to keep foam from being entrained in the exit gas. Similarly, for inhibitor studies, the dissolved inhibitor is added to the fermentor at the appropriate time via a syringe connected to a MBR 5 mm hypodermic needle that is inserted in the head plate (also see Section 5.5.5.2).

5.5.2.2 Cultivation

All fermentations are inoculated from a 1 l preculture that is cultivated in a 4 l triple baffled shaker flask for 8 to 10 h, as described in Section 5.1.2. The preculture is inoculated with a 50 ml seed culture that is grown for 10 h. Prior to fermentor inoculation, the preculture is examined for contamination, and a sterile syphon tube connected to a 8 mm MBR hypodermic needle is aseptically connected to the preculture flask. The inoculum is then driven into the fermentor under 3-4 psig of air pressure.

All fermentations are conducted at 30°C, pH 7, and under 3-4 psig of back pressure. Air flow rate is controlled at 10 l/min (1 VVM) at 21.1°C and 14.7 psia. Impeller speed is kept at 1000 RPM during exponential growth and is increased in 100 RPM increments if DO falls below 10% of saturation. Following exponential growth, impeller RPM is sometimes lowered to reduce foaming problems. Dissolved

oxygen usually ranges between 40 and 80% of saturation following exponential growth.

5.5.2.3 Sampling

Samples are removed as required from the fermentor via the side port sample valve that has been sterilized with steam after the previous sample, such that the sample valve is cool when a sample is removed. To remove stagnant fluid in the sample valve, the first 10 to 15 ml of sample removed is discarded. The collected sample is measured for optical density at 660 nm (properly diluted with water) against a water bank, and the remainder of the sample is divided into several parts for subsequent assays. To determine dry cell weight (see Section 5.5.3), a 20 ml aliquot of the sample is removed. For extracellular metabolite assays, approximately 10 ml of the sample is centrifuged at 5000 × g for 5 min to remove the cells, then the supernatant is passed through a 0.22 μm Millex-GV filter (Millipore, Bedford MA) and stored at -20°C. For intracellular protein and enzyme assays, the bacteria in 50 ml of a sample are pelletized at 5000 × g, then washed twice in extract buffer (Section 5.2.1) and resuspended in 15 ml of the same buffer before being stored at -20°C. For biomass elemental analysis, biomass in 40 ml of a sample is pelletized, washed twice with water, then stored as a pellet at -20°C.

5.5.3 Off-Line Measurements

5.5.3.1 Dry Cell Weight and Elemental Analysis

A 20 ml aliquot of a fermentation sample is centrifuged at 5000 × g for 5 min and the supernatant is discarded (or filtered and used for metabolite assays). The pellet is washed twice with water and resuspended in approximately 5 ml of water, then transferred to a pre-weighed aluminum weighing boat and placed in a 80°C oven for 24 h. Following the drying period, the boat is reweighed to determine dry cell weight. During exponential growth, the correlation between DCW and OD is given by: DCW = 0.28 OD_{660} (see Figure 6.5 (A)).

To determined elemental composition of *C. glutamicum* ATCC 21253 during a fermentation, biomass pellets stored at -20°C were lyophilized for 12 to 18 h to

remove water, then sent to MultiChem Laboratories, Inc. (Lowell, MA) for analysis of carbon, hydrogen, oxygen, and nitrogen content.

5.5.3.2 HPLC measurements

An HPLC system, consisting of a Waters (Bedford MA) 501 pump, 680 pump controller, Wisp 710B automatic injector, R401 refractive index detector, a Shimadzu C-R3A integrator (Kyoto, Japan), and a Biorad (Rockville Centre NY) column heater and columns (types discussed below), is used to determine the concentration of several components in the filtered fermentation broth sample. All chromatograms are run in an isocratic mode.

A Biorad Aminex HPX-87H reverse phase column is used to measure glucose, gluconate, trehalose, acetate, and lactate. The column is run at 45°C with a mobil phase consisting of 0.27 ml of concentrated sulfuric acid (96%) per liter of Omnisolv HPLC water (EM Industries, Inc., Gibbstown NJ) and at a flow rate of 0.6 ml/min. The mobil phase is prepared fresh for each run and is degassed and filtered through a 0.45 μm MF-Millipore filter prior to use. A sample injection volume of 30 μl is used. Although pyruvate is normally separated by the HPX-87H column, the large glucose peak associated with the FM4 medium interferes with the pyruvate peak, which renders pyruvate quantification unreliable. As a result, pyruvate is determined with the same enzymatic assay used to measure pyruvate in the oxaloacetate decarboxylase assay discussed in Section 5.2.2.8. To quantify gluconate in the presence of glucose (which has the same column residence time as gluconate), glucose concentration is determined with an enzymatic assay kit (No. 16-20, Sigma) and then subtracted from gluconate concentration overestimated from the HPLC chromatogram. Since fermentation samples must be diluted to measure glucose concentration with the HPLC, the sigma glucose assay kit is sometimes used in place of the HPLC glucose measurement.

A Biorad Aminex HPX-87C reverse phase column is used to measure trehalose, alanine, valine, leucine, and threonine in the fermentation sample. The column is run at 85°C with a mobil phase consisting of 5 mM $CaSO_4$ in Omnisolv HPLC water and at a flow rate of 1.0 ml/min. The mobil phase is prepared as above, and a sample injection volume of 30 μl is used.

The polysaccharide separated by the HPX-87H and HPX-87C columns was identified as trehalose since incubating the fermentation sample with trehalase (T 8778 Sigma) resulted in a reduction of the trehalose peak and an increase in the glucose peak. It should be noted that a second di- or trisaccharide peak often emerges close to the trehalose peak on the HPX-87C column for samples taken from the later phases of the fermentation.

Samples taken in Phase IV of the fermentation, and run on either column, often produce one or two chromatogram peaks that cannot be identified; however, they indicate the accumulation of small (3-carbon) organic acids at a level of 1-5 g/l by the end of the fermentation. As a result, rate vectors calculated from data obtained in Phase IV of the fermentation are often inconsistent.

5.5.3.3 Lysine and Glutamate

Lysine is measured enzymatically by the method described by Nakatani *et al.* (1972), which is based on the NADH plus α-ketoglutarate dependent conversion of lysine to saccharopine by saccharopine dehydrogenase.

To a 4.0 ml cuvette add:

2.5 ml	250 mM	Phosphate buffer, pH 6.8
100 µl	6.4 mM	NADH in phosphate buffer
100 µl	137 mM	α-Ketoglutaric acid
100 µl	<2.7 mM	Lysine sample, standard or blank (water)

Read absorbance at 340 nm against buffer (A_1), then add:

20 µl	25 U/ml	Saccharopine dehydrogenase (Sigma S 3633)

Reread absorbance 35 min later (A_2).

Although lysine concentration could be determined from the extinction coefficient of NADH, this is not typically done since the presence of NADH oxidase in the saccharopine dehydrogenase coupled with the long incubation period can skew the results. Instead, a standard curve is constructed at the following lysine•HCl concentrations: 0, 0.1, 0.25, 0.5 g/l. Dissolved saccharopine dehydrogenase (in water) is stored in 1 ml aliquots at -40°C.

Glutamic acid is measured with an enzymatic kit from Boehringer Mannheim Cat. No. 139 092 (Indianapolis IN). Since glutamic acid was not detected in the control fermentation, it was not assayed for in subsequent fermentations.

5.5.3.4 Ammonium

Although the ammonium assay was initially based on a phenol reaction [Weatherburn, 1967], it was later assayed enzymatically with glutamate dehydrogenase as follows:

To a 4.0 ml cuvette add:

1.68 ml		Water
1.0 ml	Buffer	0.5 M triethanolamine•HCl, plus 35 mM α-ketoglutarate, pH 8.0
100 µl	6.4 mM	NADH in 119 mM $NaHCO_3$
20 µl	<33 mM	NH_4 standard or sample

Read absorbance at 340 nm against blank (1 ml buffer, 2 ml H_2O), then add:

20 µl	1200U/ml	Glutamate dehydrogenase (Sigma G 7882) in 50% (v/v) glycerol

Reread absorbance at 340 nm after 10 min.

To improve accuracy, a standard curve, based on ammonium sulfate (0, 0.5, 1.0, and 1.5 g/l) is used to estimated ammonium in sample.

5.5.3.5 Citrate

Citrate assay is based on that of Mollering (1985), in which the sample is incubated with citrate lyase and the pyruvate and oxaloacetate formed are spectrophotometrically determined with lactate and malate dehydrogenases.

To a 4.0 ml cuvette add:

1.65 ml		Water
1.0 ml	0.5 M	Glycylglycine, 0.6 mM $ZnCl_2$, pH 7.8
100 µl	100 U/ml	Lactate dehydrogenase (Sigma L 1254)
100 µl	100 U/ml	Malate dehydrogenase (Sigma M 9004)
100 µl	10 mM	NADH in water
50 µl		Sample or blank

Read absorbance at 340 nM (A_1) after any pyruvate or oxaloacetate present in sample have been consumed, then add:

20 µl 40 U/ml Citrate lyase (Sigma C 0897)

Reread absorbance at 340 nm (A_2) after 10 min.

Citrate concentration is determined either from a standard curve, or based on the extinction coefficient of NADH.

5.5.4 Rate Calculations

Calculation of metabolite accumulation rates from the raw measurement data, required for the BRNE, are presented in this section.

5.5.4.1 OUR and CER

Oxygen uptake rate and carbon dioxide evolution rate are calculated from the following equations

$$OUR = \frac{F^{i}_{AIR}}{V}\left[y^{i}_{O_2} - \frac{y^{i}_{N_2}}{y^{o}_{N_2}} y^{o}_{O_2}\right] \tag{5.2}$$

$$CER = \frac{F^{i}_{AIR}}{V}\left[\frac{y^{i}_{N_2}}{y^{o}_{N_2}} y^{o}_{CO_2} - y^{i}_{CO_2}\right] \tag{5.3}$$

where F^{i}_{AIR} is the air inlet rate (in mmole/h), V is the fermentor volume, and y are the gas phase mole fractions of O_2, CO_2, and N_2 in the inlet (i) and exit (o) streams. At air flow rate of 10 l/min (21.1°C and 14.7 psia), F^{i}_{AIR} = 24847 mmole/h. The volume of the fermentor during the course of the fermentation is obtained from the MBR load cell. Although the load cell reading is fairly noisy, the signal is easily smoothed (Fig.P, Biosoft, Milltown NJ) after the fermentation.

As discussed by Coppella and Dhurjati (1987), the Dycor quadrupole mass spectrometer does not report mole fractions, rather it gives ion currents at a particular atomic mass unit (AMU, or mass-to-charge ratio). Consequently, response factors for selected AMUs must be backed out from a standard gas of known composition. Furthermore, the operation is based on some assumptions implicitly invoke by Coppella and Dhurjati and discussed in more detail below.

The response factor for water is assumed to be 1.0. If it is significantly different than 1.0, then the gas phase mole fractions will be corrupted. Coppella and Dhurjarti's statement that the response coefficient is "absorbed by Henry Law constant" is misleading. The second assumption made is that all significant components in the gas phase are measured; otherwise, the calculated mole fractions will be overestimated. It is easy to show that OUR and CER are overestimated by a factor of $1/(1-y_U^i)$, where y_U^i is the sum of the mole fractions for all the unaccounted for species in the feed gas (exit gas does not matter). For example, we only measured AMU channels that corresponded to O_2, CO_2, N_2, and H_2O. Fortunately, in our fermentation y_U^i appears to be negligible, even if only these four components are measured. Furthermore, the response factor of 1.0 for water does not produce significant errors, since the estimated composition of air is acceptable, even though the instrument is calibrated with a gas consisting of 2% CO_2, 20% O_2, and the balance N_2, not air.

We have encountered significant sensitivity problems in OUR with the factory settings on the Dycor mass spectrometer. The sensitivity of OUR with respect to the O_2 mole fraction (ΔOUR) at an air flow rate of 1 VVM is given approximately by: $\Delta OUR \approx -25\, y_{O2}^g\, E(y_{O2}^g)$, where $E(y_{O2}^g)$ is the percent error in the y_{O2}^g measurement. Hence, a 1% error in y_{O2}^g produces an error in OUR of 5 mmole/l/h, provided the mole fraction of O_2 in the exit gas is close to that of air. Furthermore, errors in the nitrogen measurement increase the errors in OUR. Although Dycor states that their instrument has a peak stability at a particular AMU of 2% (already quite large), we estimate errors closer to 5% or more under the factory setting. Since such errors are unacceptable for OUR measurements, we had to dramatically alter the factor setting for HI RES, HI POS, and LO SENS, to attain acceptable errors (ca. 1%) in peak

height. The improvement in sensitivity was attained at the expense of selectivity since base peak widths were broadened from 1 AMU to approximately 4 AMUs. Fortunately, good selectivity is not required for air composition measurements.

It is possible that Coppella and Dhurjati did not observe these sensitivity problems since they were using an air flow rate of 0.125 VVM, which is too low for typical aerobic fermentations. Although we were able to properly adjust the instrument to obtain acceptable results, we believe that the Dycor mass spectrometer lacks the precision required for OUR and CER measurements. For acceptable OUR and CER measurements, the mole fractions must have a precision of 1%, and preferably 0.1%. For the consistency analysis routine, a standard deviation of 10% of the mean is used for OUR and CER.

5.5.4.2 Metabolites

For all metabolites dissolved in the medium, excluding ammonium, accumulation rates are derived from the slope of a straight line connecting two sequential concentration data points. Although other interpolation methods were examined, they did not yield improved results and could not be generally applied. Standard deviations associated with the accumulation rate estimates (σ_i) are propagated from the standard deviation associated with the concentration measurements as follows

$$\sigma_i(\Delta t/2) = \frac{\left[(C_i(t_1)\,\xi_i)^2 + (C_i(t_2)\,\xi_i)^2\right]^{1/2}}{t_2 - t_1} \qquad (5.4)$$

where $C_i(t_1)$ is the concentration of metabolite i at time t_1 and ξ_i is the fractional standard deviation associated with its measurement. Errors assumed in the primary measurements are listed in Table 5.12. Errors associated with the accumulation rates of by-products (alanine, valine, lactate, etc.) are assigned a fixed value to account for the difficulties in the initial detection of these metabolites and to account for slight accumulation of unidentified metabolites, as discussed in Section 6.1.3.

The accumulation rate and error for the ammonium measurement is calculated as above, except the rate is adjusted to account for the addition of NH_4OH for pH control. The rate of NH_4OH addition is readily accounted for since the weight of NH_4OH added and the volume of the fermentor are monitored. No error is assumed in this correction factor. It should be noted that the error associated with the ammonium accumulation rate is often quite large since $(NH_4)_2SO_4$ concentration in the fermentor is quite high and does not change significantly during the fermentation. In retrospect, if the concentration of $(NH_4)_2SO_4$ in the FM4 medium was reduced, the error propagated into the rate calculation could be significantly reduced.

Table 5.12 Standard deviations associated with measurements.

Metabolite	$100 \cdot \xi_i$
Biomass	5
CER	10
Glucose	2
Gluconate	2
Lysine	2
NH3	5
OUR	10

5.5.5 Individual Fermentations

Details associated with the various fermentations are discussed in this section.

5.5.5.1 Control Fermentations

Three control lysine fermentations (F#2-4) were conducted to ensure that threonine is the limiting nutrient in the FM4 medium. The first fermentation (F#2) was conducted with a medium basically identical to the PMB medium (Table 5.2), except that the concentrations of Thr, Leu, and Met were increased to 0.733, 0.975, and 0.395 g/l, respectively. In this fermentation, lysine production started at a biomass concentration of approximately 10 g DCW/l, and reached a final lysine•HCl titer of 14 g/l. Maximum biomass titer observed was approximately 13 g DCW/l, but decayed to a final value of 7.5 g/l. Since the supplemental addition of Mg and Ca

improved respiration, it is believed one of these two elements may have been limiting. Indeed, shaker flask studies indicated that the biomass yield on Mg and Ca are 63 and 3 μmole/g-DCW, respectively, which supports the hypothesis that fermentation F#2 may have been Mg limited. Biomass samples from the F#2 fermentation were also analyzed for elemental composition, as listed in Table 5.13.

Table 5.13 Biomass elemental composition during control lysine fermentation F#2.

Culture: Phase & Time (h)		Biomass Elemental Composition (%w/w) Carbon	Hydrogen	Oxygen	Nitrogen
I	11.2	47.7	6.46	31.0	11.8
II	16.0	47.1	6.43	31.9	10.9
IV	49.5	45.2	6.59	31.1	11.4
IV	75.0	45.5	6.65	30.4	11.8

In the second control fermentation (F#3), the concentrations of NaCl, $CaCl_2$, 100x minerals salts, biotin and thiamine were doubled, $FeSO_4 \cdot 7H_2O$ was increased 2.5 times to 50 mg/l, and $MgSO_4 \cdot 7H_2O$ was quadrupled to 0.8 g/l. This fermentation also started producing lysine at approximately 10 g DCW/l of biomass; however, maximum biomass titer reached 18 g DCW/l and the final lysine•HCl titer was 18.3 g/l. Final biomass titer was 12.6 g DCW/l. The results from this fermentation indicated that one or more of the increased components might have been slightly limiting in the F#2 fermentation.

In the final control lysine fermentation (F#4), the concentrations of Leu and Met were increased; however, phosphate concentration was dropped slightly (see Table 5.11), so that the amino acids would dissolve in Part B of the medium. Also $MgSO_4 \cdot 7H_2O$ was lowered to 0.6 g/l since biomass titer in fermentation F#3 did not dramatically increase. The results obtained from this fermentation, presented in Chapter 6, are basically identical to fermentation F#3. Consequently, it was concluded that threonine is the limiting nutrient in the FM4 medium. It should be noted that the only component in the FM4 medium not significantly increased compared to the PMB medium is phosphate.

5.5.5.2 Inhibitor Experiments

Three fermentations (F#5, F#11, and F#12) were conducted under conditions identical to the control lysine fermentation F#4, except that at the start of lysine production (indicated by the drop in respiration), one of the following inhibitors was added: F#5, fluoropyruvate•Na•H_2O (Sigma); F#11, fluoroacetate•Na (Sigma); F#12, arsenite•Na. The FP and FAc were dissolved in water at concentrations of 100 and 167 g/l, respectively. Arsenite was dissolved in 1 N HCl at a concentration of 260 g/l. All inhibitors were filter sterilized and added to the fermentor via a syringe as described in Section 5.5.2.1. It should be emphasized that FAc and arsenite are extremely toxic and must be handled with care.

5.5.5.3 Gluconate Fermentation

Two gluconate fermentations were conducted in which the primary carbon source was potassium gluconate (Sigma). The first fermentation (F#8) was conducted under conditions identical to the control fermentation, except that potassium gluconate was used in place of glucose in the seed, preculture, and fermentation media (FM8 medium). In the second fermentation (F#9), the standard seed culture was used; however, the preculture medium (PMB) was modified to contain 10 g/l glucose, 20 g/l gluconate•K, and no citrate. The standard fermentation medium (FM4) was modified to contain 10 g/l glucose, 140 g/l gluconate•K, and no citrate (FM9 medium). Glucose was sterilized separately. All other conditions were the same as the control fermentation.

5.5.5.4 Strains FPS009 and NFG068

The fermentations of the *C. glutamicum* strains FPS009 (F#6) and NFG068 (F#10) were conducted under the same conditions and media as the control fermentation; however, acetate and gluconate were added during the F#6 and F#10 fermentations, respectively, to stimulate growth, as discussed in Chapter 6.

5.5.5.5 *Brevibacterium flavum* Fermentation

The fermentation (B3) of the industrial *B. flavum* strain was as follows. The fermentation was conducted in two main stages. A 500 ml preculture was used to inoculate a 10 l subculture run in the fermentor at 30 °C, at an air flow rate of 1.5 VVM, and without pH control, for 16-20 h. At the end of the subculture, 5 l of

fermentation broth was removed and replaced with 5 l of production culture medium (CM3), which defined the "start" of the lysine fermentation. The pH of the production culture was not allowed to drop below 6.5, although is was free to exceed this value. Ammonium hydroxide was used for pH control. The pre- and subcultures consisted of (in g/l): 15 Tryptone, 5 Yeast extract, 5 NaCl, 5 ammonium acetate, 20 glucose. The production culture medium (CM3) consisted of (in g/l in fermentor): 200 glucose, 5 Tryptone, 20 Yeast extract, 20 ammonium sulfate, 0.7 K_2HPO_4, 0.7 KH_2PO_4, 0.4 $MgSO_4 \cdot 7H_2O$, 15 ammonium acetate. Antifoam (PPG 2000) was added to both the sub- and production cultures initially (1 ml/l) and as needed to minimize foaming. Samples were not taken and data is not presented for the subculture.

Chapter 6

Results and Discussion

The results presented in this chapter actually address two objectives. The first, which is approached in a some what implicit manner, can basically be interpreted as a tutorial on the application of the flux analysis technique developed in Chapter 4. Although it has been demonstrated that flux distributions can readily be generated from fermentation data, the interpretation of these fluxes for the enhancement of product yield is not a trivial matter, and constitutes one of the primary objectives of the thesis. The model system chosen to demonstrate these techniques, the production of lysine by *Corynebacterium glutamicum*, actually forms the second objective, which is the identification of the limiting branch-points in the biosynthesis of lysine. An ancillary goal is to elucidate the cause of the limitation (or rigidity) and how it might be circumvented. It is the elucidation of the second objective by which the organization of this chapter is directed.

This chapter is basically broken down into three categories: 1) description, characterization and flux analysis of the standard lysine fermentation by *Corynebacterium glutamicum* ATCC 21253, hereafter referred to as the control fermentation, and for perspective, analysis of an industrial-type lysine fermentation of *Brevibacterium flavum*, Sections 6.1 and 6.2; 2) nodal flexibility assessment of the glucose-6-P (Glc6P) and pyruvate (Pyr) principal nodes from localized metabolic perturbations, Sections 6.3 and 6.4; 3) development and flexibility assessment of a kinetic model describing the PEP principal node, and a perturbation experiment based on the results found from the model, Section 6.5.

6.1 Control Lysine Fermentation

The control fermentation is not intended to outperform lysine fermentations typically conducted in industry [for instance, Nakayama, 1972] since these fermentations often employ complex media and allow autonomous operation to enhance overall lysine titer (see Section 6.2). Although industrially desirable, such complex nutrients and operating strategies hinder analysis and reproducibility. The control fermentation captures the essence of industrial fermentations, but under conditions that are easily reproduced and definable, and will represent the base case for metabolic perturbation studies examined later in the chapter. Furthermore, the AEC^s strain employed allows analysis of the pure growth phase not exhibited, or desirable, in industrial fermentations. See Section 5.5 for a complete description of the control fermentation design.

6.1.1 Fermentation Phases

Profiles of the measured extracellular on-line and off-line variables for the control fermentation of *Corynebacterium glutamicum* ATCC 21253 cultured on minimal glucose medium (FM4) are illustrated in Figures 6.1, 6.2, and 6.3. The fermentor load cell reading (*i.e.*, approximately the liquid volume of the fermentor) is presented in Figure 6.1 (E) and is used to calculate volumetric OUR and CER values as depicted in Figure 6.1 (B) and discussed in Section 5.5.4. The lysine fermentation can be broken down into four separate phases as portrayed in Figure 6.1 (A), which illustrates the profiles of biomass, glucose and lysine throughout the course of the fermentation.

6.1.1.1 Phase I

Phase I of the fermentation represents balanced growth and is marked by exponential changes in all extracellular metabolites, a respiratory quotient of one (Figure 6.2 (B)) complete glucose oxidation (Figure 6.1 (C)) and typically lasts 12 to 13 hours. RQ values above or below 1.0 during the early stages of Phase I are due to small biases in OUR and CER measurements and the consumption of supplied citrate in the first few hours. Due to the initially high glucose concentration (150 g/l), the growth rate during this phase (0.34 h^{-1}) is only half the observed maximum. The

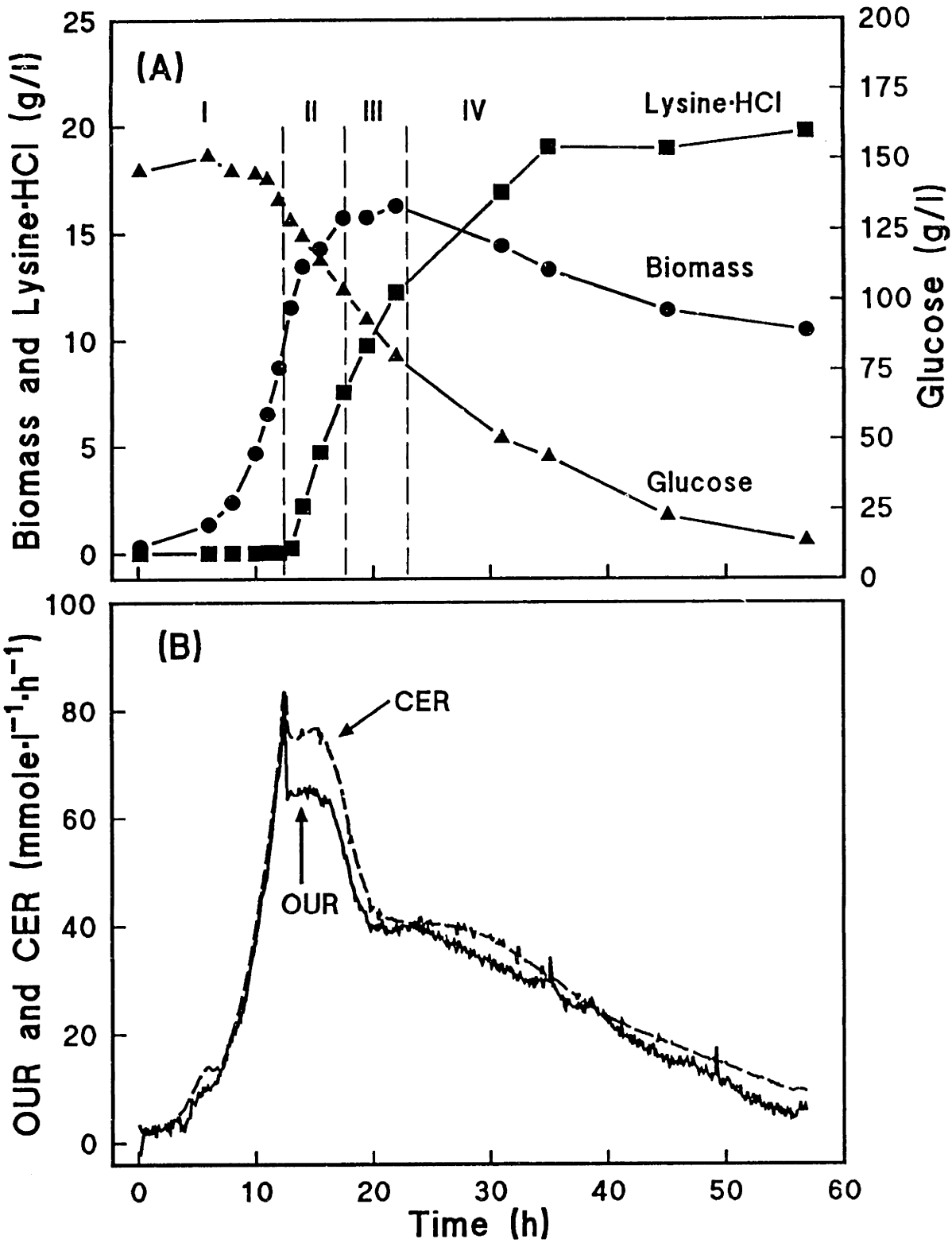

Figure 6.1 Control lysine fermentation of *Corynebacterium glutamicum* ATCC 21253 cultured on glucose minimal medium (FM4). (A) Glucose (▲), biomass (●), and lysine•HCl (■) profiles during the four phases of the culture. (B) Culture respiration: oxygen uptake rate (OUR), carbon dioxide evolution rate (CER).

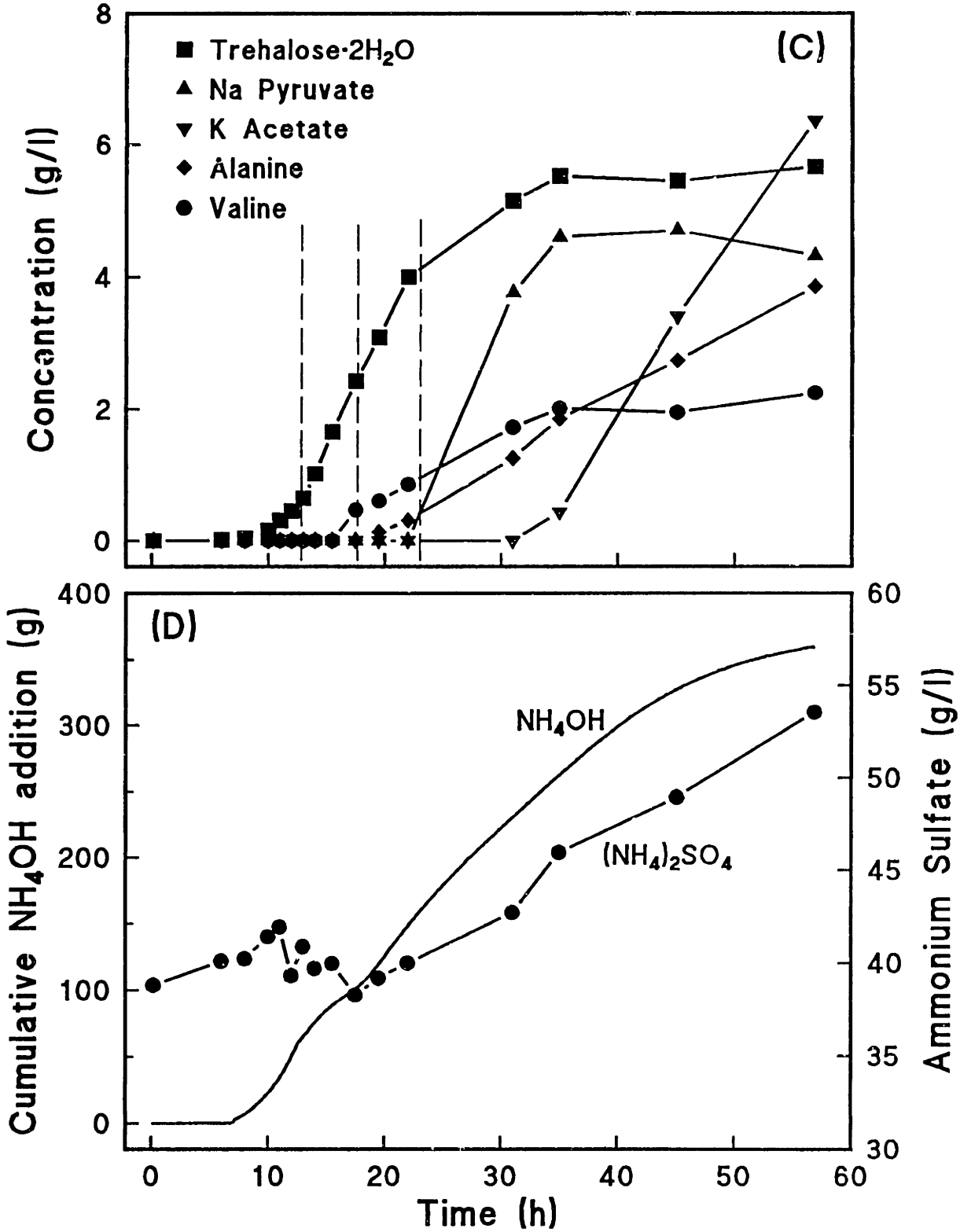

Figure 6.1 (continued) (C) Typical by-product accumulation associated with Phase IV of the culture. (D) Available ammonium in broth, as $(NH_4)_2SO_4$ (●), and amount of NH_4OH (26% (w/w) NH_3) added to maintain culture at pH 7.

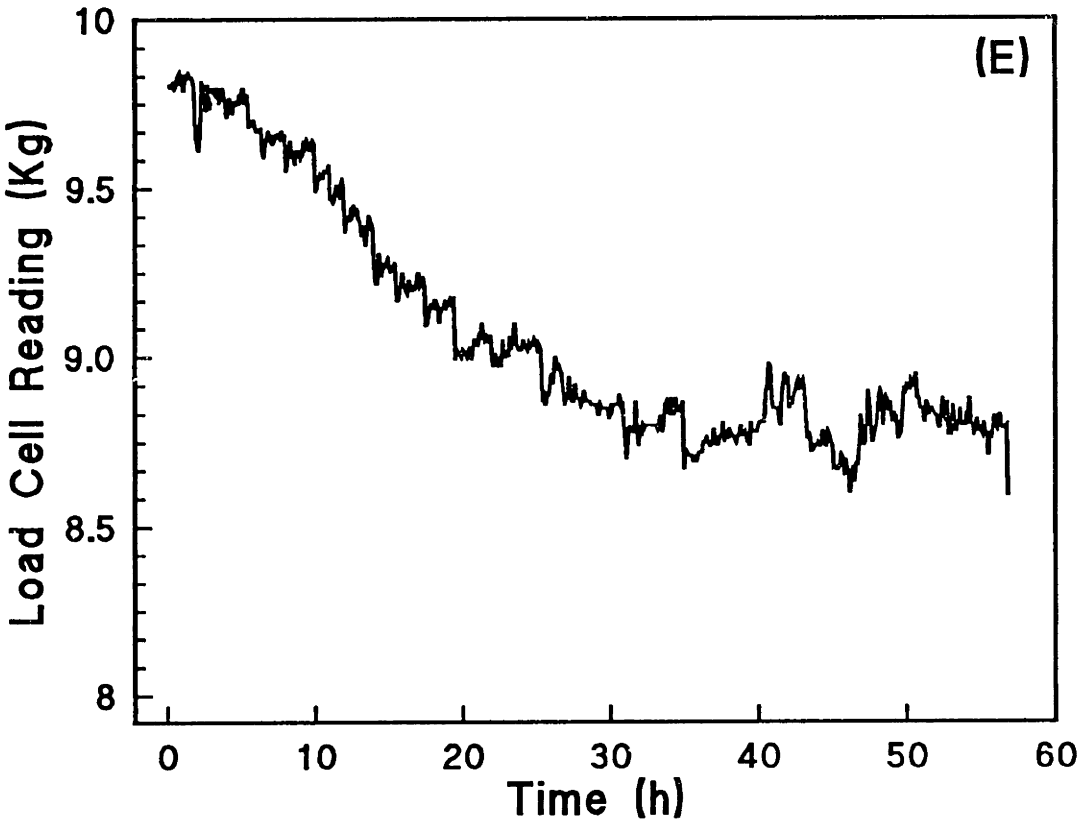

Figure 6.1 (continued) (E) On-line fermentor load cell reading (in Kg). Approximate fermentor liquid volume. Rapid decrease due to high sampling rate.

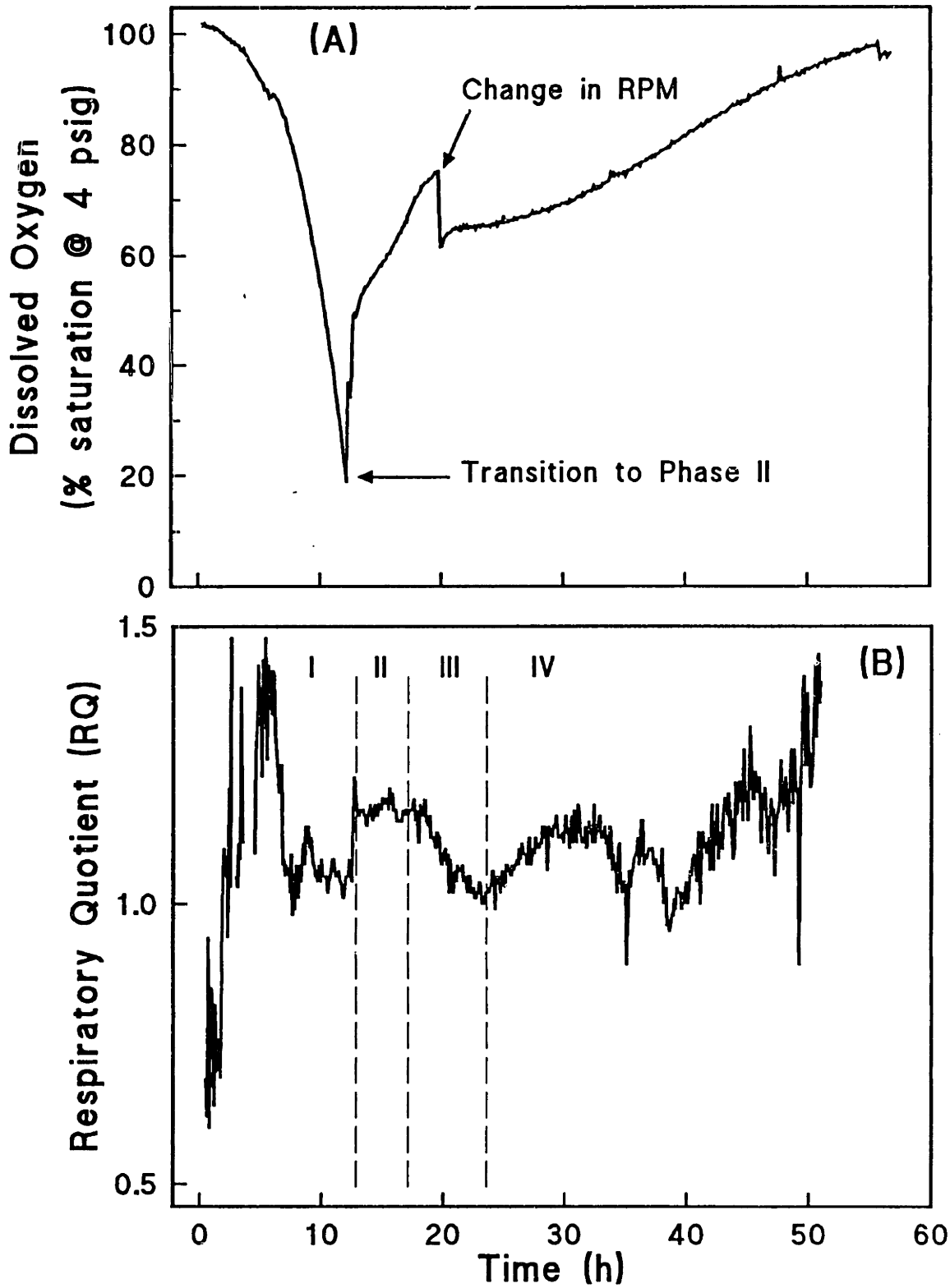

Figure 6.2 Control lysine fermentation dissolved oxygen concentration (A) and respiratory quotient (B). Elevated RQ in first few hours of fermentation is due to citrate catabolism and slight measurement biases in OUR and CER.

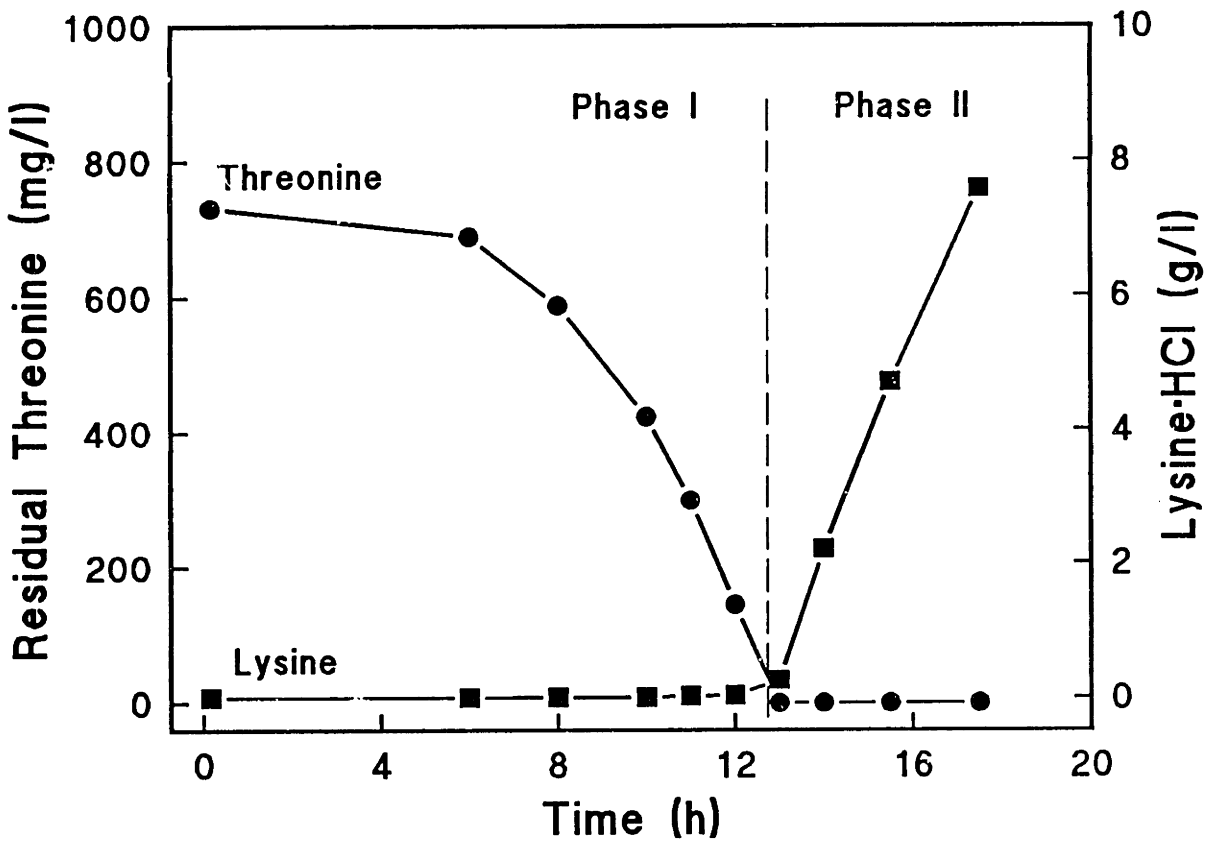

Figure 6.3 Detailed threonine (●) and lysine•HCl (▪) concentration profiles during Phases I and II of the control lysine fermentation.

duration of Phase I as well as the biomass concentration at the end of this phase is governed by the initial supply of threonine and is terminated by the exhaustion of this threonine as is evident in Figure 6.3. The initial supply of 730 mg/l threonine results in the reproducible accumulation of approximately 10 g/l DCW of biomass, Figure 6.1 (A), at the end of Phase I. The presence of excess threonine during this phase, in concert with lysine, inhibits aspartate kinase [Shiio and Miyajima, 1969] and prevents the overproduction of lysine (Figure 6.3) as discussed in Section 3.2.7.2. The end of Phase I is marked by an abrupt drop in respiration, evident in Figures 6.1 (B) and 6.2 (A), and uniquely signals the commencement of lysine production, Figures 6.1 (A) and 6.3. This telltale drop in respiration (which is monitored on-line by mass spectrometry) allows for the immediate identification of the start of lysine production and will prove quite useful in subsequent perturbation experiments.

6.1.1.2 Phase II

Phase II of the fermentation is marked by high lysine and biomass production rates (Figure 6.1 (A)), a sustained, elevated respiration (Figure 6.1 (B)) and an elevated RQ of approximately 1.17 (Figure 6.2 (B)), which is indicative of lysine production as explained in Section 4.2.1. Extracellular accumulation of the storage compound trehalose is also exhibited during this phase (Figure 6.1 (C)). The duration of Phase II in the control lysine fermentation lasts approximately four to five hours but can be extended by RQ controlled addition of threonine [Kiss, Manuscript in preparation] or by culturing an AEC^R strain as demonstrated in Section 6.2.

Phase II of the culture can be characterized as either 1) threonine scavenging or 2) the accretion of cellular constituents, or, of course, a combination of both. The first hypothesis implies that the additional increase in biomass upon the exhaustion of threonine from the medium—end of Phase I—is attributed to the scavenging of threonine from intracellular pools and denatured protein. This type of scavenging, which results in an attenuated growth phase, has been observed for trace nutrients [Brown *et al.*, 1988]. It is postulated that the organism extracts the limiting nutrient from the extracellular broth faster than it can actually incorporate the nutrient into biomass. Although the limiting nutrient is quickly exhausted from the culture medium, the organism is still able to sustain growth in a linear or diminished manner

due to intracellular reserves it has accumulated. Though the mechanism is a plausible explanation for the extended growth in Phase II of the culture, the scavenged threonine can not be present in the monomeric form since the intracellular concentration of threonine required to increase biomass from 10 to 16 g/l DCW would be high enough to completely inhibit aspartate kinase, and hence lysine production. Nevertheless, this type of mechanism may be responsible for some of the increase in biomass after extracellular threonine exhaustion.

In regards to the second hypothesis, the increase in biomass concentration during Phase II would instead be attributed to the accumulation of cell wall, cell membrane, nucleotides (DNA and RNA), storage compounds (*i.e.*, trehalose), and other cellular constituents, except protein, as observed in *Streptococcus faecalis* under amino acid limitation [Toennies *et al.*, 1963; Toennies, 1965]. Under this assumption, the exhaustion of threonine from the medium results in the termination of net protein synthesis, and the subsequent increase in biomass is attributed to a buildup of cell wall and other cellular constituents.

The actual composition of the biomass during Phase II will depending on which of the two hypotheses is true. However, unless the biomass composition changes to such an extent that the gross biomass elemental composition is affected, the net result of biomass composition change will have a negligible effect on the flux estimates due to the low sensitivity of flux estimates with respect to the biomass yield coefficients, as demonstrated in Section 4.1.8.

To ensure that the biomass elemental composition is not dramatically altered during the various culture phases, three samples from the control fermentation during Phases I, III, and IV were taken and analyzed for biomass elemental composition. The results are tabulated in Table 6.1 (also see Table 5.13). As can be seen from this table, the elemental composition of the biomass remains relatively constant throughout the fermentation and any effects of biomass composition change should not result in flux estimate discrepancies.

To investigate the second hypothesis that extracellular threonine exhaustion results in protein synthesis termination, several biomass samples during the course of the fermentation were analyzed for total soluble protein content. The results of the

Table 6.1 Biomass elemental composition during the control lysine fermentation.

Culture: Phase & Time (h)		Biomass Elemental Composition (%w/w) Carbon	Hydrogen	Oxygen	Nitrogen
I	11.0	46.8	6.41	29.1	11.0
III	19.5	46.4	6.47	34.0	9.3
IV	35.0	45.8	6.48	31.5	11.2

analysis, illustrated in Figure 6.4, indicate that protein synthesis does not completely stop after the exhaustion of available threonine, which implies that there may be some intracellular reserves available to support further protein synthesis. However, examination of Figure 6.4 reveals that the increase in soluble protein from Phase I to Phase IV is only 28%, while the increase in biomass is approximately 63% (Figure 6.1 (A)). Therefore, the percentage of cellular protein must decrease after the exhaustion of extracellular threonine, implying that both postexponential growth hypotheses are probably at work: 1) some intracellular storage of threonine; 2) relative decrease in protein synthesis. It is important to realize the implications of the second hypothesis. Since *de novo* protein synthesis dramatically diminishes after threonine exhaustion, the metabolic state of the culture will be effectively governed by the efficiency of protein turnover [Mandelstam, 1960] which has not been established or characterized in *C. glutamicum*. Consequently, subsequent metabolic flux distribution may be predominately governed by the relative stability of the metabolic enzymes. Changes in cellular morphology that accompany extracellular threonine depletion are quite complex and very important in lysine synthesis, and should be studied in future investigations. Although such morphology changes could dramatically alter flux distributions, they will not significantly affect pseudo-steady state assumptions or the accuracy of the flux estimation.

6.1.1.3 Phase III

The end of Phase II is indicated by a gradual decrease in biomass synthesis and respiration, Figure 6.1 (A,B). As discussed above, the exact cause for the transition to Phase III is unclear, but is ultimately a result of threonine depletion. Phase III of the culture is marked by termination of growth, high lysine production

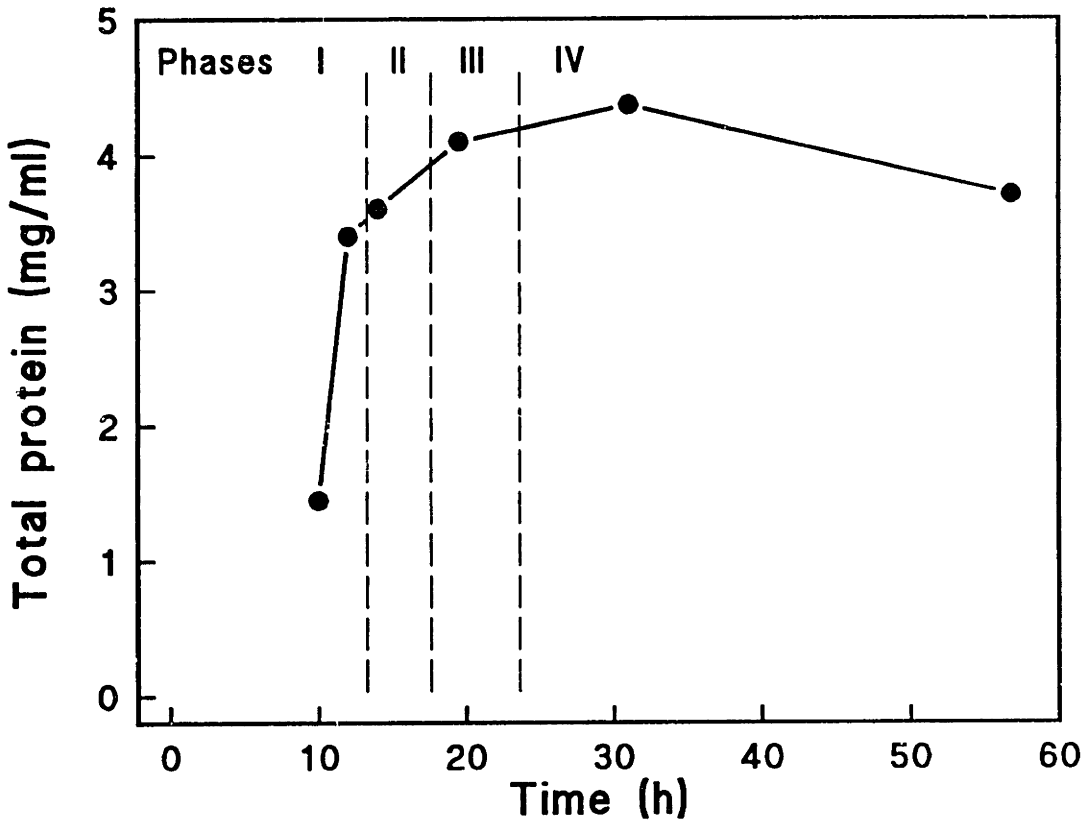

Figure 6.4 Soluble biomass-protein concentration for control lysine fermentation. See Section 5.5.2.3 assay procedure.

rates (Figure 6.1 (A)), and decreasing respiration and RQ (Figures 6.1 (B) and 6.2 (B), respectively). Phase III termination is indicated by a plateau in respiration, Figure 6.1 (B), a decrease in biomass concentration, Figure 6.1 (A), and the production of glycolysis related by-products, such as pyruvate, acetate, alanine, and valine, Figure 6.1 (C), as well as small amounts of several unidentified metabolites.

6.1.1.4 Phase IV

Phase IV of the culture basically represents the death phase and is evident by the gradual reduction in lysine production and a redirection of glucose consumption to by-product formation. An increase in RQ, Figure 6.2 (B), and ammonium sulfate concentration, Figure 6.1 (D), is also associated with Phase IV due to the production of organic acids, such as pyruvate. It is believed that the decrease in lysine synthesis in this phase results from the decay of primary enzymes that can no longer be regenerated, due to the lack of threonine and the loss of protein turnover (if operational). The excretion of glycolysis-related metabolites may be associated with the decay of the pyruvate dehydrogenase complex or TCA related enzymes, such as the α-ketoglutarate dehydrogenase complex [Shiio and Ujigawa-Takeda, 1980].

6.1.2 Lysine Yield

The overall—integrated—lysine molar yield for the control fermentation is only 15%; however, this overall number is of little value since a large fraction of the glucose is consumed in Phases I and IV of the fermentation during which little or no lysine is produced. Consequently, the overall yield is not indicative of the true instantaneous yields achieved in Phases II or III of the culture. Yet the overall yield is often cited as a measure of metabolic improvement even though yield enhancement may be the result of shortening the duration of Phases I or IV, which are not considered metabolic improvements in this study. The overall yield is no more useful than trying to assess the cellular metabolic state from measurements taken at the beginning and end of a fermentation. The integrated yield is only useful in economic feasibility studies, which are not the focus of this research.

To ascertain if primary metabolic modifications will improve lysine yields, it is necessary to examine the instantaneous yield during the various culture phases, as

Table 6.2 Lysine yields for the control lysine fermentation.

Phase	Yield (%, Molar)
I	0
II	30
III	20
IV	10
Overall	15

shown in Table 6.2. Even though lysine yield in Phase I of the culture is zero, it cannot be significantly improved through metabolic engineering since the yield in this phase will always be much lower than the theoretical maximum, due to the burden of biomass synthesis. Furthermore, yield improvements in Phase I (or removal of Phase I) can easily be accomplished if one employs an AEC^R strain of *C. glutamicum.* (From a research perspective, Phase I is quite useful since pure growth as well as the transition to lysine production can be investigated with one organism.) Similarly, the duration of Phase IV of the culture can be shortened to a negligible fraction of the entire fermentation if one uses the AEC^R strain or resorts to fed batch techniques as explained previously. The long duration of Phase IV observed in the control lysine fermentation is a result of the minimal medium and the ATCC strain used, and should not be consider indicative of industrial fermentations. An industrial-type fermentation is investigated in Section 6.2, in which the above conclusions will become quite apparent. Since Phases II and III of the culture are indicative of industrial fermentations and represent the periods over which modifications of the primary metabolism can lead to significant improvements in lysine yield, they are the phases of interest even though they comprise a relatively small fraction of the overall fermentation time. Consequently, the majority of flux analyses will focus on these two phases since the instantaneous yield in these phases is much lower than the theoretical maximum of 75%, as shown in Table 6.2. In subsequent studies, only increases in lysine yield during Phases II and III will be considered metabolic improvements. Enhancements in overall lysine yield will not be considered.

6.1.3 Metabolic State Estimation

6.1.3.1 Measurement Vector, $\mathbf{r}(t)$

As outlined in Chapter 4, the flux distribution of carbon through the primary metabolism can be estimated from the bioreaction network equation (BRNE) by determining the accumulation rate of the extracellular metabolites from the data presented in Figure 6.1 (A-E). Although flux distributions can be determined between any two sample points, it has been found that the resulting flux distributions, when normalized by glucose consumption rate, remain relatively constant throughout a particular phase of the culture. Even though the absolute magnitudes of the fluxes will change, as demonstrated in Chapter 4, it is the change in node split-ratios that are of interest and not the absolute flux magnitudes. For example, if one constructs five flux-distributions maps during Phase I of the culture based on sample points 1 through 6 from Figure 6.1 (A-E), one would find the maps statistically identical when normalized by glucose consumption. This "flux map similarity" in Phase I is not surprising since the distribution of metabolic resources—or nodal split-ratios—should not dramatically alter during balanced growth even though the absolute fluxes will increase. The flux map similarities result from the proportionality between accumulation rate vectors $\mathbf{r}(t)$ at different sample points (*i.e.*, time) throughout Phase I. For this reason, flux distributions need only be calculated for a particular culture phase or during any period in which the accumulation rate vector $\mathbf{r}(t)$ remains proportional to itself at different time points. Similarly, if $\mathbf{r}(t)$ changes in a nonproportional manner across a fermentation phase, then flux distribution maps should be discretized as needed and not integrated across the entire phase. Such discretization is required during Phase II of the culture, as discussed below.

Calculation of the metabolite accumulation vector $\mathbf{r}(t)$ for the control lysine fermentation is based on the following rationale. Flux distributions for Phase I of the culture are based on rates calculated between sample points 5 (at 11.0 h) and 6 (at 12.0 h). Although rates could have been based on earlier samples, the signal to noise ratio associated with those rates is quite large since the difference between any two measurements is very slight during the initial growth period of any fermentation. Furthermore, citrate added as a chelating agent is consumed during the first few

hours and is not present for the remainder of the fermentation. Flux characterization of Phase II of the fermentation is divided into two categories as mentioned above. Examination of Figure 6.1 (A,B) reveals that biomass accumulation rate is high in early Phase II but later drops to a lower level in late Phase II. Consequently, two accumulation rate vectors were constructed during Phase II between points 7 (at 13.0 h) and 8 (at 14.0 h), and points 8 and 10 (at 17.5 h) to capture the full dynamics of this phase. For Phase III of the fermentation, metabolite accumulation rates were calculated between sample points 10 and 12 (at 22.0 h); *i.e.*, across the entire phase. Flux distributions during Phase IV of the culture cannot be estimated with confidence since the production of unidentifiable metabolites and the difficulty in interpreting cell lysis leads to an inconsistency in the mass balance. Without such consistency analysis, discussed in Chapter 4, the flux distribution generated for Phase IV might have been deemed valid without knowledge of the consistency problems. Consequently, inclusion of the consistency analysis routine in the BRNA allows one to identify when the accuracy of the flux estimates become questionable. Elements of the metabolite accumulation rate subvector, $\mathbf{r}_E(t)$, and their associated standard deviation for the first three phases of the control lysine fermentation are presented in Table 6.3. All other metabolites of the rate vector are set to zero under the PSSA (*i.e.*, $\mathbf{r}_I(t) = \mathbf{0}$). MS1 in Appendix B contains the metabolites used in the analysis.

Examination of Table 6.3 reveals that several metabolites have been included in $\mathbf{r}_E(t)$ even though their observed accumulation rate is zero. Though certain metabolites may not be observed to accumulate in the medium at a particular instance, the probability of slight accumulation of an intracellular metabolite is more likely to arise with those metabolites that are routinely excreted. Therefore, by including such metabolites as part of the extracellular measurement vector $\mathbf{r}_E(t)$, strict closure of the mass balance can be attained in a more realistic manner if slight amounts of such metabolites are allowed to accumulate. Consequently, the metabolites Ac, Ala, Lac, Pyr, Trehal, and Val are always included in $\mathbf{r}_E(t)$ and assigned a standard deviation of 2 mM/h, which accounts for uncertainties in actual measurements and for slight intracellular accumulation. This degree of error only equates to an extracellular accumulation rate of approximately 0.2 to 0.6 $g \cdot l^{-1} \cdot h^{-1}$

Table 6.3 Extracellular metabolite accumulation rates, $\bar{\mathbf{r}}_E(t)$, based on raw data illustrated in Figure 6.1.

Elements of $\mathbf{r}_E(t)$	Accumulation Rates and Standard Deviation $\bar{\mathbf{r}}_E(t) \pm \sigma$ (mM/h)			
	Phase I Pts 5-6	Phase II Pts 7-8	Phase II Pts 8-10	Phase III Pts 10-12
Ac (1)	0. ± 2	0. ± 2	0. ± 2	0. ± 2
Ala (4)	0. ± 2	0. ± 2	0. ± 2	0.8 ± 2
Biomass (7)	21.9 ± 5.4	19.1 ± 8.9	6.5 ± 3.0	1.2 ± 2.5
CO2 (8)	61.6 ± 6.2	75.1 ± 7.5	73.5 ± 7.4	47.5 ± 4.8
Glc (14)	-40.6 ± 22	-31.1 ± 20	-30.5 ± 5.1	-29.1 ± 3.2
Lac (19)	0. ± 2	0. ± 2	0. ± 2	0. ± 2
LysE (20)	0.04 ±.01	10.7 ± 0.2	8.4 ± 0.3	5.6 ± 0.3
NH3 (25)	-64.8 ± 44	-35.3 ± 43	-18.2 ± 12	-11.8 ± 9.3
O2 (26)	-59.2 ± 5.9	-64.6 ± 6.5	-62.6 ± 6.3	-42.8 ± 4.3
Pyr (29)	0. ± 2	0. ± 2	0. ± 2	0. ± 2
Trehal (35)	0.4 ± 2	1.0 ± 2	1.1 ± 2	0.9 ± 2
Val (36)	0. ± 2	0. ± 2	0.4 ± 2	0.7 ± 2
Ave. t (h)	11.5	13.5	15.8	19.8
Δt (h)	1.0	1.0	3.5	4.5

for most metabolites and is considered to be acceptable. Although the entire measurement set could be included in the consistency analysis, allowing 37 metabolites to accumulate, even only slightly, reduces the probability of detecting inconsistencies in the mass balance. Therefore, it is preferable to constrain accumulation rates for most intracellular metabolites to identically zero, and only permit those metabolites which are typically observed to be excreted to vary. Although the entire measurement set (MS1) listed in Appendix B is used to estimate the flux distribution maps for the control lysine fermentation, only those metabolites listed in Table 6.3 are part of the consistency analysis. That is, all other metabolites—which are zero valued—are considered to have a standard deviation of zero. For a complete description of rate calculations, error estimation, and consistency analysis see Section 4.1.

As described in Section 4.1.10, it is the consistency index and the estimated measurement set, $\hat{\mathbf{r}}(t)$, that are first calculated from the BRNA. The estimated measurement set subvectors, $\hat{\mathbf{r}}_E(t)$, and the associated consistency index, h, are

Table 6.4 Weighted least-squares estimates for the metabolite accumulation rate subvectors, $\hat{\mathbf{r}}_E(t)$, based on MS1 and BS1 in Appendix B and the measurements listed in Table 6.3.

Elements of $\hat{\mathbf{r}}_E(t)$	Accumulation Rates (mM/h)			
	Phase I Pts 5-6 (11.5 h)	Phase II Pts 7-8 (13.5 h)	Phase II Pts 8-10 (15.8 h)	Phase III Pts 10-12 (19.8 h)
Ac (1)	0.04	-0.01	0.10	0.47
Ala (4)	0.16	-0.02	0.04	1.3
Biomass (7)	22.7	17.9	6.7	2.2
CO2 (8)	63.2	77.4	73.5	49.6
Glc (14)	-25.1	-35.4	-28.5	-25.5
Lac (19)	0.06	-0.02	0.15	0.70
LysE (20)	0.04	10.7	8.37	5.62
NH3 (25)	-17.0	-34.3	-22.3	-15.8
O2 (26)	-57.9	-62.8	-63.1	-42.2
Pyr (29)	0.13	0.06	0.13	0.77
Trehal (35)	0.63	0.9	1.7	3.7
Val (35)	0.06	-0.2	0.6	1.6
Consistency Index, *h*	1.84	0.25	0.40	4.38

displayed in Table 6.4. Biochemistry and metabolite sets #1 (BS1 and MS1) used to generate $\hat{\mathbf{r}}_E(t)$ and the flux estimates are listed in Appendix B. As explained in Section 4.1.9, the vectors displayed in Table 6.4 exactly satisfy mass balance constraints [$\mathbf{Z}\hat{\mathbf{r}}(t) = \mathbf{0}$]. The degree by which the raw measurement vector—listed in Table 6.3—must be displaced [$\overline{\mathbf{r}}_E(t) - \hat{\mathbf{r}}_E(t)$] to meet the balance constraints is represented by the consistency index *h*. The farther the displacement, the greater the value of *h*, where the displacement is weighted by the standard deviation of each measurement, also listed in Table 6.3. When the value of *h* exceeds the chi-square value, $\chi^2_{0.9}(\ell)$, the data is considered inconsistent (see Section 4.1.9.2). For three degrees of freedom (number of redundant equations: $\ell = 3$) and a 90% confidence interval, $\chi^2_{0.9}(3)$ equals 6.25. Examination of the consistency index for each measurement vector listed in Table 6.4 reveals that they are all statistically consistent; however, measurement vectors constructed from data points 5-6, $\overline{\mathbf{r}}_E(11.5)$, and 10-12,

$\bar{\mathbf{r}}_E(19.8)$, have a rather large consistency index. These subtle discrepancies are further investigated below.

Comparison of $\bar{\mathbf{r}}_E(11.5)$ and $\hat{\mathbf{r}}_E(11.5)$ from Table 6.3 and 6.4, respectively, indicates that the high consistency index arises from the glucose (Glc) and ammonia (NH3) measurements. If the glucose and ammonia measurements are deleted from the set, the consistency index decreases to 0.09 ($\chi^2_{0.9}(1) = 2.7$), which indicates the error resides with these two measurements. As reviewed in Section 5.5.4.2, determining the nitrogen consumption rate is inherently of poor precession, so a large discrepancy here is not alarming. The uncertainly in the glucose consumption rate can best be explained by examining the glucose profile illustrated in Figure 6.1 (A). As can be seen in this figure, the accuracy in measuring the glucose consumption rate is quite difficult for the first five or six samples; consequently, a larger than typical error during this period is understandable. Based on this rational, the updated measurement vector $\hat{\mathbf{r}}_E(11.5)$ is considered a better representation than the actual measured values and does not present any difficulties.

Consistency analysis of the rate vector at 19.8 h (Table 6.3) indicates that more glucose is consumed than can be accounted for in products. To mitigate the error, the estimated glucose consumption is slightly reduced, and synthesis of the storage compound trehalose is increased (see $\hat{\mathbf{r}}_E(19.8)$ in Table 6.4). The error can also be mitigated by deleting glucose, trehalose, acetate, or lactate from the measurement set, but such an extreme correction is not warranted. Unlike the previous analysis, measurements were taken during the period in which rates are large and the error is small due to the increased sample period. Since the profiles of all measured metabolites exhibit consistent trends (Figure 6.1), no gross measurement errors are indicated, so that the inconsistency must be associated with the accumulation of an unidentified metabolite. To achieve a consistent measurement set, the unidentified metabolite must be a carbohydrate or a metabolite whose synthesis does not alter OUR or CER. Since all typical by-products of *C. glutamicum* are assayed, and none are observed to sufficiently accumulate, the metabolite is believed to be associated with the biomass. This hypothesis is further supported by the deterioration in the correlation between dry cell weight and optical

density observed in Phase III of the fermentation, as illustrated in Figure 6.5 (A). This departure from the correlation results in an OD estimated biomass concentration that exceeds the measured DCW during Phase III, evident in Figure 6.5 (B). Since cells are microscopically observed to actually increase in diameter during this period (Phase IV as well) [Abe *et al.*, 1967], the change in optical density can not be attributed to cell shrinkage; thus, the correlation discrepancy must be caused by a change in cellular opacity or a loss in material loosely associated with the cell caused by the DCW measurement technique. Since the storage compound trehalose is known to accumulate intracellularly [Inbar *et al.*, 1985] and other unidentified di or tri saccharides have been observed to accumulate (see Section 5.5.3), the increase in the estimated trehalose synthesis rate, Table 6.4, is considered acceptable. The reproducible discrepancy between OD and DCW along with the poor consistency index during Phase III of the fermentation indicates that the culture experiences some morphological change during this period, which is undoubtedly associated with the postexponential growth phenomena discussed in Section 6.1.1.2.

It should be noted that alternate interpretations of the above analysis do not dramatically alter the resulting flux distribution estimates, due to the low sensitivity of these estimates to the measurements. The detailed explanation given above is intended to illustrate the usefulness of the consistency analysis routine coupled with the BRNE. Not only does the consistency routine indicate which measurement sets should be used with caution, but also indicates where the inconsistency occurs in the set and which measurements should be reexamined. Since the merit of any numerical routine depends on its ability to predict erroneous results, flux estimates should always be calculated in conjunction with the consistency index.

6.1.3.2 Flux Distributions

Flux distributions for the four rate vectors listed in Table 6.4 are illustrated in Figures 6.6-6.9. Before preceding with the interpretation of these fluxes, a brief discussion on how to read these diagrams is necessary. Once a flux distribution map has been constructed, it can be presented in three possible formats: 1) the absolute fluxes themselves (*i.e.*, not normalized); 2) fluxes normalized with respect to biomass concentration (*i.e.*, specific rates); 3) fluxes normalized with respect to glucose

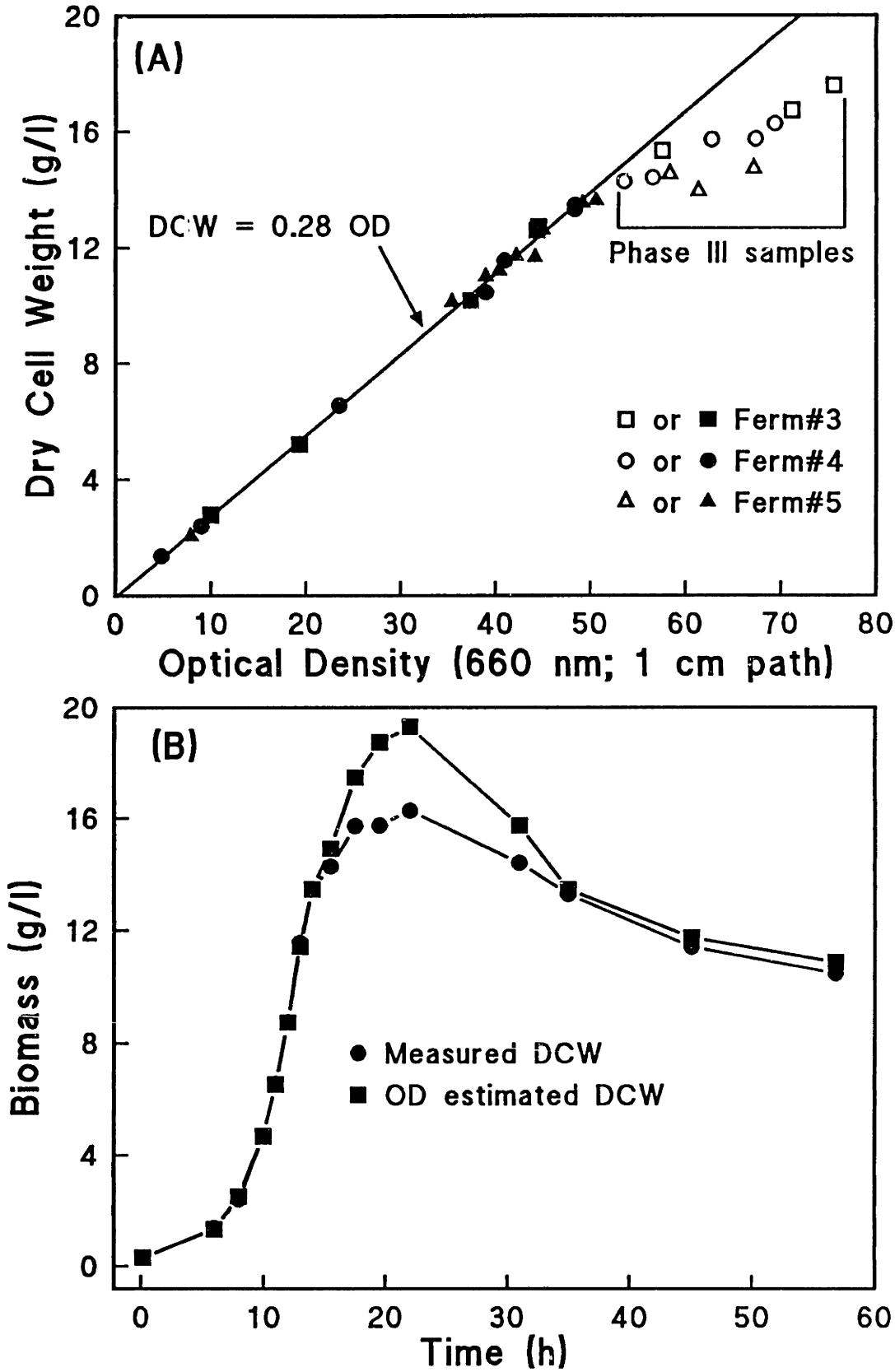

Figure 6.5 (A) Correlation between dry cell weight (DCW) and optical density (OD). Note, samples taken in Phase III of fermentations deviate from linear correlation. (B) Difference between measured DCW and OD estimated DCW in Phase III of the control lysine fermentation due to deviation in DCW versus OD correlation.

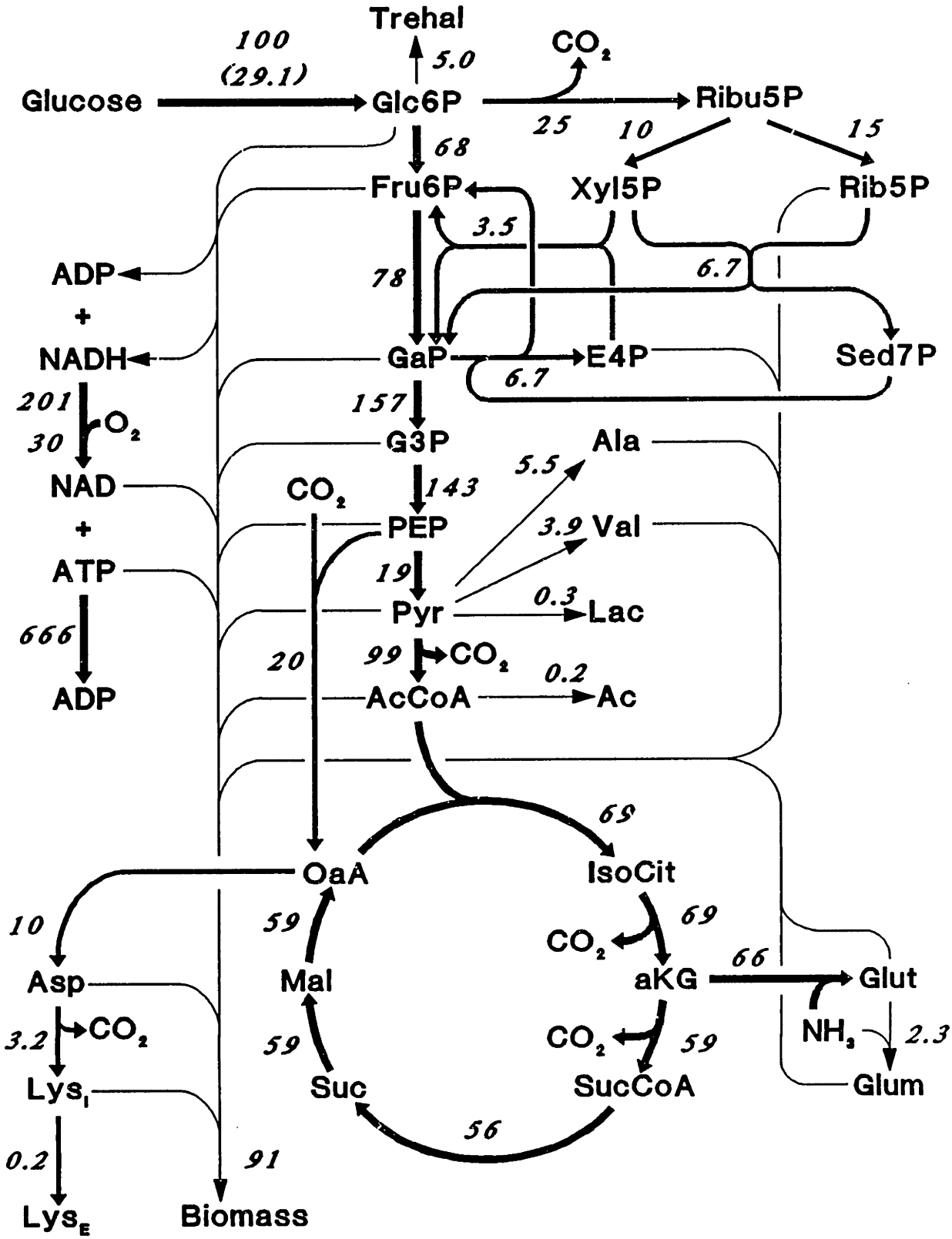

Figure 6.6 Flux distribution map for the control lysine fermentation at 11.5 h (Phase I). Fluxes estimated from measurements taken at 11.0 h and 12.0 h (see Figure 6.1 and Tables 6.3 and 6.4) and normalized by glucose uptake rate (shown in parentheses; mmole•l^{-1}•h^{-1}).

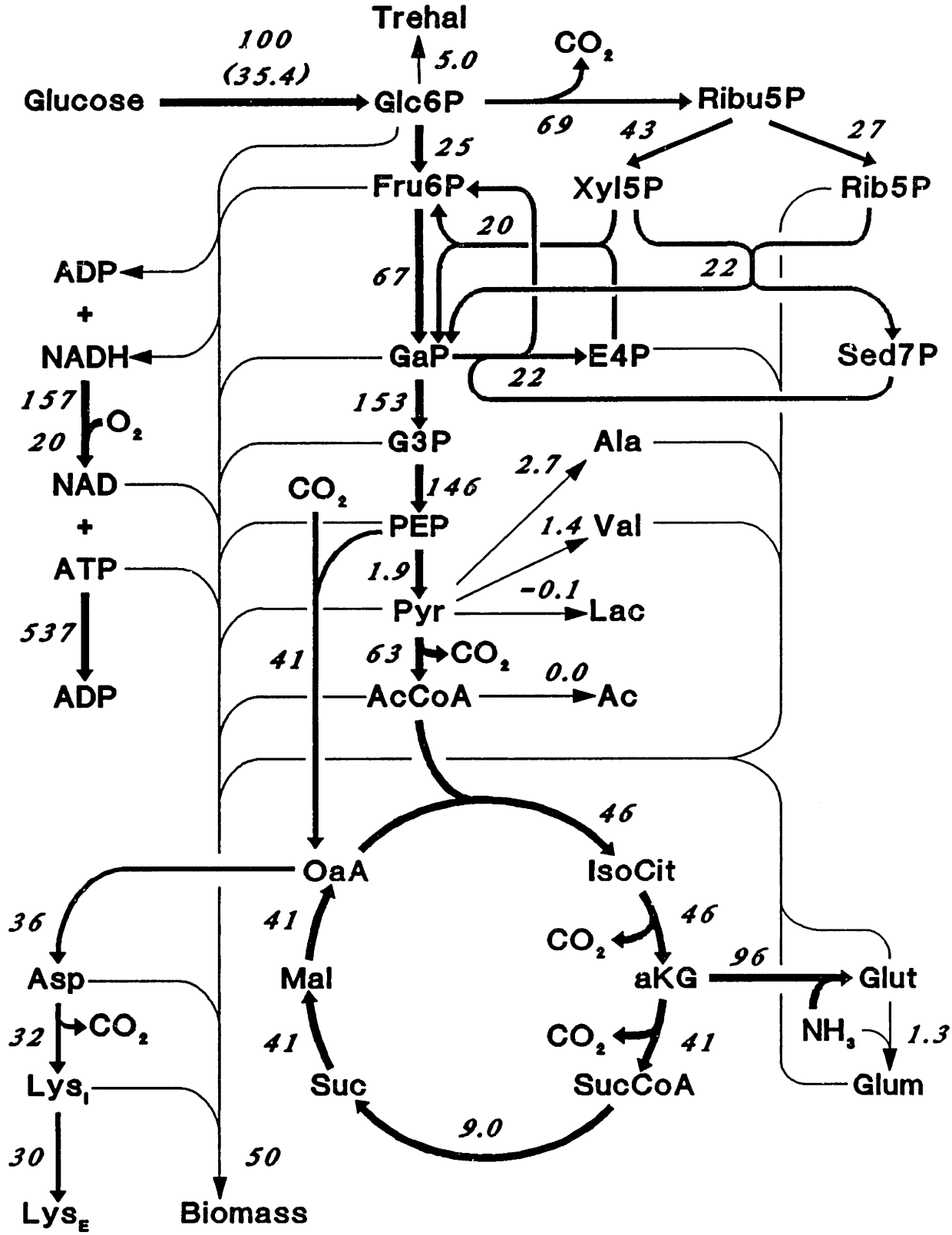

Figure 6.7 Flux distribution map for the control lysine fermentation at 13.5 h (early Phase II). Fluxes estimated from measurements taken at 13.0 h and 14.0 h (see Figure 6.1 and Tables 6.3 and 6.4) and normalized by glucose uptake rate (shown in parentheses; mmole•l^{-1}•h^{-1}).

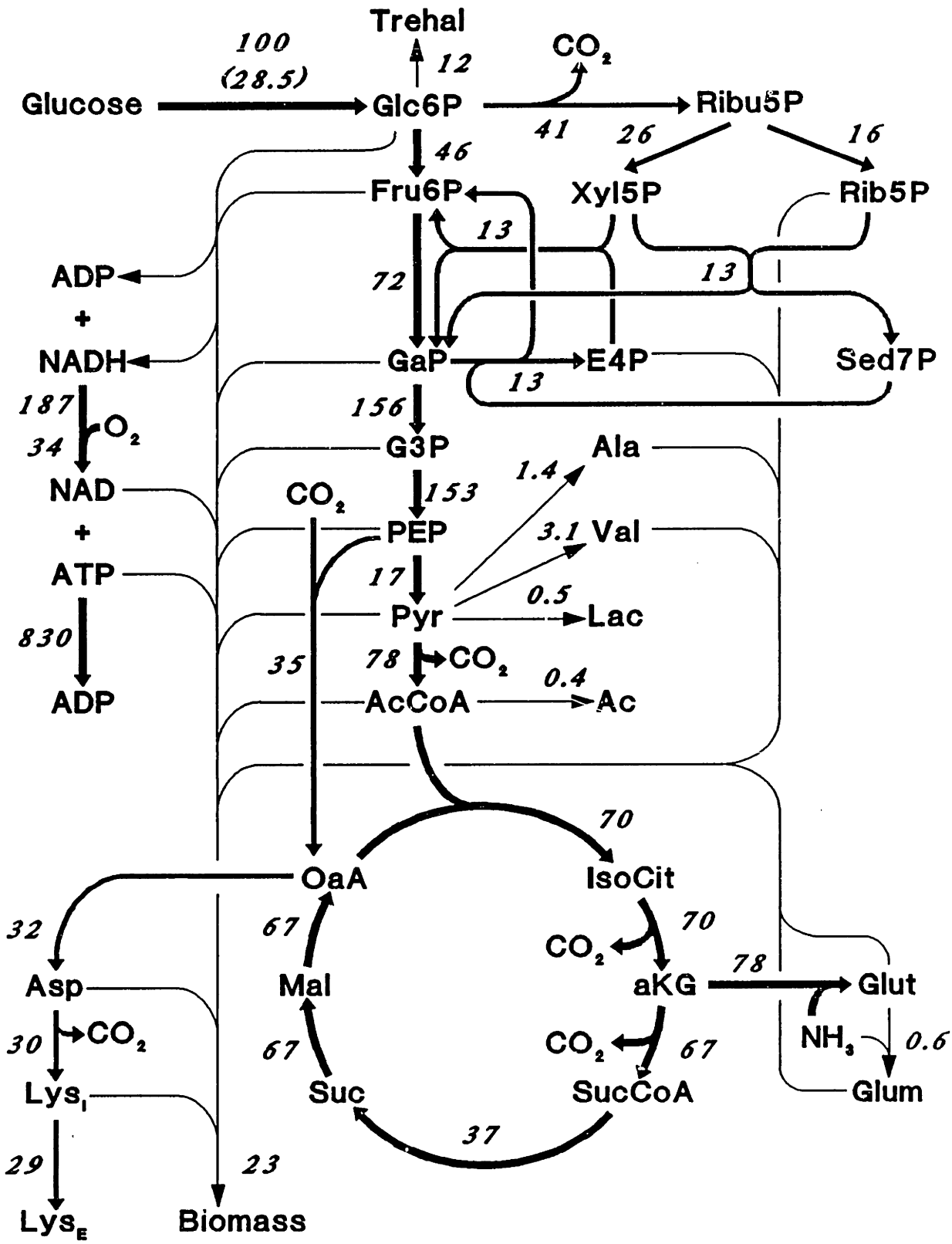

Figure 6.8 Flux distribution map for the control lysine fermentation at 15.8 h (late Phase II). Fluxes estimated from measurements taken at 14.0 h and 17.5 h (see Figure 6.1 and Tables 6.3 and 6.4) and normalized by glucose uptake rate (shown in parentheses; mmole•l^{-1}•h^{-1}).

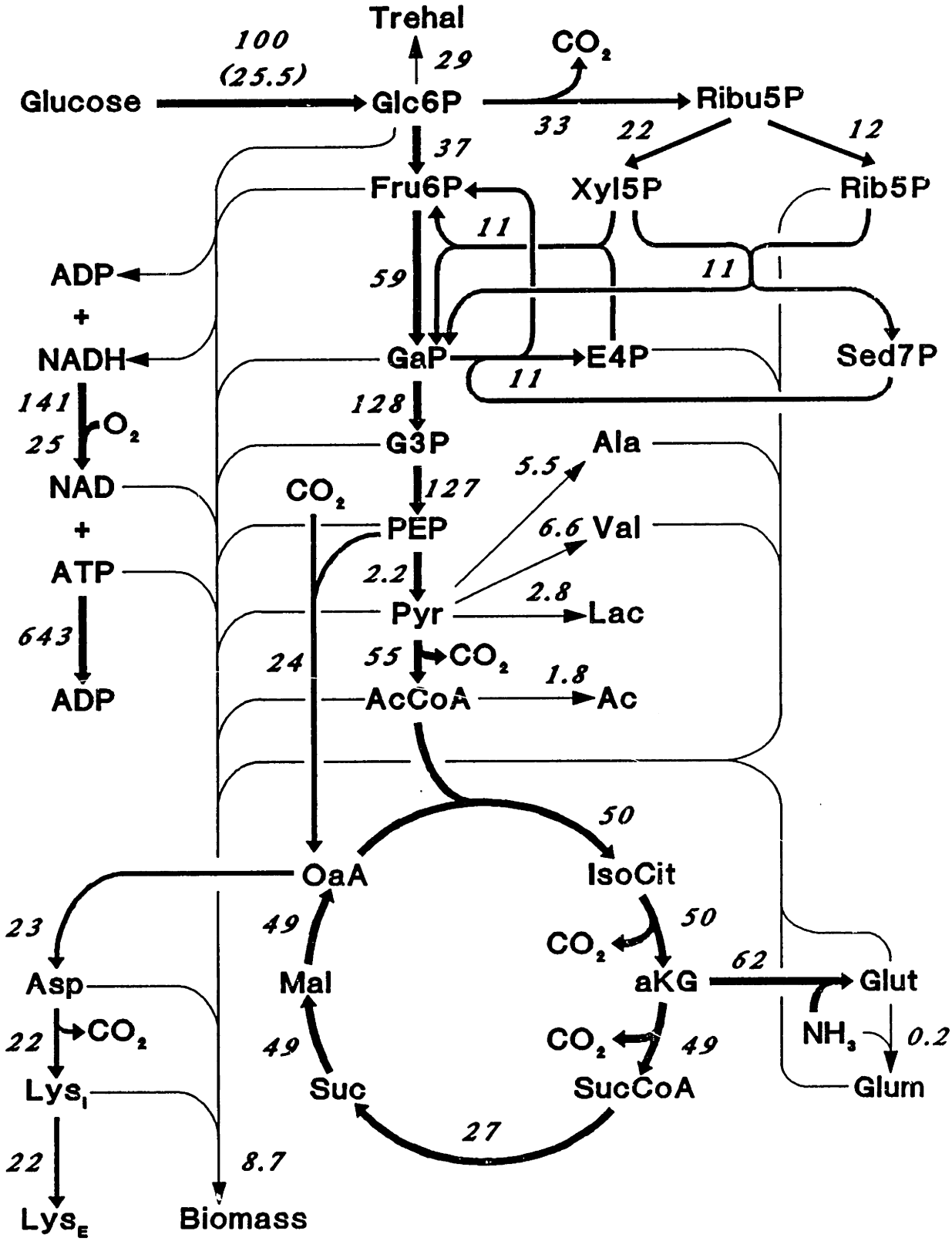

Figure 6.9 Flux distribution map for the control lysine fermentation at 19.8 h (Phase III). Fluxes estimated from measurements taken at 17.5 h and 22.0 h (see Figure 6.1 and Tables 6.3 and 6.4), and normalized by glucose uptake rate (shown in parentheses; mmole•l^{-1}•h^{-1}).

consumption rate. Clearly, Option 1 is seldom useful, except when comparing flux estimates to actual measurements. In both Options 2 and 3, all fluxes are multiplied by an arbitrarily defined constant; however, normalization by biomass concentration has been found less informative. For example, if biomass concentration remained constant yet the magnitude of $\mathbf{r}(t)$ decrease proportionally, the resulting flux distribution maps would differ even though the partitioning of carbon would remain unchanged. Furthermore, comparison of flux distribution maps normalized by biomass concentration are corrupted by noise in the biomass measurement. Since understanding and affecting the partitioning of carbon in the primary metabolism (*i.e.*, mapping and modifying principal node split-ratios) is the objective of this research, all flux distributions illustrated in Figures 6.6-6.9 are normalized with respect to glucose consumption. To obtain the absolute flux of a particular reaction (in $mmole \cdot l^{-1} \cdot h^{-1}$), divide the normalized flux by 100 and multiply it by the glucose consumption rate shown in parentheses for Reaction (1) and in Table 6.4. The biochemical reactions (BS1) and their projection onto the diagrams are detailed in Appendix B.

Since all regenerating reactions can not be clearly displayed in such diagrams, several fluxes in Figures 6.6-6.9 appear to violate the law of mass conservation. This is not the case. Reactions (18:BS1) and (14:BS1), for example, are also responsible for the regeneration of Glut and SucCoA respectively—necessary for lysine synthesis as illustrated in Figure 6.10 (A). Similarly, Reaction (7:BS1) accounts for the conversion of PEP to Pyr by pyruvate kinase only and does not account for the PTS system as shown in Figure 6.10 (B). Another illustration mirage occurs with some hydrolysis or condensation reactions, such as Reaction (4:BS1) where two GaP molecules are produced for each Fru6P molecule consumed. Also, the summation of trunk fluxes will not equal the summation of branch fluxes if the node metabolite is being consumed or produced; for instance, when pyruvate accumulates in Phase IV of the fermentation. Consequently, if what appears to be an inconsistency arises, check BS1 in Appendix B for possible connecting reactions and their stoichiometry as well as the estimated measurement vector, $\hat{\mathbf{r}}(t)$, for possible metabolite accumulation.

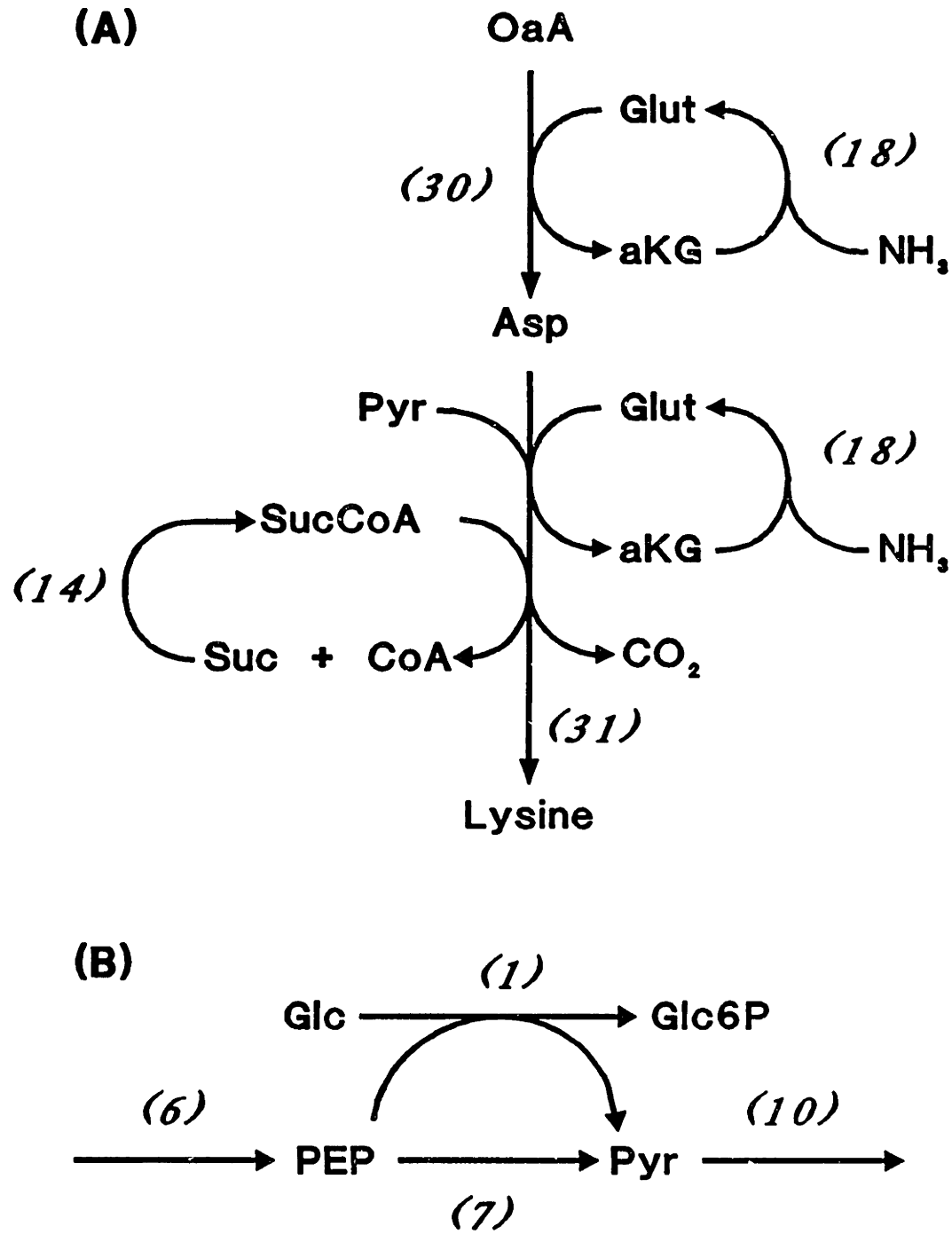

Figure 6.10 Reactions hidden in flux distribution maps. (A) Glutamate (Glut) and succinyl coenzyme A (SucCoA) regeneration and pyruvate consumption for lysine synthesis. (B) Conversion of PEP to pyruvate by PEP:glucose phosphotransferase system. For a complete listing of all reactions see BS1 in Appendix B.

The remainder of this section will focus on discernable trends in the metabolism illustrated in Figures 6.6-6.9 during the first three phases of the control fermentation based on the rate vectors listed in Table 6.4.

6.1.3.2.1 General Observations

In regards to the overall network, the most dramatic metabolic transformation is observed between flux distributions in Phase I and Phase II of the fermentation, Figures 6.6 and 6.7, respectively. This metabolic "perturbation" is induced by the sudden deregulation of lysine synthesis which causes a temporary flux redistribution in the primary metabolism from biomass towards lysine synthesis. It is during the early stages of Phase II, Figure 6.7, that the highest metabolic load is observed, as lysine and biomass yields both exhibit their maximums during Phases II-IV in this period. Subsequent flux distributions (Figures 6.8 and 6.9) reflect a slow transition of the primary metabolism back to conditions similar to Phase I, except that lysine production replaces biomass synthesis. In Phase III, glucose is diverted towards trehalose and pyruvate derived by-products and the fluxes supported by glycolysis and the TCA cycle are diminished. General trends in individual reactions that can be discerned from the four "snap shots" of metabolic activity are summarized below.

Although the flux supported by the pentose phosphate pathway (Reaction (22:BS1)) remains significant throughout all three phases of the fermentation, the transition from Phase I to Phase II (Figures 6.6 and 6.7, respectively) is accompanied by an increase in flux through this pathway to satisfy elevated NADPH requirements. The pentose phosphate flux later subsides due to the decrease in biomass yield (Figures 6.8 and 6.9).

The fraction of glucose catalyzed by PEP carboxylase (PPC, Reaction (9:BS1)) is also quite significant for the four flux distributions analyzed and experiences a similar flux increase during the transition from Phase I to Phase II; likewise, PPC flux also returns to Phase I conditions in Phase III. The PPC reaction is extremely important since it is the only anabolic reaction of the primary metabolism active when *C. glutamicum* is cultured on a minimal glucose medium (see Section 4.1.5.3) Due to the high flux supported by PPC, large amounts of CO_2 are fixed by this reaction.

Often, this CO_2 fixing is unaccounted for in metabolic tracer studies (See review in Chapter 2).

The fraction of glucose catabolized by Reactions (11-16:BS1) of the TCA cycle fluctuate around a mean and do not seem to exhibit any smooth trends. For instance, during Phase I (Figure 6.6), the TCA cycle flux is high but drops when lysine overproduction starts (Figure 6.7) due to the diversion of metabolites to lysine synthesis at the PEP and Pyr nodes. In the later stages of Phase II (Figure 6.8) the TCA cycle flux returns to its former activity, but then drops again in Phase III (Figure 6.9) due to the diversion of glucose to by-products, as mentioned above. Not surprisingly, the excess ATP generated (Reaction (34:BS1)) fluctuates in step with the TCA cycle flux. Little information can be extracted from these fluctuations; however, maintenance requirements can be inferred as discussed in Section 6.1.3.2.3.

Other reactions of interest include pyruvate kinase (Reaction (7:BS1)), which always exhibits a small flux due to the dominance of the PTS system, and glutamate dehydrogenase (Reaction (18:BS1)), which always supports a large flux since it is the only primary reaction for the incorporation of free ammonia into amino acids.

6.1.3.2.2 Flux Verification

As a preliminary check, qualitative inspection of the flux distributions illustrated in Figures 6.6-6.9 are consistent with plausible flux distributions of the primary metabolism (*i.e.*, no negative flows in irreversible reactions). This almost trivial confirmation is extremely important, for unacceptable flux distributions, constructed from consistent data, indicate errors in the biochemistry network. For example, carbon fixation by the TCA cycle would be a sure sign that certain pathways have not been included in the network or some included pathways are not operational *in vivo*. For quantitative verification, the flux distributions are compared to radio and stable isotope tracer measurement cited in the literature for glutamic acid bacteria.

As reviewed in Section 2.3.1, flux estimations from radio (^{14}C) or stable (^{13}C) isotope tracers presented in the literature are plagued by numerous uncertainties and inappropriate assumptions and are only available for a few flows. Nevertheless, such measurement techniques are the only methods currently available, and the literature

data does provide a certain amount of flux confirmation. By far the most abundant and least controversial flux measurements involve the partitioning of glucose between the pentose phosphate pathway (PPP or HMP: hexosemonophosphate pathway) and the Embden-Meyerhof-Parnas pathway (EMP or glycolysis). To review the literature on PPP flux data, the difference between actual measurements and flux estimates must be explained since tracer studies measure the fraction of glucose that enters the PPP, not the flux supported by the PPP which is estimated from the BRNE. In order to calculate the fraction of glucose that enters the PPP from the flux estimates, an assumption must be made on the fraction of carbon that is recycle through the PPP, such as 1) no Fru6P recycled, 2) all Fru6P recycled, or 3) Fru6P partially recycled—fraction of Fru6P recycled equals fraction of glucose that enters PPP. Of these three assumptions, the partial recycle of Fru6P produces the least error in multiple label experiments [Dawes *et al.*, 1958; Shiio *et al.*, 1960a]. However, in both manuscripts cited above, their calculations assume that recycled Fru6P is unlabeled, which is incorrect since some fraction of the Fru6P pool will be labeled. In actuality, they assume—unintentionally—that the fraction of label in both the Glc6P and Fru6P pools are equal. Under this assumption, the fraction of glucose that enters the PPP (f_{PPP}) as a function of network fluxes is:

$$f_{PPP} = \frac{x_{22}}{x_1 + x_{26} + x_{27}} \tag{6.1}$$

Listed in Table 6.5 is the calculated f_{PPP} from Equation (6.1) based on the flux

Table 6.5 Estimate fraction of glucose that enters the PPP from Equation (6.1) and Figures 6.6-6.9.

Phase: t_{ave} (h)	Figure	f_{PPP} (%)
I: 11.5	6.6	23
II: 13.5	6.7	49
II: 15.8	6.8	33
III: 19.8	6.9	27

Table 6.6 Summary of f_{PPP} measurements reported in the literature.

f_{PPP}(%)	Organism	Tracer*	Reference
26¶	*B. ammoniagenes*	Radio	Oishi and Aida (1965)
38§	"	"	"
18†	"	"	Oishi and Aida (1964)
36‡	"	"	"
11¶¶	*B. flavum*	Radio	Shiio *et al.* (1960a)
16-21¶¶	*B. flavum* and *C. glutamicum*	Radio	Otsuka *et al.* (1965a)
13§§	*Microbacterium ammoniaphilum*	Stable	Walker *et al.* (1982)
44††	*C. glutamicum*	Stable	Ishino *et al.* (1986)
44‡‡	*C. glutamicum*	"	Yamaguchi *et al.* (1986)

* Glucose labeled with stable of radio isotope.
¶ Stationary cells producing glutamate; low biotin.
§ Stationary cells producing glutamate; high biotin.
† As above¶ but without ammonium.
‡ As above§ but without ammonium.
¶¶ Washed cells plus arsenite; glutamate producer.
§§ Growing cells producing glutamate.
†† Growing cells producing histidine.
‡‡ Growing cells producing lysine.

distributions illustrated in Figures 6.6-6.9. Table 6.6 lists f_{PPP} reported from various literature sources. Although the conditions under which f_{PPP} was measured vary markedly in Table 6.6, the results indicate that a substantial amount of glucose is catabolized through the PPP by glutamic acid bacteria. Furthermore, the measured values of f_{PPP} are consistent with the estimated values obtained from the BRNE listed in Table 6.5, especially the last entry of Table 6.6 which was measured under conditions that closely represent those maintained in the control lysine fermentation. Consequently, it is concluded that the estimated flux distributions between the PPP and EMP, illustrated in Figures 6.6-6.9, accurately represent the true state of the metabolism at the Glc6P node.

Although Yamaguchi *et al.* (1986) and Inbar and Lapidot (1987) have investigated the flux distributions through the primary metabolism of *C. glutamicum*

and *B. flavum*, respectively, using stable isotope tracers, their results are problematic since they assume the presence of the glyoxylate shunt, "single turn" operation of pathway cycles, and do not account for label enrichment due to CO_2 fixation. Nevertheless, their results indicate that the flux supported by PEP carboxylase (Reaction (9:BS1)) is significant (40% by their analysis), which is consistent with the results presented in Figures 6.6-6.9. In conclusion, the estimated flux distributions for the control lysine fermentation are consistent with the tracer studies documented in the literature and accurately represent the true state of the metabolism.

To compare the estimated flux distributions to *in vitro* enzyme activities, several biomass samples from the control lysine fermentation where assayed for specific activities of: PEP carboxylase (PPC); NADH oxidase (NADHOX); pyruvate dehydrogenase complex (PDC); isocitrate dehydrogenase (ICDH); Glc6P isomerase (GPI); oxaloacetate decarboxylase (OAADC). The results of these assays are depicted in Figure 6.11 (A,B). Except for PPC and PDC, the assayed enzymes do not exhibit significant trends (other than slow decay), which is understandable since these enzymes are believed to be expressed constitutively. PPC exhibits a sharp increase in activity during Phase II, consistent with the increase in flux supported by Reaction (9:BS1); however, Reaction (10:BS1) exhibits a flux decrease in Phase II while the specific activity of PDC increases. (It should be noted that the activities of PPC and PDC in growing cells have been assayed at higher activities in later experiments, ca. 250 and 30 U/mg protein, respectively). Consequently, these assays indicate that flux distributions are predominately governed by enzyme inhibition or activation and not regulation. Therefore, *in vitro* enzyme activities are not indicative of flux distributions and should only be used to verify existence of metabolic pathways or to compare modified strains to parent strains.

6.1.3.2.3 ATP supply

It should be recalled from Section 4.1.3 that Reaction (34:BS1) denotes the amount of ATP that is synthesized over that which is consumed in all other reactions and also accounts for ATP required for maintenance, futile cycles, *etc.* Reaction (34:BS1) is a rough approximation of ATP requirements not easily accounted for, but it must be interpreted with caution. For instance, during rapid growth, one would

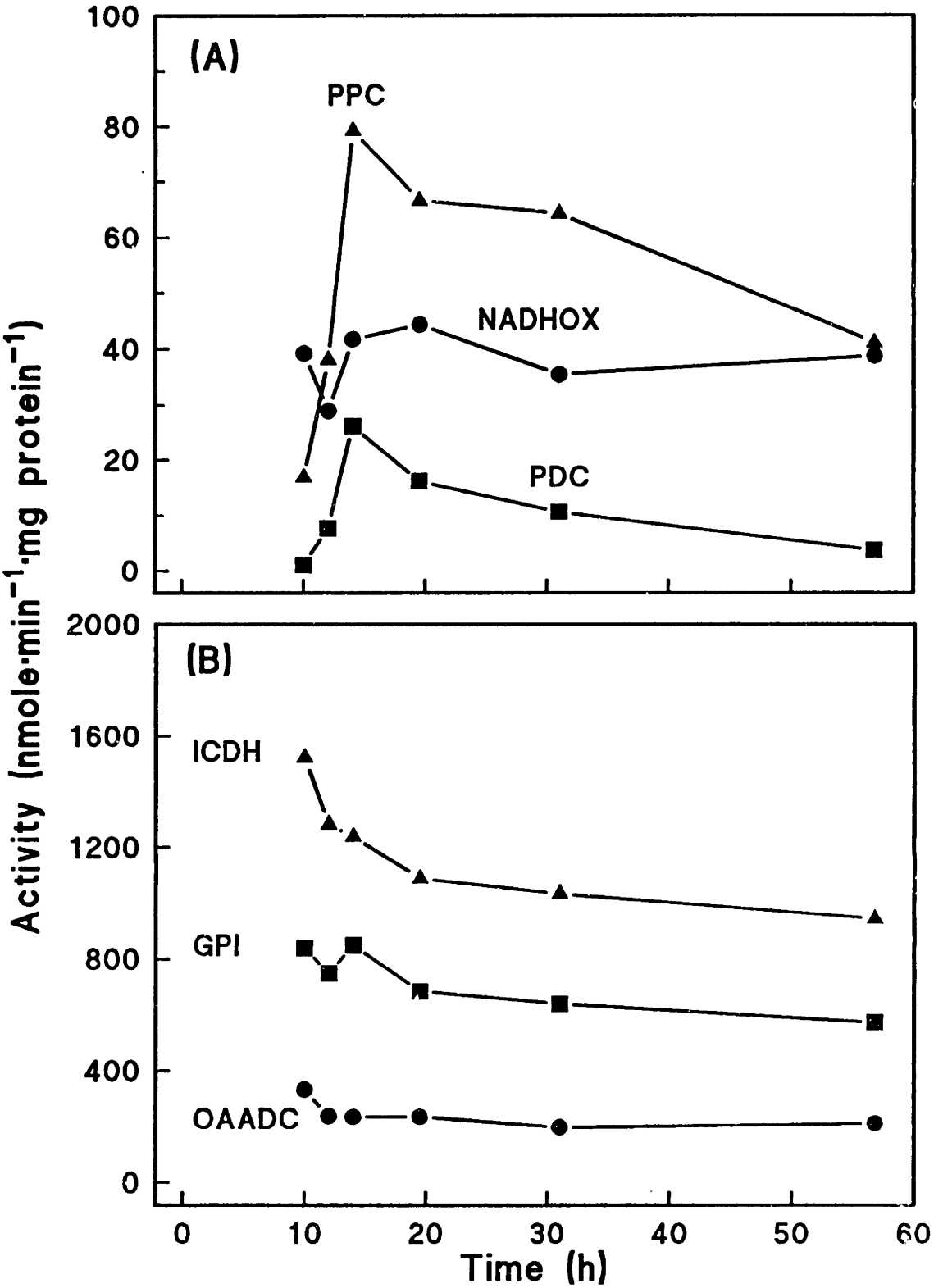

Figure 6.11 *In vitro* intracellular specific enzyme activities during the control lysine fermentation for: (A) (▲) PEP carboxylase (PPC), (●) NADH oxidase (NADHOX), (■) pyruvate dehydrogenase complex (PDC); (B) (▲) isocitrate dehydrogenase (ICDH), (●) oxaloacetate decarboxylase (OAADC), (■) glucose-6-P isomerase (GPI).

expect that futile cycle activity would be low and all ATP generated would contribute towards maintenance requirements. However, when the culture enters the stationary phase due to threonine limitation, actual ATP requirements should be low and futile cycles activity high to expend excess energy produced by the active primary metabolism. A large flux through Reaction (34:BS1) does not, therefore, always equate to high maintenance requirements; true maintenance requirements are best estimated during rapid growth or product synthesis periods when operation of futile cycles are expectedly low. Since we are interested in the maximum sustainable lysine yield, it is necessary to know what the cellular maintenance requirements are. If maintenance is extremely high, then lysine yield may be limited by energy requirements rather than suboptimal split-ratios at the principal nodes. Although the estimated excess ATP flux depicted in Figures 6.6-6.9 fluctuates around 700, the ATP flux depicted in Figure 6.7 should better reflect true maintenance requirements due to the high biomass and lysine synthesis rates associated with this period. Since the excess ATP generated during this period (537 units) may be assumed to go entirely for maintenance, this value can be used to estimate the maximum lysine yield that could be supported if biomass synthesis was close to zero. From Section 4.2 on theoretical flux distributions, a lysine yield of approximately 65% could be supported and generate enough ATP to satisfy maintenance requirements. This conclusion can also be deduced qualitatively. In early Phase II (Figure 6.7), the primary metabolism supports a high biomass yield even though the lysine yield is greater than 30%. If the energy and metabolite resources allocated to biomass were rechanneled into lysine synthesis only, a large improvement in lysine yield would result. Consequently, both analyses indicate that lysine yield in the stationary phase is not ATP limited. If not energy limited, the low observed lysine yields in Phases II and III must result from suboptimal partitioning of carbon at the principal nodes.

6.1.3.2.4 Principal Node Analysis

Principal node analysis involves the monitoring of principal node split-ratios under various conditions. If the split-ratio of a particular principal node remains unchanged during a perturbation, then the node is potentially rigid. Similarly, if a node split-ratio significantly alters under perturbations, the node is potentially flexible.

Analysis of the principal nodes during the first three phases of the fermentation, from the flux distributions illustrated in Figures 6.6-6.9, does provide some indication of their flexibility. However, because metabolite effector concentrations strongly govern nodal rigidity, the information provided from global perturbations must be interpreted with reservations. To appreciate this, it is useful to view the metabolism from a slightly different perspective. Consider the flux distribution associated with the synthesis of lysine and CO_2 only as the nominal or basal metabolism—as was done for the theoretical yield analysis. The superposition of biomass synthesis (*i.e.*, Reaction (33:BS1)) on this "basal" network can be regarded as a perturbation of the basal metabolism. However, since a vast number of metabolite pools are affected by this "biomass perturbation," it is a global perturbation, so principal node rigidity is difficult to asses. For example, if the amount of glucose catabolized by the PPP was only governed by Ribu5P concentration, then from the perspective of biomass synthesis the Glc6P node would be considered flexible since biomass synthesis affects Ribu5P concentration. From the perspective of lysine synthesis, however, the Glc6P node would be considered rigid since lysine synthesis consumes NADPH not Ribu5P. Nevertheless, principal node analysis of the control lysine fermentation is useful if viewed with proper subjectivity. Split-ratio variation for the Glc6P, PEP, Pyr, and OAA nodes are examined below.

Split-ratios at the Glc6P principal node, illustrated in Figure 6.12, are directly obtain from Figures 6.6-6.9 since they are already normalized with respect to the trunk flux (Reaction (1:BS1)). As discussed previously, the transition from Phase I to Phase II conditions results in a dramatic increase in the PPP split-ratio at the Glc6P node, as illustrated in Figure 6.12 (A,B). The 69% PPP split-ratio, as well as the specific amount of NADPH generated (1.38 moles/mole glucose), could support a lysine yield of 53% if biomass synthesis was zero. This preliminary analysis indicates that the Glc6P node is potentially flexible and not responsible for lysine yield limitations. This evidence alone, however, is not sufficient as described above, so other perturbations have been investigated as described in Section 6.3.

The split-ratios for the major flows at the PEP principal node are illustrated in Figure 6.13. The transition from growth to lysine production is exhibited by an

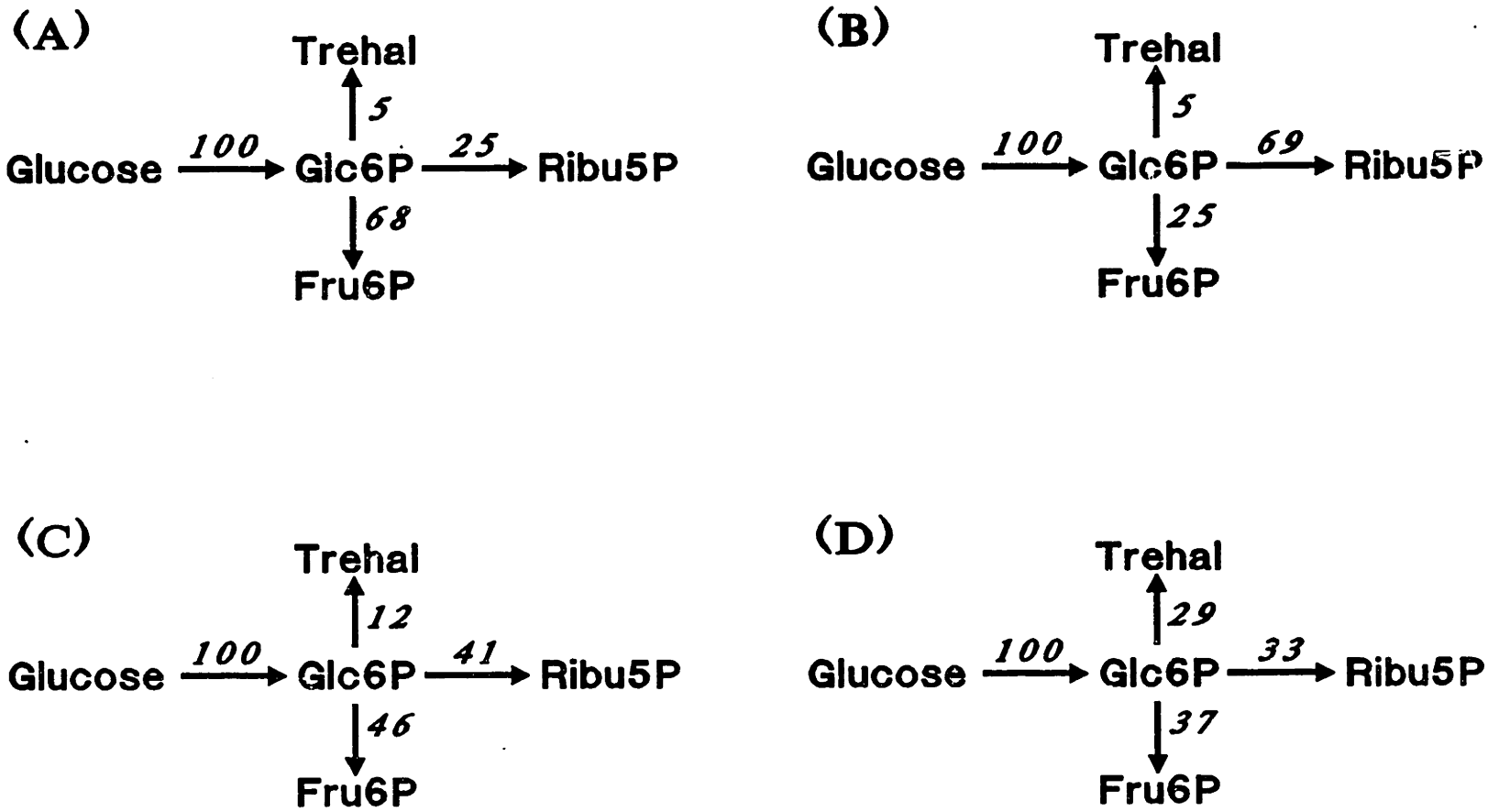

Figure 6.12 Glucose-6-P principal node split-ratios for the control lysine fermentation during: (A) Phase I (11.5 h); (B) early Phase II (13.5 h); (C) late Phase II (15.8 h); (D) Phase III (19.8 h).

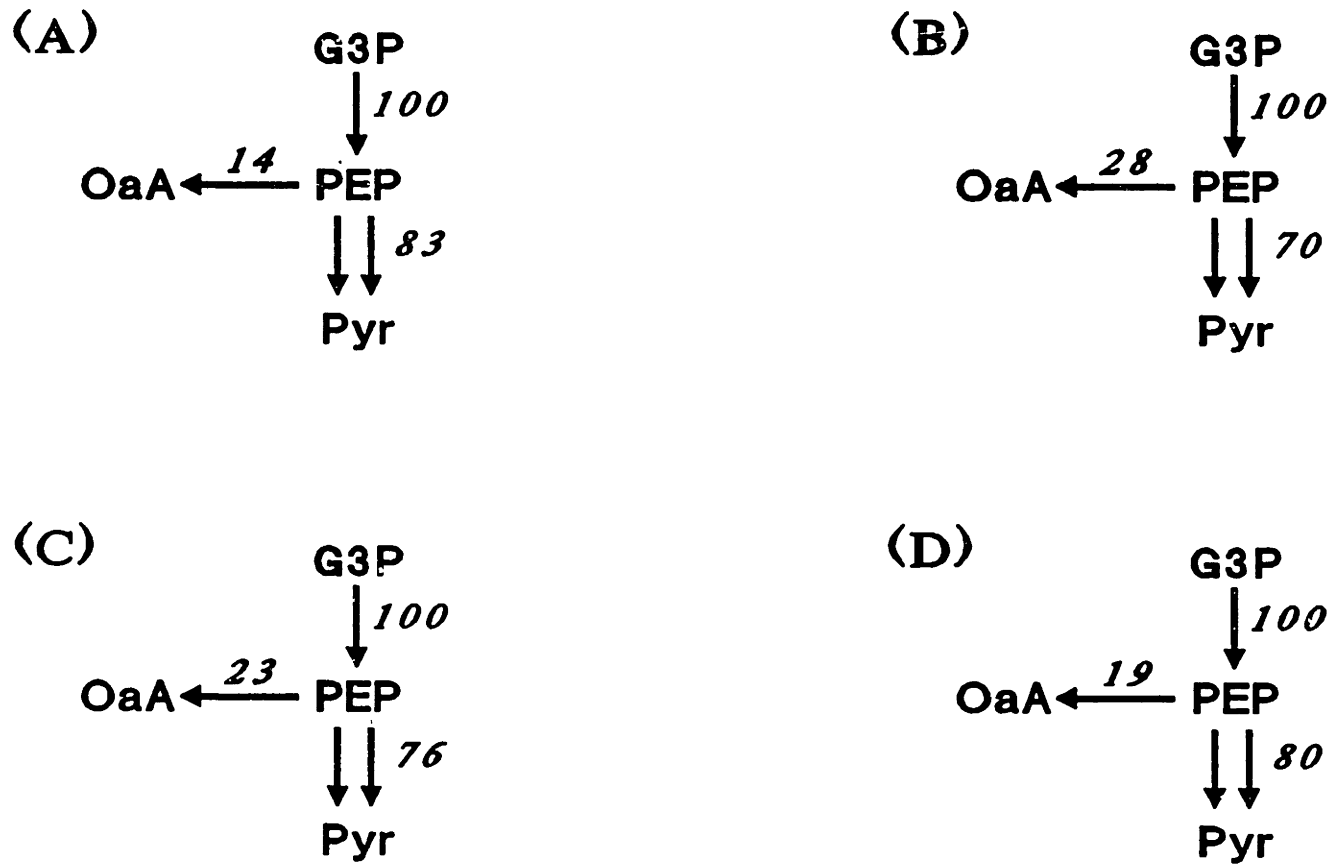

Figure 6.13 PEP principal node split-ratios for the control lysine fermentation during: (A) Phase I (11.5 h); (B) early Phase II (13.5 h); (C) late Phase II (15.8 h); (D) Phase iII (19.8 h). (Double arrows indicate summation of PK and PTS fluxes.)

increase in the OaA branch split-ratio, evident in Figure 6.13 (B). At first inspection, this increase appears slight when compared to the perturbation at the Glc6P node. Small changes in the split-ratios at the PEP node, however, can lead to significant changes in the lysine yield. For instance, the OaA branch split-ratio of 28% could produce a lysine yield of 50% under optimum conditions. Yet, if all the OaA actually synthesized by Reaction (9:BS1) during this period (shown in Figure 6.7) went towards lysine synthesis, the yield would only be 41%. The former prediction assumes zero biomass synthesis, so more glucose would reach the PEP node and the PPC flux would be 50. It cannot be determined from this analysis if the OaA branch split-ration would remain at 28% if more glucose reached this node. Although, as biomass synthesis drops, and more carbon reaches the PEP node, the OaA branch split-ratio decreases as illustrated in Figure 6.13 (C). In Phase III, less glucose reaches the PEP node and the OaA branch split-ratio drops even lower. Complications introduced by the biomass perturbation prevent a reliable flexibility assessment of the PEP node from the flux distributions obtained from the control lysine fermentation.

Split-ratio distributions about the Pyr principal node are illustrated in Figure 6.14. The maximum lysine branch split-ratio of 31%, Figure 6.14 (B), would also correspond to a theoretical lysine yield of 31%, so the Pyr node is not observed to flex beyond the observed lysine yield. This does not imply that the Pyr node is rigid, since suboptimal split-ratios at the other principal nodes would limit the lysine branch split-ratio at the Pyr node (see Section 4.3.2 on dependent networks). Furthermore, during Phase III of the fermentation, the TCA branch split-ratio decreases and the split-ratio for other amino acids (AA) increase. This implies that the TCA cycle may not out compete dihydrodipicolinate synthase (lumped in Reaction (31:BS1)) for pyruvate, although the synthesis of Val, Ala, etc, might. The degree of flexibility of the Pyr node cannot be assessed from the control lysine fermentation.

The split-ratios between the aspartate (Asp) and glutamate (Glut) branches at the OaA node are illustrated in Figure 6.15. It should be noted, Reaction (16:BS1) is not considered a trunk flux of the OaA node since this flow cannot be diverted from the TCA cycle due to mass balance constraints; that is, Reaction (16:BS1)

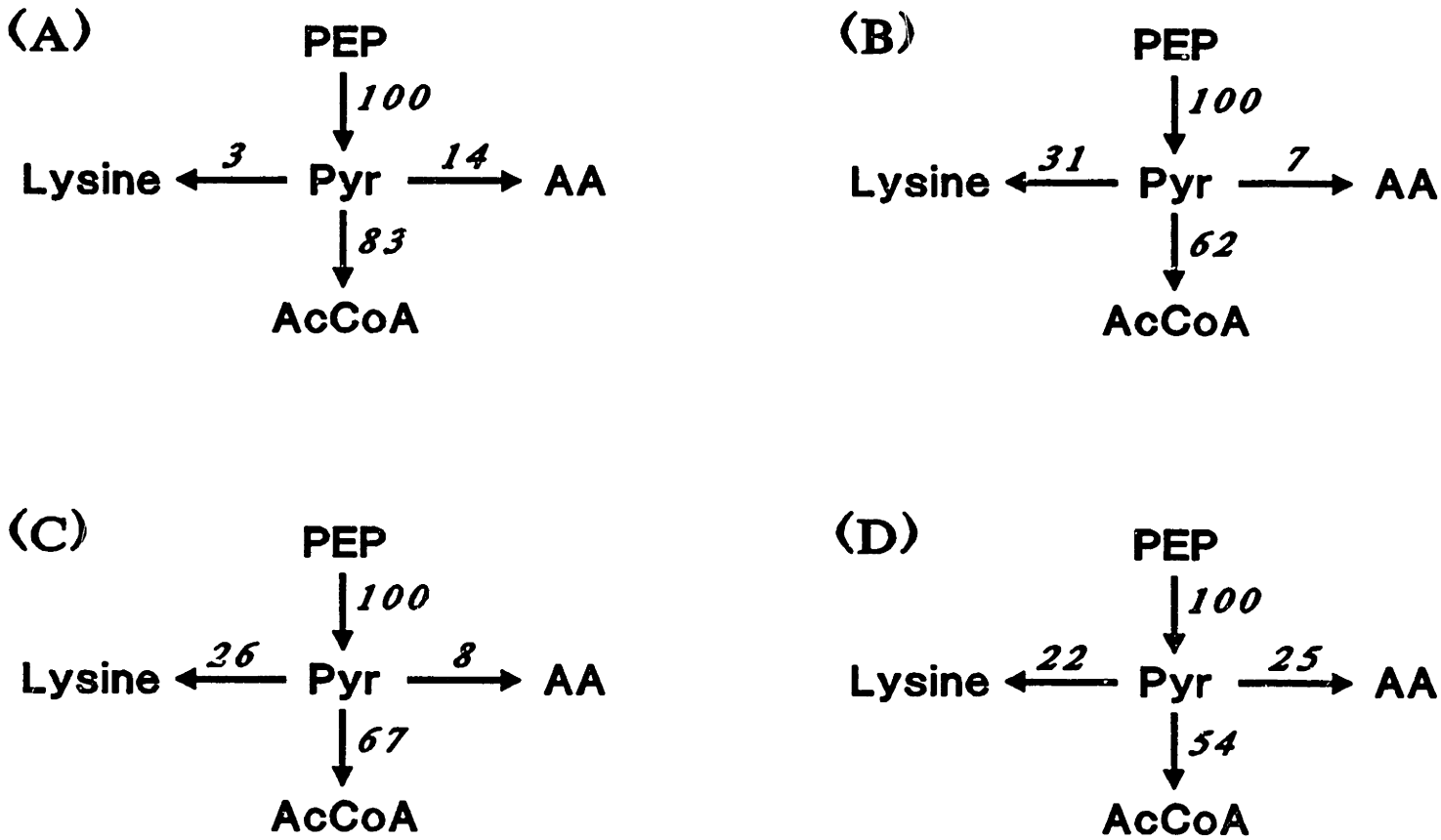

Figure 6.14 Pyruvate principal node split-ratios for the control lysine fermentation during: (A) Phase I (11.5 h); (B) early Phase II (13.5 h); (C) late Phase II (15.8 h); (D) Phase III (19.8 h). Synthesis of alanine, valine, and lactate is lumped into the AA branch flux (*i.e.*, other amino acids).

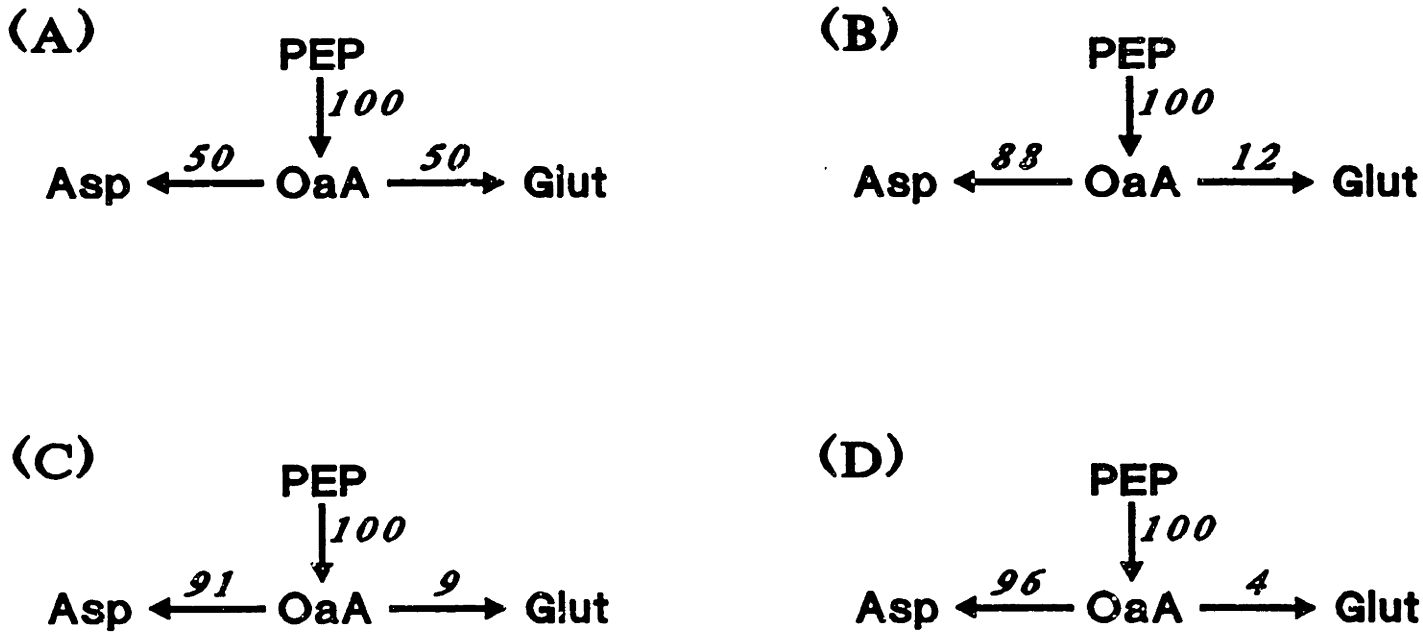

Figure 6.15 Oxaloacetate node split-ratios for the control lysine fermentation during: (A) Phase I (11.5 h); (B) early Phase II (13.5 h); (C) late Phase II (15.8 h); (D) Phase III (19.8 h). Note, Reaction (9) (PEP carboxylase) is the only true trunk of the OaA node.

represents the actual amount of flux supported by the TCA cycle which passes through OaA. The difference between Reactions (11:BS1) and (16:BS1) represent the net flux to Glut. Although under pure growth condition the split between Asp and Glut synthesis is equal (Figure 6.15 (A)), it is quite apparent that when lysine synthesis begins the majority of OaA synthesized from PEP leads to Asp formation. Consequently, it is obvious why the OaA node is not considered a principal node for the lysine fermentation.

6.1.4 Summary

The control lysine fermentation has been characterized into four phases consisting of: I) exponential growth; II) lysine overproduction and nonexponential growth; III) lysine overproduction and no growth; and IV) cell lysis, by-product excretion, and reduced lysine production. A threonine-limitation induced cellular morphology change is speculated to occur in the later stages of Phase II and in Phase III. Of the four phases, only Phases II and III are of interest for metabolic modifications since lysine yield in Phases I and IV can be easily improved by culturing an AEC^R strain, which is demonstrated in the next section.

The effectiveness of the consistency analysis routine is demonstrated, and the low consistency of the rate data in Phase III indicates potential accumulation of cellular associated constituents, such as trehalose. Flux distribution maps calculated from accumulation rates determined in Phases I, II, and III, are consistent with the established functionality of the primary metabolism. Estimated participation of the pentose phosphate pathway agrees well with radio and stable isotope tracer studies documented in the literature. The high flux supported by PEP carboxylase is also supported from stable isotope tracer studies cited in the literature. It is concluded that the estimated flux distribution maps accurately represent the metabolic state of the culture.

Analysis of the excess ATP flux reveals that the lysine yield is not energy limited. Principal node analysis demonstrates that the Glc6P node is potentially flexible, but flexibility of the PEP and Pyr nodes remains ambiguous due to metabolic alterations that result from biomass synthesis. Analysis of the OaA node conclusively

demonstrates that it is not a principal node. Localized perturbations of the three principal nodes are required to isolate network rigidity.

6.2 Industrial Type Fermentation

It was stressed in the previous section that Phases II and III of the control fermentation accurately represent the majority of industrial lysine fermentations and that Phases I and IV, although interesting, are not typically observed. To illustrate this, the results of a *Brevibacterium flavum* fermentation, cultivated on complex medium (CM3), are examined in this section. This strain, provide by Roquette Freres (Lestrem, France), is AEC resistant and auxotrophic for homoserine (and possibly other amino acids). Medium composition and operating conditions are presented in Section 5.5.5.5.

6.2.1 Characteristics

Profiles of the main extracellular metabolites are illustrated in Figure 6.16 (A-D). The biomass, glucose, and lysine profiles in Figure 6.16 (A) delineate two fundamental phases of the fermentation which closely resemble Phases II and III of the control fermentation. The first 25 hours of the *B. flavum* fermentation represents the growth phase, which, unlike the control fermentation, is accompanied by lysine overproduction due to the AEC^R phenotype of the cultured strain. Although the growth during this period is exponential, it is quite slow ($\mu = 0.076\ h^{-1}$) and indicative of growth in Phase II of the control fermentation. The drop in respiration at approximately 10 h (Figure 6.16 (B)) is due to the exhaustion of a nonessential nutrient, possibly acetate since pH is observed to increase during the first ten hours (Figure 6.16 (D)). The second stage of the fermentation starts when growth enters a stationary phase (ca. 25 h), which is accompanied by an increase in lysine synthesis rate and a plateau in respiration. This second stage lasts for approximately 30 hours before available ammonia and glucose are exhausted (Figure 6.16 (C,A, respectively)) and is suggestive of Phase III of the control fermentation.

Another noticeable difference in the *B. flavum* fermentation is the elevated respiration and the maintained culture viability in the second stage (*i.e.* no Phase IV).

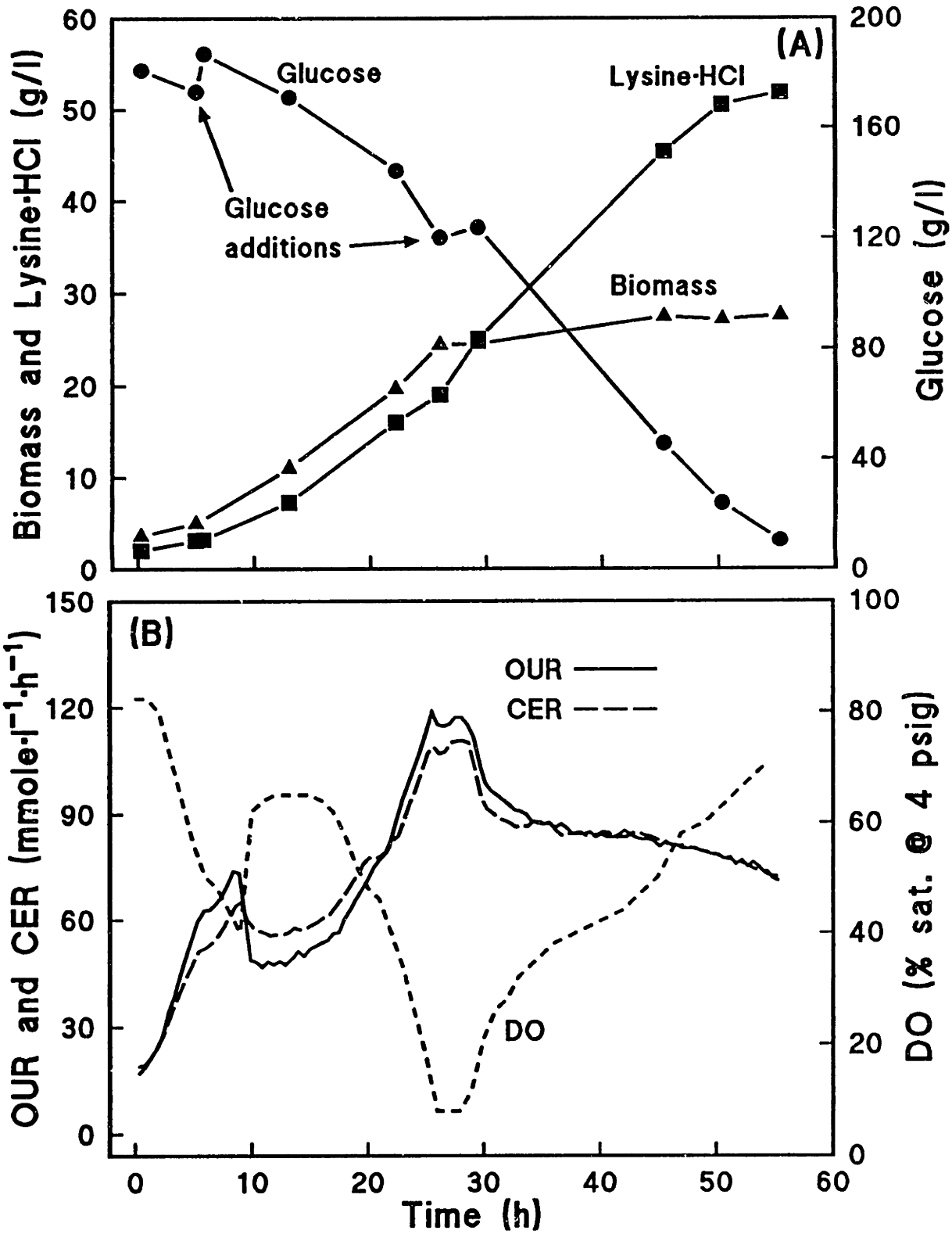

Figure 6.16 Lysine fermentation of *Brevibacterium flavum* AEC^R, Homo$^-$, cultured on complex medium (CM3). (A) Glucose (●), biomass (▲), and lysine•HCl (■) profiles in g/l. (B) Respiration: oxygen uptake rate (OUR), carbon dioxide evolution rate (CER), dissolved oxygen (DO).

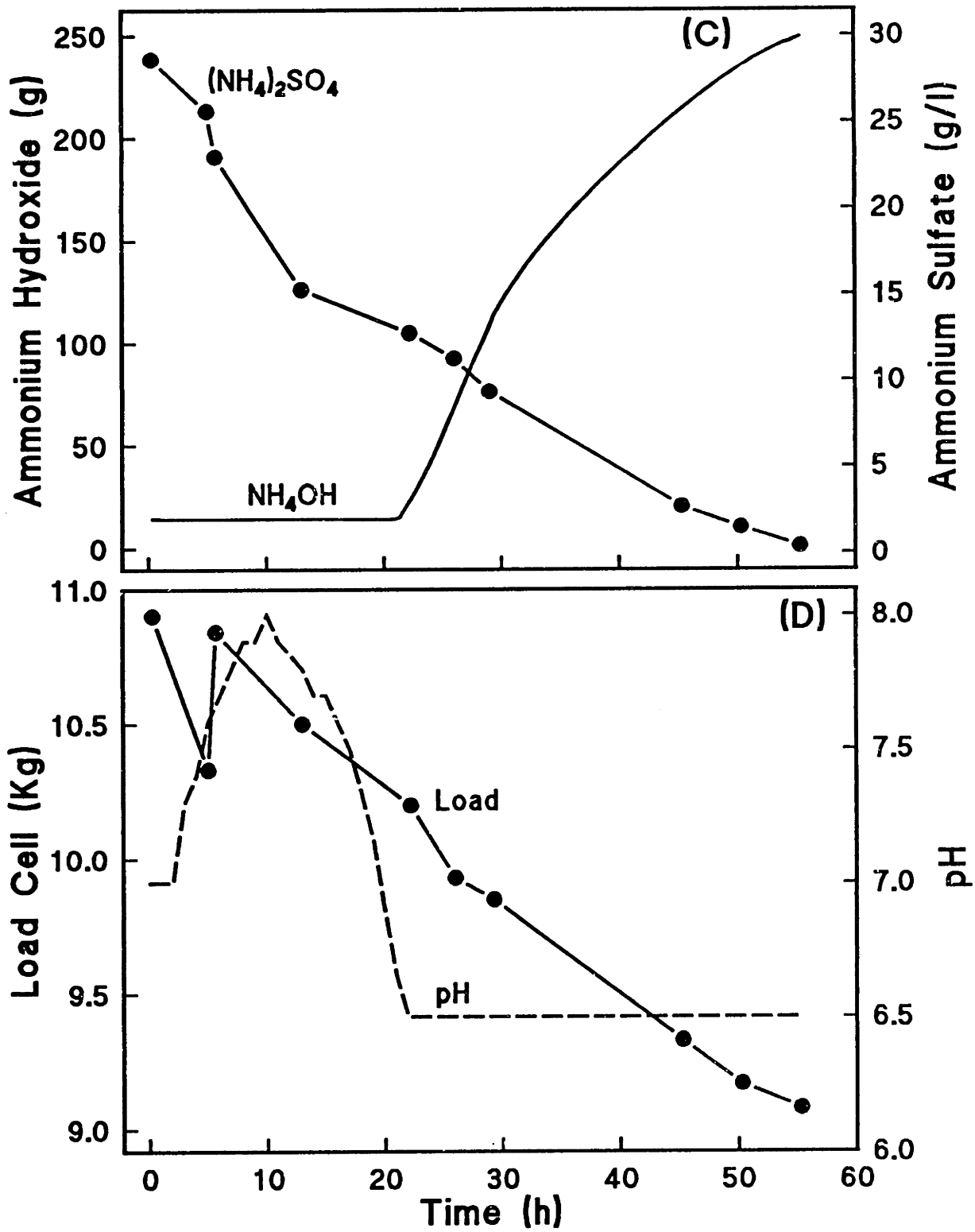

Figure 6.16 (continued) (C) Available ammonium in medium, as $(NH_4)_2SO_4$ (•), and cumulative amount of NH_4OH (26% (w/w) NH_3) added to maintain culture at pH 6.5 or above (solid curve). (D) pH (dashed curve) and fermentor load cell (volume) profiles. Note, pH is not controlled when above set point of 6.5.

What increases the viability of the culture during the last stage is unknown, but could be related to nutrients in the complex medium or efficiency of protein turnover as alluded to in Section 6.1. The complex nature of the medium also precludes identifying the growth limiting nutrient, which also might affect protein turnover. The final lysine•HCl titer (52 g/l) is more than double the control fermentation (20 g/l); however, the maximum instantaneous lysine yields of both fermentations are statistically identical (ca. 30%). The increase in lysine titer of the former is due to lysine production during growth and the maintained viability of the culture, not improvements in metabolic flux distributions.

6.2.2 Flux Distributions

Due to the consumption of unmeasured nutrients in the first stage of the fermentation (Bacto Yeast Extract and Tryptone components, and acetate), flux distributions cannot be reliably estimated. These supplied nutrients, however, are essentially exhausted by the second stage of the fermentation, so flux distributions can

Table 6.7 Accumulation rate subvectors for the *B. flavum* fermentation at 39.8 h from measurements taken at 29.3 h and 50.3 h, Figure 6.16. Based on MS1 and BS1 in Appendix B, h = 1.2.

Elements of $\mathbf{r}_B(t)$	Accumulation Rates (mM/h) $\bar{\mathbf{r}}_B(39.8) \pm \sigma$		$\hat{\mathbf{r}}_B(39.8)$
Ac (1)	0	± 2	0.23
Ala (4)	0	± 2	0.33
Biomass (7)	1.26	± 0.9	1.33
CO2 (8)	85.0	± 8.5	90.1
Glc (14)	-26.3	± 0.7	-26.2
Lac (19)	0	± 2	0.35
LysE (20)	6.64	± 0.3	6.65
NH3 (25)	-15.0	± 0.3	-15.0
O2 (26)	-86.1	± 8.6	-83.0
Pyr (29)	0	± 2	0.43
Trehal (35)	0	± 2	1.41
Val (36)	0	± 2	0.39

be calculated with acceptable consistency. Table 6.7 summarizes the accumulation rate subvector, $\overline{\mathbf{r}}_B(39.8)$, calculated from measurements taken at 29.3 h and 50.3 h. Also listed in the table is the estimated accumulation rate vector, $\hat{\mathbf{r}}_B(39.8)$, and the associated consistency index. The resulting flux distribution map is displayed in Figure 6.17.

The negative flux in the oxidative branch of the pentose phosphate pathway (Reaction (22:BS1)) is small enough to be considered zero, so the irreversibility of this pathway is not violated. The flux through the PPP is zero since the high flux through isocitrate dehydrogenase (Reaction (12:BS1)) of the TCA cycle, generates enough NADPH to satisfy lysine and biomass synthesis requirements. It is speculated that culturing the organism on a complex medium stimulates the activity of the TCA associated enzymes so that a high TCA flux can be maintained. It is also possible that the unidentified growth limiting nutrient (which need not be threonine) allows continuation of protein synthesis so that primary enzyme decay does not occur. This high TCA activity results in the elevated respiration observed throughout the fermentation (Figure 6.16 (B)). Consequently, the main difference between the *B. flavum* flux distribution and that observed in the control fermentation is the increase activity in the TCA cycle. The lower flux in the TCA cycle observed in the control fermentation results from the diversion of carbon to pyruvate derived by-products, which may indicate that PDC is losing activity in the later phases of the control fermentation. The flux comparisons also support the preliminary hypothesis that the Glc6P principal node is flexible since the loss in NADPH production associated with the lower TCA cycle flux can be compensated by an increase in PPP flux. It is interesting to note that the flux distribution associated with the *B. flavum* fermentation closely matches the expected theoretical flux distribution for the lysine yield observed.

6.2.3 Summary

It has been demonstrated that Phases II and III of the control fermentation, presented in Section 6.1, accurately capture the characteristics typically displayed in industrial lysine fermentations. Furthermore, industrial fermentations suffer the same

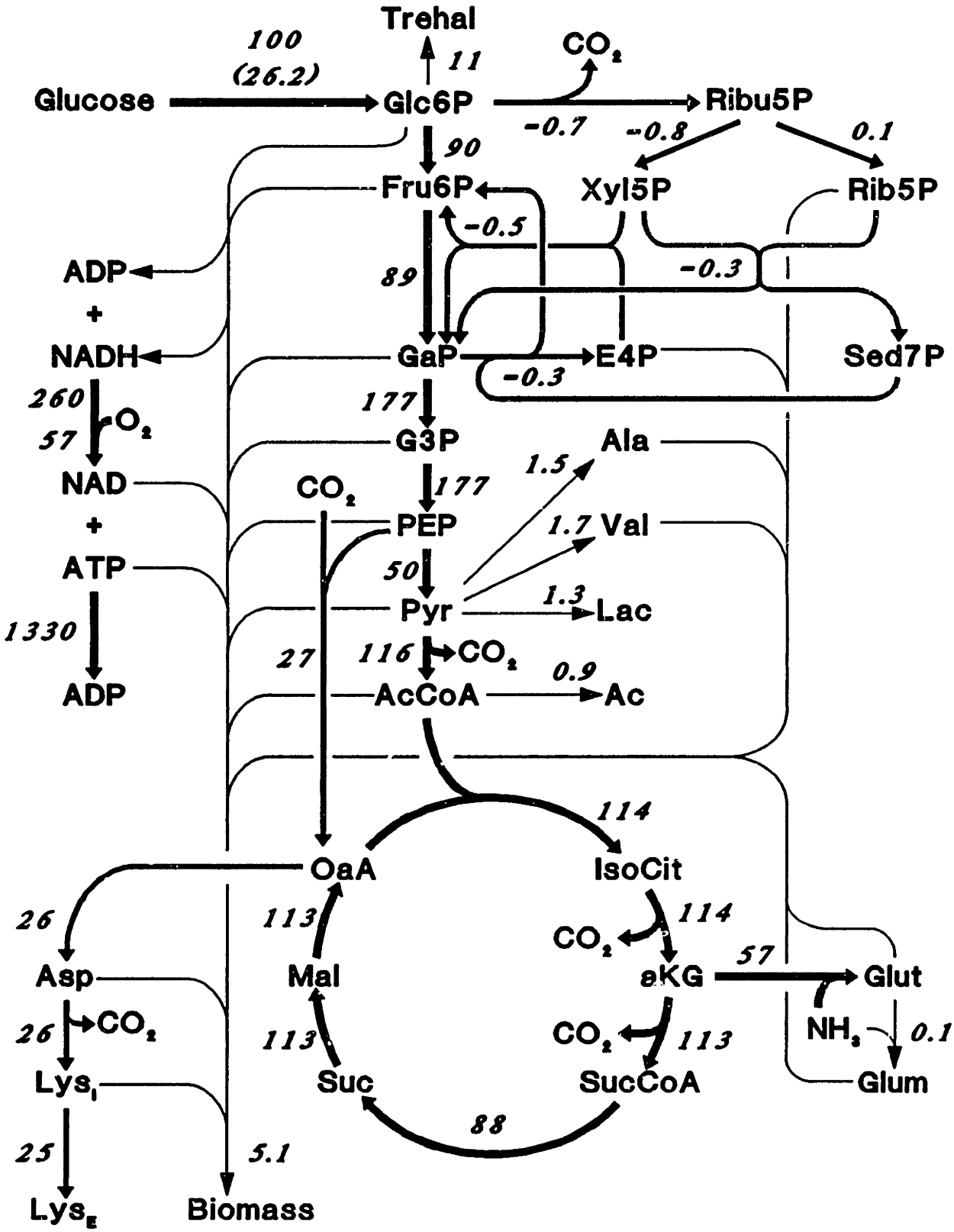

Figure 6.17 Flux distribution map for the *Brevibacterium flavum* lysine fermentation at 39.8 h. Fluxes estimated from measurements taken at 29.3 h and 50.3 h (see Figure 6.16 and Table 6.7), and normalized by glucose uptake rate (shown in parentheses; mmole•l^{-1}•h^{-1}). See BS1 in Appendix B for reaction stoichiometry.

low instantaneous lysine yields and associated suboptimal, principal node split-ratios. However, flux distributions associated with the *B. flavum* fermentation differ from those observed in the control fermentation by the higher flux supported by the TCA cycle. This high TCA cycle flux may be attributed to the complex medium which may either simulate TCA cycle enzymes or produce a favorable nutrient limitation. Nevertheless, metabolic modifications that lead to improved flux distributions in Phases II and III of the control fermentation should also enhance industrial fermentations.

6.3 Analysis of the Glc6P Principal Node

The Glc6P principal node represents the branch point between glycolysis—the main fueling pathway—and the oxidative branch of the pentose phosphate pathway, which includes two, of only three, NADPH producing primary reactions. As explained in Section 4.3.1, lysine yield may be limited by NADPH production if the Glc6P node is rigid; that is, if the fraction of glucose which enters the PPP is bounded, then the yield of NADPH produced per glucose consumed will not be high enough to meet lysine synthesis requirements, and the lysine yield will be governed by the upper bound on the PPP split-ratio. Contrary to the PEP and Pyr nodes, poor lysine yields caused by NADPH limitations—due to suboptimal glucose partitioning at the Glc6P node—has not been examined.

Preliminary analysis of the Glc6P node during the control fermentation (Section 6.1.3.2) indicates that this node is potentially flexible; however, as previously discussed, the evidence alone is not conclusive due to complications associated with biomass synthesis. Consequently, two experiments were conducted to support or refute the preliminary hypothesis governing the flexibility of the Glc6P node. The first experiment involves the fermentation and subsequent flux analysis of a Glc6P isomerase attenuated mutant of *C. glutamicum* ATCC 21253. The second experiment pertains to the fermentation and analysis of *C. glutamicum* ATCC 2125 cultured on a gluconate minimal medium.

6.3.1 Analysis of a GPI^{A} Mutant

The split-ratios for the glycolysis and PPP branches inevitably rest on the relative affinities of Glc6P isomerase and Glc6P dehydrogenase for Glc6P, respectively. In turn, the relative activities of the two enzymes depend on the intracellular environment as well as the associated enzymes of the two pathways. Nevertheless, if lysine yield is constrained by a weakly rigid Glc6P node (see Section 4.3.2), then the split-ratio of the PPP branch should increase if the activity of Glc6P isomerase is completely or partially attenuated. Even if lysine yield is unaffected, we can still conclude that the Glc6P node is not strongly rigid if a significant increase in the PPP split-ratio can be attained from the perturbation.

Isolation and characterization of *C. glutamicum* NFG068 (a GPI^{A} mutant of *C. glutamicum* ATCC 21253) is describe in Section 5.4.3. Compared to ATCC 21253, the activity of GPI in NFG068 is attenuated by 90-95%. Both strains have similar activities of G6PDH, GN6PDH, and ICDH (the only NADPH producing enzymes), and nutrient requirements. The mutation is stable and has not been observed to revert.

6.3.1.1 Fermentation of NFG068

Results of the NFG068 fermentation are depicted in Figure 6.18 (A-D). Since gluconate induces the dehydrogenases of the PPP [Sugimoto and Shiio, 1987b; Section 6.3.2.1, Table 6.10], two 50 g supplements of potassium gluconate were added early in the fermentation (Figure 6.18 (C)) in an attempt to increase the slow growth rate (μ = 0.15), but they had little to no effect other than on respiration (Figure 6.18 (B)). Profiles of biomass and lysine, illustrated in Figure 6.18 (A), exhibit phases characteristic of Phases I and III of the control fermentation; however, since growth abruptly stops and enters a stationary phase at 22.0 h, the fermentation directly enters Phase III, bypassing Phase II. Similarly, Phase IV is averted since cell lysis and by-product formation are not observed; although, lysine synthesis rate does decrease. Other notable features of the fermentation include the attenuated production and consumption rates of all extracellular metabolites (see below), the extended fermentation time, the reduced respiration, and the low final biomass titer (only 10 g/l DCW). The cause of the reduced biomass titer is still unknown, but could be

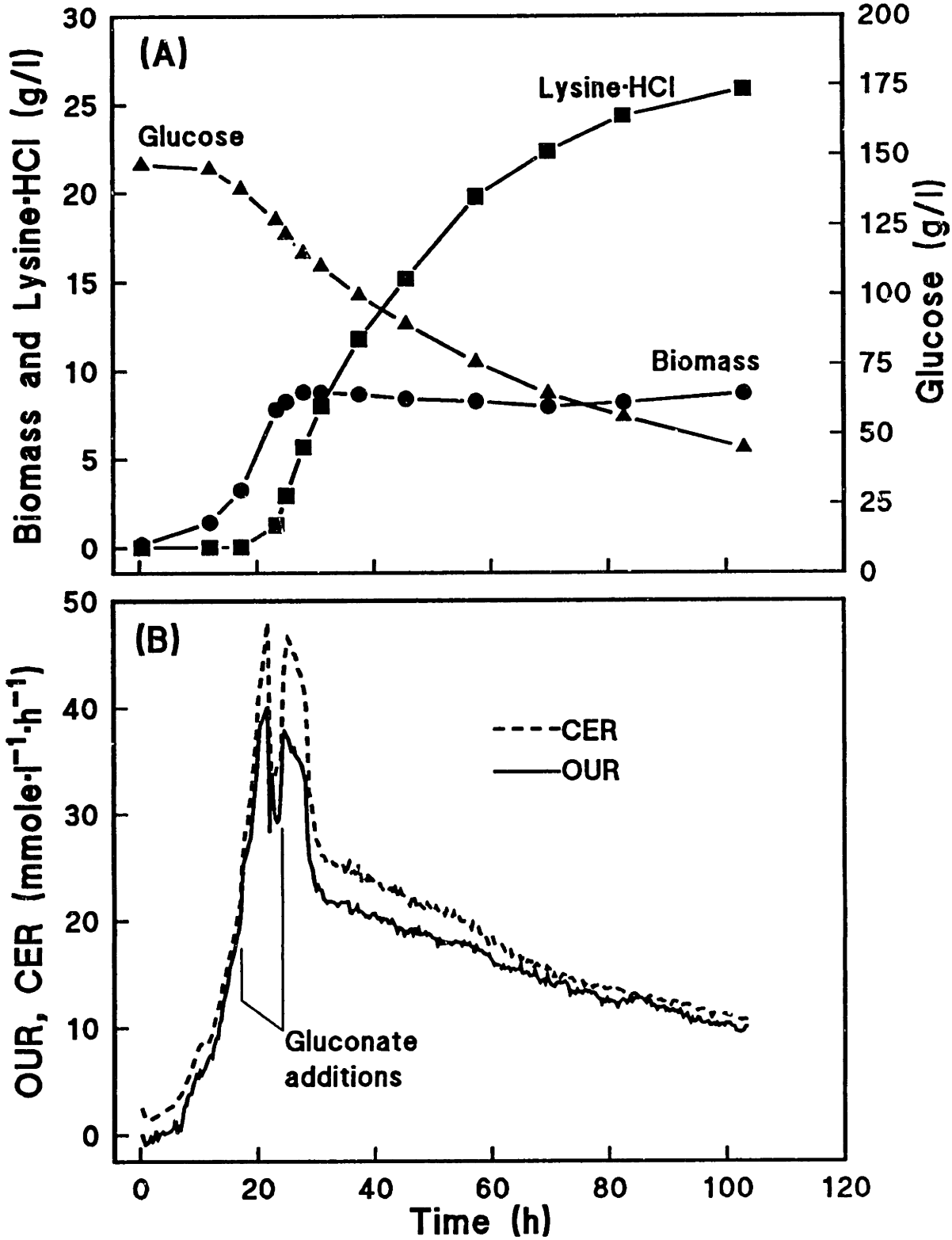

Figure 6.18 Lysine fermentation of *C. glutamicum* NFG068 (GPI^{A}) cultured on glucose medium (FM4). (A) Glucose (▲), biomass (●), and lysine•HCl (■) profiles in g/l. (B) Culture respiration: oxygen uptake rate (OUR, solid curve), carbon dioxide evolution rate (CER, dashed curve).

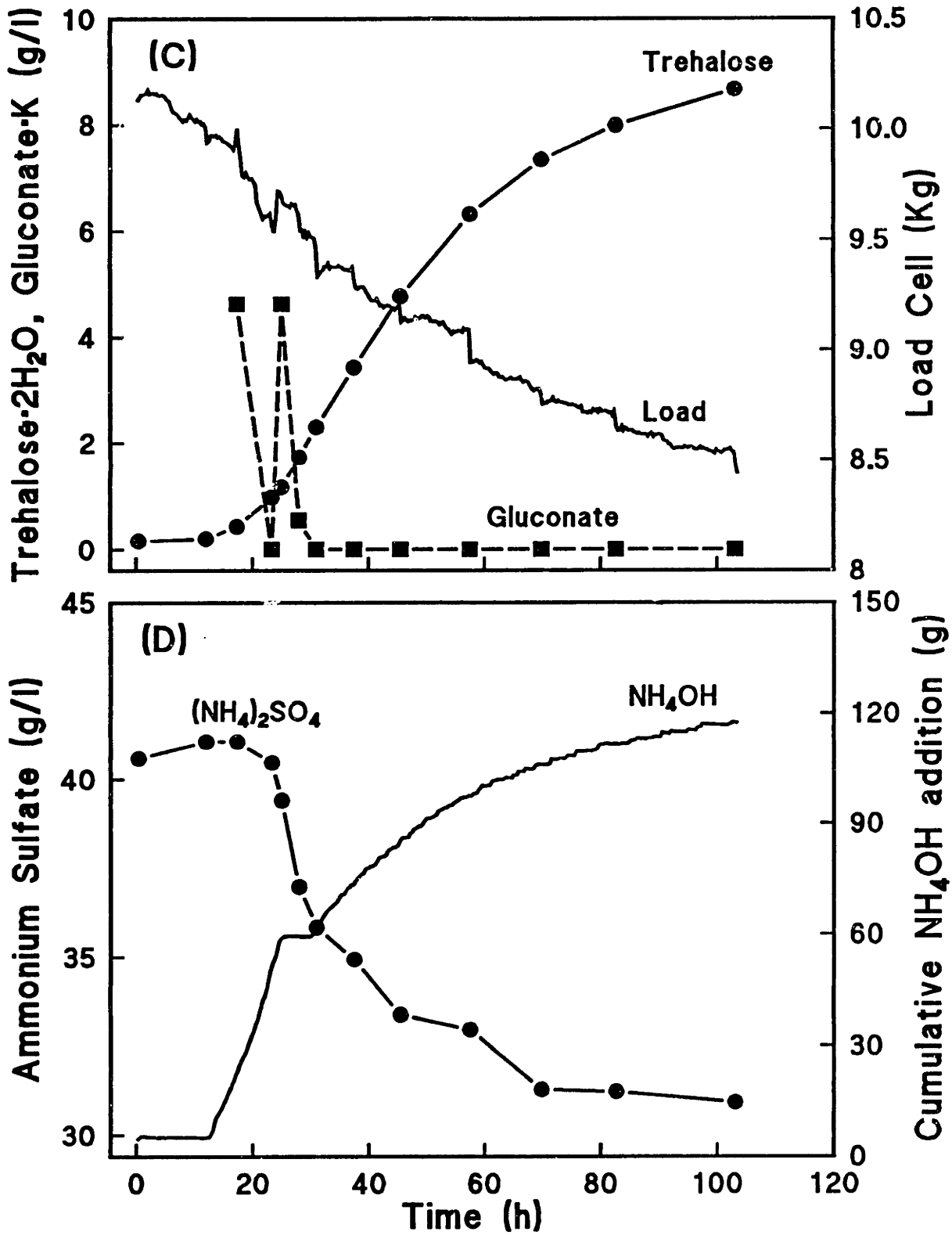

Figure 6.18 (continued) (C) Profiles of added gluconate (■) and trehalose production (●), and fermentor volume (load) used to adjust OUR and CER. (D) Available ammonium in broth, as $(NH_4)_2SO_4$ (●), and amount of NH_4OH (26% (w/w) NH_3) added to maintain culture at pH 7.

related to reduced protein turnover efficiency. Even though the final lysine titer is 25% greater than the control fermentation (25 g/l verses 20 g/l), the instantaneous yield at the start of lysine production is approximately 35%, only a slight increase over the control (see flux distribution below). Consequently, the increase in lysine titer results from an extension of phase III of the culture, and not an increase in instantaneous yield (similar to the *B. flavum* fermentation). Activity of GPI and the three NADPH-producing enzymes, assayed at 31.0 h and 57.5 h, are listed in Table 6.8. The reduced activity of GPI (11% of ATCC 21253 cultured on gluconate) confirms the stability of the mutation. The activities of GPI, G6PDH, and GN6PDH are slightly higher than nominal due to induction by added gluconate (See Section 5.4.3 and Table 6.10).

Table 6.8 Activities of selected enzymes of NFG068 during the fermentation depicted in Figure 6.18.

Time (h)	Protein (mg/ml)	Activity (nmole•min^{-1}•mg protein^{-1}) GPI	G6PDH	GN6PDH	ICDH
31.0	7.84	151	173	448	1100
57.5	7.52	146	154	443	956

6.3.1.2 Flux Analysis

To avoid flux alterations induced by gluconate consumption, the accumulation rate vector was constructed from measurements taken at 31.0 h and 37.5 h (t_{AVE} = 34.3 h), in Phase III after gluconate exhaustion. The measured and estimated rate vectors are listed in Table 6.9, along with the consistency index. Compared to the control fermentation (Table 6.4) the accumulation rates for the NFG068 fermentation are approximately three times lower. However, the flux distribution map, illustrated in Figure 6.19, is remarkably similar to those observed during the control fermentation. It is quite evident from Figure 6.19 that no perturbation of the Glc6P node split-ratios has resulted from the 90% attenuation of GPI. The mutation has not altered the instantaneous lysine yield significantly, but has dramatically reduced the absolute flux through the network. This, of course, is consistent with the

Table 6.9 Measured and estimated accumulation rate subvectors for the NFG068 fermentation at 34.3 h from measurements taken at 31.0 h and 37.5 h, Figure 6.18. Based on MS1 and BS1 in Appendix B, $h = 0.09$.

Elements of $\mathbf{r}_E(t)$	Accumulation Rates (mM/h) $\bar{\mathbf{r}}_E(34.3) \pm \sigma$		$\hat{\mathbf{r}}_E(34.3)$
Ac (1)	0	± 1	0.02
Ala (4)	0	± 1	0.00
Biomass (7)	-0.17	± 0.9	-0.15
CO2 (8)	26.5	± 2.7	26.2
Glc (14)	-9.0	± 2.5	-8.7
Lac (19)	0	± 1	0.03
LysE (20)	3.16	± 0.2	3.16
NH3 (25)	-5.5	± 5.8	-6.3
O2 (26)	-22.7	± 2.3	-23.0
Pyr (29)	0	± 1	0.00
Trehal (35)	0.46	± 1	0.57
Val (36)	0	± 1	0.08

hypothesis of a dependent network which harbors one or more rigid nodes as discussed in Section 4.3.2.

If the Glc6P node is flexible, the above results would be expected since lysine yield would be limited by the rigidity of either the PEP or Pyr nodes and network dependence would constrain the Glc6P node perturbation. On the other hand, if the Glc6P node is weakly rigid and constraining the lysine yield, the GPI perturbation should have improved the yield, as attenuation of GPI should allow more Glc6P to enter the PPP. The GPI perturbation, therefore, indicates that the Glc6P node in not weakly rigid. A third possibility does exit. The Glc6P node could be strongly rigid. If this is the case, then attenuating GPI should also result in attenuation of the PPP branch and the net result would be similar to that actually observed. To investigate the possibility that the Glc6P node might be strongly rigid, a gluconate fermentation was conducted. This fermentation is investigated in the next section.

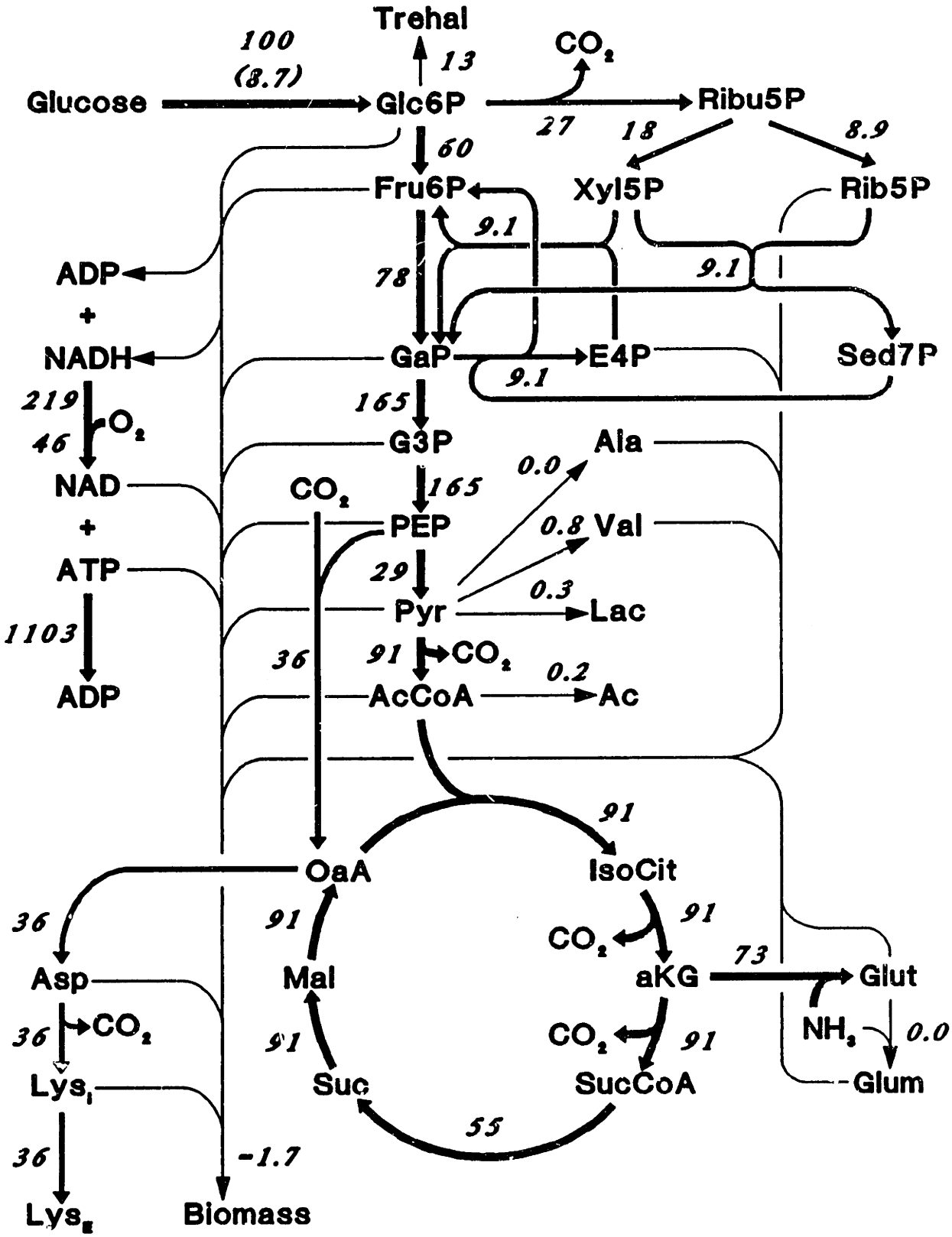

Figure 6.19 Flux distribution map for the NFG068 lysine fermentation at 34.3 h. Fluxes estimated from measurements taken at 31.0 h and 37.5 h (see Figure 6.18 and Table 6.9), and normalized by glucose uptake rate (shown in parentheses; mmole•l^{-1}•h^{-1}).

6.3.2 Analysis of Gluconate Metabolism

The Glc6P node is effectively bypassed when gluconate is used as the primary carbon source since it directly enters the PPP. Consequently, if the Glc6P node is strongly rigid and limiting lysine yield, cultivation of *C. glutamicum* ATCC 21253 on gluconate should improve lysine yield. The basis of this hypothesis and the analysis of a gluconate fermentation are examined in this section.

6.3.2.1 Gluconate Catabolism

As reviewed in Section 3.2.3, gluconate enters the PPP after phosphorylation to gluconate-6-phosphate (Glcn6P) by gluconokinase as illustrated in Figure 6.20. Since the reversal of 6-phosphogluconolactonase is thermodynamically unfavorable, $\Delta G^{\circ} = +5.0$ Kcal/mole, and its substrate (δ-6-phosphogluconolactone) spontaneously decomposes to Glc6P [Bauer *et al.*, 1983; Schofield and Sols, 1976], the reaction is considered kinetically irreversible. The overall conversion of Glcn6P to Fru6P via 6-phosphogluconolactonase is also thermodynamically unfavorable ($\Delta G^{\circ} = +5.5$ Kcal/mole (see Figure 6.20)), and the reaction cannot be driven backwards. Consequently, all gluconate phosphorylated will be converted to Ribu5P by GN6PDH and generate a minimum of one mole of NADPH for each mole of gluconate consumed, or $[\text{NADPH/gluconate}]_{MIN} = 1.0$ (this ratio is higher if recycling of Ribu5P occurs, $[\text{NADPH/gluconate}]_{MAX} = 5.0$). The corresponding minimum theoretical lysine yield on gluconate corresponds to 45% (the maximum yield is lower than glucose, 69%). For glucose catabolism $[\text{NADPH/glucose}]_{MIN} = 0$ and $[\text{NADPH/glucose}]_{MAX} = 6.0$, however, examination of the flux distributions during Phase I, late Phase II, and Phase III of the control lysine fermentation (Figures 6.6, 6.8, and 6.9, respectively) and Phase III of the NFG068 fermentation (Figure 6.19) reveals that the typical PPP flux is 30% of glucose consumption, or [NADPH/glucose] = 0.6 since two NADPH moles are produced for each Glc6P mole catabolized through the PPP. Since $[\text{NADPH/gluconate}]_{MIN}$ is greater than [NADPH/glucose] typically observed during lysine production on glucose, a fermentation on gluconate should exhibit an improved lysine yield if lysine is limited by NADPH production, due to the rigidity of the Glc6P node.

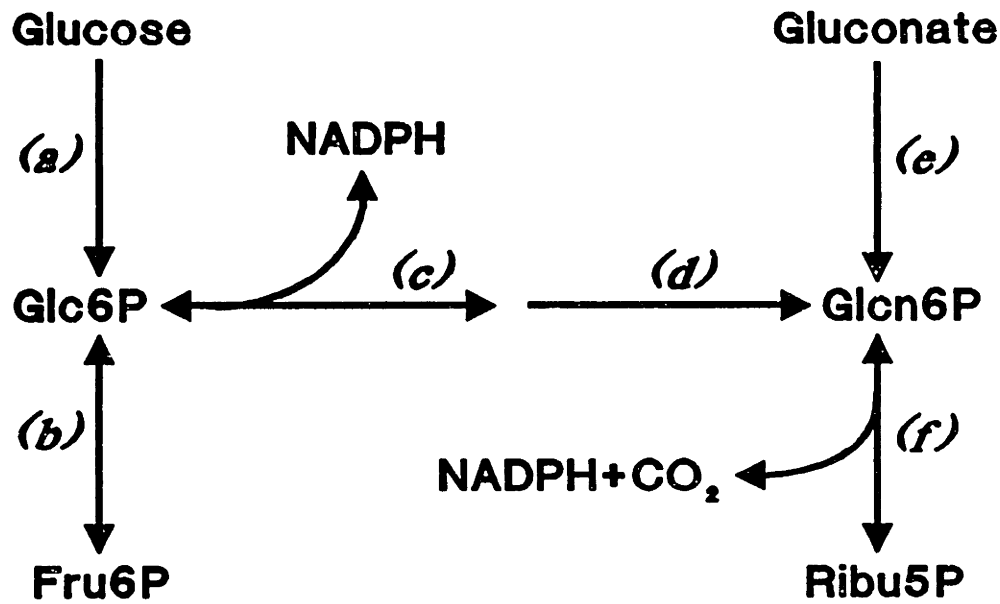

Figure 6.20 Metabolic entry points for glucose and gluconate metabolism. (a) PEP:glucose phosphotransferase system; (b) Glucose-6-P isomerase ($\Delta G^\circ = +0.4$ Kcal/mole towards Fru6P formation); (c) Glucose-6-P dehydrogenase ($\Delta G^\circ = -0.1$ Kcal/mole towards Glcn6P formation); (d) 6-Phosphogluconolactonase ($\Delta G^\circ = -5.0$ Kcal/mole towards Glcn6P formation); (e) Gluconokinase; (f) Gluconate-6-P dehydrogenase. Reaction ΔG° from Lehninger (1975).

The above biochemical analysis for gluconate metabolism assumes that 1) alternate pathways for Glcn6P catabolism are not present or induced by gluconate and 2) reactions which consume NADPH are similarly not induced. For instance, an alternate pathway for Glcn6P catabolism is the Entner-Doudoroff pathway. Although it has been demonstrated in Section 5.3.1 that this pathway is not expressed in *C. glutamicum* when cultured on glucose, its induction by gluconate was not examined then. In regards to NADPH sinks, a pyridine dinucleotide transhydrogenase has not been detected in glutamic acid bacteria (Sections 3.2.6.3 and 5.3.1), nor is a NAD specific GN6PDH induced by gluconate [Sugimoto and Shiio, 1987b]. However, it is plausible that malic enzyme, if induced by gluconate, could act as a NADPH sink (though it is not known to operate in this manner). Also, reversibility of 6-phosphogluconolactonase has not been actually checked. Consequently, intracellular assays were performed on glucose and gluconate cultured cell-free extracts to ensure that gluconate catabolism will produce more NADPH than glucose catabolism, the results of which are presented in Table 6.10. It is clear from these results that 6-phosphogluconolactonase is not reversible, and that the malic enzyme and the ED pathway are not induced by glucose or gluconate. However, GPI and G6PDH exhibit some induction and GN6PDH shows a three fold increase in activity when cultured on gluconate, which has also been observed by Sugimoto and Shiio (1987b). No noticeable induction of ICDH occurs. The dramatic increase in GN6PDH activity strongly supports the hypothesis that all gluconate is catabolized through this enzyme and that a gluconate fermentation should produce more intracellular NADPH.

6.3.2.2 Gluconate Fermentation

The first attempt to grow *C. glutamicum* on 140 g/l potassium gluconate (medium FM8; Section 5.5.5.3) resulted in linear growth and eventually ended in cell lysis after 45 h, as illustrated in Figure 6.21 (A). Although not assayed for, lysine was not believed to be produced during this peculiar fermentation. To investigate the cause of the linear growth, several shaker flask studies were conducted. It was found that *C. glutamicum* will grow exponentially on gluconate as the sole carbon source, but only at relatively low concentrations (ca. 5 g/l) and only at about half its normal

Table 6.10 Intracellular assays of *C. glutamicum* ATCC 21253 cultured on PMB medium or PMB medium with gluconate as the only carbon source.

Enzyme or Pathway	Activity (U/mg protein) Glucose	Gluconate
6-Phosphogluconolactonase, reversal	--	3. ± 3
Entner-Doudoroff	0. ± 5	0. ± 5
Malic Enzyme	1. ± 5	1. ± 5
Glucose-6-P isomerase	950. ± 50	1360. ± 50
Glucose-6-P dehydrogenase	130. ± 20	200. ± 20
Gluconate-6-P dehydrogenase	270. ± 20	830. ± 20
Isocitrate dehydrogenase	1330. ± 50	1270. ± 50

growth rate. However, if glucose is added, gluconate concentration can be dramatically increased without detrimental effects on growth rate as illustrated in Figure 6.21 (B). These seemingly insignificant results are included here, as the linear growth may be the result of NADPH overproduction and is worthy of future research as discussed in the next section.

To alleviate the linear growth problem, *C. glutamicum* was cultured on FM9 medium, which is identical to FM8 medium, except for an additional 10 g/l of glucose. The results of the gluconate fermentation are depicted in Figure 6.22 (A-D). As illustrated in Figure 6.22 (A), the additional 10 g/l glucose allows growth to proceed exponentially even in the presence of 140 g/l potassium gluconate which does not seem to effect the characteristics or growth rate (μ = 0.31 h^{-1}) of the culture. To ensure that the culture reached the lysine production phase (*i.e.*, consumed all threonine), two 50 g supplements of glucose were added as depicted in Figure 6.22 (C) and evident in the culture's respiration, Figure 6.22 (B). At 15.7 h (as documented by the drop in respiration and confirmed in Figure 6.22 (C)) all added glucose is exhausted and gluconate is the sole carbon source.

The linear growth characteristic associated with gluconate metabolism becomes evident after exhaustion of supplied glucose, as illustrated in Figure 6.22 (A). Since *C. glutamicum* does not grow exponentially on gluconate, the culture bypasses Phase II (*i.e.*, rapid biomass and lysine synthesis) and directly enters Phase III. Here

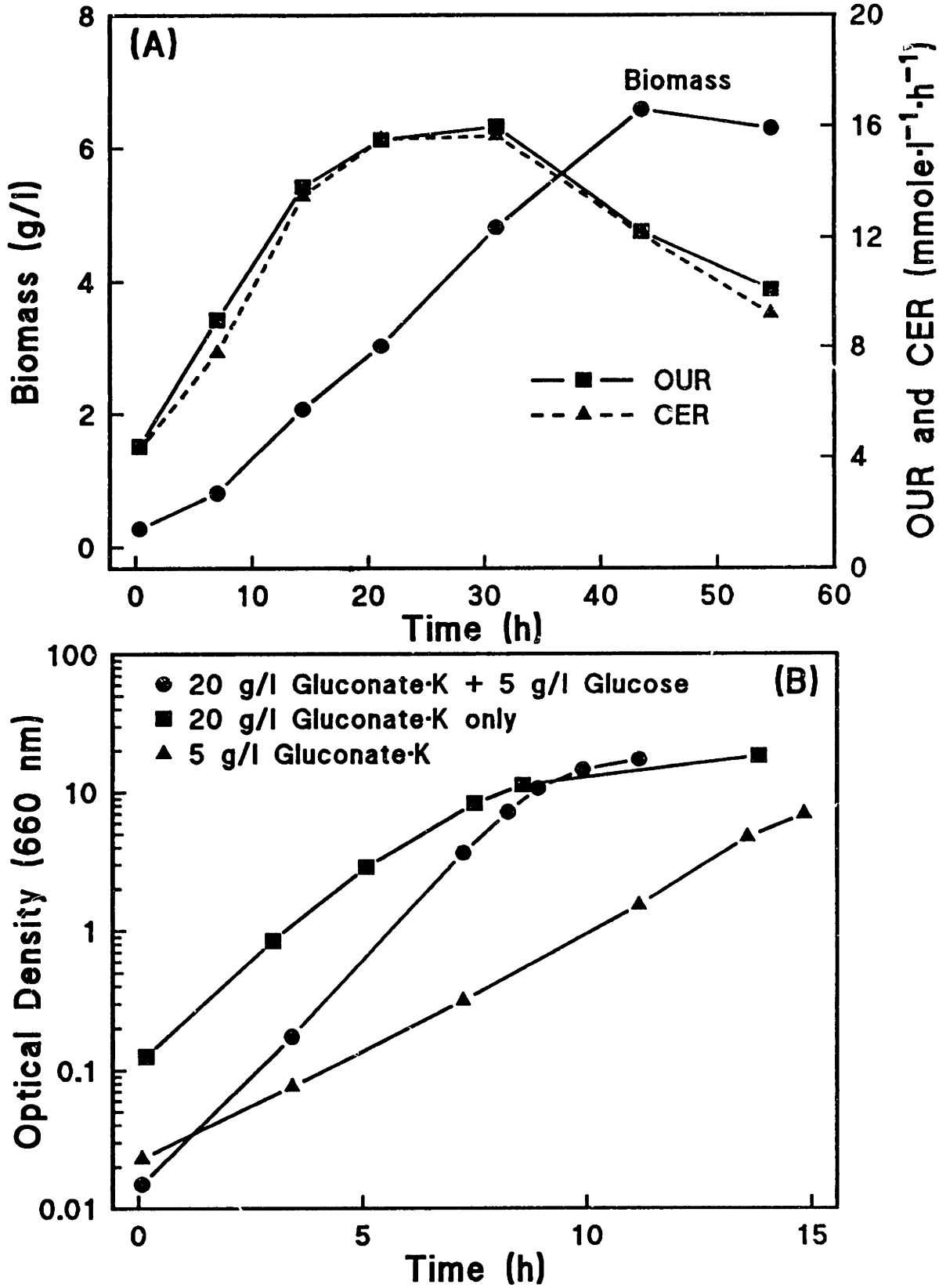

Figure 6.21 Linear growth characteristics of *C. glutamicum* ATCC 21253 when cultured on gluconate. (A) Unsuccessful fermentation on gluconate minimal medium (FM8) without glucose. (B) Growth profiles in 2 l shaker flasks cultured on modified PMB medium as illustrated. Termination of growth caused by oxygen limitation for glucose supplemented culture (●).

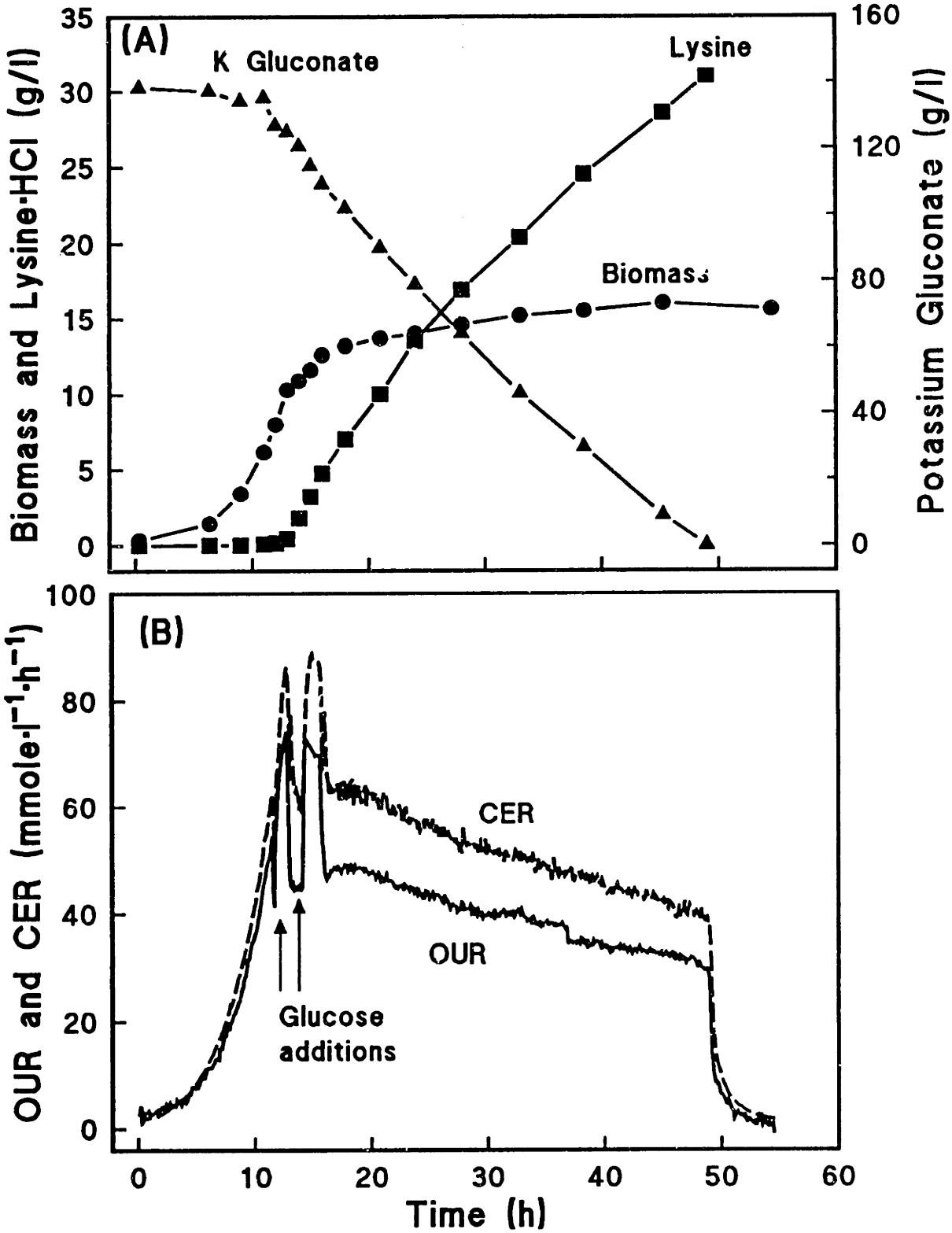

Figure 5.22 Lysine fermentation of *C. glutamicum* ATCC 21253 cultured on gluconate medium (FM9). (A) potassium gluconate (▲), biomass (●), and lysine•HCl (■) profiles in g/l. (B) culture respiration: oxygen uptake rate (OUR, solid curve), carbon dioxide evolution rate (CER, dashed curve). Note increase in respiration upon addition of glucose.

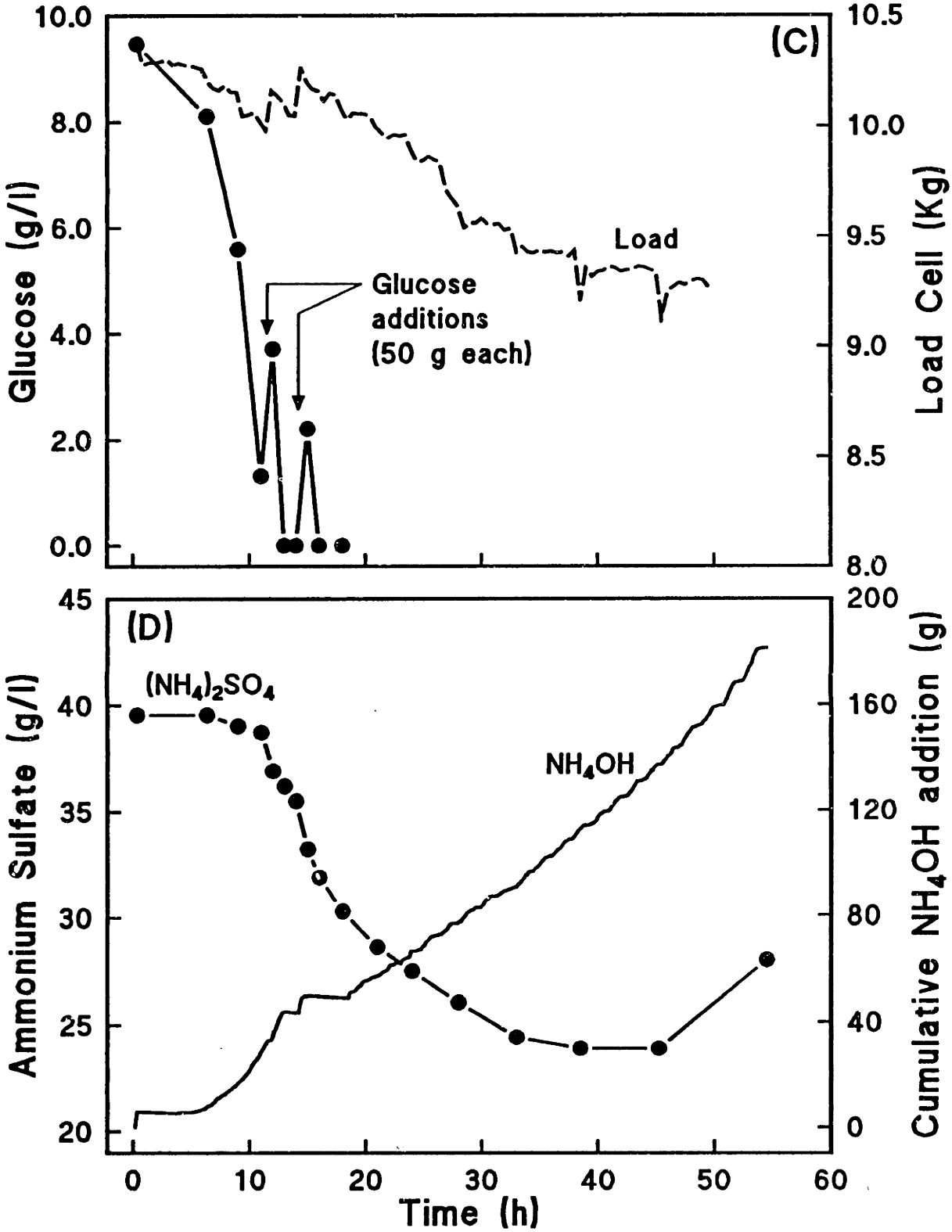

Figure 6.22 (continued) (C) Glucose concentration profile (●) illustrating points of glucose addition and fermentor volume (load) used to calculate volumetric OUR and CER. (D) Available ammonium in broth, as $(NH_4)_2SO_4$ (●), and amount of NH_4OH (26% (w/w) NH_3) added to maintain culture at pH 7.

the growth rate is linear and quite slow, but lasts for an extremely long time (35 hours) and is terminated primarily by gluconate depletion. No Phase IV conditions (*i.e.*, cell lysis and by-product formation) are exhibited. The extension of Phase III results in a lysine titer 50% greater than that observed in the control fermentation (31 g/l vs 20 g/l, respectively), however, once again the instantaneous yield is not observed to exceed 34%. Plausible explanations for the increased viability of the culture are deferred to the next section. Other notable features of the fermentation include a high respiratory quotient (ca. 1.35) and a complete lack of the typically observed by-products. The respiratory quotient is higher for gluconate catabolism since the degree of reductance of gluconate is lower than glucose, yet product formation in both fermentations is approximately equal. Consequently, a relatively lower amount of oxygen is required to balance substrate and product reducing equivalents (*i.e.*, electron balance). For a thorough description of such balances, see Roels (1983).

6.3.2.3 Flux Analysis

The accumulation rate vector is calculated from measurements taken at 18.0 h and 21.0 h (t_{AVE} = 19.5 h), so that gluconate metabolism can be examined separately from glucose consumption. The measured and estimated rate vectors are listed in Table 6.11 along with the consistency index. Inspection of these rates alone does not reveal much information, except that the metabolism of gluconate is as rapid as the glucose catabolism observed in the control fermentation, and the lack of by-product formation leads to an extremely good consistency index. To examine the resulting flux distribution map, the biochemistry set must be modified to handle gluconate metabolism.

The first biochemistry set used to represent gluconate metabolism (BS2 in Appendix B) is identical to BS1, except for the addition of the gluconokinase reaction

$$Glcn + ATP \rightarrow Glcn6P + ADP \qquad (35:BS2)$$

Table 6.11 Accumulation rate subvectors for the gluconate fermentation at 19.5 h from samples taken at 18.0 h and 21.0 h, Figure 6.22. Based on either MS2 & BS2 or MS3 & BS3 in Appendix B, h = 0.003.

Elements of $\mathbf{r}_E(t)$	Accumulation Rates (mM/h) $\bar{r}_E(19.5) \pm \sigma$		$\hat{r}_E(19.5)$
Ac (1)	0	± 2	0.00
Ala (4)	0	± 2	0.02
Biomass (7)	1.67	± 3.2	1.72
CO2 (8)	62.4	± 6.2	62.4
Glcn (16)	-17.0	± 3.9	-17.0
Lac (21)	0	± 2	0.00
LysE (22)	5.48	± 0.4	5.48
NH3 (27)	-12.8	± 11	-12.3
O2 (28)	-48.0	± 4.8	-48.0
Pyr (31)	0	± 2	0.00
Trehal (37)	0	± 2	0.02
Val (38)	0	± 2	0.03

and the breakdown of Reaction (22:BS1) into the two constituent reactions

$$\text{Glc6P} + \text{H2O} + \text{NADP} \rightarrow \text{Glcn6P} + \text{NADPH} \qquad (36{:}BS2)$$

$$\text{Glcn6P} + \text{NADP} \rightarrow \text{Ribu5P} + \text{CO2} + \text{NADPH} \qquad (22{:}BS2)$$

where 6-phosphogluconolactonase has been lumped with G6PDH in Reaction (36:BS2). However, when the flux distribution map (based on BS2) was calculated from the accumulation rate vector in Table 6.11, Reaction (36:BS2) above exhibited a negative flux (see Appendix B). This occurred because more NADPH was generated than consumed, so Reaction (36:BS2) was driven backwards in order to counterbalance excess NADPH production. Since reversal of Reaction (36:BS2) is infeasible, primarily due to irreversibility of 6-phosphogluconolactonase, a new measurement set (BS3) was constructed where Reaction (36:BS2) was deleted and replaced by :

$$2\ \text{NADPH} + \text{O2} \rightarrow 2\ \text{H2O} + 2\ \text{NADP} \qquad (36{:}BS3)$$

Although NADPH can not participate in the respiratory chain, all other NADPH sinks and alternate reaction paths have been ruled out, and it appears plausible that NADPH may be oxidized nonenzymatically. An enzyme with poor specificity for NADH could also oxidize NADPH, but this would have the same net result as inclusion of Reaction (36:BS3) on the flux distributions. The flux distribution map base on BS3, MS3 and the metabolite accumulation rates (Table 6.11) is displayed in Figure 6.23. Although the flux distribution map is remarkably similar to that observed in the control fermentation, Figure 6.8, (as well as others), catabolism of gluconate produces a substantial excess of NADPH, as evident in Reaction (36:BS3). However, this excess NADPH does not result in an increase in lysine yield. Consequently, it appears that lysine yield is not limited by NADPH availability. Another significant difference associated with gluconate metabolism is the high flux supported by pyruvate kinase, Reaction (7:BS3), due to gluconate phosphorylation by ATP and not PEP.

Although speculative, the excess NADPH production may also explain why *C. glutamicum* cannot sustain exponential growth on gluconate as the sole carbon source, except at low concentrations. Since *C. glutamicum* appears to lack adequate mechanisms for the direct oxidation of NADPH, intracellular accumulation of this reduced metabolite may perturb secondary metabolism (*i.e.*, peripheral reactions associated with biomass synthesis) to the extent that exponential growth is no longer feasible. This may also explain why a GPI lacking strain of *C. glutamicum*, that can grow on glucose, has not been isolated [Sugimoto and Shiio, 1987a] (also see Section 5.4.3). At low gluconate concentrations, the transport and phosphorylation of the sugar (which is not under the control of the PTS) may be reduced sufficiently so that NADPH can be nonspecifically oxidized fast enough to permit reduced exponential growth.

As for the increased viability of the culture, two possibilities exist. If growth in Phase II of the control fermentation is associated with scavenging of threonine reserves (Section 6.1.1.2), then the linear growth associated with gluconate metabolism may simply extend this period, as the uptake of threonine would be dramatically reduced in the linear growth mode. As for the second possibility, the

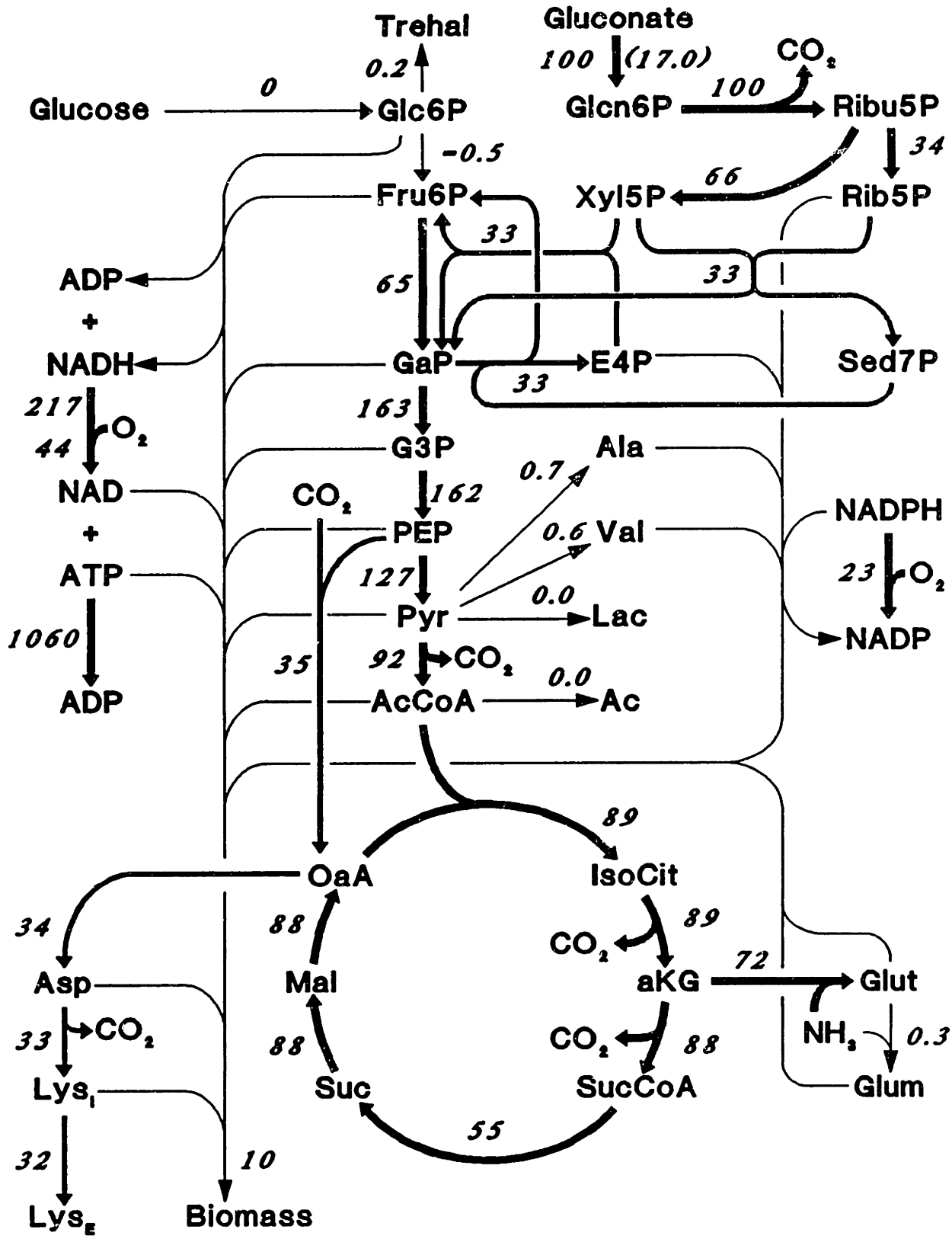

Figure 6.23 Flux distribution map for the gluconate fermentation at 19.5 h. Fluxes estimated from measurements taken at 18.0 h and 21.0 h (see Figure 6.22 and Table 6.11), and normalized by gluconate uptake rate (shown in parentheses; mmole•l^{-1}•h^{-1}). Reactions from BS3 (Appendix B) which includes direct NADPH oxidation.

increase in available reducing power (NADPH) may extend protein stability or enhance protein turnover efficiency, thereby increasing the duration of Phase III.

The reader should not be left with the feeling that the proposed mechanism regarding NADPH oxidation is the sole thread holding together the entire fabric of the bioreaction network analysis. While it is true that the flux analysis routine produces peculiar results regarding the oxidation of NADPH when *C. glutamicum* is culture on gluconate, is should no be attributed to a breakdown in the PSSA since we have demonstrated the validity of this assumption. Consequently, inconsistencies in the flux distributions (*i.e.*, negative flows) do not imply that the analysis is breaking down, but rather that the biochemistry must be functioning in a manner different than assumed since the metabolism must process all metabolites in a manner consistent with mass balance constraints. For example, if *C. glutamicum* exhibited nominal growth on high gluconate concentrations, inconsistencies would certainly exist regarding reactions involving NADPH, and the biochemistry would have to be reexamined in light of such information. Since linear growth is associated with gluconate metabolism and reasonable alternatives have not been identified to mitigate NADPH overproduction, the current assumption regarding NADPH nonspecific oxidation seems valid. Nevertheless, the BRNA is an extremely useful tool in the validation of biochemical pathways as illustrated in this section.

6.3.3 Summary

Results from the fermentation of NFG068 (GPI^A mutant) indicate that the Glc6P node is not weakly rigid, and flux analysis of the gluconate fermentation demonstrates that lysine yield is not limited by NADPH production. Therefore, the Glc6P node must be flexible and lysine yield limitations must be attributed to rigidity of either the PEP or Pyr principal nodes. The fact that attenuation of GPI resulted in flux attenuation without effecting principal node split-ratios supports the hypothesis regarding perturbations of rigid dependent-networks proposed in Section 4.3. It should be stressed that although the Glc6P node has been demonstrated to be flexible under the moderate lysine yields observed, it is possible that this node could become a limiting point if lysine yield was dramatically increased by improving split-

ratio distributions at the other principal nodes. That is, the above conclusions regarding the Glc6P node cannot be extrapolated to maximum lysine yield.

It has also been demonstrated that metabolite balances (*i.e.*, flux analysis) can be used to verify the speculated operation of a proposed primary metabolism. Analysis of gluconate catabolism, under the currently perceived biochemistry, clearly indicate that *C. glutamicum* should encounter difficulty catabolizing gluconate, due to the lack of adequate mechanisms to oxidized NADPH.

6.4 Analysis of the Pyr Principal Node

As discussed in Section 4.3.1, the Pyr node represents the branch-point between the pyruvate dehydrogenase complex (which leads into the TCA cycle and CO_2 production) and dihydrodipicolinate synthase (which, in essence, catalyzes the condensation of Pyr with OAA to form lysine). Obviously, if the Pyr node is weakly or strongly rigid, pyruvate will preferentially enter the TCA cycle instead of condensing with OAA, and lysine yield will be limited by the availability of pyruvate. Although several studies involving PDC attenuation in *B. flavum* [Shiio *et al.*, 1984b] and *B. lactofermentum* [Tosaka *et al.*, 1985] have been investigated, conclusions regarding the flexibility of the Pyr node remain uncertain for two primary reasons: 1) mutation-selection techniques employed to attenuated PDC often result in alterations of other primary metabolic enzymes [Yokota and Shiio, 1988; Shiio *et al.*, 1987; Shiio *et al.*, 1984a; Ozaki and Shiio, 1983] which may strongly affect the PEP node; and 2) the extent of the Pyr node perturbation is unknown due to the lack of adequate fermentation monitoring (*i.e.*, often only overall lysine yield is reported). Therefore, we conducted three perturbation experiments to elucidate the degree of flexibility of the Pyr Node. The first experiment involved the isolation, fermentation, and flux analysis of a PDC attenuated (PDC^A) mutant of *C. glutamicum* ATCC 21253. The second two experiments involved monitoring the response of the Pyr node split-ratios to PDC inhibition induced by either fluoropyruvate (FP) or arsenite addition at the start of lysine overproduction. The results of these experiments are described below.

6.4.1 Analysis of a PDC^{A} Mutant

If lysine yield suffers from a weak rigidity of the Pyr node, then a PDC^{A} mutant should increase the availability of pyruvate and improve lysine yield. If poor lysine yield is due to rigidity of the PEP node or a strong rigidity of the Pyr node, then PDC attenuation should result in either excretion of some intermediate or overall network-flux attenuation (see Section 4.3). To examine the effects of PDC attenuation, the mutant strain *C. glutamicum* FPS009 was selected which lacks 99% of PDC activity compared to ATCC 21253 (parent strain). Isolation and characterization of FPS009 is described in Section 5.4.2. Revertants have not been observed and the strain grows adequately on minimal glucose plates, but exhibits poor (linear) growth in minimal glucose suspensions when not supplemented with acetate.

6.4.1.1 Fermentation of FPS009

Results of the FPS009 fermentation cultured on glucose FM4 medium are depicted in Figure 6.24 (A-D). During the first 70 hours of cultivation, the strain exhibited linear growth (not shown). However, upon addition of 60 g of potassium acetate, the culture began exponential growth and continued until the biomass reached 8 g/l DCW at approximately 124 h (Figure 6.24 (A)), even though supplemented acetate was exhausted by 108 h. Growth and accumulation rates of all other extracellular metabolites during this period were severely attenuated as compared to the control fermentation (ca. 75% reduction), but the concentration profiles still resemble Phase I characteristics. At the end of the growth stage (Phase I), lysine production commenced and biomass continued to increase to 10.3 g/l DCW (120-124 h), which closely resembles Phase II characteristics of the control fermentation. At the end of Phase II, growth entered a stationary period during which lysine synthesis continued (Phase III, 124-131 h). The culture then progressed into a slow death phase where lysine synthesis dramatically decreased (Phase IV). During Phase III, 50 g of potassium acetate was added to stimulate growth, but had little effect other than on respiration (Figure 6.24 (B)). Although lysine•HCl titer only reached 12.6 g/l, the lysine yield averaged 34% during Phases II and III (based on glucose), which is a slight improvement over the control fermentation (see flux analysis below). Unlike the control fermentation, trehalose was the only by-product

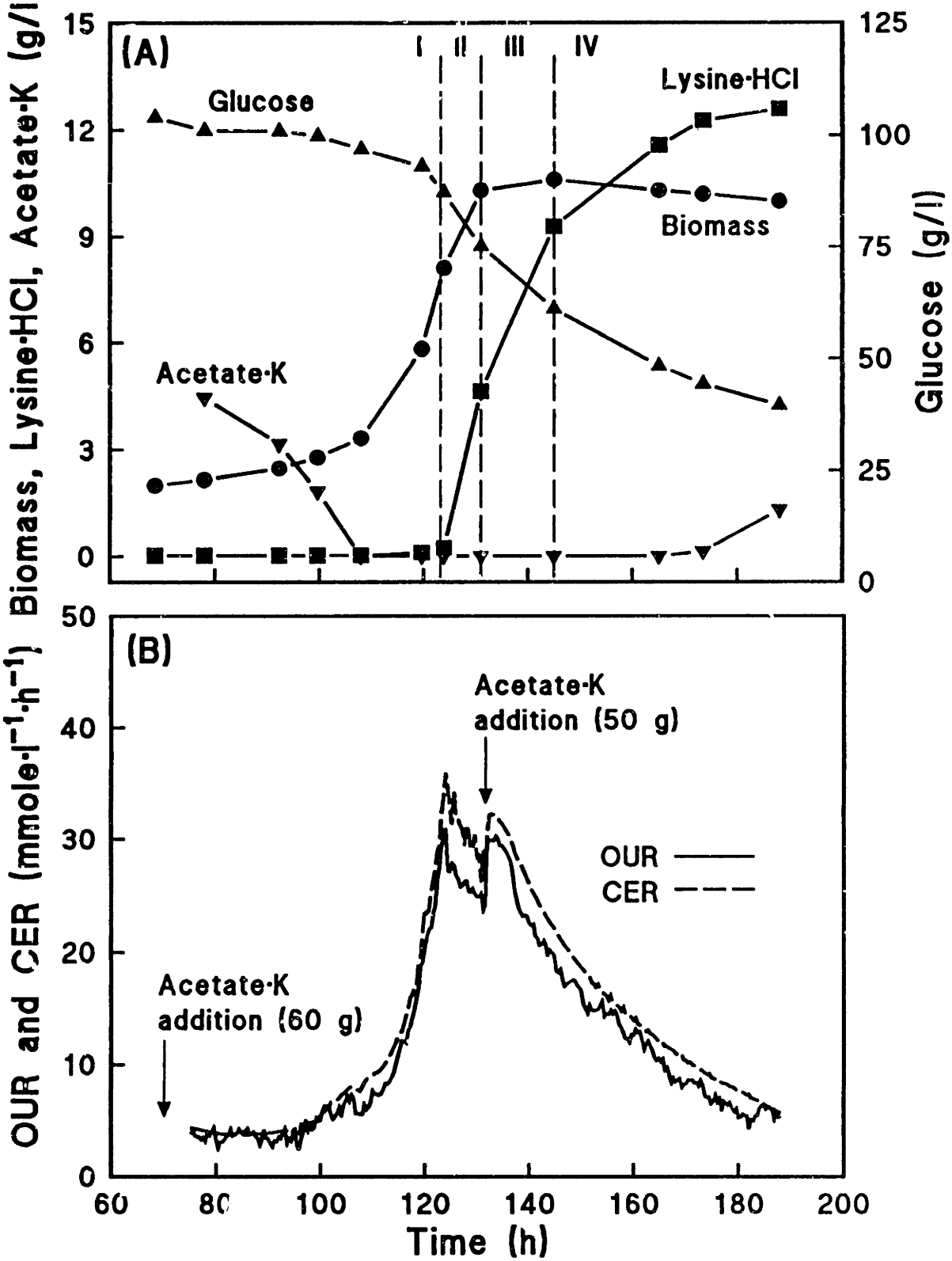

Figure 6.24 Lysine fermentation of *C. glutamicum* FPS009 cultured on glucose FM4 medium. (A) Glucose (▲), biomass (●), lysine•HCl (■), and potassium acetate (▼) profiles in g/l. Note, the first 68 h of the fermentation is not shown (linear growth), and at 70 h and 132 h, 60 g and 50 g of potassium acetate were aseptically added, respectively. (B) Culture respiration, OUR (solid curve) and CER (dashed curve). Note diminished respiration throughout fermentation.

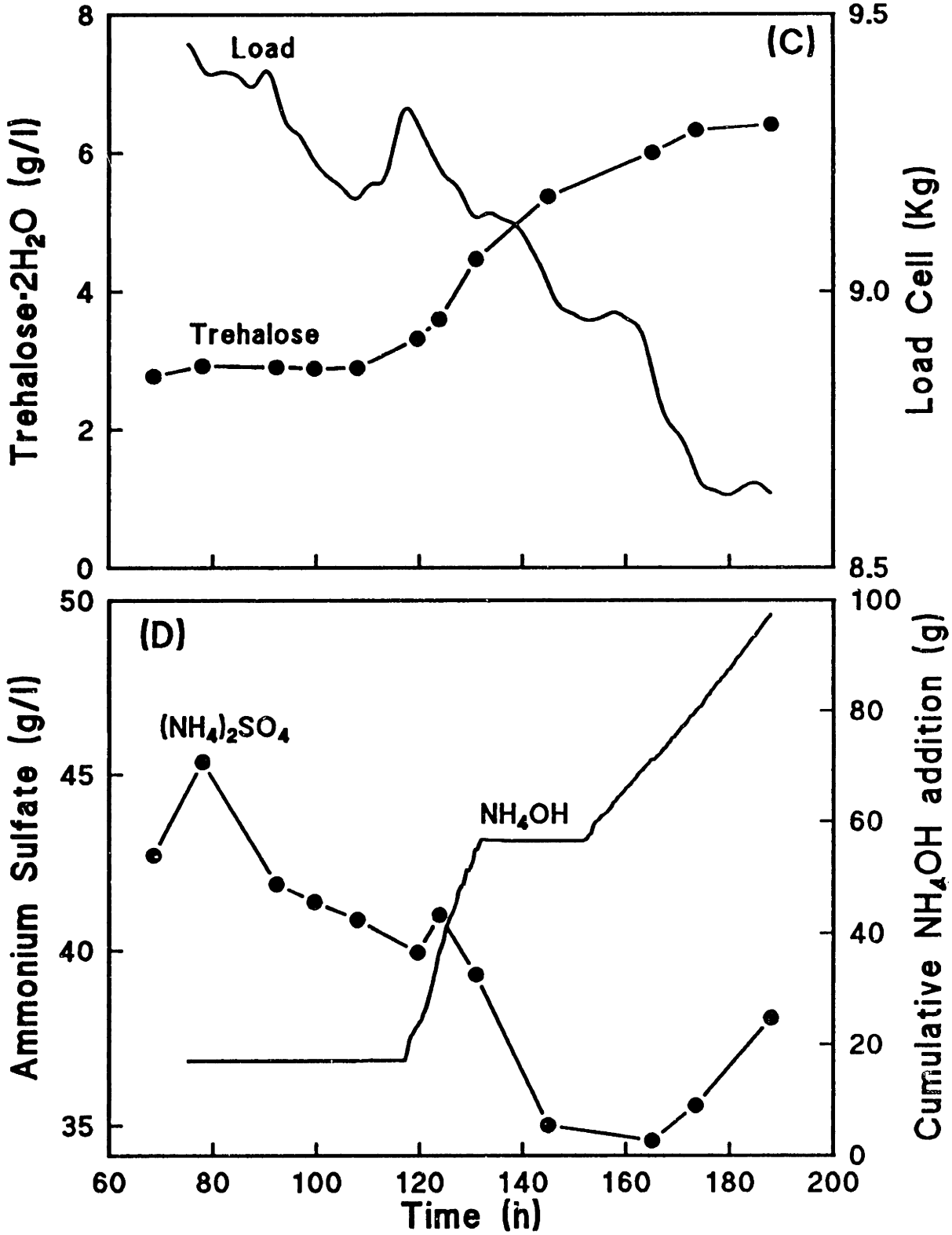

Figure 6.24 (continued) (C) Fermentor load cell reading (solid curve) and trehalose•$2H_2O$ (●) production. No other by-products were observed. (D) Available ammonium in broth, as $(NH_4)_2SO_4$ (●), and cumulative amount of NH_4OH (26% (w/w) NH_3) added to maintain culture at pH 7.0.

observed during the fermentation (Figure 6.24 (C)).

6.4.1.2 Flux Analysis

Although acetate was added twice during the fermentation, we have demonstrated in Section 5.3.2 that glucose represses the glyoxylate shunt even in the presence of acetate. Therefore, flux distributions can be calculated without the complications associated with the glyoxylate shunt. To examine glucose catabolism free from acetate consumption, metabolite accumulation rates were calculated during Phase II from measurements taken at 124 h and 131 h (t_{AVE} = 127.5 h), and are listed in Table 6.12 along with the estimated rates and consistency index. The rates listed in Table 6.12 exhibit approximately a three-fold decrease in magnitude as compared to the control fermentation; however, the resulting flux-distribution map,

Table 6.12 Accumulation rate subvectors for the FPS009 fermentation at 127.5 h from measurements taken at 123.9 h and 131.0 h (Figure 6.24). Based on MS1 and BS1 in Appendix B, h = 0.66.

Elements of $\mathbf{r}_B(t)$	Accumulation Rates (mM/h)		
	$\bar{\mathbf{r}}_B(127.5) \pm \sigma$		$\hat{\mathbf{r}}_B(127.5)$
Ac (1)	0	± 1	-0.04
Ala (4)	0	± 1	-0.07
Biomass (7)	3.09	± 0.9	3.00
CO2 (8)	27.5	± 2.8	28.8
Glc (14)	-9.48	± 1.8	-9.83
Lac (19)	0	± 1	-0.05
LysE (20)	3.41	± 0.1	3.41
NH3 (25)	-8.2	± 6.1	-8.7
O2 (26)	-26.3	± 2.6	-25.0
Pyr (29)	0	± 1	0.04
Trehal (35)	0.32	± 1	0.10
Val (36)	0	± 1	-0.29

illustrated in Figure 6.25, is remarkable similar to that observed in the control fermentation during late Phase II (Figure 6.8). Furthermore, the lysine branch split-ratio at the Pyr node of 29% is statistically identical to that observed in the control fermentation (Figure 6.14). The 99% attenuation of PDC has not resulted in flux redistributions at any of the three principal nodes, but has resulted in overall network

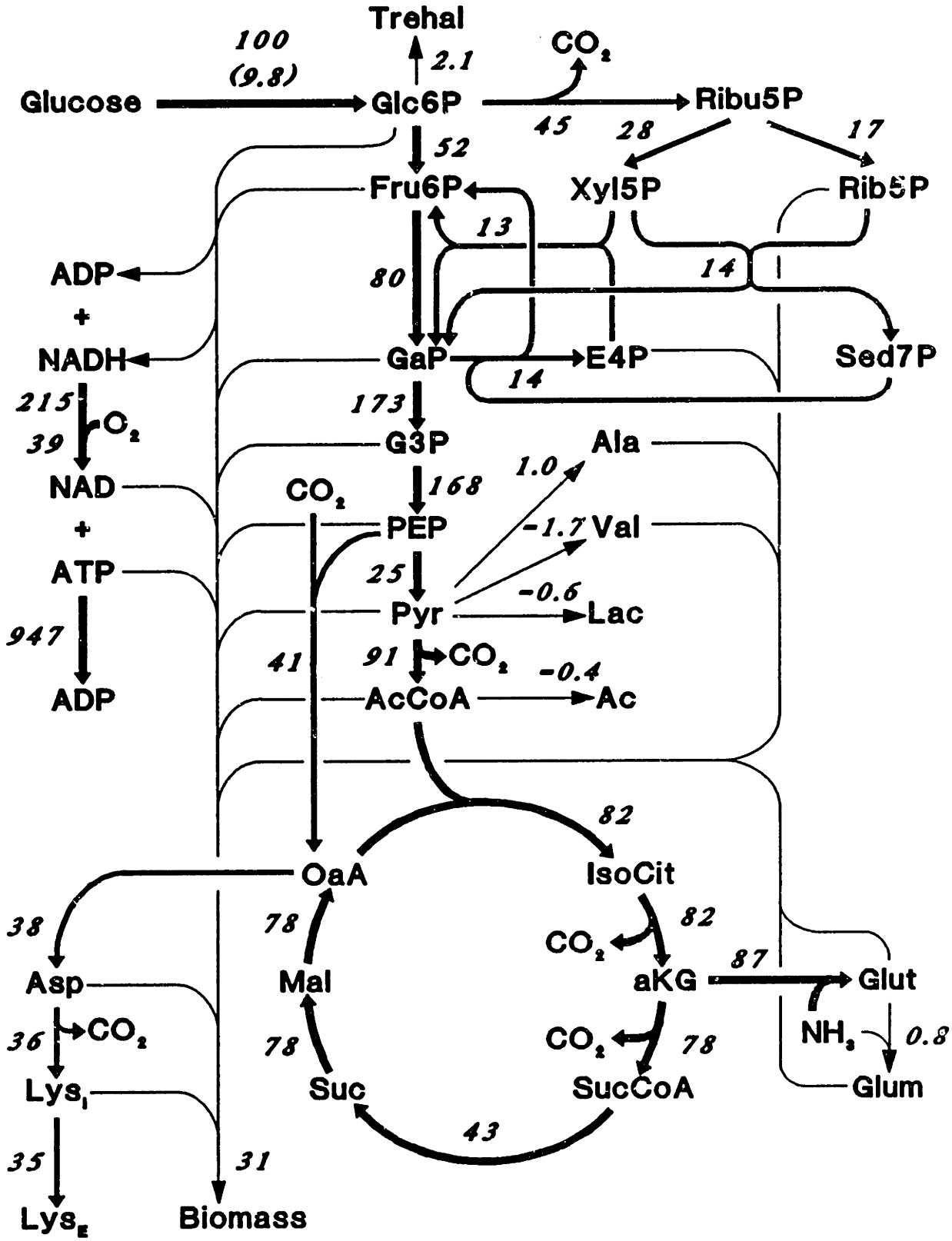

Figure 6.25 Flux distribution map for the FPS009 mutant fermentation at 127.5 h. Fluxes estimated from measurements taken at 123.9 h and 131.0 h (see Figure 6.24 and Table 6.12), and normalized by glucose uptake rate (shown in parentheses; mmole•l^{-1}•h^{-1}). Reactions are from BS1 listed in Appendix B.

attenuation, which is consistent with concepts regarding perturbations of rigid dependent-networks. Consequently, we can conclude that the Pyr node is not weakly rigid. To investigate the possibility that the Pyr may be strongly rigid, the following inhibitor studies were conducted.

6.4.2 Fluoropyruvate Perturbation

Fluoropyruvate (FP) is a strong competitive inhibitor of PDC in *B. lactofermentum* as documented by Tosaka *et al.* (1985), and is also found to inhibit PDC in *C. glutamicum* ATCC 21253 as illustrated in Figure 6.26. Although 1 mM FP inhibits 83% of PDC activity in the crude extract, it is not a perfect competitive inhibitor as it is slowly catabolize [Tosaka *et al.*, 1985], which may explain the residual PDC activity at 10 mM FP, illustrated in Figure 6.26. Nonetheless, PDC inhibition is certainly evident and the specificity of the inhibitor allows for precise perturbation of the Pyr node without altering other enzymes that often occur in mutation studies. The effects of attenuating PDC during lysine production can easily be accomplished and monitored by the addition of FP. Although not guaranteed, the resulting flux distribution may indicated whether the Pyr node is strongly rigid or flexible.

6.4.2.1 Fermentation

A standard lysine fermentation of ATCC 21253 cultured on minimal glucose medium FM4 was conducted; however, at the onset of lysine production (indicated by the telltale drop in respiration) 20 mmoles of FP was aseptically added to inhibit PDC as illustrated in Figure 6.27 (A-E). The resulting fermentor FP concentration (ca. 2.1 mM) was chosen based on the *in vitro* PDC inhibition by FP (Figure 6.26) and cost limitations.

Immediately ensuing the addition of FP, a dramatic drop in respiration occurred (Figure 6.27 (B)), and was accompanied by a decrease in growth rate (Figure 6.27 (A)) and the accumulation of extracellular pyruvate (Figure 6.27 (C)). Lysine synthesis and glucose consumption rates immediately following FP addition were unaffected (Figure 6.27 (A)); however, a few hours after FP addition, respiration resumed, excreted pyruvate was reconsumed, and glucose uptake exhibited a transient decrease, which was probably due to pyruvate reconsumption. The

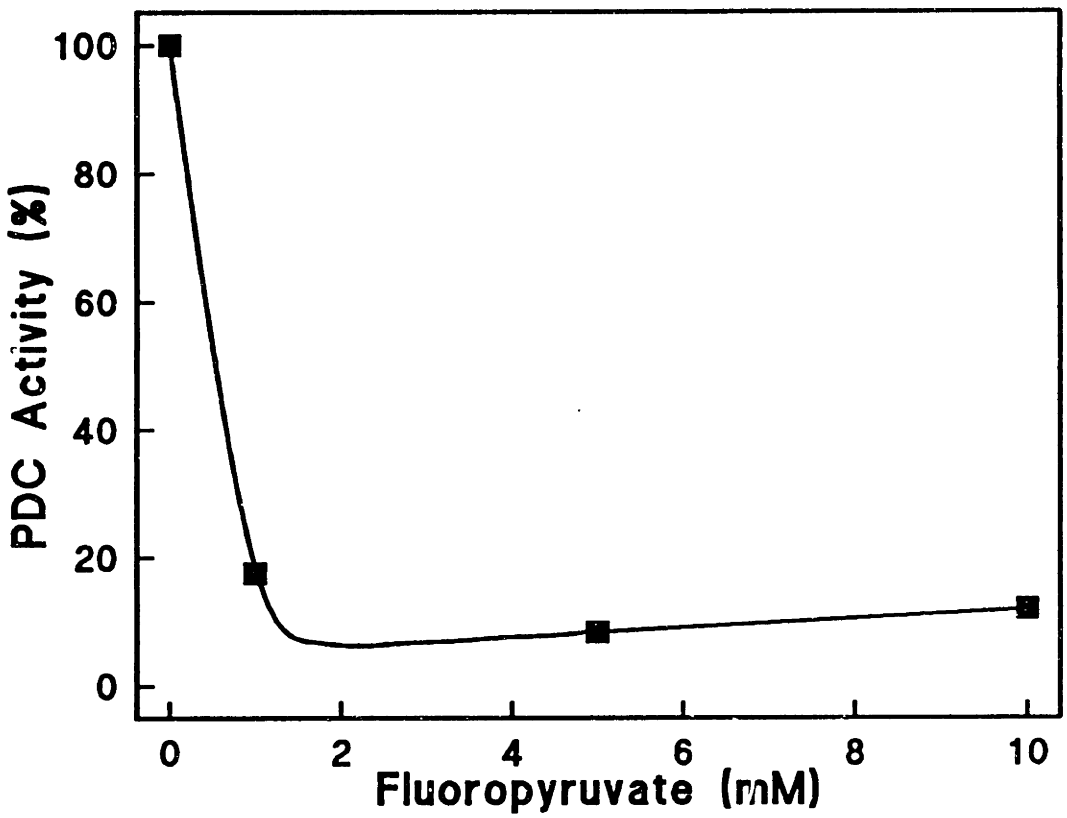

Figure 6.26 Effect of FP on PDC activity. Enzyme assay conditions described in Section 5.2.2.13. PDC activity at 100% was 27.5 U/mg-protein, where the assay contained 2 mg/ml crude-extract protein.

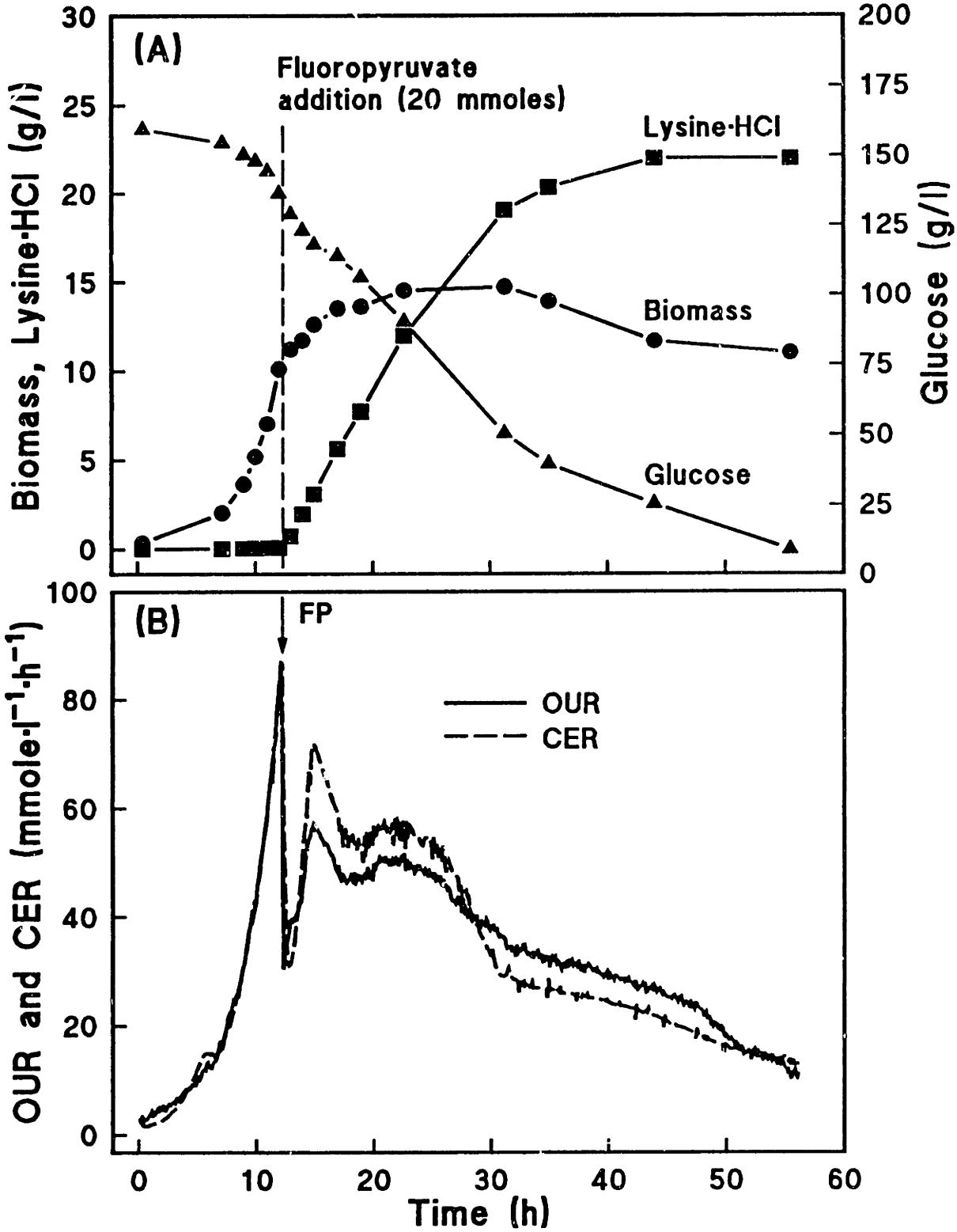

Figure 6.27 Fluoropyruvate (FP) inhibited lysine fermentation of *C. glutamicum* ATCC 21253 cultured on glucose FM4 medium. At 12.25 h 20 mmoles of fluoropyruvate•Na (Sigma, St. Louis MO) dissolved in 30 ml water was aseptically added. (A) Concentration profiles of biomass (●), glucose (▲), and lysine•HCl (■) in g/l. (B) Culture respiration, OUR (solid curve) and CER (dashed curve). Note respiration decline upon addition of FP.

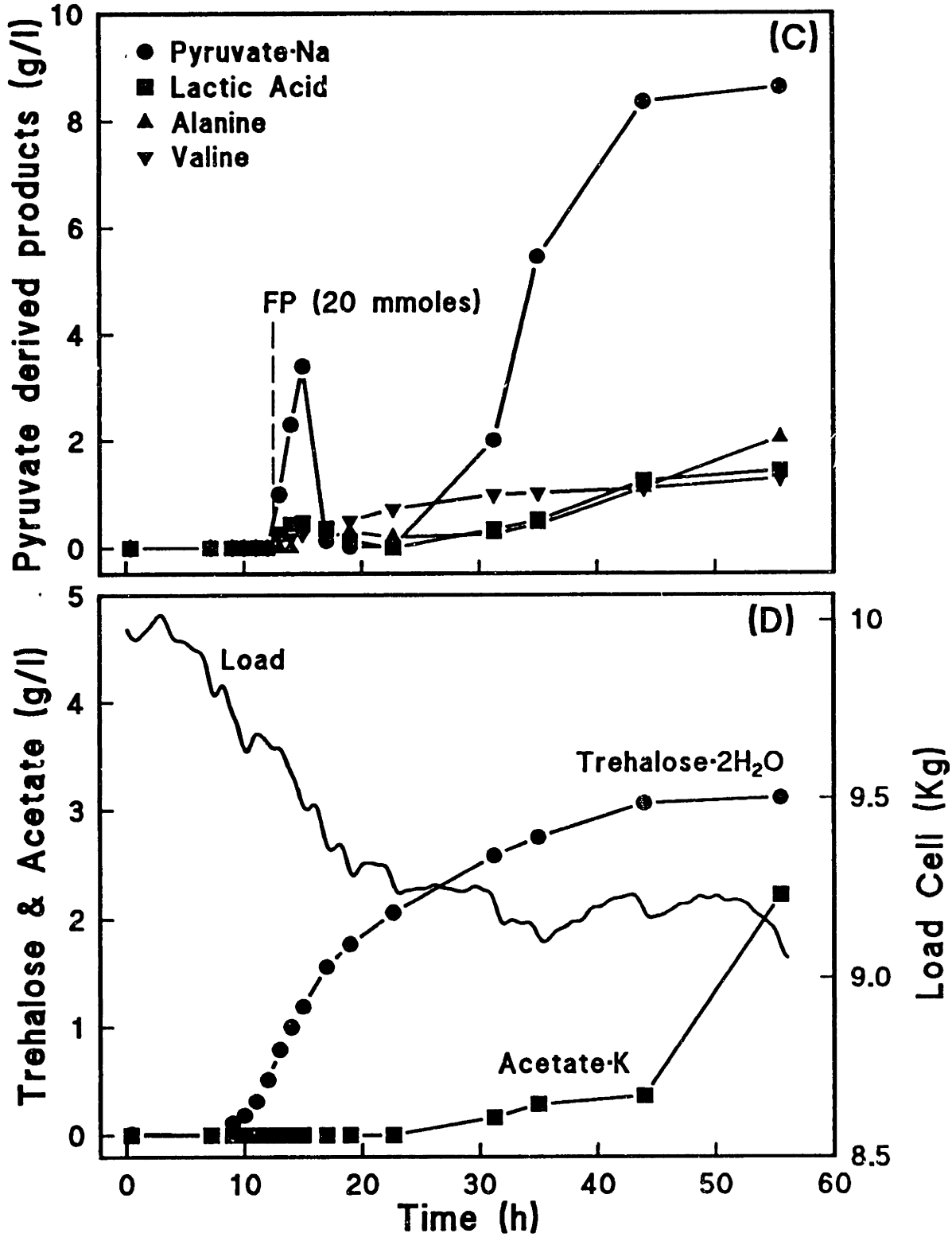

Figure 6.27 (continued) (C) Extracellular accumulation of pyruvate and pyruvate derived by-products. Note rapid increase in pyruvate accumulation upon FP addition. (D) Fermentor load cell (solid curve), trehalose (●), and potassium acetate (■) accumulation.

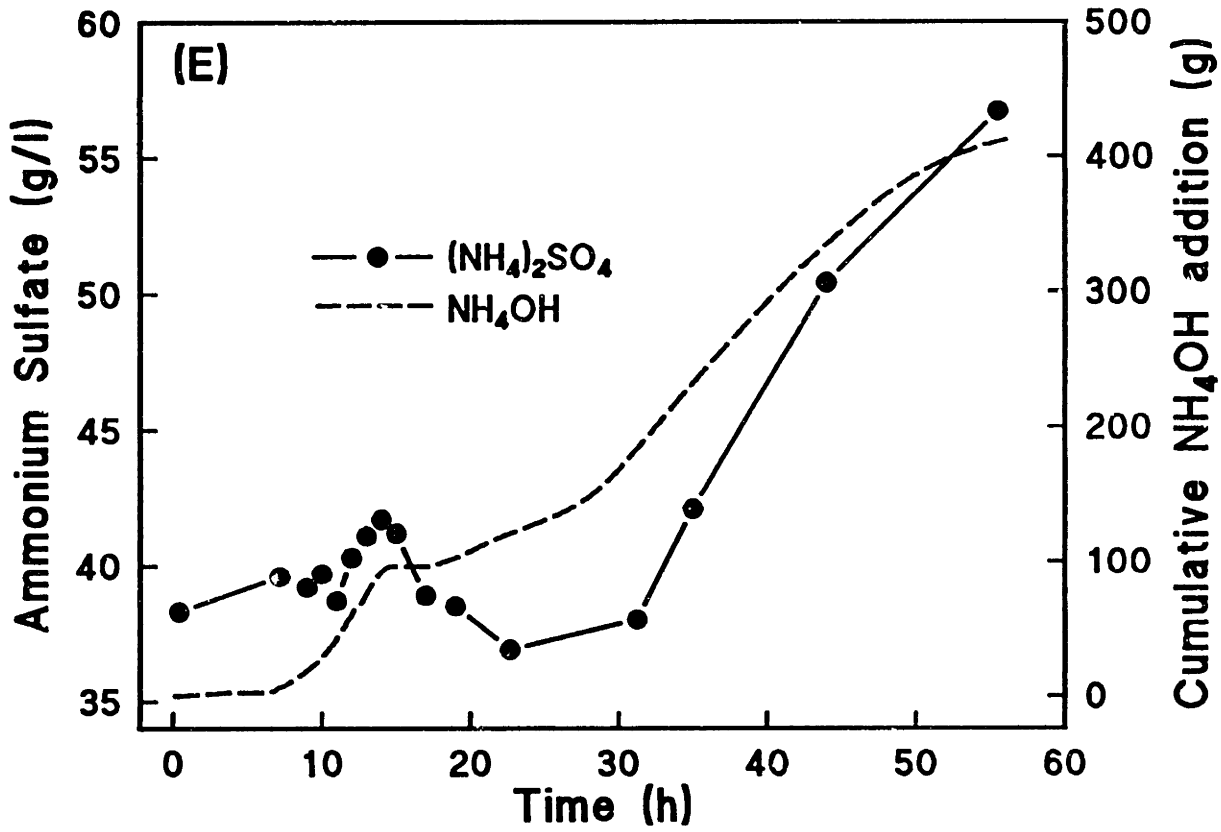

Figure 6.27 (continued) (E) Available ammonium in broth, as $(NH_4)_2SO_4$ (•), and cumulative amount of NH_4OH (26% (w/w) NH_3) added to maintain culture at pH 7.0.

temporary nature of the perturbation is undoubtedly due the breakdown of FP as mentioned above. The remainder of the fermentation exhibited characteristics similar to the control fermentation, except that extracellular pyruvate accumulation reached higher levels and the stationary period (Phase III) was extended. The excretion of pyruvate also resulted in elevating ammonium sulfate concentration due to the increase in ammonium hydroxide required to maintain the culture at ph 7 (Figure 6.27 (E)).

Although lysine•HCl titer increased by 25% compared to the control fermentation (from 20 to 25 g/l), the instantaneous lysine yield during the 13 to 19 h period (Phase II) is 30%, basically identical to the control fermentation. (Once again, the increase in lysine titer is due to the extension of Phase III.) Consequently FP perturbation of the Pyr node did not result in lysine yield improvements.

6.4.2.2 Flux Analysis

Flux distributions were calculated from measurements taken at 13.0 h and 14.0 h (Phase II, during pyruvate accumulation) in order to capture the flux perturbations induced by the addition of FP. The measured and estimated metabolite accumulation rate vectors and the associated consistency index at t_{AVE} = 13.5 h are displayed in Table 6.13. The high rate of pyruvate accumulation should be noted. The resulting flux distribution map, displayed in Figure 6.28, clearly illustrates the diversion of pyruvate from the TCA cycle (which supports a reduced flux) to extracellular excretion (Pyr_E), while the flux distributions of the remaining pathways appear relatively unaffected compared to the control fermentation in late Phase II (Figure 6.8). To highlight the effect of FP, detailed flux distributions around the PEP and Pyr nodes normalized by PEP synthesis rate for the control fermentation during late Phase II and the FP perturbed fermentation at t_{AVE} = 13.5 h are illustrated in Figure 6.29 (A, B, respectively). The inhibition of PDC by FP causes a 50% reduction in the TCA branch split-ratio at the Pyr node, while the split-ratios at the PEP node remain relatively unaffected.

If the Pyr node is strongly rigid, then attenuation of PDC should have resulted in the attenuation of lysine synthesis as well. Since pyruvate accumulates during PDC attenuation and lysine yield is unaffected, lysine yield cannot be limited by the

Table 6.13 Accumulation rate subvectors for the FP inhibited lysine fermentation at 13.5 h from measurements taken at 13.0 h and 14.0 h (Figure 6.27). Based on MS1 and BS1 in Appendix B, $h = 0.31$.

Elements of $\mathbf{r}_E(t)$	Accumulation Rates (mM/h) $\overline{\mathbf{r}}_E(13.5) \pm \sigma$		$\hat{\mathbf{r}}_E(13.5)$
Ac (1)	0	± 2	0.02
Ala (4)	0	± 2	0.04
Biomass (7)	5.0	± 8.1	4.70
CO2 (8)	41.0	± 4.1	42.2
Glc (14)	-32.2	± 20	-25.0
Lac (19)	2.0	± 2	2.0
LysE (20)	6.86	± 0.2	6.86
NH3 (25)	-17.7	± 44	-17.1
O2 (26)	-41.4	± 4.1	-40.3
Pyr (29)	11.8	± 2	12.0
Trehal (35)	0.6	± 2	0.7
Val (36)	0.1	± 2	-0.1

availability of pyruvate. Furthermore, since the split-ratios at the Pyr node can be affected by attenuating the PDC branch, we can conclude that the Pyr node is flexible and not limiting lysine yield. Since this conclusion regarding the flexibility of the Pyr node rests on a perturbation that was quite transient (only a few hours), the above perturbation experiment was repeated, with arsenite used as the inhibitor as outlined in the next section.

6.4.3 Arsenite Perturbation

To investigate the metabolic response of long-term attenuation of PDC, an arsenite perturbed fermentation was conducted. Arsenite has long been known to be a strong inhibitor of PDC [Johnstone, 1963] and has been used in several studies involving amino acid production [Shiio *et al.*, 1961b,c; Shiio *et al.*, 1962c; Fowler and Werkman, 1955]. In such studies, however, the desired information is always qualitative in nature (*i.e.*, determining if product formation requires the TCA cycle, etc.). As a result, environmental conditions are often inadequately monitored and controlled, so that extraction of quantitative information (such as, flux distributions)

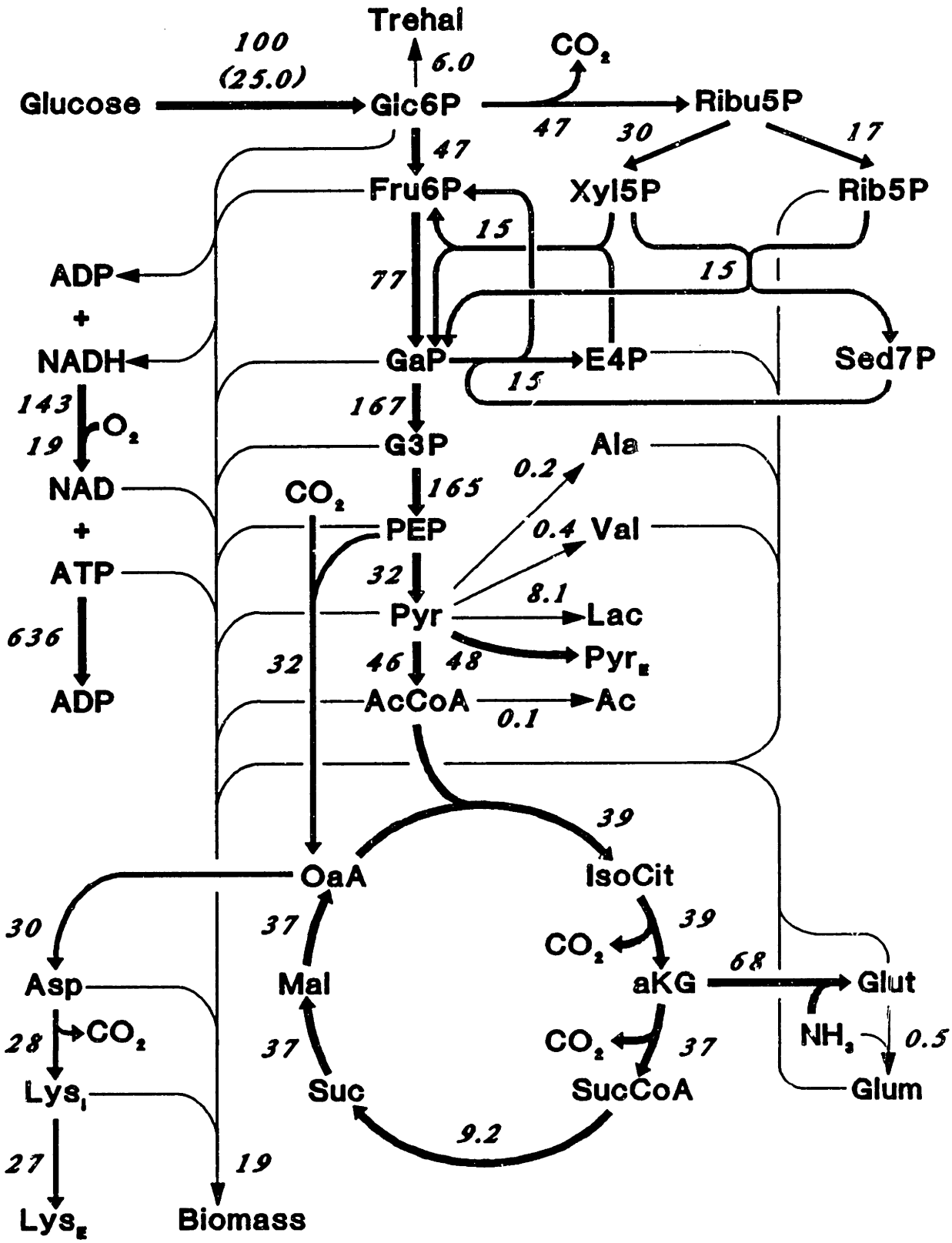

Figure 6.28 Flux distribution map for the FP inhibited fermentation at 13.5 h. Fluxes estimated from measurements taken at 13.0 h and 14.0 h (see Figure 6.27 and Table 6.13), and normalized by glucose consumption rate (shown in parentheses; mmole•l^{-1}•h^{-1}). Reactions are from BS1 listed in Appendix B. Note Pyr_B represents extracellular pyruvate accumulation and is not actually a part of BS1.

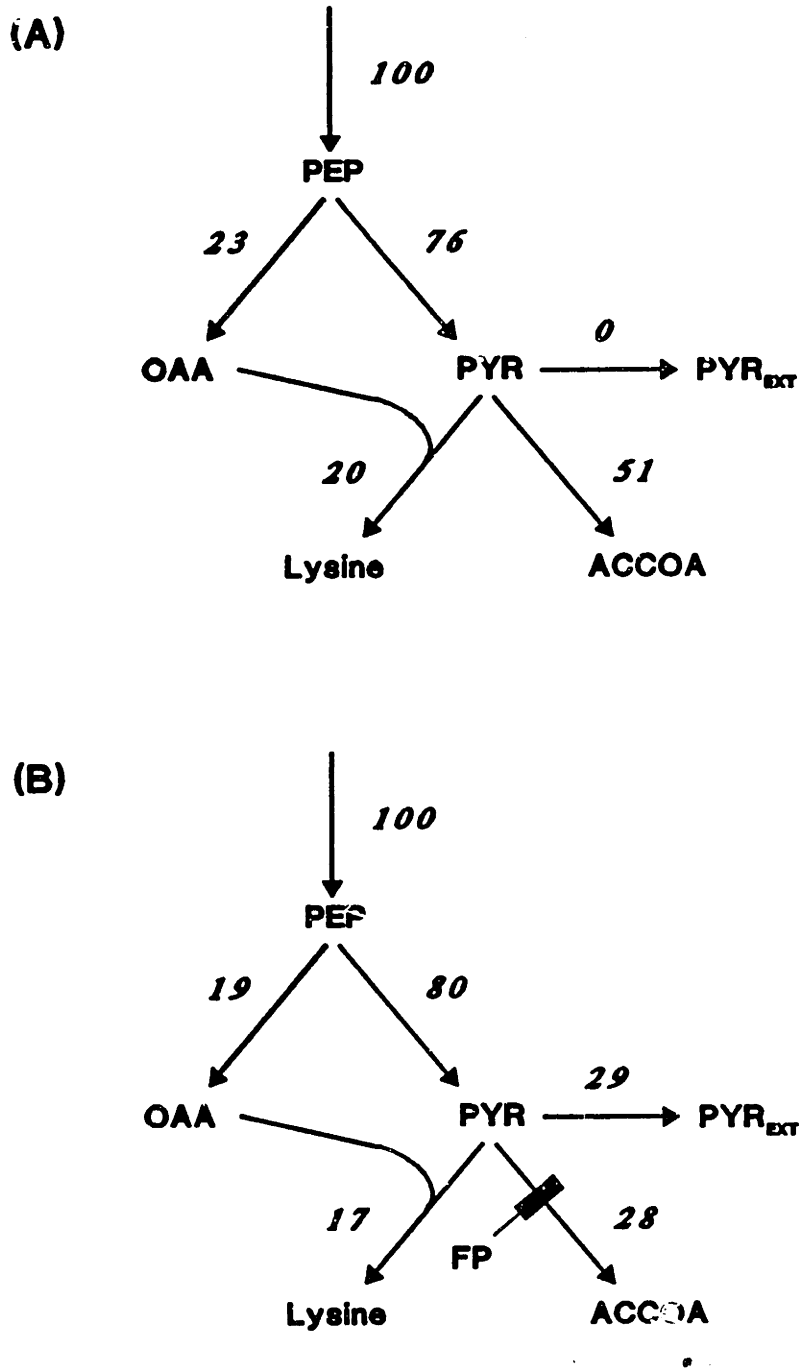

Figure 6.29 Flux distributions around the PEP and Pyr principal nodes normalized by PEP synthesis rate for the control fermentation (A) during late Phase II (extracted from Figure 6.8) and the FP inhibited fermentation (B) at 13.5 h (extracted from Figure 6.28). The solid rectangular block indicates the site of FP inhibition.

cannot be determined. The following perturbation study was required to resolve the effects of arsenite on the metabolic flux distributions.

Although the specificity of arsenite as a PDC inhibitor is not as effective as FP and may cause some inhibition of other keto acid dehydrogenases (such as, α-ketoglutarate dehydrogenase) [Webb, 1966], it is not catabolized as FP is, so its effects will persist longer. Furthermore, arsenite is inexpensive, so higher concentrations can be used. To determine the concentration of arsenite that would produce a significant metabolic perturbation, several shaker flask studies were conducted in which arsenite was added at different concentrations as illustrated in Figure 6.30. It was found that an arsenite concentration of 10 mM severely suppressed growth, while concentrations of 1 mM or below had relatively little effect on growth (Figure 6.30). Therefore, it was decided that the fermentor arsenite concentration should exceed 1 mM.

6.4.3.1 Fermentation

The arsenite perturbed fermentation, illustrated in Figure 6.31 (A-E), was conducted in a manner basically identical to the FP fermentation, except 20 mmoles of arsenite was added 45 min. after the start of lysine overproduction (Figure 6.31 (A)). A short time after the first arsenite addition (ca. 1 h), respiration began to increase (Figure 6.31 (B)) as in the FP fermentation; consequently, another 80 mmoles of arsenite was added so that sustained inhibition of PDC would ensue. The effects of the combined arsenite additions (ca. 10 mM) resulted in complete termination of growth (and even produced some lysis) and severely decrease in lysine synthesis and respiration (Figure 6.31 (A, B, respectively)). Glucose consumption, however, remained relatively unaffected, and pyruvate and pyruvate derived by-products were excreted at high rates following arsenite addition (Figure 6.31 (C)). Accumulation of pyruvate also resulted in the buildup of ammonium sulfate (Figure 6.31 (D)), as in the FP perturbed fermentation. Lysine•HCl titer was severely reduced (only 5 g/l) and lysine yield, although close to the nominal right after arsenite addition, dropped to zero seven hours after the last arsenite addition. Unlike the FP perturbation, the culture did not recover from the arsenite exposure.

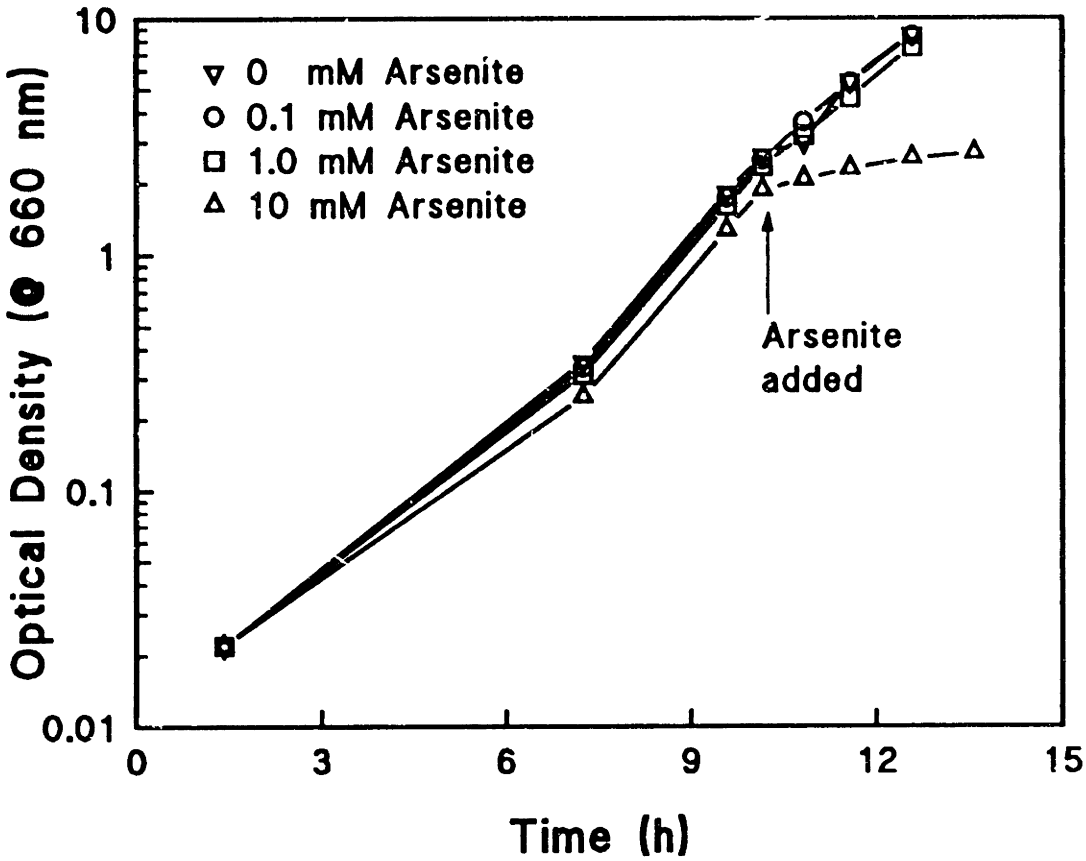

Figure 6.30 Effect of arsenite on growth of *C. glutamicum* ATCC 21253 cultured on 250 ml of glucose PMB medium in 1.0 l shaker flasks. At time 0, each flask was inoculated with 2.5 ml from an overnight (ca. 10 h) culture grown on LB5G medium. Sodium arsenite was aseptically added at 10.2 h (after sample #4) to attain the following concentrations: 0 mM (▽), 0.1 mM (○), 1.0 mM (□), 10 mM (△).

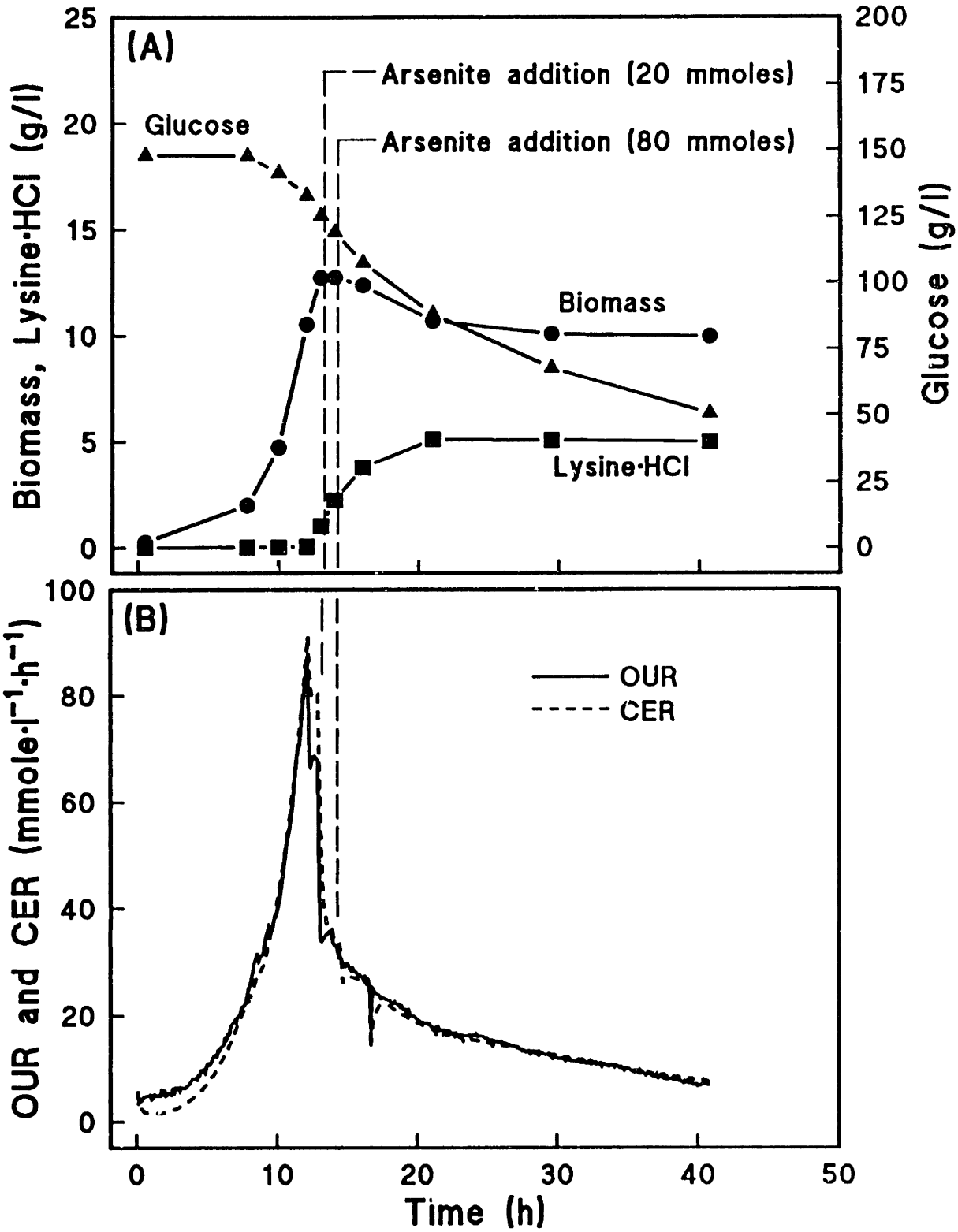

Figure 6.31 Arsenite inhibited lysine fermentation of *C. glutamicum* ATCC 21253 cultured on FM4 medium. At 13.0 h and 14.0 h, 20 and 80 mmoles of arsenite•Na dissolved in 10 ml and 40 ml water were aseptically added, respectively. (A) Concentration profiles of biomass (●), glucose (▲), and lysine•HCl (■) in g/l. (B) Culture respiration, OUR (solid curve) and CER (dashed curve). Note respiration decline upon addition of arsenite.

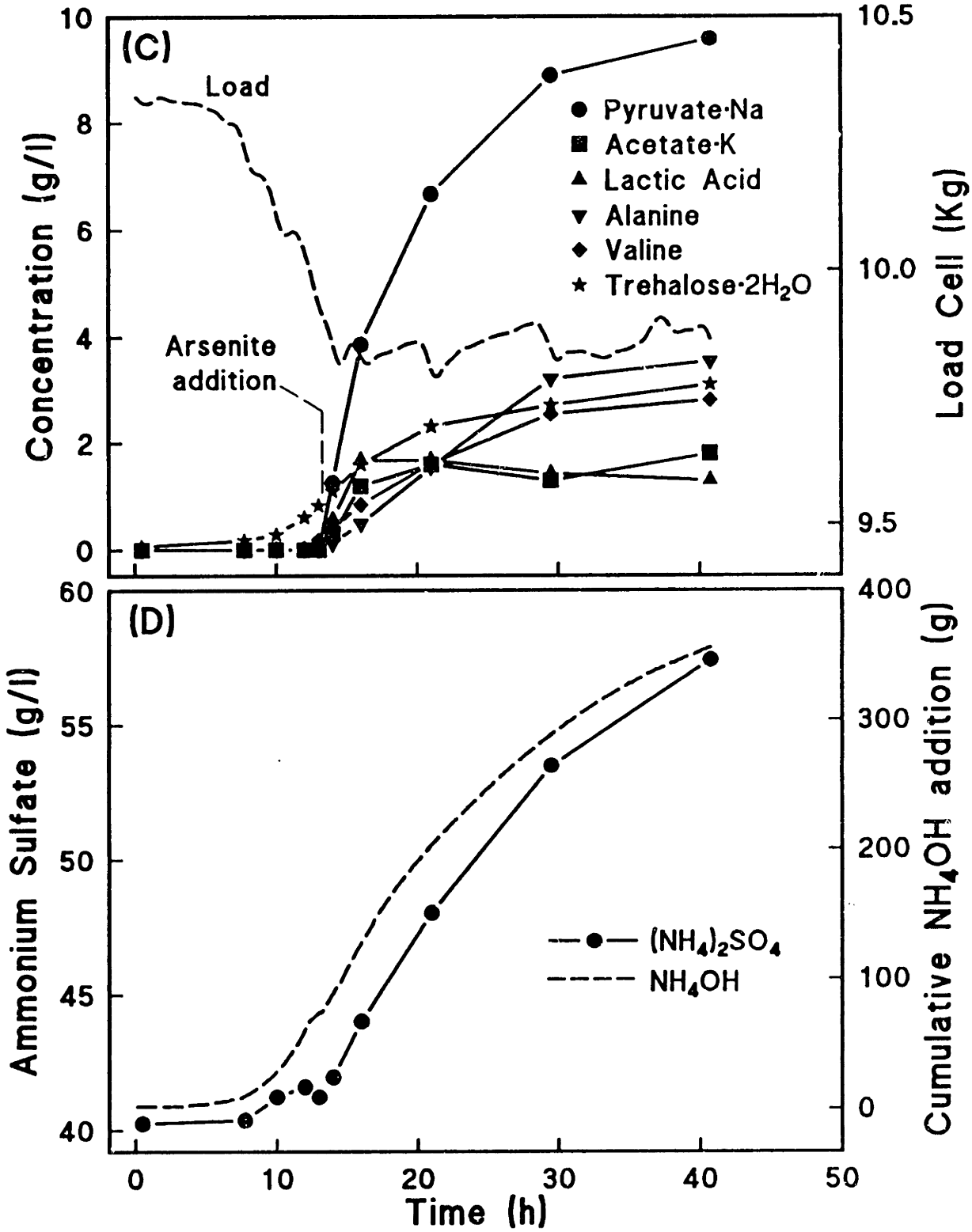

Figure 6.31 (continued) (C) Fermentor load cell (dashed curve) and by-product accumulation. The rapid increase in pyruvate concentration upon arsenite addition should be noted. (D) Available ammonium in broth, as $(NH_4)_2SO_4$ (•), and cumulative amount of NH_4OH (26% (w/w) NH_3) added to maintain culture at pH 7.0.

6.4.3.2 Flux Analysis

The metabolite accumulation rates calculated from measurements taken at 14.0 h and 16.0 h (t_{AVE} = 15.0 h) are displayed in Table 6.14 along with the estimated accumulation rates and the consistency index, and the associated flux distributions are illustrated in Figure 6.32. As evident in Figure 6.32, the effects of arsenite on the metabolism closely resembles those induced by FP, except that arsenite caused the

Table 6.14 Accumulation rate subvectors for the arsenite inhibited lysine fermentation at 15.0 h from measurements taken at 14.0 h and 16.0 h (Figure 6.31), based on MS1 and BS1 in Appendix B; h = 0.99.

Elements of $\mathbf{r}_B(t)$	Accumulation Rates (mM/h)		
	$\bar{\mathbf{r}}_B(15.0) \pm \sigma$		$\hat{\mathbf{r}}_B(15.0)$
Ac (1)	4.6	± 2	4.7
Ala (4)	2.1	± 2	2.3
Biomass (7)	-1.9	± 4.4	-1.0
CO2 (8)	28.8	± 2.9	29.4
Glc (14)	-32.2	± 8.9	-25.0
Lac (19)	6.1	± 2	6.3
LysE (20)	4.21	± 0.2	4.21
NH3 (25)	-16.9	± 23	-12.0
O2 (26)	-29.9	± 3.0	-29.4
Pyr (29)	11.8	± 2	12.1
Trehal (35)	0.7	± 2	1.4
Val (36)	1.9	± 2	2.0

collapse of lysine synthesis and an increase in pyruvate derived by-products, which lead to an even lower TCA cycle flux. Compared to the control fermentation (Figure 6.29 (A)), the arsenite perturbation not only caused the PDC branch split-ratio to drop from 67% to 24%, but also affected the OAA branch of the PEP node, as illustrated in Figure 6.33. Although the alteration of the PEP node split-ratios (Figure 6.33) is an indication of possible Pyr node rigidity, it will be demonstrated in Section 6.5 that lysine synthesis collapse is probably due to rigidity of the PEP node. In conclusion, the metabolic flux alteration due to the arsenite perturbation elicited a similar response as the perturbation induced by FP, although, TCA cycle flux may be partially attenuated due to the reduced specificity of arsenite (*i.e.*, possible

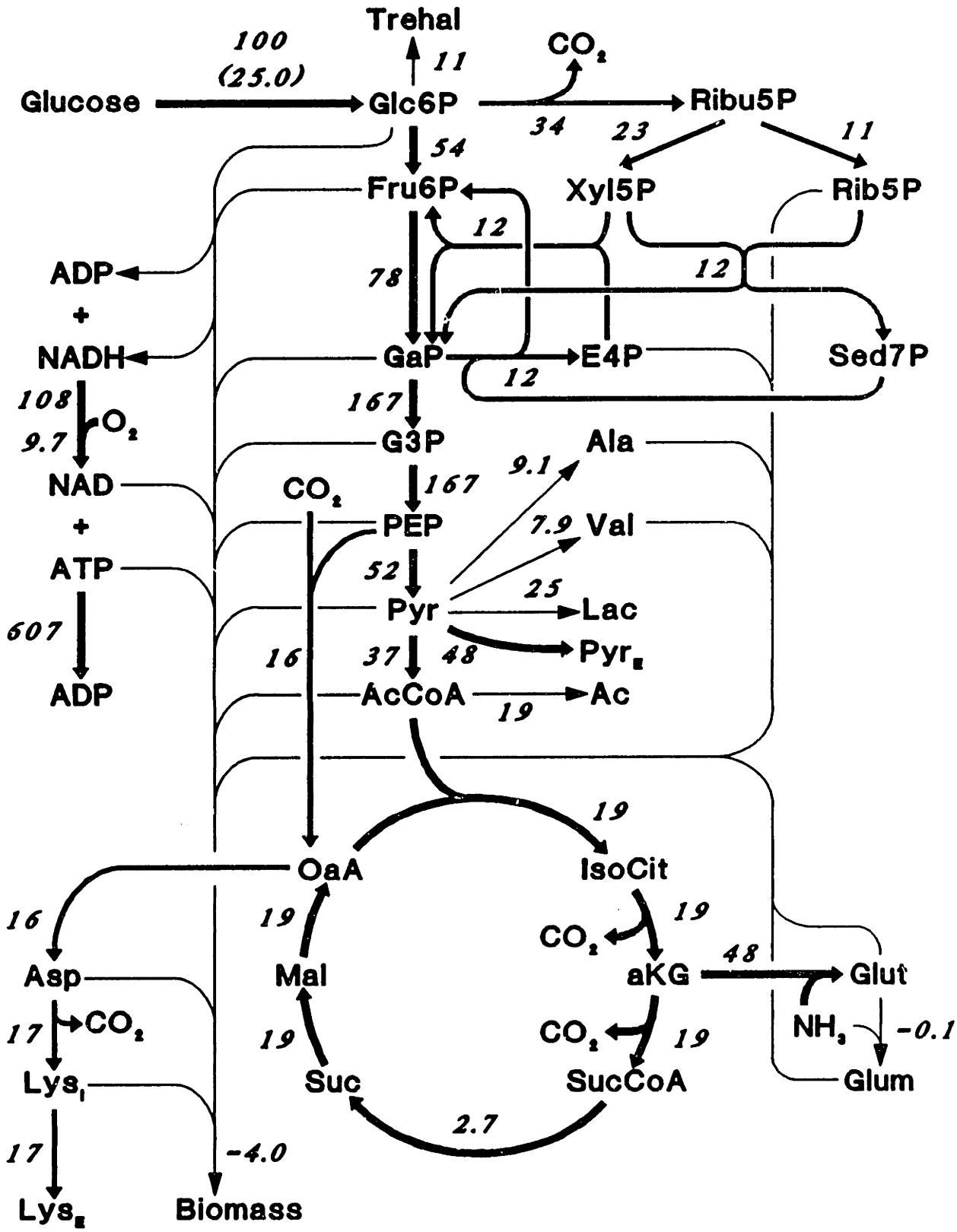

Figure 6.32 Flux distribution map for the arsenite inhibited fermentation at 15.0 h. Fluxes estimated from measurements taken at 14.0 h and 16.0 h (see Figure 6.31 and Table 6.14), and normalized by glucose consumption rate (shown in parentheses; mmole•l^{-1}•h^{-1}). Reactions are from BS1 listed in Appendix B. Note, PYR_E represents extracellular pyruvate accumulation and is not a part of BS1.

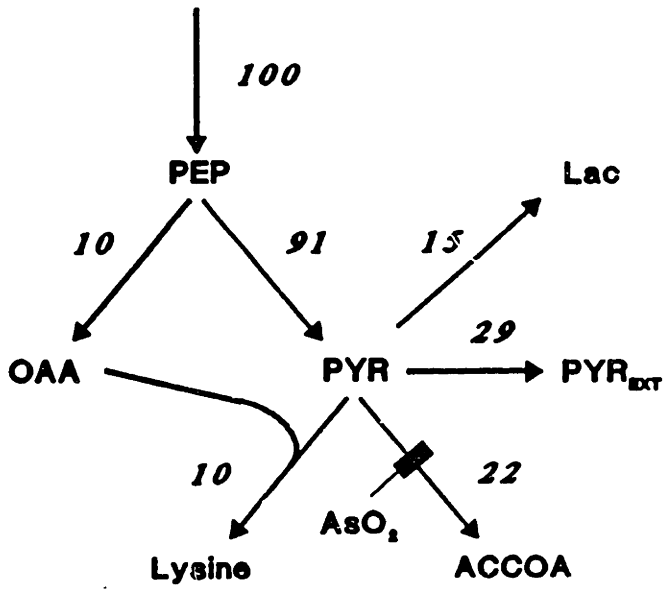

Figure 6.33 Flux distributions around the PEP and Pyr principal nodes normalized by PEP synthesis rate for the arsenite inhibited fermentation at 15.0 h (extracted from Figure 6.32). The solid rectangular block indicates the primary site of arsenite inhibition.

inhibition of αKGDH).

6.4.4 Summary

Flux analysis of FPS009 (the PDC^{A} mutant) demonstrates that the Pyr node is not weakly rigid, as improvements in lysine yield were not observed with this strain. However, the global reduction of all metabolic fluxes resulting from the PDC mutation is consistent with the hypothesis governing a dependent network that harbors one or more rigid nodes, as discussed in Section 4.3.2. Pyruvate overproduction induced by PDC inhibition by FP demonstrates that lysine yield in ATCC 21253 is not limited by pyruvate availability and indicates that the Pyr node may be flexible since alterations of the Pyr node split-ratios were achieved. However, the collapse of lysine synthesis due to PDC inhibition by high arsenite concentrations signifies the presence of a strongly rigid principal node, if we assume that arsenite did not inhibit other enzymes essential for lysine synthesis. Although strong rigidity of the Pyr node cannot be ruled out, it is unlikely in light of the results obtain from the FP perturbation. Furthermore, the proximity of the PEP node to the Pyr node means perturbations of the Pyr node may also directly affect the PEP node. Thus, it is quite conceivable that the collapse of lysine synthesis from the arsenite perturbation is due to rigidity of the PEP node.

6.5 Analysis of the PEP Principal Node

As discussed in Section 4.3.1, the PEP node represents the branch-point between pyruvate synthesis (via pyruvate kinase; PK) and oxaloacetate synthesis (via PEP carboxylase; PPC). Since both Pyr and OAA are required in equal amounts for lysine synthesis, the optimal split at the PEP node is 50-50. This optimal split, however, is not observed in the control fermentation and an excess of pyruvate is synthesized (see Figure 6.13), which is eventually oxidized to CO_2. To increase lysine yield, the carbon flux leading to pyruvate production must be attenuated; however, such a perturbation is not easily attained as specific inhibitors of PK are not known. Furthermore, the actual flux supported by PK when *C. glutamicum* is cultured on glucose is quite small due to the presence of the PEP:glucose phosphotransferase

system. Although a PK attenuated mutant (PK^{A}) of *C. glutamicum* could have been isolated and studied, the returns did not seem very promising since results regarding the Glc6P and Pyr nodes indicate that the PEP node may be strongly rigid. In all likelihood, a PK^{A} mutant would probably exhibit overall attenuated fluxes as observed in the NFG068 and FPS009 strains. Once more, several studies have investigated PK^{A} mutants [Ozaki and Shiio, 1983; Shiio *et al.*, 1984a; Mori and Shiio, 1984; Shiio *et al.*, 1987], and although some improvements in lysine yield have been observed, it is not clear that the improvements are due to PK^{A} since the enhanced strains have undergone several rounds of mutation-selection. (It is quite possible that lysine yield improvements have occurred due to modifications of PPC.)

Since the previous studies involving the Glc6P and Pyr nodes imply that the PEP node may be strongly rigid, we chose to investigate the cause of the PEP node rigidity by constructing a kinetic model from the enzymes associated with the PEP node, based on the data documented in the literature. It is important to realize that although flux analysis during perturbation events have allowed us to isolate the location of the network rigidity, the analysis does not provide any information regarding the cause of the rigidity since enzyme kinetics are not incorporated in the analysis.

The development and analysis of a kinetic model describing the PEP node is presented in Section 6.5.1. Based on the results obtained from the kinetic analysis, a final perturbation experiment was attempted and is described in Section 6.5.2.

6.5.1 Kinetic Model of the PEP Node

The goal of this section is to develop a kinetic model to describe the flux partitioning at the PEP node base on enzyme kinetics documented in the literature and to demonstrate how nodal rigidity can arise. Although flux information provided by the BRNE will prove useful, it is emphasized that the model development in this section is independent of the flux analysis developed in Chapter 4, and is intended to complement the results obtained from the BRNE.

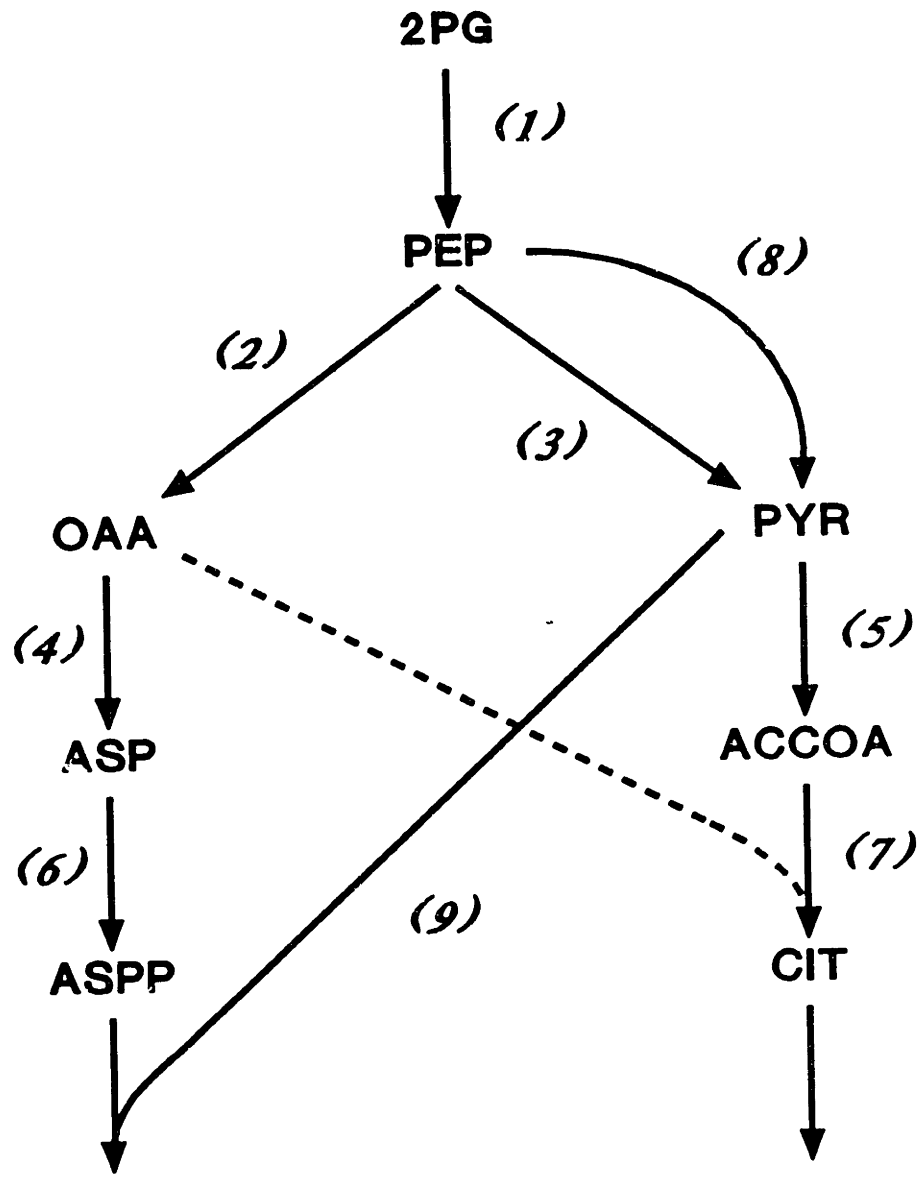

Figure 6.34 Enzymes associated with the PEP node kinetic model. (1) Enolase (ENO); (2) PEP carboxylase (PPC); (3) Pyruvate kinase (PK); (4) Aspartate aminotransferase (AT); (5) Pyruvate dehydrogenase complex (PDC); (6) Aspartate kinase (AK); (7) Citrate synthase (CS); (8) PEP:glucose phosphotransferase system (PTS); (9) Dihydrodipicolinate synthase. The dashed curve symbolizes the participation of OAA in the CS reaction; however, it does not support any flux as explained in the text.

6.5.1.1 Network and Enzymes

Although modeling the carbon-flux partitioning at some nodes would only require kinetics associated with the enzymes that directly produce or consume the node metabolite, to capture the dynamics of the PEP node, reactions leading to ASP and AcCoA formation and consumption must be included due to the kinetics of PEP carboxylase, as will be seen below. Consequently, nine reactions are used to model the kinetics of the PEP node as illustrated in Figure 6.34, as this is an open system, the concentration of 2-phosphoglycerate (2PG) is held constant and citrate (CIT) and aspartyl phosphate (AspP) are remove at their synthesis rates (which also sets Reaction (9) in Figure 6.34, see below). The model consists of five unknown metabolite concentrations (PEP, OAA, Pyr, Asp, and AcCoA) and nine unknown fluxes (Reactions (1-9) in Figure 6.34). The unknown fluxes and metabolite concentrations are determined by mass balance constraints and enzyme kinetics described below.

6.5.1.2 Enzyme Kinetics

To utilize the available literature on glutamic acid bacteria, macro-kinetic models (*i.e.*, Michaelis-Menton type [Briggs and Haldane, 1925; Dixon and Webb, 1979]) are used to express enzyme kinetics. Although micro-kinetic or detailed kinetic models (such as those that account for enzyme, enzyme-substrate and enzyme-product complexes, etc. [see Hayashi and Sakamoto, 1986]) were investigated, lack of rate constants and basic information, and the extremely large dimensions of these models (particularly if allosteric enzymes are involved), preclude their use for network descriptions. Microscopic models are best used to model the transient dynamics of single enzymes. Presented below are the macro-kinetic expressions and kinetic parameters used to represent the kinetics of the enzymes illustrated in Figure 6.34. The kinetic parameters are summarized in Table 6.15 at the end of this section. Enzyme activities (*i.e.*, V_{Mi}) are discussed in Section 6.5.1.3.

6.5.1.2.1 Enolase

Enolase is the first reaction in the network (Reaction (1) of Figure 6.34) and catalyzes the conversion of 2-phosphoglycerate to phosphoenolpyruvate as shown here,

$$2PG \rightleftarrows PEP + H_2O \qquad \text{(EC 4.2.1.11)}$$

where the equilibrium constant, K_{E1}, is 0.48 (calculated from ΔG° given by Lehninger (1975)). The kinetics of ENO have not been published for glutamic acid bacteria, so a simple Michaelis-Menton expression is used. However, since the equilibrium constant of ENO is of order (1), the reverse reaction must be accounted for, as described by Alberty (1959), which produces the following expression,

$$V_1 = \frac{V_{M1}\left([2PG] - \frac{[PEP]}{K_{E1}}\right)}{[2PG] + K_{M1}} \qquad (6.2)$$

where it is assumed that K_M of the forward reaction is much greater that K_M of the reverse reaction. (This is a minor assumption that has been invoked since K_M of the reverse reaction is not known.) The Michaelis constant used for ENO, K_{M1}, is 0.1 mM and is based on that found for Yeast [Hanlon and Westhead, 1969; Barman, 1969b, p. 771]. Although the equation used to represent ENO kinetics is unverified in glutamic acid bacteria, the enzyme has a negligible effect on the dynamics of the PEP node, so the approximations are acceptable.

6.5.1.2.2 PEP Carboxylase

PEP carboxylase (PPC; Reaction (2) of Figure 6.34) catalyzes the conversion of PEP and carbon dioxide to oxaloacetate as shown here,

$$PEP + CO_2 \rightarrow OAA + P_i \qquad \text{(EC 4.1.1.31)}$$

where ΔG° for this reaction equals -6.5 Kcal/mole [Lehninger, 1975]. The PPC catalyzed reaction can therefore be considered irreversible. Although kinetic parameters of PPC in *B. flavum* have been published [Shiio and Ujigawa-Takeda,

1979; Mori and Shiio, 1984] and several kinetic models have been proposed [Mori and Shiio, 1985a; Mori and Shiio 1985b; Mori and Shiio, 1986], they either do not capture the allosteric nature of PPC or require information not included in the PEP node model. Therefore, a generic model was fit to published data. Since PPC is an allosteric enzyme (see any of the above references), the classic Monod allosteric kinetic model [Monod *et al.*, 1965] was used to represent its kinetics as shown here†:

$$V_2 = \frac{V_{M2}\frac{[PEP]}{K_{S2}}\left(1 + \frac{[PEP]}{K_{S2}}\right)}{L_2\frac{\left(1 + \frac{[ASP]}{K_{I2}}\right)^2}{\left(1 + \frac{[ACCOA]}{K_{A2}}\right)^2} + \left(1 + \frac{[PEP]}{K_{S2}}\right)^2} \qquad (6.3)$$

The parameters of the above expression were obtained from a nonlinear least-squares fit (MINSQ, MicroMath, Salt Lake City, UT) to kinetic data published on PPC in *B. flavum* [Ozaki and Shiio, 1969] and are listed in Table 6.15. Comparison of the model predictions to the literature data is illustrated in Figure 6.35 (A).

It is quite important to understand the characteristics of PPC, for this enzyme is primarily responsible for the rigidity of the PEP node, as will be demonstrated in Section 6.5.1.6 below. As illustrated in Figure 6.35 (A), PPC exhibits sigmoidal kinetics when the effectors are absent. However, in the presence of the activator, AcCoA, the kinetics change to hyperbolic (and the apparent K_M is reduced), while addition of aspartate dramatically inhibits PPC activity, effectively increasing the apparent K_M. Furthermore, PPC activation by AcCoA can mitigate the inhibition induced by Asp. Since AcCoA is a metabolite of the PDC branch, the allosteric nature of PPC effectively couples the PPC branch to the PDC branch, a necessary condition for strong rigidity.

The kinetic expression given above for PPC is not complete, as it is well established that PPC is also strongly activated by fructose 1,6-bisphosphate [Mori and

† It is assumed that PEP and AcCoA bind only to the R state, Asp binds only to the T state, and the number of protomers (n) is 2, see Monod *et al.*, 1965.

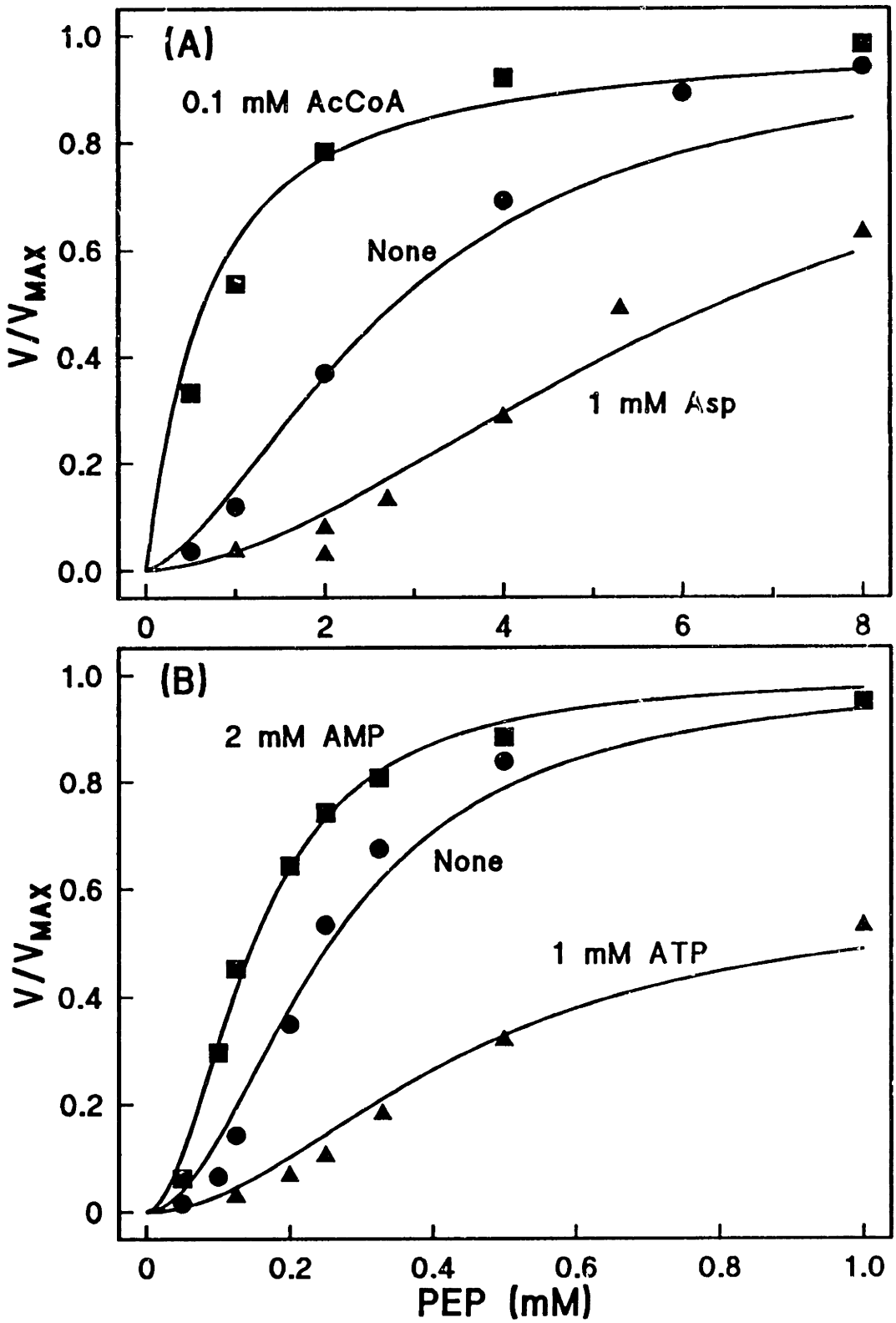

Figure 6.35 Comparison of kinetic model predictions to experimental data of Ozaki and Shiio (1969). (A) Normalized PEP carboxylase activity with no effectors (●), 0.1 mM AcCoA (■), or 1 mM Asp (▲). Solid curves are predicted kinetics from Equation (6.3). (B) Normalized pyruvate kinase activity with effectors (●), 2 mM AMP, or 1 mM ATP. Solid curves are predicted kinetics from Equation (6.4). Parameters for both equations are listed in Table 6.15.

Shiio, 1986] and inhibited (synergistically with Asp) by α-ketoglutarate [Mori and Shiio, 1985b]. These effectors were not included because it was desirable to model the PEP node with as few enzymes as possible, and it is not believed that inclusion of these other effectors would dramatically alter the response of the PEP node under the perturbations of interest. However, if a more extensive model is construct, such effectors should be accounted for.

6.5.1.2.3 Pyruvate Kinase

Pyruvate kinase (PK; Reaction (3) of Figure 6.34) competes with PPC for the node metabolite, PEP, and catalyzes the ADP dependent conversion of PEP to Pyr and ATP as shown below:

$$PEP + ADP \rightarrow Pyr + ATP \qquad \text{(EC 2.7.1.40)}$$

Here ΔG° equals -7.5 Kcal/mole [Lehninger, 1975], so the reaction is essentially irreversible. Contrary to PPC, PK has not been extensively studied, but it has been established as an allosteric enzyme in *B. flavum* [Ozaki and Shiio, 1969], where AMP is a moderate activator and ATP is a strong inhibitor. Since a kinetic model for this enzyme has not been proposed, a modified Monod allosteric kinetic expression (see PPC above) was used to represent the kinetics of PK as shown here†,

$$V_3 = \frac{V_{M3}\frac{[PEP]}{K_{S3}}\left(1 + \frac{[PEP]}{K_{S3}}\right)}{\left[L_3\frac{\left(1 + \frac{[ATP]}{K_{I3}}\right)^2}{\left(1 + \frac{[AMP]}{K_{A3}}\right)^2} + \left(1 + \frac{[PEP]}{K_{S3}}\right)^2\right]\left(1 + \frac{[ATP]}{K_{I3}}\right)} \qquad (6.4)$$

where the parameters were determined from a nonlinear least-squares fit to the data of Ozaki and Shiio (1969), illustrated in Figure 6.35 (B) and listed in Table 6.15. Although ADP certainly effects PK activity, it was not included in the above

† The additional term was added since ATP acts noncompetitively with ADP, so that V_{MAX} is effectively reduced. The number of protomers (n) is 3.

expression since ADP concentration is not part of the PEP node model and its inclusion in Equation (6.4) would only introduced another adjustable parameter.

6.5.1.2.4 Aspartate Aminotransferase

Aspartate aminotransferase (AT; Reaction (4) of Figure 6.34) catalyzes the transamination of oxaloacetate (OAA) to aspartate (Asp) via glutamate (Glut) as depicted here,

$$OAA + Glut \rightleftarrows Asp + \alpha KG \qquad \text{(EC 2.6.1.1)}$$

where the equilibrium constant, K_{E4}, for this reaction is 6.1 [Barman, 1969a]. Consequently, the reverse reaction must be accounted for. Since Glut and αKG are not represented in the PEP node model, they were removed by assuming that Glut is at saturating concentrations and that [Glut]/[αKG] = 170 (intracellular glutamate concentration is approximately 100 mM [Hoischen and Kramer, 1989] and αKG concentration† is roughly 0.6 mM). Consequently, the effective equilibrium, K'_{E4} = [Asp]/[OAA], is approximately 1000. The kinetics of AT are represented by

$$V_4 = \frac{V_{M4}\left([OAA] - \frac{[ASP]}{K'_{E4}}\right)}{[OAA] + K_{M4}} \qquad (6.5)$$

where the OAA Michaelis constant, K_{M4}, is from *B. flavum* [Shiio *et al.*, 1982c] and listed in Table 6.15.

6.5.1.2.5 Pyruvate Dehydrogenase Complex

The pyruvate dehydrogenase complex (PDC; Reaction (5) of Figure 6.34) couples glycolysis to the TCA cycle as shown here,

$$Pyr + NAD^+ + CoA \rightarrow AcCoA + NADH + H^+ + CO_2$$

† Assume αKG concentration is 10% of the αKG-Michaelis constant for glutamate dehydrogenase, which is 5.7 mM [Shiio and Ozaki, 1970].

and is catalyzed by a complex of three enzymes (EC 1.2.4.1; EC 2.3.1.12; EC 1.6.4.3). The overall reaction can be considered irreversible since the equilibrium strongly favors AcCoA formation ($\Delta G^\circ = -8.0$ Kcal/mole [Lehninger, 1975]). Although PDC kinetics in *E. coli* are quite complex [Schwartz *et al.*, 1968; Schwartz and Reed, 1970], PDC in glutamic acid bacteria has not been well characterized, so the following simple expression was used to represent its kinetics

$$V_5 = \frac{V_{M5}[PYR]}{[PYR] + K_{M5}} \tag{6.6}$$

where the Michaelis constant, K_{M5}, is from PDC in *B. flavum* [Shiio *et al.*, 1984b].

6.5.1.2.6 Aspartate Kinase

Aspartate kinase (AK; Reaction (6) of Figure 6.34) catalyzes the ATP dependent phosphorylation of aspartate

$$\text{Asp} + \text{ATP} \rightarrow \text{AspP} + \text{ADP} \qquad \text{(EC 2.7.2.4)}$$

where the equilibrium favors aspartyl phosphate formation ($K_{E6} = 3\text{x}10^3$ [Barman, 1969a]). This enzyme has been well characterized in glutamic acid bacteria, and although several studies have characterized the feedback inhibition of AK by threonine and lysine in glutamic acid bacteria [Nakayama *et al.*, 1961; Nakayama *et al.*, 1966; Miyajima *et al.*, 1968; Shiio and Miyajima, 1969; Tosaka and Takinami, 1978], feedback inhibition is not incorporated in the PEP node kinetic model as it is assumed that end-product inhibition has been removed. Consequently, the kinetic model reduces to the two substrate model proposed by Shiio and Miyajima (1969),

$$V_6 = \frac{V_{M6}}{1 + \frac{K_{MA6}}{[ASP]} + \frac{K_{MB6}}{[ATP]} + \frac{K_{DA6}K_{MB6}}{[ASP][ATP]}} \tag{6.7}$$

where the kinetic parameters are listed in Table 6.15.

6.5.1.2.7 Citrate Synthase

Citrate synthase (CS; Reaction (7) of Figure 6.34) is the first enzyme of the TCA cycle and catalyzes the condensation of OAA with AcCoA

$$AcCoA + OAA + H_2O \rightarrow Cit + CoA \qquad \text{(EC 4.1.3.7)}$$

where the equilibrium strongly favors citrate formation ($\Delta G^\circ = -7.7$ Kcal/mole [Lehninger, 1975]). This enzyme has also been well characterized in *B. flavum* [Shiio *et al.*, 1977] where its kinetics are given by the expression:

$$V_7 = \frac{V_{M7}}{\left(1 + \frac{K_{MA7}}{[OAA]}\right)\left[1 + \frac{K_{MB7}}{[ACCOA]}\left(\frac{1 + \frac{[ATP]}{K_{I7}}}{1 + \frac{[ATP]}{K_{IB7}}}\right)\right]} \qquad (6.8)$$

The model accounts for inhibition by ATP both noncompetitively with OAA and partially competitive with AcCoA.

6.5.1.2.8 PEP:glucose phosphotransferase system

The PTS (Reaction (8) of Figure 6.34) is responsible for the transport and phosphorylation of glucose

$$Glucose + PEP \rightarrow Glc6P + Pyr$$

and is the primary glucose transport system in *B. flavum* [Mori and Shiio, 1987a; Mori and Shiio, 1987b]. However, the kinetics of the reaction have not been established, nor are they really necessary to the PEP node model. Since two 2PG molecules are produced for each glucose molecule phosphorylated by PEP, the flux of PEP to Pyr due to the PTS is approximately equal to one half of the enolase catalyzed flux. Therefore, only a mass balance is used to set flux supported by Reaction (8) in the PEP node kinetic model.

6.5.1.2.9 Dihydrodipicolinate synthase

Dihydrodipicolinate synthase (Reaction (9) of Figure 6.34) catalyzes the condensation of aspartate-β-semialdehyde (ASA; not shown in Figure 6.34) with Pyr to form dihydrodipicolinate (DDP) as depicted here:

$$\text{ASA} + \text{Pyr} \rightarrow \text{DDP} \qquad \text{(EC 4.2.1.52)}$$

Since the network model developed in this section focuses on the PEP node, it is assumed that the Pyr node is completely flexible so that all AspP synthesized produces lysine. Consequently, the flux supported by DDP synthase (Reaction (9)) was set equal to the flux supported by AK (Reaction (6)), so that no kinetic expression was required. This assumption is fairly safe, as the activity of DDP synthase is relatively high (250 U/mg-protein [Cremer *et al.*, 1988; Tosaka *et al.*, 1978b]) and the apparent Michaelis constant for pyruvate is relatively low (0.6 mM [Tosaka *et al.*, 1979a]).

Table 6.15 Kinetic parameters for Equations (6.2-6.8). See text for references.

Enzyme	Parameters			Enzyme	Parameters		
ENO	K_{E1}	0.48		AT	K'_{E4}	1000	
	K_{M1}	0.1	mM		K_{M4}	0.11	mM
PPC	K_{S2}	0.54	mM	PDC	K_{M5}	89	μM
	K_{I2}	0.75	mM				
	K_{A2}	15	μM	AK	K_{MA6}	6.8	mM
	L_2	25.5			K_{MB6}	2.7	mM
					K_{DA6}	50	mM
PK	K_{S3}	3.8	μM	CS	K_{MA7}	3.9	μM
	K_{I3}	1.4	mM		K_{MB7}	54	μM
	K_{A3}	2.8	mM		K_{I7}	1.9	mM
	L_3	4560			K_{IB7}	17	mM

6.5.1.3 Enzyme Activities

All of the kinetic expressions presented in Section 6.5.1.2 require *in vivo* enzyme activity to set V_{Mi} (where i = 1 to 7). However, as evident from Table 6.16, *in vitro* enzyme activities can vary significantly. These variations can be caused by protein decay with time, variable or suboptimal assay conditions, error in total protein measurement, medium cells are cultured on, or phase of growth when cells are lysed. Consequently, enzyme activities are much more subjective than inherent kinetic parameters and do not necessarily represent *in vivo* activities. As a result, *in vitro* enzyme activities may require some adjustment to obtain realistic fluxes. Furthermore, to used the data presented in Table 6.16, they must be converted to the proper units.

Fluxes are always reported in units of mmole/l/h, while enzyme activities are in units of nmole/min/mg-protein. So that estimated flux distributions from fermentation data can be compared to (and used to fine tune) flux distributions predicted by the PEP node kinetic model, the units of enzyme activity must be converted to mmole/l/h. In order to accomplish this, protein concentration must be determined. Typical biomass concentration during lysine synthesis (where simulations will focus; *i.e.*, Phases II and III) is around 10 g/l DCW and soluble protein content is approximately 33% of DCW (see Section 6.1, Figures 6.1 (A) and 6.4). Under these conditions, the conversion factor between specific enzyme activity and measured flux is 0.2 mg-protein•min•mmole/nmole•l•h at 10 g/l DCW. Enzyme activities (in converted units), used to simulate the PEP node, are present in Section 6.5.1.5.

6.5.1.4 Kinetic Model

The kinetic model for the PEP node is easily constructed by determining the accumulation rates of each of the five state variables ([PEP], [OAA], [Pyr], [Asp], and [AcCoA]), based on the reactions illustrated in Figure 6.34. ([2PG] is an adjustable parameter and AspP and Cit are removed at their synthesis rates.) A conversion factor must be introduced as the five state variables represent intracellular concentrations while the fluxes (given by Equations (6.2-6.8)) are based on fermentor volume (see conversion factor on enzyme activities above). Consequently, the ratio of fermentor volume to intracellular volume, Φ, must be estimated. Assuming that

Table 6.16 Specific activities for enzymes associated with PEP node kinetic model, Equations (6.2-6.8). All activities reported were assayed directly from the crude cell-extract.

Enzyme	Activity†	Reference
ENO	290‡	Shiio *et al.* (1961b)
	400-1400	Maitra and Lobo (1971)
PPC	204	Mori and Shiio (1985a)
	140	Ozaki and Shiio (1969)
	90-105	Ozaki and Shiio (1983)
	351	Mori and Shiio (1984)
	20	Shiio and Ujigawa (1978)
	156	Mori and Shiio (1985b)
	250	This study, Section 5.3
PK	193	Ozaki and Shiio (1969)
	649	Ozaki and Shiio (1983)
	809	Mori and Shiio (1984)
	1243	Shiio *et al.* (1987)
	809	Mori and Shiio (1987a)
AT	376-730	Shiio *et al.* (1982c)
	400	Shiio and Ujigawa (1978)
	463	Shiio and Ozaki (1970)
PDC	20	Ozaki and Shiio (1983)
	105‡	Tosaka *et al.* (1985)
	30	This study, Section 5.3
	38	Shiio *et al.* (1984b)
AK	1.7	Ozaki and Shiio (1983)
	13.1	Shiio *et al.* (1987)
	6.3-12.6	Shiio and Miyajima (1969)
	19.2	Tosaka *et al.* (1978a)
	12-16	Cremer *et al.* (1988)
	12	Tosaka *et al.* (1978b)
CS	80-115	Ozaki and Shiio (1983)
	345-1360	Mori and Shiio (1984)
	120	Shiio and Ujigawa (1978)
	27-300	Shiio *et al.* (1977)

† $nmole \cdot l^{-1} \cdot mg\text{-}protein^{-1}$

‡ Calculated from data presented

the biomass concentration is 10 g/l DCW, the dimensions of a single cell are 1×2 μm, and the dry weight of a single cell is 2.9×10^{-13} g [Ingraham *et al.*, 1983], then $\Phi = 18$† at 10 g/l DCW. The state equations are

$$\frac{d[PEP]}{dt} = \Phi\left(\frac{1}{2}V_1 - V_2 - V_3\right) \tag{6.9}$$

$$\frac{d[OAA]}{dt} = \Phi(V_2 - V_4) \tag{6.10}$$

$$\frac{d[ASP]}{dt} = \Phi(V_4 - V_6) \tag{6.11}$$

$$\frac{d[PYR]}{dt} = \Phi\left(\frac{1}{2}V_1 + V_3 - V_5 - V_6\right) \tag{6.12}$$

$$\frac{d[ACCOA]}{dt} = \Phi(V_5 - V_7) \tag{6.13}$$

where V_i (i=1,7) are given by Equations (6.2-6.8). Although construction of the state model is fairly obvious, Equations (6.9), (6.10), and (6.12) require some explanation. The flux supported by the phosphotransferase system (Reaction (8) of Figure 6.34) accounts for the 1/2 V_1 terms in Equations (6.9) and (6.12). In Equation (6.10), V_7 is not included, as operation of the TCA cycle resynthesizes all OAA consumed by CS if no other metabolites are drawn of the cycle (which is the typically observed case). As mentioned above, because it is assumed that all AspP synthesized condenses with Pyr to form lysine, the V_6 term is added to Equation (6.12). The only adjustable parameters of the PEP node model are the concentrations of 2PG, ATP, and AMP, which are determined by tuning the predicted fluxes to the steady state fluxes obtained from the BRNE and fermentation data, discussed below.

---

† The true value of Φ is probable closer to 100 since Hoischen and Kramer (1989) have measured the intracellular water volume of *C. glutamicum* to be 1 μl/mg DCW. However, this only reduces the transient period of the simulation, which is inconsequential since we are mainly interested in the steady state solution.

6.5.1.5 Model Tuning

Model tuning is simply the adjustment of model parameters, such that the resulting steady state flux distribution matches the flux distributions observed during an actual fermentation under nominal conditions, which has already been presented in Section 6.1 for the control fermentation. There are two basic groups of adjustable parameters. The first involves setting the enzyme activities present in Section 6.5.1.3. For the first trial, the V_{Mi}'s for Reactions (6.2)-(6.8) were set (after proper units conversion) to the average *in vitro* value reported in the literature (Table 6.16). However, when this was done, the maximum activities of PDC and AK were too low to support typical fluxes observed in the control fermentation. For instance, typical lysine synthesis rates during Phase III range from 4-6 mmole/l/h (and can reach 11 mmole/l/h in Phase II) while the highest V_{M6} reported for AK (a high lysine producing strain) is only 4 mmole/l/h (Table 6.16, after units conversion). Therefore, the reported *in vitro* activity for AK cannot represent the *in vivo* activity that must exist in order to explain the observed lysine production rates. A similar argument holds for PDC. Consequently, to achieve fluxes consistent with those estimated from the BRNE during Phase III of the control lysine fermentation, it was necessary to increase V_{M5} and V_{M6} values (PDC and AK, respectively) above their reported *in vitro* activities. Activities reported for the remaining enzymes did not require any further adjustments, and the V_{Mi} used for the PEP node model are listed in Table 6.17.

The other parameters that require adjustment are the concentrations of 2PG, ATP, and AMP. As described above, these parameters were set such that the resulting steady state fluxes approximately match those observed in Phase III of the control fermentation. The values obtained for these three parameters are listed in Table 6.17. The concentration of ATP (7 mM) is on the high side, since Kornilova *et al.* (1988) has measured ATP in *Brevibacterium flavum* at approximately 1.3 mM. However, 7 mM ATP is not unreasonable, as ATP concentrations are known to fall in a range of 0.5-5 mM [Knowles, 1977] and possible higher if cellular density is higher. Shiio *et al.* (1990) have measured AMP concentrations around 1 mM, which agrees with the measurements of Kornilova *et al.* (1988). The steady state fluxes

based on the parameters listed in Table 6.15 and 6.17 are illustrated in Figure 6.37 and are discussed, along with several perturbations studies, in the next section.

Table 6.17 Range of enzyme activities reported in literature (Table 6.16) and those used for Equations (6.2)-(6.8), along with values of adjustable parameters used in the PEP node kinetic mode.

Enzyme (i)	Activity (mmole/l/h)	
	Range Reported	V_{Mi} Used
ENO (1)	58-280	80
PPC (2)	4-70	40
PK (3)	39-249	160
AT (4)	75-146	90
PDC (5)	4-21	30
AK (6)	0.3-3.8	25
CS (7)	16-272	100
Metabolite	Concentration (mM)	
2PG	4.0	
ATP	7.0	
AMP	1.0	

6.5.1.6 PEP Node Simulations

The fluxes for the reactions listed in Figure 6.34 are determined by simply integrating the state equations (6.9-6.13) forward in time. A fourth order Runge-Kutta algorithm with automatic step size adjustment was used for the integration (SIMNON; Engineering Software Concepts, Palo Alto CA) and was terminated when the state variables were at (or close to) steady state. Although we are primarily interested in steady state solutions, the transient nature of the kinetic model, based on the parameters listed in Table 6.15 and 6.17, is presented in Figure 6.36 (A-C). Figure 6.36 (B) depicts the transients of the state variables and Figure 6.36 (A) their derivatives as a function of simulation time. The profiles of the fluxes are illustrated in Figure 6.36 (C). The initial conditions for this (and all) simulation was the origin. It is apparent from Figure 6.36 that the system reaches steady state within a few minutes. Although the model is based on only seven kinetic expressions, it is quite evident that the system has response times that are consistent with the pseudo-steady

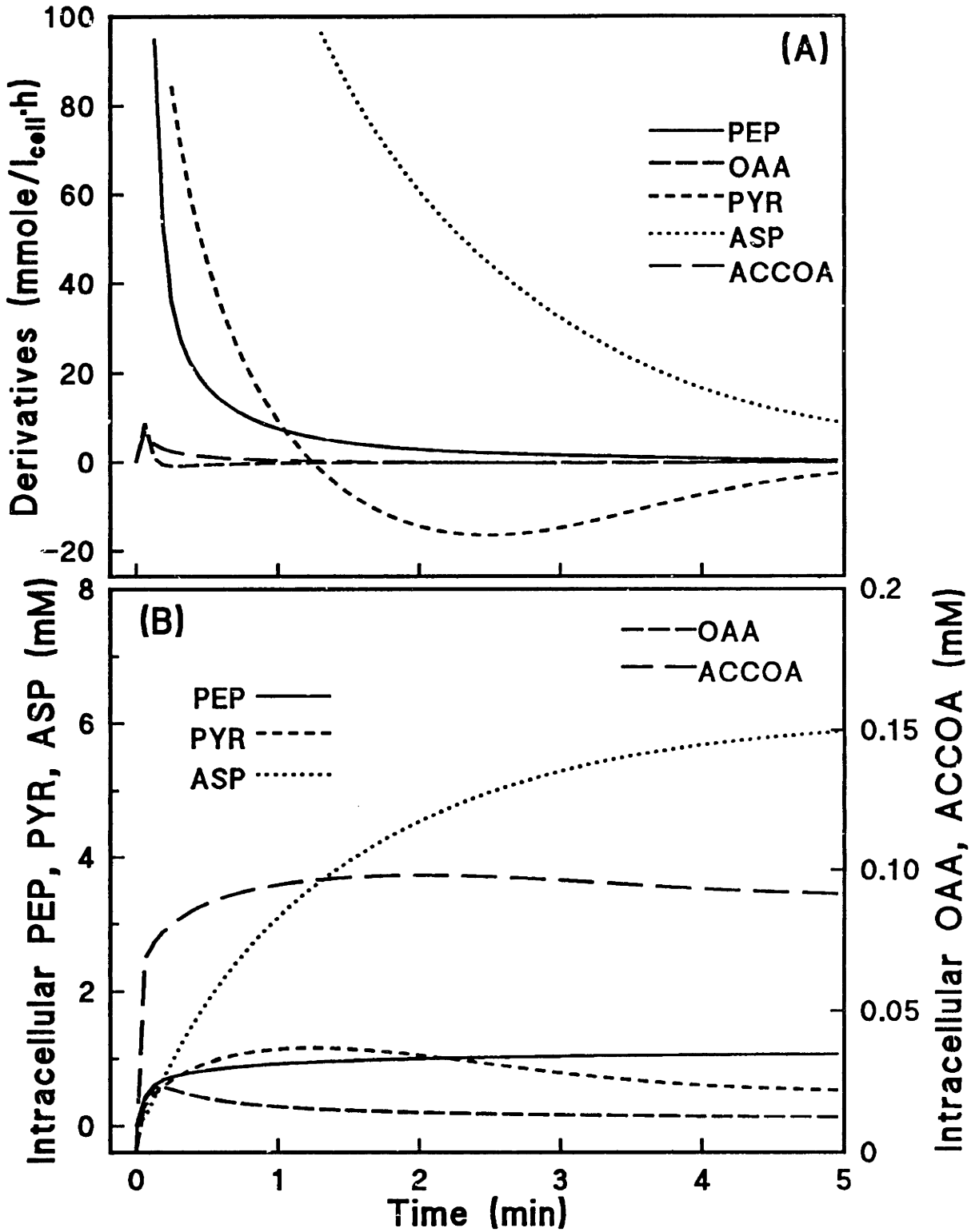

Figure 6.36 Transient dynamics of the PEP node kinetic model given by Equations (6.2)-(6.13). The initial conditions for all variables was the origin and the parameters used are listed in Tables 6.15 and 6.17. The state variables (B) and their derivatives (A) during the first 5 minutes of simulation time. Note, the state variables—intracellular concentrations—are based on cellular volume.

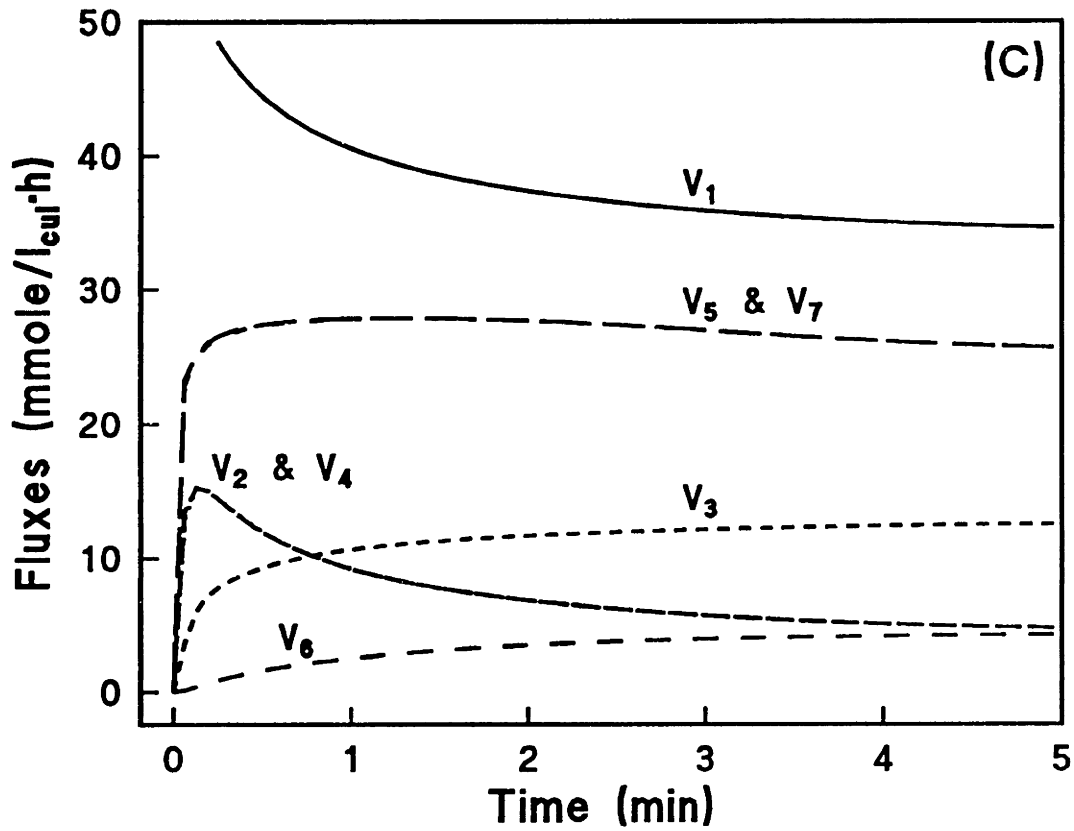

Figure 6.36 (continued) (C) Enzyme catalyzed rates—fluxes—given by Equations (6.2)-(6.8) in mmole/$l_{CULTURE}$/h during the first 5 minutes of simulation time. Note how the pseudo-steady state approximation is valid after the first few minutes.

state approximation discussed in Section 4.1 6.2. Furthermore, analysis of the transient dynamics indicates that aspartate kinase has the slowest response time and dramatically increases the time required to reach steady state operation. The dynamics of AK will become more pronounced when perturbations are examined below. In the following model studies, only steady state data will be presented as the transient behavior, although interesting, is on a time scale much shorter that we are interested in.

The goal of this section is to illustrate the presupposed rigidity of the PEP node and to determine its causes by examining the response of the PEP node to various simulated perturbations. The flux distribution under nominal conditions is illustrated in Figure 6.37. As described above, the kinetic model parameters were adjusted (tuned) such that the resulting steady state fluxes agreed with those observed in the control fermentation during Phase III (Figure 6.9), where the biomass load (yield) is quite small. In Figure 6.37, as well as in all similar diagrams, all fluxes are displayed in absolute units (mmole/l/h) and the reactions correspond to those illustrated in Figure 6.34. The numbers in brackets, [ ], are the concentrations (in mM) of the corresponding metabolites at (or near) steady state conditions. The effective lysine yield (Y_E; the projected lysine yield solely based on the split-ratios at the PEP node) is obtained by evaluating the PPC branch split-ratio ($Y_E = 150V_2/V_1$), and varies from 0 to 75%. For the nominal case (Figure 6.37), Y_E equals 20%. In subsequent perturbation studies, the goal, as it would be experimentally, is to increase the PPC branch split-ratio (hence Y_E) while maintaining a high lysine flux (*i.e.*, Reaction (6) of Figure 6.34). The first simulated perturbation examined was the attenuation of PDC activity (Reaction (5) of Figure 6.34) since the model predictions could be compared to the inhibitor experiments presented in Section 6.4.

To simulate the attenuation of PDC, V_{M5} of Equation (6.6) was reduced by 90% (from 30 to 3 mmole/l/h) and the state equations were integrated with the same initial conditions and parameters (except V_{M5}). The result of attenuating PDC, illustrated in Figure 6.38, is the accumulation of pyruvate, depicted as the flow leading to Pyr_E, which is essentially identical to the results obtained experimentally when PDC was attenuated by FP or arsenite (Section 6.4). Furthermore, examination

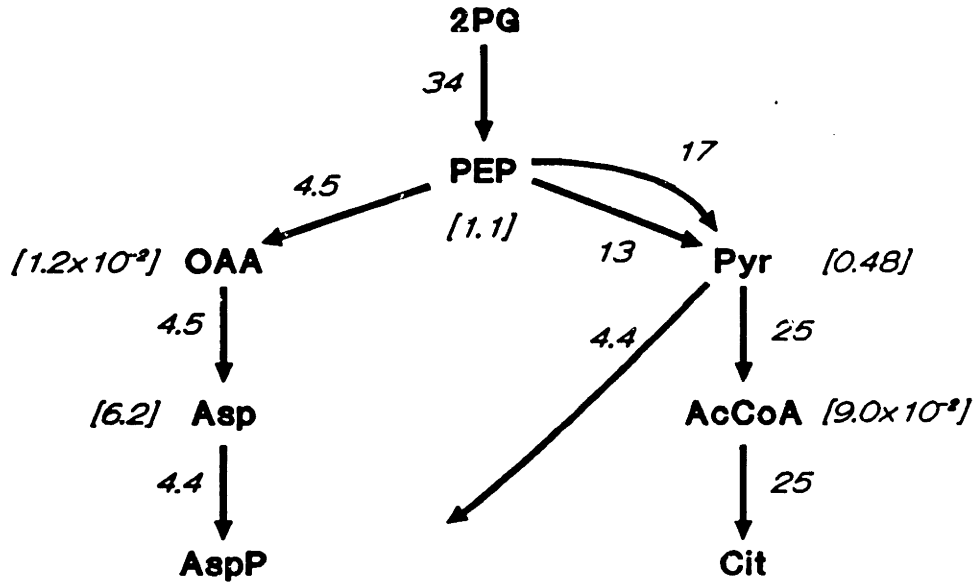

Figure 6.37 Simulated flux distribution based on Equations (6.2)-(6.13) around the PEP node, under nominal conditions given in Tables 6.15 and 6.17. Reactions correspond to those illustrated in Figure 6.34. Fluxes are in mmole/l/h; the numbers in brackets refer to the intracellular concentrations (mM) of the corresponding metabolites. The effective lysine yield (Y_B) is 20%.

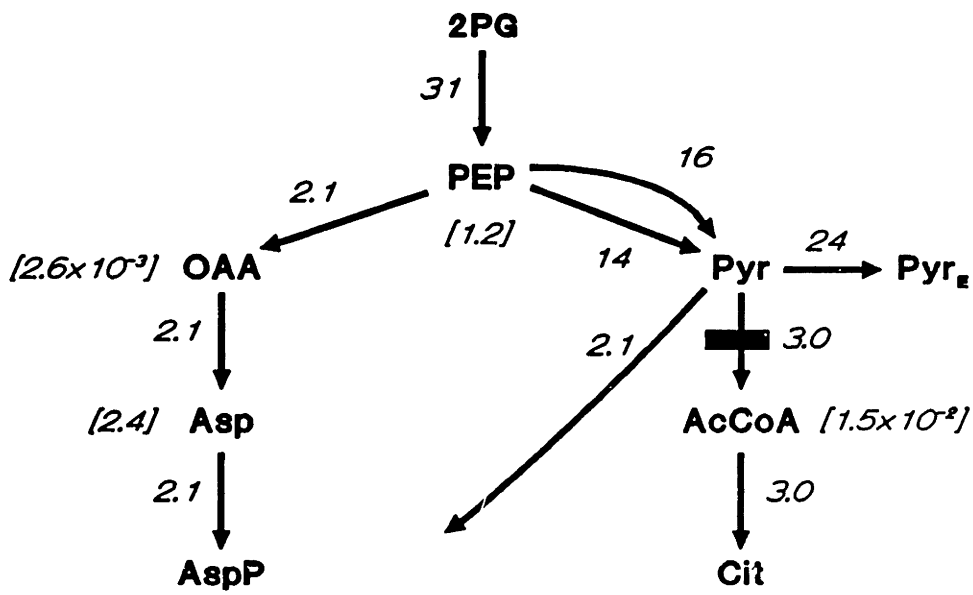

Figure 6.38 Simulated attenuation of PDC activity by 90%, indicated by solid rectangle. V_{M5} reduced to 3 mmole/l/h and Pyr_E refers to extracellular Pyr accumulation. Y_E equals 10%. Other conditions as given in Figure 6.37.

of the flux leading to AspP reveals that it has been attenuated by approximately 50%, and the effective lysine yield has dropped to only 10% since the flux to Pyr has not been affected. This, of course, symbolizes the presence of a strongly rigid node, and agrees well with that observed during the arsenite perturbation. The cause of the Pyr accumulation is attributed to the characteristics of PK. Since the equilibrium of the PK catalyzed reaction strongly favors Pyr formation, the flux of the forward reaction is not affected by Pyr accumulation, nor is Pyr known to inhibit PK. Consequently, attenuation of PDC does not significantly affect PK, so Pyr accumulation results. As for the reduction of the PPC branch split-ratio, we must consider the characteristics of PPC. Attenuation of PDC reduces the flux to AcCoA; however, CS is still quite active, so the concentration of AcCoA drops from 90 μM to 15 μM (Figures 6.37 and 6.38, respectively). Since PPC is activated by AcCoA (see Equation (6.3)), the drop in AcCoA concentration results in some loss of PPC activity, which causes the flux to AspP to drop. Consequently, the drop in Y_E caused by PDC attenuation results from the rigidity of the PEP node, and not the Pyr node.

To illustrate the strong rigidity of the PEP node, a simulation was run in which the activity of PK was attenuated 99% by reducing V_{M3} from 160 to 1.6 mmole/l/h. As evident from the flux distribution, illustrated in Figure 6.39, attenuation of PK by 99% resulted in almost complete collapse of the flux network (removal of PK did result in complete flux collapse), and although the PPC branch split-ratio was improved (Y_E reached 68%), it was at the expense of the AspP synthesis rate which dropped 60% as compared to the nominal case (Figure 6.37). Consequently, the simulation clearly exemplifies the rigidity of the PEP node. To illustrate that the allosteric nature of PPC is the causative agent behind the rigidity of the PEP node, another simulation was run where the activity of PK was attenuated (actually removed by setting V_{M3} to 0.0). In this simulation, however, the effects of Asp and AcCoA on PPC were removed by dropping the terms $[Asp]/K_{I2}$ and $[AcCoA]/K_{A2}$ from Equation (6.3). As seen in Figure 6.40, attenuation of PK activity after removing the influence of the PPC effectors not only produces the optimum PPC branch split-ration (Y_E = 75%), but actually results in a two fold increase in AspP synthesis rate (from 4.4 to 9.2 mmole/l/h) This simulation clearly demonstrates that

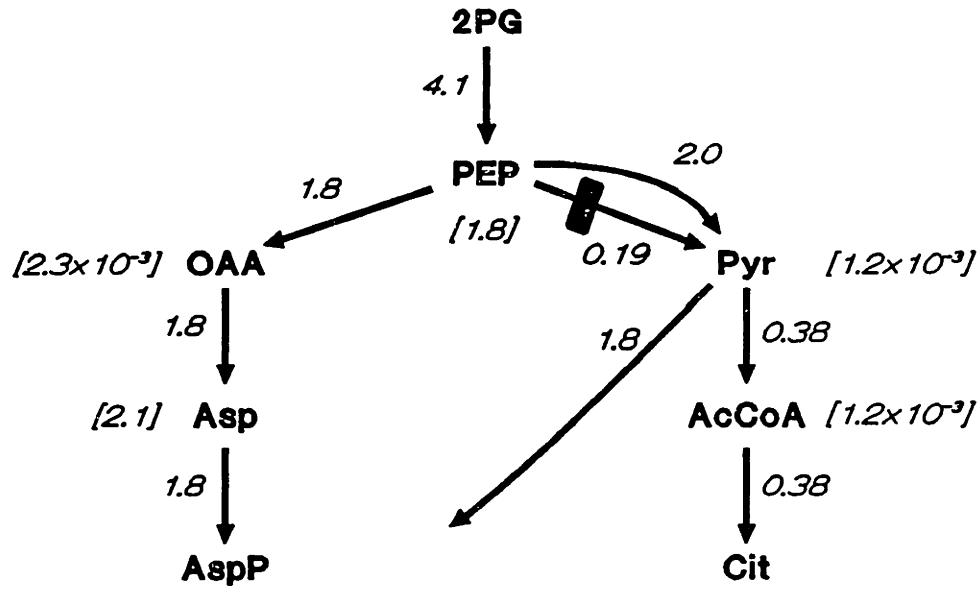

Figure 6.39 Simulated attenuation of PK activity by 99% (V_{M3} reduced to 1.6 mmole/l/h), indicated by solid rectangle. Effective lysine yield is 68%. Other conditions as given in Figure 6.37.

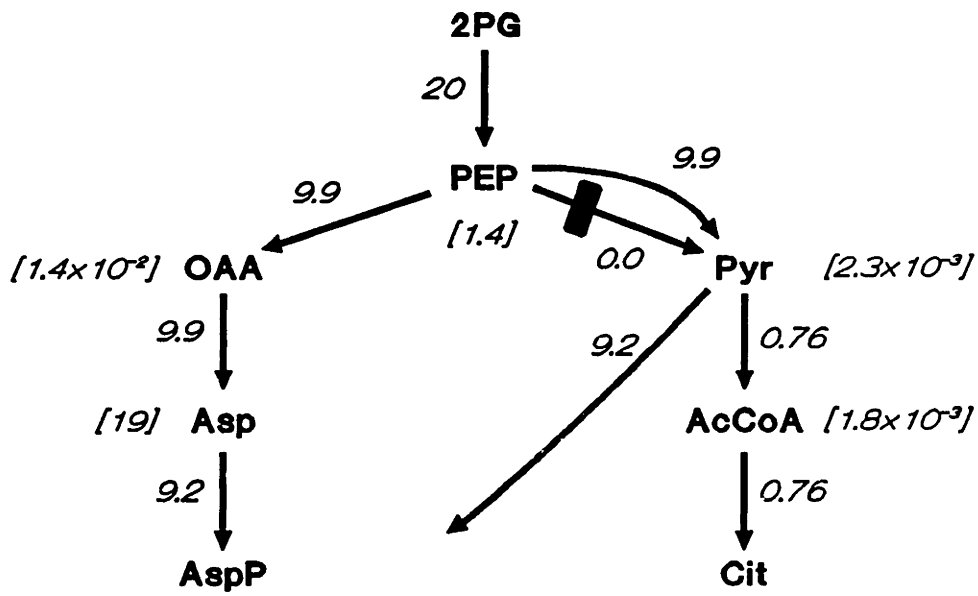

Figure 6.40 Simulated attenuation of PK activity by 100% (set V_{M3} to 0) on a network with modified PPC kinetics (removed [Asp]/K_{I2} and [AcCoA]/K_{A2} terms from Equation (6.3)). Effective lysine yield is 75%. Other conditions as given in Figure 6.37.

the strong rigidity of the PEP node is due to the allosteric nature of PPC. Removal of the PPC effectors, however, do not completely remove the rigidity of the PEP node.

To illustrate that the PEP node degenerates to a weakly rigid node after removal of the PPC effectors, a simulation was run under the same conditions as the nominal case (Figure 6.37), except the influence of the PPC effectors were removed as in the simulation described above. As portrayed in Figure 6.41, removal of the PPC effectors had an almost negligible effect on the network, except for the slight improvement in Y_E, which increased to 26%. However, as described above (Figure 6.40), attenuating PK activity in this PPC modified network dramatically increases Y_E and the AspP synthesis rate, which indicates that the PPC modified PEP node is weakly rigid as defined in Section 4.3.2.1. The cause of the weak rigidity of the PEP node after modifying PPC kinetics can best be explained by considering the kinetics of PPC and PK illustrated in Figure 6.35. As depicted in this figure, the apparent PEP K_S for PPC without AcCoA activation is approximately ten times higher than the apparent PEP K_S for PK. The lower K_S of PK, coupled with its higher activity (Table 6.17), allows PK to easily out-compete PPC for PEP; therefore, more PEP enters the PK branch over the PPC branch, which constrains the lysine yield. Furthermore, attenuation of PDC activity by 90% (Figure 6.42) or amplification of AK activity by a factor of 10 (Figure 6.43) in the PPC modified network does not result in any improvement in Y_E since these modifications are too distant from the PEP node. Though, attenuation of PDC activity does cause Pyr accumulation as it did in the previous simulation (Figure 6.38), without the influence of the PPC effectors, AspP synthesis rate is not affected (Figure 6.42).

Another set of simulations were conducted to determine the primary network modification that would lead to the single greatest improvement in lysine yield and synthesis rate. The first simulation investigated was a ten fold amplification of the wild type PPC enzyme (*i.e.*, PPC with effector influence), which can easily be achieved by introducing the cloned PPC on an active promoter. The resulting flux distribution, illustrated in Figure 6.44, exhibits a slight increase in Y_E (from 20 to 29%) and a 70% increase in AspP synthesis rate. This marginal increase is not

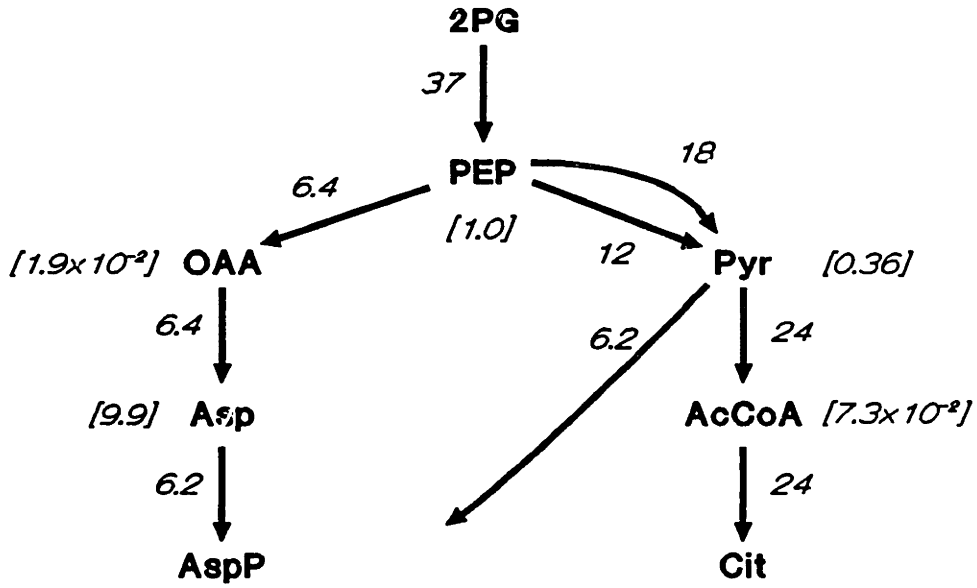

Figure 6.41 Simulated flux distribution of the PEP node with the modified PPC kinetics as described in Figure 6.40. Effective lysine yield is 26%. Other conditions as given in Figure 6.37.

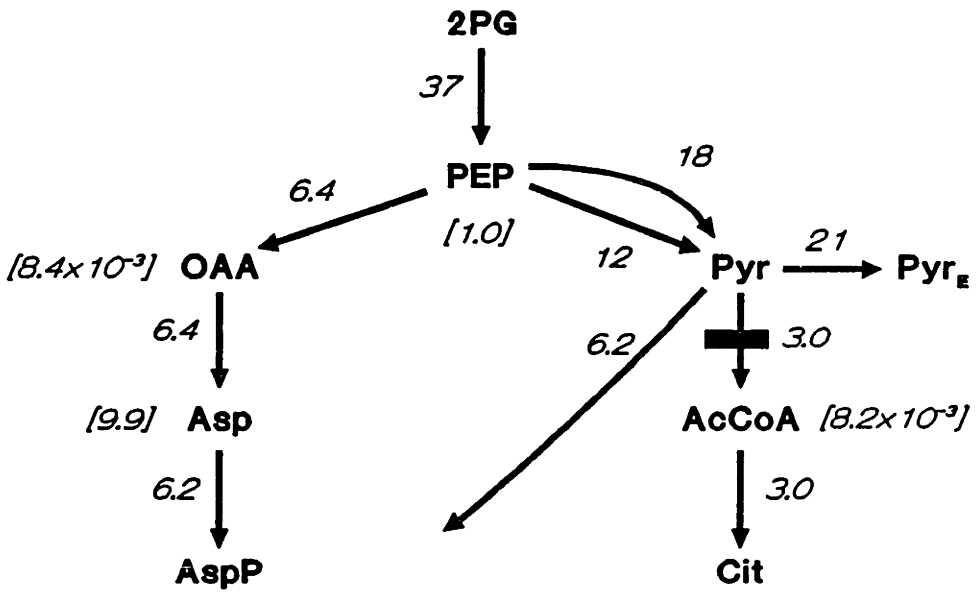

Figure 6.42 Simulated attenuation of PDC activity by 90% (set V_{M5} to 3 mmole/l/h) on a network with modified PPC kinetics as described in Figure 6.40. Pyr_E refers to extracellular pyruvate accumulation and Y_E equals 26%. Other conditions as given in Figure 6.37.

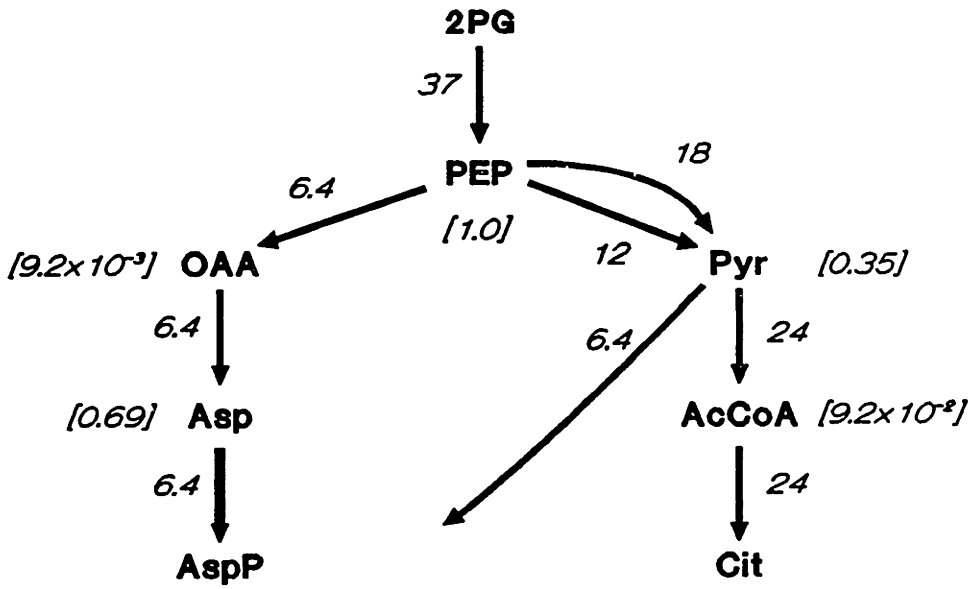

Figure 6.43 Simulated 10 fold amplification of AK activity (V_{M6} increased to 250 mmole/l/h) with modified PPC kinetics as described in Figure 6.40. Effective lysine yield is 26%. Other conditions as given in Figure 6.37.

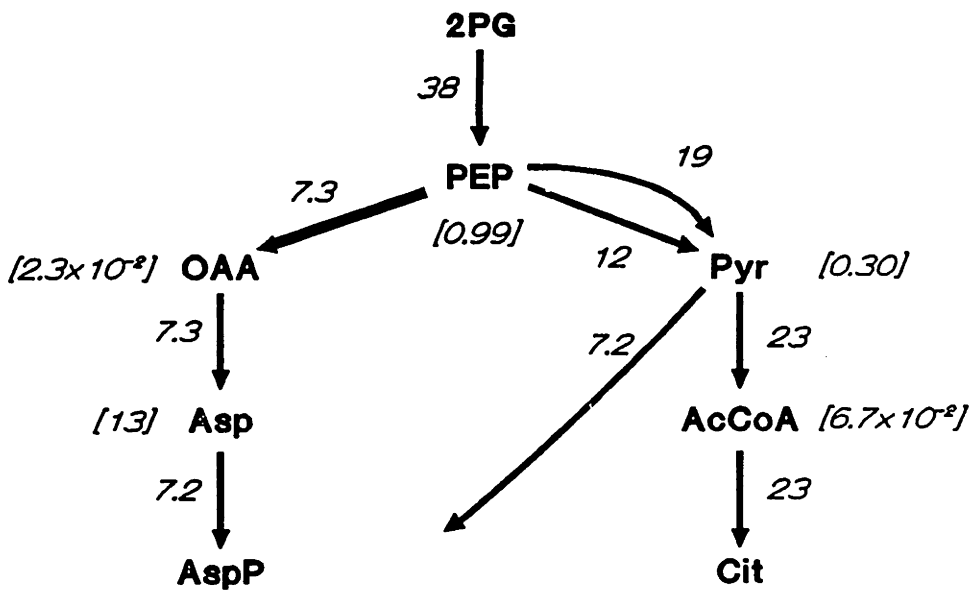

Figure 6.44 Simulated 10 fold amplification of the native PPC activity (V_{M2} increased to 100 mmole/l/h). Effective lysine yield is 29%. Other conditions as given in Figure 6.37.

surprising since PPC is still affected by Asp and AcCoA. Furthermore, the low activity of AK and its poor affinity for Asp (see Table 6.15), results in a high Asp concentration (Figure 6.44), which strongly inhibits PPC. Consequently, amplification of the native PPC should not lead to significant improvements in lysine yield, and may explain why dramatic improvements in amino acid production have not accompanied native PPC amplification [Sano *et al.*, 1987; Sugita and Komatsubara, 1989]. The next simulation investigated was the 10 fold amplification of AK activity, but with the native PPC. As portrayed in Figure 6.45, amplification of AK produces significant improvements in both Y_E (40%) and AspP synthesis rate (162% increase), so is worthy of experimental investigation. Yet, these results are quite different than those obtained when AK was amplified in the presence of the modified PPC (Figure 6.43), and requires some explanation. The amplification of AK causes the Asp concentration to decrease (Figures 6.43 and 6.45), which has no affect on the activity of the modified PPC since the influence of the effectors has been removed. However, for the network harboring the native PPC, the affinity of PPC for PEP actually increases (*i.e.*, the apparent PEP K_S is lowered) since AcCoA dramatically activates PPC when Asp concentration is low, as displayed in Figure 6.35. Consequently, amplification of AK has the added effect of lowering the apparent PEP K_S of the native PPC.

The final simulation investigated was a 10 fold amplification of the modified PPC enzyme (*i.e.*, PPC without effectors). As shown in Figure 6.46, this modification leads to the highest Y_E and AspP synthesis rate for a single modification. However, the modification also leads to the accumulation of Asp (shown as the flux to Asp_E). Although Asp accumulation can imply rigidity of the Pyr node, this is not the case here, as the Pyr node has been rendered flexible in the simulation. Aspartate accumulation is due to the low activity of AK and the lack of Asp inhibition of PPC. Aspartate accumulation could be mitigated if AK was amplified in concert with a modified PPC. Nevertheless, introduction of a PPC which is not subject to Asp inhibition or AcCoA activation leads to the greatest improvement in both lysine yield and synthesis rate that can be achieved in a single network modification. How such a PPC modification can be attained is deferred to the recommendations present in

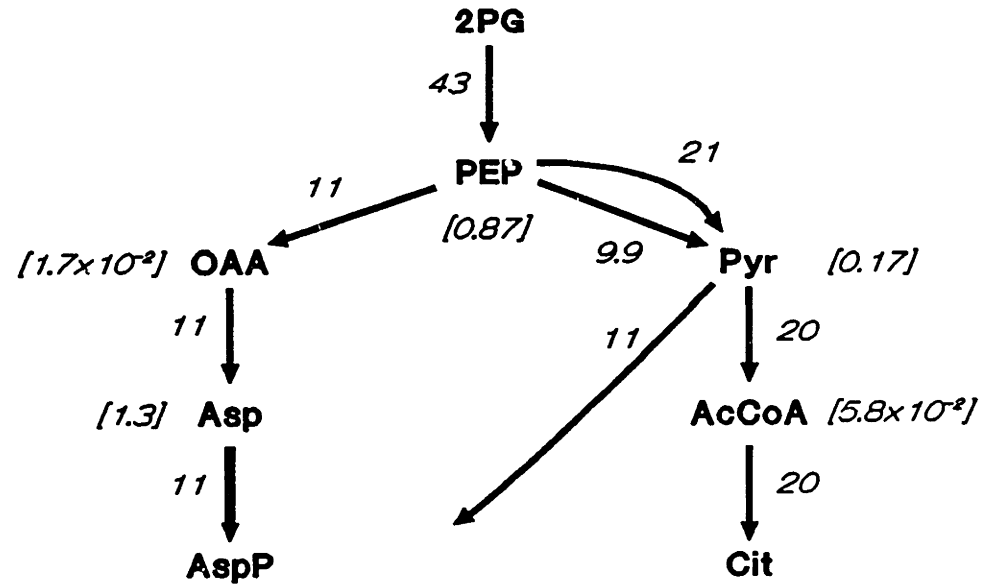

Figure 6.45 Simulated 10 fold amplification of AK activity (V_{M6} increased to 250 mmole/l/h) with native PPC kinetics. Effective lysine yield is 40%. Other conditions as given in Figure 6.37.

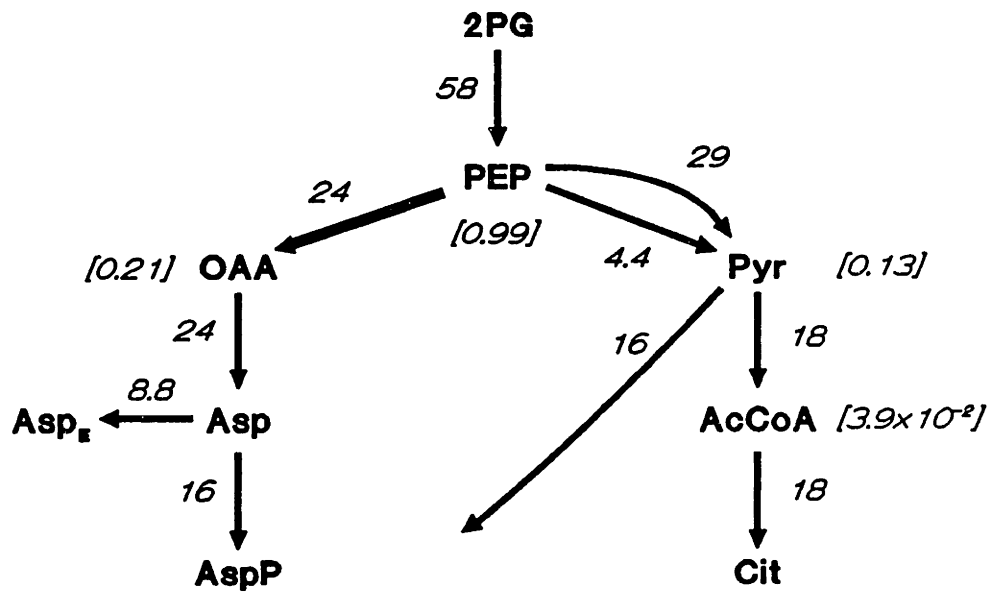

Figure 6.46 Simulated 10 fold amplification of the modified PPC activity (V_{M2} increased to 100 mmole/l/h and influence of effectors removed as explained in Figure 6.40). Asp_E symbolizes Asp extracellular accumulation and Y_E equals 75%. Other conditions as given in Figure 6.37.

Section 7.3.

Based on the outcome of the above simulations, a final perturbation experiment was conducted, as outlined in the next section.

6.5.2 Fluoroacetate Perturbation

Inspection of the PEP node kinetic model discussed in the previous section indicates that increasing AcCoA concentration, by attenuating CS, should increase the flux supported by PPC since AcCoA is a strong activator of the native enzyme. Although a simulation was conducted in which CS activity was attenuated (not shown), the network response was consider improbable, due to the following. Examination of PK and PDC kinetics (Equations (6.4) and (6.6)) reveal that neither are inhibited by AcCoA; consequently, simulated attenuation of CS (99%) resulted in an unabated increase in the intracellular concentration of AcCoA, which also allowed [Asp] and the PPC flux to increase. Since intracellular AcCoA would eventually be excreted as acetate, or removed in some other manner, in an actual culture, the simulated flux distribution was considered unrealistic due to the high intracellular accumulation of AcCoA (150 mM when simulation was terminated). Nevertheless, the simulation results still indicate that CS attenuation may be a viable mechanism for improving lysine yield. Attenuation of CS activity to improve lysine yield is not a novel idea [Shiio *et al.*, 1982a; Yokota and Shiio, 1988]; however, the effects of CS^A are difficult to interpret in these studies since the strains employed also had feedback resistent PPC enzymes, as well as possibly other nonspecific alterations associated with mutation-selection. To determine if CS attenuation will relieve the strong rigidity of the PEP node, an inhibitor study was investigated. Although a specific inhibitor of CS could not be found, a strong specific inhibitor of aconitase (the enzyme following CS) is available and was employed for the study. It was hypothesized that inhibition of aconitase would also result in attenuated CS flux and AcCoA accumulation.

Fluorocitrate (FC) is known to be a strong inhibitor of aconitase [Rokita, 1983; Kun, 1976] and was found to strongly inhibit aconitase in *C. glutamicum*, as is evident in Figure 6.47 (A). As with FP, FC also appears to act as a substrate since

some activity of aconitase can be measured at high concentrations of FC, even in the absence of citrate (Figure 6.47 (A)). The expense of FC, however, which precludes its use in large scale perturbation studies. Catabolism of the less costly monofluoroacetate (FAc), which is not known to be an inhibitor itself [Peters, 1957], results in the biosynthesis of FC in what has been called a "lethal synthesis" [Peters, 1954]. Furthermore, several early studies [Shiio *et al.*, 1961b; Shiio *et al.*, 1961c; Shiio *et al.*, 1962c] on the biochemistry of *B. flavum* employed FAc as an inhibitor and indirectly confirmed that FAc inhibits aconitase since citrate was observed to accumulate when cells were incubated in the presence of FAc. Similar results have been observed in *E. coli* as well [Kovac *et al.*, 1966]. Consequently, a fermentation was conducted in which FAc was aseptically added shortly after the start of lysine overproduction in an attempt to mitigate the strong rigidity associated with the PEP node.

6.5.2.1 Fermentation

The effect of FAc on the growth of *C. glutamicum* ATCC 21253, illustrated in Figure 6.47 (B), indicates that the concentration of FAc required to achieve a significant perturbation is on the order of 1 mM. The fluoroacetate perturbed fermentation was conducted in a manner basically identical to the FP and arsenite perturbed fermentations (Section 6.4), except 50 mmoles of monofluoroacetate•Na was aseptically added 20 minutes after (at 12.5 h) the break in respiration, as illustrated in Figure 6.48 (A-E). As depicted in Figure 6.48 (A,B), the addition of FAc caused growth to cease and severely inhibited lysine production as well as respiration. Unlike the FP or arsenite perturbations, FAc also severely suppressed the glucose consumption rate and lead to the accumulation of acetate and small quantities of citrate (Figure 6.48 (C)). Although citrate accumulation was slight, it was not observed in the control fermentation nor in the FP or arsenite perturbed fermentations. Furthermore, the level of citrate excretion is similar to that observed in *B. flavum* when exposed to FAc [Shiio *et al.*, 1961b; Shiio *et al.*, 1962c]. The only other by-products observed were lactate and trehalose (Figure 6.48 (D)). Since lysine yield was reduced to a few percent, FAc certainly did not effect the metabolism as intended. Nevertheless, flux analysis during the perturbation was investigated.

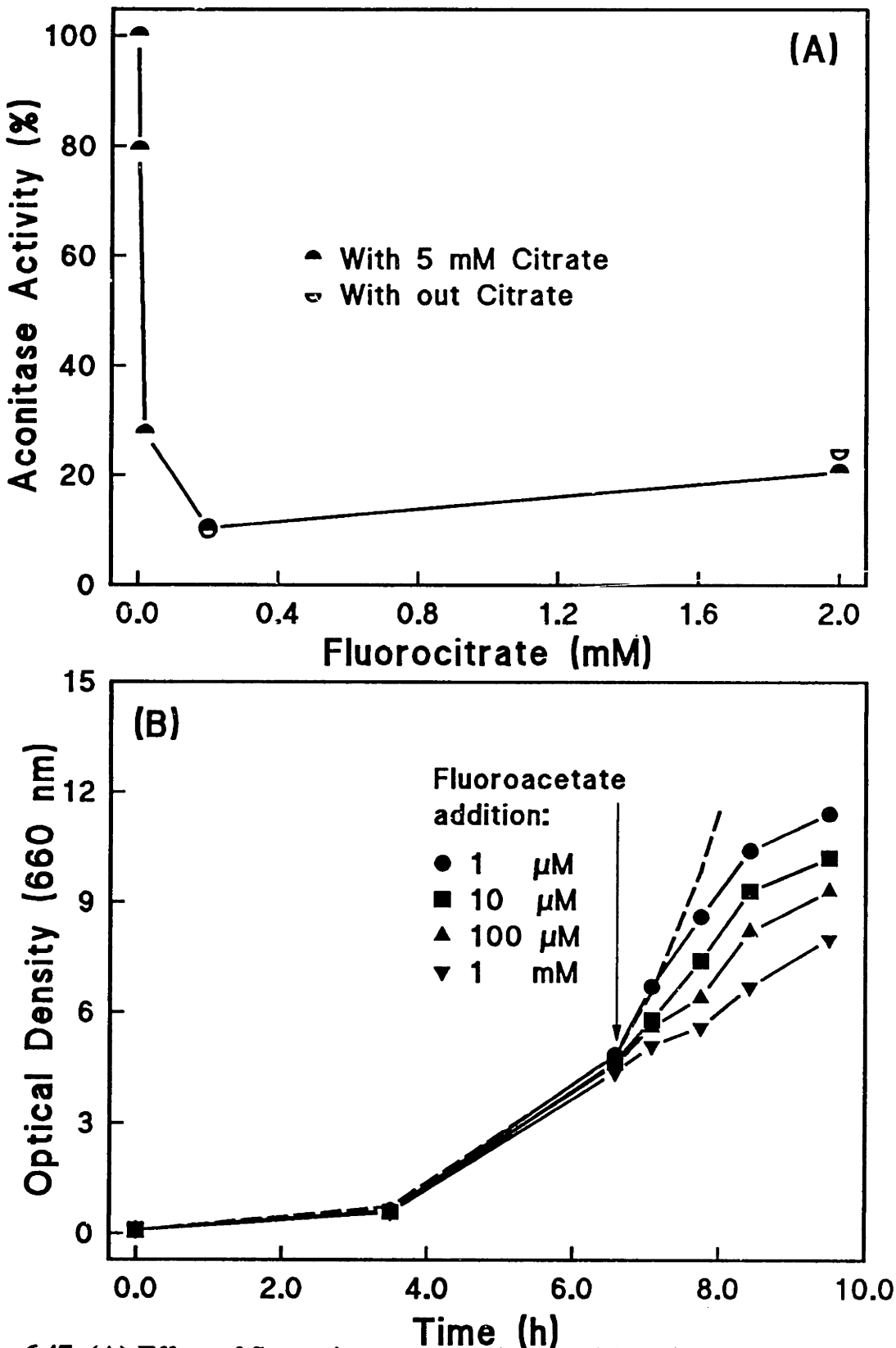

Figure 6.47 (A) Effect of fluorocitrate on aconitase activity. Assay procedure given in Section 5.2.2.6: assay contained 0.4 mg of crude cell-extract; maximum activity was 97.1 U/mg-protein. Note that assay was also conducted without citrate at 0.2 and 2 mM FC, open symbols. (B) Effect of fluoroacetate on the growth of *C. glutamicum* ATCC 21253 cultured on PMB medium. Dashed curve is an exponential profile.

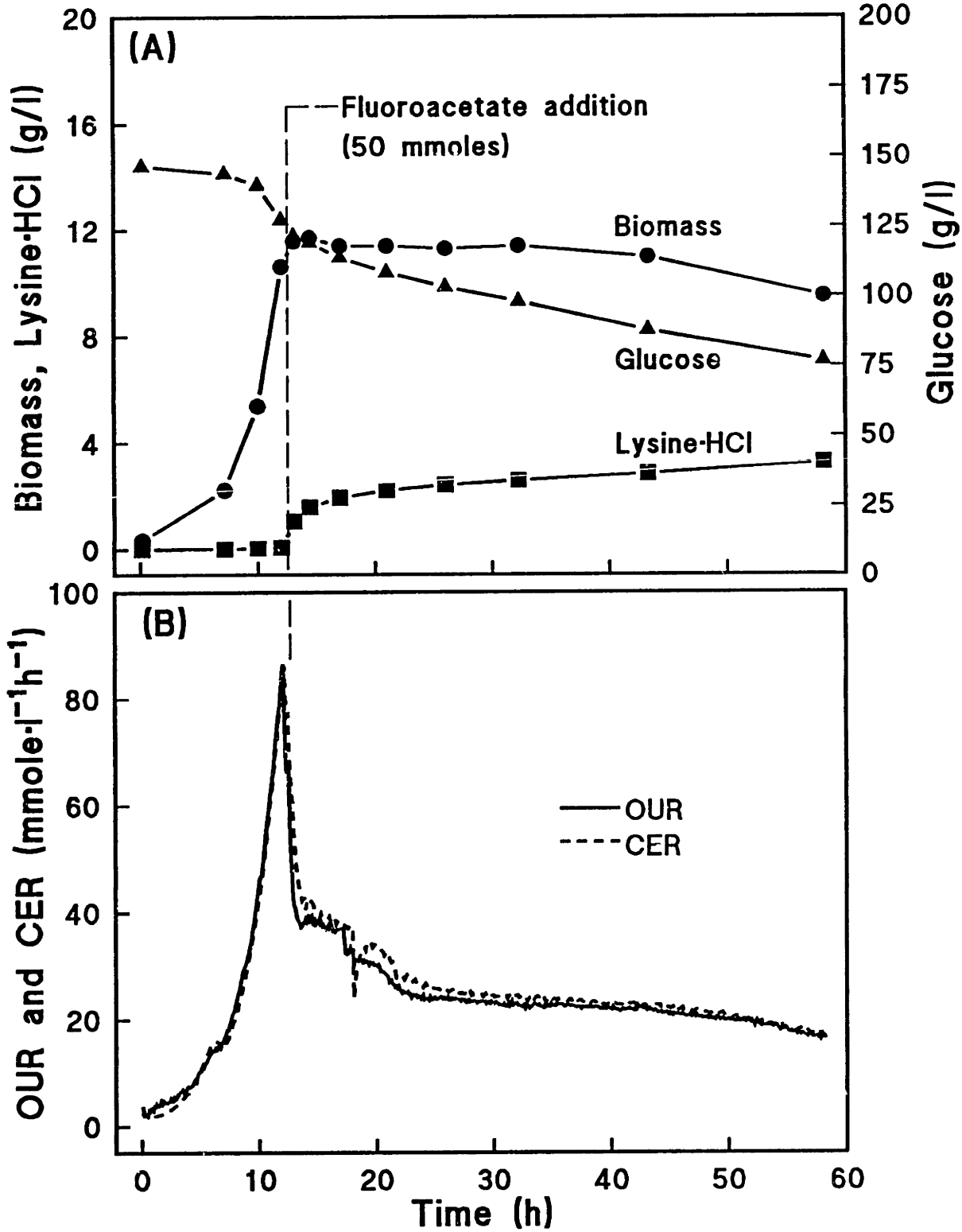

Figure 6.48 Fluoroacetate inhibited lysine fermentation of *C. glutamicum* ATCC 21253 cultured on FM4 medium. At 12.5 h 50 mmoles of monofluoroacetate•Na was aseptically added. (A) Concentration profiles of biomass (●), lysine•HCl (■), and glucose (▲) in g/l. (B). Culture respiration: OUR (solid curve) and CER (dashed curve).

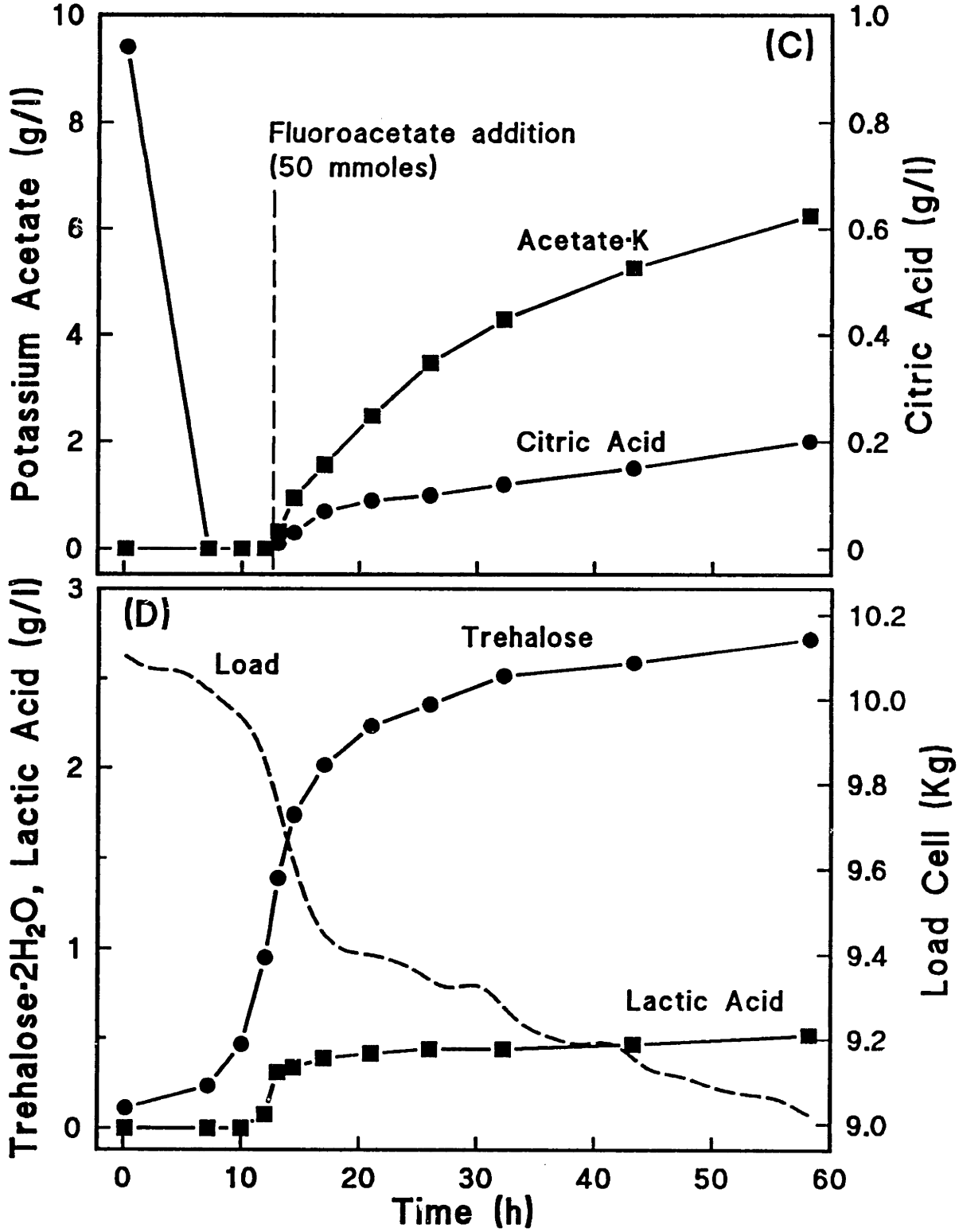

Figure 6.48 (continued) (C) potassium acetate (■) and citric acid (●) accumulation after FAc addition. (D) Profiles of trehalose•$2H_2O$ (●), lactic acid (■), and fermentor load cell reading (dashed curve).

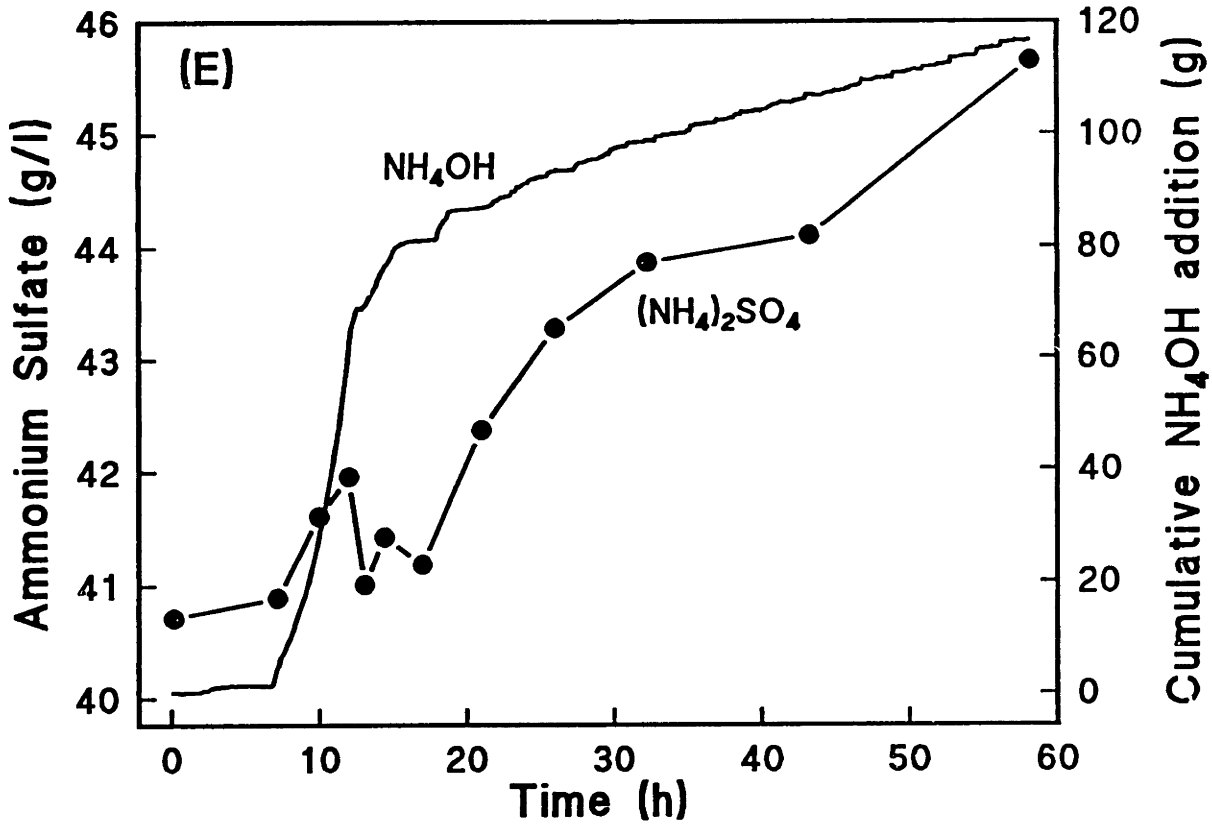

Figure 6.48 (continued) (E) Available ammonium in broth, as $(NH_4)_2SO_4$ (•), and cumulative amount of NH_4OH (26% (w/w) NH_3) added to maintain culture at pH 7.0.

6.5.2.2 Flux Analysis

Metabolite accumulation rates were calculated from measurements taken at 17.0 h and 21.0 h (t_{AVE} = 19.0 h) after the immediate transient following FAc addition. The measured and estimated accumulation rates are displayed in Table 6.18 along with the consistency index. The suppressed glucose consumption rate (as

Table 6.18 Accumulation rate subvectors for the fluoroacetate inhibited lysine fermentation at 19.0 h from measurements taken at 17.0 and 21.0 h (Figure 6.48), based on MS1 and BS4 in Appendix B; h = 0.27.

Elements of $\mathbf{r}_E(t)$	Accumulation Rates (mM/h) $\bar{\mathbf{r}}_E(19.0) \pm \sigma$	$\hat{\mathbf{r}}_E(19.0)$
Ac (1)	2.35 ± 1	2.36
Ala (4)	0.0 ± 1	-0.01
Biomass (7)	0.0 ± 1.4	0.04
CO2 (8)	33.5 ± 3.4	32.5
Glc (14)	-7.5 ± 4.4	-7.0
IsoCit (18)	0.03 ± 1	-0.08
Lac (19)	0.08 ± 1	0.09
LysE (20)	0.37 ± 0.1	0.37
NH3 (25)	1.9 ± 11	-0.8
O2 (26)	-31.0 ± 3.1	-31.9
Pyr (29)	0.0 ± 1	-0.03
Trehal (35)	0.15 ± 1	0.20
Val (36)	0.0 ± 1	0.09

well as other attenuated rates) is quite evident in Table 6.18. Isocitrate (IsoCit) was introduced as a measured variable in Table 6.18 so that citrate accumulation could be accounted for. Although a new measurement set could have been introduced, it was unnecessary, as there is no difference between citrate and isocitrate accumulation with respect to the flux analysis.

When the first set of flux distributions (not shown) were calculated from MS1 and BS1 in Appendix B, it was found that the pentose phosphate pathway (Reaction (22:BS1)) supported a large negative flux, similar to that observed in the gluconate fermentation (Section 6.3.2). As in the gluconate fermentation, the PPP was driven backwards to sequester the excess NADPH produced from ICDH in the TCA cycle.

There was an excess of NADPH since the main NADPH sinks (biomass and lysine synthesis) had been effectively eliminated by the addition of FAc, while NADPH sources (TCA cycle activity, evident in respiration), although suppressed, were not completely arrested. As explained in Section 6.3.2.1, operation of the PPP in a NADPH sequestering mode is considered infeasible; consequently, BS1 was modified by removing the oxidative branch of the PPP (Reaction (22:BS1)) and replacing it by the hypothetical NADPH oxidation reaction (see Section 6.3.2.3), to produce a new biochemistry set: BS4 (listed in Appendix B). This biochemistry modification is deemed acceptable since the direct oxidation of NADPH is considered possible when the culture is in a stationary or death phase, as discussed in Section 6.3.2.3. It should be noted that this modification has an almost negligible effect on the network as a whole, and only changes the flux in the PPP. The flux distributions based on the measurements (Table 6.18), MS1, and BS4 are displayed in Figure 6.49 where Reaction (22:BS1) (oxidative branch of the PPP) has been replaced by Reaction (22:BS4) (direct NADPH oxidation).

The most notable feature of Figure 6.49 is the large TCA cycle flux (relative to glucose consumption rate) and the associated excess ATP and NADPH fluxes (Reactions (34:BS4) and (22:BS4), respectively). Although the absolute aconitase flux (lumped in Reaction (11:BS4)) has been reduced by FAc inhibition, it is interesting to note that the FAc perturbation has actually resulted in an increase in the TCA cycle flux relative to glucose consumption, which is somewhat contrary to intuition. Although speculative, this flux paradox can be explained by considering perturbations of metabolite pools. Even though FC inhibits the aconitase flux, as FC inhibition of aconitase is reversible [Rokita, 1983], the flux can be restored, at least partially, if the intracellular citrate accumulates to the extent that it can out-compete FC for the active site of aconitase. Such intracellular accumulation of citrate from FAc catabolism has been observed [Peters, 1957], and is consistent with the slight extracellular accumulation of citrate observed during the FAc perturbed fermentation (Figure 6.48 (C)). However, since metabolites directly affect enzyme kinetics, the forced intracellular accumulation of citrate (or some other metabolite, such as AcCoA) could quite possibly result in the inhibition of other enzymes crucial for

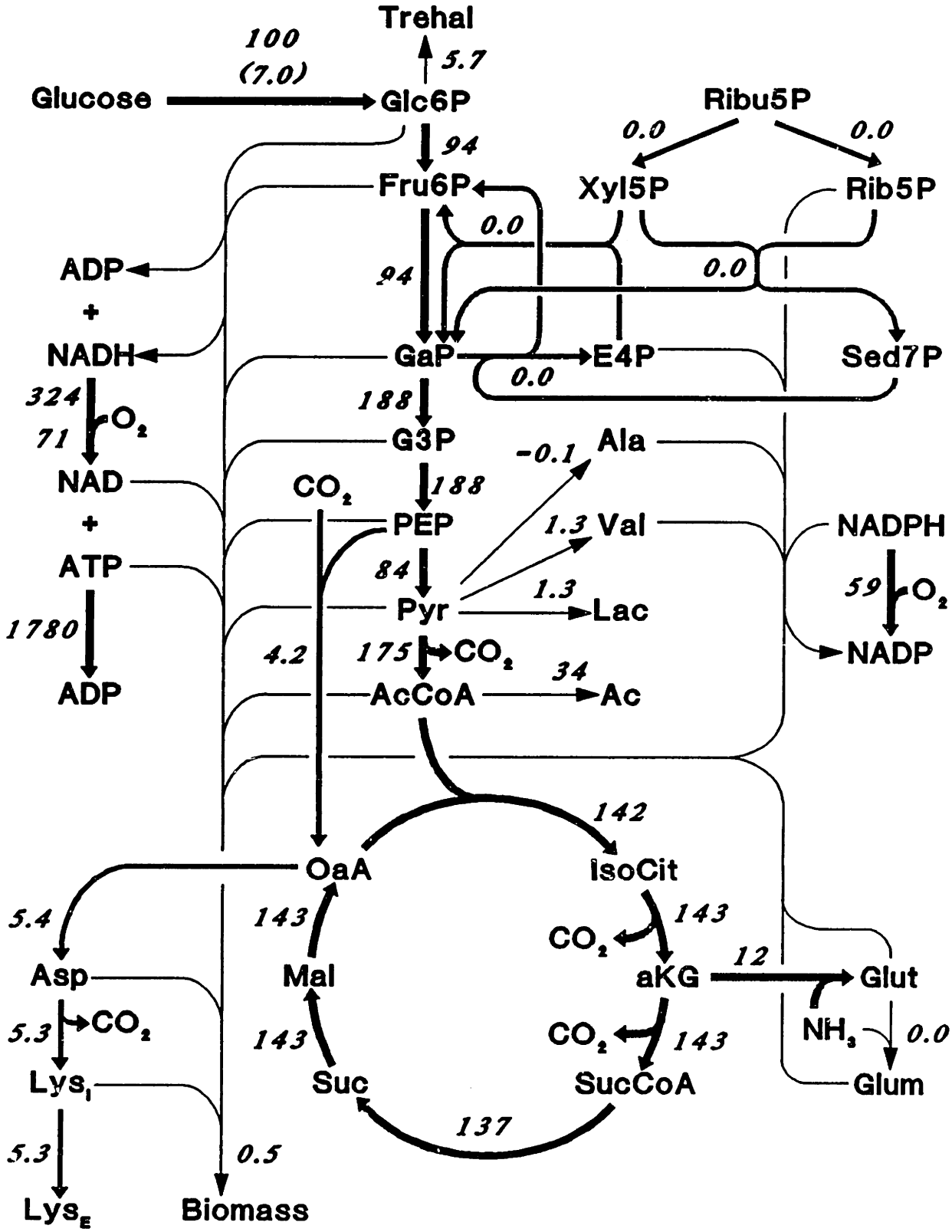

Figure 6.49 Flux distribution map for the fluoroacetate inhibited fermentation at 19.0 h. Fluxes estimated from measurements taken at 17.0 and 21.0 h (see Figure 6.48 and Table 6.19), and normalized by glucose consumption rate (shown in parentheses; mmole/l/h). Reactions are from BS4 listed in Appendix B.

biomass and lysine synthesis. It is also possible that intracellular citrate accumulation may have reduced cofactor concentrations since citrate is a strong chelating agent. Consequently, under this hypothesis, collapse of the metabolic network would not be caused by a reduced aconitase flux, but rather, alterations in intracellular metabolite pool concentrations. This may also explain why glucose consumption was severely attenuated by FAc addition but not by the addition of FP or arsenite.

Although intracellular AcCoA concentration probably increased from FAc addition, since acetate was excreted (Reaction (17:BS4)), the OAA branch split-ratio of the PEP node was reduced to 2%. The cause for this collapse is by no means clear, but could certainly be due to metabolite pool perturbations as described above since PPC is affected by many metabolites, including citrate [Ozaki and Shiio, 1969]. To investigate the possibility that citrate, FAc, or FC may have directly caused the collapse of OAA branch split-ratio, PPC activity in the presence of these compounds was investigated, and the results are listed in Table 6.19. Although FC is a potent inhibitor of PPC in the absence of AcCoA, it does not strongly inhibit PPC in its presence. Since the intracellular concentration of AcCoA should be relatively high, it is unlikely that FC inhibited the *in vivo* activity of PPC. In conclusion, attenuation of only aconitase does not appear to be a viable route for lysine yield improvement; although, in concert with other modification, it may be. This is not entirely unanticipated as aconitase is fairly distant from the PEP node.

6.5.3 Summary

A localized kinetic model of the PEP node was constructed from data available in the literature to examine the cause of the PEP node rigidity, as such information cannot be obtained from the steady state fluxes predicted from the BRNE. The steady state flux data, however, is extremely useful for tuning kinetic based models. The simulated response of the PEP node to attenuation of PK activity clearly illustrates that the node is strong rigidity, and is primarily caused by the allosteric nature of PEP carboxylase, which requires activation by AcCoA to overcome aspartate inhibition. The simulations also reveal two other characteristics of the PEP node that enhance its overall rigidity. The first involves the affinity of

Table 6.19 Inhibitors of PEP carboxylase in *C. glutamicum* ATCC 21253.

Assay modification* (+) with, (-) Without	Activity (U/mg)
Standard	270
+ 10 mM Asp	243
+ 10 mM Asp - AcCoA	26
+ 10 mM Cit	239
+ 10 mM Cit - AcCoA	205
+ 10 mM FAc	225
+ 10 mM FAc - AcCoA	214
+ 100 mM AS	208
+ 100 mM AS - AcCoA	204
+ 100 mM AS - AcCoA + 2 mM FC	78

* Abbreviations: Asp, aspartate; AcCoA, acetyl-coenzyme A; Cit, citrate; FAc, fluoroacetate; AS, ammonium sulfate; FC, fluorocitrate.

PPC and PK for the node metabolite: PEP. The apparent PEP K_M for PK is an order of magnitude less than the associated K_M for PPC. Coupled with the naturally higher activity of PK, there exists a much stronger driving force for PEP to enter the PK branch over the PPC branch, which heightens the PEP node rigidity. The other contributing factor to the PEP node rigidity is the kinetics of AK. This enzyme has relatively large K_M's for Asp and ATP, and its *in vitro* activity is low compared to PPC and AT activities. Consequently, to achieve a significant flux through AK, the intracellular Asp concentration must be maintained fairly high; however, this results in PPC inhibition and a drop in the PPC branch split-ratio. The dynamics of the PEP node rigidity can be summarized as follows.

Under nominal conditions, PEP preferentially enters the PK branch due to its higher affinity for PEP. Any attempt to redirect the flow of carbon into the PPC branch causes an increase in Asp concentration due to the AK kinetic bottleneck, and a drop in AcCoA concentration due to the high activity of CS. The combination of high Asp and low AcCoA concentrations results in a synergistic inhibition of PPC activity and a precipitous drop in the PPC flux. The net result of attempting to increase the PPC split-ratio by blocking the PK branch is the attenuation of both

branches; hence, the PEP node is strongly rigid. Furthermore, even if the Asp inhibition of PPC is removed, the kinetics of PK and AK still render the PEP node weakly rigid.

From a teleological point of view, control of the PEP node split-ratios in a feed-forward manner is a desirable property, as explained here. Due to mass balance constraints, all oxaloacetate produced from PPC must eventually leave the TCA cycle to form aspartate or glutamate derived amino acids (or some TCA related metabolite), while all carbon that enters the TCA cycle via AcCoA is oxidized to generate ATP. Since the synthesis of amino acids as well as their polymerization to protein require large amounts of ATP, the fraction of carbon that is allocated to amino acid production must be closely balanced with the fraction that leads to energy production via the TCA cycle. This flux distribution balance is controlled at the PEP node, which, by the allosteric nature PPC, regulates the fraction of carbon that enters the PPC branch against the flow of carbon to the TCA cycle. Consequently, it is not surprising that the PEP node is strongly rigid.

The PEP node simulations indicate that lysine yield can be improved by circumventing the rigidity of the PEP node by transforming *C glutamicum* with a PPC enzyme that is not inhibited by Asp nor requires AcCoA activation. The activity of the foreign PPC should be approximately ten times the activity of native PPC or have a higher affinity for PEP than PK. The simulations indicate that *C. glutamicum* transformed in this manner might also excrete Asp due to the low activity of AK; consequently, amplification of AK may also be necessary.

The attempt to increase the PPC flux by inhibiting aconitase activity through the addition of FAc resulted in lysine synthesis collapse, but it did produce some interesting effects on the flux distributions. Although the absolute aconitase flux was attenuated by FAc, the TCA cycle flux (relative to glucose consumption) was actually higher than that observed in the control fermentation. The addition of FAc did reduce the glucose consumption rate, but this should not have affected lysine synthesis since low specific glucose consumption rates during high lysine yields have been observed (see NFG068 fermentation, Figure 6.19). Consequently, it was concluded that FAc inhibition of the aconitase flux was not severe enough to

produce the collapse in lysine synthesis, but may have altered metabolite pool concentrations to the extent that enzymes distant from the perturbation were dramatically inhibited. The exact cause of the PPC flux collapse is unknown, but may be related to PPC inhibition by fluorocitrate.

Chapter 7

Conclusions and Recommendations

7.1 Summary

We have developed a general procedure by which the primary metabolism of an organism can be represented in a simple mathematical framework that permits metabolic flux distributions to be estimated from the accumulation rates of extracellular metabolites (Chapter 4). This approach is solely based on biochemically constrained metabolite balances and a pseudo-steady state approximation for intracellular metabolites (Section 4.1.6.2). Consequently, knowledge of enzyme kinetics is not required. In order to accurately distribute the burden of biomass production on the primary metabolism, we have represented biomass synthesis as an aggregate of its precursor constituents which is readily integrated into the metabolic network. Although an ATP balance is utilized in the construction of the bioreaction network equation (BRNE), the inclusion of an ATP dissipation reaction in the network circumvents ambiguities associated with futile cycles, maintenance, etc. (Section 4.1.3). The primary metabolic reactions of *Corynebacterium glutamicum*, as well as the reactions necessary to support lysine and biomass synthesis, have been compiled from literature data (Chapter 3).

Singularity analysis of the resulting BRNE allows for the identification of singular groups (*i.e.*, dependent reactions) and permits one to focus experimental efforts on identifying those reactions of the singular groups that can be rationally deleted from the network (Section 4.1.5). Similarly, sensitivity analysis is used to indicate if a nonsingular BRNE is well-conditioned, as well as to identify measurements that are essential for accurate flux estimation, and those that are not

(Section 4.1.8). Analysis of the preliminary *C. glutamicum* network (PBS; PMS) identified two major singular groups involving 1) the TCA cycle and the glyoxylate shunt, and 2) the four carboxylation reactions (Section 4.1.5.3). These singularities were removed by demonstrating that the glyoxylate shunt is not expressed in the presence of glucose, and that PEP carboxylase is the only significant anaplerotic reaction (Section 5.3). The condensed network (BS1; MS1) was found to be well-posed, with a condition number of 59 (Euclidian norm). The most sensitive measurements were identified as OUR and CER.

The solution of the BRNE is given by the well known weighted least-squares minimization. Although constraints can be imposed on the solution such that reaction irreversibilities are not violated, it was determined that such constraints are often inappropriate due to the quadratic nature of the ojective function J (Section 4.1.7). Violation of reaction irreversibilities are indicative of an inappropriate representation of the cellular metabolism. To enhance flux estimation accuracy and credibility, a consistency analysis routine was also incorporated into the analysis of the BRNE (Section 4.1.9). This routine identifies and locates inconsistencies in measurement sets and is also quite useful in detecting the accumulation of non-measured metabolites (intracellular or extracellular). Flux distributions estimated in the metabolic network defined by BS1 and MS1, calculated from rate data obtained from the control lysine fermentation, are consistent with the preconceived operation of the metabolic pathways and agree with tracer-based flux estimates documented in the literature (Section 6.1). Although certain trends can be discerned from the flux distributions, it is clear that the distributions alone are insufficient for identifying limitations in the primary metabolism. Therefore, a novel experimental approach was developed to utilize metabolic flux estimation for identifying product yield limitations.

It was demonstrated that theoretical flux distributions can be readily determined from the BRNE (Section 4.2), and that these distributions can be used to calculate maximum product yields, as constrained by the biochemistry. Analysis of theoretical flux distributions also identify key branch-points in the metabolism, referred to as principal nodes, where flux alterations must occur in order to achieve improvements in product yield (Section 4.3). It was proposed that if the flux

distribution at a principal node is actively maintained constant or is bounded, then improvements in product yield may not be realizable by simple enzyme attenuation or deletion techniques commonly employed for strain improvement, especially if the network is dependent. Although the degree by which enzyme kinetics limit flux partitioning at a node varies in a continuous manner, the type of nodal response can be classified into three general categories, as follows: 1) a node is considered flexible if flux partitioning is solely a function of metabolite demand; 2) a node is considered weakly rigid if the fraction of flux entering a branch is bounded by enzyme activity, but is not controlled; and 3) a node is considered strongly rigid if the flux partitioning is actively controlled. Since weakly and strongly rigid nodes can severely limit product yield, their identification and removal is necessary if significant improvements in product yield is to be attained. To asses principal node rigidity, the extent that nodal flux partitioning is altered from a local metabolic perturbation was examined.

Three principal nodes, at Glc6P, PEP, and Pyr, where identified in the *C. glutamicum* network (BS1 and MS1). The network is characterized as dependent and rigid since the products of the principal nodes condense to from lysine, and metabolic perturbations documented in the literature do not lead to significant metabolic flux alterations (Section 4.3).

To examine the possibility that lysine yield is limited by a weakly rigid Glc6P node, a Glc6P isomerase attenuated mutant of *C. glutamicum* ATCC 21253 was isolated (strain NFG068). Flux distributions calculated from the lysine fermentation of NFG068 exhibited 66% attenuation; however, flux partitioning at the principal nodes was unaffected compared to the parent strain. To examine the possibility that lysine yield is limited by a strongly rigid Glc6P node (*i.e.*, NADPH supply), a lysine fermentation of ATCC 21253 was conducted in which glucose was replaced by gluconate. Although more NADPH was produced on gluconate than glucose, lysine yield was not enhanced (Section 6.3).

A pyruvate dehydrogenase complex (PDC) attenuated mutant of *C. glutamicum* ATCC 21253 was isolated to examine if lysine yield is limited by a weakly rigid Pyr principal node. Analysis of the resulting metabolic flux distributions of this strain were basically identical to those observed for the NFG068 strain (*i.e.*, overall

flux attenuation without affecting partitioning at the principal nodes). To further investigate the rigidity of the Pyr node, two PDC inhibitor experiments were examined. In these experiments, either fluoropyruvate or arsenite were added at the onset of lysine production. Subsequent flux analysis from both metabolic perturbations revealed that pyruvate was diverted from the TCA cycle; however, the surplus pyruvate did not enhance lysine yield and was simply excreted into the culture medium (Section 6.4).

Since the perturbation experiments of the Glc6P and Pyr principal nodes indicate that they do not limit lysine yield, it was concluded that the PEP node is the source of the network rigidity. To support this hypothesis, as well as identify the causative agent, a kinetic based model was developed to examined the control of flux partitioning at the PEP node. The PEP node model incorporates kinetic expressions for enolase, PEP carboxylase, pyruvate kinase, aspartate aminotransferase, pyruvate dehydrogenase complex, aspartate kinase, and citrate synthase. Model parameters were adjusted such that the steady state flux distribution agreed with that observed in the control lysine fermentation. To examine the cause of the PEP node rigidity, several simulated "perturbations" were examined. The results of the perturbations indicated that the PEP node is strongly rigid due to the kinetics of PEP carboxylase and its effectors (Section 6.5).

7.2 Conclusions

1) Isocitrate lyase in *C. glutamicum* ATCC 21253 is not expressed in the presence of glucose, and PEP carboxylase is the only significant anaplerotic reaction present when *C. glutamicum* is cultured on a minimal glucose medium. Some activity of PEP synthetase has also been detected.

2) Metabolite balances can be used to estimate flux distributions in the primary metabolic network of an organism.

3) The metabolic network of *C. glutamicum*, defined by BS1 and MS1, is nonsingular. The estimated flux distributions during the standard lysine

fermentation are consistent with the preconceived operation of the metabolic pathways and agree well with tracer-based flux estimates reported in the literature.

4) Theoretical flux analysis of the lysine network indicates that the maximum theoretical lysine yield (mole lysine/mole glucose) is 75%, provided PEP synthetase can support a significant flux. Three principal nodes are identified at the glucose-6-P, phosphoenolpyruvate, and pyruvate branch-points.

5) Flux analysis of the GPI^{A} mutant (NFG068) indicates that lysine yield is not limited by a weakly rigid Glc6P node, and the gluconate fermentation indicates that lysine yield is not limited by NADPH supply. It is concluded that the Glc6P node is flexible.

6) Flux analysis of the FPS009 strain (PDC^{A}) indicates that lysine yield is not limited by a weak rigidity of the Pyr node. Pyruvate accumulation, induced by PDC inhibition by either fluoropyruvate or arsenite, indicates that pyruvate availability does not limit lysine yield. It is concluded that the Pyr node is flexible, which implicates the PEP node as the cause of the network rigidity.

7) Kinetic simulations of the PEP node demonstrate that the PEP node is strongly rigid. This rigidity is predominately caused by the allosteric kinetics of PEP carboxylase which requires activation by AcCoA to overcome inhibition induced by aspartate. The overall rigidity of the PEP node is enhanced by the poor affinity of aspartate kinase for Asp, as well as the high affinity of pyruvate kinase for PEP.

7.3 Recommendations

In order to enhance lysine yield, the strong rigidity of the PEP node must be removed, which can be partially accomplished by removing aspartate inhibition of PPC. The most promising approach to accomplish this is to introduce a foreign gene

into *C. glutamicum* that encodes for a PPC enzyme which is not inhibited by aspartate, nor requires activation by AcCoA. Effectorless PPC enzymes can be found in organisms that utilized radically different metabolic control architectures, such as photosynthesizers. In particular, the cyanobacterium *Synechococcus* sp. has been reported to harbor such an enzyme [Kodaki *et al.*, 1985]. Simulations indicate that the cloned enzyme should be amplified by a factor of 10, so that it can effectively compete with PK for PEP. A slightly different approach is to transform *C. glutamicum* with a gene that encodes for a pyruvate carboxylase that is similarly resistent to the effects of Asp and AcCoA. This approach is quite promising since it effectively removes the PEP principal node and localizes the flux partitioning control at the Pyr node. Furthermore, from the FP and arsenite inhibitor experiments, it is known that pyruvate can be forced to accumulate. Also, the affinity of PDC for Pyr is relatively weak. Pyruvate carboxylase enzymes with the desired properties have been reported in strains of *Pseudomonas* [Higa *et al.*, 1976; Scrutton and Young, 1970], as well as in *Brevibacterium lactofermentum* [Tosaka *et al.*, 1979c].

As indicated by the simulations, the rigidity of the PEP node is also attributed to the properties of aspartate kinase and pyruvate kinase. Consequently, if the above modifications do not radically increase lysine yield, then amplification of AK activity (by a factor of ca. 10) and attenuation or deletion of PK activity (if the deregulated PPC approach is followed) should be investigated. It is important to realize, however, that the flexibility of the Glc6P and Pyr nodes may be bounded; that is, after the PEP node is rendered flexible, it is possible that lysine yield will be constrained by the rigidity at the Glc6P or Pyr node before reaching the maximum yield. Consequently, the rigidity of these nodes must be reinvestigated, in the manner described in this thesis, if only marginal improvements in lysine yield are achieved by modifying the PEP node.

Although there are no fundamental improvements that can be recommended for the flux analysis technique developed in Chapter 4, improvements on effective metabolic perturbation techniques could dramatically increase the usefulness of the flux analysis approach. A few suggestions are as follows. Although we employed mutant strains to assess nodal rigidity, in hindsight, this approach is undesirable for

two reasons: 1) isolation of mutants with the desired genotype is a laborious and time consuming task; and 2) it is always conceivable that the isolated strain harbors multiple mutations. However, if the desired mutant strains are available, they should be employed in metabolic studies. If metabolic perturbations can only be achieved via genetic alterations (and mutants are not available), then methods in molecular biology should be utilized, rather than mutation/selection. Specific enzyme inhibitors are powerful tools in metabolic perturbation studies; unfortunately, there are relatively few specific enzyme inhibitors known. However, if such inhibitors are available or can be fabricated, they are certainly the method of choice in perturbations studies. Metabolic perturbation can also be achieved by deregulating by-product synthesis, provided the synthesis of the by-product consumes a metabolite that is a product of a principal node. For example, if significant amounts of valine can be synthesized without effecting lysine yield, then this would indicate that pyruvate and NADPH availability do not limit lysine yield, and that the Glc6P and Pyr principal nodes are flexible. Another possible technique would be to examine flux distributions in the control fermentation following the supplemental addition of a principal node metabolite. For example, the addition of aspartate (or a TCA intermediate) would effectively by-pass the rigidity of the PEP node. Although several techniques exist for the perturbation of metabolic networks, the implementation of such techniques is still rather *ad hoc* and is in need of further advancement.

7.4 Tangents

During the course of this research several interesting questions arose (predominately related to the biochemistry of *C. glutamicum*) that could not be investigated due to time constraints. They are the following:

- Which enzymes are responsible for by-passing PDC and PK in the gluconeogenesis pathway? Although it is proposed that they might be OAA decarboxylase and PEP synthetase, respectively, this has not been conclusively shown.

- OAA decarboxylase was found to be expressed constitutively and at relatively high activity; however, its role in the primary metabolism remains uncertain.

- Does *C. glutamicum* lack adequate mechanisms for the direct oxidation of NADPH, and does this inadequacy cause the linear growth observed on the minimal gluconate medium? Similarly, does *C. glutamicum* possess an active dinucleotide transhydrogenase (this was not examined in depth in this thesis)?

- Although the addition of fluoropyruvate or arsenite inhibits the flow of carbon into the TCA cycle, glucose consumption is basically unaffected. However, the addition of fluoroacetate not only inhibits the TCA cycle flux but also results in severe attenuation of glucose assimilation. What is the control architecture of glycolysis that explains these results?

- Phase IV of the control fermentation resembles that observed in the arsenite inhibited fermentation. Is Phase IV of the control fermentation brought about by the decay of either the pyruvate or α-ketoglutarate dehydrogenase complexes?

- What are the optimal activities of PEP carboxylase (or pyruvate carboxylase) and dihydrodipicolinate synthase for lysine synthesis, and how does one control them on-line?

8. References

ABE, S. AND TAKAYAMA, K. (1972). Amino Acid-producing Microorganisms: Variety and Classification. In: *The Microbial Production of Amino Acids.* Yamada *et al.* (eds.), Wiley, New York, pp. 3-38.

ABE, S., TAKAYAMA, K-I., AND KINOSHITA, S. (1967). Taxonomical Studies on Glutamic Acid-Producing Bacteria. *J. Gen. Appl. Microbiol.* **13**, 279-301.

ACHS, M. J. AND GARFINKEL, D. (1977a). Computer Simulation of Energy Metabolism in Anoxic Perfused Rat Heart. *Am. J. Physiol.* **232**, R164-R174.

ACHS, M. J. AND GARFINKEL, D. (1977b). Computer Simulation of Rat Heart Metabolism After Adding Glucose to the Perfusate. *Am. J. Physiol.* **232**, R175-R184.

ACHS, M. J., ANDERSON, J. H., AND GARFINKEL, D. (1971). Gluconeogenesis in Rate Liver Cytosol. I. Computer Analysis of Experimental Data. *Comput. Biomed. Res.* **4**, 65-106.

AIBA, S. AND MATSUOKA, M. (1979). Identification of Metabolic Model: Citrate Production from glucose by *Candida lipolytica. Biotechnol. Bioeng.* **21**, 1373-1386.

AKASHI, K., IKEDA, S., SHIBAI, H., KOBAYASHI, K., HIROSE, Y. (1978). Determination of Redox Potential Levels Critical for Cell Respiration and Suitable for L-Leucine Production. *Biotechnol. Bioeng.* **20**, 27-41.

AKASHI, K., SHIBAI, H., AND HIROSE, Y. (1979a). Inhibitory Effects of Carbon Dioxide and Oxygen in Amino Acid Fermentation. *J. Ferment. Technol.* **57**, 317-320.

AKASHI, K., SHIBAI, H., AND HIROSE, Y. (1979c). Effect of Oxygen Supply on L-Lysine, L-Threonine and L-Isoleucine Fermentations. *Agric. Biol. Chem.* **43**, 2087-2092.

ALBERTY, R. A. (1959). The Rate Equation for an Enzymatic Reaction. In: *The Enzymes*, Vol. I., Second Edition. Boyer, P. D., Lardy, H., and Myrback, K. (eds.), Academic Press Inc., New York, pp. 143-155.

ALGER, J. R. AND SHULMAN, R. G. (1984). NMR Studies of Enzymatic Rates *in vitro* and *in vivo* by Magnetization Transfer. *Q. Rev. Biophys.* **17**, 83-124.

ANDERSON, J. H., ACHS, M. J., AND GARFINKEL, D. (1971). Gluconeogenesis in Rat Liver Cytosol. II. Computer Simulation of Control Properties. *Comput. Biomed. Res.* **4**, 107-125.

ARIS, R. AND MAH, R. H. S. (1963). Independence of Chemical Reactions. *IEC Fund.* **2**, 90-94.

ATKINSON, D. E. (1977). *Cellular Energy Metabolism and its Regulation.* Academic Press, New York.

BAILEY, J. E. AND OLLIS, D. F. (1977). *Biochemical Engineering Fundamentals.* McGraw-Hill, Inc., New York.

BARMAN, T. E. (1969a). *Enzyme Handbook*, Vol. I. Springer-Verlag, New York.

BARMAN, T. E. (1969b). *Enzyme Handbook*, Vol. II. Springer-Verlag, New York.

BARYSHNIKOVA, L. M. AND LOGINOVA, N. V. (1979). Carboxylases of Coryneform Bacteria. *Microbiol.* **48**, 787-789.

BARYSHNIKOVA, L. M., REZNIK, G. I., AND GOLOVLEV, E. L. (1979). Enzymes of Intermediary Metabolism in *Corynebacterium*-Like Microorganisms. *Microbiol.* **48**, 146-151.

BAUCHOP, T. AND ELSDEN, S. R. (1960). The growth of Micro-Organisms in Relation to Their Energy Supply. *J. Gen. Microbiol.* **23**, 457-469.

BAUER, H. P., SRIHARI, T., JOCHIMS, J. C., AND HOFER, H. W. (1983). 6-Phosphogluconolactonase: Purification, Properties and Activities in Various Tissues. *Eur. J. Biochem.* **133**, 163-168.

BEKER, M., MEZHINA, G., RUKLISHA, M., VIESTURE, U., SELGA, S., ALEXANDROVA, M., APSITE, A. AND SAVENKOV, V. (1973). Correlation Between Aeration and Physiological Activity of the Producer of Extracellular L-Lysine. *Biotechnol. Bioeng. Symp.* **4**, 233-239.

BLUM, J. J. AND STEIN, R. B. (1982). On the Analysis of Metabolic Networks. In: *Biological Regulation and Development*, Vol. 3A. Goldberger, R. F. and Yamamoto, K. R. (eds.), Plenum Press, New York, pp. 99-125.

BOOT, J. C. G. (1963a). On Sensitivity Analysis in Convex Quadratic Programming Problems. *Operations Res.* **11**, 771-786.

BOOT, J. C. G. (1963b). Binding Constraint Procedures of Quadratic Programming. *Econometrica* **31**, 464-498.

BRIGGS, G. E. AND HALDANE, J. B. S. (1925). A Note on the Kinetics of Enzyme Action. *Biochem. J.* **19**, 338-339.

BRINDLE, K. M. AND CAMPBELL, I. D. (1987). NMR Studies of Kinetics in Cells and Tissues. *Q. Rev. Biophys.* **19**, 159-182.

BROWN, D. E. AND GADDUM, R. N. (1988). Linear Growth in Batch Culture Caused by Conservative Trace Nutrient Limitations. *Biotechnol. Letters* **10**, 525-530.

CABIB, E. AND LELOIR, L. F. (1958). The biosynthesis of Trehalose Phosphate. *J. Biol. Chem.* **231**, 259-275.

CASCANTE, M., FRANCO, R., AND CANELA, E. E. (1989a). Use of Implicit Methods from Geneeral Sensitivity Theory to Develop a Systematic Approach to Metabolic Control. I. Unbranched Pathways. *Math. Biosci.* **94**, 271-288.

CASCANTE, M., FRANCO, R., AND CANELA, E. E. (1989b). Use of Implicit Methods from Geneeral Sensitivity Theory to Develop a Systematic Approach to Metabolic Control. II. Complex Systems. *Math. Biosci.* **94**, 289-309.

CAVALLINI, D., DEMARCO, C., MODOVI, B., AND AZZONE, G. F. (1955). A New Synthetic Sulfur-Containing Amino Acid: S-Aminoehtylcysteine. *Experientia* **11**, 61-62.

CHANCE, B. AND WILLIAMS, G. R. (1956). The Respiratory Chain and Oxidative Phosphorylation. *Adv. Enzymol.* **17**, 65-134.

CHANCE, B., WILLIAMS, G. R., HOLMES, W. F., AND HIGGINS, J. (1955). Respiratory Enzymes In Oxidative Phosphorylation. V. A Mechanism for Oxidative Phosphorylation. *J. Biol. Chem.* **217**, 439-451.

CHANCE, B., HOLMES, W., AND HIGGINS, J. (1958). Localization of Interaction Sites in Multi-Component Transfer Systems: Theorems Derived from Analogues. *Nature* **182**, 1190-1193.

CHANCE, B., GARFINKEL, D., HIGGINS, J., AND HESS, B. (1960). Metabolic Control Mechanisms. V. A Solution for the Equations Representing Interaction Between Glycolysis and Respiration in Ascites Tumer Cells. *J. Biol. Chem.* **235**, 2426-2439.

CLEMENT, Y. AND LANEELLE, G. (1986). Glutamate Excretion Mechanism in *Corynebacterium glutamicum*: Triggering by Biotin Starvation or by Surfactant Addition. *J. Gen. Microbiol.* **132**, 925-929.

COHEN, G. N. (1965). Regulation of Enzyme Activity in Microorganisms. *Annu. Rev. Microbiol.* **19**, 105-126.

CONNETT, R. J. AND BLUM, J. J. (1971). Metabolic Pathways in *Tetrahymena*: Distribution of Carbon Label by Reactions of the Tricarboxylic Acid and Glyoxylate Cycles in Normal and Desmethylimipramine-Treated Cells. *Biochemistry* **10**, 3299-3309.

COONEY, C. L., WANG, H. Y., AND WANG, D. I. C. (1977). Computer-Aided Material Balancing for Prediction of Fermentation Parameters. *Biotechnol. Bioeng.* **19**, 55-67.

COOPER, R. A. AND KORNBERG, H. L. (1969). Phosphoenolpyruvate Synthetase. *Methods Enzymol.* **13**, 309-314.

COPPELLA, S. J. AND DHURJATI, P. (1987). Low-Cost Computer-Coupled Fermentor Off-Gas Analysis via Quadrupole Mass Spectrometer. *Biotechnol. Bioeng.* **29**, 679-689.

CORNISH-BOWDEN, A. (1989). Metabolic Control Theory and Biochemical Systems Theory: Different Objectives, Different Assumptions, Different Results. *J. Biol. Chem.* **136**, 365-377.

CORWIN, L. M. (1959). Oxaloacetic Decarboxylase from Rat Liver Mitochondria. *J. Biol. Chem.* **234**, 1338-1341.

CRABTREE, B. AND NEWSHOLME, E. A. (1987). A Systematic Approach to Describing and Analysing Metabolic Control Systems. *Trends Biochem. Sci.* **12**, 4-12.

CREMER, J., TREPTOW, C., EGGELING, L., AND SAHM, H. (1988). Regulation of Enzymes of Lysine Biosynthesis in *Coyrnebacterium glutamicum. J. Gen. Microbiol.* **134**, 3221-3229.

CRAWFORD, J. M. AND BLUM, J. J. (1983). Quantitative Analysis of Flux Along the Gluconeogenic, Glycolytic and Pentose Phosphate Pathways Under Reducing Conditions in Hepatocytes Isolated From Fed Rats. *Biochem. J.* **212**, 595-598.

DAOUST, D. R. AND STOUDT, T. H. (1961). The Biosynthesis of L-Lysine in a Strain of *Micrococcus glutamicus. Develop. Industrial Microbiol.* **7**, 22-34.

DARTON, H. H. AND GUNSALUS, I. C. (1969). Citratase and Isocitratase. *Methods Enzymol.* **5**, 622-633.

DAWES, E. A. AND HOLMS, W. H. (1958). Metabolism of *Sarcina lutea.* II. Isotopic Evaluation of the Routes of Glucose Utilization. *Biochim. et Biophys. Acta* **29**, 82-91.

DEMAIN, A. L. AND BIRNBAUM, M. J. (1968). Alteration of Permeability for the Release of Metabolites from Microbial Cells. *Current Topics Microbiol. Immunol.* **46**, 1-25.

DEUTSCH, J. (1983). Glucose-6-Phosphate Dehydrogenase. In: *Methods of Enzymatic Analysis*, Third Edition, Vol. 3. Bergmeyer (ed.), Verlag Chemie, Weinheim, pp. 190-197.

DIXON, M. AND WEBB, E. (1979). *Enzymes*, Third Edition. Academic Press, New York.

DOMACH, M. M., LEUNG, S. K., CAHN, R. E., COCKS, G. G., AND SHULER, M. L. (1984). Computer Model for Glucose-Limited Growth of a Single Cell of *Escherichia coli* B/r-A. *Biotechnol. Bioeng.* **26**, 203-216.

EIKMANNS, B. J., GRIOT, M. U., FOLLETTIE, M. T., AND SINSKEY, A. J. (1989). The Phosphoenolpyruvate Carboxylase Gene of *Corynebacterium glutamicum*: Molecular Cloning, Nucleotide Sequence, and Expression. *Mol. Gen. Genet.* **218**, 330-339.

ENEI, H., SHIBAI, H., AND HIROSE, Y. (1982). Amino Acids and Nucleic Acid-Related Compounds. In: *Annual Reports on Fermentation Processes*, Vol 5. Perlman, D. (eds.), Academic Press, New York, pp. 79-100.

ENTNER, N. AND DOUDOROFF, M. (1952). Glucose and Gluconic Acid Oxidation of *Pseudomonas saccharophila*. *J. Biol. Chem.* **196**, 853-862.

FANSLER, B. AND LOWENSTEIN, J. M. (1969). Aconitase from Pig Heart. *Methods Enzymol.* **13**, 26-30

FELL, D. A. AND SAURO, H. M. (1985). Metabolic Control and Its Analysis. *Eur. J. Biochem.* **148**, 555-561.

FERNANDEZ, E. J. AND CLARK, D. S. (1987). NMR Spectroscopy: A Non-Invasive Tool for Studying Intracellular Processes. *Enzyme Microb. Technol.* **9**, 259-271.

FOWLER, E. B. AND WERKMAN, C. H. (1955). Synthesis of Amino Acids by *Aerobacter aerogenes*. *Arch. Biochem. Biophys.* **56**, 22-27.

FRAENKEL, D. G. AND LEVISOHN, S. R. (1987). Glucose and Gluconate Metabolism in an *Escherichia coli* Mutant Lacking Phosphoglucose Isomerase. *J. Bacteriol.* **93**, 1571-1578.

FRANCO, C. M. M., SMITH, J. E., AND BERRY, D. R. (1984). Effect of Nitrogen and Phosphate on the Levels of Intermediates in Bakers' Yeast Grown in Continuous Culture. *J. Gen. Microbiol.* **130**, 2465-2472.

GARFINKEL, D. (1964). Metabolic Control Mechanisms. VII. A Detailed Computer Model of the Glycolytic Pathway in Ascites Cells. *J. Biol. Chem.* **239**, 971-983.

GARFINKEL, D. (1971a). Simulation of the Krebs Cycle and Closely Related Metabolism in Perfused Rat Liver. I. Construction of a Model. *Comput. Biomed. Res.* **4**, 1-17.

GARFINKEL, D. (1971b). Simulation of the Krebs Cycle and Closely Related Metabolism in Perfused Rat Liver. II. Properties of the Model. *Comput. Biomed. Res.* **4**, 18-42.

GARFINKEL, D. (1981). Computer Modeling of Metabolic Pathways. *Trends Biochem. Sci.* **6**, 69-71.

GERHARDT, P., *et al.* (eds.) (1981). *Manual of Methods for General Bacteriology.* American Society for Microbiology, Washington.

GOLDBERG, D. M. AND ELLIS, G. (1983). Isocitrate Dehydrogenase. In: *Methods of Enzymatic Analysis*, Third Edition, Vol. 3. Bergmeyer (ed.), Verlag Chemie, Weinheim, pp. 183-190.

GOTTSCHALK, G. (1986). *Bacterial Metabolism*, Second Edition. Springer-Verlag, New York.

GROEN, A. K. AND TAGER, J. M. (1988). Control Analysis Provides a Simple Means of Understanding the Control Structure of a Metabolic Pathway. *Biochem. J.* **253**, 619-623.

GROSZ, R., STEPHANOPOULOS, G., AND SAN, K.-Y. (1984). Studies on On-Line Bioreactor Identification. III. Sensitivity Problems with Respiratory and Heat Evolution Measurements. *Biotechnol. Bioeng.* **26**, 1198-1208.

GURR, J. A. AND JONES, K. M. (1977). Purification and Characterization of Pyruvate Carboxylase from *Arthrobacter globiformis*. *Arch. Biochem. Biophys.* **179**, 444-455.

HADDOCK, B. A. AND JONES, C. W. (1977). Bacterial Respiration. *Bacteriol. Rev.* **41**, 47-99.

HADJ, S. A., QUERIC, M. P., DESCHAMPS, A. M., AND LEBEAULT, J. M. (1988). Optimization of L-Lysine Production by *Corynebacterium* sp. in Fed-Batch Cultures. *Biotechnol. Let.* **10**, 583-586.

HANEL, F., HILLIGER, M., AND GRAFE, U. (1981). Effect of Oxygen Limitation on Cellular L-Lysine Pool and Lipid Spectrum of *Corynebacterium glutamicum*. *Biotechnol. Let.* **3**, 461-464.

HANLON, D. P. AND WESTHEAD, E. W. (1969). Kinetic Studies on the Activation of Yeast Enolase by Divalent Cations. *Biochemisty* **8**, 4255-4260.

HAYASHI, K. AND SAKAMOTO, N. (1986). *Dynamic Analysis of Enzyme Systems: An Introduction.* Springer-Verlag, New York.

HEINRART, R. AND SONNTAG, I. (1982). Dynamics of Non-Linear Biochemical Systems and the Evolutionary Significance of Time Hierarchy. *BioSystems* **15**, 301-316.

HEINRICH, R. AND RAPOPORT, T. A. (1974a). A Linear Steady-State Treatment of Enzymatic Chains. General Properties, Control and Effector Strenght. *Eur. J. Biochem.* **42**, 89-95.

HEINRICH, R. AND RAPOPORT, T. A. (1974b). A Linear Steady-State Treatment of Enzymatic Chains. Critique of the Crossover Theorem and a General Procedure to Identify Interaction Sites with an Effector. *Eur. J. Biochem.* **42**, 97-105.

HEINRICH, R., RAPOPORT, S. M., AND RAPOPORT, T. T. (1977). Metabolic Regulation and Mathematical Models. *Prog. Biophys. Molec. Biol.* **32**, 1-82.

HIGA, A. I., MILRAD DE FORCHETTI, S. R., AND CAZZULO, J. J. (1976). CO_2-Fixing Enzymes in *Pseudomonas fluorescens. J. Gen. Microbiol.* **93**, 69-74.

HIGGINS, J. (1965). Dynamics and Control in Cellular Reactions. In: *Control of Energy Metabolism.* Chance, B., Estabrook, R. W., and Williamson, J. R. (eds.), Academic Press, New York, pp. 13-46.

HILLIGER, M. AND HANEL, F. (1981). Process Analysis of L-Lysine Fermentation Under Different Oxygen Supply. *Biotechnol. Let.* **3**, 219-224.

HINMAN, L. M. AND BLASS, J. P. (1981). An NADH-Linked Spectrophotometric Assay for Pyruvate Dehydrogenase Complex in Crude Tissue Homogenates. *J. Biol. Chem.* **256**, 6583-6586.

HIRAO, T., NAKANO, T., AZUMA, T., SUGIMOTO, M., AND NAKANISHI, T. (1989). L-Lysine Production in Continuous Culture of an L-Lysine Hyperproducing Mutant of *Corynbacterium glutamicum. Appl. Microbiol. Biotechnol.* **32**, 269-273.

HIROSE, Y. AND OKADA, H. (1979). Microbial Production of Amino Acids. In: *Microbial Technology*, second edition, Vol I. Peppler, H. J. (eds.), Academic Press, New York, pp. 211-240.

HIROSE, Y., SONODA, H., KINOSHITA, K., AND OKADA, H. (1967). Studies on Oxygen Transfer in Submerged Fermentations. Part VI. The Effect of Aeration on Glutamic Acid Fermentation.

HIROSE, Y., SANO, K., AND SHIBAI, H. (1978). Amino Acids. In: *Annual Reports on Fermentation Processes*, Vol 2. Perlman, D. (eds.), Academic Press, New York, pp. 155-189.

HOEK, J. B. AND RYDSTROM, J. (1988). Physiological Roles of Nicotinamide Nucleotide Transhydrogenase. *Biochem. J.* **254**, 1-10.

HOISCHEN, C. AND KRAMER, R. (1989). Evidence for an Efflux Carrier System Involved in the Secretion of Glutamate by *Coynebacterium glutamicum*. *Arch. Microbiol.* **151**, 342-347.

HORTON, A. A. AND KORNBERG, H. L. (1964). Oxaloacetate 4-carboxylase from *Pseudomonas ovalis* Chester. *Biochim. Biophys. Acta* **89**, 381-383.

HSU, R. Y. AND LARDY, H. A. (1969). Malic Enzyme. *Methods Enzymol.* **13**, 230-235.

INBAR, L. AND LAPIDOT, A. (1987). ^{13}C-NMR, ^{1}H-NMR and Gas-Chromatography Mass-Spectrometry Studies of the Biosynthesis of ^{13}C-Enriched L-Lysine by *Brevibacterium flavum*. *Eur. J. Biochem.* **162**, 621-633.

INBAR, L., KAHANA, Z. E., AND LAPIDOT, A. (1985). Natural-Abundance ^{13}C Nuclear Magnetic Resonance Studies of Regulation and Overproduction of L-Lysine by *Brevibacterium flavum*. *Eur. J. Biochem.* **149**, 601-607.

INGRAHAM, J. L., MAALOE, O., AND NEIDHARDT, F. C. (1983). *Growth of the Bacterial Cell*. Sinauer Associates, Inc., Sunderland.

ISHINO, S., YAMAGUCHI, K., SHIRAHATA, K., AND ARAKI, K. (1984). Involvement of *meso*-α,ϵ-Diaminopimelate D-Dehydrogenase in Lysine Biosynthesis in *Corynebacterium glutamicum*. *Agric. Biol. Chem.* **48**, 2557-2560.

ISHINO, S., KUGA, T., YAMAGUCHI, K., SHIRAHATA, K., AND ARAKI, K. (1986). ^{13}C NMR Studies of Histidine Fermentation with a *Corynebacterium glutamicum* Mutant. *Agric. Biol. Chem.* **50**, 307-310.

JEONG, J. W., SNAY, J., ATAAI, M. M. (1990). A Mathematical Model for Examining Growth and Sporulation Processes of *Bacillus subtilis*. *Biotechnol. Bioeng.* **35**, 160-184.

JOHNSTONE, R. M. (1963). Sulfhydryl Agents: Arsenicals. In *Metabolic Inhibitors: A Comprehensive Treatise*, Vol. II. Hochster, R. M. and Quastel, J. H. (eds.), Academic Press, New York, pp. 99-118.

JOSHI, A. AND PALSSON, B. O. (1989a). Metabolic Dynamics in the Human Red Cell. Part I—A Comprehensive Kinetic Model. *J. Theor. Biol.* **141**, 515-528.

JOSHI, A. AND PALSSON, B. O. (1989b). Metabolic Dynamics in the Human Red Cell. Part II—Interactions with the Environment. *J. Theor. Biol.* **141**, 529-545.

JOSHI, A. AND PALSSON, B. O. (1990a). Metabolic Dynamics in the Human Red Cell. Part III—Metabolic Reaction Rates. *J. Theor. Biol.* **142**, 41-68.

JOSHI, A. AND PALSSON, B. O. (1990b). Metabolic Dynamics in the Human Red Cell. Part IV—Data Prediction and Some Model Computations. *J. Theor. Biol.* **142**, 69-85.

KACSER, H. AND BURNS, J. A. (1973). The Control of Flux. *Symp. Soc. Exp. Biol.* **27**, 65-104.

KACSER, H. AND BURNS, J. A. (1979). Molecular Democracy: Who Shares the Controls. *Biochem. Soc. Trans.* **7**, 1149-1161.

KACSER, H. AND PORTEOUS, J. W. (1987). Control of Metabolism: What Do We Have to Measure. *Trends Biochem. Sci.* **12**, 5-14.

KALNENIEKS, U. Z., SAULITIS, J. B., GALININA, N. I., LIEPINS, E. E., AND SHVINKA, J. E. (1989). Protonmotive Force in *Brevibacterium flavum*: the Lack of Intracellular pH Homeostasis. *Arch. Microbiol.* **151**, 213-219.

KATZ, J. AND ROGNSTAD, R. (1976). Futile Cycles in the Metabolism of Glucose. *Curr. Top. Cell Regu.* **10**, 237-289.

KAWAHARA, Y., TANAKA, T., IKEDA, S., AND SONE, N. (1988). Coupling Sites of the Respiratory Chain of *Brevibacterium lactofermentum*. *Agric. Biol. Chem.* **52**, 1979-1983.

KIKUCHI, M. AND NAKAO, Y. (1986). Glutamic Acid. *Prog. Indust. Microbiol.* **24**, 101-116.

KIMURA, K. (1963). The effect of Biotin of the Amino Acid Biosynthesis by *Micrococcus glutamicus*. *J. Gen. Appl. Microbiol.* **9**, 205-212.

KINOSHITA, S. (1962). Production of Amino Acids with Special Consideration of the Function of Biotin. *Recent Progess in Micobiol.* **8**, 334-340.

KINOSHITA, S. (1972). Glutamic Acid. In: *The Microbial Production of Amino Acids*. Yamada *et al.* (eds.), Wiley, New York, pp. 3-38.

KINOSHITA, S. (1985). Glutamic Acid Bacteria. In: *Biology of Industrial Microorganisms*. Demain, A. L. and Solomon, N. A. (eds.), The Benjamin/Cummings Publishing Co., Inc., London, pp.115-142.

KINOSHITA, S. AND NAKAYAMA, K. (1978). Amino Acids. In: *Economic Microbiology*, Vol 2. Rose, A. H. (eds.), Academic Press, New York, pp. 209-261.

KINOSHITA, S., UDAKA, S., AND SHIMONO, M. (1957a). Studies on the Amino Acid Fermentation. Part I. Production of L-Glutamic Acid by Various Microorganisms. *J. Gen. Appl. Microbiol.* **3**, 193-205.

KINOSHITA, S., TANAKA, K., UDAKA, S., AND AKITA, S. (1957b). Glutamic Acid Fermentation. In: *Proceedings of the International Symposium on Enzyme Chemistry*, Vol. 2, Tokyo and Kyoto, pp. 464-468.

KINOSHITA, S., NAKAYAMA, K., AND KITADA, S. (1958a). L-Lysine Production Using Microbial Auxotroph. *J. Gen. Appl. Microbiol.* **4**, 128-129.

KINOSHITA, S., NAKAYAMA, K., AND AKITA, S. (1958b). Taxonomical Study of Glutamic Acid Accumulating Bacteria, *Micrococcus glutamicus* nov. sp. *Bull. Agr. Chem. Soc. Japan* **3**, 176-185.

KINOSHITA, S., TANAKA, K., AND AKITA, S. (1960). L-Glutamic Acid Fermentation. III. Distribution and Activity of L-Glutamic Acid Dehydrogenase in Microorganisms. *Nippon Nogei Kagaku Kaishi* **34**, 589-593. In: *Chem. Abs.* **59**, 1051e (1963).

KISS, R. (In preparation). Ph.D. thesis, Chemical Engineering, Massachusetts Institute of Technology, Cambridge Massachusetts.

KNOWLES, C. J. (1977). Microbial Metabolic Regulation by Adenine Nucleotide Pools. In: *Microbial Energetics*, 27th Symposium of the Society for General Microbiology. Haddock, B. A. and Hamilton, W. A. (eds.), Campridge University Press, Cambridge, pp. 241-283.

KODAKI, T., KATAGIRI, F., ASANO, M., IZUI, K., AND KATSUKI, H. (1985). Cloning of Phosphoenolpyruvate Carboxylase Gene from a Cyanobacterium, *Anacystis nidulans*, in *Escherichia coli*. *J. Biochem.* **97**, 533-539.

KORNBERG, H. L. (1966). Anaplerotic Sequences and Their Role in Metabolism. *Essays in Biochem.* **2**, 1-31.

KORNILOVA, I. G., MISHNEVA, V. G., SHATS, V. D., AND SHVINKA, YU. E. (1988). Change in Nucleotide Pool of *Brevibacterium flavum* Cells that Oxidize Molecular Hydrogen, Established by High-Performace Liquid Chromatography. *Microbiology* **57**, 142-146.

KOVAC, L., BERTA, F., PSENAK, M, AND SLEZARIKOVA, V. (1966). Metabolic Differences between *Escherichia coli* Cultures Growing Aerobically and Anaerobically in the Presence of Fluoroacetate. *Fol. Microb.* **11**, 263-270.

KOVACHEVICH, R. AND WOOD, W. A. (1955a). Carbohydrate Metabolism by *Pseudomonas fluorescens*. III. Purification and Pr ɔperties of a 6-Phosphogluconate dehydrase. *J. Biol. Chem.* **213**, 745-756.

KOVACHEVICH, R. AND WOOD, W. A. (1955b). Carbohydrate Metabolism by *Pseudomonas fluorescens*. IV. Purification and Properties of 2-Keto-3-deoxy-6-phosphogluconate Aldolase. *J. Biol. Chem.* **213**, 757-767.

KRULWICH, T. A. AND PELLICCIONE, N. J. (1979). Catabolic Pathways of Coryneforms, Nocardias, and Mycobacteria. *Ann. Rev. Microbiol.* **33**, 95-111.

KUN, E. (1976). Fluorocarboxylic Acids as Enzymatic and Metabolic Probes. In: *Biochemistry Involving Carbon-Fluorine Bonds*. Filler, B. (ed.), ACS Symposium Series 28, American Chemical Society, Washington, D. C., pp. 1-21.

KURGANOV, B. I. (1982). *Allosteric Enzymes: Kinetic Behaviour*. Wiley, New York.

KVASHNIKOV, E. I., NOGINA, T. M., NESTERENKO, O. A., PANCHENKO, L. P., ROZYNOV, B. V., AND KORONELLI, T. V. (1984). Systemmatic Position of Lysine-Producing *Brevibacterium flavum*. *Microbiol.* **53**, 75-78.

LAPORTE, D. C., WALSH, K., AND KOSHLAND, D. E. JR. (1984). The Branch Point Effect. *J. Biol. Chem.* **259**, 14068-14075.

LEADLAY, P. F. (1979). Free (S,S)-Diaminopimelate is not an Obligatory Intermediate in Lysine Biosynthesis in *Corynebacterium glutamicum*. *FEBS lett.* **98**, 399-402.

LEDERBERG, J. (1950). Isolation and Characterization of Biochemical Mutants of Bacteria. *Methods Med. Res.* **3**, 5-22.

LEHNINGER, A. L. (1975). *Biochemistry*, Second Edition. Worth Publishers, Inc., New York.

LEISER, J. AND BLUM, J. J. (1987). On the Analysis of Substrate Cycles in Large Metabolic Systems. *Cell Biophys.* **11**, 123-138.

LIAO, J. C. AND LIGHTFOOT, E. N. (1987). Extending the Quasi-Steady State Concept to Analysis of Metabolic Networks. *J. Theor. Biol.* **126**, 253-273.

LIAO, J. C. AND LIGHTFOOT, E. N. (1988a). Characteristic Reaction Paths of Biochemical Reaction Systems with Time Scale Separation. *Biotechnol. Bioeng.* **31**, 847-854.

LIAO, J. C. AND LIGHTFOOT, E. N. (1988b). Lumping Analysis of Biochemical Reaction Systems with Time Scale Separation. *Biotechnol. Bioeng.* **31**, 869-879.

LIAO, J. C., LIGHTFOOT, E. N., JOLLY, S. O., AND JACOBSON, G. K. (1988). Application of Characteristic Reaction Paths: Rate-Limiting Capability of Phosphofructokinase in Yeast Fermentation. *Biotechnol. Bioeng.* **31**, 855-868.

LIEW, C. K. (1976). Inequality Constrained Least-Squares Estimation. *J. Am. Stat. Assoc.* **71**, 746-751.

LUENBERGER, D. G. (1979). *Introduction to Dynamic Systems: Theory, Models, and Applications.* John Wiley & Sons, New York.

LUNTZ, M., ZHDANOVA, N. I., AND BOURD, G. I. (1986). Transport and Excretion of L-Lysine in *Corynebacterium glutamicum. J. Gen. Microbiol.* **132**, 2137-2146.

MACFADDIN, J. F. (1985). *Media for Isolation-Cultivation-Identification-Maintenance of Medical Bacteria*, Vol. 1. Williams & Wilkins, Baltimore.

MAITRA, P. K. AND LOBO, Z. (1971). A Kinetic Study of Glycolytic Enzyme Synthesis in Yeast. *J. Biol. Chem.* **246**, 475-488.

MAJEWSKI, R. A. AND DOMACH, M. M. (1985). Consideration of the Gain, Enzymatic Capacity Utilization, and Responce Time Properties of Metabolic Networks as a Function of Operating Point and Structure. *BioSystems* **18**, 15-22.

MAJEWSKI, R. A. AND DOMACH, M. M. (1990a). Simple Constrained-Optimization View of Acetate Overflow in *E. coli. Biotechnol. Bioeng.* **35**, 732-738.

MAJEWSKI, R. A. AND DOMACH, M. M. (1990b). Effect of Regulatory Mechanism on Hyperbolic Reaction Network Properties. *Biotechnol. Bioeng.* **36**, 166-178.

MAJEWSKI, R. A. AND DOMACH, M. M. (1990c). Chemostat-Cultivated *Escherichia coli* at High Dilution Rate: Mulitple Steady States and Drift. *Biotechnol. Bioeng.* **36**, 179-190.

MALLETTE, M. F. (1963). Validity of the Concept of Energy of Maintenance. *Ann. NY Acad. Sci.* **102**, 521-535.

MANDELSTAM, J. (1960). The Intracellular Turnover of Protein and Nucleic Acids and Its Role in Biochemical Differentiation. *Bacteriol. Rev.* **24**, 289-308.

MANDELSTAM, J., MCQUILLEN, K., AND DAWES, I. (EDS.) (1982). *Biochemistry of Bacterial Growth*, Third Edition. Halsted Press, New York.

MARAUSKA, D. F., RUKLISH, M. P., AND GALYNINA, N. I. (1981). Energy-Dependence of Glucose Transport in *Brevibacterium flavum* Cells. *Microbiol.* **50**, 560-565.

MARR, A. G., NILSON, E. H., AND CLARK, D. J. (1963). The Maintenance Requirement of *Escherichia coli*. *Ann. NY Acad. Sci.* **102**, 536-548.

MENKEL, E., THIERBACH, G., EGGELING, L., AND SAHM, H. (1989). Influence of Increased Aspartate Availability on Lysine Formation by a Recombinant Strain of *Corynebacterium glutamicum* and Utilization of Fumarate. *Appl. Microbiol. Biotechnol.* **55**, 684-688.

MILLER, G. A. (1956). The Magical Number Seven, Plus or Minus Two: Some Limits On Our Capacity for Processing Information. *Pyschol. Rev.* **63**, 81-97.

MILNER, J. L., VINK, B., WOOD, J. M., (1987). Transmembrane Amino Acid Flux in Bacterial Cells. *CRC Critical Rev. Biotechnol.* **5**, 1-47.

MINKEVICH, I. G. AND EROSHIN, V. K. (1973). Productivity and Heat Generation of Fermentation Under Oxygen Limitation. *Folia Microbiol.* **18**, 376-385.

MINNIKIN, D. E., GOODFELLOW, M., AND COLLINS, M. D. (1978). Lipid Composition in the Classification and Identification of Coryneform and Related Taxa. In: *Coryneform Bacteria*. Bousfield, I. J. and Callely, A. G. (eds.), Academic Press, New York, pp. 85-160.

MINODA, Y. (1986). Raw Materials for Amino Acid Fermentation. *Prog. Indust. Microbiol.* **24**, 51-66.

MISONO, H., TOGAWA, H., YAMAMOTO, T., AND SODA, K. (1979). *meso*-α,ϵ-Diaminopimelate D-Dehydrogenase: Distribution and the Reaction Product. *J. Bacteriol.* **137**, 22-27.

MISONO, H., OGASAWARA, M., AND NAGASAKI, S. (1986). Characterization of *meso*-Diaminopimelate Dehydrogenase from *Corynebacterium glutamicum* and Its Distribution in Bacteria. *Agric. Biol. Chem.* **50**, 2729-2734.

MIYAJIMA, R. AND SHIIO, I. (1970a). Regulation of Aspartate Family Amino Acid Biosynthesis in *Brevibacterium flavum*. III. Properties of Homoserine Dehydrogenase. *J. Biochem.* **68**, 311-319.

MIYAJIMA, R. AND SHIIO, I. (1970b). *Agric. Biol. Chem.* **34**, 1275.

MIYAJIMA, R. AND SHIIO, I. (1971). Regulation of Aspartate Family Amino Acid Biosynthesis in *Brevibacterium flavum*. Part IV. Repression of the Enzymes in Threonine Biosynthesis. *Agric. Biol. Chem.* **35**, 424-430.

MIYAJIMA, R., OTSUKA, S.-I., AND SHIIO, I. (1968). Regulation of Aspartate Family Amino Acid Biosynthesis in *Brevibacterium flavum*: I. Inhibition by Amino Acids of the Enzymes in Threonine Biosynthesis. *J. Biochem.* **63**, 139-148.

MOLLERING, H. (1985). Citrate. In: *Methods of Enzymatic Analysis*, Third Edition, Vol. 7. Bergmeyer (ed.), Verlag Chemie, Weinheim, pp. 2-12.

MONOD, J., WYMAN, J., AND CHANGEUX, J.-P. (1969). On the Nature of Allosteric Transitions: A Plausible Model. *J. Mol. Biol.* **12**, 88-118.

MORI, M. AND SHIIO, I. (1984). Production of Aspartic Acid and Enzymatic Alteration in Pyruvate Kinase Mutants of *Brevibacterium flavum*. *Agric. Biol. Chem.* **48**, 1189-1197.

MORI, M. AND SHIIO, I. (1985a). Purification and Some Properties of Phosphoenolpyruvate Carboxylase from *Brevibacterium flavum* and Its Aspartate-Overproducing Mutant. *J. Biochem.* **97**, 1119-1128.

MORI, M. AND SHIIO, I. (1985b). Synergistic Inhibition of Phosphoenolpyurvate Carboxylase by Aspartate and 2-Oxoglutarate in *Brevibacterium flavum*. *J. Biochem.* **98**, 1621-1630.

MORI, M. AND SHIIO, I. (1986). Multiple Ineraction of Fructose 1,6-Bisphosphate and Other Effectors on Phosphoenolpyruvate Carboxylase from *Brevibacterium flavum* and Its Aspartate-producing Mutant. *Agric. Biol. Chem.* **50**, 2605-2614.

MORI, M. AND SHIIO, I. (1987a). Pyruvate Formation and Sugar Metabolism in an Amino Acid-Producing Bacterium, *Brevibacterium flavum*. *Agric. Biol. Chem.* **51**, 129-138.

MORI, M. AND SHIIO, I. (1987b). Phosphoenopyruvate:Sugar Phosphotransferase Systems and Sugar Metabolism in *Brevibacterium flavum*. *Agric. Biol. Chem.* **51**, 2671-2678.

NAKATANI, Y., FUJIOKA, M., HIGASHINO, K. (1972). Enzymic Determination of L-Lysine in Biological Materials. *Anal. Biochem.* **49**, 225-231.

NAKAYAMA, K. (1972). Lysine and Diaminopimelic Acid. In *The Microbial Production of Amino Acids*, 369-397, K. Yamada, S. Kinoshita, T. Tsunoda, and K. Aida (eds.), Kodansha, Tokyo.

NAKAYAMA, K. (1982). Amino Acids. In: *Prescott and Dunn's Industrial Microbiology*, forth edition. Reed, G. (ed.), AVI Pub. Co., Westport, pp. 748-801.

NAKAYAMA, K. AND KINOSHITA, S. (1961a). Studies on Lysine Fermentation II. α, ϵ-Diaminopimelic Acid and its Decarboxylase in Lysine Production Strain and Parent Stain. *J. Gen. Appl. Microbiol.* **7**, 155-160.

NAKAYAMA, K. AND KINOSHITA, S. (1961b). Studies on Lysine Fermentation III. α, ϵ-Diaminopimelic Acid Accumulation and Diaminopimelic Acid Decarboxylase. *J. Gen. Appl. Microbiol.* **7**, 161-172.

NAKAYAMA, K., KITADA, S., AND KINOSHITA, S. (1961). Studies on Lysine Fermentation: I. The Control Mechanism on Lysine Accumulation by Homoserine and Threonine. *J. Gen. Appl. Microbiol.* **7**, 145-154.

NAKAYAMA, K., KITADA, S., SATO, Z., AND KINOSHITA, S. (1961b). Induction of Nutritional Mutants of Glutamic Acid Bacteria and Their Amino Acid Accumulation. *J. Gen. Appl. Microbiol.* **7**, 41-51.

NAKAYAMA, K., SATO, Z., AND KINOSHITA, S. (1964a). Growth of a Glutamic Acid Producing Bacterium and Related Bacteria. I. Effects of Iron Salts, Ferrichrome, Amino Acids and Some Other Compounds. *J. Gen. Appl. Microbiol.* **10**, 143-155.

NAKAYAMA, K., SATO, Z., TANAKA, H., AND KINOSHITA, S. (1964b). Growth of a Glutamic Acid Producing Bacterium and Related Bacteria. II. Effect of Chelating Agent and Its Relation to Inorganic Salt. *J. Gen. Appl. Microbiol.* **10**, 181-199.

NAKAYAMA, K., TANAKA, H., AND HAGINO, H. (1966). Studies on Lysine Fermentation: Part V. Concerted Feedback Inhibition of Aspartokinase and the Absence of Lysine Inhibition on Aspartic Semialdehyde-Pyruvate Condensation in *Micrococcus glutamicus*. *Agric. Biol. Chem.* **30**, 611-616.

NARA, T., SAMEJIMA, H., FUJITA, C., ITO, M., NAKAYAMA, K., AND KINOSHITA, S. (1961). L-Homoserine Fermentation. Part VI. Effect of Threonine and Methionine on L-Homoserine in Dehydrogenase in *Micrococcus glutamicus* 534-Co147. *Agric. Biol. Chem.* **25**, 532-541.

NASRI, M., DHOUIB, A, ZORGUANI, F., KRIAA, H., AND ELLOUZ, R. (1989). Production of Lysine by Using Immobilized Living *Corynebacterium* sp. Cells. *Biotechnol. Let.* **11**, 865-870.

NIRANJAN, S. C. AND SAN, K.-Y. (1989). Analysis of a Framework Using Material Balances in Metabolic Pathways to Elucidate Cellular Metabolism. *Biotechnol. Bioeng.* **34**, 496-501.

NOBLE, B. AND DANIEL, J. W. (1977). *Applied Linear Algebra*, Second Edition. Prentice-Hall, Inc., Englewood Cliffs.

NOLTMAN, E. A. (1966). Phosphoglucose Isomerase. *Methods Enzymol.* **9**, 557-575.

OISHI, K. AND AIDA, H. (1964). Studies on Amino Acid Fermentation. Part XII. Effect of NH_4^+ on the Catabolism of Glucose by a Glutamic Acid-Producing Bacterium, *Brevibacterium ammoniagenes* 317-1. *Amino Acid and Nucleic Acid* **10**, 6-11 (in Japanese, except for abstract).

OISHI, K. AND AIDA, H. (1965). Studies on Amino Acid Fermentation. Part XI. Effect of Biotin on the Embden-Meyerhof-Parnas Pathway and the Hexose-

Monophosphate Shunt in a Glutamic Acid-Producing Bacterium, *Brevibacterium ammoniagenes* 317-1. *Arg. Biol. Chem.* **29**, 83-89.

O'REGAN, M., THIERBACH, G., BACHMANN, B., VILLEVAL, D., LEPAGE, P., VIRET, J.-F., AND LEMOINE, Y. (1989). Cloning and Nucleotide Sequence of the Phosphoenolpyruvate Carboxylase-Coding Gene of *Corynebacterium glutamicum* ATCC 13032. *Gene* **77**, 237-251.

OSHIMA, K., TANAKA, K., AND KINOSHITA, S. (1964). Dehydrogenation of α,ϵ-Diaminopimelic Acid by the Highly Purified L-Glutamic Acid Dehydrogenase from *Micrococcus glutamicus*. *J. Gen. Appl. Microbiol.* **10**, 175-177.

OTSUKA, S-I., MIYAJIMA, R., AND SHIIO, I. (1965a). Comparative Studies on the Mechanism of Microbial Glutamate Formation. I. Pathways of Glutamate Formation From Glucose in *Brevibacterium flavium* and in *Micrococcus glutamicus*. *J. Gen. Appl. Microbiol.* **11**, 285-294.

OTSUKA, S-I., MIYAJIMA, R., AND SHIIO, I. (1965b). Comparative Studies on the Mechanism of Microbial Glutamate Formation. II. Effect of Biotin. *J. Gen. Appl. Microbiol.* **11**, 295-301.

OZAKI, H. AND SHIIO, I. (1968). Regulation of the TCA and Glyoxylate Cycles in *Brevibacterium flavum*. I. Inhibition of Isocitrate Lyase and Isocitrate Dehydrogenase by Organic Acids Related to the TCA and Glyoxylate Cycles. *J. Biochem.* **64**, 355-363.

OZAKI, H. AND SHIIO, I. (1969). Regulation of the TCA and Glyoxylate Cycles in *Brevibacterium flavum*. II. Regulation of Phosphoenolpyruvate Carboxylase and Pyruvate Kinase. *J. Biochem.* **66**, 297-311.

OZAKI, H. AND SHIIO, I. (1983). Production of Lysine by Pyruvate Kinase Mutants of *Brevibacterium flavum*. *Agric. Biol. Chem.* **47**, 1569-1576.

PALSSON, B. O. AND JOSHI, A. (1987). On the Dynamic Order of Structured *Escherichia coli* Growth Models. *Biotechnol. Bioeng.* **29**, 789-792.

PALSSON, B. O. AND LIGHTFOOT, E. N. (1984). Mathematical Modeling of Dynamics and Control in Metabolic Networks. I. On Michaelis-Menten Kinetics. *J. Theor. Biol.* **111**, 273-302.

PALSSON, B. O. AND LIGHTFOOT, E. N. (1985a). Mathematical Modeling of Dynamics and Control in Metabolic Networks. IV. Local Stability Analysis of Single Biochemical Control Loops. *J. Theor. Biol.* **113**, 261-277.

PALSSON, B. O. AND LIGHTFOOT, E. N. (1985b). Mathematical Modeling of Dynamics and Control in Metabolic Networks. V. Static Bifurcations in Single Biochemical Control Loops. *J. Theor. Biol.* **113**, 279-298.

PALSSON, B. O., JAMIER, R., AND LIGHTFOOT, E. N. (1984). Mathematical Modeling of Dynamics and Control in Metabolic Networks. II. Simple Dimeric Enzymes. *J. Theor. Biol.* **111**, 303-321.

PALSSON, B. O., PALSSON, H., AND LIGHTFOOT, E. N. (1985). Mathematical Modeling of Dynamics and Control in Metabolic Networks. III. Linear Reaction Sequences. *J. Theor. Biol.* **113**, 231-259.

PETERS, R. (1954). Biochemical Light Upon an Ancient Poison: A Lethal Synthesis. *Endeavour* **13**, 147-154.

PETERS, R. (1957). Mechanism of the Toxicity of the Active Constituent of *Dichapetalum cymosum* and Related Compounds. *Advances Enzymol.* **18**, 113-159.

PAPOUTSAKIS, E. T. (1984). Equations and Calculations for Fermentations of Butyric Acid Bacteria. *Biotechnol. Bioeng.* **26**, 174-187.

PAPOUTSAKIS, E. T. AND MEYER, C. L. (1985). Equations and Calculations of Product Yields and Preferred Pathways for Butanediol and Mixed-Acid Fermentations. *Biotechnol. Bioeng.* **27**, 50-66.

PERETTI, S. W. AND BAILEY, J. E. (1986). Mechanistically Detailed Model of Cellular Metabolism fro Glucose-Limited Growth on *Escherichia coli* B/r-A. *Biotechnol. Bioeng.* **28**, 1672-1689.

REARDON, K. F., SCHEPER, T.-H., AND BAILEY, J. E. (1987). Metabolic Pathway Rates and Culture Fluorescence in Batch Fermentations of *Clostridium acetobutylicum*. *Biotechnol. Prog.* **3**, 153-167.

REED, L. J. AND WILLMS, C. R. (1966). Purification and Resolution of the Pyruvate Dehydrogenase Complex (*Escherichia coli*). *Methods Enzymol.* **9**, 247-265.

REICH, J. G. AND SELKOV, E. E. (1975). Time Hierarchy, Equilibrium and Non-Equilibrium in Metabolic Systems. *BioSystems* **7**, 39-50.

RODWELL, V. W. (1969). Biosynthesis of Amino Acids and Related Compounds. In: *Metabolic Pathways*, Third Edition, Vol. 3. Greenberh, D. M. (ed.), Academic Press, Inc., New York, pp. 334-351.

ROELS, J. A. (1983). *Energetics and Kinetics in Biotechnology.* Elservier Biomedical Press, New York.

ROKITA, S. E. (1983). *Enzymatic Processing of Fluorinated Citrate Analogues.* PhD thesis, Chemistry, Massachusetts Institute of Technology, Cambridge Massachusetts.

ROMAGNOLI, J. A. AND SEPHANOPOULOS, G. (1981). Rectification of Process Measurement Data in the Presence of Gross Errors. *Chem. Eng. Sci.* **36**, 1849-1863.

RUKLISH, M. P. (1987). Kinetic Characteristics of Glucose Transport in *Brevibacterium flavum*. *Microbiol.* **56**, 14-18.

RUKLISH, M. P., MARAUSKA, D. F., AND VIESTUR, U. E. (1978). Nature of the Regulation of Enzymes of Glucose and Acetic Acid Metabolism in Lysine-Forming *Brevibacterium flavum*. *Microbiol.* **47**, 804-808.

RUKLISHA, M., MARAUSKA, D., SHVINKA, J., TOMA, M., AND GALYNINA, N. (1981). Coordination of Energy and Carbon Metabolism in Lysine Producing *Brevibacterium* strains. *Biotechnol. Letts.* **3**, 465-470.

RUKLISH, M. R., MARAUSKA, D. F., AND LABANE, L. YA. (1982). Characteristics of the Functioning of Phosphoenol Pyruvate Carboxylase in Bacteria Producing Lysine. *Microbiol.* **51**, 12-15.

SAN, K.-Y. AND STEPHANOPOULOS, G. (1984a). Studies on On-Line Bioreactor Identification. II. Numerical and Experimental Results. *Biotechnol. Bioeng.* **26**, 1189-1197.

SAN, K.-Y. AND STEPHANOPOULOS, G. (1984b). Studies on On-Line Bioreactor Identification. IV. Utilization of pH Measurements for Product Estimation. *Biotechnol. Bioeng.* **26**, 1209-1218.

SANO, K. AND SHIIO, I. (1967). Microbial Production of L-Lysine. I. Production by Auxotrophs of *Brevibacterium flavum*. *J. Gen. Appl. Microbiol.* **13**, 349-358.

SANO, K. AND SHIIO, I. (1970). Microbial Production of L-Lysine. III. Production by Mutants Resistant to S-(2-Aminoethyl)-L-Cysteine. *J. Gen. Appl. Microbiol.* **16**, 373-391.

SANO, K., ITO, K., MIWA, K., AND NAKAMORI, S. (1987). Amplicication of the Phosphoenol Pyruvate Carboxylase Gene of *Brevibacterium lactorfermentum* to Improve Amino Acid Production. *Agric. Biol. Chem.* **51**, 597-599.

SAVAGEAU, M. A. (1969a). Biochemical Systems Analysis. I. Some Mathematical Properties of the Rate Law for the Component Enzymatic Reactions. *J. Theor. Biol.* **25**, 365-369.

SAVAGEAU, M. A. (1969b). Biochemical Systems Analysis. II. The Steady-State Solutions for an *n*-Pool System Using a Power-Law Approximation. *J. Theor. Biol.* **25**, 370-379.

SAVAGEAU, M. A. (1970). Biochemical Systems Analysis. III. Dynamic Solutions Using a Power-Law Approximation. *J. Theor. Biol.* **25**, 365-369.

SAVAGEAU, M. A., VOIT, E. O., AND IRVINE, D. H. (1987a). Biochemical Systems Theory and Metabolic Control Theory: 1. Fundamental Similarities and Differences. *Math. Biosci.* **86**, 127-145.

SAVAGEAU, M. A., VOIT, E. O., AND IRVINE, D. H. (1987b). Biochemical Systems Theory and Metabolic Control Theory: 2. The Role of Summation and Connectivity Relationships. *Math. Biosci.* **86**, 147-169.

SCHENDEL, F. J., BREMMON, C. E., FLICKINGER, M. C., GUETTLER, M., AND HANSON, R. S. (1990). L-Lysine Production at 50°C by Mutants of a Newly Isolated and Characterized Methylotrophic *Bacillus* sp. *Appl. Environ. Microbiol.* **56**, 963-970.

SCHMITT, A., BOTTKE, I., AND SEIBERT, G. (1966). Eigenschaften einer Oxalacetat-Decarboxylase aus Dorschmuskulatur. *Hoppe-Seyler's Z. Physiol. Chem.* **347**, 18-34.

SCHOFIELD, P. J. AND SOLS, A. (1976). Rat Liver 6-Phosphogluconolactonase: A Low K_m Enzyme. *Biochem. Biophys. Res. Commum.* **71**, 1313-1318.

SCHWARTZ, E. R. AND REED, L. J. (1970). Regulation of the Activity of the Pyruvate Dehydrogenase Complex of *Escherichia coli*. *Biochemistry* **9**, 1434-1439.

SCHWARTZ, E. R., OLD, L. O., AND REED, L. J. (1968). Regulatory Properties of Pyruvate Dehydrogenase from *Escherichia coli*. *Biochem. Biophys. Res. Commun.* **31**, 495-500.

SCRUTTON, M. C. (1978). Fine Control of the Conversion of Pyruvate (Phosphoenolpyruvate) to Oxaloacetate in Various Species. *FEBS Lett.* **89**, 1-9.

SCRUTTON, M. C. AND YOUNG, M. Y. (1970). Pyruvate Carboyxylase. In: *The Enzymes*, 3rd ed., Vol. 6. Boyer, P. D., (ed.), Academic Press, New York, pp. 1-122.

SEGEL, I. H. (1975). *Enzyme Kinetics: Behavior and Analysis of Rapid Equilibrium and Steady-State Enzyme Systems.* John Wiley & Sons, New York.

SEGEL, L. A. (1988). On the Validity of the Steady State Assumption of Enzyme Kinetics. *Bull. Math. Biol.* **50**, 579-593.

SHANKS, J. V. AND BAILEY, J. (1990). Comparison of Wild-Type and reg1 Mutant *Saccharomyces cerevisiae* Metabolic Levels During Glucose and Galactose Metabolism Using ^{31}P NMR.

SHIIO, I. (1960). Bacterial Formation of Glutamic Acid from Acetic Acid. I. Glutamate Formation and Its Related Enzymes in *Brevibacterium flavum*, No. 2247. *J. Biochem.* **47**, 273-283.

SHIIO, I. AND MIYAJIMA, R. (1969). Concerted Inhibition and Its Reversal by End Products of Aspartate Kinase in *Brevibacterium flavum*. *J. Biochem.* **65**, 849-859.

SHII, I. AND NAKAMORI, S. (1970). Microbial Production of L-Threonine. Part II. Production by α-Amino-β-hydroxyvaleric Acid Resistant Mutants of Glutamate Producing Bacteria. *Agric. Biol. Chem.* **34**, 448-456.

SHIIO, I. AND OZAKI, H. (1968). Concerted Inhibition of Isocitrate Dehydrogenase by Glyoxylate Plus Oxalacetate. *J. Biochem.* **64**, 45-53.

SHIIO, I. AND OZAKI, H. (1970). Regulation of Nicotinamide Adenine Dinucleotide Phosphate-specific Glutamate Dehydrogenase from *Brevibacterium flavum*, a Glutamate-producing Bacterium. *J. Biochem.* **68**, 633-647.

SHIIO, I. AND SANO, K. (1969). Microbial Production of L-Lysine. II. Production by Mutants Sensitive to Threonine or Methionine. *J. Gen. Appl. Microbiol.* **15**, 267-287.

SHIIO, I. AND TSUNODA, T. (1961a). Bacterial Formation of Glutamic Acid from Acetic Acid. II. Formation of Glutamic Acid from C^{14}-Labelled Acetic Acid in *Brevibacterium flavum*, No. 2247. *J. Biochem.* **49**, 141-147.

SHIIO, I. AND TSUNODA, T. (1961b). Bacterial Formation of Glutamic Acid from Acetic Acid. III. Incorporation of Labelled Acetate and Kinetic Relationships of the Metabolites in *Brevibacterium flavum*, No. 2247. *J. Biochem.* **49**, 148-153.

SHIIO, I. AND UJIGAWA, K. (1978). Enzymes of the Glutamate and Aspartate Synthetic Pathways in a Glutamate-Producing Bacterium, *Brevibacterium flavum*. *J. Biochem.* **84**, 647-657.

SHIIO, I. AND UJIGAWA-TAKEDA, K. (1979). Regulation of Phosphoenolpyruvate Carboxylase by Synergistic Action of Aspartate and 2-Oxoglutarate. *Agric. Biol. Chem.* **43**, 2479-2485.

SHIIO, I. AND UJIGAWA-TAKEDA, K. (1980). Presence and Regulation of α-Ketoglutarate Dehyrogenase Complex in a Glutamate-Producing Bacterium, *Brevibacterium flavum*. *Agric. Biol. Chem.* **44**, 1897-1904.

SHIIO, I., OTSUKA, S.-I., AND TSUNODA, T. (1959a). Glutamic Acid Formation from Glucose by Bacteria. I. Enzymes of the Embden-Meyerhof-Parnas Pathway, the Krebs Cycle, and the Glyoxylate Bypass in Cell Extracts of *Brecibacterium flavum* No. 2247. *J. Biochem.* **46**, 1303-1311.

SHIIO, I., OTSUKA, S.-I., AND TSUNODA, T. (1959b). Glutamic Acid Formation from Glucose by Bacteria. II. Glutamic Acid and α-Ketoglutaric Acid Formation by *Brevibacterium flavum* No. 2247. *J. Biochem.* **46**, 1597-1605.

SHIIO, I., OTSUKA, S.-I., AND TSUNODA, T. (1960a). Glutamic Acid Formation from Glucose by Bacteria. III. On the Pathway of Pyruvate Formation in *Brevibacterium flavum* No. 2247. *J. Biochem.* **47**, 414-421.

SHIIO, I., OTSUKA, S.-I., AND TSUNODA, T. (1960b). Glutamic Acid Formation from Glucose by Bacteria. IV. Carbon dioxide fixation and Glutamate Formation in *Brevibacterium flavum* No. 2247. *J. Biochem.* **48**, 110-120.

SHIIO, I., OTSUKA, S.-I., AND TAKAHASHI, M. (1961a). Effect of Growth Substrate on Levels of Glyoxylate By-pass Enzymes in a Glutamate Forming Bacterium, *Brevibacterium flavum* No. 2247. *J. Biochem.* **49**, 262-263.

SHIIO, I., OTSUKA, S.-I., AND TAKAHASHI, M. (1961b). Glutamic Acid Formation from Glucose by Bacteria: V. Oxidative Metabolism of Glucose in *Brevibacterium flavum* No. 2247. *J. Biochem.* **49**, 397-403.

SHIIO, I., OTSUKA, S.-I., AND TAKAHASHI, M. (1961c). Glutamic Acid Formation from Glucose by Bacteria. VI. Metabolism of the Intermediates of the TCA Cycle and of the Glyoxylate Bypass in *Brevibacterium flavum* No. 2247. *J. Biochem.* **50**, 34-40.

SHIIO, I., OTSUKA, S.-I., AND TAKAHASHI, M. (1961d). Significance of α-Ketoglutaric Dehydrogenase on the Glutamic Acid Formation in *Breivbacterium flavum. J. Biochem.* **50**, 164-165.

SHIIO, I., OTSUKA, S.-I., AND KATSUYA, N. (1962c). Effect of Biotin on the Bacterial Formation of Glutamic Acid. II. Metabolism of Glucose. *J. Biochem.* **52**, 108-116.

SHIIO, I., MOMOSE, H., AND OYAMA, A. (1969). Genetic and Biochemical Studies on Bacterial Formation of L-Glutamate. I. Relationship Between Isocitrate Lyase, Acetate kinase, and Phosphate Acetyltransferase Levels and Glutamate Production in *Brevibacterium flavum. J. Gen. Appl. Microbiol.* **15**, 27-40.

SHIIO, I., OZAKI, H., AND UJIGAWA, K. (1977). Regulation of Citrate Synthase in *Brevibacterium flavum*, a Glutamate-Producing Bacterium. *J. Biochem.* **82**, 395-405.

SHIIO, I., OZAKI, H., AND UJIGAWA-TAKEDA, K. (1982a). Production of Aspartic Acid and Lysine by Citrate Synthase Mutants of *Brevibacterium flavum. Agric. Biol. Chem.* **46**, 101-107.

SHIIO, I., OZAKI, H., AND MORI, M. (1982b). Glutamate Metabolism in a Glutamate-Producing Bacterium, *Brevibacterium flavum. Agric. Biol. Chem.* **46**, 493-500.

SHIIO, I., MORI, M., AND OZAKI, H. (1982c). Amino Acid Aminotransferases in an Amino Acid-producing Bacterium, *Brevibacterium flavum*. *Agric. Biol. Chem.* **46**, 2967-2977.

SHIIO, I., SUGIMOTO, S.-I., AND TORIDE, Y. (1984a). Studies on Mechanisms for Lysine Production by Pyruvate Kinase-Deficient Mutants of *Brevibacterium flavum*. *Agric. Biol. Chem.* **48**, 1551-1558.

SHIIO, I., TORIDE, Y., AND SUGIMOTO, S.-I. (1984b). Production of Lysine by Pyruvate Dehydrogenase Mutants of *Brevibacterium flavum*. *Agric. Biol. Chem.* **48**, 3091-3098.

SHIIO, I., YOKOTA, A., AND SUGIMOTO, S.-I. (1987). Effect of Pyruvate Kinase Deficiency on L-Lysine Productivities of Mutants with Feedback-resistant Aspartokinases. *Agric. Biol. Chem.* **51**, 2485-2493.

SHIIO, I., SUGIMOTO, S.-I., AND KAWAMURA, K. (1990). Effects of Carbon Source Sugars on the Yield of Amino Acid Production and Sucrose Metabolism in *Brevibacterium flavum*. *Agric. Biol. Chem.* **54**, 1513-1519.

SHIOTA, T., FOLK, J. E., AND TIETZE, F. (1958). Inhibition of Lysine Utilization in Bacteria by S-(β-Aminoethyl)cysteine and Its Reversal by Lysine Peptides. *Arch. Biochem. Biophy.* **77**, 372-377.

SHVINKA, YU. E., VIESTUR, U. E., AND TOMA, M. K. (1979). Alternative Pathways of Oxidation in the Respiratory Chain of *Brevibacterium flavum*. *Microbiol.* **48**, 4-10.

SHVINKA, J., VIESTURS, U., AND RUKLISHA, M. (1980). Yield Regulation of Lysine Biosynthesis in *Brevibacterium flavum*. *Biotechnol. Bioeng.* **22**, 897-912.

SHVINKA, YU. E., BABURIN, L. A., AND VIESTUR, U. E. (1982). Sensitivity of the Process of Oxygen Uptake in *Brevibacterium flavum* to Changes in the pH of the Medium and the Action of an Uncoupler of Oxidation and Phosphorylation. *Microbiol.* **51**, 728-734.

SIMON, J.-L., ENGASSER, J.-M., AND GERMAIN, P. (1984). Substrate Flux Mapping in Corynebacteria for Amino Acids Production. In: *Third European Congress on Biotechnology*, Vol II. Verlag Chemie GmbH, Weinheim, pp. 10-14.

SMALL, J. R. AND FELL, D. A. (1989). The Matrix Methods of Metabolic Control Analysis: its Validity for Complex Pathway Structures. *J. Theor. Biol.* **136** 181-197.

SORRIBAS, A. AND SAVAGEAU, M. (1989a). A Comparison of Variant Theories of Intact Biochemical Systems. I. Enzyme-Enzyme Interactions and Biochemical Systems Theory. *Math. Biosci.* **94**, 161-193.

SORRIBAS, A. AND SAVAGEAU, M. (1989b). A Comparison of Variant Theories of Intact Biochemical Systems. II. Flux-Oriented and Metabolic Control Theories. *Math. Biosci.* **94**, 195-238.

STEIN, R. B. AND BLUM, J. J. (1979). Quantitative Analysis of Intermediary Metabolism in *Tetrahymena* Cells Grown in Proteose-Peptone and Resuspended in a Defined Nutrient-Rich Medium. *J. Biol. Chem.* **254**, 10385-10395.

STEPHANOPOULOS, G. AND SAN, K. Y. (1984). Studies on On-Line Bioreactor Identification. I. Theory. *Biotechnol. Bioeng.* **26**, 1176-1188.

STOUTHAMER, A. H. (1973). A Theoretical Study of the Amount of ATP Required for Synthesis of Mircobial Cell Material. *Antonie van Leeuwenhoek* **39**, 545-565.

STOUTHAMER, A. H. (1978). Energy-Yielding Pathways. In: *The Bacteria; a Treatise on Structure and Function*, Vol. VI: *Bacterial Diversity.* Ornston, L. N. and Sokatch, J. R. (eds.), Academic Press, New York, pp. 389-462.

STOUTHAMER, A. H. AND BETTENHAUSSEN, C. (1973). Utilization of Energy for Growth and Maintenace in Continuous and Batch Cultures of Microorganisms. *Biochim. Biophys. Acta* **301**, 53-70.

STRANG, G. (1980). *Linear Algebra and its Applications*, Second Edition. Academic Press, Inc., Orlando.

SUGIMOTO, S.-I., AND SHIIO, I. (1987a). Regulation of Glucose-6-Phosphate Dehydrogenase in *Brevibacterium flavum*. *Agric. Biol. Chem.* **51**, 101-108.

SUGIMOTO, S.-I., AND SHIIO, I. (1987b). Regulation of 6-Phosphogluconate Dehydrogenase in *Brevibacterium flavum*. *Agric. Biol. Chem.* **51**, 1257-1263.

SUGIMOTO, S.-I., AND SHIIO, I. (1989). Fructose Metabolism and Regulation of 1-Phosphofructokinase and 6-Phosphofructokinase in *Brevibacterium flavum*. *Agric. Biol. Chem.* **53**, 1261-1268.

SUGIMOTO, S.-I. AND SHIIO, I. (1989b). Regulation of Enzymes for Erythrose 4-Phosphate Synthesis in *Breviacterium flavum*. *Agric. Biol. Chem.* **53**, 2081-2087.

SUGITA, T. AND KOMATSUBARA, S. (1989). Construction of a Threonine-Hyperproducing Strain of *Serratia marcescens* by Amplifying the Phosphoenolpyruvate Carboxylase Gene. *Appl. Microbiol. Biotechnol.* **30**, 290-293.

SUGIYAMA, Y., KITANO, K., AND KANZAKI, T. (1973). Role of Copper Ions in the Regulation of L-Glutamate Biosynthesis. *Agric. Biol. Chem.* **37**, 1873-1847.

SUZUKI, K., KANEKO, T., AND KOMAGATA, K. (1981). Deoxyribonucleic Acid Homologies Among Coryneform Bacteria. *Int. J. Syst. Bacteriol.* **31**, 131-138.

TANG, R. T., ZHU, X. Z., AND GONG, C. S. (1989). Effect of Dimethyl Sulfoxide on L-Lysine Production by a Regulatory Mutant of *Brevibacterium flavum. Can. J. Micorbiol.* **35**, 668-670.

TOENNIES, G. (1965). Role of Amino Acids in Postexponential Growth. *J. Bacteriol.* **90**, 438-442.

TOENNIES, G., SHOCKMAN, G. D., AND KOLB, J. (1963). Differential Effects of Amino Acid Deficiencies on Bacterial Cytochemistry. *Biochemisty* **2**, 294-296.

TOSAKA, O. AND TAKINAMI, K. (1978). Pathway and Regulation of Lysine Biosynthesis in *Brevibacterium lactorfermentum. Agric. Biol. Chem.* **42**, 95-100.

TOSAKA, O., TAKINAMI, K., AND HIROSE, Y. (1978a). L-Lysine Production by S-(2-Aminoethyl) L-Cysteine and α-Amino-β-hydroxyvarelic Acid Resistant Mutants of *Brevibacterium lactcfermentum. Agric. Biol. Chem.* **42**, 745-752.

TOSAKA, O., HIRAKAWA, H., TAKINAMI, K, AND HIROSE, Y. (1978b). Regulation of Lysine Biosynthesis by Luecine in *Brevibacterium lactofermentum. Agric. Biol. Chem.* **42**, 1501-1506.

TOSAKA, O., HIRAKAWA, H., YOSHIHARA, Y., TAKINAMI, K., AND HIROSE, Y. (1978c). Production of L-Lysine by Alanine Auxotrophs Derived from AEC Resistant Mutants of *Brevibacterium lactofermentum. Agric. Biol. Chem.* **42**, 1773-1778.

TOSAKA, O., TAKINAMI, K., AND HIROSE, Y. (1978d). Production of L-Lysine by Leucine Auxotrophs Derived from AEC Resistant Mutants of *Brevibacterium lactofermentum. Agric. Biol. Chem.* **42**, 1181-1186.

TOSAKA, O., ISHIHARA, M., MORINAGA, Y., AND TAKINAMI, K. (1979a). Mode of Conversion of Asparto β-Semialdehyde to L-Threonine and L-Lysine in *Brevibacterium lactofermentum. Agric. Biol. Chem.* **43**, 265-270.

TOSAKA, O., MORIOKA, H., AND TAKINAMI, K. (1979c). The Role of Biotin Dependent Pyruvate Carboxylase in L-Lysine Production. *Argic. Biol. Chem.* **43**, 1513-1519.

TOSAKA, O., YOSHIHARA, Y., IKEDA, S., AND TAKINAMI, K. (1985). Production of L-Lysine by Fluoropyruvate-Sensitive Mutants of *Brevibacterium lactofermentum. Agric. Biol. Chem.* **49**, 1305-1312.

TSAI, S. P. AND LEE, Y. H. (In preparation). Application of Gibbs' Rule and a Simple Pathway Method to Microbial Stoichiometry.

TSAI, S. P. AND LEE, Y. H. (1988). Application of Metabolic Pathway Stoichiometry to Statistical Analysis of Bioreactor Measurement Data. *Biotechnol. Bioeng.* **32**, 713-715.

TSUCHIDA, T. AND MOMOSE, H. (1975). Genetic Changes of Regulatory Mechanisms Occurred in Leucine and Valine Producing Mutants Derived from *Brevibacterium lactofermentum* 2256. *Agric. Biol. Chem.* **39**, 2193-2198.

UMBARGER, H. E. (1969). Regulation of Amino Acid Metabolism. *Annu. Rev. Biochem.* **38**, 323-370.

VALLINO, J. J. AND STEPHANOPOULOS, G. N. (1987). Intelligent Sensors in Biotechnology: Applications for the Monitoring of Fermentations and Cellular Metabolism. *Ann. NY Acad. Sci.* **506**, 415-430.

VALLINO, J. J. AND STEPHANOPOULOS, G. N. (1989). Flux Determination in Cellular Bioreaction Networks: Applications to Lysine Fermentations. In: *Frontiers in Bioprocessing.* Sikdar, S. K., Bier, M., and Todd, P. (eds.), CRC Press, Inc., Boca Raton, pp. 205-219.

VANDECASTEELE, J. P., LEMAL, J., AND COUDERT, M. (1975). Pathways and Regulation of Glutamate Synthesis in a *Corynebacterium* sp. Overproducing Glutamate. *J. Gen. Mirobiol.* **90**, 178-180.

VERGONET, G. AND BERENDSEN, H. J. C. (1970). Evaluation of the Steady-State Approximation in a System of Coupled Rate Equations. *J. Theor. Biol.* **28**, 155-173.

VERHOFF, F. H. AND SPRADLIN, J. E. (1976). Mass and Energy Balance Analysis of Metabolic Pathways Applied to Citric Acid Production by Aspergillus niger. *Biotechnol. Bioeng.* **18**, 425-432.

VON DER OSTEN, C. H., GIOANNETTI, C., AND SINSKEY, A. J. (1989). Design of a Defined Medium for Growth of *Corynebacterium glutamicum* in Which Citrate Facilitates Iron Uptake. *Biotechnol. Let.* **11**, 11-16.

WALKER, T. E. AND LONDON, R. E. (1987). Biosynthetic Prepartion of L-[^{13}C]- and [^{15}N] Glutamate by *Brevibacterium flavum. Appl. Envir. Microbiol.* **53**, 92-98.

WALKER, T. E., HAN, C. H., KOLLMAN, V. H., LONDON, R. E., AND MATWIYOFF, N. A. (1982). ^{13}C Nuclear Magnetic Resonance Studies of the Biosynthesis by *Microbacterium ammoniaphilum* of L-Glutamate Selectively Enriched with Carbon-13. *J. Biol. Chem.* **257**, 1189-1195.

WANG, N. S. AND STEPHANOPOULOS, G. (1983). Application of Macroscopic Balances to the Identification of Gross Measurement Errors. *Biotechnol. Bioeng.* **25**, 2177-2208.

WANG, H. Y., COONEY, C. L., AND WANG, D. I. C. (1977). Computer-Aided Baker's Yeast Fermentation. *Biotechnol. Bioeng.* **19**, 69-86.

WEATHERBURN, M. W. (1967). Phenol-Hypochlorite Reaction for Determination of Ammonia. *Anal. Chem.* **39**, 971-974.

WEBB, J. L. (1966). *Enzymes and Metabolic Inhibitors*, Vol. III. Academic Press, New York, pp. 595-790.

WEIBEL, K. E., MOR, J.-R., AND FIECHTER, A. (1974). Rapid Sampling of Yeast Cells and Automated Assays of Adenylate, Citrate, Pyruvate, and Glucose-6-phosphate Pools. *Anal. Biochem.* **58**, 208-216.

WELCH, G. R., KELETI, T., FELL, D. A., CANELA, E. I., FRANCO, R., SAVAGEAU, M. A., VOIT, E. O., SORRIBAS, A., KACSER, H., PORTEOUS, J. W. CRABTREE, B., AND NEWSHOLME, E. A. (1987). In Discussion Forum. *Trends Biochem. Sci.* **12**, 216-224.

WESTERHOFF, H. V., GROEN, A. K., AND WANDERS, R. J. A. (1984). Modern Theories of Metabolic Control and Their Applications. *Biosci. Rep.* **4**, 1-22.

WHITE, P. J. (1983). The Essential Role of Diaminopimelate Dehydrogenase in the Biosynthesis of Lysine by *Bacillus sphaericus*. *J. Gen. Microbiol.* **129**, 739-749.

WIFLING, K. AND DIMROTH, P. (1989). Isolation and Characterization of Oxaloacetate Decarboxylase of *Salmonella typhimurium*, a Sodium Ion Pump. *Arch. Microbiol.* **152**, 584-588.

YAMAGUCHI, K., ISHINO, S., ARAKI, K., AND SHIRAHATA, K. (1986). ^{13}C NMR Studies of Lysine Fermentation with a *Corynebacterium glutamicum* Mutant. *Agric. Biol. Chem.* **50**, 2453-2459.

YEH. P., SICARD, A. M., AND SINSKEY, A. J. (1988). General Organization of the Genes Specifically Involved in the Diaminopimelate-Lysine Biosynthetic Pathway of *Corynebacterium glutamicum*. *Mol. Gen. Genet.* **212**, 105-111.

YOKOTA, A. AND SHIIO, I. (1988). Effects of Reduced Citrate Synthase Activity and Feedback-resistant Phosphoenolpyruvate Carboxylase on Lysine Productivities of *Brevibacterium flavum*. *Agric. Biol. Chem.* **52**, 455-463.

ZAKI, D., GALAL, O., WAHBA, A. E.-A., MORSI, K., AND EL-WAKEIL, F. A. (1982). Microbiological Production of Lysine. *Nutrition Rep. Internal.* **26**, 537-546.

Appendix A

Abbreviations and Nomenclature

A.1 Abbreviations

αKGDH	α-ketoglutarate dehydrogenase
AA	Amino acids (generic)
Ac	Acetic acid
AcCoA	Acetyl coenzyme A
ADP	Adenosine 5'-diphosphate
AEC	S-(2-aminoethyl) L-cysteine (lysine analog)
AEC^R	A strain resistant to AEC
AEC^S	A strain sensitive to AEC
AH	Aconitase
AHV	α-Amino-β-hydroxyvaleric acid (threonine analog)
AK	Aspartate kinase
AK^R	Strain with AK resistant to inhibition by Lys+Thr
AKAP	N-acetyl (or succinyl)-ε-keto-α-aminopimelate
AKG, αKG	α-Ketoglutaric acid
AKP	2-Amino-6-ketopimelate
Ala	Alanine
Ala^-	Alanine auxotroph
AMP	Adenosine 5'-monophosphate
AMU	Atomic mass unit
ASA	Aspartate-β-semialdehyde
Asp	Aspartate
AspP	Aspartyl phosphate
AT	Aminotransferase
ATP	Adenosine 5'-triphosphate
ATCC	American Type Culture Collection
BIOMAS	Biomass
BRNE	Bioreaction network equation
BRNA	Bioreaction network algorithm
BST	Biochemical systems theory
BS#	Biochemistry Set number # (Appendix B)
B&T	Biotin and Thiamine solution (Table 5.2)
CER	Carbon dioxide evolution rate

Cit	Citrate
CM3	Complex medium 3 (Section 5.5.5.5)
CoA	Coenzyme A
CO2	Carbon dioxide
CRP	Characteristic reaction path
CS	Citrate synthase
CS^A	Attenuated CS activity
CS^L	Citrate synthase lacking strain
Cyt	Cytochrome
DAP	Diaminopimelate
DCA	Dicarboxylic acid (*i.e.* modified TCA)
DCW	Dry cell weight (g/l)
DDP	Dihydrodipicolinate
DHAP	Dihydroxyacetone phosphate
DMSO	Dimethyl sulfoxide
DNA	Deoxyribonucleic acid
DO	Dissolved oxygen
EC	Enzyme catalog number
ED	Entner-Doudoroff pathway
EDTA	(Ethylenedinitrilo)-tetraacetic acid
EMB	Eosin Y/Methylene blue (Table 5.3)
EMP	Embden-Meyerhof-Parnas pathway
ENO	Enolase
E4P	Erythrose-4-phosphate
FAc	Fluoroacetate
FAD	Flavin adenine dinucleotide (oxidized)
FADH	Flavin adenine dinucleotide (reduced)
FC	Fluorocitrate
FM4	Fermentation medium 4 (Table 5.11)
FM8	Fermentation medium 8 (Section 5.5.5.3)
FM9	Fermentation medium 9 (Section 5.5.5.3)
FP	Fluoropyruvate
FP^S	A strain which is FP sensitive
Frc	Fructose
Fru1P	Fructose-1-phosphate
Fru16dP	Fructose-1,6-diphosphate
Fru6P, F6P	Fructose-6-phosphate
Fum	Fumarate
GAP	Glyceraldehyde-3-phosphate
GDH	Glutamate dehydrogenase
Glc	Glucose
Glcn	Gluconate
Glcn6P	Gluconate-6-phosphate
Glum	Glutamine
Glut	Glutamate
Glyox	Glyoxylate
GN6PDH	Gluconate-6-phosphate dehydrogenase

GOGAT	Glutamine: α-ketoglutarate aminotransferase
GPI	Glucose-6-phosphate isomerase
GPI^A	Strain with attenuated GPI activity
GS	Glutamine synthetase
G3P	3-Phosphoglycerate
G6P, Glc6P	Glucose-6-phosphate
G6PDH	G6P dehydrogenase
HDH	Homoserine dehydrogenase
HMP	Hexosemonophosphate pathway
Homo	Homoserine
$Homo^-$	Homoserine auxotrophic strain
H2O	Water
ICDH	Isocitrate dehydrogenase
ICLY	Isocitrate lyase
Ile	Isoleucine
IsoCit	Isocitrate
KDPG	2-keto-3-deoxy-6-phosphogluconate
Lac	Lactate
LB5G	Seed culture medium (Table 5.1)
LDH	Lactate dehydrogenase
Leu	Leucine
Leu^-	Leucine auxotroph
LysE	Lysine, Extracellular
LysI	Lysine, Intracellular
Mal	Malate
Mann	Mannitol
MCT	Metabolic Control Theory
mDAP	*meso*-Diaminopimelate
MDH	Malate dehydrogenase
ME	Malic enzyme
Met	Methionine
Met^S	A strain sensitive to Met
MQ	Menaquinone
MS#	Metabolite Set number # (Appendix B)
MW	Molecular weight
MWCO	Molecular weight cut-off
NAD	Nicotinamide adenine dinucleotide (oxidized)
NADH	Nicotinamide adenine dinucleotide (reduced)
NADHOX	NADH oxidase
NADP	Nicotinamide adenine dinucleotide phosphate (oxidized)
NADPH	Nicotinamide adenine dinucleotide phosphate (reduced)
NH3	Ammonia
NMR	Nuclear magnetic resonance
NTG	N-methyl-N'-nitro-N-nitrosoguanidine
Oaa	Oxaloacetate
OAADC	Oxaloacetate decarboxylase
OD	Optical density

OUR	Oxygen uptake rate
O2	Oxygen
P_i	Inorganic phosphate
P-enzyme	Succinate thiokinase
PBS	Preliminary biochemistry set (Appendix B)
PC	Pyruvate carboxylase
PDC	Pyruvate dehydrogenase complex
PDC^A	Strain with attenuated activity of PDC
PDH	Pyruvate dehydrogenase
PEP	Phosphoenolpyruvate
PGP	3-Phosphoglyceroyl phosphate
PK	Pyruvate kinase
PK^A	Strain with attenuated activity of PK
PMB	Preculture medium, basal (Table 5.2)
PMS	Preliminary metabolite set (Appendix B)
PPC	PEP carboxylase
PPC^R	Strain with PPC resistant to inhibition by Asp
PPG	Poly(propylene glycol) MW 2000
PPP	Pentose phosphate pathway
PPS	PEP synthetase
PRED	Phenol red (Table 5.8)
PSS	Pseudo-steady state
PSSA	Pseudo-steady state approximation
PTS	Phosphotransferase system
Pyr	Pyruvate
PyrE	Pyruvate, extracellular
Rib5P	Ribose-5-phosphate
Ribu5P	Ribulose-5-phosphate
RNA	Ribonucleic acid
RPM	Revolutions per minute
RQ	Respiratory quotient: CER/OUR
Sed7P	Sedoheptulose-7-phosphate
SLB	Super LB medium (Table 5.6)
Suc	Succinate
SucCoA	Succinyl coenzyme A
TA	Transaldolase
TCA	Tricarboxylic acid
Thr	Threonine
Thr^-	Threonine auxotroph
TK	Transketolase
Trehal	Trehalose
Tris	Tris(hydroxymethyl)aminomethane
Trp	Tryptophan
Trp^-	Tryptophan auxotroph
U	Unit of enzyme activity (nmole product/min)
UDPG	Uridine diphosphate glucose
Val	Valine

VVM	Volume of air per volume of fermentation broth per min.
WLS	Weighted least squares
Xyl5P	Xylulose-5-phosphate
2PG	2-Phosphoglycerate
6PGL	6-Phosphogluconolactone

A.2 Nomenclature

A.2.1 Roman

$\mathbf{A}$	Biochemistry matrix ($m \times n$)
a_{ij}	Element of $\mathbf{A}$
$\mathbf{b}$	Constraint vector (k)
$\mathbf{C}$	Constraint matrix ($k \times n$)
C_j^E	Extracellular concentration of metabolite j
$\mathbf{C}^E$	Concentration vector of all C_j^E (mM)
C_j	Intracellular concentration of metabolite j
C_j^T	Total concentration of metabolite j
C($\mathbf{A}$)	Condition number of $\mathbf{A}$ (Equation (4.17))
D($\mathbf{M}$)	Row and column dimensions of Matrix $\mathbf{M}$
f_{PPP}	Faction of glucose that enters the PPP
ΔG°	Free energy of reaction (Kcal/mole)
h	Consistency index
H^+/O	Proton translocation efficiency
$\mathbf{I}$	Identity matrix
J	Ojective function
$\mathbf{J}$	Jacobian matrix
k	Number of reaction fluxes constrained, as given by $\mathbf{C}$
K_M	Michaelis or saturation constant
ℓ	Number of dependant equations (rows) in $\mathbf{A}$
m	Number of metabolites in measurement set
$\mathbf{m}$	Modal vector (Equation (2.8))
$\mathbf{M}$	Modal matrix (Equation (2.9))
n	Number of reaction fluxes in biochemistry set
$\mathbb{P}$	Permutation matrix (Equation (4.20))
P/O	ADP phosphorylation efficiency
p	Confidence level, see $\chi_p^2(\chi)$.
q	Number of singular groups in $\mathbf{A}$
R($\mathbf{M}$)	Rank of a matrix $\mathbf{M}$
$\mathbf{r}(t)$	Metabolite accumulation rate vector at time t (mM/h) (m)
$r_i(t)$	Element of $\mathbf{r}(t)$
$\hat{\mathbf{r}}(t)$	Estimated $\mathbf{r}(t)$
$\overline{\mathbf{r}}(t)$	Actually measured $\mathbf{r}(t)$
$\mathbf{r}_E(t)$	Extracellular metabolite accumulation rate vector at time t
$\mathbf{r}_I(t)$	Intracellular metabolite accumulation rate vector

$\mathbf{S}$	As defined in Equation (4.21)
t	Time (units as indicated)
t_{AVE}	Average time between two samples
$\mathbf{U}$	Upper triangular matrix (Equation (4.20))
$V(t)$	Fermentor volume (l)
V_i	Reaction rates defined by Equations (6.2)-(6.8)
$\mathbf{x}(t)$	Vector of metabolic fluxes at time t (mmole/l/h) (n)
$\hat{\mathbf{x}}(t)$	Estimated $\mathbf{x}(t)$ (mmole/l/h)
$\mathbf{x}_G$	General solution of BRNE when $\mathbf{A}$ is singular
$\mathbf{x}_{N,i}$	Flux vector which falls in the null space of $\mathbf{A}$
$\mathbf{x}_R$	Solution of BRNE with the minimum norm (Equation (4.4))
x_i	Element of $\mathbf{x}$
Y_{ATP}	Biomass yield on ATP (g DCW/mole ATP)
Y_{ATP}^{MAX}	Theoretical maximum of Y_{ATP}
Y_{LYS}	Lysine yield (mole lysine/mole substrate)
Y_{LYS}^{MAX}	Theoretical maximum lysine yield
$\mathbf{Z}$	Redundancy matrix ($\ell \times m$)

A.2.2 Greek

ϵ	Residual vector (Equation (4.23))
ϵ_{340}	Molar absorptivity of NADH or NADPH at 340 nm
$\theta_{MAX}(\mathbf{A})$	Maximum singular value of $\mathbf{A}$
$\theta_{MIN}(\mathbf{A})$	Minimum singular value of $\mathbf{A}$
λ	Eigenvalue
$\mathbf{\Lambda}$	Matrix of eigenvalues
μ	Specific growth rate (h^{-1})
ν_{CELL}	Specific cellular volume (μl/mg DCW)
ξ_i	Fractional standard deviation of measurement i
ρ_{CELL}	Density of packed cells (mg DCW/ml)
$\sigma_i(t)$	Standard deviation of $r_i(t)$ (mM/h)
τ	Time constant
Φ	Fermentor volume to intracellular volume.
$\chi^2(\ell)$	Chi-square variate with ℓ degrees of freedom.
$\chi_p^2(\ell)$	The value given by $P\{\chi^2(\ell) < \chi_p^2(\ell)\} = p$
$\mathbf{\Psi}$	Measurement noise covariance matrix ($m \times m$)

A.2.3 Operators

$E\{\ \}$	Expectation operator
$P\{\ \}$	Probability operator
^{T}	Matrix transpose
$^{-1}$	Matrix inverse
$\lvert\ \rvert$	Absolute value
$\lVert\ \rVert$	Matrix or vector norm, Euclidian norm unless specified
[ ]	Metabolite concentration

Appendix B

Biochemistry and Metabolite Sets

This appendix contains the biochemistry and metabolite sets used to represent the cellular metabolism of *C. glutamicum*. To avoid ambiguities, reactions are referenced in the thesis by number and biochemistry set. For example Reaction (23:BS1) refers to Reaction (23) in biochemistry set BS1. Reversible reactions listed below are indicated by an "=" sign, while irreversible reactions are indicated by ">" or "<" signs. However, as discussed in Chapter 4, reaction irreversibility was not used to constrain metabolic fluxes. Metabolite abbreviations are listed in Appendix A.

B.1 Preliminary Sets (PBS, PMS)

The preliminary biochemistry and metabolite sets (PBS, PMS) reflect the biochemical reactions that have been reported (independent of conditions or magnitude of activity) in the cell-free extract of glutamic acid bacteria, as reviewed in Chapter 3. As a result, there are several reactions listed in the PBS that either introduce singularities in **A** (Chapter 4) and/or are not expressed under the standard fermentation conditions (Chapter 5).

B.1.1 PBS

PEP:Glucose Phosphotransferase System

1) GLC + PEP > GLC6P + PYR

Storage Compounds; Trehalose

2) GLC6P + 0.5 ATP = 0.5 TREHAL + 0.5 ADP

Embden-Meyerhof-Parnas Pathway

3) GLC6P = FRU6P
4) FRU6P + ATP > 2 GAP + ADP
5) GAP + ADP + NAD = NADH + G3P + ATP
6) G3P = PEP + H2O
7) PEP + ADP > ATP + PYR
8) PYR + NADH = LAC + NAD

Carboxylation Reactions

9) PEP + CO2 > OAA
10) PYR + CO2 + ATP > OAA + ADP
11) OAA > PYR + CO2
12) PYR + CO2 + NADPH = MAL + NADP

Tricarboxylic Acid Cycle

13) PYR + COA + NAD > ACCOA + CO2 + NADH
14) ACCOA + OAA + H2O = ISOCIT + COA
15) ISOCIT + NADP = AKG + NADPH + CO2
16) AKG + COA + NAD > SUCCOA + CO2 + NADH
17) SUCCOA + ADP = SUC + COA + ATP
18) SUC + H2O + FAD = MAL + FADH
19) MAL + NAD = OAA + NADH

Acetate Production or Consumption

20) ACCOA + ADP = AC + COA + ATP

Glyoxylate Shunt

21) ISOCIT = SUC + GLYOX
22) ACCOA + GLYOX + H2O > MAL + COA

Glutamate, Glutamine, Alanine, and Valine Production

23) NH3 + AKG + NADPH = GLUT + H2O + NADP
24) GLUT + NH3 + ATP > GLUM + ADP
25) PYR + GLUT > ALA + AKG
26) 2 PYR + NADPH + GLUT > VAL + CO2 + H2O + NADP + AKG

Pentose Phosphate Cycle

27) GLC6P + H2O + 2 NADP > RIBU5P + CO2 + 2 NADPH
28) RIBU5P = RIB5P
29) RIBU5P = XYL5P
30) XYL5P + RIB5P = SED7P + GAP
31) SED7P + GAP = FRU6P + E4P
32) XYL5P + E4P = FRU6P + GAP

Oxidative Phosphorylation; P/O = 2

33) 2 NADH + O2 + 4 ADP > 2 H2O + 4 ATP + 2 NAD
34) 2 FADH + O2 + 2 ADP > 2 H2O + 2 ATP + 2 FAD

Aspartate Amino Acid Family

35) OAA + GLUT = ASP + AKG
36) ASP + PYR + 2 NADPH + ATP > AKP + 2 NADP + ADP + H2O
37) AKP + SUCCOA + H2O + GLUT > MDAP + COA + AKG + SUC
38) MDAP > LYSI + CO2

Alternate Lysine Pathway
39) AKP + NADPH + NH3 = MDAP + NADP + H2O

Lysine Transport
40) LYSI = LYSE

Biomass Synthesis; $C_{3.97}H_{6.46}O_{1.94}N_{0.845}$ and 3.02% Ash
41) 0.021 GLC6P + 0.007 FRU6P + 0.09 RIB5P + 0.036 E4P + 0.013 GAP
+ 0.15 G3P + 0.052 PEP + 0.03 PYR + 0.332 ACCOA + 0.08 ASP
+ 0.033 LYSI + 0.446 GLUT + 0.025 GLUM + 0.054 ALA
+ 0.04 VAL + 3.82 ATP + 0.476 NADPH + 0.312 NAD = BIOMAS
+ 3.82 ADP + 0.364 AKG + 0.476 NADP + 0.312 NADH
+ 0.143 CO2

ATP Dissipation Reaction
42) ATP > ADP

Dinucleotide Transhydrogenase
43) NADH + NADP = NAD + NADPH

B.1.2 PMS

1) AC	11) FADH	21) LAC	31) PEP
2) ACCOA	12) FRU6P	22) LYSE	32) PYR
3) AKG	13) G3P	23) LYSI	33) RIB5P
4) AKP	14) GAP	24) MAL	34) RIBU5P
5) ALA	15) GLC	25) MDAP	35) SED7P
6) ASP	16) GLC6P	26) NADH	36) SUC
7) ATP	17) GLUM	27) NADPH	37) SUCCOA
8) BIOMAS	18) GLUT	28) NH3	38) TREHAL
9) CO2	19) GLYOX	29) O2	39) VAL
10) E4P	20) ISOCIT	30) OAA	40) XYL5P

B.2 Basic Sets (BS1, MS1)

As discussed in Section 4.1.5.3, the PBS and PMS were condensed to remove singularity problems in the associated biochemistry matrix, **A**. The resulting sets, BS1 and MS1, reflect these modifications and are the predominate sets from which the BRNE is complied.

B.2.1 BS1

PEP:Glucose Phosphotransferase System
1) GLC + PEP > GLC6P + PYR

Storage Compounds; Trehalose

2) GLC6P + 0.5 ATP = 0.5 TREHAL + 0.5 ADP

Embden-Meyerhof-Parnas Pathway

3) GLC6P = FRU6P
4) FRU6P + ATP > 2 GAP + ADP
5) GAP + ADP + NAD = NADH + G3P + ATP
6) G3P = PEP + H2O
7) PEP + ADP > ATP + PYR
8) PYR + NADH = LAC + NAD

Anaplerotic Reactions; PEP carboxylase

9) PEP + CO2 > OAA

Tricarboxylic Acid Cycle

10) PYR + COA + NAD > ACCOA + CO2 + NADH
11) ACCOA + OAA + H2O = ISOCIT + COA
12) ISOCIT + NADP = AKG + NADPH + CO2
13) AKG + COA + NAD > SUCCOA + CO2 + NADH
14) SUCCOA + ADP = SUC + COA + ATP
15) SUC + H2O + FAD = MAL + FADH
16) MAL + NAD = OAA + NADH

Acetate Production or Consumption

17) ACCOA + ADP = AC + COA + ATP

Glutamate, Glutamine, Alanine, and Valine Production

18) NH3 + AKG + NADPH = GLUT + H2O + NADP
19) GLUT + NH3 + ATP > GLUM + ADP
20) PYR + GLUT > ALA + AKG
21) 2 PYR + NADPH + GLUT > VAL + CO2 + H2O + NADP + AKG

Pentose Phosphate Cycle

22) GLC6P + H2O + 2 NADP > RIBU5P + CO2 + 2 NADPH
23) RIBU5P = RIB5P
24) RIBU5P = XYL5P
25) XYL5P + RIB5P = SED7P + GAP
26) SED7P + GAP = FRU6P + E4P
27) XYL5P + E4P = FRU6P + GAP

Oxidative Phosphorylation; P/O = 2

28) 2 NADH + O2 + 4 ADP > 2 H2O + 4 ATP + 2 NAD
29) 2 FADH + O2 + 2 ADP > 2 H2O + 2 ATP + 2 FAD

Aspartate Amino Acid Family

30) OAA + GLUT = ASP + AKG
31) ASP + PYR + 2 NADPH + SUCCOA + GLUT + ATP > SUC

+ AKG + CO2 + LYSI + 2 NADP + COA + ADP
32) LYSI = LYSE

Biomass Synthesis; $C_{3.97}$ $H_{6.46}$ $O_{1.94}$ $N_{0.845}$ and 3.02% Ash
33) 0.021 GLC6P + 0.007 FRU6P + 0.09 RIB5P + 0.036 E4P + 0.013 GAP
+ 0.15 G3P + 0.052 PEP + 0.03 PYR + 0.332 ACCOA + 0.08 ASP
+ 0.033 LYSI + 0.446 GLUT + 0.025 GLUM + 0.054 ALA
+ 0.04 VAL + 3.82 ATP + 0.476 NADPH + 0.312 NAD = BIOMAS
+ 3.82 ADP + 0.364 AKG + 0.476 NADP + 0.312 NADH
+ 0.143 CO2

ATP Dissipation Reaction
34) ATP > ADP

B.2.2 MS1

1) AC	11) FRU6P	21) LYSI	31) RIBU5P
2) ACCOA	12) G3P	22) MAL	32) SED7P
3) AKG	13) GAP	23) NADH	33) SUC
4) ALA	14) GLC	24) NADPH	34) SUCCOA
5) ASP	15) GLC6P	25) NH3	35) TREHAL
6) ATP	16) GLUM	26) O2	36) VAL
7) BIOMAS	17) GLUT	27) OAA	37) XYL5P
8) CO2	18) ISOCIT	28) PEP	
9) E4P	19) LAC	29) PYR	
10) FADH	20) LYSE	30) RIB5P	

B.2.3 Flux Diagrams

In order to facilitate interpretation of flux distributions, reaction fluxes are displayed on flux diagrams, such as that shown in Figure B.1. The numbers on Figure B.1 correspond, on a one-to-one basis, with the reactions listed above in BS1. Fluxes are reported in absolute (mmole/l/h) or relative units and represent the extent of a reaction as given by its stoichiometry. For a further discussion on flux diagrams, see Section 6.1.3.2.

B.3 Modified Sets

B.3.1 BS2 and MS2

In order to handle gluconate metabolism, the following two reactions were add to BS1

GLCN + ATP > GLCN6P + ADP (35:BS2)
GLC6P + H2O + NADP > GLCN6P + NADPH (36:BS2)

and Reaction (22:BS1) was modified to:

GLCN6P + NADP = RIBU5P + CO2 + NADPH (22:BS2)

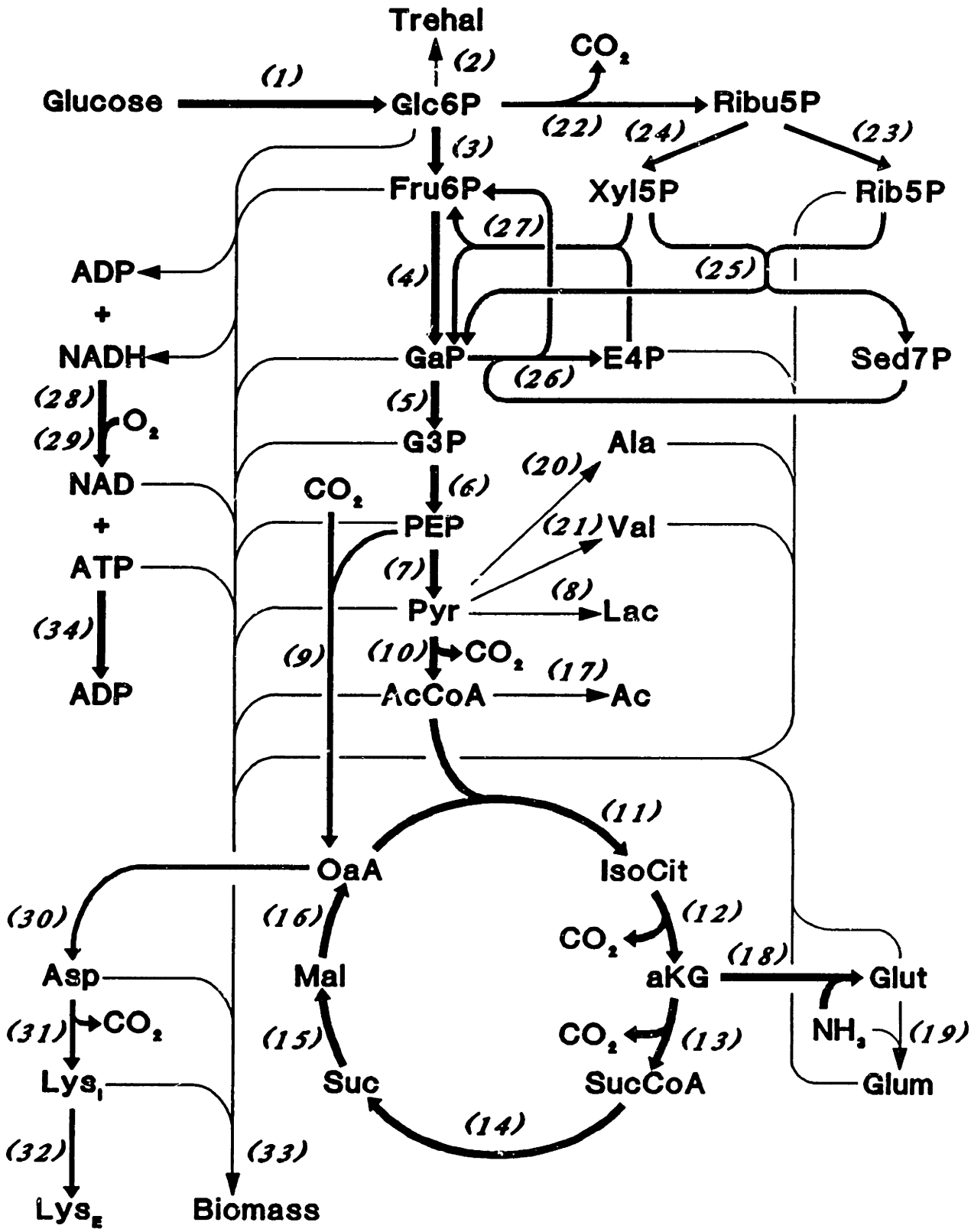

Figure B.1 Diagram of the biochemical reactions used to represent the primary metabolism of *Corynebacterium glutamicum*, as well as the peripheral reactions necessary to support lysine and biomass synthesis. Numbers correspond to the reactions listed in BS1. For clarity, cofactor requirements are not illustrated, and substrates and products for some reactions are not completely displayed.

All other reactions in BS2 are the same as those in BS1. The corresponding metabolite set (MS2) is the same as MS1, except that two addition metabolite balances are included for GLCN and GLCN6P.

When flux distributions for the gluconate fermentation were calculated from BS2 and MS2, it was found that the lactonase supported a negative flux, as illustrated in Figure B.2. Since thermodynamic constraints prohibit the reversal of lactonase (see Section 6.3.2), the biochemistry and metabolite sets were modified as described below.

B.3.2 BS3 and MS3

In order to dissipate the excess NADPH produced by gluconate catabolism, Reaction (36) in BS2 was replaced by:

$$2\ NADPH + O2 > 2\ H2O + NADP \qquad (36{:}BS3)$$

The metabolite set, MS3, was left unchanged from MS2.

B.3.3 BS4 and MS4

Excess NADPH also resulted in the flux distributions (based on BS1 and MS1) calculated from the *C. glutamicum* fermentation in which fluoroacetate was added (Section 6.5.2). As a result, BS1 was modified by replacing Reaction (22:BS1) with Reaction (36:BS3) to produce BS4. The metabolite set, MS4, was left unmodified from MS1.

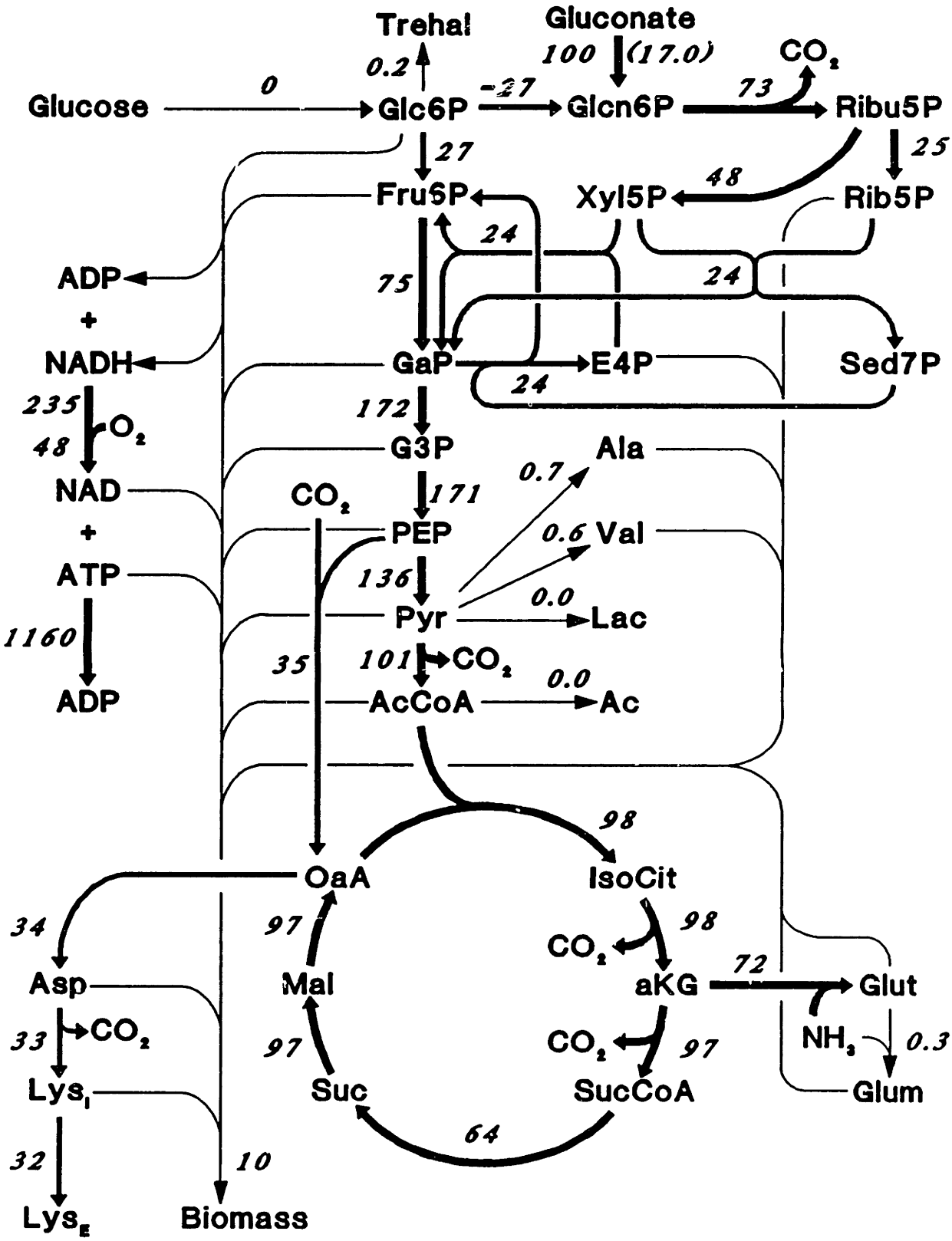

Figure B.2 Flux distribution map for the gluconate fermentation at 19.5 h. Fluxes estimated from measurements taken at 18.0 and 21.0 h (see Figure 6.22 and Table 6.11), and normalized by gluconate uptake rate (shown in parentheses in mmole/l/h). Fluxes based on BS2 and MS2.

Appendix C

BIONET Program

The program BIONET was written to facilitate the construct and analysis of metabolic bioreaction networks and to estimate flux distributions in such networks from experimental measurements. It is assumed that the reader is familiar with the theory (presented in Chapter 4) and the objectives of flux estimation. This appendix is simply a manual for this program. A copy of this program is available, free of charge, by contacting either Joe Vallino or Greg Stephanopoulos in the Chemical Engineering Department at the Massachusetts Institute of Technology, Cambridge, MA 02139. Since the source code, written in FORTRAN (ouch), consists of several thousand lines, it is not included here. However, most of the code is also available upon request.

The program runs on an IBM PC/XT/AT (or clone) equipped with 550 K of memory (preferably 640 K), a math coprocessor, and a 1.2 M floppy drive or a hard drive. A graphics card is not required, but the menus are more easily read on a color monitor.

The file README.1ST is included on the system disk that describes the installation of the BIONET program, as well as information on the other files included on the system disk.

C.1 Program Overview

BIONET consists of four main menus, which are typically executed in a sequential manner. Following the title screen, the program starts at Menu 1. This menu simply shows the current status of the system variables, and allows the user to change directories and/or drives. The options under Menu 2 are used to construct the bioreaction network equation (BRNE) either manually or from user defined biochemistry files. Following construction of the BRNE, the options under Menu 3 can be used to analyze the BRNE for singularity or sensitivity problems, as well as to construct the matrix used in the consistency routine (more on this later). Finally, options under Menu 4 allow the user to construct the measurement vector, to check the measurements for consistency, and to solve the BRNE for the metabolic fluxes.

At the top-level of any of the four main menus, the following global keys are active:

Function Keys

F1 - F4	Displays the options of the corresponding top-level menu.
F9	Temporarily exits the program and enters a DOS shell. This is useful for examining files. To return to the program, 'EXIT' is typed at the DOS prompt. It should be noted that the DOS file COMMAND.COM must be in the top level director of the drive (this is standard for a hard drive).
F10	Displays a non-context sensitive help menu.

Other Keys

<CR>	(Carriage Return) Transfers control to the top-level of the next menu.
ESC	Exits the program.

To execute a menu option, the corresponding number is entered. In general, the escape key (ESC) is used to exit submenus, as well as to gracefully exit options that require further input, such as file names. In regard to file names, most options will except the wild card characters '*' and '?' and display all files in the current directory that match. The desired file can be selected by highlighting it with the arrow keys and hitting <CR>. The wild card characters can only be used in options that read files, not in ones which write files. In options that require further input, the arrow and back space keys can be used to edit the input prior to hitting <CR>.

The rest of this manual describes the options that are available under each of the four top-level menus.

C.2 Menu 1: Default Settings and System Status

Currently, Menu 1 serves only two purposes. The first is to be able to change the default directory and drive, and the second is to display the status of system variables. Option 1 is used to change the drive specifier, while Option 2 is used to change the default directory path. Normal DOS protocols govern both options. Since the BIONET program generates or requires files containing rate measurements, flux estimates, biochemical reactions, and balance metabolites (as well as others), it is useful to create many separate directories that contain all the files for a given set of data. As such, it is best to execute the BIONET program from its home directory and then change to the desired subdirectory via the options of Menu 1.

The status window displayed in Menu 1 indicates if a system matrix or vector has been defined (set). Also displayed are the current dimensions of the system matrices and vectors, which are briefly described below:

Variable	Dimension	Description
A	m × n	Contains the bioreaction network stoichiometry. This matrix is constructed in Menu 2.
x	n	Vector of flux estimates, which is generated in Menu 4.
r	mr	Vector of metabolite accumulation rates, which is constructed in Menu 4.
Z	ℓ × mz	Redundancy matrix constructed in Menu 3.
b	k	Reaction constraint vector, constructed in Menu 2.
C	k × n	Constraint matrix, constructed in Menu 2.

Further information on each system variable is given in the section corresponding to the appropriate menu. The status or dimension of the system matrices or vectors cannot be modified from Menu 1.

C.3 Menu 2: System Construction Routines

The options under Menu 2 are used to construct the BRNE, $\mathbf{Ax} = \mathbf{r}$, and the constraint equation, $\mathbf{Cx} \geq \mathbf{b}$ (if used), either from user supplied files or directly from the keyboard. Options are also included to store the system or recall a previously constructed system. Menu 2 can be reached by pressing the F2 function key or by pressing the <CR> key from Menu 1. The details for the Menu 2 options are discussed below.

C.3.1 Option 1: Construction of BRNE from files

Option 1 of Menu 2 invokes the Biorxn Matrix Compiler: Menu 2.1. This routine constructs **A**, **C**, and **b** from user supplied biochemistry (*.BIO) and metabolite (*.CMP) files. The biochemistry file contains the biochemical reactions used to represent the network, and must be written, with a standard text (ASCII) editor, prior to the initiation of the BIONET program. Furthermore, the file must meet the following matrix compiler specifications:

- A record† with the '!' character in column 1 is treated as a comment, as well as any record that is blank.
- Columns 1-6 are used by the matrix compiler for numbering and comments, and so, should not be used.
- Reaction data are read starting from column 7 and ending at column 80.
- Each record can only be 80 characters long (including the first 6 characters).
- A reaction can be continued on the next record only if the '&' character is placed in column 80. However, a reaction cannot be longer than 254 characters in total (i.e. 3 full records plus up to column 41 of 4th record).
- Upper and lower case characters can be used as well as numerical characters to construct metabolite names; however, all alpha characters are converted to upper case before processing.

† A record is one line of text.

- All metabolite names must be equal to or less than 8 characters and can only begin with an alpha character.
- All stoichiometric coefficients must be in decimal format (*i.e.*, scientific notation is not supported).
- Direction of a reaction is specified by the following symbols:
  - = Specifies a reversible reaction.
  - > Specifies an irreversible forward reaction.
  - < Specifies an irreversible backwards reaction.
- The end of a metabolite name is delimited by a '+', '−', space or one of the directional specifiers given above. Spaces, however, are treated as a '+'; that is, numbers are assumed positive. A coefficient is assumed negative if it is preceded by a minus sign '−'.
- Reaction numbers need not be entered since the compiler automatically generates them.

The file EXAMPLE.BIO provided with the system disk is an example of a typical biochemistry file. The metabolite file (*.CMP) must also be written before initiation of the BIONET program, and contains the list of metabolites that balances will be constructed for. This file must meet the following specifications:

- A record is treated as a comment if the '!' character is placed in column 1.
- Metabolite names must abide by the specifications given for the biochemistry file described above.
- No more than one metabolite name can occupy any single record.
- Metabolite names are read starting at column 7.
- The list does not need to be capitalized, alphabetized, or numbered since this is done by the compiler.

The file EXAMPLE.CMP is an example of a *.CMP file.

Option 1 of Menu 2.1 is used to select the biochemistry and metabolite files used in the compilation of the BRNE. Option 2 of this menu is used to specify whether the matrix **C** and vector **b** of the constraint equation, $\mathbf{Cx} \geq \mathbf{b}$, are to be constructed as well (this is described below). If the output from the compilation is to be stored in a file, then Option 3 can be used to specify the file name. Pressing the <CR> key begins the compilation, described below.

The metabolite names list in the specified *.CMP file are first read and are converted to capitals, alphabetized, then rewritten to the *.CMP file with the comment lines (those preceded with the character '!') pushed to the bottom of the file. The compiler then begins to read the *.BIO file, record by record, to construct **A**. During this construction, the compiler lists those names found in the *.BIO file which it cannot find in the *.CMP file. For example, the metabolite H2O may be listed in the biochemistry file; however, this metabolite is seldom included in the *.CMP file because the rate of H2O accumulation cannot be measured. These metabolites are displayed to ensure that a typographical error has not occurred. After the compiler finishes constructing the biochemistry matrix, **A**, it lists those metabolites in the *.CMP file that were not found in the *.BIO file. For a properly constructed system, no metabolites will be listed. However, if any metabolites are

reported in this list, then the resulting **A** matrix will be singular since it will contain zero rows. This problem is usually caused by typographical errors in either the *.CMP or *.BIO files. In any case, the BIONET program must be exited and the biochemistry files corrected, so that all metabolites listed in the *.CMP file participate in at least one reaction listed in the *.BIO file. Next, the compiler list those metabolites that are involved in only one reaction since the pseudo-steady state approximation cannot be invoked for these metabolites. Typically, the metabolites listed here should correspond to extracellular compounds. After this report, the compiler displays the system dimensions, given by the values of k, m, and n. If Option 2 is invoked, then the compiler also constructs the constraint matrix, **C**, and vector, **b**. Listed below is an example of what the compiler does.

Compiler Example:

Let the *.BIO and *.CMP files contain:

	*.BIO file	*.CMP file
1)	GLC6P = FRU6P	ATP
2)	FRU6P + ATP > 2 GAP + ADP	FRU6P
3)	GAP + ADP + NAD < NADH + G3P + ATP	G3P
		GAP
		NADH

From these files the matrix compiler would construct the following system (provide Option 2 was set to invoke the constraints):

$$\mathbf{A} = \begin{bmatrix} 0 & -1 & 1 \\ 1 & -1 & 0 \\ 0 & 0 & 1 \\ 0 & 2 & -1 \\ 0 & 0 & 1 \end{bmatrix} \quad \mathbf{C} = \begin{bmatrix} 0 & 1 & 0 \\ 0 & 0 & -1 \end{bmatrix} \quad \mathbf{b} = \begin{vmatrix} 0 \\ 0 \end{vmatrix} \qquad \begin{matrix} k = 2 \\ m = 5 \\ n = 3 \end{matrix}$$

The elements of the measurement vector, **r**, would correspond to the metabolites listed in the *.CMP file, and the vector **x** would represent the three unknown reaction fluxes given in the *.BIO file.

At the end of the compilation and following the status and system reports, the matrix compiler routine returns control over to the top-level of Menu 2. If all metabolites listed in the *.CMP file were used in the *.BIO file (so that **A** does not contain any zero rows), then the status of **A** will be "defined"; otherwise, it will be left as "undefined". Also, **the number of equations must be equal to or greater than the number of unknowns** (*e.g.*, $m \geq n$); otherwise, **A** will remain undefined. The status window will also display the current values of k, m, and n. If the constraints were invoked, then the status of **C** and **b** will also be "defined". The constraint matrix, **C**, specifies those fluxes that are unidirectional. It should be noted that the matrix compiler always produces a constraint vector, **b**, that is identically **0**. However, this vector can be modified if desired as described below.

C.3.2 Option 2: Modify Elements of A, C, b

Option 2 of Menu 2 calls up the System Modification: Menu 2.2. This menu can be used to modify individual elements of **A**, **C**, or **b**, completely define the system matrices (element by element), or to add additional constraints or equations to the system. The options displayed in Menu 2.2 are fairly obvious and do not require much explanation. However, if the system matrices are to be created from scratch, then the system dimensions must be defined (Option 1) and the system matrices must be initialized (usually to zero; Option 2) before individual elements of **A**, **C**, or **b** can be entered. Unfortunately, to set or modify an element of **A**, **C**, or **b** (Options 3, 4, and 5), its row and column (for **A** and **C**) position must be entered first, followed by the new element value (sorry, but I did not have the time to write a spread sheet routine; .... FORTRAN remember). Pressing the ESC key at the menu prompt returns control to Menu 2.

C.3.3 Storage and Recall of System

Once a system has been constructed, it is often used repeatedly. Consequently, Options 3, 4 and 5 allow the user to store and recall the system, so that it does not need to be compiled from the biochemistry files each time the BIONET program is initiated. Option 3 specifies the file storage format (in FORTRAN), which can be toggled between "UNFORMATTED" and "FORMATTED". If Option 3 specifics "FORMATTED" then the file will be stored in ASCII (*i.e.*, normal text) format; otherwise, the file will be stored in binary code. The advantage to the formatted file structure is that it can be easily examined like any other text file, the disadvantage is that a formatted file takes more disk space and more time to store and read. Once the file structure is specified (default is unformatted), the system can be stored with Option 4. This option requires a file name, for which the extension *.ACB is usually used, and stores the following information into the designated file:

*.BIO file name used to construct the system
*.CMP file name used to construct the system
k, m, n
A(1,1) ... A(1,n)
⋮
A(m,1) ... A(m,n)
C(1,1) ... C(1,n)
⋮
C(k,1) ... C(k,n)
b(1) ... b(k)

It should be noted that Option 4 does not check for existence of the specified file; consequently, any file with the same file name will be overwritten without warning! It is also possible to construct or edit a *.ACB file with a text editor, provided the file is recalled with the formatted file structure. Option 5 is used to recall a previously stored system from disk. However, the file structure specified by Option 3 must match the file's format, otherwise an error will occur.

When a system is recalled from disk, the *.CMP file name is restored; however, the *.CMP file is not read. Since it is helpful in the redundancy routine (Menu 4) to have the metabolite names that correspond to the elements of **r**, Option 6 of Menu 2 is provided, so that the metabolite names can also be recalled from the *.CMP file. It should be noted that both Options 5 and 6 support wild card characters.

Option 7 is used to print the system to a specified file. The difference between Option 7 and Option 4 is that only elements whose absolute values are greater than zero are printed. This is quite useful since the system matrices are usually quite sparse (*i.e.*, most elements have zero values).

C.4 Menu 3: System Analysis and Redundancy Matrix

Menu 3 is entered either by pressing the F3 function key or by hitting the <CR> key from Menu 2. Once a system has been constructed (Menu 2), the options under Menu 3 can be used to examine the rank of **A**, as well as its condition number and singular values. During the singularity analysis, the redundance matrix, **Z**, is also constructed; **Z** can also be constructed or edited from the keyboard, as well as stored and recalled to/from disk. Menu 3 options are explained below.

C.4.1 Option 2: Singularity Analysis Routine

Option 2 of Menu 3 invokes the Singularity Analysis Routine: Menu 3.2. This routine is used to calculate the rank of **A**, provided **A** is defined, as well as to construct the redundancy matrix, **Z**. This routine uses Gaussian elimination (with partial pivoting) to determine the number of dependent rows in **A**. In so doing, the routine generates the permutation matrix, **P**, which transforms the BRNE as follows:

$$\mathbf{PAx} = \mathbf{Ux} = \mathbf{Pr} \tag{C.1}$$

Depending on the setting of Option 2, **PA** (= **U**) will be either an upper triangular matrix (the default setting) or an upper diagonal matrix. (It should be noted that **U**, as defined by Equation (C.1), is slightly different than the **U** defined by Equation (4.20) in Chapter 4.) The number of dependent rows in **A**, represented by ℓ, is given by the number of zero rows at the bottom of **U**. The rank of **A** is given by $m - \ell$. If the rank of **A** is less than n, then **A** is singular and the BRNE cannot be solved. It is acceptable (actually desirable if **A** is nonsingular) for the rank of **A** to be less than m. Since the Gaussian elimination routine needs to know what to consider as absolute zero, Option 1 is provided so that the tolerance may be adjusted. All elements whose absolute value are less than the tolerance are treated zero. Finally, the redundancy matrix, **Z**, is given by the last ℓ rows of **P**; *e.g.*, $\mathbf{P} = [\mathbf{S}\ \mathbf{Z}]^T$. Of course, if ℓ equals 0, then the redundancy matrix is not defined and the redundancy routine cannot be used.

To summarize, Option 1 is used to adjust the tolerance for the Gaussian elimination routine (the default value usually works fine). Next, Option 2 is used to determine the form of **U**. The Gaussian elimination proceeds slightly faster if **U** is made upper triangular; however, if **U** is upper diagonal, it is easier to identify singular groups. The form of **U** does not affect **Z**. Option 3 is used to store **U** and

P in a user specified file for later examination (if desired); however, elements of **U** or **P** whose absolute value are less than the tolerance (Option 1) are not stored. To initiate the Gaussian elimination, the <CR> key is hit. At the end of the calculations, a window is displayed in which the results of the analysis are given. The ESC key is used to return to the top-level of Menu 3 (if you hit <CR>, the analysis will start again; sorry about that).

To identify singular groups in **A** (assuming **A** is singular) the form of **U** should be set to upper diagonal, and Option 3 should be used to store **U** and **P** (to reduce ambiguity, the *.UP file extension is suggested). To examine the *.UP file, the BIONET program must be exited, either through the ESC or the DOS shell (F9) options executable at the top-level of any menu. The matrices are stored in the file as shown below:

Example output of a sparse matrix:

```
ROW 1
--------------------------------
 1) 1

ROW 2
--------------------------------
 2) 1     10)-5

ROW 3
--------------------------------
 3) 1
```

And so on.

This output displays the nonzero elements (*i.e.*, elements that are greater than or equal to the tolerance) of **U** in a row-by-row format. In the above example, the elements of **U** displayed are: U(1,1) = 1; U(2,2) = 1; U(2,10) = -5; and U(3,3) = 1. All other elements in the first three rows of **U** are zero with respect to the tolerance. The singular groups can be identified as those fluxes (represented by **x**) that are not uniquely defined by **U**. For example, since the BRNE can be express as, **Ux** = **Pr**, the above example output would produce the following set of equations:

$$\begin{aligned} x(1) &= \Sigma_i P(1,i)r(i) \\ x(2) - 5\,x(10) &= \Sigma_i P(2,i)r(i) \\ x(3) &= \Sigma_i P(3,i)r(i) \end{aligned}$$

Although fluxes 1 and 3 are uniquely defined by the measurements, fluxes 2 and 10 are not. Consequently, fluxes 2 and 10 constitute a singular group. As discussed in Chapter 4, there are as many singular groups as there are dependent columns of **A**, or $n - m + \ell$. It should be noted that some singular groups may only involve a couple of reaction fluxes, while others may consist of many. In any case, singularities

in **A** can only be removed by modifying the biochemistry files (*.BIO and *.CMP) or by directly modifying **A** via Menu 2.2.

Hence, when developing a bioreaction network, the procedure is to construct the *.BIO and *.CMP files, compile them via Menu 2, and then check the resulting biochemistry matrix for singularities. If singularities are identified, the output of **U** is employed to identify the reactions in the *.BIO file whose deletion would remove the singularities. When **A** is nonsingular, only the diagonal elements of **U** (*i.e.*, U(i,i)) will be nonzero. Although the elements of **P** (which includes **Z**) are also stored in the *.UP file, they are of little use in identifying singular groups.

C.4.2 Option 3: Singular Value Decomposition

Option 3 of Menu 3 invokes the Singular Value Decomposition Routine: Menu 3.3. This routine is predominately used to calculate the condition number of **A** from its maximum and minimum singular values. It can also be used to examine the singular values and the singular vectors of **A** as well (I have not examined the implications of the singular vectors of **A**, as yet). An option is also provided to calculate the condition number of **A** based on the 1-norm (maximum absolute column sum); however, to do so, the pseudo-inverse of **A** [given by $(\mathbf{A}^T\mathbf{A})^{-1}\mathbf{A}^T$] must also be calculated.

Singular values less that the tolerance, Option 1, are treated as zero. If the singular vectors, pseudo-inverse, or 1-norm condition of **A** are to be calculated in addition to the singular values, then Options 2, 3 or 4 should be toggled to 'YES'; otherwise, these options will not be invoked. Since the routine only displays the maximum and minimum singular values, a file must be opened if the values of the other singular values are also required. This can be accomplished with Option 5. If the singular vectors are also to be examined (both right and left), then Option 6 must be toggled to 'YES'. The singular value decomposition of **A** begins after the <CR> key is pressed. Results from the decomposition are then displayed in a window and stored to a file, if requested. The singular value decomposition routine is from the LINPACK library. The ESC key returns control to Menu 3.

C.4.3 Option 4: Sensitivity Analysis

Option 4 of Menu 3 initiates Menu 3.4 from which the partial derivatives, $\partial\mathbf{x}/\partial\mathbf{r}$ and $\partial\mathbf{x}/\partial a_{ij}$, of the solution to the BRNE (Menu 4) can be calculated. (These derivatives are given by Equations (4.18) and (4.19) in Chapter 4.) Due to the amount of data generated by either of these derivatives, all output is directed to a user specified file given by Option 1 (with file extensions *.dxr and *.dxa). After the output file is specified, invoking Option 2 calculates $\partial\mathbf{x}/\partial\mathbf{r}$, which produces an n × m matrix (the pseudo-inverse). Option 3 requires additional input of the element of **A** that the derivative is to be taken with respect to. Note, since **r** may not have been calculated yet, it is not used. Therefore, the derivative $\partial\mathbf{x}/\partial a_{ij}$ generates an n × m matrix for each element of **A**. In other word, the derivative is given by, $\partial\mathbf{x}/\partial a_{ij} = \boldsymbol{\Theta}\mathbf{r}$, but only $\boldsymbol{\Theta}$ is reported. The ESC key is used to exit Menu 3.4.

C.4.4 Manipulation of Z

After the redundancy matrix, **Z**, has been constructed via the singularity analysis routine (Option 2, Menu 3), the matrix can be stored or recalled to/from a user specified file with Options 5 and 6 from Menu 3 (the file extension *.Z is suggested). As with the storage of the system matrices (Section C.3.3), the user must also specify the file structure for the *.Z file. This is accomplished with Option 7. The *.Z file is stored as:

ℓ, mz
Z(1,1) ... Z(1,mz)
⋮
Z(ℓ,1) ... Z(ℓ,mz)

So as to keep tract of the current dimensions of **Z**, the variable mz is used instead of m for the column dimension. The *nonzero* elements of the **Z** matrix can be printed to a user specified file with Option 8 (also see Section C.4.1).

Although the **Z** matrix is automatically calculated in the singularity analysis routine, the matrix can be constructed or edited from the keyboard with Options 9, 10, and 11 of Menu 3. These three options work identically to those described under Menu 2.2 (Section C.3.2), so their use will not be explained here.

C.5 Menu 4: Measurements and Solution of BRNE

Menu 4 servers the follow three main functions: 1) to construct the measurement vector, **r**; 2) to check the measurement vector for proper consistency; and 3) to solve the BRNE for the reaction fluxes. Menu 4 can be called up with either the F4 function key or by pressing the <CR> key from the top-level of Menu 3.

C.5.1 Construction of r

Option 2 allows the user to specify the time that the measurement vector corresponds to. The input to this option is not used by the program, but is merely stored with the measurement file. This option accepts up to 13 characters, which can be alphanumeric. When a measurement vector is read from disk, this option displays the 13 character string that was stored with that file. If the option is not called, the string defaults to 'UNSPECIFIED'.

Option 3 is used to specify or change the dimension of **r**, which is represented by the variable mr. In general, mr should have the same value as m, which corresponds the row dimension of **A**. Next, Option 4 is used to initialize the vector, usually to zero. At this point the measurement vector is defined as displayed in the status window. Finally, Option 5 is used to enter the elements of **r** (the values corresponding to the metabolite accumulation rates). It is usually helpful to have a copy of the corresponding *.CMP file since this file contains the names and element numbers of the metabolites. This file can also be examined by leaving the program via the DOS shell (F9 key).

Once the measurement vector is constructed, it can be stored onto disk with Option 6. The extension suggested for this file is *.r. Before the file is stored, the

program allows the user to enter one 80 character comment line that will be stored with the file. The file is stored in a standard ASCII (*i.e.*, text) file. This file can also be created with any standard text editor; however, the file format must match that of the programs. To examine the file format, simply examine a file that has been previously stored via Option 6.

Option 7 is used to recall a previously stored measurement vector file. This option excepts wild card characters. If the file is properly recovered, then the status window should display the value of mr and **r** should read 'DEFINED'. Once a measurement vector is constructed or recovered from disk, the redundancy routine can be called up to check the measuremen vector for consistency. However, if the measurement vector has been constructed or modified, *the vector should be stored prior to invoking Option 8* since the vector may be updated (overwritten) by the redundancy routine.

C.5.2 Option 8: Redundancy Analysis

Option 8 of Menu 4 invokes Menu 4.8, the Redundancy Analysis Routine†. For this routine to be executed, the measurement vector, **r**, and the redundancy matrix, **Z**, must both be defined, mr must equal mz, and ℓ must be greater than zero. This information can be obtained from the status window displayed under Menu 1 (if you have any doubts). Before the options of Menu 4.8 are displayed, however, a preliminary screen is displayed that informs the user of the measurements that will not be involved in the consistency analysis. The measurements displays at this point are not expressed in any of the constraint equations contain within **Z**. Consequently, if a gross measurement error is in one of these measurements, it will not be identifiable, nor will it produce any inconsistencies (although the fluxes calculated will be incorrect). At this point control can be return to Menu 4 by pressing the ESC key, or transferred to the main display of Menu 4.8 by pressing the <CR> key. It should be noted that if the *.CMP file has been previously read (Menu 2, Section C.3.3), then the actual metabolite names will be displayed in all menus under Menu 4.8; otherwise, only the metabolites elemental position in **r** will be displayed. Thus, it is always useful to read in the *.CMP file prior to calling the redundancy routine. It should also be noted that the options under Menu 4.8 are not necessarily executed in the order that they are listed (see Sections C.5.2.5 and C.6).

C.5.2.1 Confidence Level

Option 1 of Menu 4.8 is used to change the confidence level of the consistency routines. In essence, measurements vectors that *fail* the consistency check have a {confidence level}% probability of harboring a gross measurement error, where {confidence lever}% is given by Option 1. Therefore, as the confidence level is increased, the value of Chi-square, used to test the consistency index, h, increases. Hence, as the confidence level is increased, fewer and fewer measurement vectors *fail* the consistency check. (This does make sense, just think about it a while.) Standard values used for the confidence level are typically 90% (default value) or 95%. The tolerance specified by Option 2 is identical to that discussed for the singularity

† The algorithm for this routine is based on that presented by Wang, N. S. and Stephanopoulos, G. (1983). *Biotechnol. Bioeng.* **25**, 2177-2208.

analysis routine, Menu 3.2 (Section C.4.1). The default value for the tolerance usually performs just fine.

C.5.2.2 Measurement Variance

Option 3 invokes yet another menu: Measurement Variance Routine: Menu 4.8.3. This menu is used to construct, or recover from disk, the variance associated with the measurements. Although measurement variance is what is used in the redundancy routine and stored on to disk, *the user enters measurement* ***standard deviation*** *from the keyboard,* ***not*** *measurement variance.* (The standard deviation is simply squared by the routine to get measurement variance.) Option 1 of Menu 4.8.3 is used to initialize the standard deviation of all the measurements in **r**. The initial value used is typically some small number, but not usually zero since this will introduce singularities when the inverse of the variance is taken. Option 2 is used to enter the standard deviations associated with specific measurements. This option displays a window which prompts the user to enter the element number, then its standard deviation. This process is repeated until all values are entered. The ESC key can be used back out of this window. Once the standard deviations are entered, they can be stored to disk with Option 3. Prior to storage, the program prompts the user to enter one line of comments. As stated above, the measurement variance and not the standard deviation is written to the file specified. This file can also be constructed from a standard text editor, but the file format must match that which the program is expecting. The extension *.VAR is suggested for the variance file. Previously stored *.VAR files can be recovered with Option 4. Wild card characters are supported by this option. The ESC key returns control to Menu 4.8. Note, the measurement variance must be set before Options 4-8 of the redundance routine, Menu 4.8, can be invoked.

C.5.2.3 Automatic Error Identification

Option 4 of Menu 4.8 is used to begin the Automatic Error Identification Routine: Menu 4.8.4. This routine is used to check the consistency of the measurement vector and to identify measurements that cause inconsistencies, provided inconsistencies are detected. Before this routine can be called, the measurement variance must be set. Menu 4.8.4 has four options. Option 1 allows the output to be sent to a printer as well as to the screen; Option 2 specifies the amount of information to display during the consistency analysis; Option 3 determines if the automatic iteration process should stop when the test function passes; and Option 4 designates the maximum number of measurements that can be deleted from **r** at one time. Although the maximum number of measurement deletions possible is ℓ-1 (usually the default value of Option 4), a maximum of five is placed on the number of measurements that can be deleted due to display limitations. After the four options are set, the automatic error analysis is started by hitting the <CR> key.

The analysis first displays the consistency index, h, and the Chi-square value for the case when no measurements are deleted. Depending on the settings of Menu 4.8.4, the program may pause to allow the user to either continue or exit the analysis. The analysis continues by systematically deleting one measurement at a time and reporting the test results for each deletion until the set of all **r** with one measurement deleted have been displayed. The analysis proceeds by displaying the test results for all sets of **r** in which two measurements have been deleted. This deletion process

continues until the maximum number of measurements that can be deleted, given by Option 4, is reached. At any time during this process, whether prompted or not, hitting the ESC key returns control to Menu 4.8. However, upon exiting Menu 4.8.3, the information on the measurements that were currently deleted when ESC was executed is retained and is used by Option 8 of Menu 4.8, if invoke (see details on Option 8 below).

If the calculated consistency index for any set of deletions is greater than the Chi-square value, then the measurement set is said to fail the consistency check, and there is a {confidence lever}% probability that the measurement set harbors a gross measurement error. If the complete measurement set fails the consistency test, then the cause of the inconsistency can sometimes be identified by examining the test results under different measurement deletion cases. If the deletion of one particular measurement (*i.e.*, metabolite) alleviates the inconsistency in the resulting measurement set (that is, the consistency index significantly decreases, so that the reduced set passes the consistency test), then there is a strong possibility that the deleted measurement is grossly in error (*i.e.*, the variance assigned to the deleted measurement is much smaller than that indicated by its residual). Deleting a measurement is equivalent to setting its standard deviation to infinity. In any case, this routine allows the user to examine the change in the consistency index as various measurements are deleted from the measurement vector, **r**.

C.5.2.4 User Directed Error Identification

Option 5 of Menu 4.8 invokes the User Directed Error Identification routine: Menu 4.8.5. This routine is vary similar to the automatic error identification routine discussed above, except that in this routine the user directly specifies the measurements that are to be deleted. As in Menu 4.8.4, the ESC key is used to exit this routine and the current set of deleted measurements are retained for Option 8 of Menu 4.8.

C.5.2.5 Measurement Set Modification

Option 6 of Menu 4.8 invokes the Measurement set Reduction/Expansion Routine: Menu 4.8.6. Although the complete measurement set can be used in the error identification routines discussed above, it is often useful to limit the consistency analysis to a subset of the complete measurement set. For example, one may wish to examine the consistency of only those metabolites that are observed to accumulate extracellularly. It is easy to show that metabolites whose rate of accumulation equal zero (*i.e.*, r(i) = 0) can be legitimately removed from the measurement set. In effect, removal of a zero-valued measurement is equivalent to setting its variance or standard deviation to zero. (This is not actually implemented; instead, the columns of **Z**, which correspond to zero-valued measurements, are deleted as specified.) The net result is that only those measurements that are included in the active measurement set (displayed in the window of Menu 4.8.6) are involved in the consistency analysis or updated when Menu 4.8 is exited via Option 8. Measurements that are *not* zero-valued *cannot* be removed from the measurement set.

There are four options available under Menu 4.8.6. Option 1 removes all metabolites from the measurement set that have an accumulation rate of zero. Option 2 is used to remove user specified zero-valued measurements. Once Option 2 is invoked, enter the value of a zero-valued measurement then hit return. Continue to enter numbers followed by a return until finished, then exit via ESC. The window

will then be updated to display the currently active measurements. Option 3 is used to restore the complete measurement set (excluding those measurements that are not involved in the consistency analysis). Option 4 is used to restore previously removed measurements. This option works as Option 2 does. Once the measurement set is properly reduced or expanded, the ESC key returns control to Menu 4.8. It should be noted that those metabolites that were listed in the preliminary menu upon initiation of the redundancy routine are not listed since they are not involved in the consistency routine. If an attempt is made to add these metabolites to the measurement set, it will not be permitted and an error message will be displayed. Also, Menu 4.8.6 is usually called after the measurement variance routine has been called, but before initiating one of the error identification routines. Therefore, Option 6 is somewhat out of sequence.

C.5.2.6 Updating Measurement Vector

The redundancy routine may be exited via two routes. If Menu 4.8 is left via the ESC key, then the measurement vector, **r**, that was passed to this routine from Menu 4 is **not** updated or changed in any way. As far as Menu 4 is concerned, it would be as if the redundancy routine had never been called. If the measurement vector is to be updated, then the redundancy routine must be left via Option 8, which calls the Measurement Estimation Routine: Menu 4.8.8.

This routine is used to update the measurement vector, such that the measurement constraints are exactly satisfied, as given by, $\mathbf{Z}\hat{\mathbf{r}} = \mathbf{0}$, where $\hat{\mathbf{r}}$ represents the updated vector (note, in general $\mathbf{Zr} \neq \mathbf{0}$). When the measurement vector is updated, via Option 1 of Menu 4.8.8, all measurements (that are currently active) are adjusted, so that the constraints are exactly satisfied with an updated measurement vector that produces the smallest consistency index, h (also see Equation 4.26 in Chapter 4 and Section 4.1.9). The net result, of course, is simply the weighted least-squares solution applied to the measurement vector. Those metabolites that are currently deleted from the measurement set, which are displayed at the bottom of Menu 4.8.8, are free to take on any value; hence, this explains why deleting measurements reduces the value of consistency index (recall that the standard deviation of a deleted measurement is effectively infinite). If the measurements currently deleted are not the ones of choice, then Option 2 can be used to delete different measurements (Option 2 calls the User Directed Error Identification Routine discussed in Section C.5.2.7). Also, only those measurements that are currently active are affected by the measurement update routine (recall that zero-valued measurements that have been removed have an effective standard deviation of zero; also see Option 6 of Menu 4.8 and Section C.5.2.5). It is important to realize that the Measurement Estimation Routine (Menu 4.8.8) is the only way by which a *weighted* least-squares solution of the BRNE can be obtained. If the redundancy routine is left via Option 1 of Menu 4.8.8, then the measurement vector that was passed to the redundancy routine is replace with the updated measurement vector, $\hat{\mathbf{r}}$. Consequently, *the measurement vector passed to the redundancy routine should be store beforehand.* It should be noted that once the redundancy routine is left (*i.e.*, control is returned to Menu 4 either by the ESC key or Option 8), the measurement variance vector, as well as all other information is lost (yes, this *is* stupid, but there was some memory allocation problems). Consequently, each time the redundancy routine is called, the measurement variance vector must be recalled

from disk, the measurement set must be reduced (if desired), and the error identification routine must be run.

C.5.3 Flux Estimates

Once the measurement vector has been constructed, tested for consistency, and updated via Option 8 of Menu 4 (updating the measurement vector is desirable, but not required), the BRNE can be solved for the reaction flux estimates, $\hat{\mathbf{x}}$, provided mr equals m. Before calculating the fluxes, however, Options 9-11 must be considered. If Option 9 is invoked, then the residuals, given by, $\mathbf{r} - \mathbf{A}\hat{\mathbf{x}}$, are also calculated and stored with the flux estimates. However, if the measurement vector has been updated via the redundancy routine (Option 8), then Option 9 will calculate, $\hat{\mathbf{r}} - \mathbf{A}\hat{\mathbf{x}}$, which equals 0. Consequently, Option 9 should only be used if the measurement vector has not been updated via Option 8. If the measurement vector has been updated via Option 8, then the residuals can be calculated by comparing the raw measurement vector with the updated measurement vector (this must be done outside of the BIONET program since it is not supported). Option 10 imposes the flux constraints on the solution to the BRNE (provided that $\mathbf{C}$ and $\mathbf{b}$ were constructed in Menu 2). If the constraints are invoked (which is not usually desirable; see Chapter 4), then the following nonlinear programming problem is solved†:

$$\text{Find } \mathbf{x} \text{ that minimizes } (\mathbf{Ax} - \mathbf{r})^T(\mathbf{Ax} - \mathbf{r})$$
$$\text{Subject to: } \mathbf{Cx} \geq \mathbf{b} \tag{C.2}$$

Otherwise, the standard least-squares solution, given by $\hat{\mathbf{x}} = (\mathbf{A}^T\mathbf{A})^{-1}\mathbf{A}^T\mathbf{r}$ (or $\hat{\mathbf{r}}$), is used to solve the BRNE (a QR decomposition is used to solve this problem). It is reiterated that if the measurement vector has not been updated via the redundancy routine, then the solution is *not* weighted by the measurement variances. Since the error (*i.e.*, standard deviation) associate with each measurement can, in general, vary significantly, the weight least-squares solution is usually preferable to the least-squares solution. Consequently, the redundancy analysis routine (Option 8) should always be used to calculate the updated measurement vector, even if the measurement set is consistent! It should be noted that the solution to the inequality constrained least-squares problem, Equation (C.2), does not use the measurement variance vector; consequently, the measurement vector should *not* be updated if constraints are to be invoked. (Since the constraints are seldom invoked, I have not investigate how the redundancy routine can be used with the flux constraints). Finally, Option 11 can be used so that flux estimates normalized (divided by) by a user specified flux are reported in addition to the absolute flux values.

Option 12 is used to solve the BRNE (with or without constraints) and Option 13 specifies the file to which the fluxes (and additional information if requested) are to be stored (the file extension *.FLX is suggested for the flux estimates). Before the

---

† The algorithm used to solve the nonlinear programming problem is given by Liew, C. K. (1976). *J. Am. Stat. Assoc.* **71**, 746-751, and Boot, J. C. G. (1963). *Econometrica* **31**, 464-498.

fluxes are stored, the user is prompted to enter one line of comments. Unlike all other storage routines, Option 13 checks for the existence of the file before storing the fluxes.

C.6 Typical Implementation

Described below is a brief account of how the BIONET program is used. There are basically two main iteration loops that are followed in the flux analysis of bioreaction networks. The first loop consists of constructing and analyzing the bioreaction network, so that the final network is nonsingular and well-posed. This is usually accomplished via Menus 1-3 of the BIONET program and without the input from measurements. In the second iteration, the measurement vector is constructed, then checked for consistency. Once a consistent measurement vector is obtained, the flux estimates are calculated from the updated measurement vector. The process is repeated for each measurement vector. The second loop predominately relies on the options under Menu 4.

C.6.1 Construction of Bioreaction Network

Once the biochemistry (*.BIO) and metabolite (*.CMP) files are constructed (with a standard text editor) the BIONET program is initiated, and the directory options of Menu 1 are used to change the default director to that which contains the *.BIO and *.CMP files. Next, Option 1 of Menu 2 is used to construct the biochemistry matrix, **A**, and the constraints, **C** and **b**, if they are to be used. Option 4 of Menu 2 is then used to store the system in a user specified *.ACB file. Options under Menu 3 are then used to examine the biochemistry matrix, **A**. Option 2 of Menu 3 is first used to see if **A** is singular or not. If **A** is singular, then the matrix **U** is examined (after storing to a *.UP file) to identify the singular groups in **A**. At this point the BIONET program is usually exited, so that the *.BIO and *.CMP file can be edited (reactions lumped or deleted) to removed the singularities in **A**. This process is repeated until a bioreaction network is constructed that is nonsingular. Once the biochemistry matrix, **A**, is rendered nonsingular, Option 3 of Menu 3 is used to calculate the condition number of **A**. If the condition number is unacceptable (around 1000 or more), then the biochemistry files must be modified again, so that the condition number of **A** is acceptable (approximately 100 or less). The detailed sensitivity routine (Option 4 of Menu 3) can also be used to identify the measurements that may introduce sensitivity problems. Finally, once the biochemistry files are modified such that **A** is nonsingular and well-conditioned, the singularity routine (Option 2, Menu 3) is used to construct the redundancy matrix, **Z**. This matrix is then stored to a file *.Z with Option 6 of Menu 3. At this point the first iteration loop is completed.

C.6.2 Flux Estimation

Once a nonsingular, well-conditioned biochemistry matrix is constructed from the *.BIO and *.CMP files, flux estimates can be calculated from the measurements. To start, the metabolite accumulation rates, and their associated standard deviation, at a specified time are calculated from experimental data (see Chapters 4 and 5). After the rate measurements have been obtained, the BIONET program is initiated.

As before, Menu 1 is used to set the default directory to that which contains the system files. Option 5 of Menu 2 and Option 5 of Menu 3 are then used to recall the system file *.ACB and the redundancy file *.Z previously stored from the first iteration loop. Options 2-5 of Menu 4 are then used to enter the measurement rate data, and Option 6 is used to store this data. The redundancy routine, Option 8, is then invoked.

Under Menu 4.8, Option 3 is used to enter the standard deviations for the measurements (typically, only the standard deviations of actually measured metabolites are known; consequently, the rest of the measurements are usually assigned a small, but acceptable, standard deviation). Next Option 6 of Menu 4.8 is used to reduce the measurement set, so that only those metabolites that are actually measured are left active. Following the reduction, Option 4 is used to initiate the automatic error analysis. If the measurement set *passes* the consistency test (no deletions) then Option 8 is used to exit the redundancy routine and update the measurement vector. If the measurement set is inconsistent, but the inconsistency can be removed by deleting a measurement, then the measurement is deleted (or its standard deviation increased) and the routine is exited via Option 8 as above. If the measurement set is inconsistent, and the inconsistency *cannot* be removed by deleting a measurement, then the entire measurement set is restored via Option 6, and the automatic consistency routine stared again. If the inconsistency can now be removed by deleting a previously removed measurement, then Option 8 is once again used to update the measurement vector. Finally, if the inconsistency cannot be legitimately removed, then the use of the measurement vector should be questioned. If inconsistencies routinely arise that cannot be identified, then there is a strong probability that the biochemistry may be in error or a metabolite is accumulating that is not properly accounted for in the measurement set. It should be noted that outright deleting a measurement is rather drastic. Consequently, an alternative is to increase the standard deviation of the questionable measurement(s) to an acceptable level before actual measurement deletion is invoked. As you might agree, the redundancy routine requires some experience to use; however, once mastered, the technique is quite powerful for identifying questionable measurements and their legitimate elimination.

Once the updated measurement vector is returned from the redundancy routine, Options 9-13 of Menu 4 are used to calculate the fluxes and to store the results. The flux estimates may be examined by leaving the BIONET program via the DOS shell (F9 function key). The above process is repeated for each measurement vector, **r**.

C.6.3 Miscellaneous

It often occurs that one would like to estimate fluxes with an incomplete measurement set. For example, O_2 and CO_2 may not have been measured for a particular run. To do so, those measurements in the *.CMP file that correspond to the non-measured metabolites can be removed from the balance by placing the '!' character in column one of the record that corresponds to the metabolite to be deleted. The number of metabolites that can be deleted from the *.CMP file is given by m − n. Once the *.CMP file is modified, the system must be rechecked for

singularity and sensitivity problems as described above since deleting measurements can introduce singularities even if m > n. This deletion procedure can also be used to calculate theoretical flux distributions. Simply stated, metabolites are deleted from the *.CMP file until the biochemistry matrix, **A**, is render square (m = n). At this point, the remaining measurements can be set to arbitrary values since inconsistencies cannot arise (of course, **A** must be nonsingular). Therefore, on can examine theoretical flux distributions for any arbitrarily defined measurement vector (see Chapter 4 for more details on theoretical flux distributions).

C.7 Libraries Used in BIONET

All matrix manipulations in the BIONET program were handled in double precision. The following libraries were used in the BIONET program for the indicated function:

Screen Drivers	ASMUTIL2 and BUTILE (Impulse Engineering, San Francisco, CA)
Matrix Inverse QR decomposition SVD decomposition	LINPACK (National Energy Software Center, Argonne IL)
Chi-Square values	IMSL (IMSL, Houston TX)

C.8 File Extensions

Due to the large number of files that the BIONET program interacts with, the following file extensions are suggested for use with the BIONET program:

File Extension:	File Contains:
*.BIO	Biochemical reactions of network.
*.CMP	List of compound names use to construct metabolite balances.
*.ACB	System file which contains the elements of **A**, **C**, and **b**.
*.Z	Redundancy matrix.
*.UP	Matrices from singularity analysis.
*.SVD	From singular value decomposition routine.
*.DXR	From sensitivity analysis routine, dx/dr.
*.DXA	From sensitivity analysis routine, dx/da.
*.R	Raw or updated measurement vector.
*.VAR	Variance of measurements.
*.FLX	Reaction flux estimates.